GEOLOGY, HYDROTHERMAL ALTERATION AND GEOCHEMISTRY OF THE IAMALELE (D'ENTRECASTEAUX ISLANDS, PAPUA NEW GUINEA) AND WAIRAKEI (NORTH ISLAND, NEW ZEALAND) GEOTHERMAL AREAS

A dissertation

submitted in partial fulfilment

of the requirements for the Degree

of

Doctor of Philosophy in Geology

in the

University of Canterbury

by

Peter Ashley Mitchell

University of Canterbury

1989

"In this age of cheap and expeditious travel when a voyage round the world is looked upon as an undertaking of less magnitude than a journey of a few hundred miles would have appeared to our fathers..."

Thomas Bracken

1879

ABSTRACT

The geothermal system at Iamalele is hosted by a series of late Quaternary high-silica dacite to rhyolite ignimbrite, air-fall tuff and related volcaniclastic rocks. The ignimbrite flows are intercalated with calc-alkalic andesite and low-silica dacite lavas, some of which are high-Mg varieties. The Iamalele Volcanics may be related to caldera collapse and post-caldera volcanism. Geothermal activity occurs over 30 km^2 of the Iamalele area. Chemical analyses of water from hot springs indicate that the near-surface reservoir is dominated by an acid-sulphate fluid, and that the deeper reservoir fluid probably has a significant seawater component. Analyses of rock and soil samples within the limits of geothermal activity identified several areas of above background values in Au, Hg, As and Sb. A diamond drill hole was completed to a depth of ~200 m in one of these areas. Hydrothermal alteration identified in the drill core indicates that the upper 200 m of the geothermal reservoir is well-zoned and contains a trace element signature characteristic of high-level, epithermal precious metal deposits. With increasing depth mineral assemblages indicative of advanced argillic, intermediate argillic and potassic alteration were observed in the recovered core.

The Wairakei geothermal system is hosted by a voluminous sequence of late Quaternary rhyolitic ignimbrite, air fall tuff and related volcaniclastic rocks intercalated with andesite to rhyolite lavas. The volcanic sequence was deposited during formation of the Maroa and Taupo caldera volcanoes, and geothermal activity is localized within a diffuse border zone between these two volcanic centres. The high-temperature reservoir at Wairakei is primarily restricted to porous pyroclastic rocks of the Waiora Formation. Geothermal activity is exposed over ~25 km^2 of the Wairakei area. Chemical analyses of well discharge indicate that the fluid is a low salinity, low total sulphur, near-neutral pH chloride water with a local meteoric source. Temperature profiles for ~60% of the Wairakei wells were used to construct a c. 1950 view of the thermal zoning of the reservoir. When compared to the estimated preproduction isotherms, reconnaissance fluid inclusion homogenization temperatures indicated that the deeper portion of the reservoir had cooled by ~45°C prior to production discharge. Hydrothermal rock alteration within the reservoir is systematically zoned and may be separated into four principal assemblages: propylitic, potassic, intermediate argillic and advanced argillic. Calcium

zeolites, mainly wairakite, mordenite and laumontite, occur throughout the reservoir and, with the exception of laumontite, form an integral part of either the propylitic or potassic assemblage. Intermediate argillic alteration is widespread but is not strongly developed. The distribution of advanced argillic alteration is sporadic and restricted to depths less than 65 m. Below a depth of ~500 m potassic alteration commonly overprints propylitic alteration. The location of the "average" Wairakei fluid on several activity diagrams drawn for 100°, 200°, 250° and 300°C indicates that propylitic and potassic alteration probably formed in equilibrium with a hydrothermal fluid chemically equivalent to the modern reservoir fluid at temperatures between ~275° and ~210°C. Assays of drill samples indicate that trace amounts of gold (<0.04 g/t) and other metals permeate the reservoir. Samples of siliceous sinter collected from wellhead production equipment contain significant quantities of precious metals and also platinum group and base metals. Metal-rich scale from a back pressure plate (well 66) was analysed by optical microscopy and by electron microprobe analysis. The scale is composed of several discrete mineral phases which show a distinct paragenesis.

Hydrothermal alteration and metallization identified within the reservoirs at Iamalele and Wairakei are similar to hydrothermal alteration and metallization identified within the epithermal precious metal deposits of Rawhide and Round Mountain (Nevada, U.S.A.). The major difference between these systems is the much greater abundance of gold and silver at Rawhide and Round Mountain. Conclusions drawn from these comparisons include: (1) within high-temperature active systems gold remains in solution or is dispersed at low grades; (2) boiling does not appear to be a viable means of producing a gold ore deposit within deep (>500 m) hydrothermal reservoirs and (3) the formation of a major precious metal ore deposit may require the superposition of a structural event on a waning geothermal system to initiate an extended period of fluid mixing.

High-Mg lavas similar to ones identified at Iamalele occur elsewhere in the late Cenozoic arc-type volcanic associations of southeastern Papua New Guinea. Detailed geochemical studies of these rocks have revealed the presence of relatively aphyric lavas which are high in MgO, Cr, and Ni and form an integral part of the arc-type association. The high concentrations of these elements relative to typical arc-related rocks are thought to reflect the chemical composition of the initial melt. High-Mg lavas occur in other volcanic arcs of Papua New Guinea as well as in several other circum-Pacific volcanic arcs, and it is likely that high-Mg lavas form a fundamental component of most, if not all, volcanic arcs.

ACKNOWLEDGMENTS

Many people have contributed to the production of this dissertation. Among those to whom I am most deeply indebted are Steve D. Weaver (my advisor), Terry M. Seward, Marco T. Einaudi, Ian E. M. Smith and Jim W. Cole who have encouraged me and supported my efforts over the past years.

Steve Weaver, Pat Browne and Pat Muffler were subjected to an early, and poorly contrived version of this dissertation. To them my condolences and sincere apologies.

Naomi Oreskes and John Black for providing the motivation to finish the first and second editions of this dissertation respectively. Both appeared in those final dark days when the possibility of finishing takes on a surreal quality. An additional note of gratitude goes to John, for he is the only person, other than the formal reviewers and my wife, who had to suffer through reading the initial draft. John's comments contributed substantially to the final format of this dissertation.

I would like to express my appreciation to the Geology Department staff at the University of Canterbury, past and present, for their patience and perseverance. Most of all, my appreciation goes to Wendy Nuttall, Davey Jones, Arthur Nicolas and Arthur Alloway and Kay Card.

My stay in New Zealand was very pleasant and memorable thanks to the efforts of Steve and Rosemary Weaver, Ray Crawford, Jarg Pettinga, Jim Cole, Yosuke Kawachi, Rod Sewell, Anthony Coote, John and Karla Marra, Joy and Colin Harrison, Hekmat and Sana Yousif whom I think of frequently during these difficult days in the Middle East.

Special thanks go to Tony Mahon for field and office assistance from the Department of Scientific and Industrial Research Wairakei, and to Doug Hattersley, Paul Bixby, John Leaver, and Lynell at the Ministry of Works

and Development for openly providing reservoir engineering and drilling data. Many other people, in true Kiwi fashion, were overwhelmingly helpful during my work in the North Island. I am particularly thankful to Terry and Di Seward, Mike Mongillo, Malcolm Grant, Bruce and Di Christensen, Ray Merchant, Peter Roberts, Ralph Krupp, Toni Cottle, Ernie Allen, Billy Duncan, Jim Healy, George Grindley and Bill Waters.

A word of thanks goes to Pat Browne, Dick Henley, Jeff Hedenquist, Rick Allis, Kevin Brown and Doug Sheppard for thoughtful comments, suggestions and support over the duration of my work in the North Island. Gareth Newton with the Department of Lands and Survey, Wellington helped me to acquire copies of the Wairakei area orthophoto maps, which Mark Lehman compiled into a single topographic base map of the Wairakei area.

Turning now to the topic of laboratory work, several people provided me with hours of night-time fun and entertainment interspersed with burned out filaments, broken vacuum lines and overloaded computers. In this regard I would like to express my appreciation to Yosuke Kawachi (University of Otago), Arthur Alloway and Kay Card (University of Canterbury), Julie Paque (Stanford University), Allan Campbell (Lincoln College) and Roger Nielsen (Oregon State University), your patience was appreciated.

I am also indebted to the staff of the Department of Applied Earth Sciences at Stanford University. Jan Moffat was particularly helpful during my year as a visiting scholar. This year I enjoyed very much. My sincere appreciation for this opportunity goes to Marco Einaudi and Gordon Brown.

To the Stanford contingent: John Black, Naomi Oreskes, Barb Bakken, Carey Peabody, Mark Sander and Eric Seedorff, your encouraging (at first, then threatening) phone calls and pleasant dinner conversation helped me survive the final push, which like Eric Seedorff I finished on Guam time. Carey, our days (and nights) on the Stanford probe made the final writing seem a pleasant task! For Barb I have mixed emotions. The time we spent

reminiscing about Montana and touring the California wine country were some of the best times I can recall. But Barb also introduced me to Stanford's Vax computer during my hour of need, which, as luck would have it, corresponded to the transition period between operating systems--supcript gave us the data, but the lines never met. Additional thanks go to Dave Boden, John Dilles, and Anita Grunder; all provided helpful discussions and reviews of various aspects of this dissertation.

Most of the drafting presented in this thesis was done by Lee Leonard (Christchurch), Mark Lehman (Missoula, Montana), Debbie Montgomery (Palo Alto, California) and Lisa Walsh (Reno, Nevada).

This work was partially supported by the City Resources Pty. Ltd. (Australia), Coeur d'Alene Mines Corporation, Esso Papua New Guinea, Inc., Exxon Minerals Company, U.S.A., Exxon Production Research Company, the Geological Society of America, Spectrum Resources and United Gold Pty. Ltd.

Special thanks go to Myron Goldstein and the upper management of Coeur d'Alene Mines Corporation for allowing me to take time off from work to complete my dissertation. With any luck, Myron will never notice the impact preparing my dissertation (drafting and reproduction) has had on our 1990 and 1991 reconnaissance budgets.

As I near the end of this endeavour, I would like to express my sincere gratitude to Julie Smith for taking the time to colour many of the figures in this volume while on holiday in the U.S.A., to Rob Noble for helping Julie colour and for fixing the back door to the house, and to Shirene Urton for formatting and printing Volume II and for teaching Ann to operate the laser printer. With regard to my dissertation, John Black and Mark Sander graciously provided copies of figures from their respective (recent) publications so that I could use them in Chapter 4. I suspect they did this to protect the quality of their work.

Several other people were very helpful during the course of my studies - among these are Jon Thorson, Bob and Rosemary McNeil, Eric Braun, Ian

Lange, Phil Ganz, Elizabeth Miller, Roger Nielsen, Jim Wright, Gail Mahood, Colin Wilson, Dennis Bird, J.G. Liou, Johnny Walker, Ted Bence, Joe Wagner and Millar Kesipik.

To the rest of you whose name should appear here but does not, you are not forgotten, simply preempted by the University deadline.

The one I owe the most to is my wife, Ann, first for putting up with this protracted (even for me) ordeal, and secondly for proof reading, rereading, typing, formatting, reformatting and printing the dissertation.

With one final comment, I conclude 38 years of formal, and sometimes not so formal, schooling. The only compliment that I have ever had in my life that was worth repeating came from Hyland Morrow when he reported that I have the best friends of anyone he has ever known--it's true.

TABLE OF CONTENTS

Page

ABSTRACT v

ACKNOWLEDGMENTS vii

VOLUME I:

TABLE OF CONTENTS xi

LIST OF TABLES xix

LIST OF FIGURES xxiii

VOLUME II:

TABLE OF CONTENTS xxix

LIST OF TABLES xxxv

LIST OF FIGURES xxxvii

VOLUME III - MAPS

LIST OF PLATES xxxix

CHAPTER

1. INTRODUCTION 1

Purpose of Study 1
Study Areas 3
Iamalele Geothermal Area,
D'Entrecasteaux Islands, Papua New Guinea 3
Wairakei Geothermal Area, North Island, New Zealand 4
Dissertation Format and Scope 6
Chapter 1 7
Chapter 2 7
Chapter 3 8
Chapter 4 9
Appendices. 10

2. IAMALELE GEOTHERMAL AREA, D'ENTRECASTEAUX ISLANDS,
PAPUA NEW GUINEA: GEOLOGY, HYDROTHERMAL
ALTERATION AND METALLIZATION 11

Introduction 11
Location and Geologic Setting 11
Previous Work 14

CHAPTER Page

2. IAMALELE GEOTHERMAL AREA, D'ENTRECASTEAUX ISLANDS, PAPUA NEW GUINEA: GEOLOGY, HYDROTHERMAL ALTERATION AND METALLIZATION (continued)

Regional Geology 16
Southeastern Papua New Guinea 16
Tectonic Setting 16
Volcanic Geology 17
D'Entrecasteaux Islands 17
Geologic Setting 17
Geophysics 19
Gravity Data 19
Airborne Magnetic Data 20
Geothermal Activity 21
Western Fergusson Island 22
Geology and Geomorphology 22
Structural Geology 23
Regional Tilting 23
Major Faults 24
Seymour Bay Caldera(?) 24
Geothermal Activity 27
Iamalele Geothermal Area 28
Volcanic Geology 28
Fagalulu Volcanics 31
I'wa'ur Basaltic Andesite 31
I'wa'ur Dacite 33
I'wa'ur Andesite 33
I'wa'ur Ignimbrite 34
Miapuya Ignimbrite 34
Iamalele Volcanics 35
Kilugaba Rhyolite 35
Iamalele Ignimbrite 36
Aloai and Wameai Andesite 37
Mona Malala Rhyolite 38
Yaluwana Tuff 38
Uluwa Obsidian 39
Uluwa Tuffaceous Siltstone 39
Surficial Deposits 40
Geochemistry 41
Andesite and Low-Silica Dacite 41
High-Silica Dacite and Rhyolite 42
Geophysics 45
Airborne Radiometric Data 46
Airborne Magnetic Data 47
High-Level Hydrothermal Alteration 48
Introduction 48
Surface Features 50
Tuffaceous Breccia 51
Stockwork Fracturing 53
Soil and Rock Geochemistry 53
High-Level Reservoir Conditions 55
Fluid Chemistry 55
Porosity and Permeability 58
Faults 60

CHAPTER Page

2. IAMALELE GEOTHERMAL AREA, D'ENTRECASTEAUX ISLANDS, PAPUA NEW GUINEA: GEOLOGY, HYDROTHERMAL ALTERATION AND METALLIZATION (continued)

Iamalele Geothermal Area (continued)
High-Level Hydrothermal Alteration (continued)
Diamond Drilling 60
Hydrothermal Alteration 60
Propylitic Alteration 64
Potassic Alteration 65
Intermediate Argillic Alteration 66
Advanced Argillic Alteration 67
Metallization 69
Discussion. 70

3. WAIRAKEI GEOTHERMAL AREA, NORTH ISLAND, NEW ZEALAND: GEOLOGY, THERMAL ZONING, HYDROTHERMAL ALTERATION AND METALLIZATION 71

Introduction 71
Location and Geologic Setting 72
Production History 74
Previous Work 75
Regional Geology 76
Taupo Volcanic Zone 76
Maroa and Taupo Caldera Volcanoes 79
Maroa Caldera Volcano 79
Taupo Caldera Volcano 81
Geothermal Activity 82
Wairakei Geothermal System 83
Tauhara Geothermal System 83
Wairakei Geothermal Area 84
Volcanic Stratigraphy 84
Pre-Tertiary Basement 84
Ohakuri Group 89
Wairakei Ignimbrite 90
Waiora Formation 92
Member 1 92
Member 2 93
Waiora Valley Andesite 94
Member 3 95
Member 4 95
Member 4 (Haparangi Rhyolite) 96
Karapiti Rhyolite 97
Haparangi Rhyolite 98
Te Mihi Rhyolite 99
Member 5 99
Huka Falls Formation 100
Members 1-4 100
Western Breccias 100
Wairakei Formation 102
Wairakei Breccia 102
Taupo Pumice 102

CHAPTER Page

3. WAIRAKEI GEOTHERMAL AREA, NORTH ISLAND, NEW ZEALAND: GEOLOGY, THERMAL ZONING, HYDROTHERMAL ALTERATION AND METALLIZATION (continued)

Wairakei Geothermal Area (continued)
Structural Development 103
Tectonic Components 103
Wairakei High 103
Taupo-Reporoa Basin 105
Te Mihi Basin 105
Volcano-Tectonic History 106
Geothermal Reservoir 108
Surface Expression 108
Preproduction Reservoir 110
Thermal Zoning 112
Fluid Inclusion Homogenization Temperatures 115
Production-Modified Reservoir 117
Duration of Geothermal Activity 117
Hydrothermal Alteration 119
Propylitic Alteration 121
Alteration Mineral Assemblage 122
Textural Relationships 122
Spatial Distribution 123
Potassic Alteration 125
Alteration Mineral Assemblage 126
Apatite 127
Monazite 127
Biotite 128
Zircon 131
Textural Relationships 140
Spatial Distribution 141
Transitional Propylitic-Potassic Alteration 142
Zeolite Alteration 148
Alteration Mineral Assemblage and Textural Relationships 149
Spatial Zoning 152
Carbonate Alteration 154
Textural Relationships 155
Spatial Zoning 156
Mineral-Fluid Equilibria 156
Reservoir Chemistry 157
Calculated Reservoir Fluid Composition 157
Activity Diagrams 164
Propylitic Alteration 165
Low-Temperature Alteration 165
Alkali Feldspar Equilibrium 176
Low Temperature Hydrothermal Biotite 178
Metallization 180
Steam Production Equipment 180
Siliceous Precipitates 181
Metal-Rich Scale 183
Hydrothermal Reservoir 189
Rare Earth Elements 191
Discussion 198

TABLE OF CONTENTS - VOLUME I (CONTINUED)

CHAPTER — Page

4. DISCUSSION AND CONCLUSIONS 201

Introduction 201
Active Geothermal Systems as the Precursors of Epithermal Gold-Silver Deposits 202
Introduction 202
Potential for the Discovery of Economic Precious Metal Mineralization in High-Temperature Geothermal Systems 203
Lihir Island, Papua New Guinea 207
Metal Loss through Surface Discharge in High-Temperature Geothermal Systems 209
Tectonic Setting and Geochemical Environment of Active and "Fossil" Hydrothermal Systems 210
Selection of Areas for Comparison 210
Tectonic Setting and Regional Geology 214
Iamalele 214
Wairakei 217
Rawhide 220
Round Mountain 223
Discussion 223
High-Level Hydrothermal Systems 228
Hydrothermal Alteration 229
Structural Controls 229
Potassic Alteration 230
Iamalele 230
Wairakei 231
Rawhide 231
Intermediate Argillic Alteration 231
Iamalele 232
Wairakei 232
Rawhide 233
Advanced Argillic Alteration 233
Iamalele 234
Wairakei 236
Rawhide 236
Metallization 237
Iamalele 239
Wairakei 240
Rawhide 241
Discussion 245
Intermediate-Level Hydrothermal Systems 247
Hydrothermal Alteration 248
Structural Controls 249
Propylitic Alteration 249
Wairakei 250
Round Mountain 253
Potassic Alteration 254
Wairakei 256
Round Mountain 257
Metallization 258
Wairakei 258
Round Mountain 259
Discussion 259

CHAPTER Page

4. DISCUSSION AND CONCLUSIONS (continued)

Active Geothermal Systems as the Precursors of Epithermal Gold-Silver Deposits (continued)
Tectonic Setting and Geochemical Environment of Active and "Fossil" Hydrothermal Systems (continued)
Implications for Precious Metal Exploration 266
Geochemical Anomalies Related to Surface Discharge Features 266
Conclusions 270
High-Mg Lavas in the Late Cenozoic Volcanic Arc Associations of Papua New Guinea 271
Introduction 271
High-Mg Lavas in Arc-Type Associations 273
Nomenclature of Magnesium-Rich Arc-Type Lavas 274
High-Mg Lava or Boninite? 276
Tectonic Setting of Papua New Guinea 277
Papua New Guinea Mainland and New Britain 277
Southeastern Papua New Guinea 278
Late Cenozoic Volcanism in Southeastern Papua New Guinea . . 279
Calvados Islands 280
Egum Atoll 281
Normanby Island 281
Amphlett Islands 284
Western D'Entrecasteaux Islands 284
East Papuan Volcanic Arc 285
Northern Volcanic Belt 285
Southern Volcanic Belt 289
High-Mg Lavas in Arc-Type Settings of Papua New Guinea . . . 292
Petrology of High-Mg Lavas, Northern Volcanic Belt, East Papuan Volcanic Arc 294
Bulk Rock Chemistry 295
Major Elements 295
Minor and Trace Elements 295
Rare Earth Elements 296
Radiogenic Isotopes 299
Neodymium and Strontium 299
Lead. 301
Mineral Chemistry 302
Spinel 302
Olivine 304
Clinopyroxene 308
Orthopyroxene 309
Iron-Titanium oxides 312
Plagioclase 314
Petrogenesis of the Southeastern Papua New Guinea Lavas . 316
Modified Mantle Source 316
Delayed Magmatism 319
Contamination 320
Fractional Crystallization 321
Crystal Accumulation 322
Two Component Mixing 324
Primary Magma 324
Conclusions 325

CHAPTER Page

REFERENCES CITED 327

LIST OF TABLES - VOLUME I

TABLE		Page
2.1.	Representative chemical analyses of lavas and pyroclastic rocks exposed in the Iamalele area of western Fergusson Island	32
2.2.	Chemical analyses of water samples from Fergusson and Normanby Islands	56
2.3.	Reservoir temperatures calculated using alkali geothermometers for water samples from Fergusson and Normanby Islands, D'Entrecasteaux Islands, Papua New Guinea and Wairakei, North Island, New Zealand	57
2.4.	Porosity of hydrothermally altered samples from Iamalele drill hole IA-1	59
2.5.	Chemical analysis of alunite from Iamalele drill hole IA-1, sample number 125838	68
3.1.	Summary of the stratigraphy of the Wairakei geothermal area	85
3.2	Microprobe analysis of hydrothermal biotite replacing groundmass microlites and glass in Haparangi Rhyolite	129
3.3	Representative fluorine, chlorine and F/Cl values for hydrothermal biotite from selected mineral deposits and active geothermal areas, and for magmatic biotite from selected unaltered igneous rocks	130
3.4.	Partial chemical analyses of reservoir fluid and steam for selected Wairakei wells	158
3.5.	Partial chemical analyses of Wairakei well discharge used to calculate activity ratios plotted in Figure 3.27	161
3.6.	Calculated total discharge fluid composition for well discharge data reported in Table 3.5	161
3.7.	Calculated reservoir pH values for well discharge data reported in Table 3.5	162
3.8.	Ion activities calculated from well discharge data presented in Table 3.6	162
3.9.	Activity ratios calculated from Wairakei water and steam analyses given in Table 3.5	163
3.10.	Hydrolysis reactions and log K values for minerals used in constructing Figure 3.27	166
3.11.	Reactions and log K values used to construct phase boundaries in Figure 3.27	167

TABLE		Page
3.12.	Partial trace element composition of siliceous precipitate collected from silencers and hot water drains at Wairakei	184
3.13.	Composition and textural characteristics of minerals contained in metal-rich scale from the back pressure plate of Wairakei Well 66	185
3.14.	Composition of electrum inclusions in tetrahedrite Ni-arsenides and bornite contained in metal-rich scale from Well 66	188
3.15.	Selected rare earth element data for representative bulk rock and siliceous precipitate samples	196
4.1.	Volcano-tectonic and structural setting of the Iamalele and Wairakei geothermal areas and the Rawhide and Round Mountain epithermal precious metal deposits	215
4.2.	Geology of the geothermal reservoirs at Iamalele and Wairakei and the palaeoreservoirs at Rawhide and Round Mountain	216
4.3.	Characteristics of hydrothermal alteration occurring in the geothermal reservoirs at Iamalele and Wairakei and in the palaeoreservoirs at Rawhide and Round Mountain	227
4.4.	Characteristics of metallization occurring in the geothermal reservoirs at Iamalele and Wairakei and in the palaeoreservoirs at Rawhide and Round Mountain	238
4.5.	Occurrence of high-Mg lavas, circum-Pacific rim	275
4.6.	Mean chemical composition of calc-alkalic and boninite lavas from southeastern Papua New Guinea	277
4.7.	Chemical analyses of andesitic rocks from the northern volcanic belt of the east Papuan volcanic province	288
4.8.	Chemical analyses of high-Mg lavas from the northern volcanic belt of the east Papuan volcanic province	296
4.9.	Rare earth element data for andesitic lavas from the northern volcanic belt of the east Papuan volcanic province	299
4.10.	Chemical analyses of spinel in high-Mg lavas from the northern volcanic belt of the east Papuan volcanic province	303
4.11.	Chemical analyses of olivine in high-Mg lavas from the northern volcanic belt of the east Papuan volcanic province	304

TABLE Page

4.12. Chemical analyses of clinopyroxene in high-Mg lavas from the northern volcanic belt of the east Papuan volcanic province 308

4.13. Chemical analyses of coexisting phenocrysts and groundmass pyroxene in high-Mg lavas from Watota Island, northern volcanic belt, east Papuan volcanic province . . . 312

4.14. Analyses of coexisting iron-titanium oxide minerals in high-Mg lavas from the northern volcanic belt of the east Papuan volcanic province 314

LIST OF FIGURES - VOLUME I

FIGURE		Page
1.1.	Location of the D'Entrecasteaux Islands and the Iamalele geothermal area	3
1.2.	Location of the Taupo Volcanic Zone and the Wairakei geothermal area	5
2.1.	Location of the D'Entrecasteaux Islands and the Iamalele area and the simplified geology of Fergusson Island and the southeastern tip of Goodenough Island	12
2.2.	Photographs of the Iamalele area	13
2.3.	Structural geology of west central Fergusson Island	15
2.4.	Bouguer anomaly map for Fergusson Island and the southeastern tip of Goodenough Island	20
2.5.	General geology of the Iamalele area	29
2.6.	Variation diagrams for rhyolitic rocks from the Iamalele area of western Fergusson Island	43
2.7	Map of the Iamalele area showing the limits of the airborne geophysical surveys, volcanic eruptive centres and active thermal areas	44
2.8	Simplified and contoured airborne radiometric data for the Iamalele area	45
2.9	Simplified and contoured airborne magnetic data for the Iamalele area	47
2.10.	Distribution of thermal features within the Iamalele area of western Fergusson Island	49
2.11.	Characteristic expression of strong hydrolytic alteration	50
2.12.	Surface expression of geothermal activity	52
2.13.	Geology and soil geochemical anomalies of the Uluwa dome and southern end of the Yaluwana plateau	54
2.14.	Summary log for Iamalele diamond drill hole IA-1	62
2.15.	Summary cross section through Iamalele drill hole IA-1	63
3.1.	Photograph of the eastern "bore field" at Wairakei	72
3.2.	Location of the Wairakei geothermal area with respect to the Taupo Volcanic Zone and the major caldera volcanoes and geothermal systems within the TVZ	73

FIGURE		Page
3.3.	Principal tectonic components of the New Zealand segment of the Indo-Australian Plate and Pacific Plate boundary	78
3.4.	Approximate location of major calderas of the southern Taupo Volcanic Zone	80
3.5.	Wairakei geologic cross sections	88
3.6.	Location of the geologic cross sections for Wairakei relative to selected geothermal wells.	89
3.7.	Geology of the Wairakei-Rotokawa region	104
3.8.	Location of the major thermal features and the traces of the major and minor faults within the Wairakei geothermal area	109
3.9.	Apparent resistivity contours for the Wairakei geothermal area	111
3.10.	Estimated preproduction thermal zoning for three cross sections through the Wairakei geothermal reservoir	114
3.11.	Location of the cross sections shown in Figure 3.10	115
3.12.	Location of wells for which fluid inclusion homogenization temperature data were determined from drilling samples	116
3.13.	East-west thermal cross sections for the Wairakei reservoir	118
3.14.	Spatial distribution of propylitic (pericline) alteration within the Wairakei hydrothermal reservoir	125
3.15.	Textures and mineral assemblages characteristic of potassic alteration	132
3.16.	Textures and mineral assemblages characteristic of potassic alteration overprinting propylitic alteration	134
3.17.	Textures and mineral assemblages characteristic of magnetite-destructive (potassic) alteration	136
3.18.	Textures and mineral assemblages characteristic of zircon (potassic) alteration	138
3.19.	Spatial distribution of potassic alteration within the Wairakei hydrothermal reservoir	141
3.20.	Spatial distribution of transitional propylitic-potassic alteration within the Wairakei hydrothermal reservoir	143
3.21.	Textures and mineral assemblages characteristic of transitional propylitic-potassic alteration	144

FIGURE		Page
3.22.	Textures and mineral assemblages characteristic of oxidized and reduced environments within potassic and transitional propylitic-potassic alteration	146
3.23.	Compositions of the calc-silicate phases identified at Wairakei	149
3.24.	Textures and mineral assemblages characteristic of zeolite alteration	150
3.25.	Spatial distribution of mordenite and laumontite alteration within the Wairakei hydrothermal reservoir	153
3.26.	Spatial distribution of calcite alteration within the Wairakei hydrothermal reservoir	155
3.27.	Activity diagrams for the aqueous species at 100°C, 200°C, 250°C and 300°C and quartz saturation	168
3.28.	Relation between Na/K and temperature in fluid coexisting with alkali feldspars	177
3.29	Photograph of production wellhead equipment in the central bore field at Wairakei	181
3.30.	Gold and silver content of siliceous precipitate collected from silencers and hot water drains at Wairakei	182
3.31	Schematic drawing of the wellhead production equipment required to separate steam from the two-phase fluid	183
3.32	Photomicrographs and back scatter electron images of metal-rich scale removed from a back pressure plate from well 66	186
3.33.	Graph of gold content versus depth and temperature for 225 core and cuttings samples collected from the Wairakei reservoir.	190
3.34.	Typical occurrences of gold-palladium and hydrothermal monazite in transitional propylitic-potassic alteration	192
3.35.	Examples of precious, platinum group, base and rare earth element mineralization associated with potassic alteration	194
3.36.	Chondrite normalized REE patterns for one representative bulk rock sample from each lithologic unit and five siliceous precipitate samples	197
4.1.	World map showing the location of several well-known high-temperature geothermal fields	204

FIGURE		Page
4.2.	Hot spring at the northwestern edge of Acid Lake in the Yaluwana thermal area at Iamalele	208
4.3.	Eastern bore field at Wairakei	208
4.4.	Comparison of the Wairakei geothermal reservoir with schematic representations of the ore zones at Rawhide and Round Mountain	212
4.5.	Location of the Iamalele geothermal area and simplified geology of Fergusson Island and the southeastern tip of Goodenough Island	218
4.6.	Structural setting of west-central Fergusson Island	218
4.7.	Location of the Wairakei geothermal area with respect to the Taupo Volcanic Zone and the major caldera volcanoes and geothermal systems within the TVZ	219
4.8.	Location map and regional geology in the vicinity of the Rawhide gold-silver deposit	221
4.9.	Location map and simplified geology of the Rawhide gold-silver deposit	222
4.10.	Location of the Round Mountain gold-silver mine with respect to Nevada, U.S.A., and the Toquima caldera complex	224
4.11.	Generalized geology of the Round Mountain gold-silver mine	225
4.12.	Relationship between geology, hydrothermal alteration and gold mineralization at the Rawhide precious metal deposit	234
4.13.	Down-hole distribution of selected trace and minor elements determined from drill cuttings and core from Wairakei well 48	242
4.14.	Gold geochemical data for core and cuttings samples from four Wairakei wells	244
4.15.	Characteristic rock alteration occurring at intermediate levels within the hydrothermal reservoir at Wairakei and the palaeoreservoir at Round Mountain	251
4.16.	Characteristic rock alteration occurring at intermediate levels within the hydrothermal reservoir at Wairakei and the palaeoreservoir at Round Mountain	251
4.17.	Photomicrographs of key feldspar replacement textures	252
4.18.	Spatial distribution of hydrothermal alteration assemblages at the Round Mountain epithermal gold-silver deposit	255

FIGURE Page

4.19. Relationship between hydrothermal alteration and precious metal mineralization at the Round Mountain epithermal gold-silver deposit 260

4.20. Log fO_2 -pH diagrams constructed for fluid composition typical of carbon- and sulphur-poor (low gas) geothermal systems and consistent with broad compositional constraints at Round Mountain 263

4.21. Model for the development of the Round Mountain hydrothermal system in space and time 264

4.22. Schematic cross section through the Uluwa flow dome showing the relationship between active thermal springs and the spatial distribution of gold in stream sediment samples . . 267

4.23. Isothermal log fO_2 -pH diagrams constructed for temperatures of 225°C and 150°C 268

4.24. Log fO_2 -pH diagram simplified from Figure 4.23 and showing the expected decrease in the solubility of gold bisulphide as the activity of H^+ and the relative oxidation state of the fluid increase 270

4.25. Distribution of late Cenozoic arc-type rocks in Papua New Guinea 272

4.26. Location of high-Mg lavas summarized in Table 4.5 274

4.27. Generalized geology of the D'Entrecasteaux Islands, Calvados Islands and Egum Atoll 282

4.28. K_2O-SiO_2 variation in late Cenozoic arc-type volcanic rocks from the east Papuan volcanic province 287

4.29. Variation in MgO, Cr and Ni with respect to SiO_2 in lavas from the northern volcanic belt of the east Papuan volcanic province 290

4.30. Variation in major oxides and trace elements with respect to SiO_2 in lavas from the northern volcanic belt of the east Papuan volcanic province 291

4.31. Variation in MgO, Cr and Ni with respect to SiO_2 in lavas from the southern volcanic belt of the east Papuan volcanic province 292

4.32. Variation in MgO with respect to SiO_2 in rocks from the Bismarck volcanic arc and the Fly-Highlands province 293

4.33. Chondrite normalized rare earth element abundance patterns for andesitic rocks from the northern volcanic belt of the east Papuan volcanic province 298

FIGURE		Page
4.34.	$^{143}Nd/^{144}Nd$ and $^{87}Sr/^{86}Sr$ ratios for lavas from the east Papuan volcanic province	300
4.35.	$^{207}Pb/^{204}Pb$ and $^{208}Pb/^{204}Pb$ ratios plotted against $^{206}Pb/^{204}Pb$ for lavas from the east Papuan volcanic province	301
4.36.	Compositional range of spinel in high-Mg lavas from the northern volcanic belt of the east Papuan volcanic province	302
4.37.	Compositional range of olivine phenocrysts in high-Mg lavas from the northern volcanic belt of the east Papuan volcanic province	306
4.38.	Partitioning of Fe^{2+} and Mg between olivine phenocrysts and the magma for high-Mg lavas from the northern volcanic belt of the east Papuan volcanic province	307
4.39.	Compositional range of pyroxene phenocrysts in high-Mg lavas from the northern volcanic belt of the east Papuan volcanic province	310
4.40.	fO_2T-X diagram for olivine phenocrysts in high-Mg lavas from the northern volcanic belt of the east Papuan volcanic province	313
4.41.	Chondrite normalized rare earth element abundance patterns for andesite rocks from the northern volcanic belt of the east Papuan volcanic province and for Pacific Ocean sea water	319
4.42.	Composition of pyroxene in "normal" series calc-alkalic andesitic lavas from the northern volcanic belt of the east Papuan volcanic province	323

TABLE OF CONTENTS - VOLUME II

APPENDIX — Page

1. SAMPLE LOCATIONS, USES AND DESCRIPTIONS 1

General Statement 1
Data Format and Abbreviations 1
East Papuan Volcanic Arc 3
Iamalele Geothermal Area 14
Wairakei Geothermal Area 154

2. LIST OF DRILL CORE AND CUTTINGS AND WELLHEAD SILICEOUS PRECIPITATE SAMPLES 299

General Statement 299
Data Format and Abbreviations 299
Iamalele Drill Core 300
Wairakei Drill Core and Cuttings 304

3. BULK ROCK CHEMISTRY 321

General Statement 321
Analytical Methods 321
X-ray fluorescence spectrometry 321
Sample preparation 321
Fusion beads 322
Pressed powder pellets 323
Instrumentation, software and operating conditions 324
Data quality 325
Accuracy, precision and sensitivity 325
Bead "shelf life" 325
Ferric and ferrous iron determination 328
Wet chemical methods 329
Alkali-based calculation 329
Norm calculation 331
Rare Earth Element Normalization Data 332
Data Format and Abbreviations 333
Trace and Minor Element Data
Iamalele geothermal area
Iamalele geochemistry 336
Diamond drill hole IA-1 geochemistry 381
Submittal information and analytical methods for samples submitted to commercial laboratories 386
Wairakei geothermal area
Wairakei geochemistry 389
Well 12 geochemistry 425
Well 48 geochemistry 427
Well 54 geochemistry 438
Well 67 geochemistry 441
Well 121 geochemistry 444
Well 205 geochemistry 445
Well 206 geochemistry 446
Well 212 geochemistry 447
Well 219 geochemistry 448
Well 221 geochemistry 449

APPENDIX — Page

3. BULK ROCK CHEMISTRY (continued)

Trace and Minor Element Data (continued)
Wairakei geothermal area (continued)
Production equipment geochemistry 450
Surface sample geochemistry 464
Replicate geochemistry 468
Submittal information and analytical methods for samples submitted to commercial laboratories 477
Major, Minor, Trace and Rare Earth Element Data
East Papuan volcanic arc
East Papuan volcanic arc geochemistry 480
East Papuan volcanic arc C.I.P.W. norms 487
Iamalele geothermal area
Iamalele geothermal area geochemistry 494
Iamalele geothermal area C.I.P.W. norms 500
Wairakei geothermal area
Wairakei geothermal area geochemistry 504
Wairakei geothermal area C.I.P.W. norm 505

4. MINERAL CHEMISTRY 507

General Statement 507
Analytical Method 507
Sample preparation 507
Instrumentation and software 508
University of Otago 508
Stanford University 509
Detection limits, accuracy and precision 510
University of Otago 510
Stanford University 512
Ferric and ferrous iron calculation 513
Standardization and cation calculations 515
University of Otago 515
Stanford University 515
Olivine 516
Iddingsite 516
Pyroxene 519
Plagioclase 520
Spinel group minerals 520
Ferric and ferrous iron calculation 521
Calculation of wt % ulvospinel 522
Ilmenite 524
Ferric and ferrous iron calculation 526
Calculation of wt % M_2O_3 526
Groundmass glass 528
Rare earth element-bearing minerals 528
Electrum, sulphide, sulphosalt and selenide minerals . . . 533
Data Format and Abbreviations 534
East Papuan Volcanic Arc Mineral Chemistry
Egum Atoll
Sample number 33607: Egum Island 538
Amphlett Islands
Sample number 33628: Wamea Island 539
Sample number 33630: Wawasi Island 547

APPENDIX Page

4. MINERAL CHEMISTRY (continued)

East Papuan Volcanic Arc Mineral Chemistry (continued)
Amphlett Islands (continued)
Sample number 33631: Wawasi Island 552
Sample number 33636: Tuboa Island 556
Sample number 33637: Wawiwa Island 559
Sample number 33638: Watota Island 560
Sample number 33639: Noupoi Island 570
Sample number 33640: Wata Island 575
Sample number 33642: Watota Island 578
Fergusson Island
Sample number 33645: Kukuia Peninsula 579
Sample number 33660: Kukuia Peninsula 590
Sample number 33667: Kukuia Peninsula 592
Goodenough Island
Sample number 33647: Bolubolu 593
Sample number 33648: Bwaido Peninsula 602
Sample number 33649: Bwaido Peninsula 612
Sample number 33655: Mud Bay 617
Sample number 33657: Wagipa Island 624
Sample number 33669: Wagipa Island 630
Sample number 33670: Mount Oiava'ai 633
Iamalele Geothermal Area Mineral Chemistry
Fergusson Island
Sample number 33652: Wameai Plateau 640
Sample number 33662: Wameai Plateau 646
Sample number 125802: Aloai Volcanic Cone 647
Sample number 125805: I'wa'ur River 654
Sample number 125806: Wameai Plateau 660
Sample number 125810: Wameai Plateau 664
Sample number 125827: Aloai Volcanic Cone 667
Sample number 125828: I'wa'ur River 672
Sample number 125830: I'wa'ur River 674
Sample number 125832A: Aloai Volcanic Cone 676
Sample number 125832B: Aloai Volcanic Cone 679
Sample number 125833: Wameai Plateau 685
Sample number 125834: Wameai Plateau 690
Sample number 139015: I'wa'ur River 696
Wairakei Geothermal Area Mineral Chemistry
Sample number 125275: Well 121 699
Sample number 125296: Well 202 701
Sample number 125768: Well 66 702
Replicate Mineral Chemistry
East Papuan volcanic arc
Amphlett Islands
Sample number 33628: Wamea Island 708
Sample number 33638: Watota Island 710
Fergusson Island
Sample number 33645: Kukuia Peninsula 713
Goodenough Island
Sample number 33648: Bwaido Peninsula 715
Sample number 33670: Mount Oiava'ai 718

APPENDIX Page

4. MINERAL CHEMISTRY (continued)

Replicate Mineral Chemistry (continued)
Iamalele geothermal area
Fergusson Island
Sample number 125802: Aloai Volcanic Cone 721
Sample number 125805: I'wa'ur River 723
Sample number 125833: Wameai Plateau 725
Sample number 125834: Wameai Plateau 726
Sample number 139015: I'wa'ur River 727

5. X-RAY DIFFRACTION DATA 729

General Statement 729
Analytical Method 729
Sample preparation 729
Instrumentation and software 730
University of Canterbury 730
Lincoln College 730
Stanford University 731
Specific analytical techniques 731
D-spacing calculations 731
Mineral abundance estimates 732
Beidellite 732
Mixed-layer illite-smectite 732
Vermiculite 732
Mixed-layer illite-vermiculite 734
Hydrous silica phases 735
Data Format and Abbreviations 736
Iamalele Geothermal Area
Iamalele diamond drill hole IA-1 x-ray diffraction data . . . 737
Wairakei Geothermal Area
Wairakei x-ray diffraction data 738

6. BULK ROCK PHYSICAL PROPERTIES
(Iamalele Geothermal Field) 741

General Statement 741
Analytical Method 741
Porosity, rock density and particle density 741
Particle density 742
Precision and accuracy 742
Data Format and Abbreviations 743
Iamalele Geothermal Area
Iamalele porosity and rock density data 745
Iamalele particle density data 748

7. ESTIMATED PREPRODUCTION RESERVOIR TEMPERATURES
(Wairakei Geothermal Field) 751

General Statement 751
Hydrothermal Reservoir 751
Physical characteristics 751
Production history 752

APPENDIX Page

7. ESTIMATED PREPRODUCTION RESERVOIR TEMPERATURES (Wairakei Geothermal Field) (continued)

Hydrothermal Reservoir (continued)
Reservoir engineering data 754
Temperature measurements 754
Pressure measurements 754
Estimated Preproduction Temperatures 755
Downhole temperature profiles 755
Boiling point-with-depth relationship 755
Preproduction temperatures 757
Wairakei well 54 758
Temperature gradients 760
Two-phase zone 761
Cold water intrusion 762
Permeability 763
Characteristic temperature profiles 763
Well 34 764
Well 44 765
Well 48 766
Reliability of temperature estimates 766
Data Format 768
Wairakei Estimated Preproduction Reservoir Temperatures 770

8. FLUID INCLUSION HOMOGENIZATION TEMPERATURES 779

General Statement 779
Analytical Method 779
Sample preparation 779
Instrumentation 779
Institute for Nuclear Sciences 779
Stanford University 780
KRTA Limited 780
Data Format and Abbreviations 781
Iamalele Geothermal Area
Iamalele fluid inclusion data 782
Wairakei Geothermal Area
Wairakei fluid inclusion data 783

9. AIRBORNE GEOPHYSICAL DATA 785

General Statement 785
Equipment and Technique 785
Magnetometer 786
Spectrometer 786
Magnetic susceptibility measurements 786
Qualitative Data Interpretation 787
Airborne magnetic data 787
Airborne radiometric data 788
Ground magnetic susceptibility measurements 788

REFERENCES CITED 789

LIST OF TABLES - VOLUME II

TABLE		Page
3.1.	Summary of geochemical data reported by commercial laboratories	323
3.2.	Comparison of measured major and trace element abundances in bulk rock standards to preferred values	326
3.3.	Comparison of measured trace element abundances in bulk rock standards to preferred values	327
3.4.	Replicate XRF data for Iamalele bulk rock samples	328
3.5.	Lower limits of detection for XRF data	328
3.6.	Replicate XRF analyses of bulk rock samples	331
3.7.	Summary of measured and calculated Fe^{3+}/Fe^{2+} ratios for four rocks from the Kukuia Peninsula	332
3.8.	Rare earth element normalization data	333
3.9.	Symbols used in Appendix 3	335
4.1.	Comparison of energy dispersive X-ray data to reported values	511
4.2.	Detection limits for wavelength dispersive X-ray analyses	513
4.3.	Chemical formula calculation for iddingsite	518
4.4.	Calculation of ferrous and ferric iron and wt % ulvospinel from microprobe data for spinel group minerals	523
4.5.	Summary of Fe species calculations for microprobe analysis G.84	524
4.6.	Calculation of wt % M_2O_3 from microprobe data for ilmenite	527
4.7.	Summary of Fe species calculations for microprobe analysis 23	528
4.8.	Summary of microprobe operating parameters	530
4.9.	Empirical correction factors for microprobe analysis of REE-bearing minerals	532
4.10.	Electron microprobe analyses of Olympic Dam monazite	533
4.11.	Symbols used in Appendix 4	537

LIST OF TABLES - VOLUME II (CONTINUED)

TABLE		Page
5.1.	Symbols used in Appendix 5	736
6.1.	Symbols used in Appendix 6	744
8.1.	Symbols used in Appendix 8	781

LIST OF FIGURES - VOLUME II

FIGURE		Page
4.1.	Compositional fields and chemical composition of the end members of the spinel group	521
4.2.	Solid solution series in the system FeO-Fe_2O_3-TiO_2	525
5.1.	X-ray diffraction patterns for oriented K^+-saturated clay separated from sample 125849	733
5.2.	X-ray diffraction patterns for oriented, heat-treated and glycerol-treated clay separated from sample 125849	734
5.3.	X-ray diffraction patterns for oriented, Mg^{2+}-saturated clay separated from sample 125849	735
7.1.	Annual and cumulative mass and heat discharged from the Wairakei reservoir between 1952 and 1984	752
7.2.	Temporal variations in downhole temperature profiles for Wairakei well 12	753
7.3.	Potential uncertainty in the boiling point-with-depth relationship	757
7.4.	Locations of Wairakei wells 12, 34, 44, 48 and 54	759
7.5.	Selected temperature profiles, estimated preproduction temperature profile and drill hole geology for Wairakei well 54	759
7.6.	Selected temperature profiles for the upper portion of Wairakei well 54	761
7.7.	Selected temperature profiles for Wairakei well 34	764
7.8.	Selected temperature profiles for Wairakei well 44	765
7.9.	Selected temperature profiles for Wairakei well 48	767

LIST OF PLATES - VOLUME III

PLATE	
1	Iamalele Surface Geology
1A	Iamalele Airborne Radiometric Survey
1B	Iamalele Airborne Magnetic Survey
1C	Iamalele Sample Locations
1D	Iamalele Flight Path Recovery
2	Yaluwana and Kilugaba Thermal Areas
3	Iamalele Airport Breccia
4	Iamalele Diamond Drill Hole IA-1
5	Wairakei Cross Section Locations
6	Wairakei Geology
6A	Wairakei Estimated Preproduction Reservoir Temperatures
6B	Wairakei Hydrothermal Alteration and Metallization
6C	Wairakei Sample Locations and Metallization

CLASSIFICATION OF HYDROTHERMAL ALTERATION ASSEMBLAGES USED IN THIS THESIS

The nomenclature of hydrothermal alteration used in this thesis is based on the occurrence of characteristic indicator minerals and replacement textures. Adhering to the usage of Meyer and Hemley (1967), hydrothermal alteration is divided into four principal equilibrium assemblages. In order of decreasing temperature and increasing hydrogen ion activity these assemblages are referred to as propylitic, potassic, intermediate argillic and advanced argillic.

Propylitic alteration is characterized by the replacement of magmatic andesine by pericline ± wairakite, epidote, adularia and illite-sericite together with the alteration of primary ferromagnesian minerals to clinochlore and anatase-rutile ± epidote and pyrite. During propylitic alteration the groundmass is replaced by varying proportions of quartz, pericline, wairakite, adularia, illite-sericite, smectite and pyrite. Other minerals which may occur in the propylitic equilibrium assemblage are clinozoisite, zoisite, prehnite, magnetite, leucoxene and calcite.

Potassic alteration is identified by the replacement of pericline and magmatic andesine by adularia, and replacement of the groundmass by quartz, adularia, grothite, illite-sericite and pyrite. Other minerals which may occur in the propylitic assemblage are clinochlore, smectite, mordenite, chlorapatite, monazite, magnetite, ilmenite, anatase-rutile, calcite, anhydrite, barite, biotite and zircon. Laumontite veins form either during or slightly after the last stages of potassic alteration.

Intermediate argillic alteration is manifested by the replacement of primary and secondary feldspar, ferromagnesian minerals and portions of the groundmass by smectite, kaolinite and/or illite accompanied by quartz and/or hydrous silica. Other minerals which may occur in the intermediate argillic assemblage are mixed-layer illite-smectite, vermiculite, barite and pyrite.

Advanced argillic alteration is defined by the replacement of illite-sericite, smectite and vermiculite by kaolinite which is typically accompanied by alunite and hydrous silica. Other minerals which may occur in the advanced argillic assemblage are gibbsite, brucite, barite and pyrite

Chapter 1

INTRODUCTION

PURPOSE OF STUDY

During the past decade the minerals industry has directed most of its exploration efforts toward the discovery of large-tonnage (bulk mineable) precious metal deposits which can be economically mined at very low grades (~0.03 troy ounce Au-equivalent/tonne). Although precious metal deposits occur in a variety of tectonic settings and widely varying host lithologies, they are particularly abundant in areas of regional extension, and are commonly hosted by thick sequences of calc-alkalic (rhyolitic) ignimbrite. In this environment gold-silver mineralization is localized by caldera margins, by basin-bounding faults and in particular by the spatial coincidence of these features.

Fluid inclusion and stable isotope studies have shown that volcanic-hosted precious metal deposits characteristically are formed at shallow crustal levels by the interaction of rock with low salinity, metal-bearing fluids at temperatures between 150° and 300°C (see for example, Taylor, 1974; O'Neil and Silberman, 1974; Roedder, 1979; Sander and Einaudi, 1990; Field and Fifarek, 1984). The mineralizing fluids are dominated by meteoric water which migrates through the rock in response to an abnormally high geothermal gradient induced by crustal thinning and/or magmatic activity. At depth and in rocks of low permeability the rising hydrothermal fluids are typically confined to major faults and formational contacts, but at shallow levels they may expand into subhorizontal volcanic and/or sedimentary aquifers to form large hydrothermal reservoirs.

Because the physical conditions which characterize the epithermal ore-forming environment are remarkably similar to the conditions prevailing in active geothermal systems, most exploration models for epithermal precious metal deposits (e.g., Henley and Ellis, 1983; Henley, 1985; Hayba et al., 1985) are firmly based on chemical and hydrologic data collected from liquid-dominated geothermal systems such as Wairakei (Grindley, 1965; Steiner, 1977), Broadlands (Browne, 1969; Browne and Ellis, 1970; Eslinger and Savin, 1973), Cerro Prieto (Elders et al., 1978; Schiffman et al., 1984; Schiffman et al., 1985), Salton Sea (Helgeson, 1968; Muffler and White, 1969) and Steamboat Springs (White, 1955; Schoen and White, 1967; Schoen et al., 1974). However, as noted by White (1981), despite extensive exploitation, substantial quantities of gold ore are not known to occur within the geothermal systems from which the precious metal "models" were developed.

Two fundamental questions which arise from White's observation provided the stimulus for undertaking my doctoral research. These questions are (1) why do significant quantities of gold at economic grades not occur within the high-temperature reservoirs of active geothermal systems and (2) to what extent are the current geothermal-based models applicable to the genesis of epithermal precious metal deposits? To answer these questions two active, gold-bearing geothermal systems were investigated, Iamalele in the D'Entrecasteaux Islands of Papua New Guinea and Wairakei in the North Island of New Zealand. The major emphasis of this dissertation is directed toward evaluating hydrothermal alteration and metallization occurring within the Wairakei reservoir, but because detailed data pertaining to the near-surface environment of the reservoir are limited, data from the upper 200 metres of the Iamalele reservoir are also included.

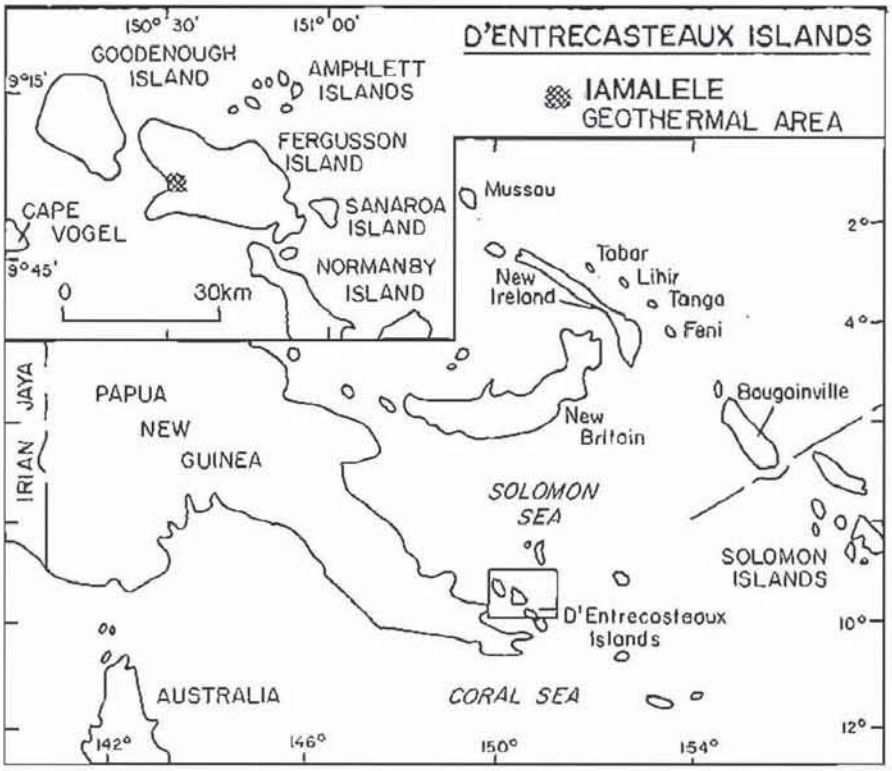

Figure 1.1. Location of the D'Entrecasteaux Islands and the Iamalele geothermal area.

STUDY AREAS

Iamalele Geothermal Area, D'Entrecasteaux Islands, Papua New Guinea

The D'Entrecasteaux Islands are located in the southern Solomon Sea approximately 50 kilometres east of the Papuan peninsula (Fig. 1.1). Regional mapping (Davies, 1973) indicates that the main islands, Normanby, Fergusson and Goodenough, form a series of metamorphic core complexes which occur in a very complex boundary zone between the Indo-Australian and Pacific plates. Fragments of a once spatially extensive sequence of mafic and ultramafic rock occur along the flanks of the tectonic domes where they are in fault contact and/or locally overlie the high-grade metamorphic terrane. In areas of low topographic relief on the southwestern and south-eastern ends of Fergusson Island Pliocene to Holocene calc-alkalic and peralkaline volcanic rocks cover significant segments of the metamorphic terrane and may fill regional volcano-tectonic depressions.

The Iamalele geothermal area encompasses the coastal plains and low hills on the western side of Fergusson Island (Fig. 1.1). Late Pleistocene to Holocene volcanic rocks are exposed in the Iamalele area and range in composition from basaltic andesite to rhyolite, with high-silica dacite and rhyolite the most abundant. Outcrops are dominated by ignimbrite, lava domes and at least one obsidian flow which may be related to caldera collapse and post-caldera volcanism.

Solphataras, acid lakes and rare sinter deposits are exposed over more than 30 km^2 of the Iamalele area. Detailed sampling of both soil and rock exposures within the limits of geothermal activity revealed several areas which contained anomalous values of gold, mercury, arsenic and antimony. One diamond drill hole was completed to a depth of ~200 metres in the centre of the geothermal area. The core recovered from the drill hole indicated that hydrothermal rock alteration within the upper portion of the geothermal reservoir is well-zoned and contains a trace element signature (As, Bi, Hg, Se, Te, Tl and Au) characteristic of high-level, epithermal precious metal deposits. Mineral assemblages and textural relationships indicative of potassic, intermediate argillic and advanced argillic alteration (usage of Meyer and Hemley, 1967) were observed in the core. Down-hole temperatures were not measured, but rock temperatures increased with depth and by ~100 metres asbestos gloves were needed to remove the core from the core barrel.

Wairakei Geothermal Area, North Island, New Zealand

New Zealand is located in the South Pacific Ocean, where it straddles a well-defined boundary between the Indo-Australian and Pacific plates. Regional extension and magmatism associated with westward subduction of the Pacific plate beneath the North Island have resulted in the formation of a regional volcano-tectonic depression referred to as the Taupo Volcanic Zone. Volcanic rocks related to the Taupo Volcanic Zone are

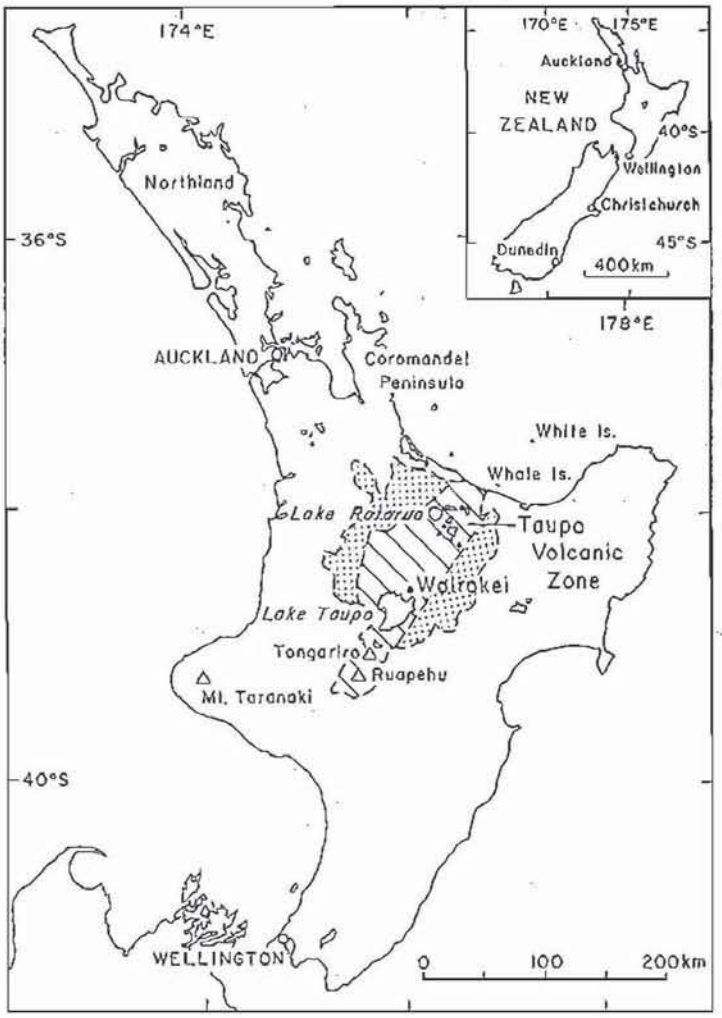

Figure 1.2. Location of the Taupo Volcanic Zone and the Wairakei geothermal area. Stippled area shows the approximate distribution of volcanic rocks which are related to the Taupo Volcanic Zone but occur outside the area of basin subsidence.

calc-alkalic and predominantly rhyolitic in composition, although mafic to intermediate compositions are not uncommon.

Wairakei is located near the centre of the North Island of New Zealand (Fig. 1.2) and is a liquid-dominated geothermal system. The high-temperature reservoir is localized within a voluminous sequence of rhyolitic ignimbrite and air fall tuff intercalated with volcaniclastic rocks and andesite to rhyolite lavas. The primary production reservoir is underlain by a series of massive ignimbrite sheets, within which permeabilities are generally low, and overlain by relatively impermeable tuffaceous mudstone and siltstone intercalated with minor pumiceous ignimbrite.

Steaming ground, hydrothermal eruption craters and intense hydrolytic alteration are exposed over ~25 km^2 of the Wairakei area. The results of extensive drilling indicate that hydrothermal rock alteration within the reservoir is systematically zoned and may be separated into four major assemblages, propylitic, potassic, intermediate argillic and advanced argillic (usage of Meyer and Hemley, 1967). Mineral assemblages characteristic of propylitic alteration occur at depth, whereas potassic alteration is the dominant alteration type at high levels (less than ~500 m deep) within the reservoir. At intermediate depths the potassic assemblage overprints propylitic alteration. Calcium zeolites occur throughout the reservoir, and although their distribution appears to be controlled by lithology and temperature, in general their occurrence may be genetically related to either propylitic or potassic alteration. Intermediate argillic alteration is widespread, but overall is weakly developed. Advanced argillic alteration occurs in the upper 65 metres of the reservoir and may be intense, but its distribution is sporadic. Assays of drill core and cuttings indicate that trace amounts of gold and other metals permeate the reservoir. Samples of siliceous sinter collected from wellhead production equipment contain significant quantities of precious, platinum group and base metals. Downhole temperature logs show that temperatures within the production reservoir varied initially from ~240° to ~265°C.

DISSERTATION FORMAT AND SCOPE

The information presented in this dissertation has been organized into four chapters (Volume I) and nine appendices (Volume II). A third volume marked Maps contains a series of maps and cross sections on which I have summarized much of the data collected during my research.

Chapter 1

Chapter 1 is a general introduction to the dissertation. It includes an explanation of the purpose of the study, an introduction to the study areas and a description of the format and scope of the dissertation.

Chapter 2

Chapter 2 contains a discussion of the geology and geochemistry of the Iamalele geothermal area, with emphasis on high-level hydrothermal alteration and metallization. The petrologic descriptions are very preliminary, but are included because they are the most detailed and up-to-date information available for western Fergusson Island.

Iamalele was included in this dissertation as a secondary study area for three reasons. The principal reason is that the diamond drill core from Iamalele provided very important data about the type and extent of hydrothermal alteration occurring in the upper levels of geothermal reservoirs. Secondly, the geologic setting of the Iamalele area is similar to that of Wairakei, thus data obtained at Iamalele complements the data obtained at Wairakei. The third reason is that the information provided by the Iamalele core could not be readily obtained from the Wairakei drilling samples. This is primarily because only the early drill holes at Wairakei were cored continuously and most of these drill holes were located along the cooler northern periphery of the reservoir. Furthermore most of the core had not been split and equipment for splitting extensive intervals of the core was not available.

In total about three months were spent mapping, sampling and logging core at Iamalele. From this work a reconnaissance geologic map covering about 90 km^2 of the Iamalele area was completed (Plates 1, 1C, 2, 3 and 4). Airborne magnetic and radiometric surveys were conducted concurrently with the field mapping and diamond drilling, and the results of these surveys

are contoured on Plates 1A and 1B. Flight lines for the airborne geophysical survey are plotted on Plate 1D.

Chapter 3

Chapter 3 concerns the Wairakei geothermal area, and is the focal point of this dissertation. Wairakei was selected as my primary study area because it is a major liquid-dominated geothermal field for which extensive geology, hydrology, fluid chemistry, and temperature and pressure data bases are available. In addition Wairakei is one of the geothermal systems from which the exploration model for epithermal precious metal deposits was developed. However, before Wairakei could be realistically compared to a volcanic-hosted epithermal precious metal deposit, a more complete understanding of the paragenesis and spatial distribution (zoning) of hydrothermal alteration minerals, equilibrium mineral assemblages, and gold and silver occurring within the reservoir was needed.

The information presented in Chapter 3 complements and expands upon the work of Grindley (1965), Steiner (1977), Grant (1980) and Healy (1984). The chapter is divided into three main sections. The first section (Introduction) includes a brief history of the geothermal field and comments on the available data base for the geothermal reservoir. Then (in Regional Geology) the reader is introduced to the volcano-tectonic history of the Taupo Volcanic Zone. The final section (Wairakei Geothermal Area) contains a detailed description of the geology of the Wairakei area and of the types and extent of hydrothermal alteration and metallization identified within the Wairakei geothermal reservoir.

Approximately three months were spent at Wairakei. Most of this time was utilized logging drill core and cuttings and studying drilling records and reservoir engineering data. Because the surface had been mapped in relative detail (Grindley, 1965; Allis, 1981; Allis and Webber, 1984), mapping was given a low priority and field work was restricted to checking the

existing maps and collecting samples of siliceous precipitate from the production equipment (silencers, weir boxes and hot water drains). The results of core logging and subsequent alteration and mineralization studies are shown on a series of cross sections which accompany this dissertation (Plates 6, 6A, 6B and 6C). To facilitate locating and drawing these cross sections it was necessary to construct a topographic base map (Plate 5) from the Ministry of Works and Development orthophotos for the Wairakei geothermal area (Department of Lands and Survey, Orthophoto Plan Nos. 1298/1-7, 1:5,000).

The most significant results to come out of my research at Wairakei include (1) the development of a series of cross sections showing the thermal zoning and corresponding hydrothermal alteration zoning of the preproduction hydrothermal reservoir, (2) the identification of several previously unreported hydrothermal minerals including gold-palladium alloys, argentite, monazite, biotite and zircon, (3) the documentation of the transport of gold, silver and a variety of other metals by the reservoir fluid, (4) the identification of trace amounts of gold and other metals pervading the geothermal reservoir and (5) the determination of quantitative chemical compositions for "ore" minerals precipitated on wellhead production equipment.

Chapter 4

Chapter 4 is divided into two parts and contains most of the discussion and conclusions of this dissertation. In the first part of the chapter the regional and district-scale geology and the characteristics of hydrothermal alteration and metallization identified at Wairakei, and to a lesser degree at Iamalele, are compared to similar aspects of the epithermal gold-silver deposits at Rawhide and Round Mountain in Nevada (U.S.A.). Conclusions arrived at from the comparison of these four areas are used to develop a genetic model which provides a viable explanation for

the absence of significant quantities of gold and silver at economic grades within the high-temperature reservoirs of active geothermal systems.

The second part of Chapter 4 is an expanded version of an article entitled "High-Mg lavas in the late Cenozoic volcanic arc associations of southeastern Papua New Guinea" by Smith and Mitchell (1989). A copy of the article is contained in the pocket at the back of this volume. Although of a regional nature, this work is the most important scientific contribution to come out of my research at Iamalele, and is included because (1) the information presented contributes substantially to the existing published data base on high-Mg lavas and (2) the existence of high-Mg lavas may have significant implications for volcanic arc petrogenesis. The discussion includes comments on the nomenclature of the high-Mg lavas and detailed descriptions of the occurrence and the bulk rock and mineral chemistry of the high-Mg lavas identified in southeastern Papua New Guinea. These data are then used to generate a tectonic model for genesis of the high-Mg lavas.

Appendices

All of the data collected during the course of preparing this dissertation are presented in Volume II. Each appendix begins with a description of the equipment used, the methods followed and the assumptions made to generate the data.

Chapter 2

IAMALELE GEOTHERMAL AREA, D'ENTRECASTEAUX ISLANDS, PAPUA NEW GUINEA: GEOLOGY, HYDROTHERMAL ALTERATION AND METALLIZATION

INTRODUCTION

Chapter 2 contains a discussion of the volcanic geology of the coastal lowlands surrounding the villages of Iamalele and Fagalulu on western Fergusson Island (Fig. 2.1b) and of the hydrothermal alteration and metallization occurring at the surface and within the upper ~300 metres of the Iamalele geothermal system. The data presented in this chapter are the results of a three month long reconnaissance-style evaluation of the region, which culminated in the completion of a ~200 metre deep diamond drill hole. Although of a general nature, the information provided is the most complete data base available for the Iamalele area. Stable isotope data and age dates for the various rock units were not determined during the course of this study and consequently the discussion of the Holocene volcanic geology of west-central Fergusson Island is mainly descriptive. The section on hydrothermal alteration is also primarily descriptive because only one relatively shallow drill hole was completed. However, the importance of the Iamalele data is enhanced when put in context with observations made at Wairakei (Chapter 3) and compared to data from the Rawhide epithermal gold-silver deposit (Chapter 4).

Location and Geologic Setting

Iamalele is located on the west coast of Fergusson Island in the D'Entrecasteaux Islands of Papua New Guinea (Fig. 2.1). The area is a

roughly elliptical topographic basin bordered by rugged mountainous terrain to the north, hills and low mountains of moderate relief to the east and

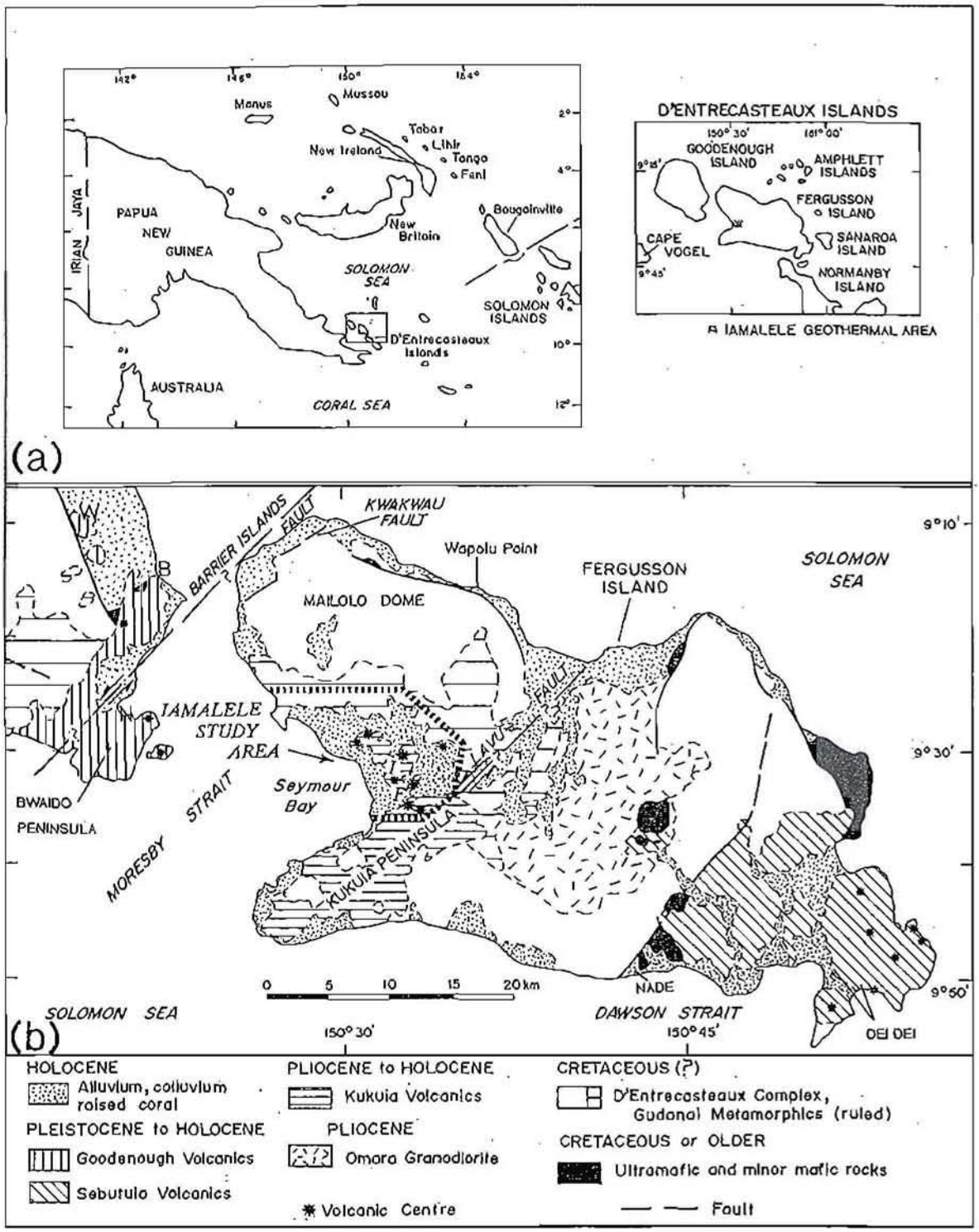

Figure 2.1. Location of the D'Entrecasteaux Islands and the Iamalele area (a) and the simplified geology of Fergusson Island and the southeastern tip of Goodenough Island (b). The following place names have been abbreviated: Bolu Bolu (B), Nou Nou (N), Wakala Hill (W). Geology after Davies (1973).

Figure 2.2. Photographs of the Iamalele area. Top photograph is a view to the east from Seymour Bay. The prominent hill in the left centre of the picture is the Wameai dome. Iamalele village is ~1.7 km southeast of the dome in the topographically low area which appears 2.5 cm to the right of the dome in the photograph. The bottom photograph is a view to the northeast across the Iamalele area showing several volcanic landforms (domes and plateaus) and active thermal areas which can be identified by rising steam and areas of grey-white hydrothermal alteration. The large tree-covered hill in the right centre of the photograph is the Uluwa dome. The high ridge in the background is the southeastern flank of the Mailolo metamorphic core complex.

south, and Seymour Bay to the west (Figs. 2.2 and 2.3). High-grade metamorphic rocks occur along the northern and eastern boundaries of the Iamalele area, and along the southern boundary of the area a thick sequence of calc-alkalic volcanic rocks is exposed. The floor of the topographic basin was initially a planar feature which has been disrupted by relatively recent block faulting. These faults were the locus for the emplacement of numerous volcanic domes and small cones composed of pyroclastic debris and

lava. Although detailed subsurface data are limited, a large, liquid-dominated hydrothermal system appears to have developed in a relatively thick sequence of dacite to rhyolite pyroclastic rocks which underlie the Iamalele area. The physiography of the region and the occurrence of abundant volcanic eruptive centres localized by high-angle normal faults may be the result of caldera collapse and post-caldera volcanism.

Previous Work

Historical notes about the early geologic investigations of the D'Entrecasteaux Islands were provided by Davies (1973). The earliest geologic reports which mention Iamalele are those of Thompson (1889) and Stanley (1920). Edwards (1950) completed the first site-specific geologic investigation of the area when he evaluated the near-surface sulphur potential of the Iamalele thermal area. Pritchard (1963) visited the Iamalele area in 1960 during a reconnaissance geologic mapping programme which covered Fergusson and Goodenough Islands. The most extensive geological reconnaissance of Fergusson Island was carried out by Davies and Ives (1965). The results of this work are presented on a 1:250,000 scale geologic map (Sheet SC 56-5) covering Goodenough, Fergusson and the northern half of Normanby Islands. The Davies and Ives (1965) report also contains a ~1:1,000,000 scale Bouguer anomaly map of the area. These data and the results of a regional airborne magnetic survey covering the D'Entrecasteaux Islands were discussed by Milsom and Smith (1975). Detailed petrologic and geochemical data pertaining to samples collected on western Fergusson Island and in the Iamalele area by geologists of the Australian Bureau of Mineral Resources, Geology and Geophysics during the years 1968 to 1970 are contained in Davies and Smith (1971), Smith (1973), Smith (1976b), Smith (1982) and Smith and Compston (1982). Recent volcanic activity which has occurred in the Iamalele area was described by Smith (1981).

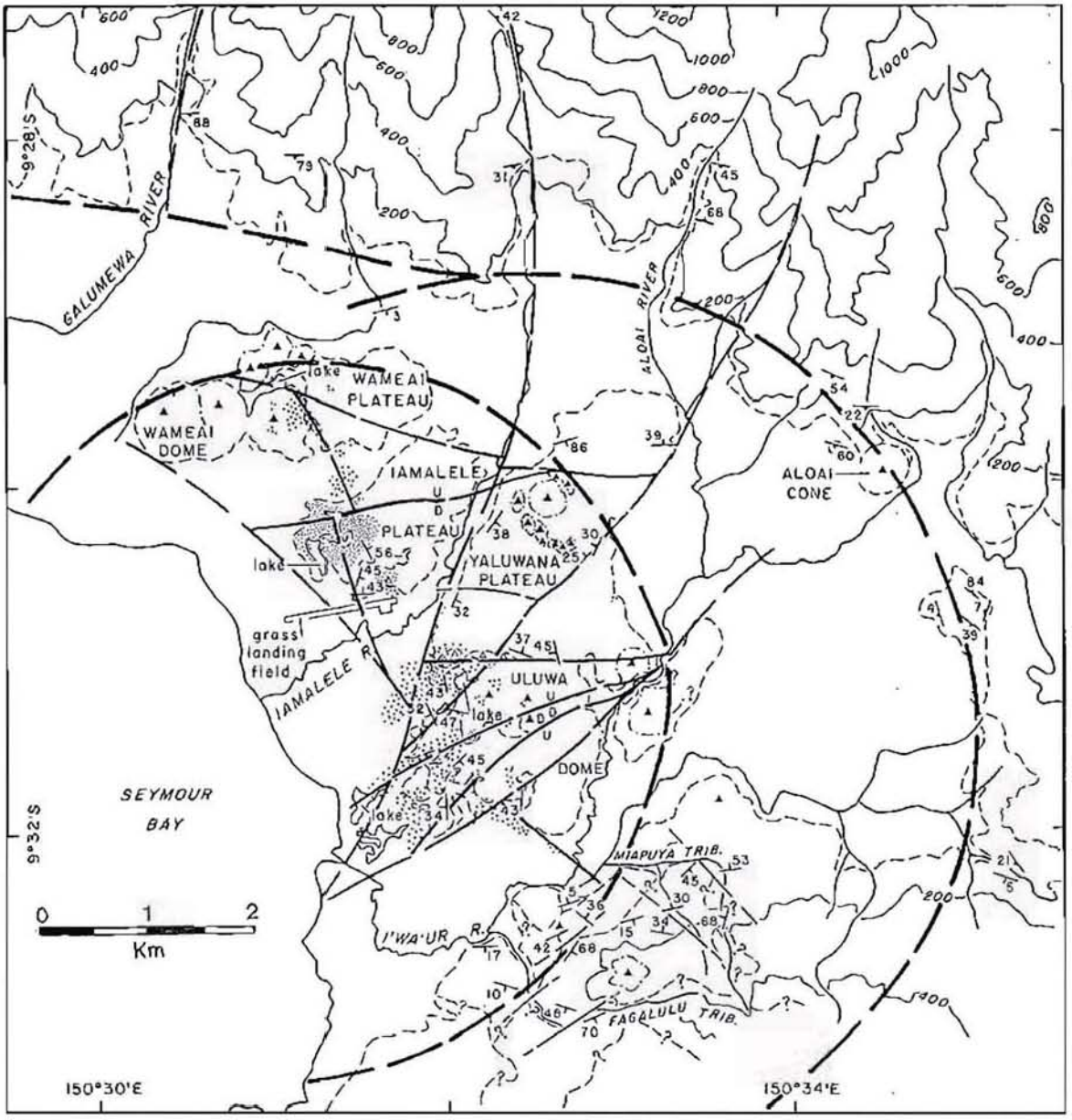

Figure 2.3. Structural geology of west central Fergusson Island. Fault trends interpreted from air photographs and airborne geophysical data, supported by field mapping. Heavy dashed lines are inferred ring structures, thinner long dashed lines are normal faults. See Plates 1A and 1B for geophysical data. Geologic units can be identified by comparing the figure to Plate 1.

The only detailed geologic and geochemical investigations of western Fergusson Island were carried out by geologists of Esso Papua New Guinea, Inc. during the period 1982 to 1985. The bulk of this work is unpublished, but much of it may be recovered from the data files maintained by the

Geological Survey of Papua New Guinea; this information is contained in the data file for Prospecting Authority 544 (Kukuia Peninsula).

REGIONAL GEOLOGY

The Iamalele area lies in one of the tectonically more complex regions of the world (see, for example, Davies et al., 1984). Post-Cretaceous tectonic activity and associated volcanism have resulted in the emplacement of a wide variety of lithologies throughout southeastern Papua New Guinea, and in particular on Fergusson Island. In order to provide a more complete understanding of the relationship between the late Cenozoic volcanic rocks and the underlying geologic basement on Fergusson Island and elsewhere in the D'Entrecasteaux Islands, this section begins with brief descriptions of the tectonic setting and volcanic geology of southeastern Papua New Guinea. A more detailed description of the regional geologic framework of southeastern Papua New Guinea is given in the section on High-Mg Lavas in the Late Cenozoic Volcanic Arc Associations of Papua New Guinea in Chapter 4.

Southeastern Papua New Guinea

Tectonic Setting

Late Cenozoic tectonism in Papua New Guinea involved several micro-plates caught up in a major zone of interaction between the Pacific and Indo-Australian plates (e.g., Curtis, 1973). In southeastern Papua New Guinea tectonic interaction between the Indo-Australian plate and the Solomon Sea microplate was particularly complex and involved subduction, obduction and rifting (Davies et al., 1984; Smith and Milsom, 1984). These processes have resulted in the juxtaposition of an unusual variety of late Mesozoic and Cenozoic rock associations including ultramafic, mafic, plutonic, metamorphic and tholeiitic to peralkaline volcanic rocks. The

geological basement of southeastern Papua New Guinea consists of a core of moderate- to high-grade metamorphic rocks overlain by an obducted veneer of ultramafic rocks and associated mid-ocean ridge basalts (Davies and Smith, 1976).

Volcanic Geology

Late Cenozoic arc-type volcanic rocks are widely distributed in southeastern Papua New Guinea. The oldest of these rocks are Miocene in age (12 to 11 Ma; Smith, 1972; Smith and Compston, 1982) and occur in the Louisiade Archipelago and near the southeastern tip of the Papuan peninsula (Fig. 2.1). Pliocene and younger volcanic rocks are found in the D'Entrecasteaux Islands and in the central part of the Papuan peninsula. The spatial distribution and ages of the post-Miocene volcanic terrane indicate a general westward migration of volcanic activity through the late Cenozoic, a trend which may indicate that magma generation is related to tensional stresses associated with the westward migration of spreading in the Woodlark Basin (Smith and Mitchell, 1989).

As in other modern island arcs the volcanic terrane of southeastern Papua New Guinea is characterized by the predominance of andesite accompanied by subordinate basalt, dacite and rhyolite. However, in several locations in the D'Entrecasteaux Islands and on the Papuan peninsula rhyolite is the dominant lithology. One of the areas where rhyolite is particularly abundant is on the Kukuia Peninsula of southwestern Fergusson Island (Fig. 2.1).

D'Entrecasteaux Islands

Geologic Setting

Late Cenozoic uplift resulted in doming of the metamorphic basement, which on Normanby, Fergusson and Goodenough Islands culminated in the

emplacement of several metamorphic domes and anticlines (core complexes) composed of Mesozoic schist, amphibolite and gneiss (Davies, 1973). The metamorphic core complexes are flanked and overlain by Cretaceous mafic and ultramafic rocks of the Papuan Ultramafic Belt (Davies, 1973). The pre-Tertiary rocks are locally overlain by calc-alkalic to peralkaline volcanic rocks and volcaniclastic and clastic sedimentary rocks.

The dominant metamorphic lithology is quartzofeldspathic gneiss which is intercalated with varying percentages of amphibolite and calcic gneiss. The rocks are metamorphosed to the amphibolite facies, but mineralogies characteristic of the granulite and eclogite facies are also present (Davies, 1973). It is possible that Normanby, Fergusson and Goodenough Islands and parts of the Papuan peninsula are the faulted remains of a single metamorphic complex which exceeded 165 kilometres in length and 30 kilometres in width (Davies and Ives, 1965).

Late Cenozoic calc-alkalic and peralkaline volcanic rocks are exposed along the margins of the metamorphic domes and anticlines and overlie the metamorphic terrane in low-lying areas; peralkaline rocks were identified only on Fergusson Island (Smith, 1973, 1976a). The oldest of these rocks occur in the central and western portions of Normanby Island, on the Amphlett Islands and on the Kukuia Peninsula of Fergusson Island (Smith, 1973; Smith and Compston, 1982). Pleistocene to Holocene calc-alkalic rocks form the bulk of the lithologic units exposed on the Kukuia Peninsula and on the Bwaido Peninsula of Goodenough Island. The youngest volcanic centres occur on the Bwaido Peninsula, in the Iamalele area and on the southeastern end of Fergusson Island, and on Dobu Island (Figs. 2.1 and 4.27). Smith (1981) estimates that the volcanic landforms exposed on the northeastern tip of the Bwaido Peninsula (Fig. 2.1) are only a few hundred years old. The age of the most recent eruptions in the Iamalele area is unknown, but very youthful landforms, including a composite volcanic cone composed of basaltic andesite scoria and lava suggest relatively recent

eruption. The most recent eruptions at Iamalele are probably time-equivalent to the youngest volcanic activity on the Bwaido Peninsula. Taylor (personal communication in Davies, 1973) estimates that the most recent eruptions of peralkaline rhyolite may have occurred ~600 years ago.

Geophysics

The only published geophysical data for the D'Entrecasteaux Islands include small-scale regional gravity (Bouguer anomaly) (Davies, 1973; Milsom and Smith, 1975) and airborne magnetic (Milsom and Smith, 1975) contour maps. The following comments are meant to augment the discussion of the data presented by Davies (1973) and Milsom and Smith (1975), but are my own interpretations.

Gravity Data

The Bouguer anomaly map for the D'Entrecasteaux Islands shows two prominent features, the Amphlett High and the D'Entrecasteaux Low (Davies, 1973). Although the Amphlett High is open to the east, it generally coincides with the spatial distribution of the Amphlett Islands which are probably the remnants of a large andesitic stratovolcano. Davies (1973) believes that the Amphlett High reflects a relatively dense pluton of intermediate to mafic composition beneath the Amphlett Islands. The D'Entrecasteaux Low is a broad gravity low (<50 mGal) which approximates the outline of Fergusson and Goodenough islands. In part, the low probably reflects thicker sialic crust beneath these islands as suggested by Davies (1973). However, the coincidence of the maximum Bouguer low (<30 mGal) with Pleistocene to Holocene volcanic centres suggests that these areas contribute to the magnitude and shape of the D'Entrecasteaux Low (Fig. 2.4). The maximum lows may reflect relatively near-surface magma chambers,

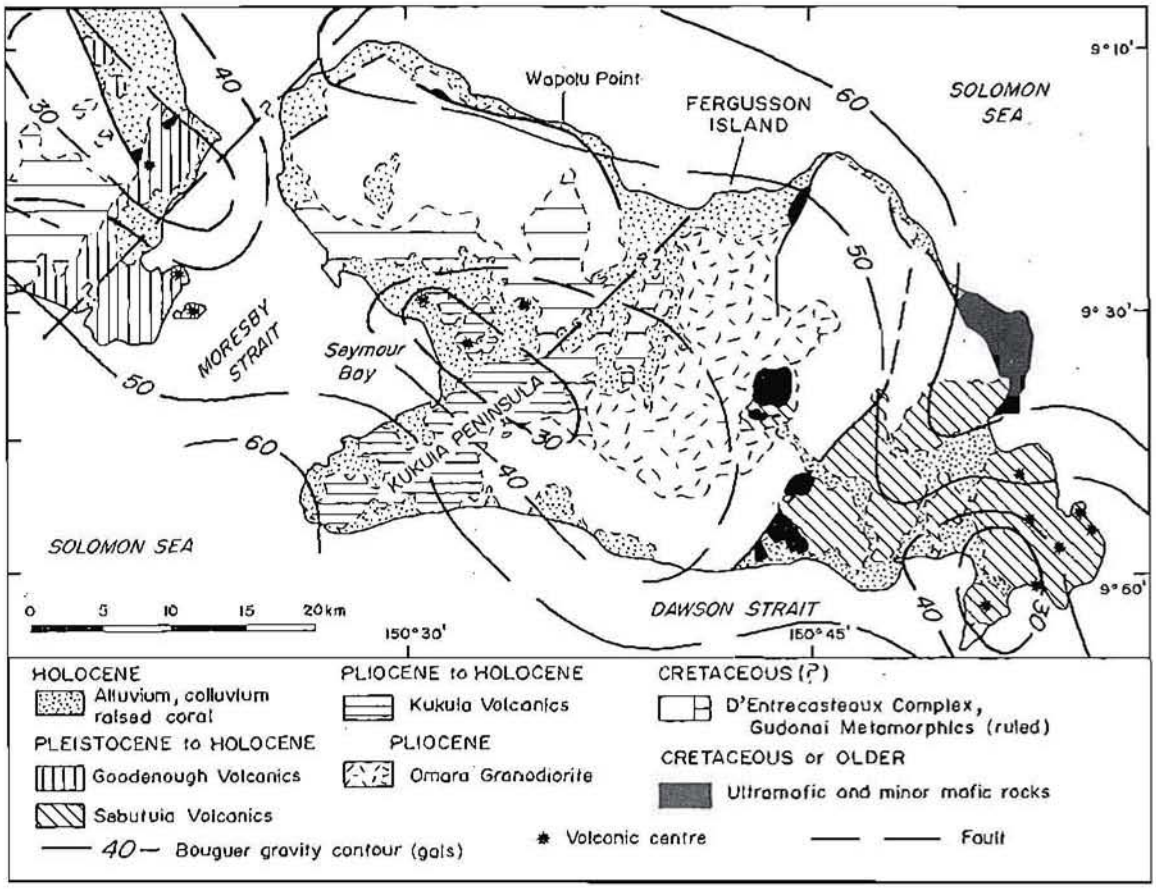

Figure 2.4. Bouguer anomaly map for Fergusson Island and the southeastern tip of Goodenough Island, D'Entrecasteaux Islands, Papua New Guinea. Data from Davies (1973).

or in the case of the Iamalele and Dawson Strait areas of Fergusson Island, large volumes of low density pyroclastic material filling major volcano-tectonic depressions, i.e., calderas.

Airborne Magnetic Data

The airborne magnetic survey of southeastern Papua New Guinea was flown at relatively high altitudes with a nominal terrain clearance of at least 2,130 metres (Milsom and Smith, 1975). Because of the high level at which the survey was flown, only very large geological features are visible in the data. The following comments relating to the contoured airborne magnetic map published by Milsom and Smith (1975) are based on the interpretation methods described in Appendix 9.

In general the D'Entrecasteaux Islands are represented by a broad, relatively low amplitude pattern reflecting the predominance of sialic rock forming and underlying the islands. The magnetic data do identify a relatively magnetic body underlying the Bwaido Peninsula. Presumably this feature is a major intrusive body of mafic to intermediate composition. A small magnetic low occurs immediately east of the Dei Dei thermal area on the southeastern end of Fergusson Island. Two relatively large magnetic highs occur along the south coast of Fergusson Island and between Fergusson Island and Sanaroa Island which lies to the east. These magnetic highs may be related to very large reversely magnetized intrusive bodies.

One very curious feature of the contoured magnetic data is the coincidence of a magnetic low with the major belt of ultramafic and mafic rock which transects the central portion of Normanby Island. The reason for this low is not clear.

Geothermal Activity

The two largest geothermal areas in the D'Entrecasteaux Islands are located at Iamalele and Dei Dei on Fergusson Island (Fig. 2.1). Less extensive thermal areas occur at Nade on the south coast of Fergusson Island, on the north coast of Dobu Island (see Fig. 4.27) and at Nou Nou, Bolu Bolu and near Wakala Hill (Fig. 2.1) on Goodenough Island (Davies, 1973). In addition, hot springs are present along many of the dome-building faults and major transcurrent faults. Examples of this type of occurrence are the hot springs near Wapolu Point on Fergusson Island (Fig. 2.1) and at Bwasiyiyi on the central west coast of Normanby Island (slightly south of the southern edge of the map in Fig. 4.27). In most of these areas the hydrothermal fluids have been mixed to some degree with seawater; see Table 2.2.

Western Fergusson Island

Western Fergusson Island includes the Kukuia Peninsula, Iamalele lowlands and the Mailolo metamorphic dome (Fig. 2.1), however, most of the discussion in this section is limited to the Iamalele lowlands and adjacent areas.

Geology and Geomorphology

The coastal lowlands of western Fergusson Island are bounded by a highland metamorphic core complex (Mailolo gneiss dome) of probable Cretaceous age (Davies, 1973) on the north and east and by a Pliocene to Holocene calc-alkalic volcanic terrane (Kukuia Volcanics) of moderate relief on the south. The Mailolo gneiss dome is a fault-bounded segment of a regional gneissic terrane which may have extended from Normanby Island to the Papuan peninsula during early Pliocene time (Davies and Ives, 1965). The northeastern boundary of the Mailolo gneiss dome is a well-defined, low- to moderate-angle ($\leq 32°$) normal fault, and the northwestern end of the dome is clearly offset by the Barrier Islands transcurrent fault (Fig. 2.1). The southwestern boundary of the dome was removed either by erosion (Davies, 1973) or by block faulting (gravity slide?) associated with recent volcanism and possibly caldera collapse. The southeastern end of the dome was probably removed by erosion which progressed more rapidly along the Lavu fault zone than on the main mass of the dome.

Volcanism began on the Kukuia Peninsula between 6 and 4 Ma, with the most recent activity occurring in the coastal lowlands surrounding the village of Iamalele (Smith and Compston, 1982; Smith and Milsom, 1984). The very youthful volcanic landforms which abound around Iamalele are considered by Smith (1981) to indicate that the area is still volcanically active.

The present physiography of the Iamalele lowlands is the result of differential uplift, both tectonic and volcanic, and fluvial erosion

operating on originally planar ignimbrite deposits (Mitchell and Yousif, 1985). Several circular to oval-shaped topographic highs are spread throughout the Iamalele area, although most of these features are poorly exposed due to the combined effects of erosion and thick vegetation. These topographic features were tentatively identified as volcanic domes and associated eruptive centres. Field mapping and diamond drilling confirmed that some of these features are very young volcanic centres (e.g., Aloai Cone and Uluwa dome; Fig. 2.3), but most of the volcanic centres were identified from their geomorphology and geophysical characteristics.

Structural Geology

Field mapping in the coastal areas of western Fergusson Island is difficult because most of the low-lying areas are covered by dense growths of kunai grass or sago swamps. Mapping is somewhat easier at slightly higher elevations on the domes and on some of the plateaus where the grasslands give way to dense forests, but structural detail is still difficult to obtain due to a thick accumulation of organic matter. Because of the paucity of good rock exposures much of the structural information presented in this section was interpreted from colour air photographs (1:20,000) and geophysical data (Plates 1A and 1B).

Regional Tilting

The morphology of the active and ancestral channels of the major rivers (Iamalele, Aloai and I'wa'ur) draining the Iamalele lowlands document their progressive rotation and southward migration through time (Mitchell and Yousif, 1985). The ancestral rivers eroded the rising Iamalele plateau forming wide valleys which parallel the strike of the ignimbrite units (Plate 1). Southward migration of the major rivers is indicated by the existence and location of ancestral river channels. The progressive changes in the location of the major rivers is consistent with

the interpretation that uplift either began or was more rapid in the northwestern part of the Iamalele area (Mitchell and Yousif, 1985). The modern rivers have broad, flat floors indicating that the Iamalele region is now tectonically quiescent.

Major Faults

Several major faults were identified from air photographs and the air magnetic contour map. In general, the traces of these structures trend in three principal directions, east, northeast and northwest (Fig. 2.3). The east- and northeast-trending faults separate the region into a series of fault-bounded blocks which, in part, contribute to the topographic expression of the volcanic plateaus. The northeast-trending faults also control the distribution of several of the major river drainages, particularly those draining the metamorphic highlands north of Iamalele. Although very few northwest-trending faults were recognized within the Iamalele lowlands, these structures are prominent in the central portion of the Kukuia Peninsula south of the I'wa'ur River (T.V. Weis, written communication). The northern extensions of two of these northwest-trending faults were mapped in the low hills just south of the I'wa'ur River (Fig. 2.3). If these faults were extended into the Iamalele lowlands, their traces would coincide with the distribution of geothermal activity, and it is possible that these northwest-trending faults are related to basement structures which guide rising hydrothermal fluids into the Iamalele reservoir.

Seymour Bay Caldera(?)

Two very subtle structural features which may be potentially very important in reconstructing the volcanic history of western Fergusson Island are reflected by the arcuate boundaries of the Iamalele lowlands and in the spatial distribution of the recent volcanic eruptive centres. The trace of the outermost of these structures coincides with the contact

between the high-grade metamorphic terrane and the Iamalele volcanics (Fig. 2.3). A smaller arcuate structure was inferred from the distribution of cumulodomes, hypabyssal intrusions and eruptive centres within the Iamalele lowlands. These two arcuate structures are centred near the mouth of the Iamalele river and have radii of approximately 4 and 5 kilometres respectively. These arcuate features may represent the (caldera) structures along which basement subsidence occurred during the eruption cycle that produced the Iamalele ignimbrite and ash fall deposits, and along which post-caldera volcanism was localized.

The presence of more than 250 metres of subhorizontal ignimbrite deposits (Iamalele Volcanics) in the Iamalele lowlands requires the existence of a major depression within which the erupted material could accumulate; the most likely means of creating this depression is caldera collapse. Volume calculations based on the present surface exposures of the Iamalele ignimbrite deposits within the topographic basin alone suggest that the eruption had a minimum volume of 1.5 km^3, which is statistically large enough to cause caldera collapse (Smith, 1979). Late-stage lava domes and geothermal activity are commonly associated with post-caldera volcanism (Smith and Bailey, 1968; Wilson et al., 1984).

Relatively thick sequences of ignimbrite, erupted in association with caldera collapse, are generally deposited over a wide area which may easily extend 20 to 30 miles outward from the caldera, especially for larger, directed eruptions. Such outflow deposits should be present if the Iamalele topographic depression formed during caldera collapse. Possible outflow deposits were identified south of the I'wa'ur River overlying andesite on the northwestern flank of the Kukuia Peninsula. However, this is near the edge of the mapped area and insufficient work was completed to correlate these units with the ignimbrite deposits within the Iamalele lowlands. Outflow deposits were not identified on the flanks of the Mailolo dome which, considering the steep topography, is not surprising.

Additional outflow deposits may be present to the east, but this area was outside the limits of my study.

It is also significant that the young volcanic centres (Goodenough Volcanics) on Bwaido Peninsula at the southeastern end of Goodenough Island are similar in age and style of volcanism to the young volcanic centres in the Iamalele area (Smith and Johnson, 1981). It is possible that the rocks exposed in these areas are genetically related. However, most of the exposed volcanic rocks on the Bwaido Peninsula are andesitic and rhyolite is rare (Smith, 1976b). It may be that recent andesitic pyroclastic rocks and lava cover an underlying rhyolite terrane, but additional field work will be required before this possibility can be confirmed or rejected. If the Iamalele and Goodenough Volcanics are related, then their spatial distribution and consequently their inferred eruption volumes would imply the existence of a major caldera system. Considering the spatial distribution of the Iamalele and Goodenough Volcanics the only viable source for their pyroclastic members lies under Seymour Bay and Moresby Strait. For these reasons I believe that the most probable source for the Iamalele ignimbrites and the depression within which they accumulated is volcanism associated with caldera collapse. In this scenario rhyolitic pyroclastic rocks exposed on the Kukuia Peninsula may be outflow facies related to the collapse of the inferred Seymour Bay caldera.

An alternative to caldera-related volcanism was described by Roobol et al. (1983) to explain the occurrence of ignimbrite-filled arcuate basins in the Lesser Antilles. These authors considered the volcano-tectonic basins to be the result of large gravity slides related to magmatic dilation and subsequent volcanic eruption. The features described by Roobol et al. (1983) are nearly identical in size and morphology to those of the Iamalele area and this possibility cannot be ruled out. If one or more major gravity slides are responsible for the subsidence and related volcanism of southwestern Fergusson Island and southeastern Goodenough

Island, then the direction of mass movement would have to be to the southwest (see Figure 4.27).

Geothermal Activity

As mentioned earlier, the largest areas of geothermal activity are Iamalele and Dei Dei on the southeastern tip of Fergusson Island (Fig. 2.1). Hot springs related to dome-building and major transcurrent faults occur along the northeast flank of the Mailolo dome and at Nade on the southern coast of Fergusson Island in the Dawson Strait area. Water samples were collected from two thermal springs at Dei Dei and from a small hot spring about 0.75 kilometre west of Wapolu point.

The waters collected from the Dei Dei springs were near-neutral-pH chloride (Cl^- >4500 mg/kg) fluids which contained relatively high concentrations of Na^+ (>3500 mg/kg) and K^+ (>400 mg/kg), see Table 2.2. The abundance of Na^+, K^+ and Cl^- may reflect a small seawater component in the geothermal fluid. This in fact is expected considering the proximity of Dei Dei to the ocean. Chemical geothermometers applied to these fluids indicate a deep "reservoir" temperature of approximately 240°C (Table 2.3). Neither the extent of hydrothermal activity nor the geologic potential for the existence of a major high-temperature reservoir was investigated.

Fluid collected from the Wapolu Point spring was slightly alkaline and contained moderate SO_4^{2-} (856 mg/kg), relatively high Cl^- (6160 mg/kg), Na^+ (4670 mg/kg), HCO_3^- (691 mg/kg) and Ca^{2+} (159 mg/kg) and very high Mg^{2+} (331 mg/kg) concentrations (Table 2.2). The abundance of Cl^- and Na^+ may reflect the presence of a seawater component to the fluid. However, the high concentrations of Cl^- and Na^+ may be related to the abundance of amphibolite and weakly metamorphosed ultramafic and mafic rocks through which the fluid traveled. The Ca^{2+} and Mg^{2+} content of the fluid is most likely the result of hydrothermal leaching of mafic and ultramafic rocks. Chemical geothermometers indicate a maximum temperature for the "deep"

fluid of 140°C (Table 2.3). The Wapolu Point spring occurred along a very well exposed dome-building fault. The fault plane and, to a lesser degree ultramafic rocks on the hanging wall, were silicified and, at least locally, contained significant quantities of gold (>1 g/t).

IAMALELE GEOTHERMAL AREA

The following material pertains to the post-Pliocene volcanic geology and geothermal activity occurring in the lowlands surrounding the village of Iamalele (Fig. 2.5). The volcanic rocks exposed in the region are the youngest units of the Kukuia Volcanics which range in age from Miocene to Holocene (Smith and Compston, 1982). The majority of the volcanic rocks exposed in the Iamalele area are ignimbrite flows and air-fall tuffs of dacite to rhyolite composition. These pyroclastic units are intercalated with and intruded by minor andesitic to rhyolitic lavas, and are locally overlain by volcanic cones composed of andesite scoria and lava domes composed of flow-banded rhyolite and rhyolite obsidian flows. Approximately 60% of the Iamalele lowlands are covered by boulder terrace and other fluvial deposits.

Geothermal activity is widespread in the Iamalele area, and probably reflects the existence of a large liquid-dominated hydrothermal reservoir at depth. Outcrops commonly show the effects of hydrolytic alteration which may be accompanied by strongly anomalous concentrations of mercury, arsenic, antimony and locally gold.

Volcanic Geology

The volcanic rocks exposed in the Iamalele area range in age from Late Pleistocene to Holocene (Smith, 1981; Smith and Compston, 1982). When considered together these rocks form a calc-alkalic assemblage which ranges from basaltic andesite to rhyolite. In general, the volume of rocks of

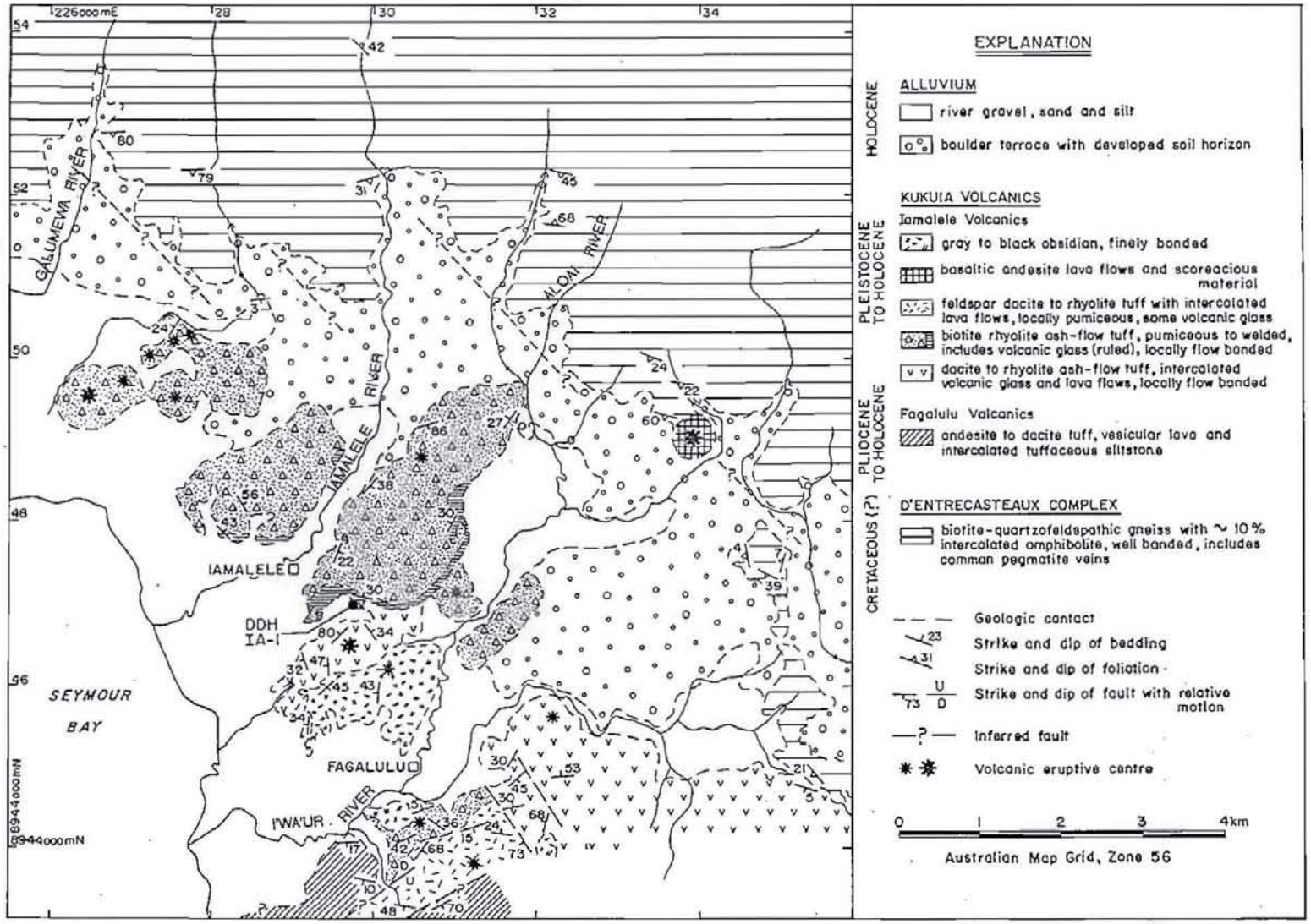

Figure 2.5. General geology of the Iamalele area. Additional information is shown on Plate 1.

mafic to intermediate compositions (basaltic andesite to low-silica dacite) decreases as the age of the rock units decreases.

Davies and Ives (1965) tentatively separated these rocks into two sequences which they referred to as the Fagalulu Volcanics (older) and the Iamalele Volcanics. At the present time there are insufficient field or laboratory data to support this subdivision in any detail. However, the relatively massive andesite to dacite lavas and tuffs which are exposed on the south side of the I'wa'ur River are uncommon elsewhere in the Iamalele area (Fig. 2.5; Plate 1). Considering this the terminology proposed by Davies and Ives (1965) is retained herein.

Because of the abundance of volcanic units within the Iamalele area it was necessary to assign informal names to mappable rock sequences to clarify the discussion of the volcanic geology. Although the unit names are of local origin, it is not proposed that they be considered for adoption as formal names. Much additional geochemical data and a detailed evaluation of the spatial distribution of the units is required before any formal name can be proposed. Because the unit names are informal the first letters of the name are capitalized only if the word is a proper name.

The stratigraphy and spatial distribution of the rock units described in this section are based on field mapping and bulk rock chemistry. Poor exposures and the lack of radiometric age dates make correlation of the rock units difficult and consequently the unit descriptions which follow are of a general nature. However, these descriptions are important because past geologic investigations (Davies and Ives, 1965; Smith, 1976a) did not elaborate on the stratigraphy of Iamalele Volcanics.

The following units are discussed in stratigraphic order starting with the oldest known unit. Samples for which thin sections were analysed are listed in parentheses in the relevant sections.

Fagalulu Volcanics

Andesitic lavas and high-silica dacite account for more than half of the outcrops classified as Fagalulu Volcanics, with high-silica dacite and rhyolite ignimbrite and air fall tuff (I'wa'ur ignimbrite) deposits forming the remainder of the unit. On the geologic map (Fig. 2.5; Plate 1) rock units belonging to both the Fagalulu Volcanics and the Iamalele Volcanics are shown south of the I'wa'ur River. Initially all of the ignimbrite units were considered to belong to the Iamalele Volcanics. However, the I'wa'ur ignimbrite appears to be more mafic than nearly all of the ignimbrites of the Iamalele Volcanics. Because of the close spatial relationship between the unit and the surrounding massive lavas and tuffs, the I'wa'ur ignimbrite is now considered to be the youngest member of the Fagalulu Volcanics. The physical appearance and mineralogy of the Miapuya ignimbrite are also similar to those of rocks exposed north of the I'wa'ur River and the unit was initially thought to be a member of the Iamalele Volcanics. However, considering the rock chemistry of these units, particularly the abundances of Zr and K_2O (Table 2.1; Appendix 3), which were not available when the map was constructed, it appears that the I'wa'ur and Miapuya ignimbrites are components of the same pyroclastic sequence, and both of these units are now considered to be members of the Fagalulu Volcanics.

I'wa'ur Basaltic Andesite

A very limited exposure of vesicular basaltic andesite lava occurs in the Fagalulu tributary to the I'wa'ur River (Fig. 2.3, Plate 1; at sample location 125805). The lava is the oldest stratigraphic unit identified in the Iamalele area. It is overlain by the I'wa'ur dacite and may be in fault contact with the I'wa'ur ignimbrite.

The basaltic andesite is unaltered and contains phenocrysts of clinopyroxene, plagioclase and minor olivine (locally replaced by iddingsite)

Table 2.1. Representative chemical analyses of lavas and pyroclastic rocks exposed in the Iamalele area of western Fergusson Island

SAMPLE NO.	125832	125802	125805	125834	125810	125833	125828	139015	125826	125812	139003	125816	125814	125807	125823	139021	125801	125809	139039
(wt %)																			
SiO_2	53.79	54.93	55.74	56.25	57.50	57.71	61.28	63.11	64.23	67.48	68.18	68.82	68.83	70.34	71.15	72.55	73.62	74.18	74.37
TiO_2	0.98	0.97	1.18	0.94	1.11	1.02	0.99	0.87	0.92	0.43	0.29	0.41	0.43	0.32	0.28	0.22	0.24	0.21	0.24
Al_2O_3	15.80	15.72	18.49	14.70	17.42	16.75	18.32	16.82	17.15	16.11	16.19	15.47	15.80	15.49	14.77	13.31	13.96	13.45	14.15
Fe_2O_3	7.13	6.90	6.96	6.77	6.31	6.32	5.05	4.55	4.71	2.37	1.74	2.20	2.30	1.93	1.61	1.16	1.17	1.16	1.19
MnO	0.10	0.11	0.12	0.10	0.10	0.10	0.08	0.09	0.04	0.07	0.07	0.03	0.04	0.07	0.04	0.06	0.05	0.05	0.05
MgO	8.48	8.67	3.25	6.59	3.47	3.90	1.47	1.11	0.41	0.68	0.51	0.59	0.66	0.67	0.16	0.23	0.21	0.17	0.23
CaO	6.60	7.56	7.32	8.15	6.74	6.72	3.63	3.72	3.42	1.88	1.16	1.72	1.91	1.68	0.65	0.64	0.78	0.68	0.81
Na_2O	3.33	3.67	3.90	2.91	3.72	3.68	5.20	5.15	5.35	4.44	3.93	4.26	4.29	4.15	4.59	3.11	4.84	4.33	4.96
K_2O	1.82	1.75	1.53	2.08	2.52	2.52	2.15	2.41	2.56	3.67	3.31	3.96	4.07	3.50	4.49	4.51	4.09	4.20	4.07
P_2O_5	0.31	0.32	0.25	0.29	0.44	0.37	0.34	0.29	0.33	0.12	0.03	0.05	0.10	0.03	0.05	0.02	0.04	0.02	0.04
SO_3	nd	nd	nd	nd	nd	nd	nd	0.01	nd	nd	nd	nd	nd	nd	nd	nd	nd	nd	nd
LOI	0.53	-0.67	0.90	0.49	0.67	0.20	0.67	1.03	0.80	1.50	3.87	2.07	1.57	1.43	2.00	3.60	0.57	0.98	-0.10
Total	98.87	99.93	99.64	99.27	100.00	99.29	99.19	99.17	99.92	98.76	99.29	99.57	100.00	99.60	99.76	99.41	99.58	99.44	100.01
(ppm)																			
Ba	706	609	585	962	964	1057	791	1891	1181	815	776	779	808	757	841	615	737	642	1341
Rb	53	48	37	45	57	54	28	66	73	111	108	125	114	107	121	150	124	129	127
Sr	514	582	609	910	1209	1127	532	560	566	294	170	271	292	234	86	83	106	84	108
Pb	15	16	11	16	15	18	17	16	18	23	37	24	25	26	25	29	30	26	30
Th	5	6	5	10	11	11	9	7	8	11	19	11	11	15	13	18	17	19	17
Zr	206	195	201	252	303	304	262	229	243	330	184	315	320	167	348	168	206	161	207
Nb	6	11	8	6	5	6	4	7	4	5	6	5	4	4	8	7	6	7	7
Y	21	22	36	96	22	25	27	26	45	24	11	15	16	12	24	18	21	17	19
La	28	31	63	361	86	110	31	36	68	33	24	28	31	24	33	31	35	29	35
Ce	50	61	46	367	129	141	61	60	92	60	66	56	58	46	75	65	75	56	72
Nd	22	32	50	218	44	50	39	28	54	26	10	18	24	11	24	21	26	18	25
V	132	159	130	169	187	162	57	54	49	23	18	21	23	23	6	11	9	9	10
Cr	403	472	69	260	23	77	6	4	3	6	5	6	7	8	3	4	3	2	4
Ni	225	301	28	89	24	36	4	5	4	5	4	3	5	6	1	1	2	3	1
Zn	59	106	73	62	68	62	63	76	57	39	30	39	37	32	40	27	30	25	30
Ga	16	16	19	17	20	21	22	18	18	17	17	17	18	16	18	14	16	15	16

The data were determined by X-ray fluorescence spectrometry and are for samples of I'wa'ur basaltic andesite (125805), I'wa'ur andesite (125828), Aloai andesite (125802, 125832), Wameai andesite (125810, 125833, 125834), I'wa'ur dacite (125826, 139015), I'wa'ur ignimbrite (125816, 125823), Miapuya ignimbrite (125812, 125814), Iamalele ignimbrite (125807, 125809, 139003, 139021) and Uluwa obsidian (125801, 139039). See Appendix 3 for additional data.

in a fine-grained groundmass containing abundant brown glass. Small crystals and microlites of feldspar, clinopyroxene and Fe-Ti oxide minerals occur in the groundmass. Microxenoliths or micro-mineral clusters consisting of aggregates of predominantly groundmass crystals mixed with a few microphenocrysts are also present. Bulk rock and mineral chemical data for this sample are given in Appendices 3 and 4 respectively.

I'wa'ur Dacite

The I'wa'ur dacite tuff is exposed along the I'wa'ur River south of Fagalulu village (Fig. 2.5). The unit strikes westerly and generally dips at shallow angles (10° to 17°) to the south. Very well-developed platy cleavage, possibly related to bedding, is characteristic of the unit.

Only one thin section (139015) of the I'wa'ur dacite was prepared. At this locality the tuff is unaltered and contains phenocrysts and microphenocrysts of plagioclase, orthopyroxene, rare clinopyroxene and an unidentified opaque mineral in a fine-grained groundmass of plagioclase, Fe-Ti oxide minerals and orthopyroxene. The I'wa'ur dacite differs from other members of the Fagalulu volcanics in that it contains a particularly high abundance of Ba (1181 and 1891 ppm for samples 125826 and 139015 respectively) and in this regard is more like sample 139039 of the Iamalele Volcanics (Table 2.1) than the Fagalulu volcanics.

I'wa'ur Andesite

The I'wa'ur andesite is composed of blocky lava flows intercalated with andesitic tuff and tuff breccia. Bedding or flow banding was tentatively identified in only one location within the unit. However, this attitude is subparallel to a nearby fault and it is likely that in this area the unit has been displaced by faulting.

Thin sections of two andesite lavas (125828, 125830) contained phenocrysts of plagioclase, and microphenocrysts of plagioclase, Fe-Ti oxide and

other opaque minerals, orthopyroxene and rare apatite in a fine-grained feldspathic groundmass containing minor clinopyroxene.

I'wa'ur Ignimbrite

Unconsolidated to poorly welded pumiceous biotite rhyolite and dacite tuff and tuff breccia are exposed in the low hills south of the I'wa'ur River in the vicinity of the Miapuya stream (Fig. 2.3; Plate 1). The unit is overlain by the Miapuya ignimbrite to the south and covered by a sago swamp to the north. The I'wa'ur ignimbrite consists of a series of grey to pink, glassy and pumiceous ignimbrite and poorly consolidated, locally sandy air fall tuff deposits. All of the flows that make up this unit contain biotite phenocrysts and locally may contain clasts of biotite rhyolite tuff.

One distinctive characteristic of the I'wa'ur ignimbrite is its relatively high (greater than ~300 ppm) zirconium content, which may indicate a genetic link between the I'wa'ur and Miapuya ignimbrites and earlier andesitic volcanism. See sample 125823 in Table 2.1 and samples 125816 and 125823 to 125825 in Appendix 3.

Miapuya Ignimbrite

The Miapuya ignimbrite is intermittently exposed south of the I'wa'ur River and east of Fagalulu stream. The unit is composed of at least four separate ignimbrite and air-fall(?) deposits. The rocks are generally unconsolidated to poorly welded, but contain several thin beds of volcanic glass and vitrophyre. Volcanic glass and glass-rich tuff horizons are more abundant and much thicker (locally >2 m) in the eastern exposures of the Miapuya ignimbrite. The dominant lithologies are pumiceous biotite rhyolite and dacite tuff and tuff breccia. The tuff breccia contains clasts that vary from <2 to >10 centimetres in diameter. The best exposures of

the tuff breccia are in the lower reaches of the Fagalulu stream, where clast-supported beds are more than 3 metres thick. The Miapuya ignimbrite overlies the I'wa'ur ignimbrite and is overlain by the Uluwa obsidian. Bedding planes measured within the Miapuya ignimbrite have moderate dips (36° to 53°) and variable strikes suggesting some tectonic deformation has occurred.

Iamalele Volcanics

The Iamalele Volcanics is the youngest member of the Kukuia Volcanics and, because of youthful landforms, is interpreted to be Holocene in age (Smith, 1982; Smith and Milsom, 1984). The rocks are predominantly high-silica dacite and rhyolite ignimbrite and air-fall tuff intercalated with andesitic lava and pyroclastic material. The pyroclastic units are relatively flat-lying except where intruded and uplifted by small hypabyssal igneous bodies which are related to a late dome-building event.

Andesitic rocks, including high-Mg varieties, account for less than 10% percent of the exposed Iamalele Volcanics. The spatial distribution of the andesites is restricted to (1) a small volcanic cone east of the Aloai River, (2) thin lavas on the Wameai plateau and (3) three small volcanic cones on the north side of the Wameai plateau.

Kilugaba Rhyolite

The oldest identified member of the Iamalele Volcanics is probably the lithic-rich ignimbrite which was intersected by drilling at a depth of 179 metres (~160 m below mean sea level). The unit, referred to as the Kilugaba rhyolite, is a very distinctive lithic-rich, flow-banded ash-flow tuff containing a high percentage of glass shards and poorly-sorted, heterogeneous rock fragments supported by an ash matrix, and characterized by highly contorted flow-banding. Lithic fragments consist of dominantly rounded clasts of coarse-grained biotite dacite(?) and fine-grained rhyo-

lite(?) which vary in size from a few millimetres to ~6 centimetres in maximum dimension. Compaction textures are common, particularly adjacent to the larger lithic fragments.. Much of the flow-banding and flattened pumice dips between 10 and 30° indicating that the Kilugaba rhyolite may be a relatively flat-lying sheet. However, internal contacts, determined by the relative abundance of fragmental material, may dip as steeply as 70°. The thickness of the Kilugaba rhyolite is not known because its upper contact is with the intrusive Mona Malala rhyolite and the drill hole was terminated (202.2 m) in the unit. The Kilugaba rhyolite may be the basal(?) cooling unit of the Iamalele ignimbrite, but this could not be confirmed because the upper depositional contact of the unit was not intersected by the drill hole and there are no known outcrops of the Kilugaba Rhyolite.

Pervasive hydrothermal alteration has extensively modified the chemical composition of the rock while preserving its texture. A chemical analysis of a less altered portion of the Kilugaba rhyolite (125846) suggests that the unit may have been a dacite (Table 2.1).

Iamalele Ignimbrite

The youngest and most widespread ignimbrite is a pumiceous biotite rhyolite ash-flow tuff which caps the Yaluwana and Iamalele plateaus and many of the low-lying hills to the east (Fig. 2.5; Plate 1). In outcrop the Iamalele ignimbrite varies from a basal, partially devitrified glass, through a middle, moderately welded tuff, to an upper pumiceous tuff. The unit is relatively flat lying with a composite thickness of at least 50 metres.

The Iamalele ignimbrite is typically a fine-grained pumiceous ash-flow containing a few oligoclase phenocrysts or, more commonly, microphenocrysts in an ash matrix. Iron-titanium oxide minerals, minor amphibole and rare orthopyroxene occur in the Iamalele ignimbrite, but the

most notable feature of this unit is the abundance of thin to thick "books" of primary, black biotite.

Aloai and Wameai Andesite

The Aloai andesite is a massive to scoriaceous high-Mg basaltic andesite (125802, 125827 and 125832) which forms a small cone along the contact between the Iamalele Volcanics and the Gudanai Metamorphics east of the Aloai River (Fig. 2.5). The contact between the andesite cone and the Iamalele ignimbrite is concealed by alluvium and thick vegetation, and consequently it was not possible to determine the relative age relationship between the units.

The Wameai andesite (125806, 125810, 125833 and 125834) crops out in several locations on the Wameai plateau and is composed of calc-alkalic and high-Mg calc-alkalic andesite (Fig. 2.5). The distribution of the float suggests that these andesitic rocks are remnants of lava flows, but the stratigraphic relationship between the lava and ignimbrite flows is not clear because most of the rock exposures are concealed by a dense growth of kunai grass. Locally, the andesites appear to be intercalated with the upper unit of the Iamalele ignimbrite, but elsewhere they seem to overlie the Iamalele ignimbrite.

Both the Aloai and Wameai andesites are typically hypocrystalline and sparsely porphyritic. Phenocrysts of olivine, diopside and labradorite comprise less than 15% of the rocks, and are dispersed in a trachytoid groundmass of labradorite to andesine plagioclase, clinopyroxene, olivine and interstitial brown glass. Glomerocrysts of clinopyroxene, olivine, plagioclase and Cr-spinel, and, less commonly, autoliths of olivine or clinopyroxene comprise 5 to 15 percent of the phenocryst content of the rock.

The bulk rock chemistry and mineral chemistry of the Aloai and Wameai andesites are discussed under the heading Petrology of High-Mg Lavas, Northern Volcanic Belt, East Papuan Volcanic Province in Chapter 4.

Mona Malala Rhyolite

At the end of the small ridge just west of Acid Lake (125829; Plate 1) flow-banded rhyolite occurs as float and sub-outcrop. The rock exposed on the ridge is identical to the flow-banded Mona Malala rhyolite intersected at depths between 64 and 170 metres by the Iamalele diamond drill hole. Both of these rhyolites are finely banded, have similar phenocryst contents and lack the fragmental material which is common in the ignimbrites. Banding in these rocks rarely exceeds a few centimetres in width and is commonly contorted. In the drill core the flow-banding dips between 45° and 90°. Considering the spatial distribution of the Mona Malala rhyolite, the unit intersected in the drill hole is probably a feeder zone for the Uluwa dome and for the flow-banded rhyolite exposed west of Acid Lake.

The Mona Malala rhyolite contains rare to ~1% microphenocrysts of plagioclase, minor Fe-Ti oxide minerals, trace phenocrysts of biotite, and small lithic fragments dispersed in a trachytoid groundmass. Intense hydrothermal alteration has modified the chemical composition of the flow-banded rhyolite so that its original composition is unknown. Chemical analyses of the Mona Malala rhyolite are given in Appendix 3 (see samples 125839 to 125845, 125848, 125849 and 125852).

Yaluwana Tuff

A crystal-poor, air-fall tuff is present in the diamond drill core at depths between 20 and 64 metres. Outcrops of mineralogically and texturally similar tuff occur across the northern flank of the Uluwa dome and in a few small outcrops on the southern flank. The Yaluwana tuff is

strongly altered making identification of the primary mineralogy difficult, but the unit was probably a pumiceous rhyolite tuff containing a small percentage (-1%) of phenocrysts of oval-shaped quartz, feldspar, hornblende and rare pyroxene. The tuff is relatively flat-lying with dips varying between 30° at the base and 10° near the top. The systematic decrease in the dip of the beds suggests that the tuff was deposited in, and partially filled, a small basin or lake.

Chemical analyses of two samples of the Yaluwana tuff (125837 and 125838) are given in Appendix 3.

Uluwa Obsidian

The southern flank of the Uluwa dome is covered by a late finely-banded, grey to black rhyolite obsidian flow. The flow is relatively extensive, covering approximately 1.5 km^2. Major and trace element data for two unaltered samples of the Uluwa obsidian (125801 and 139039) are similar (except for barium). The variation in the abundances of barium may indicate that the unit is actually composed of multiple flows. However, there is no field evidence to support this and it is likely that the unit is a single obsidian flow. Obsidian also occurs in the lowlands and caps many of the higher ridges on the south side of the I'wa'ur River. The small outcrop of obsidian south of Fagalulu village is probably part of the Uluwa obsidian flow, but the chemical data needed to confirm this are not available. A source area for the obsidian capping the southern ridges was not located.

Uluwa Tuffaceous Siltstone

The youngest unit of the Iamalele Volcanics is a tuffaceous siltstone which overlies the Yaluwana tuff. The unit was initially identified in the drill core, where it was present from the surface to a depth of 20 metres. Poorly exposed outcrops of the unit were subsequently located in the small

valley separating the Uluwa dome from the Yaluwana plateau. In drill core bedding in the tuffaceous siltstone dips at -24° and appears conformable to the Yaluwana tuff. The contact between the Yaluwana tuff and Uluwa tuffaceous siltstone may be gradational, but compositional differences between the units are significant enough to warrant their separation. The most notable differences are the presence in the Uluwa tuffaceous siltstone of black obsidian fragments (<1 mm) and a small percentage of strongly altered biotite phenocrysts, neither of which is found in the Yaluwana tuff. A further difference is a lower percentage of feldspar phenocrysts in the Uluwa tuffaceous siltstone when compared with the Yaluwana tuff. The tuffaceous siltstone is probably a reworked crystal-poor, pumiceous rhyolite tuff which contained <2% phenocrysts comprised of quartz, feldspar, biotite, hornblende and rare pyroxene. The obsidian fragments were probably contributed by the Uluwa obsidian.

The Uluwa tuffaceous siltstone is intensely altered and in places is totally replaced by secondary hydrothermal minerals. Chemical analyses of two samples of the tuffaceous siltstone (125835 and 125836) are given in Appendix 3.

Surficial Deposits

Recent alluvium consists of extensive boulder terrace deposits and minor talus deposits. Boulder terraces of fluvial and possibly shallow marine origin occur throughout the Iamalele region, and are primarily composed of unaltered Gudanai Metamorphics. Remnants of these terraces occur on all areas of topographic relief, suggesting that the entire region was a low-lying plain which postdated the ignimbrite eruptions. The geologic map presented in Figure 2.5 shows two ages of boulder terrace deposits. Different ages are indicated by the development of extensive soil profiles on the boulder terraces located closer to the metamorphic terrane.

Talus deposits are restricted to narrow zones immediately below the higher cliffs which occur along the margins of the major plateaus and, less commonly, adjacent to the volcanic domes.

Geochemistry

Andesite and Low-Silica Dacite

Lavas and pyroclastic deposits ranging in composition from basaltic andesite to low-silica dacite occur as isolated units intercalated with and overlying high-silica dacite to rhyolite ignimbrite and air fall tuff throughout the Iamalele area (Table 2.1, Plate 1). Because the andesites and low-silica dacites are rarely in contact with each other definitive stratigraphic relationships are difficult to perceive. Initial correlations were made by relating the intermediate composition rocks to spatially extensive and chemically distinct high-silica dacite and rhyolite horizons. Once established it was relatively easy to refine the preliminary stratigraphy for the intermediate composition rocks because their chemistry is remarkably diverse, especially considering the limited area in which they occur and the short period of time over which they were deposited.

Two fundamental types of calc-alkalic andesites occur in the Iamalele area, those with compositions considered typical of arc-type rocks (e.g., Irvine and Baragar, 1971; Jakes and White, 1972), and those with distinctively high abundances of Mg, Cr and Ni. All of the intermediate composition rocks are high-K calc-alkalic (Fig. 4.28), but to simplify the following discussion rocks with "typical" arc-type compositions are referred to as high-K andesites (HKA), whereas rocks with high Mg, Cr and Ni contents are referred to as high-Mg andesites (HMA). The low-silica dacites are referred to simply as dacites. Chapter 4 contains a detailed description of the occurrence of high-Mg andesites and dacites in southeastern Papua New Guinea, including a comparison of the high-Mg rocks to more "typical" arc-type compositions, see High-Mg Lavas in the Late

Cenozoic Volcanic Arc Associations of Papua New Guinea. The discussion on high-Mg lavas contains detailed information on several HKA and HMA samples collected in the Iamalele area.

The andesites with less than ~60% SiO_2 have distinctly higher CaO and lower Na_2O contents than intermediate composition rocks with higher silica contents. With the exception of the I'wa'ur basaltic andesite, which is the oldest andesite exposed south of the I'wa'ur river, the above division clearly separates the andesites and dacites of the Fagalulu Volcanics from the andesites of the Iamalele Volcanics. Since there is no clear chemical distinction between the I'wa'ur basaltic andesite and the HKAs of the Iamalele Volcanics, it is possible that the I'wa'ur basaltic andesite is actually the oldest exposed member of the Iamalele Volcanics.

Andesites which crop out on the plateau immediately east of the Wameai dome (Fig. 2.7, Plate 1) contain distinctively high levels of Ba, Sr and the rare earth elements (REEs) La, Ce and Nd when compared to other andesites of the Iamalele Volcanics. It is interesting to note that both the HKA and HMA Wamaei andesites are enriched in Ba, Sr and the REEs; see Table 2.1 and Appendix 3. Andesites from the Aloai and Wameai areas may be separated further based on their MgO, K_2O, Cr, Ni and Zr contents.

High-Silica Dacite and Rhyolite

There are insufficient chemical data from the rhyolitic rocks exposed in the Iamalele area to establish conclusive patterns for the different rock units, but a few preliminary comments are warranted. Variation diagrams for the rhyolitic rocks show a systematic decrease in the major element oxides, Al_2O_3, TiO_2, total iron as FeO*, MgO and CaO, with increasing SiO_2 (Fig. 2.6). Levels of Na and K are relatively high and the abundance of each correlates with that of SiO_2, although the abundance of K_2O increases much more rapidly than that of Na_2O. The trace elements, Sr, Ba and Zn and to a lesser extent Ce and Zr, decrease with increasing SiO_2,

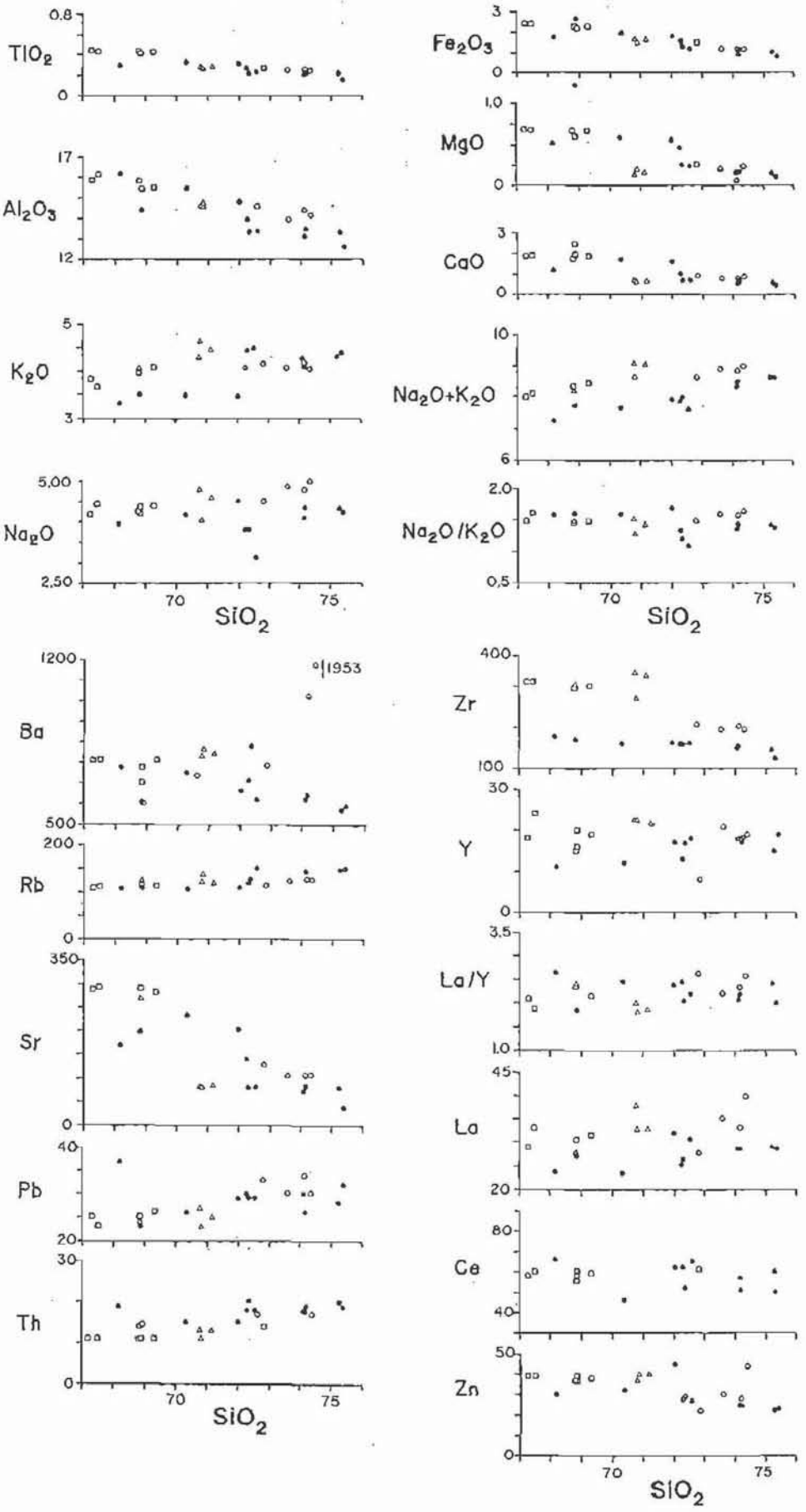

Figure 2.6. Variation diagrams for rhyolitic rocks from the Iamalele area of western Fergusson Island. The data are for the I'wa'ur ignimbrite (△), Miapuya ignimbrite (□), Iamalele ignimbrite (●) and Uluwa obsidian and Yaluwana tuff (○). Major element data in wt %, trace element data in ppm.

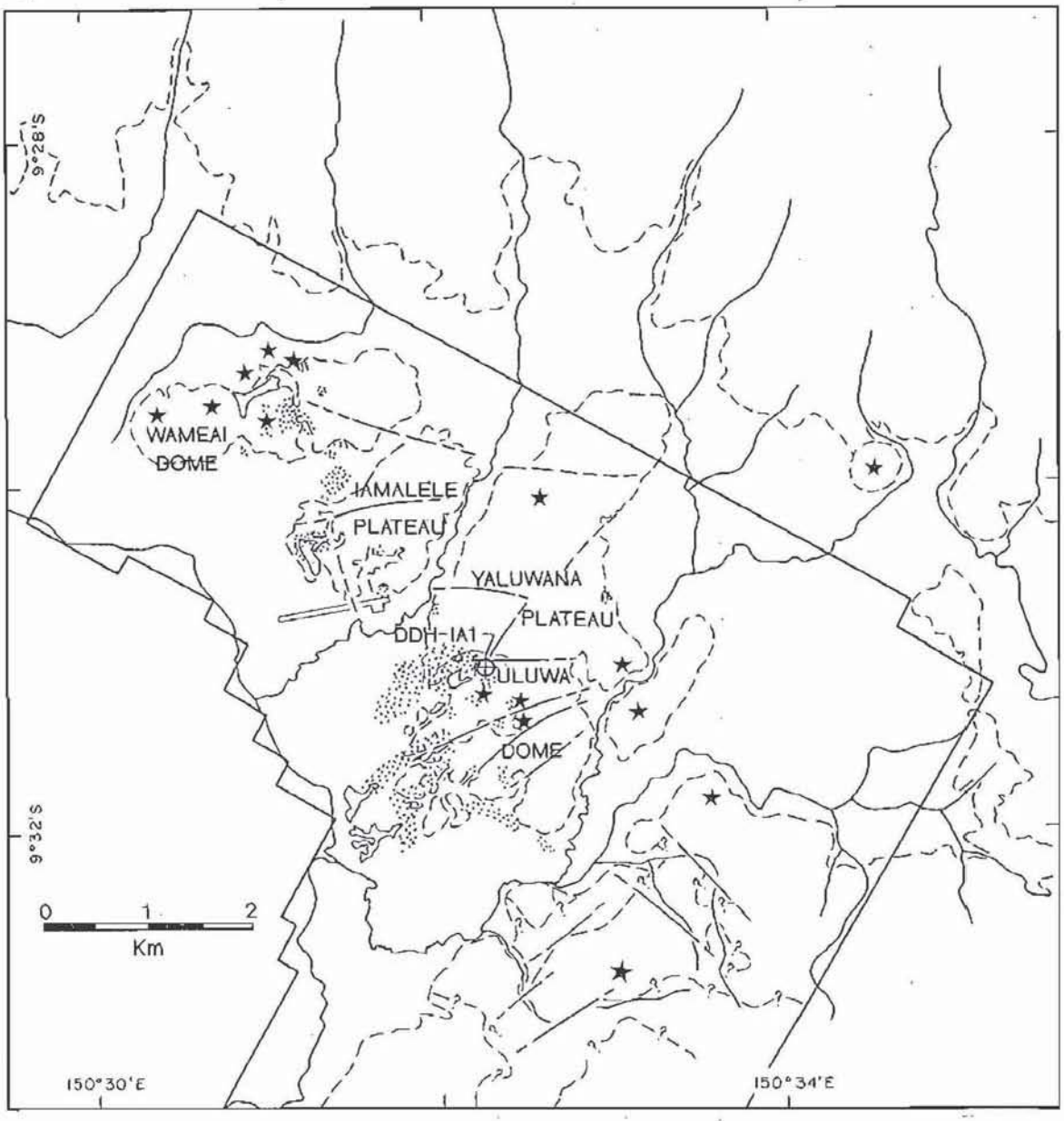

Figure 2.7. Map of the Iamalele area showing the limits of the airborne geophysical surveys (solid outline), volcanic eruptive centres (stars) and active thermal areas (dot pattern). Several of the major topographic features are named. For additional geographical information see Figure 2.3 or Plate 1. Geologic units may be located by comparing the figure to Plate 1.

whereas Rb, Pb, Th and, although there is more scatter, La and Nb increase as SiO_2 increases. The abundances of Cr and Ni are consistently very low in all of the rhyolitic rocks.

The variation diagrams clearly separate the Iamalele ignimbrite from the remainder of the rhyolitic rocks. The remaining rock units all may be members of a second rhyolitic suite of rocks, but more data are needed to conclusively confirm this grouping. The two "suites" of rhyolitic rocks

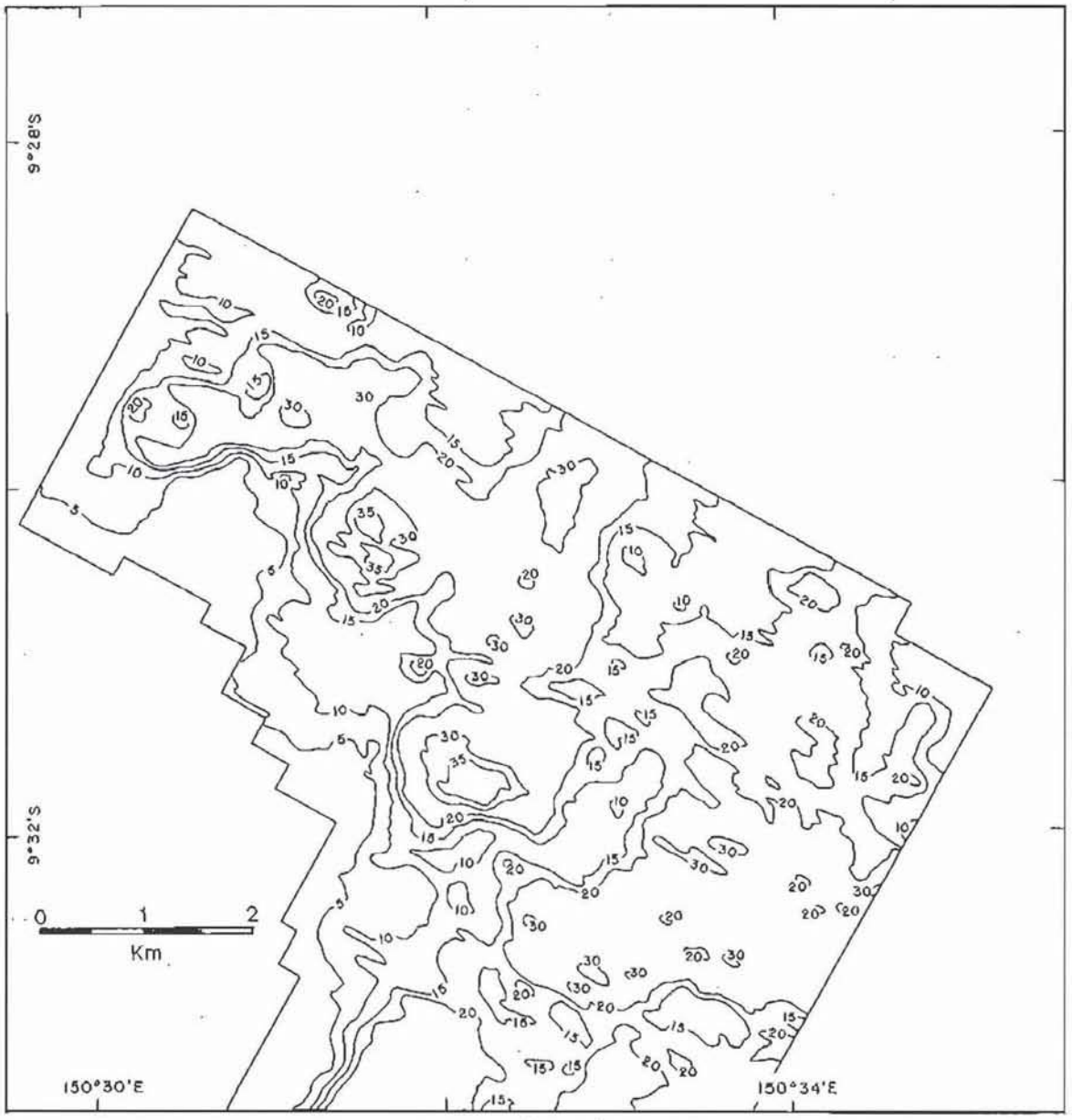

Figure 2.8. Simplified and contoured airborne radiometric data for the Iamalele area. Values are total counts (U, Th, K) x 10^2. For geographic locations see Figure 2.7 or Plate 1.

are most obviously separated on the variation diagrams for Zr, Y, (Na_2O + K_2O), K_2O and Th. Less clear separations can be seen on the diagrams for Ba, La and Na_2O.

Geophysics

The detailed airborne air magnetic and radiometric surveys discussed below are parts of regional surveys which cover most of the Kukuia Peninsula. These surveys were flown by Esso Papua New Guinea, Inc., during 1985

and the contoured data are on file with the Geological Survey of Papua New Guinea (Prospecting Authority 544, Kukuia Peninsula). Simplified contour maps for the portion of this survey that covers the Iamalele area are included with this dissertation (Figs. 2.8 and 2.9; Plates 1A and 1B). Details of the airborne surveys and discussions of the criteria employed in interpreting the data are given in Appendix 9.

Airborne Radiometric Data

The radiometric signature of the high-K rhyolite and high-silica dacite in the Iamalele area contrasts strongly with that of the high-grade metamorphic rocks, andesite, low-silica dacite and alluvium. Outcrops of the high-K rhyolite to dacite are effectively outlined by the 2000 total count (U, Th, K) contour (Fig. 2.8, Plate 1A). The radiometric data for the Wameai plateau are particularly interesting in that they suggest that the Iamalele ignimbrite is a relatively thin veneer over the Wameai dome, thickening slightly to the east and south. The close spacing of the contours suggests that the Iamalele ignimbrite may not be present west of the Wameai dome or that it may be covered by thick alluvial deposits. The shape of the radiometric contours over the Wameai dome indicates that the main mass of the dome is much less radiogenic than the Iamalele ignimbrite, and that it is probably andesite.

Active thermal areas correlate very well with the 3000 total count contour. Whether the radiometric anomalies are related to radioactive isotopes carried by the geothermal fluid or to potassium-rich alteration products, such as alunite and adularia, is not clear. Several small areas outlined by the 3000 total count contour are not known to be associated with active geothermal features. These areas may represent very near-surface geothermal activity or unidentified hydrothermal alteration.

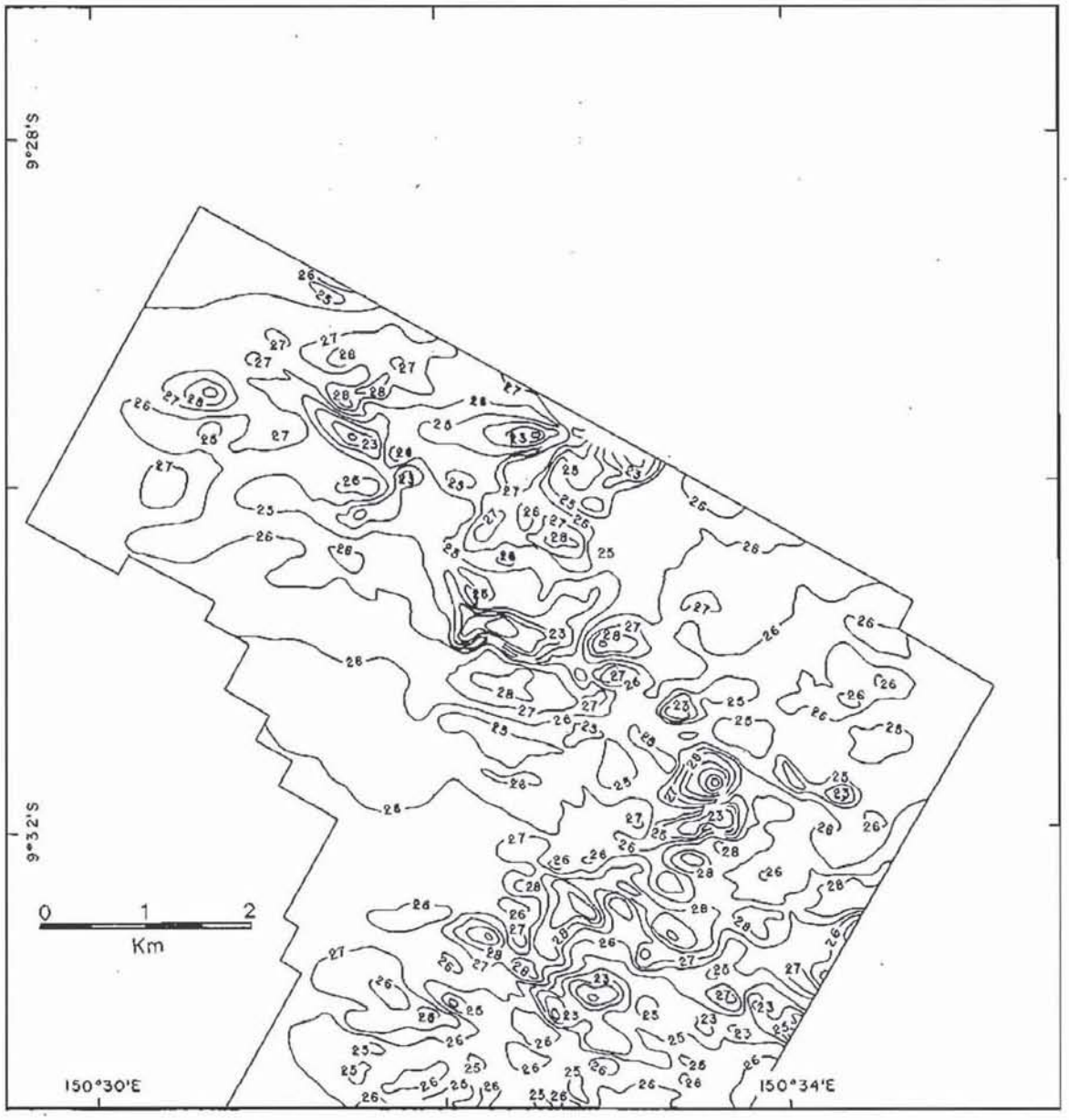

Figure 2.9. Simplified and contoured airborne magnetic data for the Iamalele area. Values are nt (nanotesla) x 10^2. For geographic locations see Figure 2.7 of Plate 1.

Airborne Magnetic Data

Several major geological features are indicated on the residual magnetic contour map. These features include igneous intrusions, faults, magnetite-destructive hydrothermal alteration and variable thicknesses of alluvial deposits (see Figure 2.9, Appendix 9 and Plate 1B). The magnetic data confirmed faults tentatively mapped in the field and from air photographs and indicated the location of several additional structural discontinuities near the northern end of the Kukuia Peninsula. Most of these

structures are probably major block faults, but some may reflect a major caldera-related ring fracture zone.

An evaluation of the magnetic data for the areas east of the Uluwa dome indicates that the boulder terraces are relatively thick, whereas, near the northern end of the Yaluwana plateau, the Iamalele ignimbrite appears to continue to the east under relatively shallow alluvial cover. The alluvial deposits which occur west of the Uluwa dome, Iamalele plateau and Wameai dome are probably very thick indicating that the contact between these volcanic features and the alluvial plane may parallel a major basin-bounding fault.

Magnetic lows reflecting magnetite-destructive hydrothermal alteration associated with geothermal activity occur along the southern edge of the Iamalele plateau near the drill hole location, on the south side of the Wameai plateau and possibly associated with the southernmost eruptive centre shown on Figure 2.7 and Plate 1. The spatial distribution of magnetite-destructive alteration occurring on the south side of the Wameai plateau appears to be fault-controlled.

High-Level Hydrothermal Alteration

Introduction

Active thermal features are exposed over ~30 km^2 of the coastal lowlands surrounding the villages of Iamalele and Fagalulu on western Fergusson Island (Fig. 2.10). Surface expressions of the underlying geothermal reservoir include boiling springs, mud pools, sinter terraces and areas of strong to intense hydrothermal rock alteration. Chemical analyses of soil and rock samples taken from hydrothermally altered areas indicated anomalously high values of gold, arsenic, antimony and mercury. To gain a more thorough understanding of the subsurface geology and the extent of precious and toxic metal mineralization a vertical diamond drill hole was completed to a depth of 202 metres. The results obtained from reconnaissance geolo-

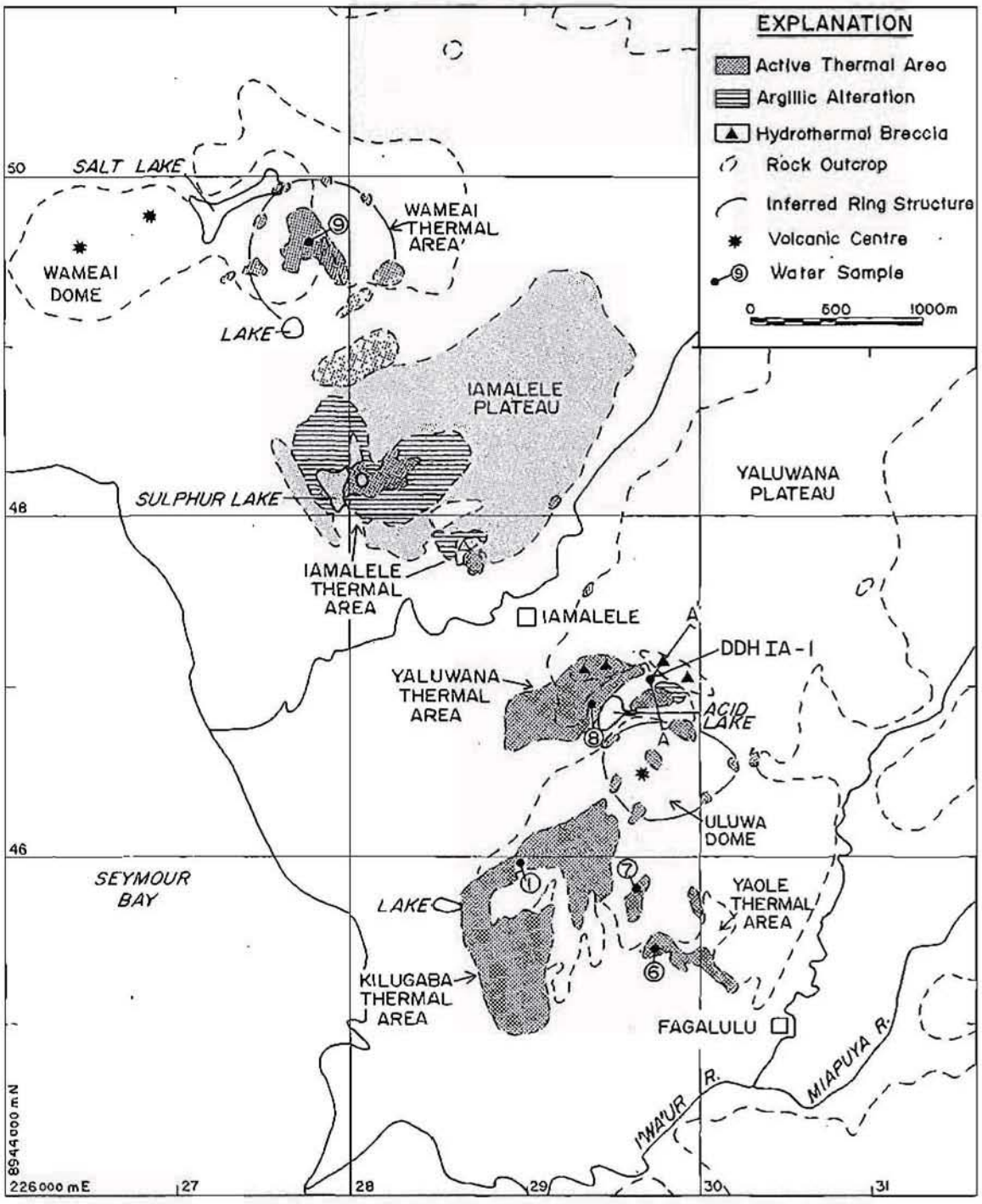

Figure 2.10. Distribution of thermal features within the Iamalele area of western Fergusson Island.

gic mapping within the geothermal area and from the drill core are discussed below. Most of the data pertaining to hydrothermal rock alteration were acquired from the drill core.

Figure 2.11. Characteristic expression of strong hydrolytic alteration. Top photograph taken at water location 9 (Fig. 2.10); view is to the south. The strong bleaching of the Iamalele ignimbrite seen in the photograph is characteristic of kaolinite-cristobalite-alunite ± sulphur alteration, as is the shallow depression caused by dissolution of the rock by the acidic fluid (see Table 2.2). Bottom photograph was taken at water sample location 8 (Fig. 2.10); view is to the north. The strong bleaching of the Iamalele ignimbrite exposed on the low ridge and the flow-banded Mona Malala rhyolite in the foreground is the result of intense hydrolytic alteration. Note the concentration of sulphur crystals around fumaroles. Collapse features in foreground are the result of acid leaching associated with kaolinite-cristobalite-alunite-sulphur alteration.

Surface Features

Hydrothermal alteration of exposed rock is characterized by strong hydrolytic leaching and is associated with toxic and precious metal mineralization. Thermal areas commonly occur in shallow depressions formed by the dissolution of rock by strongly acidic near-surface fluids (Fig. 2.11). Within these areas the rock that remains is intensely replaced (>90%) by

a mixture of kaolinite, cristobalite, alunite and native sulphur, any one of which may be the dominant phase. Halos of kaolinite ± cristobalite alteration extend outward from most active thermal areas for a distance of from 10 to more than 300 metres. Samples collected from several mud pools indicate that the mud consists predominantly of kaolinite, but typically contains some cristobalite and alunite. Sinter terraces are relatively rare and only occur in and around areas of active hot springs (Fig. 2.12).

Tuffaceous Breccia

Two tuffaceous breccias are exposed along the southern margin of the Yaluwana plateau (hydrothermal breccias in Fig. 2.10). The westernmost of these features is an oval-shaped breccia less than 100 metres in diameter (Fig. 2.12). The breccia lies within an active geothermal area and was not investigated in detail. However, it is worth noting that it contains abundant cobbles and boulders (≤1 m in diameter) of gneiss and amphibolite. The origin of the metamorphic clasts is not clear, but most likely they are fluvial material that was entrained in the breccia. The metamorphic material may be a surface (boulder terrace) deposit laid down on top of a hydrothermal breccia and later hydrothermally altered. A less likely possibility is that the pebbles and cobbles are fragments of the metamorphic basement which were rounded by gas streaming in a breccia pipe. However, for this to be true the metamorphic material must have been originated at depths exceeding 225 metres (the depth of the drill hole plus the elevation of the outcrop above the collar of the drill hole).

The second breccia is intermittently exposed for about 500 metres along the southern edge of the Yaluwana plateau where it partially fills a small depression. The breccia consists of a coarse fraction which varies from fine sand to pebble-size clasts set in a poorly consolidated tuffaceous matrix. The unit contains angular to subrounded clasts of unaltered gneiss, amphibolite, rhyolitic pumice and ignimbrite, and andesite lava

Figure 2.12. Surface expression of geothermal activity. Top photograph was taken about 700 m southeast of water sample location 1; view is to the northwest. The photograph shows the development of a large sinter terrace which surrounds intensely altered (kaolinite-cristobalite-alunite ± sulphur) Yaluwana tuff. Note arsenic-antimony-silica precipitate coating bottom of the small thermal pool behind (left side of photograph) the field assistants. Bottom photograph was taken from the top of the small ridge to the west of water sample 1 (Fig. 2.10 and Fig. 2.11, bottom photograph); view is to the south-southwest across Seymour Bay and toward the Kukuia Peninsula. The field assistants are standing on a tuffaceous hydrothermal breccia. "Mounds" in the brownish altered area are rounded cobbles of high-grade metamorphic rocks set in a tuffaceous matrix. Cobbles and matrix are strongly altered to kaolinite-cristobalite-alunite ± sulphur.

mixed with argillically altered volcanic rock fragments. The origin of the unit is not clear because of the occurrence of locally well developed bedding. It is possible that the feature is of fluvial or shallow marine origin, but because of the isolated nature of the unit and the close spatial association of clasts of amphibolite and very delicate clay-altered volcanic rocks this interpretation seems unlikely. A second possibility

is that the breccia may be part of a tuff ring related to hypabyssal intrusive activity. However, the occurrence of hydrothermally altered clasts in the central portion of the breccia suggests that it at least postdates early geothermal activity, and it is unlikely that tuff rings can form in a geothermal environment (Lorenz, 1986). The bedded deposits are, therefore, considered to be remnants of an ejecta apron related to a hydrothermal eruption. Nonbedded and chaotic portions of the unit may have been deposited in the vent portion of the breccia pipe.

Stockwork Fracturing

Areas of highly fractured (15 to 70 fractures/linear metre) and brecciated rock were identified north of the northeast end of the Iamalele runway (Fig. 2.7; Plate 3) and adjacent to the south side of the large (eastern) tuffaceous breccia described in the previous section, see Figure 2.10. Both areas occur in active geothermal centres and are associated with pervasive kaolinite-alunite-cristobalite ± sulphur alteration. The breccia north of the runway is surrounded by a halo of argillic alteration (kaolinite-cristobalite ± vermiculite) which extends outward ~50 metres from the breccia-ignimbrite contact. Silica (opal or cristobalite) veins are locally abundant with the intensity of veining related to the fracture density of the rock. The breccias are probably dilation features (crackle breccias), as indicated by the angularity and paucity of rotation of the clast.

Soil and Rock Geochemistry

Trace element data (Au, Hg, Sb, As) were determined for more than 600 soil and rock chip samples collected along traverse lines throughout the Iamalele lowlands and in a 50 by 100 metre grid pattern surrounding the drill site; see Appendix 3 for geochemical data and Plates 1C, 2 and 3 for

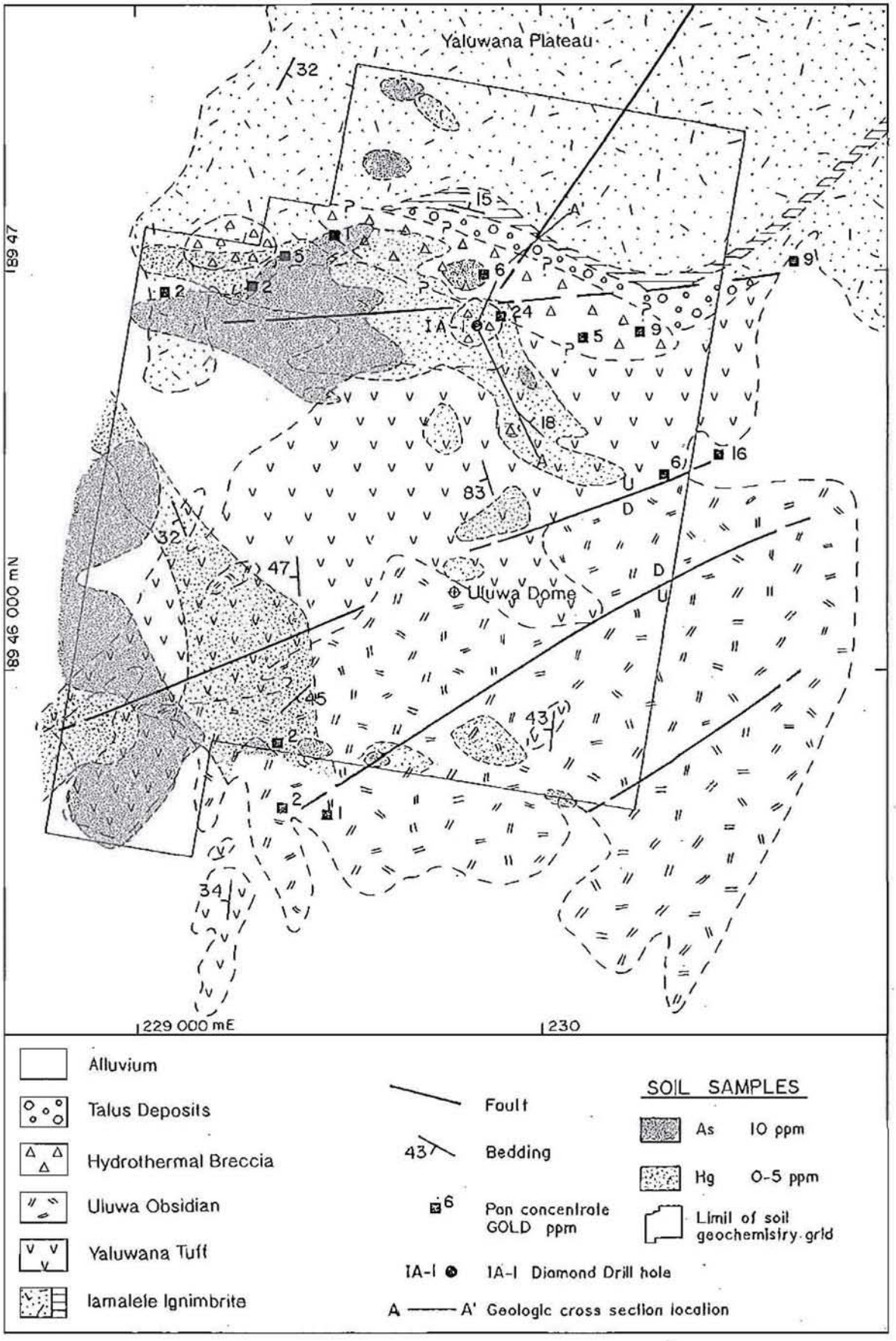

Figure 2.13. Geology and soil geochemical anomalies of the Uluwa dome and southern end of the Yaluwana plateau; see Plate 1C and 2 for sample locations and Appendix 3 for geochemical data.

sample locations. These data indicate several areas which are enriched in one or more of the assayed elements, and show a particularly good correlation between surface geothermal activity and the presence of these metals. The strongest mercury anomalies (>100 ppm) consistently occur in areas of intense kaolinite alteration. Arsenic and antimony sols(?) mixed with a siliceous precipitate commonly form a bright yellow to rust-coloured, fluffy coating up to 4 centimetres thick on the bottom and walls of many acid hot pools and shallow springs (Figs. 2.12 and 4.2), indicating that arsenic and antimony may be deposited directly from the hydrothermal fluid. Surface sand (sample 131840, Plate 2) collected at the northeast edge of Acid Lake in the Yaluwana thermal area and containing a similar yellow-brown precipitate assayed 8.25% As, 34 parts per million (ppm) Sb and 121 ppm Hg. The largest consistent arsenic and mercury anomalies occur on the southwest and northwest flanks of the Uluwa dome (Fig. 2.13).

Pan concentrate samples were collected from most of the streams and dry gullies that drain the southern portion of the Iamalele plateau and the Uluwa dome (Fig. 2.13; Plate 2). Fifty percent (29) of these samples contained between 0.1 and 23.6 ppm gold. All of the samples assaying greater than 0.2 ppm gold occurred within, or were related to, dispersion trains that were traced to active geothermal features. The distribution of gold and silver in both soil and rock chip samples is sporadic with concentrations rarely exceeding 0.1 and 1 ppm respectively.

High-Level Reservoir Conditions

Fluid Chemistry

Water samples were collected from eight thermal springs on Fergusson Island and one on Normanby Island (Table 2.2) in May, 1984. The data indicate that the surface discharge from the Iamalele area is dominated by hot (~45° to 101°C), acidic water which is enriched in sulphate. In contrast to these data, other thermal areas on Fergusson Island are discharging

Table 2.2. Chemical analyses of water samples from Fergusson and Normanby Islands

Sample Number	Location	Surface Outflow T°C	pH	SiO_2	SO_4	NH_3	HCO_3	Cl	Na	K	Mg	Ca	F	Li	B	Rb	Cs
									(mg/kg)								
	Iamalele, western Fergusson Island:																
125878	Kilugaba (ws-1)	101	1.9	308	1337	4.2	--	3494	2600	132	77.5	98	0.29	1.9	44	1.01	0.47
125910	Mana Yaole (ws-6)	94	4.0	379	398	2.1	--	28	176	54	0.5	8	0.69	<	<	0.19	<
125911	Mana Yaole (ws-7)	86	2.1	269	989	3.7	--	6	68	31	1.1	7	0.26	<	<	0.13	<
125912	Yaluwana (ws-8)	90	1.7	268	6020	9.8	--	2	11	2	2.4	5	0.20	<	6	0.02	<
125913	Buatabutu (ws-9)	88	1.7	359	3527	3.0	--	3	26	22	0.8	3	0.23	<	8	0.06	<
	Dei Dei, southeastern Fergusson Island:																
125899	Geyser (ws-2)	100	6.7	332	127	0.3	--	4534	3530	510	0.09	28	43.00	4.3	9	2.76	0.67
125907	Still Pool (ws-3)	86	6.9	227	115	0.5	10	4832	4050	440	0.04	30	47.00	4.7	15	2.70	0.72
	Wapolu, northern Fergusson Island:																
125908	Near DDH-3 (ws-4)	76	8.0	134	856	1.0	691	6160	4670	210	331.0	159	0.54	2.8	21	0.84	0.16
	Bwasiyiyi, Normanby Island:																
125909	Bwahu (ws-5)	82	7.6	144	227	6.0	156	9019	5280	490	96.0	498	0.97	1.9	20	2.41	0.51

< = below detection limit, -- = analysis not completed, (ws-1), etc. = water sample location, DDH-3 = diamond drill hole number 3. Analyses completed by D.S. Sheppard, Chemistry Division, DSIR, Petone. pH data measured at ~35°C. See Appendix 1 for sample descriptions and locations; Iamalele sample locations plotted on Plates 1C and 2.

Table 2.3. Reservoir temperatures calculated using alkali geothermometers for water samples from Fergusson and Normanby Islands, D'Entrecasteaux Islands, Papua New Guinea and Wairakei, North Island, New Zealand

Sample Number	Location	Surface Outflow Temperature (°C)	(mg/kg) Na	K	Ca	Calculated Reservoir Temperature (°C) — Calculation Method — Fournier and Truesdell (1973)	Fournier (1981)	Truesdell (1984)
	Dei Dei, southeastern Fergusson Island							
125899	Geyser (ws-2)	100	3530	510	28	266	251	231
125907	Still Pool (ws-3)	86	4050	440	30	247	224	197
	Wapolu, northern Fergusson Island							
125908	Near DDH-3 (ws-4)	76	4670	210	159	178	157	115
	Bwasiyiyi, Normanby Island							
125909	Bwahu (ws-5)	82	5280	490	498	212	211	180
	Wairakei, North Island, New Zealand							
--	Well 67 (12/59)	--	1260	228	26	264	274	262
--	Well 67 (3/60)	--	1260	210	--	--	265	250
--	Well 67 (12/60)	--	1295	215	--	--	265	249

-- = data not available or not determined, (ws-1), etc. = water sample location, (12/59), etc. = water sample collection date.

near-neutral chloride waters. High molal concentrations of Na^+, Cl^-, K^+ and Mg^{2+} at many of the thermal areas suggest that the fluids may be partially derived from seawater.

Alkali geothermometers developed by Fournier and Truesdell (1973), Fournier (1981) and Truesdell (1984) were used to calculate[1] a "source" temperature for the water analyses given in Table 2.2. The results of these calculations appear to be reasonable and relatively consistent for the springs at Dei Dei and Wapolu (Table 2.3). However, temperatures determined for the Iamalele springs were highly variable and in many cases unrealistically high. This is most likely due to fluid-rock disequilibrium and may indicate that only near-surface acid-"sulphate" waters were sampled. Chemical disequilibrium in the upper portions of the Iamalele reservoir may have resulted from (1) vapour condensation producing acidic and possibly sulphate-rich fluids, (2) ion exchange between the hydrothermal fluid and alteration-related clay minerals, a process which may be accentuated if the "deep" fluid temperature is less than 200°C (Truesdell, 1984), and/or (3) incorporation of seawater into the hydrothermal fluid (e.g., Giggenbach et al., 1983).

Porosity and Permeability

The primary porosity of the ignimbrite flows and related rocks varies from ~10 to >30% in the nonwelded units to less than 1% in the glassy units (Appendix 3). Pores and open spaces are generally connected by small fractures resulting in very high permeability, even in the welded tuffs. All of the drill core is pervasively altered, indicating that the rock remained relatively permeable during hydrothermal alteration. Table 2.4 lists the

[1]A computer program was written to perform the alkali geothermometer calculations. To verify that the program was written correctly reservoir temperatures were calculated for fluid analyses for the Wairakei geothermal system using water analyses from well 67. The results of these calculations (Table 2.3) are in good agreement with the high-temperature inflow (~260°C) to the well.

Table 2.4. Porosity of hydrothermally altered samples from Iamalele drill hole IA-1

Sample Number	Depth (m)	Porosity (%)	Rock Type	Alteration Mineralogy
125835	9.3	56.83	Tuffaceous siltstone	Ka(96), Ct(4)
125836	19.2	8.38	Tuffaceous siltstone	Ct(86), Al(7), Ka(7)
125837	34.0	20.57	Yaluwana tuff	Ka(60), Ct(29), Al(10), Py(1)
125838	49.3	8.49	Yaluwana tuff	Al(100)
125848	60.0	10.99	Mona Malala rhyolite	Ct > Ka > Al
125839	74.3	17.89	Mona Malala rhyolite	Ct(54), Ka(44), Py(2)
125840	81.2	7.64	Mona Malala rhyolite	Ct(40), Ad(22), Bd(16), Py(11), Ka(7), Il-Vm(2), Qz(2)
125841	99.9	8.41	Mona Malala rhyolite	Bd(45), Qz(37), Ad(9), Ka(4), Ab(2), Py(2), Il-Bd(1)
125842	118.6	14.01	Mona Malala rhyolite	Ad(35), Qz(27), Ct(19), Bd(13), Py(4), Il(2)
125844	139.7	7.21	Mona Malala rhyolite	Qz(58), Ad(33), Ab(6), Py(2), Il-Vm(1)
125845	160.9	5.71	Mona Malala rhyolite	Qz(60), Ad(28), Ab(6), Il-Bd(2), Il-Vm(2), Py(2)
125846	181.4	24.37	Kilugaba rhyolite	Qz(43), Ad(37), Ab(10), Il-Bd(6), Il-Vm(6), Py(3)
125850	186.0	21.45	Kilugaba rhyolite	Qz(63), Il(16), Ad(12), Vm(6), Py(2), Ab(1)
125847	199.8	10.03	Kilugaba rhyolite	Qz(50), Ad(30), Ab(13), Il(4), Py(2), Vm(1)

Ab = albite, Ad = adularia, Al = alunite, Bd = beidellite, Ct = cristobalite, Il = illite, Ka = kaolinite, Py = pyrite, Qz = quartz, Vm = vermiculite. Percent mineral present in sample given in ( ). See Appendix 6 for additional information.

measured porosities for several samples of hydrothermally altered drill core. An important observation from these data is that strongly clay-altered core remains relatively porous. This fact indicates that clay gouge-filled fault zones still may be useful channels for migrating hydrothermal fluids.

The rocks intersected by drilling are moderately well fractured. Fractures generally dip between 45° and 80° and are typically subparallel to flow banding in the Mona Malala rhyolite. Except in areas of brecciation, which dominate the upper 65 metres of the core, the fracture density of the rocks increases slightly with depth. In nonbrecciated core the fracture density increases rapidly from ~10 to ~20 fractures per linear metre at a depth of about 140 metres.

Hydrothermal breccias occur in the upper and lower parts of the cored interval. The breccias are generally matrix supported and composed of very angular clasts of intensely altered rock. The alteration mineral assemblage of the clasts is similar to that of the wall rocks, which in conjunction with the angularity of the clasts and the common occurrence of crackle breccias suggests that the fragments have undergone limited transport.

Rock textures in the relatively near-surface breccias indicate multiple periods of brecciation. These hydrothermal breccias are described in greater detail under their respective alteration types.

Faults

Most of the faults intersected by the drill hole occur as single fractures with little or no clay gouge. Where present, slickensides indicate nearly total dip-slip motion. Major fault zones containing more than one metre of highly fractured rock and clay gouge occur at four locations (Fig. 2.14), but the displacement on these faults appears to be minor. The fault at ~85 metres is the most significant, in that it may juxtapose different types of hydrothermal alteration. There is an increase in the abundance of adularia on both sides of the fault which may be related to increased permeability and fluid movement near the fault. This fault also occurs at the transition from hydrous silica to quartz.

Diamond Drilling

The drill site was selected on the basis of overlapping soil geochemical (Hg, Sb, As) anomalies, very high values (0.4 to ~23.6 ppm) of gold in the p[illegible] concentrate samples and the presence of (1) strong kaolinite-cristobalite ± alunite alteration and associated fracturing, (2) local brecciation associated with strong silicification (cristobalite stockwork veining) exposed in several rock outcrops and (3) remnant hypogene silica-pyrite and pyrite stringers.

Hydrothermal Alteration

With the exception of early propylitic alteration which is only weakly developed at depths greater than 128 metres, the major hypogene mineral assemblages are the result of either potassic alteration or a

subsequent hydrolytic event. The diamond drill hole intersected an alunite ± silica breccia around which particularly well developed hydrolytic alteration is concentrically zoned (Fig. 2.15). Advanced argillic alteration represented by the assemblage kaolinite-cristobalite ± alunite occurs closest to the alunite breccias, and the intermediate argillic assemblage smectite ± vermiculite forms an outer and possibly earlier halo on the breccias. Alternatively, the zoned alteration halo on the alunite breccia may be the result of prograde alteration. Potassic alteration occurs outside the limits of intense intermediate argillic alteration. Silica and sulphate minerals, and the metals Hg, As and Sb, are well zoned with respect to depth and type of alteration (Fig. 2.14).

The major types of rock alteration described below are a pervasive feature of the core. However, because only one drill hole was completed, the spatial extent of these alteration assemblages and their relationship to major structural features is not known. The alunite-bearing breccias are certainly structurally controlled and probably do not extend to great depths. Pervasive smectite (beidellite) alteration is associated with the upper fault zones and pervades the rock between 80 and 115 metres. Feldspar (adularia and below 128 m adularia ± pericline (albite)) alteration may be widespread within the geothermal reservoir, but an alternate interpretation is that potassic alteration is actually a large, pervasive alteration halo surrounding the hydrothermal breccias, see Figure 2.15.

The silica species identified in the drill core include lussatite (opal-CT), α-cristobalite (opal-C) and quartz; opal (opal-A) occurs only in surface exposures. Hydrous silica is most abundant adjacent to the alunite breccias and, with the exception of the alunite core of the lower breccia, is the dominant mineral at depths between 20 and 85 metres. Quartz is the principal form of silica below ~85 metres and is the only silica phase below a depth of 125 metres.

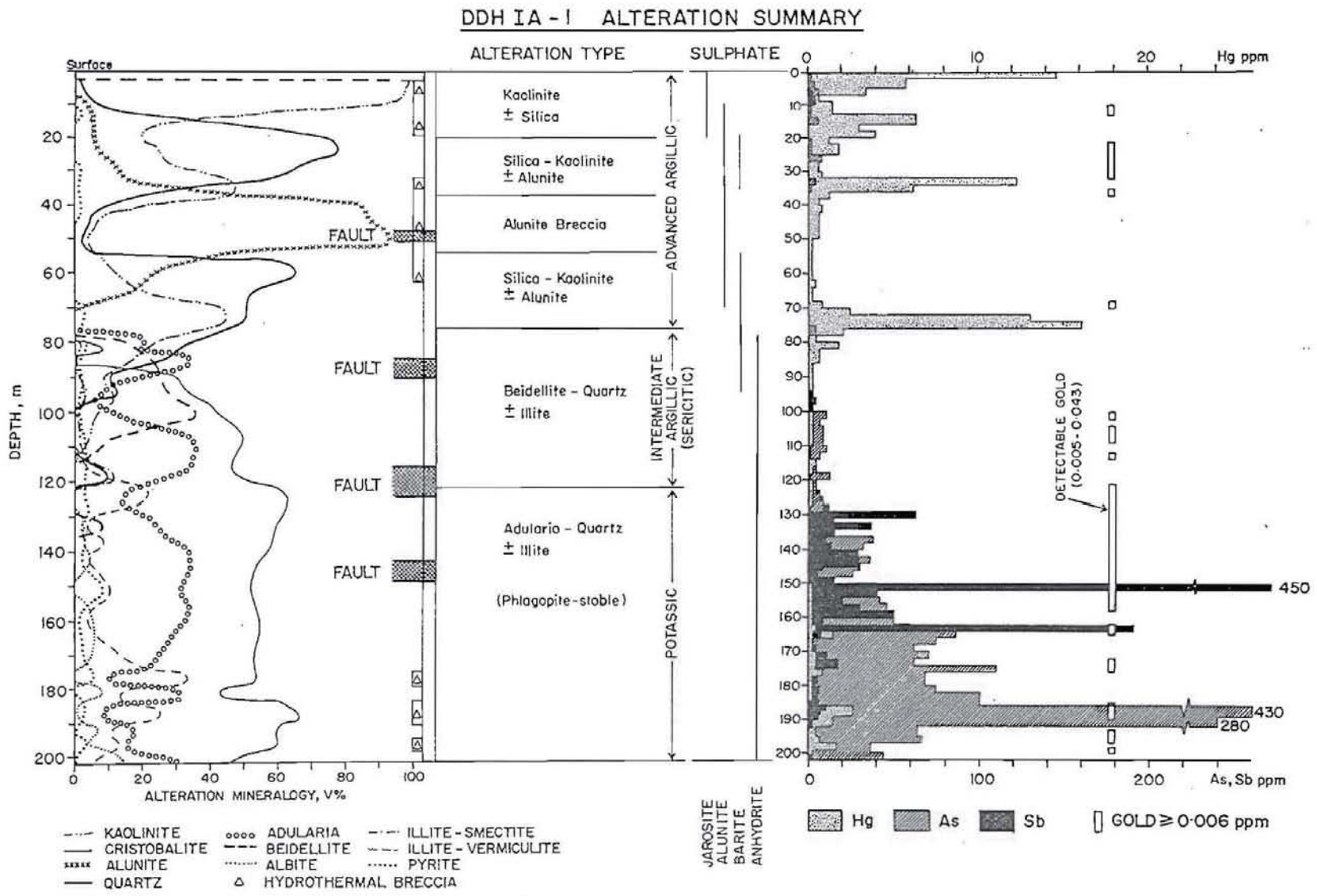

Figure 2.14. Summary log for Iamalele diamond drill hole IA-1.

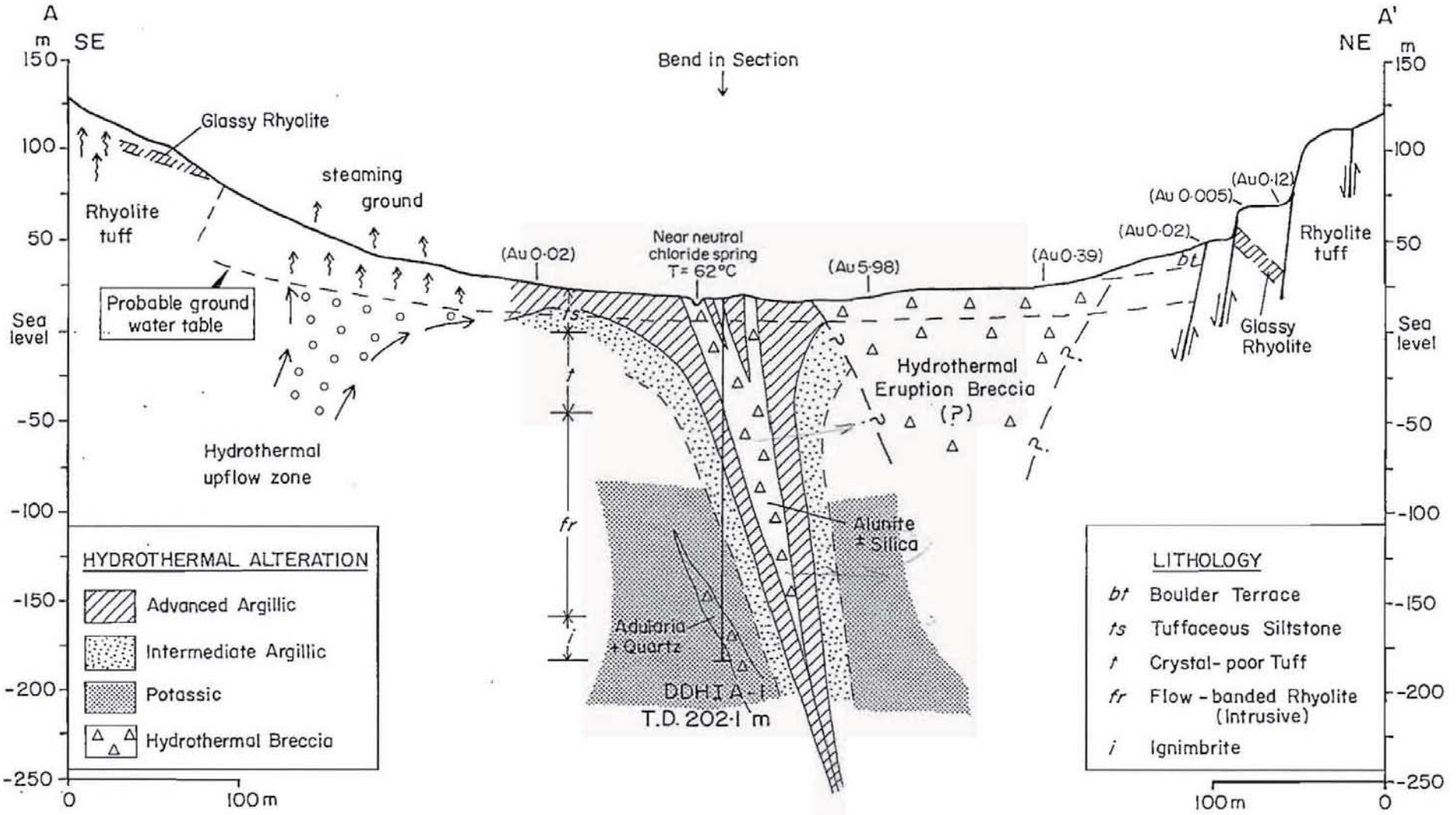

Figure 2.15. Summary cross section through Iamalele drill hole IA-1. Alteration mineral assemblages are described in the text. See Figure 2.13 and Plate 2 for cross section location and additional information.

Sulphate minerals are present throughout the cored interval and include jarosite (Fe), alunite (K), barite (Ba) and anhydrite (Ca). Jarosite is only present in the upper 20 metres of the core, where it is associated with hematite and goethite. Alunite is a major constituent of the core between ~10 and ~70 metres where it occurs as a monomineralic fracture filling, is a major component of the hydrothermal breccias and occurs as disseminated alteration. Barite in association with kaolinite occurs along late fractures between 28 and 100 metres. Anhydrite is present in the core below 75 metres and is characteristically associated with adularia.

Propylitic Alteration

Below a depth of 128 metres trace to minor amounts (<5%) of pericline[2] are present in the core. Adhering to the usage of Meyer and Hemley (1967), the occurrence of pericline ± adularia replacing plagioclase and the groundmass signifies propylitic alteration. Studies at Wairakei (Chapter 3) indicate that propylitic alteration is uncommon in the reservoir at depths less than ~300 metres. The presence of weakly developed pericline alteration below 128 metres indicates that the drill hole penetrated the upper fringe of propylitic alteration. The occurrence of propylitic alteration at very high levels in the Iamalele reservoir may be related to the relatively high activity of Na^+ in the fluid. It is possible that pericline represents an earlier period of alteration and is either metastable with or is being replaced by adularia. However, there is insufficient textural evidence to confirm an early propylitic event.

---

[2]Low temperature Na- and K-feldspar which crystallize from hydrothermal solutions, particularly as open-space or vein filling, are termed pericline and adularia respectively (Shelley, 1985; p. 247).

Energy dispersive x-ray analysis (EDXA) data indicate that, although stoichiometric pericline and adularia are present, isomorphic substitution of Ba and Na for K in adularia and K for Na in pericline is prevalent.

Potassic Alteration

Potassic alteration is represented by the assemblage quartz-adularia-illite/sericite-anhydrite-pyrite (usage of Meyer and Hemley (1967)). These minerals occur as pervasive rock alteration and as vein filling. Adularia was first identified at a depth of ~78 metres and is always a major component (>20%) of potassic alteration (Fig. 2.14). Together quartz and adularia may locally comprise more than 50% of the core.

Hydrothermal biotite is present in the core between 130 and 150 metres, where it replaces rare primary amphibole (hornblende) and forms overgrowths on magmatic biotite. Semiquantitative EDXA of hydrothermal biotites indicates that they are a Mg-rich variety, probably phlogopite. The occurrence of secondary biotite overgrowths on magmatic biotite confirms that biotite, at least locally, is a stable phase within the zone of potassic alteration. The occurrence of secondary biotite at depths of 150 metres is unexpected since hydrothermal biotite normally does not form at temperatures less than ~300°C (see for example, Bird and Norton, 1981) and it is very unlikely that reservoir temperatures were ever this high at a depth of 150 metres. The occurrence of low-temperature hydrothermal biotite at high levels within hydrothermal systems is discussed in Chapter 3, see section on Hydrothermal Biotite under Potassic Alteration.

Below 75 metres anhydrite is present as a vug or fracture filling, where it is intergrown with quartz, adularia and albite. EDXA indicates that minor Ba-Ca substitution occurs, but in general anhydrite is stoichiometric calcium sulphate.

Illite commonly replaces plagioclase, but is in equilibrium with adularia and possibly pericline. This is suggested by the apparent coexis-

tence of these minerals in vugs and open fractures, where illite coats alteration feldspar without evidence of replacement. The volume ratio of adularia, quartz and illite remains relatively constant (Ad:Qz:Is ~ 25:45:10) below a depth of ~130 metres. An exception to this abundance ratio occurs in the hydrothermal breccias, where illite-smectite and vermiculite replace secondary feldspar.

Hydraulic fracturing occurs in six intervals between 165 and 195 metres. The breccias consist of very angular fragments composed of a mixture of adularia (~50%), quartz (~35%) and illite-smectite (~15%) supported in a matrix consisting of quartz (>50%), pyrite (~10%), adularia (~10%) and illite-vermiculite (>25%). Crackle breccias consisting of angular fragments of potassically altered rock surrounded by quartz veins and open space filling 1 to 7 millimetres thick occur on the margins of the larger breccias. The breccias probably formed during a fracturing event which accompanied potassic alteration, and have subsequently been replaced by smectite and vermiculite (intermediate argillic alteration).

Intermediate Argillic Alteration

Intermediate argillic alteration (usage of Meyer and Hemley, 1967) is ubiquitous below a depth of ~75 metres, but is most well developed in a narrow (~35 m) interval separating potassic alteration from the "overlying" kaolinite-cristobalite ± alunite alteration. The clay minerals characteristic of intermediate argillic alteration, smectite (K- and Na-beidellite ± montmorillonite) and mixed-layer illite-smectite ± K-vermiculite, coexist with silica in fractures and replace plagioclase, alteration feldspars and illite/sericite. Barite is a minor component of intermediate argillic alteration and probably reflects Ba lost from feldspar as it is altered to clay.

Smectite first appears at 75 metres and is a major (>20%) constituent of the core between 80 and 115 metres. Smectite replaces primary and

secondary feldspar and the groundmass, and is particularly well developed along fault planes. X-ray diffraction and EDXA data indicate that the clay fraction at 100 metres is a (K,Na)-beidellite mixed with a small (<5%) portion of K-vermiculite.

K-vermiculite occurs as an alteration product of smectite below 110 metres. The volume ratio of mixed-layer vermiculite-smectite varies from ~50 to ~100% vermiculite, with vermiculite being a major mineral phase in the hydrothermal breccias below 170 metres. Mixed-layer illite-vermiculite coexisting with quartz occurs in the last ~30 metres of the core. There is an inverse correlation between the abundances of vermiculite and pyrite, indicating that the minerals may not coexist.

Advanced Argillic Alteration

Alunite, kaolinite, lussatite and cristobalite are the major components of advanced argillic alteration (usage of Meyer and Hemley (1967). At depths less than 15 metres kaolinite and hydrous silica (lussatite + cristobalite) are the dominant minerals, occurring with trace to minor amounts of gibbsite, brucite, jarosite, goethite and hematite. Initially kaolinite, alunite and lussatite-cristobalite replace illite-sericite and primary and secondary feldspar, but as the intensity of alteration increases, the entire rock including quartz may be replaced. Hydrothermal breccias containing a high percentage of alunite are characteristic of advanced argillic alteration, and within these breccias some of the alunite and lussatite in the matrix appears to have precipitated directly from the fluid. Intergrown alunite and lussatite occur as very fine-grained bedded sediment locally filling voids in the alunite breccias.

Alunite first appears in the core at ~10 metres and remains a volumetrically significant phase to a depth of ~70 metres. The abundance of alunite shows an inverse relationship to that of kaolinite and cristobalite. Below a depth of ~52 metres alunite changes colour from a light

Table 2.5. Chemical analysis of alunite from Iamalele drill hole IA-1, sample number 125838

Oxide	wt %	Oxide	wt %	Oxide	wt %	Element	ppm
Al_2O_3	36.82	SiO_2	1.05	CaO	0.01	Rb	172
K_2O	10.29	TiO_2	0.02	Na_2O	0.27	Sr	109
SO_3	36.64	Fe_2O_3*	0.01	P_2O_5	0.56	La	218
LOI	13.70	MnO	0.02	BaO	0.52	Ce	230

Fe_2O_3* = total Fe as Fe_2O_3, LOI = loss on ignition. See Appendix 3 for additional data.

tannish brown to dark greyish black. The reason for this colour change is not clear, but it does not appear to be due to either a leaching phenomenon or the inclusion of very fine-grained pyrite. Data from an X-ray fluorescence spectrometry analysis of pure alunite taken from the core at 49 metres are given in Table 2.5.

Kaolinite is a major component of advanced argillic alteration, comprising a significant portion of the core between ~15 and ~45 metres and between ~60 and ~110 metres. Kaolinite is a pale yellow-green colour when the rock is removed from the core barrel, but the colour begins to darken shortly after the core is exposed to the atmosphere, suggesting that the colour of kaolinite is a function of oxidation.

Cristobalite is the dominant hydrous silica phase associated with advanced argillic alteration and forms envelopes on the alunite breccia. Lussatite is the most abundant silica phase at shallow depths (less that ~20 m).

Barite is a minor component of advanced argillic alteration, occurring as a late fracture filling intergrown with kaolinite, lussatite, pyrite and, below 80 metres, quartz. Barite is not present in the main alunite zone, possibly because barium is strongly partitioned into alunite (see Table 2.5).

Hydrothermal breccias genetically related to advanced argillic alteration occur at depths between 32 and 62 metres. The breccias are composed of clasts of cristobalite, lussatite and alunite supported in a lussatite-alunite matrix. Near the base, the breccia becomes clast supported, and cristobalite is the dominant alteration mineral comprising >50% of the rock. Open spaces within the breccias are typically coated or filled with a fine horizontally banded mixture of lussatite (40%), kaolinite (40%) and alunite (20%). Alunite makes up >40% of the breccia and locally constitutes 100% of the core. The distribution of pyrite in these breccias is irregular.

Metallization

Pyrite is the most abundant sulphide mineral and occurs throughout the core as fracture coatings, as fine disseminated grains and as small stringers. Disseminated pyrite may locally exceed 5% of the rock. Pyrite is found in association with quartz, illite and stibnite in fault gouge; the matrix of both the "alunite" and "adularia" breccias may contain pyrite in excess of 10%.

Stibnite (Sb_2S_3) is present in the core between 129 and 185 metres, where it locally accounts for as much as 0.5% of the rock. However, the maximum Sb assay value for a metre of core was 450 ppm. Stibnite occurs as radiating clusters of very fine, acicular crystals intergrown with illite ± smectite in late fractures, and much less commonly, disseminated through the rock.

Rare crystals of arsenopyrite (FeAsS) were visually identified in the core below a depth of 160 m but were not identified in thin section.

Mercury occurs in the upper portion of the drill core where its abundance is roughly proportional to that of kaolinite (Fig. 2.14). Antimony and arsenic are most abundant within the zone of potassic alteration, and although the data are limited by the depth of the drill hole, it appears

that the main antimony anomaly occurs above that of arsenic (Fig. 2.14). Trace amounts of gold occur sporadically throughout the core. The most continuous gold anomalies occur within the zone of potassic alteration.

Discussion

The occurrence of numerous surface geochemical anomalies and the degree of metallization of the drill core clearly indicate that the reservoir fluid at Iamalele is transporting gold, mercury, arsenic and antimony. The reasons for the absence of significant concentrations of precious metals at Iamalele are not clear. Since only one drill hole was completed it is possible that economic gold mineralization does exist, but was not identified during reconnaissance exploration. A second possibility is that the Iamalele geothermal system has not evolved to the stage at which ore-grade quantities of precious metals are deposited. This possibility is difficult to assess because there are limited chemical, thermal, rock alteration and metallization data pertaining to the high-temperature reservoir.

Although it may not be possible to determine the extent and timing of precious metal mineralization at Iamalele because of the limited data base, some inferences may be made by comparing the Iamalele geothermal system to an epithermal precious metal deposit. This is done in the first part of Chapter 4 where Iamalele is compared to the Rawhide gold-silver deposit.

Chapter 3

WAIRAKEI GEOTHERMAL AREA, NORTH ISLAND, NEW ZEALAND: GEOLOGY, THERMAL ZONING, HYDROTHERMAL ALTERATION AND METALLIZATION

INTRODUCTION

Chapter 3 deals with the spatial and temporal relationships between the minerals formed during hydrothermal alteration, their primary and secondary hosts and the temperatures at which these reactions occur. Recognition of these relationships permits grouping of the alteration minerals into equilibrium assemblages which more fully describe the physicochemical conditions prevailing within the geothermal reservoir during the relatively recent past. The information presented in this chapter builds on the works of Grindley (1965), Steiner (1977), Grant (1979, 1980) and Healy (1984), but differs significantly from these earlier works in that this study is directed from the point of view of mineral exploration. That is, what, if any, are the similarities between hydrothermal alteration and metallization at Wairakei and at epithermal precious metal deposits which have formed in similar volcano-tectonic environments?

Important aspects of this study include (1) development of a set of cross sections which show the distribution of preproduction isotherms within the Wairakei hydrothermal reservoir, (2) classification of the minerals formed during hydrothermal alteration into paragenetic assemblages that are consistent with the usage of Meyer and Hemley (1967), (3) development of a set of cross sections which show the spatial distribution of the hydrothermal alteration mineral assemblages within the Wairakei reservoir and (4) documentation of metal mobility and metal deposition within the Wairakei hydrothermal reservoir and wellhead production equipment.

Location and Geologic Setting

Wairakei is located near the centre of the North Island of New Zealand and is one of several large, liquid-dominated geothermal systems which are associated with the major caldera volcanoes of the Taupo Volcanic Zone (Figs. 3.1 and 3.2). The northern boundary of the hydrothermal system at Wairakei coincides with the southeastern periphery of the Maroa volcanic complex, but the majority of the geothermal reservoir lies within a diffuse border zone between the Maroa and Taupo volcanoes. The Wairakei reservoir is localized in a voluminous sequence of rhyolitic ash-flow and air-fall tuffs intercalated with lacustrine deposits and lava flows of andesite to rhyolite composition. The high temperature reservoir is mainly restricted to the Waiora Formation which is underlain by less permeable ash-flow tuffs (Wairakei Ignimbrite) and capped by relatively impermeable volcaniclastic rocks (Huka Falls Formation).

Figure 3.1. Photograph of the eastern "bore field" at Wairakei. View is to the southeast from the public lookout. The pipeline carries steam to the power station which is located along the Waikato River ~3 km east-southeast of the lookout. Mounds of yellowish-tan material are piles of siliceous precipitate removed from the main hot water drain.

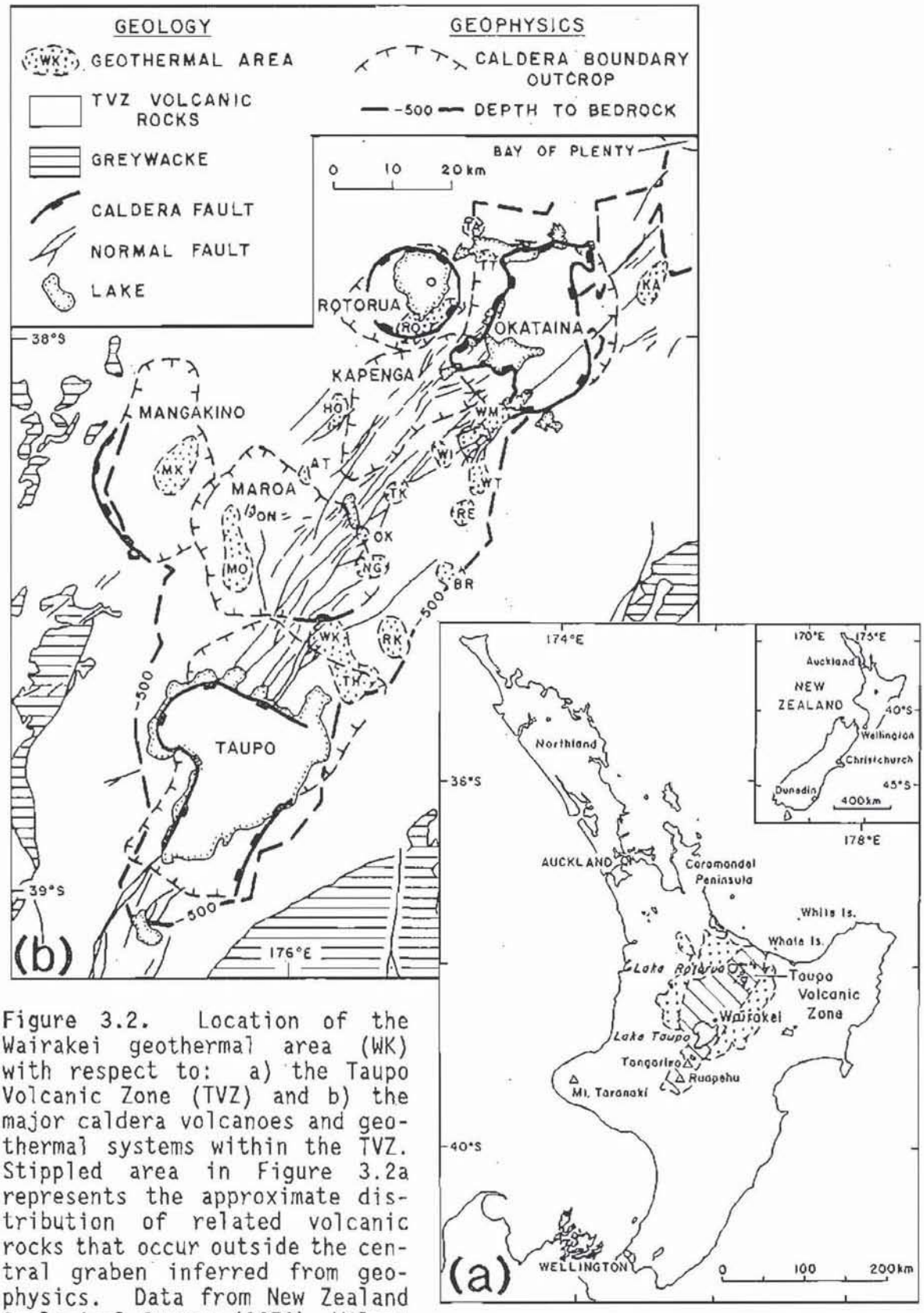

Figure 3.2. Location of the Wairakei geothermal area (WK) with respect to: a) the Taupo Volcanic Zone (TVZ) and b) the major caldera volcanoes and geothermal systems within the TVZ. Stippled area in Figure 3.2a represents the approximate distribution of related volcanic rocks that occur outside the central graben inferred from geophysics. Data from New Zealand Geological Survey (1972), Wilson et al. (1984) and Mongillo and Clelland (1984). Geothermal areas: Atiamuri (AT), Broadlands (BR), Horohoro (HO), Kawerau (KA), Mangakino (MK), Mokai (MO), Ngatamariki (NG), Ongaroto (ON), Orakeikorako (OK), Reporoa (RE), Rotokawa (RK), Rotorua (RO), Tahara (TH), Taheke (TA), Te Kopia (TK), Tikitere (TT), Wairakei (WK), Waikite (WI), Waimangu (WM) and Waiotapu (WT).

Production History

Potential for the commercial development of geothermal resources within the Taupo Volcanic Zone was recognized in the 1930's (Bruce and Shorland, 1932; Grange, 1937), but it was 1948 before geothermal energy was considered a viable alternative to hydroelectric power in New Zealand (Grindley, 1965). In 1950, buoyed by the prospect of supplying heavy water for England's fledgling nuclear weapons programme, the New Zealand government initiated a study to assess the feasibility of large-scale power production from the geothermal reservoir at Wairakei (Grange, 1955). By 1956 drilling results indicated a resource sufficient to support a 250 megawatt (MW) power station and construction began that year (Grindley, 1965; Ministry of Energy, 1985). Subsequent reservoir testing indicated that the level of sustained steam production had been overestimated by about 40%, and the Wairakei power plant was ultimately constructed with maximum power production capacity of ~193 MW.

When commissioned in November 1958, Wairakei became the world's second geothermal power station and the first to exploit a liquid-dominated reservoir. Approximately 200 exploration, production and monitor wells have been completed to depths varying from <100 metres to 2,240 metres. Current annual mass discharge (liquid water and steam) from the reservoir is approximately 47 million tonnes. The discharged fluid has an average apparent enthalpy of ~1049 joules per gram (J/g), corresponding to liquid water at a temperature of 242°C. Peak steam production was attained in 1964 when ~65 million tonnes of fluid were extracted from the reservoir to produce 173 MW of power. Although the hydrothermal system was unable to sustain the 1964 rate of production, Wairakei has proven to be a reliable source of electrical power for more than 30 years, and currently supplies approximately 5 percent (1170 GWh) of New Zealand's power requirement, energy worth about NZ$70 million per annum (1984 dollars).

Previous Work

The Wairakei geothermal field has been written about extensively. Many of the articles are unpublished reports, including drilling, production and maintenance data retained at Wairakei by the Ministry of Works and Development, Department of Industrial and Scientific Research and Ministry of Energy. An early description of the geology and thermal activity at Wairakei was presented by Grange (1937). Details of the geology, rock structure and hydrothermal alteration determined from Wairakei drilling data were described by Grindley (1959, 1965) and Steiner (1953, 1955, 1968, 1977). More recently Grindley (1982) discussed the results of deep drilling at Wairakei and Healy (1984) reinterpreted the volcanic stratigraphy and structural history of the Wairakei area.

Field geophysical surveys at Wairakei and in the surrounding areas collected data on residual Bouguer gravity (Robertson, 1951; Hunt, 1970, 1975, 1977), magnetic force (Baird, 1951; Studt, 1951; Cullington, 1954; Modriniak and Studt, 1959), electrical resistivity (Banwell and MacDonald, 1965; Hatherton et al., 1966; Risk et al., 1983), seismic refraction (Modriniak and Studt, 1959; Pritchett et al., 1976) and surface heat flow (Ellis and Wilson, 1955; Healy, 1956; Gregg, 1958; Banwell and Thompson, 1959; Benseman, 1959; Thompson et al., 1961; Fisher, 1964; Dawson and Fisher, 1964; Dawson and Dickinson, 1970; Glover, 1977; Allis, 1979, 1981; Allis and Webber, 1984). These surveys were supported by laboratory analyses of core samples which provided specific data on porosity, permeability and rock density (Banwell, 1955; Bolton, 1982; Robertson, 1984), rock magnetism (Studt, 1951) and seismic velocities (Modriniak and Studt, 1959; Pritchett et al., 1976).

The initial state of the reservoir and production-related changes were described by Grant and Horne (1980). Reservoir recharge was discussed by Hunt (1977) and Grant (1982) and factors controlling hydrology and thermal zoning within the Wairakei reservoir were discussed by Banwell

(1955), Grindley (1965), Bolton (1970), Allis (1982a) and Grant (1984). The physical characteristics and performance of exploration, production and monitor wells were described in detail by Bolton (1970) and Grant (1977, 1980). Numerical models of the reservoir including production-induced changes and the potential responses to reinjection of waste fluid were presented by Bolton (1970), Mercer et al. (1975), Pritchett et al. (1980) and Grant (1984).

Summaries of production data for Wairakei covering the years 1953 to 1976 and 1978 to 1984 were compiled by Pritchett et al. (1978, 1979) and the Ministry of Works and Development (1984) respectively. Henley et al. (1984) compiled chemical analyses and physical measurements determined for fluid samples collected from natural features and wells at Wairakei between 1950 and 1982. Additional data pertaining to the chemical composition and physical properties of the liquid and vapour phases discharged from the Wairakei reservoir were provided by Wilson (1955), Ellis and Wilson (1960), Mahon (1962, 1966), Ellis (1962, 1970), Mahon and Glover (1965), Glover (1970, 1971) and Steiner (1977). The isotopic composition and residency time of Wairakei fluids were discussed by Stewart (1978), Craig (1963) and Torgersen et al. (1982).

Historical details of the Wairakei project were summarized by Grange (1955), Fisher (1955), Grindley (1965) and the Ministry of Energy (1984).

REGIONAL GEOLOGY

Taupo Volcanic Zone

New Zealand straddles the boundary between the Indo-Australian and Pacific plates (Fig. 3.3). In the North Island, the major manifestation of this boundary is the Taupo Volcanic Zone (TVZ), a wedge-shaped volcano-tectonic depression interpreted as a volcanic front related to westward-directed subduction of the Pacific Plate (J. Gamble, personal communication). Cole (1984, 1989) considers the TVZ to be the southern extension

of the Kermedec-Tonga volcanic arc and separates the volcanic front into a dominantly andesitic volcanic arc (east) and an associated ensialic marginal basin (west).

The TVZ began forming about 2 Ma (Wilson et al., 1984). During the past 600 ka the central portion of the TVZ, which is an active graben-like structure (~125 km long, ~60 km wide and 1 to 4 km deep; Rogan, 1982; Wilson et al., 1984), has been the focal point of numerous, dominantly rhyolitic, pyroclastic eruptions related to regional extension and subsidence (Cole, 1979, 1986). The TVZ is still volcanically and structurally active. Wilson et al. (1984) estimate that >1.7 m^3 of magma intrude the crust below the central graben every second, and current rates of extension and subsidence are estimated to be ~7 millimetres per year (mm/yr) (Cole, 1986; Grapes et al., 1987) and ~3 mm/yr (Pullar, 1981) respectively. Considering the rate of basin expansion there is surprisingly little topographic relief within the central graben. This reflects the relative state of equilibrium existing between basin subsidence and eruption volumes (~0.27 m^3s^{-1}; Wilson et al., 1984) coupled with an erosion rate of ~1 mm/yr (Pullar, 1981).

Within the central graben, movement along near-surface faults is characteristically normal, but en echelon offsets in the axis of the TVZ and fault-plane solutions for major earthquakes document actively forming deep-seated transcurrent (transform) faults (Cole, 1986; Smith and Webb, 1986). Although poorly constrained, the transcurrent faults may be important in localizing the abundant, high-temperature geothermal systems by providing conduits for rising magma and deeply circulating meteoric water.

The TVZ hosts at least six major, non-resurgent caldera volcanoes (Fig. 3.2b), which are characterized by complex histories of multiple eruptions and associated caldera collapse (Wilson et al., 1984). Collectively, the volcanic complexes of the TVZ form a nested caldera system comparable in size to the major caldera systems of the western U.S.A., e.g.,

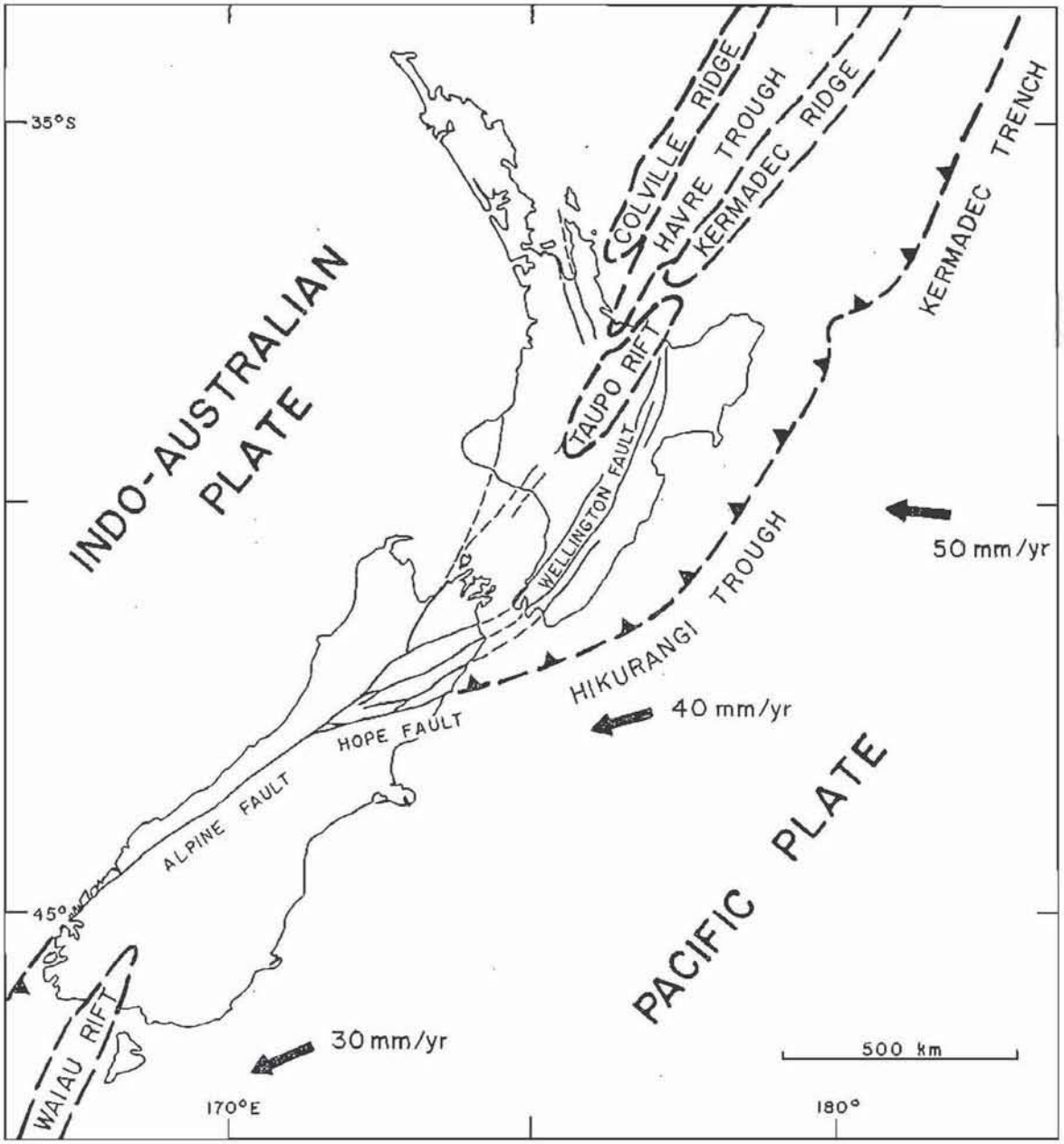

Figure 3.3. Principal tectonic components of the New Zealand segment of the Indo-Australian Plate and Pacific Plate boundary. Arrows indicate relative motion of the Pacific Plate. After Cole and Lewis (1981) and Cole (1986).

the Yellowstone (Christiansen, 1979) and San Juan (Smith and Bailey, 1968; Steven and Lipman, 1976) volcanic fields. Volcanic eruptions from the central TVZ differ from those overlying a stable craton in that the TVZ eruptions were less voluminous but more frequent than eruptions from similar size caldera volcanoes in the western U.S.A. (Smith, 1979; Wilson et al., 1984). This may reflect the inability of the young, highly faulted

crust of the TVZ to support large high-level magma chambers (Wilson et al., 1984). An important implication of this is that associated geothermal activity may be more common, but of shorter duration, than would be expected in areas of older, more stable basement.

Maroa and Taupo Caldera Volcanoes

Explosive volcanism and related sedimentation in the Wairakei area began prior to 330 ka, but the most extensive eruptions occurred between 330 and 230 ka and from 22.7 ka to the present (Wilson et al., 1984; P.R.L. Browne, personal communication). The 330 to 230 ka events produced the most voluminous ignimbrite deposits identified within the TVZ, and culminated in the formation of the Whakamaru caldera (Wilson et al., 1986). Between 230 ka and the present two satellite caldera volcanoes, Maroa and Taupo, formed along the northern and southwestern peripheries (respectively) of the Whakamaru caldera (Fig. 3.4). The major pyroclastic eruptions between 22.7 ka and the present were derived from the Taupo volcano and, in part, contributed to the formation of the Lake Taupo caldera (Wilson et al., 1984).

Maroa Caldera Volcano

The Maroa volcano was active from 230 to about 14 ka, with most of the eruptions occurring between 200 and 40 ka (Wilson et al., 1984). Volcanic activity began with a sequence of small to moderate volume, caldera-forming pyroclastic eruptions, but around 140 ka explosive activity gave way to relatively passive effusive eruptions which resulted in the emplacement of a series of simple to complex domes and voluminous lava flows (Wilson et al., 1986).

Physiographically, the Maroa volcano consists of a central dome complex ~15 kilometres in diameter and widely distributed peripheral domes which define an outer ring fracture system ~45 kilometres in diameter

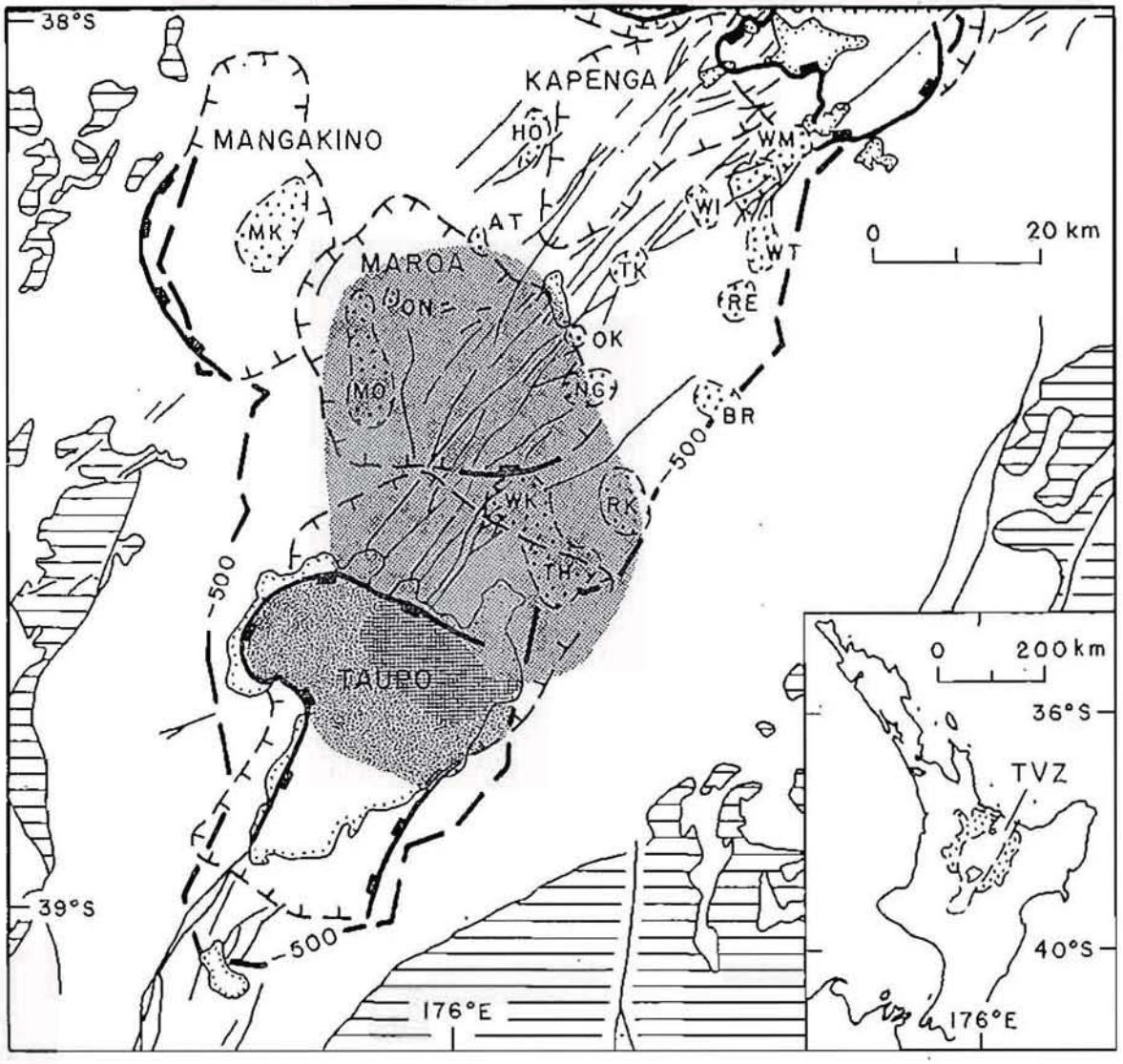

Figure 3.4. Approximate location of major calderas of the southern Taupo Volcanic Zone: (1) the Whakamaru caldera (stippled), (2) the inferred outlines of the Maroa and Taupo calderas (dashed lines with tick marks) and (3) Taupo calderas produced during the 22.7 ka (irregular pattern) and 1800a (cross hatched pattern) eruptions. For a description of the abbreviations see Figure 3.2. Data from New Zealand Geological Survey (1972), Wilson et al. (1984), Mongillo and Clelland (1984) and Wilson et al. (1986).

(Healy, 1962). The lava domes and associated flows overlie at least four locally derived ignimbrite sheets (Healy, 1962; Wilson et al., 1984). Together these features conceal a complex basement depression, 10 by 15 kilometres in area and extending to a depth of ~2.5 kilometres, which is interpreted as an infilled caldera (Rogan, 1982; Wilson et al., 1986).

The boundary of the Maroa volcano (Fig. 3.4) is poorly constrained and relies heavily on the interpretation of geophysical data which is

supported by the spatial distribution and abundance of rhyolite domes and active geothermal systems (Healy, 1962; Rogan, 1982; I.E.M. Smith, personal communication). The location of the southern boundary of the Maroa volcanic complex is particularly obscure because of the intricate spatial and temporal interfingering of volcanic domes derived from both the Maroa and Taupo caldera volcanoes (Wilson et. al., 1984).

Taupo Caldera Volcano

The following summary of the eruptive history of the Taupo volcano was extracted primarily from papers by Wilson et al. (1984) and Wilson et al. (1986). For a more detailed description the reader is referred to these works and those of Froggatt (1983) and Northey (1982).

Volcanic activity contributing to the formation of the Taupo caldera volcano was episodic with respect to both time and eruption style. The initial eruptions from Taupo occurred about 230 ka and produced at least 3 small to moderate volume unwelded rhyolitic ignimbrites (Wilson et al., 1986). Volcanic quiescence followed until c. 140 ka when small scale, relatively passive dome building began. Between 140 and about 50 ka several small rhyolitic domes were emplaced at the north end of Lake Taupo (Wilson et al., 1984), and at 30 ka successive dacite flows contributed to the formation of the Tauhara dome (Lewis, 1968; Stipp, 1968). Around 50 ka volcanic activity reverted to dominantly pyroclastic eruptions, and at least five explosive events preceded the major 20 ka eruption (Wilson et al., 1986). Approximately 10,000 years of relative volcanic quiescence followed the 20 ka event, but since 10 ka a minimum of nine pyroclastic events and two periods of dome building have occurred (Healy, 1964; Wilson et al., 1986). The most recent pyroclastic eruptions occurred at 3.44 ka and 186 A.D. (Wilson et al., 1984). The most spectacular feature of the Taupo volcanic complex is the central caldera, which is a well-defined

fault-bounded basin ~50 kilometres across and more than 4 kilometres deep (Wilson et al., 1984), now partly occupied by Lake Taupo.

Geothermal Activity

Major liquid-dominated geothermal systems are spatially and temporally associated with the caldera volcanoes of the TVZ, the eastern graben-bounding fault, and several of the northeast-trending intragraben faults (Fig. 3.2). Within the TVZ hydrothermal fluids migrate through the rock in response to abnormally high thermal gradients induced by crustal thinning and/or magmatic activity. In all known cases, magma chambers supporting convection are at least a few thousand metres below the surface, an idea supported by the minor amount of magmatically derived solutes present in the fluids. The high-temperature (T=~250°C) reservoirs of the major geothermal systems are commonly 3 to 5 kilometres in diameter and 400 metres or more below the land surface. These "near-surface" geothermal systems form as upwelling thermal plumes, which are guided by faults and/or formational contacts, and expand into large subhorizontal volcanic aquifers. Reservoir geometry is ultimately determined by local hydrologic conditions, principally permeability and hydraulic gradients.

Fluids collected from the deeper, higher temperature zones of several of the explored geothermal reservoirs in the TVZ are characteristically very dilute meteoric water with a near-neutral pH and containing low concentrations of carbon and sulphur. The results of detailed studies completed at many of the high-temperature geothermal systems in the TVZ have shown that these fluids are transporting and depositing many economically important elements, e.g., Au, Ag, Pt, Pd, Pb, Zn, As, Sb, and the rare earth elements (Henley and Ellis, 1983; Brown, 1986; Brown, 1988); also see Henley et al. (1986) and the section entitled Metallization in this chapter.

Wairakei Geothermal System

The northern boundary of the Wairakei geothermal system approximates the southern boundary of the Maroa caldera, but the majority of the hydrothermal system lies within the complex border zone between the Maroa and Taupo caldera volcanoes. Prior to production discharge at Wairakei, the geothermal system was characterized by a well-developed thermal column which widened out within ~1.5 kilometres of the surface. Fluid entered the high-temperature reservoir in the west-central and western portions of the field and migrated eastward forming a well-defined outflow zone (Elder, 1981; Grant, 1984). Massive production-related withdrawal of fluid from the high-temperature reservoir at Wairakei during the past 25 years has caused substantial changes in the thermal zoning pattern of both the Wairakei (Grant, 1984) and the Tauhara (Henley and Stewart, 1983) geothermal reservoirs.

Tauhara Geothermal System

The Tauhara geothermal system is located approximately 6 kilometres southeast of Wairakei and is associated with the northern margin of the Taupo volcanic complex. Although Wairakei and Tauhara have independent high temperature upflow zones, resistivity data (Risk et al., 1983) and fluid chemistry data (Henley et al., 1984) provide evidence that the high-temperature reservoirs of the two systems are interconnected to form a large "dumbbell-shaped" composite hydrothermal system (Fig. 3.4). Since significant quantities of high temperature fluid were not extracted from the Tauhara reservoir prior to commercial production from Wairakei, it is unlikely that fluid migration within the Tauhara reservoir affected the preproduction thermal zoning pattern within the high-temperature reservoir at Wairakei.

WAIRAKEI GEOTHERMAL AREA

Volcanic Stratigraphy

The Wairakei stratigraphy consists of a relatively flat-lying sequence of interbedded Pleistocene to Holocene felsic pyroclastic and lacustrine volcaniclastic rocks intercalated with rhyolite and andesite lava. The petrology and petrographic characteristics of individual units were described in detail by Grindley (1965; 1982) and Steiner (1977). The results of these investigations and of petrologic observations made during the course of this study are summarized in Table 3.1. A series of three cross sections are included with this chapter (Figure 3.5; Plate 6). The cross sections were drawn from information contained in geologic well logs constructed by Healy (unpublished data), Grindley (1965; 1982) and Steiner (1977), following the stratigraphic and structural interpretation of Healy (1984). Many of the important contacts, in particular where discrepancies between previous interpretations are significant, and drill holes 48 and 54 were relogged in detail, but in general the data used to construct the cross sections are equivalent to those presented in the above mentioned works. The geologic cross sections accompanying this chapter are important because they provide the geological control required for an internally consistent interpretation of preproduction zoning patterns for both reservoir temperatures and hydrothermal alteration.

Pre-Tertiary Basement

Pre-Tertiary basement was not intersected by any of the wells drilled at Wairakei; well 121 was drilled to a depth of 2.240 kilometres. Ellis (1969) believed that the Wairakei volcanic succession overlay clastic rocks of the Mesozoic Torlesse Supergroup and estimated that the volcanic pile was ~3.7 kilometres thick. Applying more sophisticated geophysical models to a much larger data base, Stern (1985) predicted that a thick sequence

Table 3.1. Summary of the stratigraphy of the Wairakei geothermal area.

FORMATION (AGE)	MEMBERS	LITHOLOGY	ESTIMATED THICKNESS (m)		WELL	REFERENCES
WAIRAKEI FORMATION (Wr) (post early Hawera)	Taupo Pumice	Ash fall deposits and subsequent alluvium consisting of pumice ash and lapilli.	30-300	0-100	3	G65, S77 H84
	Wairakei Breccia	Two similar units consisting of an upper zone of vitric tuff breccia and a basal zone of locally diatomaceous vitric tuff (locally containing accretionary lapilli horizons) and underlying tuffaceous sandstone. The upper vitric tuff contains pumice and rhyolite lapilli, broken crystals of andesine, oligoclase, quartz, hypersthene, hornblende, and accessory magnetite; lacustrine deposits. The pyroclastic units are locally overlain by interbedded mudstone and siltstone which does not contain diatoms or sponge spicules.		0-165	6	
HUKA FALLS FORMATION (Hu) (late Castlecliffian to early Hawera)	Member 4	Tuffaceous sandstone containing rhyolite and pumice lapilli, abundant quartz grains and thin mudstone bands; lacustrine deposits.	50-300+	<40	225	G65, S77 H84
	Member 3	Locally diatomaceous mudstone with thin carbonaceous layers interbedded with siltstone, sandstone and diatomite. Clastic units contain abundant pumice glass, minor diagenetic pyrite and rare sponge spicules; lacustrine deposits.		<155	225	
	Member 2	Siltstone, mudstone and tuffaceous sandstone, interbedded with pumice breccia, silty and sandy pumiceous tuff, vitric tuff and a diatom-bearing basalt tuff. Vitric tuffs contain detrital oligoclase, andesine, hypersthene, hornblende and magnetite, and minor sponge spicules; lacustrine deposits.		<215	2A	
	Hydrothermal Breccia	Hydrothermal eruption breccia composed of hydrothermally altered angular to subrounded fragments of pumice breccia, sandstone, siltstone, rhyolite and quartz-bearing ignimbrite randomly mixed with angular to subrounded clasts of unaltered sandstone, siltstone, mudstone, and pumice breccia, and set in a matrix of unaltered pumiceous silt- and sand-sized debris including crystals of andesine and quartz. Hydrothermal breccias are locally intercalated with siltstone and pumiceous sandstone; subaerial deposits except where locally reworked.		0-205	215	
	Member 1	Well-bedded lacustrine mudstone with thin siltstone and sandstone bands. Mudstones are finely stratified and contain minor carbonaceous material, very fine organic-derived pyrite and rare diatoms.		<200	225	

Table 3.1. Summary of the stratigraphy of the Wairakei geothermal area (Continued)

FORMATION (AGE)	MEMBERS		LITHOLOGY	ESTIMATED THICKNESS (m)		WELL	REFERENCES
WAIORA FORMATION (Wa) (Castlecliffian ?)	Member 5		Quartz-bearing pumiceous ignimbrite, pumice-breccia and vitric tuff (locally contain-accretionary lapilli horizons) interbedded with silty water-laid tuff, and minor mud-stone. Quartz, andesine and rare hypersthene and hornblende phenocrysts, and access-ory magnetite occur in the pumiceous ignimbrite, but are rare or absent in the tuffs and breccias. Variable amounts of subangular to subrounded pumice and xenoliths of rhyolite and rare granite and dolerite occur in most of the pyroclastic units. The rocks are subaerial and lacustrine in origin.	400-1075+	0-180	215	G65, H84, S77
	Haparangi Rhyolite	Te Mihi Rhyolite (Tm)	Typically quartz-bearing rhyolite dykes, flows and domes containing phenocrysts of andesine, quartz, hornblende, hypersthene, rare biotite and accessory magnetite in a cryptocrystalline, hyalopilitic or glassy spherulitic groundmass; flows are locally pumiceous, and generally lack flow-banding.		0-250+	208	
		Karapiti Rhyolite (Kp)	Generally quartz-free, flow-banded rhyolite lava containing phenocrysts of andesine to oligoclase, hornblende, hypersthene, rare biotite and quartz, and accessory magnetite in a perlitic, hyalopilitic, spherulitic or cryptocrystalline groundmass. Flows commonly grade inward from pumiceous tops and margins through perlitic and/or spherulitic zones into cores of cryptocrystalline, flow-banded rhyolite.		0-520	208	
		Haparangi Rhyolite (Ha)	Generally quartz-free rhyolite flows containing phenocrysts of fractured andesine, minor hypersthene and hornblende, rare biotite and quartz, and accessory magnetite in a cryptocrystalline, hyalopilitic or glassy spherulitic groundmass; ferromagnesian minerals may be absent. Flow may be pumiceous, perlitic, spherulitic or flow-banded; multiple textures are common.		0-170	212?	
	Member 4		Subaerial to subaqueous, massive pumice and rhyolite breccias, vitric tuff (locally containing accretionary lapilli horizons) and tuffaceous sandstone interbedded with minor lacustrine siltstone. Pyroclastic units contain varying amounts of angular to rounded pumice, minor andesine and rare hypersthene, hornblende and quartz pheno-crysts, common accessory magnetite, and xenoliths of rhyolite and rare granite and dolerite.		0-495	221	
	Member 3		Massive pumice breccia, tuffaceous sandstone and rhyolitic breccias interbedded with minor siltstone, ignimbrite and rare vitric tuff (locally containing accretion-ary lapilli horizons). Breccia beds contain pumice, quartz and plagioclase crystals and minor rhyolite clasts; quartz is rare in the upper portion of the unit. Rocks are of subaerial and lacustrine origin.		40-275+	226	

Table 3.1. Summary of the stratigraphy of the Wairakei geothermal area (Continued)

FORMATION (AGE)	MEMBERS	LITHOLOGY	ESTIMATED THICKNESS (m)		WELL	REFERENCES
WAIORA FORMATION (Wa) (Castlecliffian ?)	Waiora Valley Andesite (Wv)	Flow-banded, quartz-free andesite with abundant phenocrysts of andesine and relatively smaller ferromagnesian minerals set in a hyalopilitic to cryptocrystalline groundmass containing disseminated magnetite.	400-1075+	0-200	48	G65, S77 H84
	Member 2	Well-sorted silty and sandy water-laid tuff, tuffaceous sandstone and siltstone, well-bedded sandstone, siltstone and mudstone consisting of pumice, perlitic rhyolite, and plagioclase with variable amounts of quartz, ferromagnesian minerals, magnetite, glass shards and clay interbedded with pumice breccia. Rare lithic fragments include andesite, basalt, microdolerite and granite; lacustrine deposits.		0-150+	207	
	Member 1	Quartz-bearing pumiceous ignimbrites containing minor andesine, hypersthene, and hornblende phenocrysts and accessory magnetite in a vitroclastic groundmass; xenoliths include rhyolite, granite, microdolerite, andesite and Wairakei Ignimbrite.		0-275+	37	
WAIRAKEI IGNIMBRITE (Wk) (Upper Nukumaruan ?)	Member 3	Moderately welded, crystal-rich rhyolitic ignimbrite with abundant, commonly broken phenocrysts of andesine and strongly embayed quartz, and minor hornblende and hypersthene in a vitroclastic groundmass. Inclusions of basalt, microdolerite, granoblastic quartz and glassy rhyolite occur in each member. Distinction between members is based on the abundance of biotite which is rare in Member 1, common in Member 2, and absent in Member 3, the presence of a basal glassy unit to Member 2, and the presence of pumiceous sediments between Members 2 and 3.	255-1020	<300	121	B76, E65, F83, G59, G65, G82, H84, K73, M61, S77
	Member 2			<380		
	Member 1			<340		
OHAKURI GROUP (Oh) (Nukumaruan ?)		Interbedded pumiceous tuff breccia, thin-bedded sandy water-laid tuff, and tuffaceous siltstone and sandstone intercalated with andesitic lava and associated breccia. Clastic rocks contain small, subangular pumice and rhyolite and rounded graywacke (rare) fragments; lacustrine deposits.	200-575+	>575	121	G59, G65 H84, M61, S77

Note: Thicknesses estimated from cross sections drawn from well logs published by Grindley (1965), structure contour maps published by Healy (1964) and author's unpublished data. The well in which the maximum unit thickness was intersected is indicated under the heading WELL. References: Briggs (1976), B76; Ewart (1965), E65; Froggatt (1983), F83; Grindley (1959), G59: Grindley (1965), G65; Grindley (1982), G82; Healy (1984), H84; Kohn (1973), K73; Martin (1961), M61; Steiner (1977), S77.

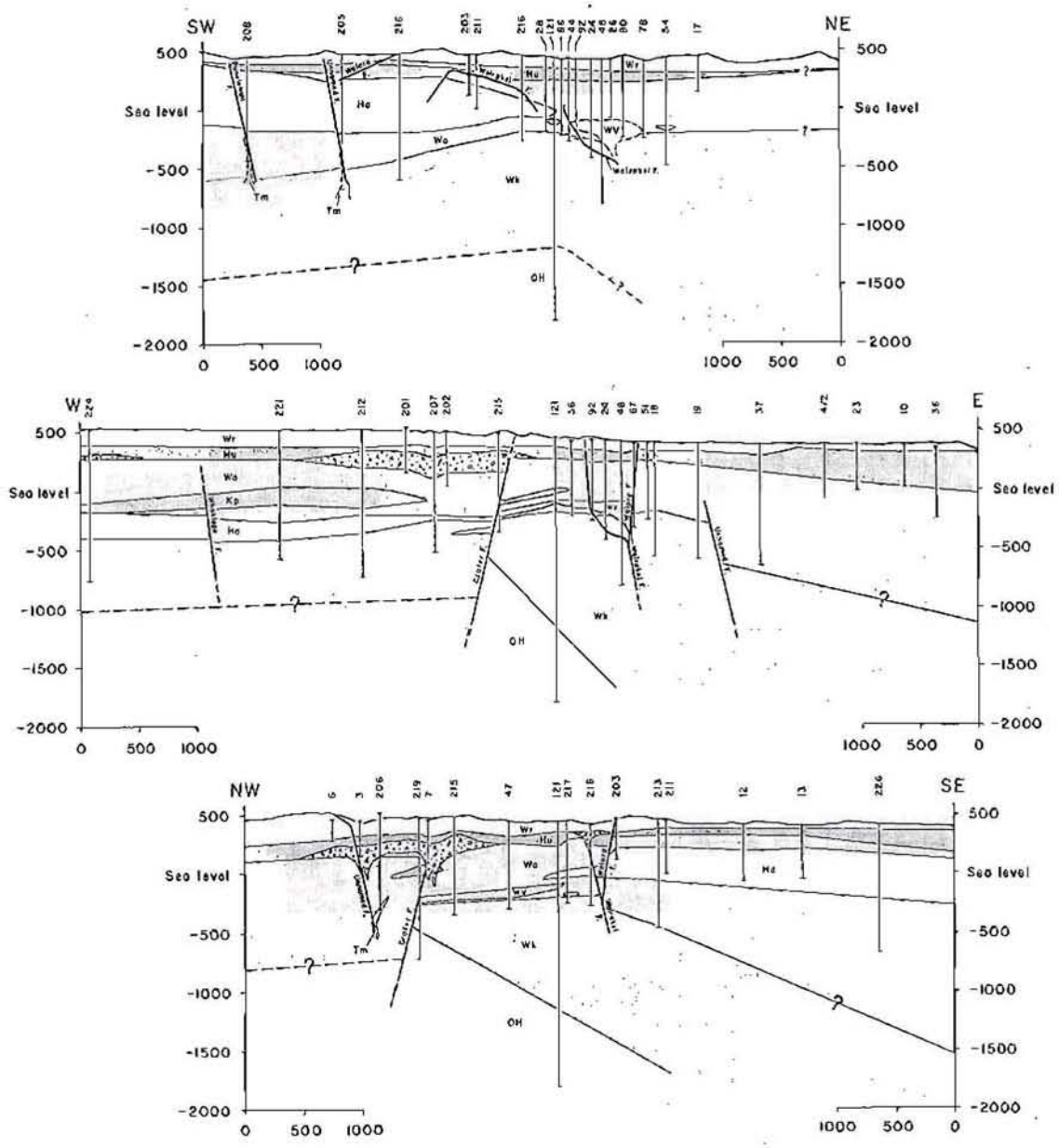

Figure 3.5. Wairakei geologic cross sections. Rock units are: Ohakuri Group (Oh, not coloured), Wairakei Ignimbrite (Wk, grey), Waiora Formation (Wa, lavender), Waiora Valley Andesite (Wv, green), Haparangi Rhyolite (Ha, orange), Karapiti Rhyolite (Kp, rose), Te Mihi Rhyolite (Tm, wine), Huka Falls Formation (Hu, brown) and Wairakei Formation (Wr, yellow). Pattern indicates the distribution of hydrothermal eruption breccias (Huka Falls Formation). Well number shown above the respective well. See Figure 3.6 for the locations of the cross sections, and Table 3.1 and Plate 6 for additional detail.

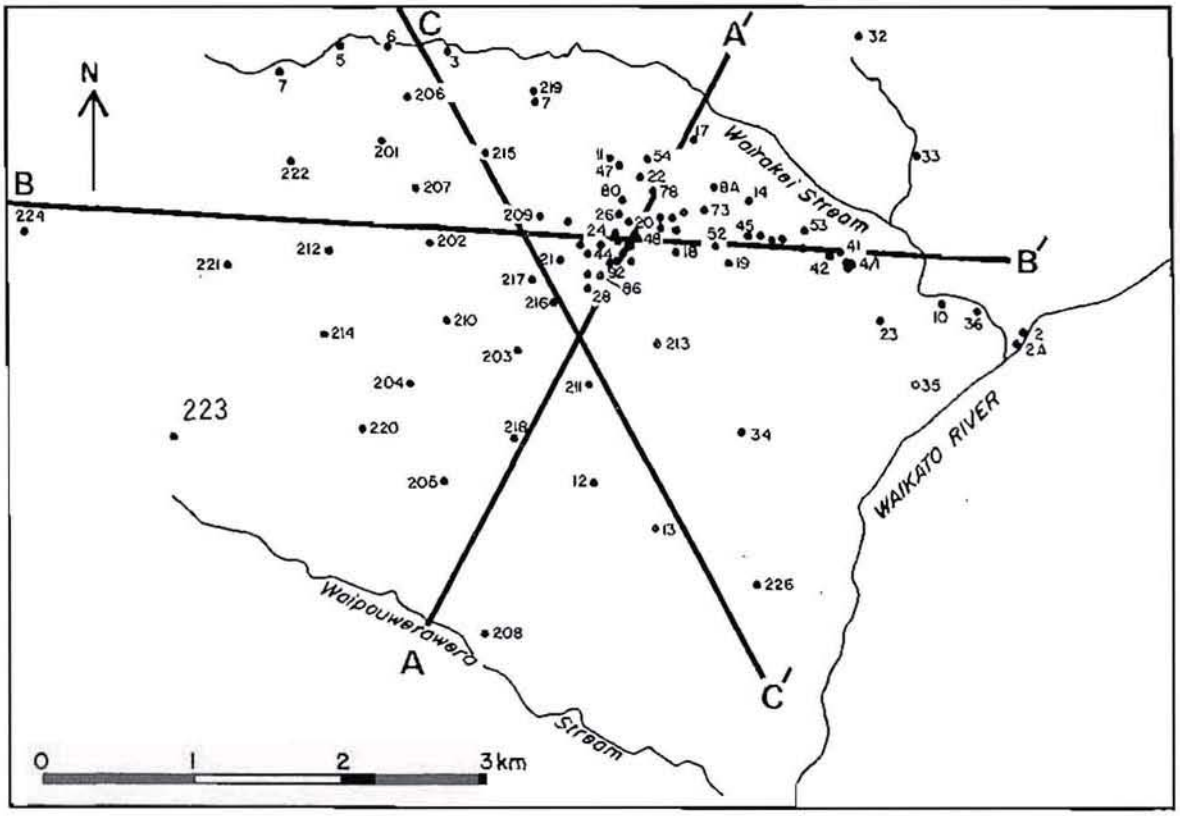

Figure 3.6. Map showing the location of the geologic cross sections for Wairakei relative to selected geothermal wells.

of andesitic lavas and related pyroclastic rocks separated the overlying rhyolitic pyroclastic sequence (Ohakuri Group through the Wairakei Breccia) from pre-Tertiary basement and cautioned that basement rocks may not be metaclastic rocks of the Torlesse Supergroup. Stern's hypothesis is supported by the presence of thick andesite lavas in the Ohakuri Group (well 121 bottomed in andesite) and by deep (~2.70 km) drilling within the Rotokawa geothermal area (Fig. 3.4) where more than 600 metres of andesite was penetrated beneath ~2.0 kilometres of rhyolitic ignimbrite and related lacustrine volcaniclastic rocks (P.R.L. Browne, personal communication).

Ohakuri Group

The oldest stratigraphic unit identified by drilling at Wairakei consists of more than 640 metres of interbedded pumiceous pyroclastic and tuffaceous sedimentary rocks intercalated with thick andesite lava flows

(Grindley, 1965; 1982). Considering the thickness of the unit and the presence of well bedded sandy tuff and tuffaceous siltstone and sandstone, it is likely that the unit accumulated in a continually subsiding volcano-tectonic basin, which at least intermittently contained water. Because only two drill holes (121 and 219) penetrated Ohakuri Group rocks their spatial distribution is unknown, and evidence for their structural orientation is sparse. However, bedding plane dips (30° to 35°) measured in core samples of the sedimentary units (Grindley, 1965) are similar to the dip of the Ohakuri Group-Wairakei Ignimbrite contact determined from drill hole intercepts. From this information and the relative locations of the wells it is assumed that the Ohakuri Group rocks dip ~35° to the southeast.

The origin of the Ohakuri Group ignimbrite and volcaniclastic deposits is poorly understood. Grindley (1965) correlated the pumiceous ignimbrites and interbedded volcaniclastic rocks underlying the Wairakei Ignimbrite at Wairakei with the pumice breccias and associated volcaniclastic rocks exposed at Ohakuri, the type section for the Ohakuri Group. Based on data obtained during outcrop studies of the Ohakuri Group north of Wairakei, Wilson et al. (1986) concluded (1) that the pyroclastic units were most likely extruded during the caldera-forming eruptions of the Maroa volcano and (2) that explosive activity associated with the formation of the Maroa caldera only produced small to moderate volume ignimbrites. Thus, the substantial thickness of the Ohakuri Group sequence within the Wairakei area probably reflects ponding of the erupted material in a relatively restricted basin, possibly the newly formed Maroa caldera.

Wairakei Ignimbrite

The Wairakei Ignimbrite consists of at least three moderately welded crystal-rich ash-flow tuffs with a composite thickness exceeding 960 metres (Fig. 3.5, well 121). Grindley (1965, 1982) separated the Wairakei Ignimbrite into three members based on mineralogy and rock texture. The key to

the identification of these members is the occurrence of andesite inclusions and magmatic biotite in only the middle member (Grindley, personal communication). Additionally, Members 1 and 2 are separated by interbedded volcaniclastic rocks. Member 3 is the thickest and spatially most extensive of the three ignimbrite sheets (Grindley, 1982).

The Wairakei Ignimbrite is one of several moderately welded ash-flow tuff deposits which were deposited during the initial eruptive phase (330 to 230 ka) of the Taupo volcano (Wilson et al., 1986). Because of its stratigraphic position and mineralogical and textural similarities to several major ash-flow tuffs also considered to be related to the early eruptive phase of the Whakamaru volcano, the Wairakei Ignimbrite was tentatively correlated with the Whakamaru and Manunui ignimbrites and with the Te Whaiti and Rangitaiki ignimbrites which crop out to the west and east of Wairakei respectively (Martin, 1961; Healy, 1964; Grindley, 1965; Wilson et al., 1984). Collectively these five ignimbrites and related volcaniclastic rocks are referred to as the Whakamaru Group, and are thought to be related to the collapse of the Whakamaru caldera (Wilson, 1986).

The nature of the contact between the Ohakuri Group and the Wairakei Ignimbrite is crucial to the interpretation of the structural history of the Wairakei region. Healy (1984) believes that the Wairakei Ignimbrite was deposited as a series of horizontal sheets which conformably overlie the Ohakuri Group, whereas Grindley (personal communication) considers the contact between the two units to be an unconformity. Grindley based his conclusion on the orientation of Member 2 (Wairakei Ignimbrite) within the Wairakei geothermal area. Geologic cross sections constructed from drilling data confirm that Member 2, and consequently the Wairakei Ignimbrite, is relatively flat-lying. Since the Ohakuri Group dips at ~35°, Grindley concluded that its contact with the Wairakei Ignimbrite must be an unconformity.

Waiora Formation

The Waiora Formation consists of interbedded pyroclastic and lacustrine sedimentary rocks intercalated with dacite to rhyolite and minor andesite lava flows and domes(?). The formation is subdivided into five members (Table 3.1) which record a history of explosive volcanism followed by volcanic quiescence and erosion. Most of the pyroclastic deposits are nonwelded, locally massive pumiceous tuffs and breccias generally containing phenocrysts of andesine and quartz in a vitroclastic groundmass. Additional phenocryst phases which are locally present include oligoclase, hypersthene, hornblende, biotite and accessory magnetite (Grindley, 1965; Steiner, 1977). Vitric and accretionary lapilli (chalazoidite) tuffs and perlitic rhyolite are also common constituents of the Waiora Formation. Lacustrine sedimentary rocks, including sandy to silty water-laid tuff, tuffaceous sandstone, siltstone and mudstone, are locally interbedded with the pyroclastic units.

Member 1

Member 1 consists of two quartz-bearing ignimbrites which grade from a basal lenticular ignimbrite into an upper pumiceous tuff (Grindley, 1965). The ignimbrites contain minor phenocrysts of andesine, hypersthene and hornblende which, along with accessory magnetite, are suspended in a vitroclastic groundmass (Steiner, 1977). Mineralogically the ignimbrites are indistinguishable and contain common xenoliths of rhyolite, andesite and basalt, however, rare xenoliths of granite, microdolerite and Wairakei Ignimbrite are found only in the lenticular ignimbrite (Steiner, 1977). The ignimbrites are locally separated by a sequence of silty and sandy tuffs which Steiner (1977) considered to be water-laid tuffs deposited during an erosional period between eruptions. But because the contact between the two ignimbrites is gradational where the tuffs are missing, the sandy tuffs may be an intra-event base surge deposit. Pumice is more

abundant in the upper portion of the unit, and to the east and southeast a thick (>300 m) sequence of pumice breccias occurs beneath Member 2 of the Waiora Formation (Plate 6). Grindley (1965) considers these pumice breccias to be the stratigraphic equivalent of Member 1, and in part aggradational deposits.

Member 1 forms a thin layer covering the Wairakei Ignimbrite in the centre of the reservoir and thickens relatively abruptly to the east of the Unnamed fault and to the west of the Crater fault. The maximum thickness of Member 1 is not known. Drill holes in the eastern and western areas have not penetrated the base of the unit. The maximum drilled thickness of Member 1 is ~170 metres in the west and ~290 metres in the east.

Member 2

The lacustrine clastic and volcaniclastic rocks of Member 2 were deposited during a period of erosion and reduced volcanic activity. The rocks consist of generally well-sorted and locally well-bedded silty and sandy water-laid tuff, tuffaceous sandstone and siltstone, sandstone, siltstone, and mudstone interbedded with pumice breccia. The rocks contain detrital grains of plagioclase and variable amounts of quartz, strongly altered ferromagnesian minerals, magnetite and glass shards (Steiner, 1977). There are two main pumice breccia interbeds which contain clasts of a wide range of lithologies. The lower pumice breccia contains clasts of andesite, basalt, microdolerite, granophyric granite and greywacke, whereas the upper breccia contains predominantly perlitic rhyolite fragments (Grindley, 1965; Steiner, 1977).

The distribution of Member 2 is similar to that of Member 1 in that the unit thins in the central portion of the reservoir and thickens to the east and west. In the western portion of the reservoir Member 2 is thickest near the Crater fault and thins westward (Plate 6). The unit is the thinnest in the north and northeast parts of the reservoir and thickest in

the southern half of the reservoir. In the central portion of the reservoir the unit was deeply eroded prior to extrusion of the Waiora Valley Andesite. The maximum thickness of Member 2 is not known because none of the drill holes in the southern peripheral portion of the reservoir, where the unit is thickest, penetrated the clastic sequence. The maximum drilled thickness is ~130 metres.

Waiora Valley Andesite

Extrusion of the Waiora Valley Andesite occurred during a period of subdued volcanic activity and sedimentation prior to deposition of Member 3. The Waiora Valley Andesite is composed of at least two locally flow-banded, andesite lavas which were probably erupted from a vent near the centre (well 48) of the reservoir (Grindley, 1965; Healy, 1984). Andesite breccias, possibly aa-lava flows, are locally intercalated with pumiceous volcaniclastic rocks (Grindley, 1965). In thin section the andesite is quartz-free, but contains abundant phenocrysts of andesine and small phenocrysts to microphenocrysts of ferromagnesian minerals set in a hyalopilitic to cryptocrystalline groundmass containing disseminated magnetite (Steiner, 1977).

Eruption of the Waiora Valley Andesite apparently was localized by the Wairakei and Waiora fault systems. The thickest section of andesite (~180 m) occurs in well 48. This thick section of andesite is thought to be the result of ponding, possibly in an eruption-related crater (Healy, 1984). The spatial distribution of the Waiora Valley Andesite shown on the E-W cross section in Plate 6 supports this theory, but the enhanced thickness also could be related to the formation of a small cone at the vent site. Once erupted, the andesite lava flowed to the west and northwest. The small occurrence of andesite underlying Member 2 near well 48 (Plate 6) is probably an intrusive phase (dyke) of the Waiora Valley Andesite flow.

Member 3

Member 3 of the Waiora Formation consists of massive pumice breccia, tuffaceous sandstone and rhyolitic breccias interbedded with minor siltstone, ignimbrite and rare accretionary lapilli tuff (Grindley, 1965). The basal contact of Member 3 typically grades downward into Member 2, but locally the unit rests directly upon the Waiora Valley Andesite. The upper contact of Member 3 coincides with the base of a distinctive grey siltstone bed (Grindley, 1965).

Member 3 is present throughout the reservoir forming a continuous horizon except where downdropped along the Crater fault. The unit appears to be a planar sheet of relatively uniform thickness in the north and northeast portions of the reservoir. Member 3 thins over the central high where it was eroded, and dips gently into the basins lying to the northwest, southwest and east. The maximum drilled thickness of Member 3 is ~290 metres in the eastern portion of the reservoir.

Member 4

Member 4 is a complex unit containing massive pumice and rhyolite breccias, vitric tuff (containing accretionary lapilli) and tuffaceous sandstone interbedded with locally thick (~20 m) lacustrine siltstone and intercalated with massive composite rhyolite lavas. The pyroclastic rocks contain rounded pumice, a few phenocrysts of andesine and less commonly hypersthene and hornblende and accessory magnetite supported by a vitroclastic groundmass. All of the rocks contain varying amounts of angular to rounded pumice and xenoliths of rhyolite, and some contain granite and dolerite. The paucity of phenocrysts and the vitroclastic texture are characteristic of Member 4 (Grindley, 1965; Steiner, 1977).

The massive lava flows of the Haparangi Rhyolites reach their maximum drilled thickness of ~500 metres in the southern part of the reservoir. The lava flows are absent in the eastern and northern parts of the reser-

voir and split into two major flows in the western part of the reservoir (see Plate 6). Healy (1984) attributes the thickness of the rhyolite lavas to ponding in a small basin, but this is not obvious from the spatial distribution of the lava flows and surrounding units on the cross sections (Fig. 3.5). It does appear that the Haparangi Rhyolite was in part channelized by one or more small basins. The thickest section (~650 m) of Member 4 was intersected by well 221.

Member 4 (Haparangi Rhyolite)

The Haparangi Rhyolite is subdivided into the Karapiti, Haparangi and Te Mihi Rhyolites (Table 3.1), all three of which appear to be time equivalent to Member 4 of the Waiora Formation (Fig. 3.5). The spatial distribution of the Haparangi Rhyolite is poorly constrained, particularly in the western portion of the reservoir, because of the compositional and textural variability (both horizontally and vertically) of the units. The problem is enhanced by the shortage of samples resulting from wide-spaced drilling and limited coring in the deeper and more recent drill holes.

Major correlation problems also exist because different authors have used somewhat different criteria when defining the units, and have placed different emphases on unit characteristics. Steiner (1977) relied solely on the presence or absence of quartz to differentiate the rhyolite bodies regardless of their stratigraphic position. Grindley (1965) and Steiner (1977) disagreed on the mode of emplacement of the major Haparangi Rhyolite bodies and gave different names to the same units. Grindley (1965) named the largest body of rhyolite the Karapiti Rhyolite, while referring to the other rhyolite bodies as Haparangi Rhyolite. Steiner (1977) subdivided the Haparangi Rhyolite on the basis of mineralogy into two Karapiti Rhyolite (quartz-free) bodies and four Te Mihi Rhyolite (quartz-bearing) bodies.

Grindley (1965) considered all of the rhyolites to be intrusive, whereas Steiner (1977) considered the upper Karapiti Rhyolite to be a lava

flow and the lower Karapiti Rhyolite and the four Te Mihi Rhyolite bodies to be intrusive. It is apparent from structure contour maps constructed for several of the Haparangi Rhyolite bodies (Healy, 1984) that the main Karapiti and Haparangi Rhyolites are extrusive, but that the Te Mihi Rhyolite bodies are most likely intrusive (dykes?). Because of the thickness, areal extent and compositional and textural variability of the Haparangi and Karapiti Rhyolites it is likely that they are composite lava flows and/or domes.

If the rhyolites are considered to be primarily lava flows, and drill hole intercepts are connected disregarding minor compositional variations, then the main mass of Haparangi Rhyolite is older than the Karapiti Rhyolite (see Figure 3.5)[3]. Age relationships cannot be determined conclusively from drill core and cuttings for the Te Mihi Rhyolite. Because of the generally isolated nature of these "quartz-bearing" rhyolites and their common association with major fault zones, the Te Mihi Rhyolites are most likely dyke-like bodies, and are arbitrarily shown to be younger than the overlying "quartz-free" rhyolite lavas.

Karapiti Rhyolite

The following petrographic and textural description of the Karapiti Rhyolite was compiled from Grindley (1965) and Steiner (1977). The Karapiti Rhyolite is generally quartz-free, flow-banded rhyolite lava containing phenocrysts of andesine to oligoclase, hornblende, hypersthene, rare biotite and quartz, and accessory magnetite in a perlitic, hyalopilitic, spherulitic or cryptocrystalline groundmass. Flows commonly grade inward

[3]The morphology of the Karapiti and Haparangi Rhyolite bodies shown in the cross sections (Fig. 3.5; Plate 6) reflects my belief that stratigraphic relationships are at least as important as textural and minor mineralogical variations when correlating thick, composite lavas between drill holes.

from pumiceous tops and margins through perlitic and/or spherulitic zones into cores of cryptocrystalline, flow-banded rhyolite.

Haparangi Rhyolite

The following petrographic description was compiled from Grindley (1965) and Steiner (1977). The Haparangi Rhyolite consists of generally quartz-free rhyolite flows containing phenocrysts of fractured andesine, minor hypersthene and hornblende, rare biotite and quartz, and accessory magnetite in a cryptocrystalline, hyalopilitic or glassy spherulitic groundmass; ferromagnesian minerals may be absent. Multiple rock textures are characteristic of the Haparangi Rhyolite and probably reflect the existence of individual lava flows within the unit. A consistent sequence of rock textures was not apparent from the drill core and cuttings which I logged. However, it was possible to trace several "textural" horizons through multiple drill holes. The most common rock textures are spherulitic, flow-banded, massive, vesicular, perlitic and pumiceous.

The cross sections presented in Figure 3.5 and Plate 6 show the Haparangi Rhyolite to be thickest in the southern part of the reservoir and to thin relatively abruptly near the centre of the reservoir. Considering the cross sections it appears that the lava entered the Wairakei area from the southwest. Part of the flow fanned out toward the east, but the main mass flowed northward into a shallow (western) basin. The rhyolite lava filled the western basin and then flowed eastward into the central part of the Wairakei area. This is essentially the hypothesis of Healy (1984) except that Healy believes that the western depression was a relatively deep fault-bounded basin within which the lava flow ponded, and considers the thin eastern extension of the flow to have originated from vents along the fractured margin of the basin.

Gravity (Gerard and Lawrie, 1955) and aeromagnetic (Beck and Robertson, 1955) data indicate that the most likely source for the

Haparangi Rhyolite is a major vent system (Tukairangi Volcanic Complex (Healy, 1984)) along the northern flank of the Taupo caldera.

Te Mihi Rhyolite

The name Te Mihi was given to several thin quartz-bearing rhyolite dykes and/or thin lava flows by Steiner (1977). The Te Mihi Rhyolite contains phenocrysts of andesine, quartz, hornblende, hypersthene, rare biotite and accessory magnetite suspended in a cryptocrystalline, hyalopilitic or glassy spherulitic groundmass (Steiner, 1977). Three of these bodies are shown on the cross sections (Fig. 3.5). There is insufficient drilling to determine the morphology of any of these units, although the two occurrences of Te Mihi Rhyolite in wells 205 and 208 may indicate the presence of a thin lava flow rather than dykes. Because of the spatial association of the Te Mihi Rhyolite with major faults it seems more likely that these rhyolites are dykes.

Member 5

Member 5 is the youngest member of the Waiora Formation. Steiner (1977) separated Member 5 into four units: (1) fine-grained vitric tuff with accretionary lapilli beds grading upward into tuff breccia (oldest), (2) vitric tuff locally grading into pumice breccia, (3) matrix-poor pumice breccia interbedded with silty and sandy water-laid tuffs and (4) pumiceous ignimbrite (youngest). Most of the volcanic rocks contain andesine phenocrysts, accessory magnetite and rhyolite xenoliths set in a vitroclastic groundmass. Minor to trace amounts of quartz, hypersthene and hornblende and rare xenoliths of granite and dolerite may be present. The volcaniclastic units generally contain fragments of pumice and rhyolite set in a matrix consisting of fine pumice, volcanic glass, andesine and quartz.

Member 5 attains its maximum thickness (~180 m) in the west-central portion of the Wairakei area and, with the possible exception of the north-

west area, thins rapidly outward in all directions. Member 5 was eroded from several topographic highs and redeposited in lowlying areas prior to deposition of the Huka Falls Formation.. One of these areas occurs in the vicinity of well 212 (Fig. 3.5) where Member 5 was completely eroded and the detritus was redeposited in a small tectonic "basin" lying to the east between the well and the Crater fault.

Huka Falls Formation

Members 1-4

The Huka Falls Formation consists of four members (1-4) which define a locally thick (≤300 m) sequence of tuffaceous siltstone and sandstone interbedded with siltstone, mudstone, diatomaceous mudstone and rhyolite tuff which was deposited in a shallow glacial lake (Grindley, 1965). Argillaceous rocks are most abundant in the northern and eastern parts of the Wairakei area and water-laid silty to sandy tuffs predominate in the southern and western areas (Steiner, 1977). Diatomaceous units are common in the eastern half of the area, but are absent in the west (Healy, 1984). In the western portion of the Wairakei area conglomerate-like beds are locally interbedded with the volcaniclastic rocks of the Huka Falls Formation. Grindley (1965) and Steiner (1977) recognized these units and, because they contained sub-rounded clasts, they referred to them as conglomerates. However, after considering the composition and spatial distribution of the "conglomerate" beds, Healy (1984) thought that they were most likely hydrothermal eruption deposits and as such should be referred to as breccias.

Western Breccias

Several breccia beds containing sub-rounded to angular clasts occur in Member 1 of the Huka Falls Formation. The breccias are locally inter-

bedded with mudstone, tuffaceous siltstone and sandstone, and pumice breccias. The rocks are composed of hydrothermally altered fragments of pumice, sandstone, siltstone, mudstone, tuff, rhyolite and quartz-bearing ignimbrite randomly mixed with angular clasts of unaltered sandstone, siltstone and pumice and supported by a matrix of unaltered silt- and sand-sized grains which include pumice and crystals of andesine and quartz. In general, the matrix of the breccias is only altered in the vicinity of faults which tap the high-temperature reservoir.

The thickest and most extensive breccias developed in the western part of the reservoir, where their localization appears to be controlled by the western Unnamed fault and the Crater fault. Fault control is also indicated by a small breccia whose location coincides with the trace of the Wairakei fault near well 216. A major breccia horizon more than 1300 metres long and 110 metres thick occurs in the west-central part of the area (Fig. 3.5), and a thinner breccia horizon occurs at the base of the Huka Falls Formation in well 224.

The occurrence of highly friable (clay altered) to silicified hydrothermally altered clasts associated with unaltered rock fragments in an unaltered clastic matrix limits the origin of these breccias to two main possibilities: (1) lahars and (2) hydrothermal eruptions. The major problem with the lahar mechanism is locating a source area. Mudflows of the proportion of the Huka Falls breccias would require a source area both larger in acreage and higher in elevation than that which existed in the Wairakei area during the time the Huka Falls Formation was deposited. The occurrence of the thin breccia intersected by well 224 may be a remnant of a lahar which entered the Wairakei area from the west or possibly the southwest, a possibility which cannot be discounted. However, considering the spatial distribution of the breccias and their intimate association with several of the major faults in the western area, the breccias are most likely the result of hydrothermal eruptions. The occurrence of the

breccias above the area where the high-temperature fluid enters the reservoir also supports a hydrothermal origin for the breccias.

Wairakei Formation

Wairakei Breccia

The Wairakei Breccia was deposited during the 22.7 ka Taupo eruption (Wilson et al., 1984). The unit is composed of two pyroclastic flows each consisting of vitric tuff with a basal tuffaceous sandstone containing abundant accretionary lapilli (Grindley, 1965). The vitric tuffs both contain common fragments of andesine to oligoclase plagioclase, quartz, hypersthene, hornblende and accessory magnetite and minor xenoliths of rhyolite in hyalopilitic groundmass (Steiner, 1977). The occurrence of diatoms within the tuffaceous sandstone indicates that the Wairakei Breccia was deposited in a lacustrine environment.

The Wairakei breccia blankets most of the Wairakei area varying from ~30 to ~100 metres in thickness. The unit is thicker in the northern part of the Wairakei area where its thickness may exceed 250 metres (Plate 6). In the eastern part of the area the Wairakei breccia either was not deposited or was completely eroded.

Taupo Pumice

The Taupo Pumice was deposited during the 186 A.D. eruption from the Taupo volcano (Wilson et al., 1984). The unit is composed of ash fall deposits and related alluvium which consists primarily of pumice ash and lapilli (Grindley, 1965). Local mudstone and siltstone beds occur at the base of the Taupo Pumice, but no diatoms or sponge spicules have been identified (Steiner, 1977).

The Taupo Pumice blankets the Wairakei area except in the northwest where it has been eroded off of a topographic high. The thickness of the

unit is relatively uniform, varying between 30 and 50 metres, although in local depressions the unit may be as much as 100 metres thick.

Structural Development

Tectonic Components

Regionally, the Wairakei geothermal area occurs within a sigmoidal bend in the northeast-striking "Wairakei" fault system (Fig. 3.7). This regional flexure is probably attributable to the combined influence of left-lateral shear and major basement structures (e.g., caldera margin or transcurrent faults) on the northeast-trending faults.

Three major structural components of the Wairakei geothermal area are apparent on structural contour maps (Healy, 1984). They are the central Wairakei ridge, eastern Taupo-Reporoa basin and western Te Mihi basin. The relative locations of these features are indicated in Figure 3.5.

Wairakei High

Early mathematical models of gravity data for the Wairakei region (Beck and Robertson, 1955; Modriniak and Studt, 1959) depicted the central ridge as an elliptical basement (horst) block approximately 2 miles long and elongated in a northeasterly direction. Structure contour maps (Healy, 1984) and geological cross sections (Fig. 3.5) constructed from drill hole intercept data confirm the ridge-like form of the Wairakei high and provide detailed information pertaining to the geometry of the structure. Within the boundaries of the geothermal area the Wairakei high is an elongated, mesa-like horst block made up of Ohakuri Group rocks and Wairakei Ignimbrite. The ridge supports a minor amount of topographic relief, but in general slopes gently to the south or southwest (Healy, 1984). To the west and southeast the Wairakei high is bounded by two major northeast-trending faults, the Crater fault and the Unnamed fault respectively (Fig. 3.5).

WAIRAKEI – ROTOKAWA

Regional Geology

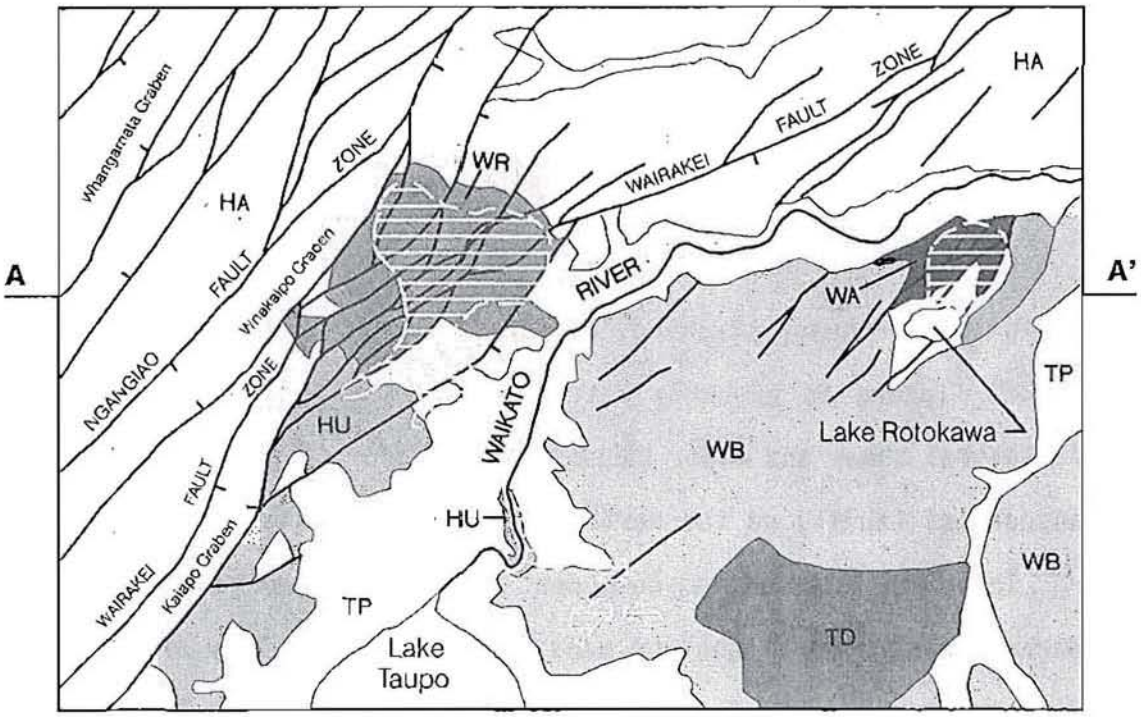

Cross Section A–A'

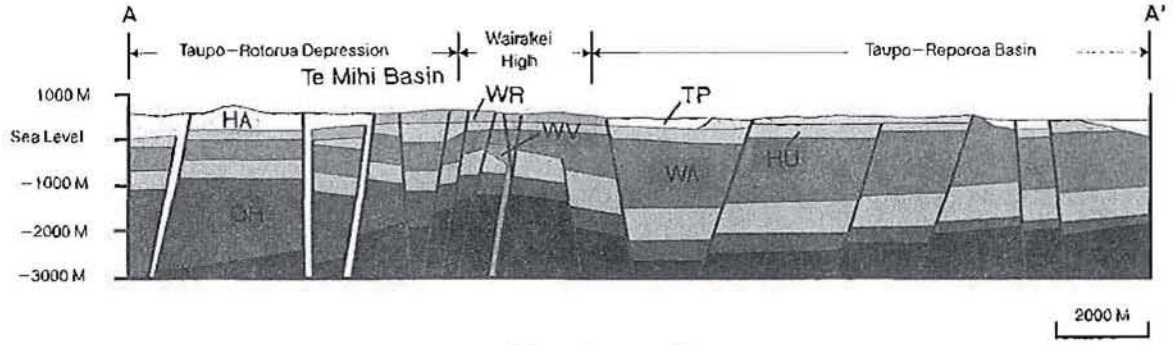

Explanation

(TP) Taupo Pumice/Alluvium

(WB) Waitahanui Breccia

(TD) Tauhara Dacite

(WR) Wairakei Fm

(HA) Haparangi Rhyolite

(HU) Huka Falls Fm

(WA) Waiora Fm

(WV) Waiora Valley Andesite

(WK) Wairakei Ignimbrite

(OH) Ohakuri Group

Greywacke

Active Thermal Area

Figure 3.7. Geology of the Wairakei-Rotokawa region. Simplified and redrawn from Geological Map of New Zealand, Sheet N94-Taupo (in Grindley, 1965).

Taupo-Reporoa Basin

The Taupo-Reporoa Basin is a complex, north-northeast-trending basement depression identified by gravity data modeling (Beck and Robertson, 1955; Modriniak and Studt, 1959). Subsidence progressed more rapidly in the east producing an asymmetrical basin apparently hinged on the western side. As the basin deepened the Ohakuri Group was progressively tilted to the southeast. At about 230 ka (Wilson et al., 1986) voluminous pyroclastic flows (Wairakei Ignimbrite) were deposited in and partially filled the Taupo-Reporoa basin. Prior to (or during) deposition of Member 1 (Wairoa Formation), the Ohakuri Group and overlying Wairakei Ignimbrite were down-dropped at least 250 metres along the Unnamed fault which forms the southeastern margin of the Wairakei ridge (Fig. 3.5). Movement along the eastern Unnamed fault stopped prior to deposition of Member 4 (Wairoa Formation), but other northeast-trending, eastward-dipping normal faults which lie east of the Unnamed fault displace the Huka Falls Formation, documenting relatively recent subsidence within the Taupo-Reporoa Basin.

Te Mihi Basin

The Te Mihi Basin is a relatively small elliptical basin elongated in an east-northeast direction and is part of the much larger Taupo-Rotorua Depression (Grindley, 1965). Subsidence of the Ohakuri Group rocks and possibly the Wairakei Ignimbrite in the western and northwestern portions of the Wairakei geothermal area occurred along the northeast-trending Crater fault (Fig. 3.5). Significant normal displacement had occurred along the Crater fault prior to or during deposition of Member 1 of the Waiora Formation. Basin subsidence in the northern portion of the Te Mihi Basin ceased prior to deposition of Member 4 (Waiora Formation), whereas subsidence in the southern portion of the basin continued after deposition of Member 5 (Waiora Formation), possibly continuing to the present.

Volcano-Tectonic History

The geologic history of the Wairakei area is characterized by repeated magmatic events and associated caldera development followed by periods of volcanic quiescence and basin subsidence. The earliest known event resulted in the deposition of the Ohakuri Group which consists of a thick sequence of interbedded pyroclastic and related volcaniclastic rocks. The origin and age of the Ohakuri Group identified by drilling at Wairakei is obscure, but the occurrence of thick ignimbrites interbedded with ash-rich clastic rocks indicates that the rocks are most probably related to a caldera-forming (Whakamaru ?) event. Regardless of the unit's origin, the Ohakuri Group provides a time-stratigraphic base line upon which to reconstruct the recent volcano-tectonic history of the Wairakei area.

As subsidence began in the Taupo-Reporoa Basin, a large block of the Ohakuri Group was tilted southeastward. About 230 ka (Wilson et al., 1986) the Wairakei Ignimbrite flows were deposited in and progressively filled the actively subsiding Taupo-Reporoa tectonic basin. Deposition of Member 2 of the Wairakei Ignimbrite apparently filled the western portion of the Taupo-Reporoa Basin (Grindley, 1965), so that Member 3 was deposited as a relatively planar sheet draped over Member 2 in the east and over the Ohakuri Group in the west.

Following emplacement of the Wairakei Ignimbrite a north-northeast-trending (normal) fault system began to develop in the southern portion of the TVZ central graben. At Wairakei two particularly important faults which formed at this time were the eastern Unnamed fault and the Crater fault (Fig. 3.5). Repetitive movement along these two basin-bounding faults controlled the structural development and palaeophysiography of the Wairakei area.

A "central" horst, the Wairakei high, began to emerge as the western portion of the Taupo-Reporoa Basin continued to subside along the eastern Unnamed fault and as the eastern portion of an incipient Te Mihi Basin

began to subside along the Crater fault. Prior to deposition of Member 1 of the Waiora Formation, the Wairakei high was a pronounced topographic ridge with steep margins possibly rising more than 400 metres above the adjoining valley floors. However, deposition of a sequence of major pyroclastic flows (Member 1 of the Waiora Formation) which were probably related to the initial collapse of the Taupo caldera (Healy, 1984) quickly filled the adjoining basins and covered the Wairakei high. Subsidence of the Taupo-Reporoa Basin along the eastern Unnamed fault effectively ceased prior to (or during) deposition of Member 1 (Waiora Formation), whereas significant subsidence of the Te Mihi Basin along the Crater fault preceded deposition of Member 2 (Waiora Formation) (see Plate 6). A period of relative tectonic quiescence began concurrently with deposition of Member 2 of the Waiora Formation.

Following minor erosion of Member 2 (Wairoa Formation), volcanic activity resumed when the Waiora Valley Andesite, which apparently ascended the Wairakei fault system, was erupted from a vent near the centre of the Wairakei high. The ensuing lava flowed ~1500 metres down the gently dipping western and northwestern slope of the ridge resulting in a fan-shaped flow elongated in a northwesterly direction (see Plate 6; Healy (1984), Figs. 6 and 7).

The pyroclastic deposits of Member 3 and the lower portion of Member 4 of the Waiora Formation progressively filled the Te Mihi and Taupo-Reporoa basins while minor subsidence occurred along the eastern Unnamed fault and the Crater fault. At c. 140 ka (Wilson et al., 1986), the Haparangi Rhyolite was extruded from a vent located to the south of the Wairakei area. Extrusion of the Karapiti Rhyolite was preceded and followed by deposition of ignimbrite and associated volcaniclastic debris.

Significant (>150 m) subsidence along the Crater fault occurred immediately following deposition of Member 5 (Waiora Formation). During this time a glacial lake covered the Wairakei area, depositing the Huka

Falls Formation (Grindley, 1965). Geothermal activity was well under way by the time the Huka Falls Formation was deposited, as evidenced by the occurrence of hydrothermal eruption breccias at the base of and within the Huka Falls Formation.

The c. 20 ka pyroclastic flows and tuffs (Wairakei Breccia) were erupted from vents along the north side of Lake Taupo (Self and Healy, 1987; Wilson et al,. 1984). The last significant pyroclastic eruption occurred at 186 A.D. with the extrusion of the Taupo Pumice.

The northern part of the Taupo volcanic centre, the Tukairangi volcanic complex (Healy, 1984), is the most probable source for the pyroclastics of the Waiora Formation and Huka Falls Formation (Grindley, 1965).

Geothermal Reservoir

Surface Expression

The distribution of thermal springs and steaming ground at Wairakei covers an area of approximately 25 km^2 (Fig. 3.8). Many of the thermal springs are concentrated along minor, nonproductive structures which did not significantly influence the development of the geothermal reservoir. However, most of the larger thermal features, with the notable exception of Hot Hill (~1 km north of Alum Lake), are localized in the structurally more complex areas. The north-south lineation defined by the location of the Karapiti, Alum Lake and Hot Hill thermal areas may reflect an unrecognized basement structure which was important to the formation of the reservoir. Similarly, the northwest-trending elongation of the Geyser Valley thermal area is almost certainly structurally controlled, and may be related to one of the deep-seated regional transcurrent faults noted earlier (see section of Taupo Volcanic Zone).

Prior to steam production active hot springs and steaming ground occurred at Geyser Valley, in the Waiora valley, at Karapiti and along the Waikato river (Allis, 1982b). The hot springs occurred in low-lying areas

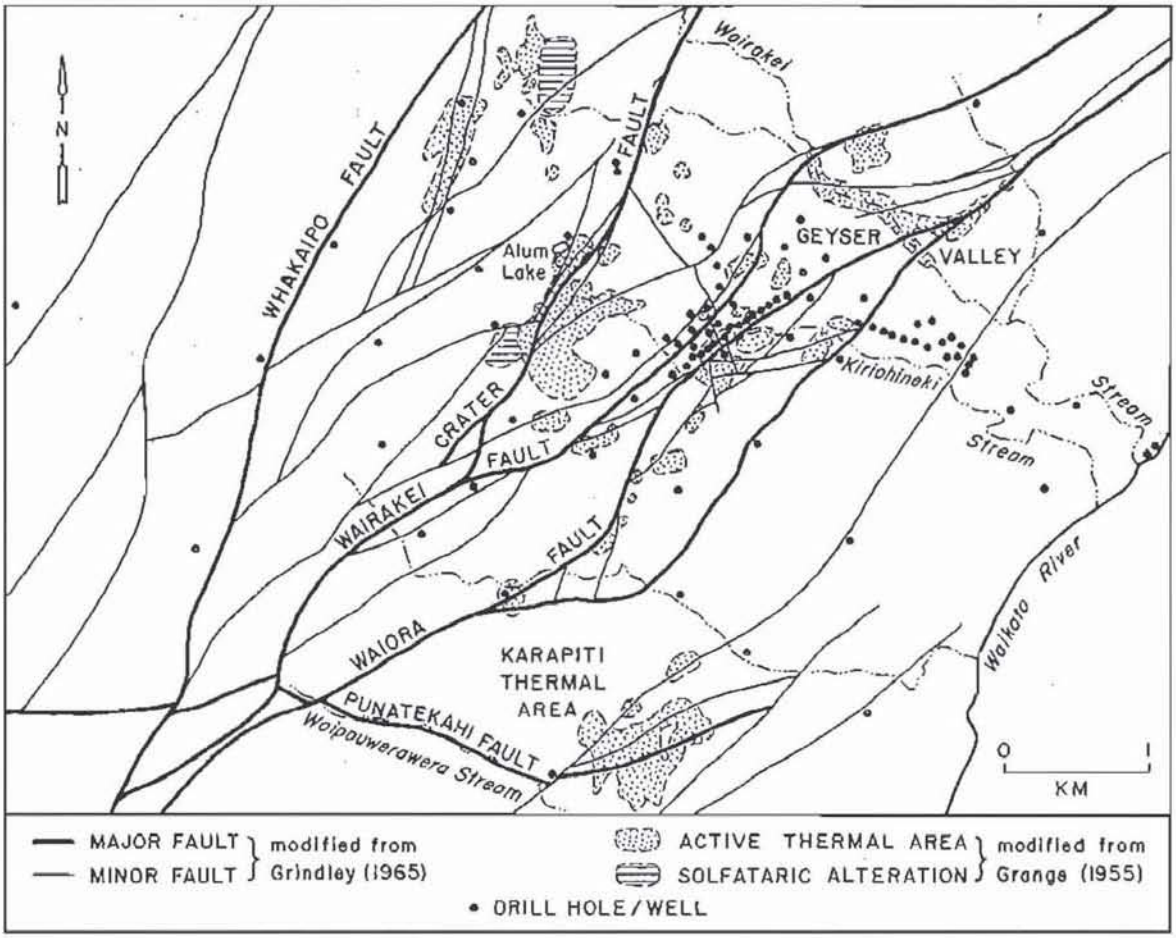

Figure 3.8. Map showing the location of the major thermal features and the traces of the major and minor faults within the Wairakei geothermal area.

and discharged near-neutral pH chloride water (NaCl ≈ 3300 ppm), whereas steam vents occurred on areas of topographic relief and above structural highs and expelled acid-sulphate water (condensed steam) or a mixture of acid-sulphate and chloride waters (Ellis and Mahon, 1982).

A production-related drop in reservoir pressure has resulted in the formation of a vapour-dominated zone immediately below the Huka Falls Formation (Allis, 1982a). The establishment of the vapour-dominated zone was concurrent with the cessation of flow from most of the hot springs, a change from near-neutral pH, chloride water to acid-sulphate or acid-sulphate chloride water and the inception of steam vents as surface discharge ceased (Ellis and Mahon, 1982). Water table drawdown induced by

production discharge has affected both reservoir monitor wells and groundwater wells over an area of ~100 km^2 (R.G. Allis, personal communication).

Preproduction Reservoir

The preproduction Wairakei geothermal system may be envisioned as an upwelling hydrothermal plume which widens out within ~1500 metres of the surface. The rising column of hot water enters the reservoir in the west and migrates eastward as a result of both gravity-induced flow in the highly permeable Waiora Formation and a reduction in permeability (Hochstein, 1982) near the western boundary of the reservoir. The maximum reservoir temperature recorded was ~275°C, but the majority of the higher temperature reservoir varied from 240° to 265°C. In general the fluid within the upper ~500 metres of the reservoir was boiling.

The topology of the hydrothermal reservoir may be represented by the apparent resistivity of the rocks. Figure 3.9 shows the distribution of apparent resistivity contours at a depth of ~350 metres (AB/2 = ~500 m). The 100 ohm metre (Ω•m) contour roughly coincides with the edge of the hydrothermal system (T ≤100°C), with the area inside the 20 Ω•m contour corresponding to the high-temperature (T ≥240°C) portion of the reservoir (Risk et al., 1983). Using Figure 3.9 as a guide, the area of the reservoir can be seen to be ~50 km^2 at a depth of about 350 metres. Risk et al. (1983) also present apparent resistivity data for a depth of ~700 metres (AB/2 = ~1000m) which, on the basis of the 100 Ω•m contour, indicates that the reservoir covers an area of ~45 km^2 at that depth. Excluding the hydrothermal column and assuming an average vertical dimension of the reservoir of ~1000 metres, the volume of the reservoir is about 48 km^3. The high temperature (T ≥ 250°C) portion of the reservoir, approximated by the 20 Ω•m contours, covers a much smaller area, which Ellis and Mahon (1982) estimate to be ≥8 km^2. Using an average vertical dimension of ~400

metres (see Plate 6A) for the high-temperature reservoir, the volume of rock-containing ≥240°C fluid is ~3 km³. If the volume of the high-temperature portion of the thermal column is included then the total volume of rock at temperatures ≥240°C exceeds 7 km³.

The high-temperature reservoirs of Wairakei and Tauhara are connected at depth (Henley and Stewart, 1983). Ellis and Mahon (1982) estimated that for the two reservoirs combined the total volume of rock saturated with a high-temperature (200° to 270°C) fluid varies from 22 to 25 km³. In spite of the connection between the two reservoirs there is apparently little fluid movement between the two. This is indicated by the minimal pressure changes which occurred in the Tauhara field in response to production at Wairakei (R.G. Allis, personal communication).

The Wairakei geothermal reservoir exists because the highly permeable Waiora formation rests upon rocks of lower permeability at depth (Ohakuri Group and Wairakei Ignimbrite) and is overlain by relatively impermeable clastic rocks of the Huka Falls Formation (see section on Permeability in

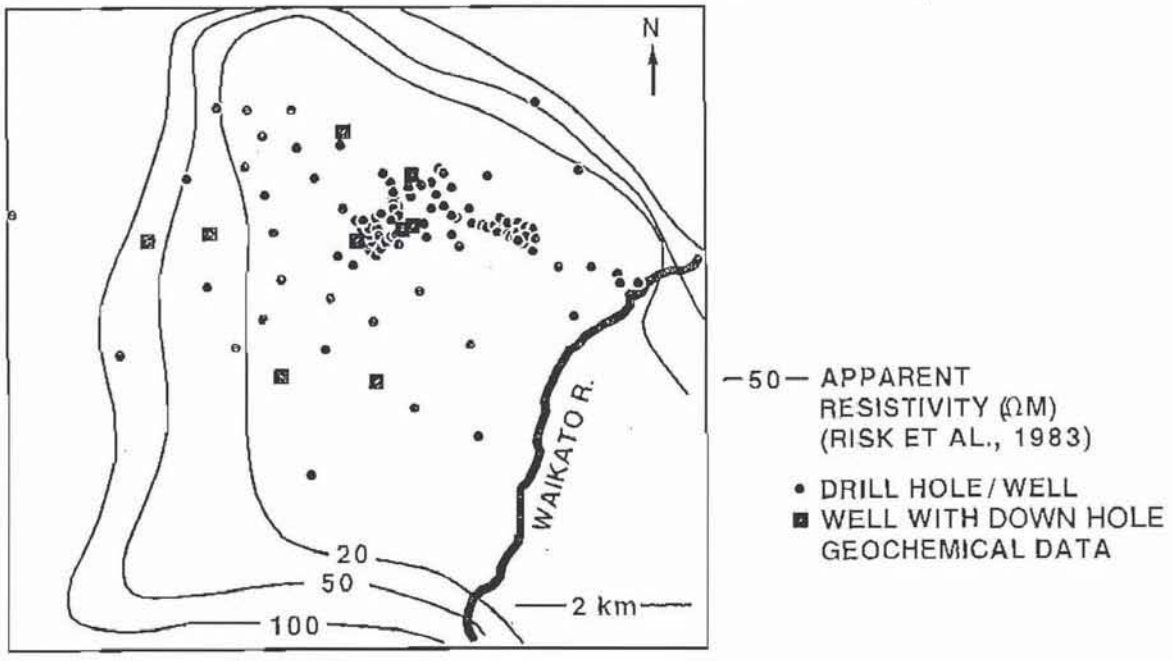

Figure 3.9. Apparent resistivity (AB/2 = ~550 m) contours for the Wairakei geothermal area. 100 Ω•m contour approximates the limit of the hydrothermal reservoir. Area within the 20 Ω•m contours approximately corresponds to the high-temperature reservoir. The contours correspond to a depth of ~350 m. Data from Risk et al. (1983).

Appendix 7). At depth, and in other areas of low permeability, fluid migration is controlled by fault and formational contacts, whereas within the reservoir these conduits are of secondary importance and fluid migration is controlled by intrastratal porosity and permeability. Strong evidence for the existence of well developed horizontal permeability within the Waiora Formation is the fact that well 223 (Fig. 3.11) responds very rapidly to the production from the central portion of the reservoir in spite of the fact that the two areas are not connected by a fault or fault system (R.G. Allis, personal communication).

Permeability in the Waiora Formation is partly the result of the high porosity of the pumiceous volcaniclastic and ignimbrite units. However, laboratory testing has indicated that matrix permeabilities for the Waiora Formation are lower than the minimum needed to maintain reservoir production, suggesting the presence of additional fracture permeability (Pritchett et al., 1979; 1980). The importance of fracture permeability over porosity is illustrated by the fact that the eastward-trending lobe of high-temperature outflow crosscuts formational boundaries (see Plates 6 and 6A). In order to form a large, productive geothermal reservoir the unit(s) hosting the reservoir (1) must have a relatively large volume to provide sufficient fluid storage and (2) must be highly permeable to allow rapid fluid migration. The Waiora Formation meets both of these criteria, whereas the underlying Wairakei Ignimbrite appears to have a much lower fluid storage capacity and the overlying Huka Falls Formation is much less permeable.

Thermal Zoning

Cross sections showing the preproduction thermal zoning patterns for the Wairakei reservoir were constructed by Banwell et. al. (1957), Elder (1981) and Grant (1984). Banwell et. al. (1957) described the thermal zoning of the northern edge of the reservoir in detail, but their work was

generally limited to shallow, lower temperature wells. The cross section drawn by Banwell et al. (1957) was very detailed, but their section covered only a small segment of the northern portion of the reservoir. The descriptions by Elder (1981) and Grant (1984) incorporate thermal data from much deeper and higher temperature wells, but their published cross sections lack detail and are inadequate for the purpose of comparing the preproduction thermal zoning with the distribution of hydrothermal rock alteration within the reservoir. Therefore, it was necessary for me to construct three thermal cross sections (Fig. 3.10; Plate 6A), which correspond to the geologic cross sections discussed earlier (Fig. 3.5; Plate 6). The location of the cross sections and of the wells for which reservoir temperatures were estimated are shown in Figure 3.12.

This was a nontrivial endeavour because the procedure for estimating reservoir temperatures from the measured thermal profile of a well is an iterative process which incorporates data from several years and from all of the adjacent wells during the same time period. The preproduction reservoir temperatures which are represented by the isotherms in Figure 3.10 were estimated following the methods described by Grant (1979) and incorporate well characterization data presented in Grant (1980). Reconstruction of preproduction thermal zoning was particularly difficult because reliable bottom-hole temperatures were not taken while the wells were being drilled and the direction of fluid flow was not measured during the majority of the down-hole temperature runs. Nevertheless, it is possible to make reasonable predictions about the reservoir conditions from temperature-pressure profiles (Grant, 1979) and, providing that the production related changes in the thermal zoning of the reservoir are known, these data may be extrapolated to preproduction conditions. The method used to estimate the preproduction reservoir temperatures is discussed in Appendix 7.

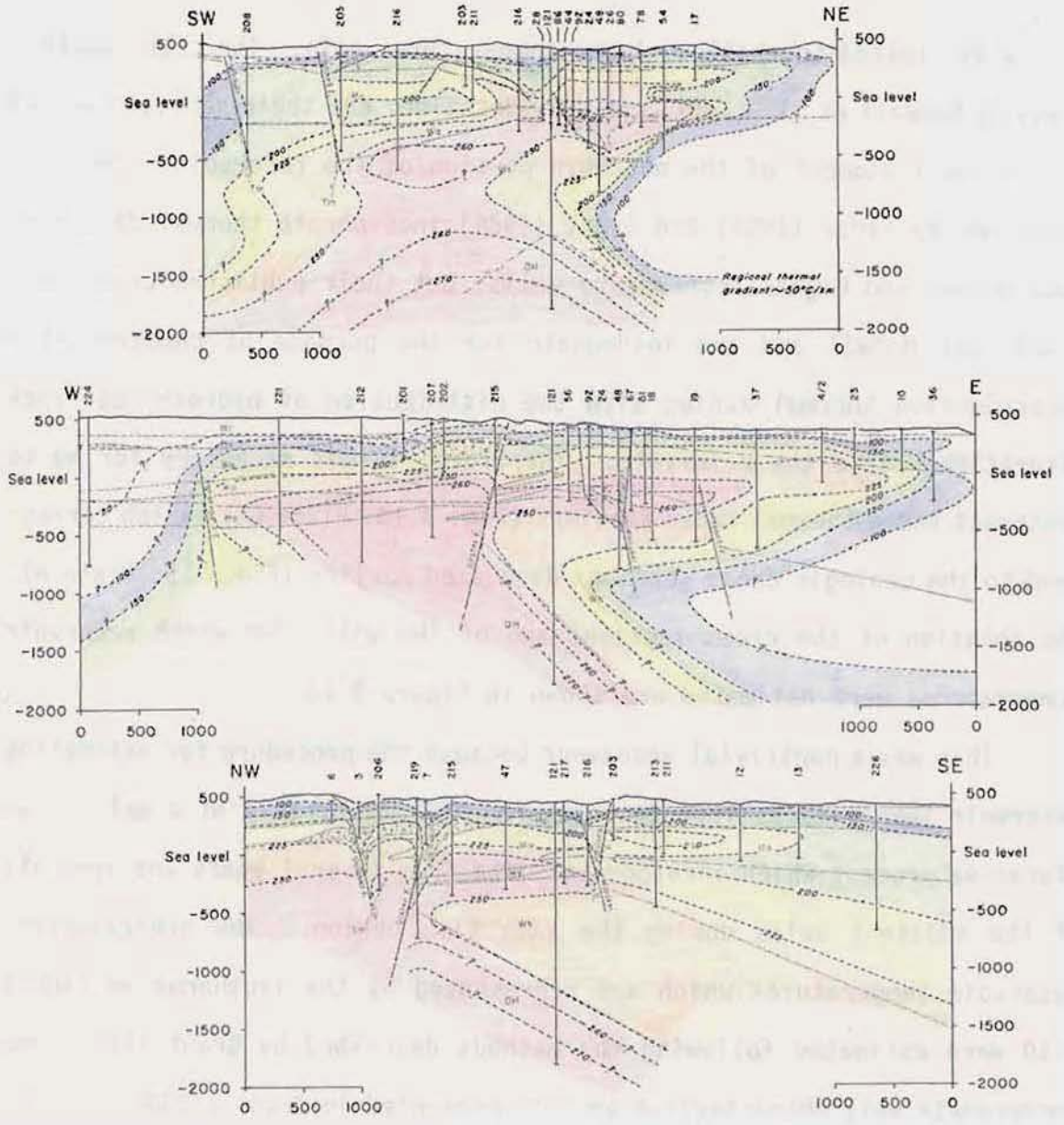

Figure 3.10. Estimated preproduction thermal zoning (T°C) for three cross sections through the Wairakei geothermal reservoir. See Figure 3.11 for cross section locations and Plate 6A for enlargement of the cross sections. Appendix 7 contains additional data and an explanation of the method used to estimate the preproduction reservoir temperatures.

The interpreted preproduction temperatures provide a c. 1950 look at the thermal zoning of the Wairakei reservoir. Two important observations about the preproduction reservoir are (1) that unit contacts and bulk permeability (porosity and fracture permeability), and to a lesser degree major structures, control the migration of the high-temperature fluid and

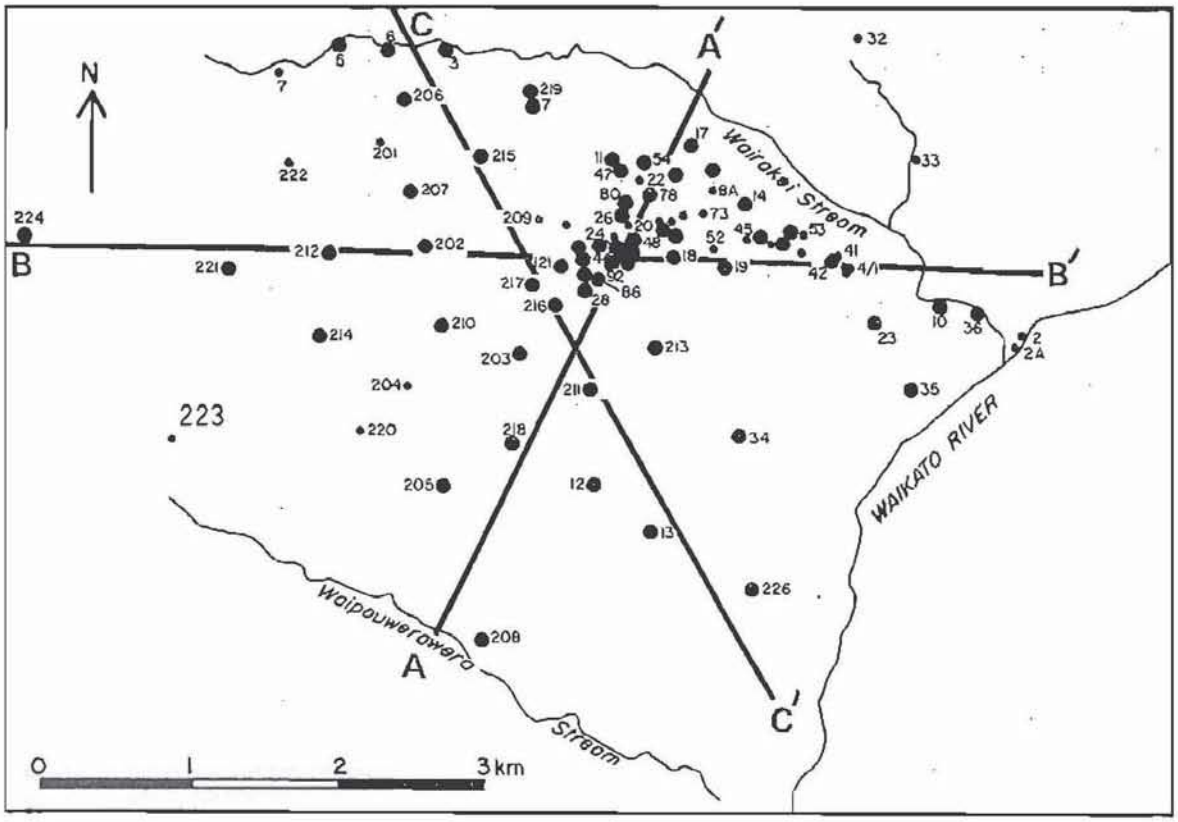

Figure 3.11. Map showing the location of the cross sections shown in Figure 3.10. Large dots indicate the wells for which preproduction reservoir temperatures were estimated. See Appendix 7 for a discussion of the method and the data.

(2) that the major structures appear to be the primary control on cold water invasion of the reservoir.

Fluid Inclusion Homogenization Temperatures

One of the main reasons for constructing the thermal cross sections (Fig. 3.10; Plate 6A) was to use them as a guide for interpreting the corresponding hydrothermal rock alteration. In order to evaluate the compatibility between the estimated temperatures and the temperatures at which the major types of rock alteration occurred, it was necessary to acquire a minimal amount of microthermometric data for the hydrothermal minerals. At the time that I was studying the distribution of and controls on hydrothermal alteration and metallization at Wairakei another Ph.D. student from

the University of Auckland (K.J. Youngman) began a major investigation of fluid inclusions contained in hydrothermal alteration minerals collected from the Wairakei reservoir. Consequently, I deliberately avoided an extensive evaluation of fluid inclusions, collecting only the bare minimum of data required to obtain a general representation of the relationship of fluid inclusion homogenization temperatures to preproduction thermal zoning and to estimate the spatial extent of the preproduction 2-phase (boiling) zone. It is my belief that the fluid inclusion homogenization temperature (T_H) data presented in Appendix 8 are reasonably representative of the temperatures at which the major alteration assemblages formed (Figure 3.12 shows the wells which were sampled for T_H measurements).

Although there is clearly insufficient data to form any conclusions, the magnitude and distribution of the T_H data warrant a few preliminary comments. (1) The T_H data suggest that the reservoir attained a maximum

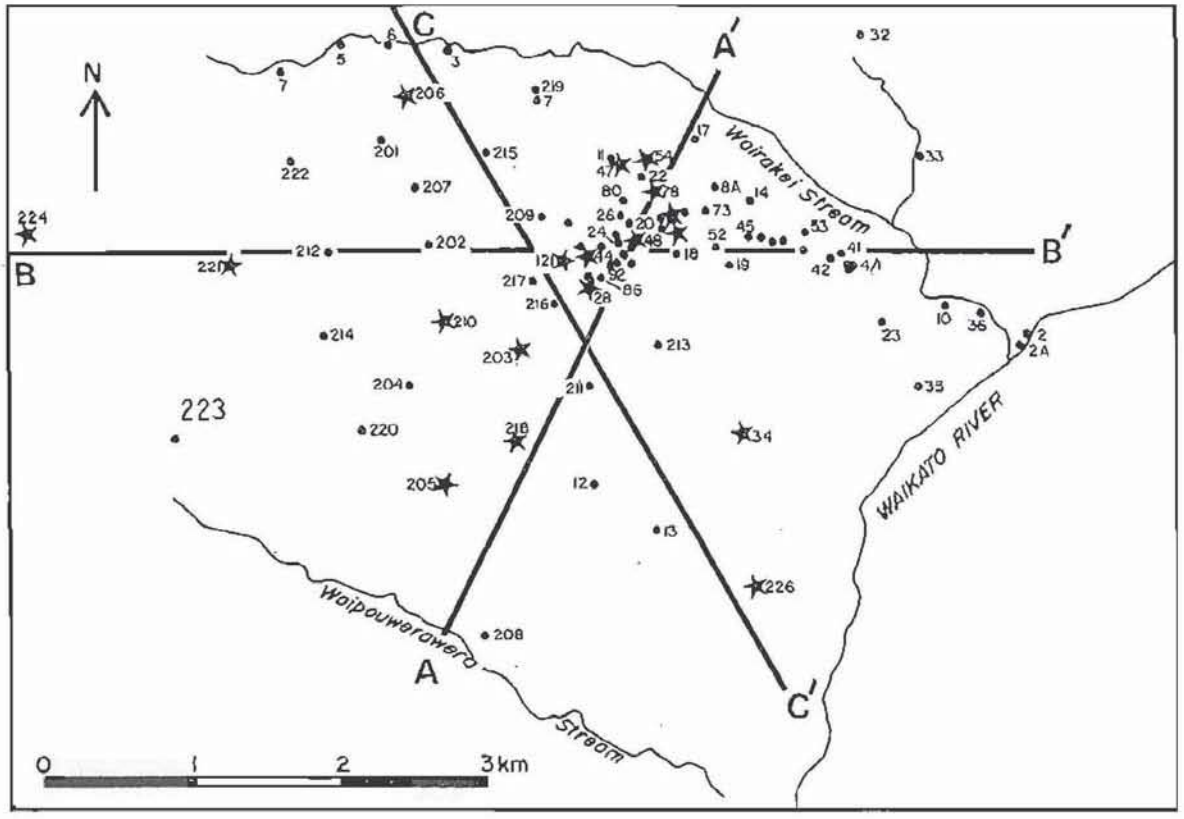

Figure 3.12. Map showing the location of wells (stars) for which fluid inclusion homogenization temperature data were determined from drilling samples. See Appendix 8 for a discussion of the method and the data.

temperature of ~310°C at depths below 1.3 kilometres. (2) Comparison of the estimated preproduction temperatures and T_H data for well 224 indicate that the extreme western part of the field has cooled by ~200°C at depths >1000 metres. (3) T_H values for the upper 500 metres of the reservoir equate with the estimated preproduction temperature data, but below 500 metres the T_H values are significantly higher than the estimated preproduction temperatures. The similarity between the two sets of data for the upper 500 metres indicates that the reservoir is not cooling from the top down, but from the bottom up. (4) The reduction in deep fluid temperature from ~310° to ~265°C caused the base of the 2-phase zone to migrate upward by more than 700 metres.

Production-Modified Reservoir

Production-induced changes in the thermal zoning within the Wairakei reservoir have been well documented (e.g., see Grant, 1980; 1984 and Grant and Horne, 1980). Figure 3.13 shows schematically the magnitude of the disruption of preproduction thermal zoning as a result of the extraction of ~1.5 billion tonnes of fluid, ~20 wt % of which is steam, from the high-temperature reservoir.

Initial fluid residency times for the deep reservoir fluid were estimated by Elder (1981) to be ~10^4 years. More recently Stewart (1984) estimated that at the present rate of production (~45 million tonnes per annum; Ministry of Works and Development, 1984) the fluid recycling time for the reservoir is ~1000 years. High-temperature reservoir recharge is deeply circulating meteoric water which originates within 10 kilometres of Wairakei, apparently in the western catchment for Lake Taupo, although water is not supplied by the lake (Ellis and Mahon, 1982).

Duration of Geothermal Activity

The maximum age of the Wairakei geothermal system is constrained by the age of the Wairakei Ignimbrite (230 ka; Wilson et al., 1986), which is

tentatively correlated with the Whakamaru, Rangitaiki and Peroa ignimbrites (Healy, 1984, p. 12). The presence of hydrothermal eruption breccias within the lower members of the Huka Falls Formation indicates that the geothermal activity certainly predates the Huka Falls Formation. The Wairakei Formation has been dated at 22.7 ka (P.R.L. Browne, personal communication) which provides an "absolute" minimum age for the Huka Falls

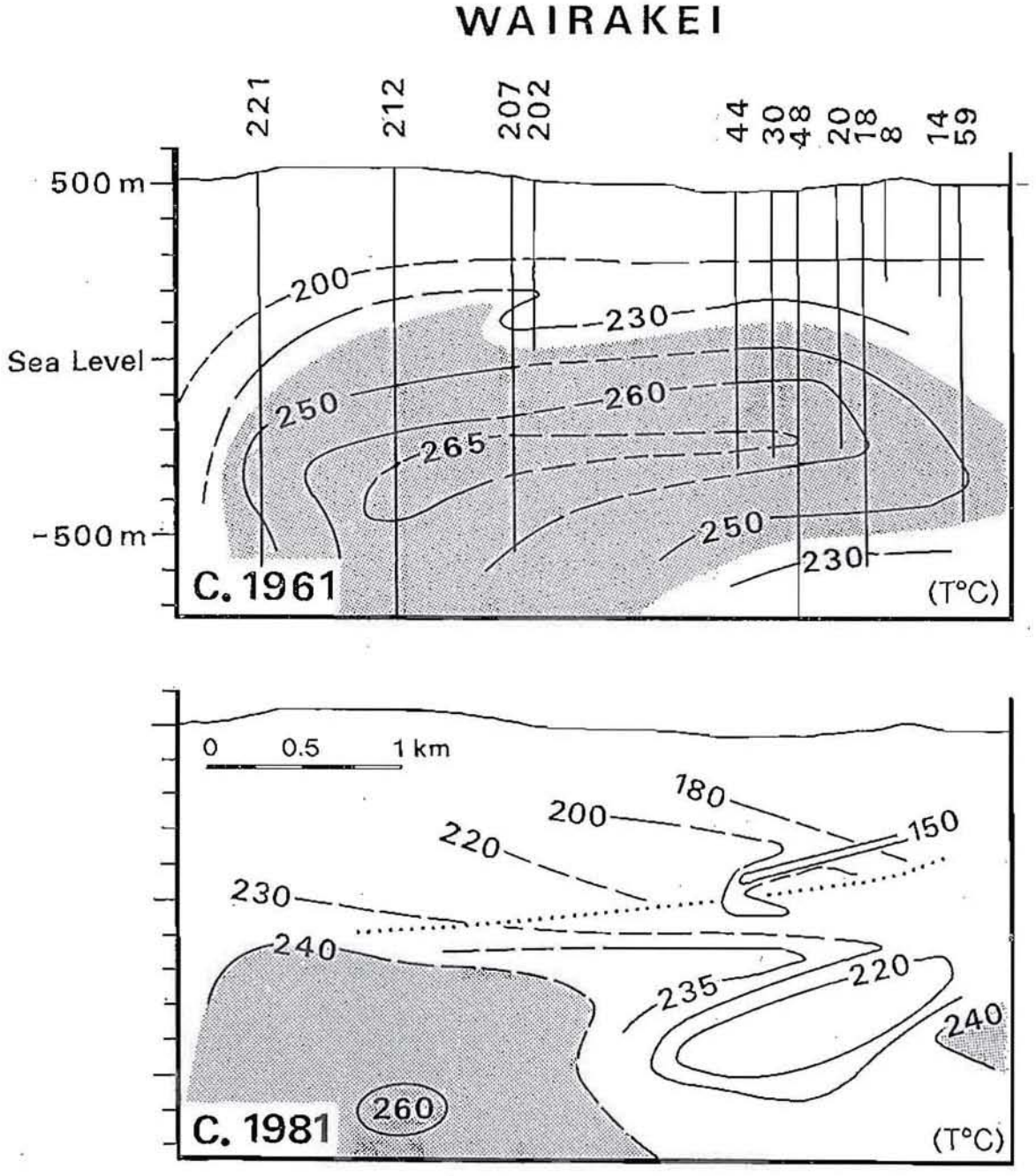

Figure 3.13. East-west thermal cross sections for the Wairakei reservoir. Stippled area indicates the distribution of ≥240°C water. Figure is redrawn from Grant (1984, Figure 4, page 6).

Formation. Eight miles south of Wairakei the Huka Falls Formation is overlain by the K-Trig basalt which was dated by Stipp (1968) at 137 ka. However, outcrops of the Huka Falls Formation beneath the K-Trig basalt and at Wairakei cannot be directly correlated. Therefore, the minimum age of the Huka Falls Formation is between 137 and 20 ka, probably closer to the older date.

The 45°C temperature drop from the maximum reservoir temperature estimated from the T_B data to the maximum measured temperature of the main body of the high-temperature reservoir is consistent with thermal decay trends expected from a 90,000 year-old hydrothermal system produced by the emplacement of a small impermeable pluton at a depth of 2.5 to 4.5 kilometres (Norton, 1982). This model age falls within the range of possible ages of the Huka Falls Formation. However, mathematical modelling by Cathles (1977) indicates that the life span of an individual hydrothermal convection cell is unlikely to exceed 20,000 years. Based on this work Cathles believes that the continuation of geothermal activity at Wairakei most likely is due to the continuous emplacement of small intrusive bodies.

Hydrothermal Alteration

Detailed petrographic descriptions of the hydrothermal alteration at Wairakei were published by Steiner (1968, 1977). His classification of hypogene alteration was based on (1) temperature, (2) the common association of certain secondary minerals and (3) the extent to which magmatic minerals were hydrothermally altered. Using these parameters Steiner divided hydrothermal alteration into three "ranks" of variable "intensity." Low-rank alteration was most common where temperatures were below 230°C and was defined by the formation of montmorillonite followed by the progressive crystallization of illite-montmorillonite, mordenite, laumontite, chlorite, apatite, calcite and pyrite with increasing temperature. Initially one or more of these minerals replaced the groundmass of the rock but, as altera-

tion intensity increased, mafic minerals (pyroxene and hornblende) and primary feldspar were also replaced. Medium-rank alteration formed at temperatures between 230° and 240°C and was identified by the replacement of primary plagioclase by wairakite and pericline[4] (albite) with or without epidote and micaceous clay. The crystallization of adularia and quartz, locally accompanied by albite and wairakite, defined high-rank alteration, which was only present in areas where temperatures exceeded 240°C. High-rank alteration was typically restricted to areas surrounding major structures.

Steiner (1968, 1977) also documented the common occurrence of pyrite and pyrrhotite at Wairakei. He described pyrite as being widespread and observed that it characteristically replaces magnetite and ferromagnesian minerals. Steiner noted that pyrrhotite was commonly associated with pyrite, but that it also occurred separately. The most common occurrence of pyrrhotite was as an alteration product of magnetite.

In my study of Wairakei, I have also classified bulk rock hydrothermal alteration on the basis of certain indicator minerals which typify the alteration mineral assemblage and are consistently present. I restricted my classification to four major alteration mineral assemblages which (1) could be related to relatively simple chemical reactions and (2) were mappable on a reservoir scale. The major types of alteration and the diagnostic mineral or minerals which characterize the alteration assemblage, adhering to the usage of Meyer and Hemley (1967), are (1) propylitic (pericline, wairakite, prehnite, epidote, clinozoisite-zoisite), (2) potassic (adularia, grothite (Al-titanite), apatite), (3) zeolite (laumontite, mordenite) and (4) carbonate (calcite).

---

[4]Low temperature Na- and K-feldspar which crystallize from hydrothermal solutions, particularly as open-space or vein filling, are termed pericline and adularia respectively (Shelley, 1985; p. 247).

The nomenclature presented here is similar to the alteration nomenclature used to describe several epithermal gold-silver deposits (e.g., see Sander and Einaudi, 1990; Black et al., 1991). The major departure from these studies is the occurrence of the zeolites (wairakite, laumontite and mordenite) at Wairakei. My classification also resembles Steiner's (1977) alteration classification with propylitic alteration being equivalent to a combination of Steiner's "high" and "medium" rank assemblages and potassic and zeolite alteration equivalent to Steiner's "medium" and "low" rank assemblages. The use of the scanning electron microscope and electron microprobe during my study allowed me to expand and refine Steiner's alteration scheme. Without the use of these tools it would have been difficult for Steiner to identify fine-grained adularia which is the principal component of potassic alteration.

It will be shown in the following sections that Steiner's classification sequence of temperature-dependent alteration minerals is generally correct, with only the "medium" rank minerals being out of sequence. It will be shown through thermodynamic constraints that wairakite, clinozoisite and, by inference, epidote only form at temperatures in excess of ~250°C. Other expansions of Steiner's work presented in this chapter are the addition to his classification of additional accessory phases and the construction of three cross sections showing the spatial distribution of the alteration assemblages.

Propylitic Alteration

Propylitic alteration is characterized by the replacement of magmatic andesine by either pericline (stoichiometric hydrothermal albite) or wairakite. Evidence for the direct precipitation of pericline and wairakite from the geothermal fluid (open space- or fracture-filling) is rare although microveinlets of pericline are a common feature of plagioclase alteration. The degree of host rock replacement and equilibrium mineral

assemblage varies, but in general propylitic alteration tends to occur at deeper levels within the high-temperature reservoir and becomes more pervasive as the fluid/rock ratio increases.

Alteration Mineral Assemblage

The minerals which most commonly occur in equilibrium with pericline (in approximate order of frequency and abundance) are: quartz, adularia, "white mica" (illite/sericite), pyrite, epidote, clinochlore, montmorillonite, clinozoisite, wairakite, prehnite and magnetite. In addition to these minerals, pericline locally occurs in apparent textural equilibrium with anatase-rutile, zoisite, and leucoxene(?).

Textural Relationships

During propylitic alteration plagioclase (andesine) and lithic fragments are replaced to varying degrees by irregular intergrowths of quartz, pericline and/or wairakite which may be accompanied by adularia, epidote, clinochlore, prehnite, and magnetite. Examples of propylitic alteration textures and associated alteration minerals are shown in Figures 3.16d, 3.21c and 3.22a. In a few samples andesine is almost totally replaced by either epidote ± pericline or wairakite ± epidote ± pericline. Where plagioclase phenocrysts are replaced by the assemblages pericline-wairakite or pericline-adularia, pericline characteristically replaces phenocryst rims, whereas wairakite or adularia replace phenocryst cores. It is possible that wairakite may locally replace pericline, but unequivocal textural evidence for this was not observed. When twinned plagioclase is replaced by pericline or the assemblage pericline-adularia the twin planes are generally preserved (Fig 3.20a), but if adularia alone (potassic alteration) replaces feldspar phenocrysts, twinning is generally destroyed.

Clinochlore typically replaces ferromagnesian minerals and groundmass, but also replaces andesine phenocrysts in association with pericline

± epidote. When replacing mafic minerals, clinochlore most commonly forms irregular fibrous veinlets or spherulitic clusters (Figs. 3.15e and f).

During propylitic alteration the groundmass is replaced by intergrown quartz, pericline and adularia, which is commonly accompanied by epidote, clinochlore and white mica. Unless the alteration is particularly strong and the groundmass is replaced by relatively large grains, it is difficult to differentiate between quartz, pericline, adularia and wairakite with the optical microscope. In several examples of propylitic alteration the dominant alteration determined optically was very fine-grained "silicification" of the groundmass. However, when these areas were scrutinized with the scanning electron microscope and several grains were analysed by energy dispersive X-ray techniques, pericline and adularia commonly formed a high percentage of the altered rock.

At depth, particularly in the Wairakei Ignimbrite, where permeability is low, andesine and the groundmass are more commonly replaced by quartz than by pericline ± adularia, and the degree of replacement is limited. In these areas secondary feldspar is generally restricted to the groundmass.

Calcite is a common alteration product of lithic fragments, phenocrysts and the groundmass in the deeper portions of the reservoir. In general calcite appears to be relatively late, replacing both magmatic and secondary minerals, but at least part of the calcite is related to propylitic alteration. However, since the distribution of calcite does not coincide directly with the distribution of propylitic alteration, the occurrence and spatial distribution of calcite is discussed later under a separate heading.

Spatial Distribution

The spatial distribution of propylitic alteration appears to be controlled by temperature and permeability (Fig. 3.14; Plate 6B). In the

central and southern parts of the reservoir the upward limit of pericline approximates the 250°C isotherm, but to the north and east the upper limit of pericline converges toward the surface. The reason for this convergence is not clear. However, the northwestern "bulge" (Fig. 3.14, NW-SE cross section) overlies the high-temperature upflow for the reservoir. Although reservoir temperatures in this area once exceeded those shown in Figure 3.10, it is unlikely that the 250°C contour coincided with the maximum upper limit of propylitic alteration. It is possible that higher heat flow in this area plus a possible slight increase in the activity of Na^+ may have contributed to the formation of pericline at temperatures <250°C. Likewise, the upward convergence of propylitic alteration in the northeast may reflect a structurally controlled palaeo high-temperature upflow zone. These "northwestern" and "northeastern" bulges in the upper level of pericline may actually extend across the northern edge of the reservoir reflecting an unrecognized east-northeast trending high-temperature upflow zone which was active in the past. This zone may be related to the inferred fault which controlled the trend of the Wairakei stream and Geyser Valley.

The major control on the distribution of pericline in the southern part of the reservoir is the occurrence of the Haparangi Rhyolite which forms a relatively impermeable ceiling to the high temperature fluid. Pericline is restricted to the lower 50 metres of the Haparangi Rhyolite and below. The zoning pattern is more complicated in the central portion of the reservoir (Fig. 3.14, E-W cross section) where the upper limit of pericline is influenced by several small structurally-controlled upflow and downflow zones. Pericline is absent in the upper 700 metres of the extreme western portion of the Wairakei reservoir (see well 224), and its absence suggests that the high temperature fluid never infiltrated this portion of the reservoir.

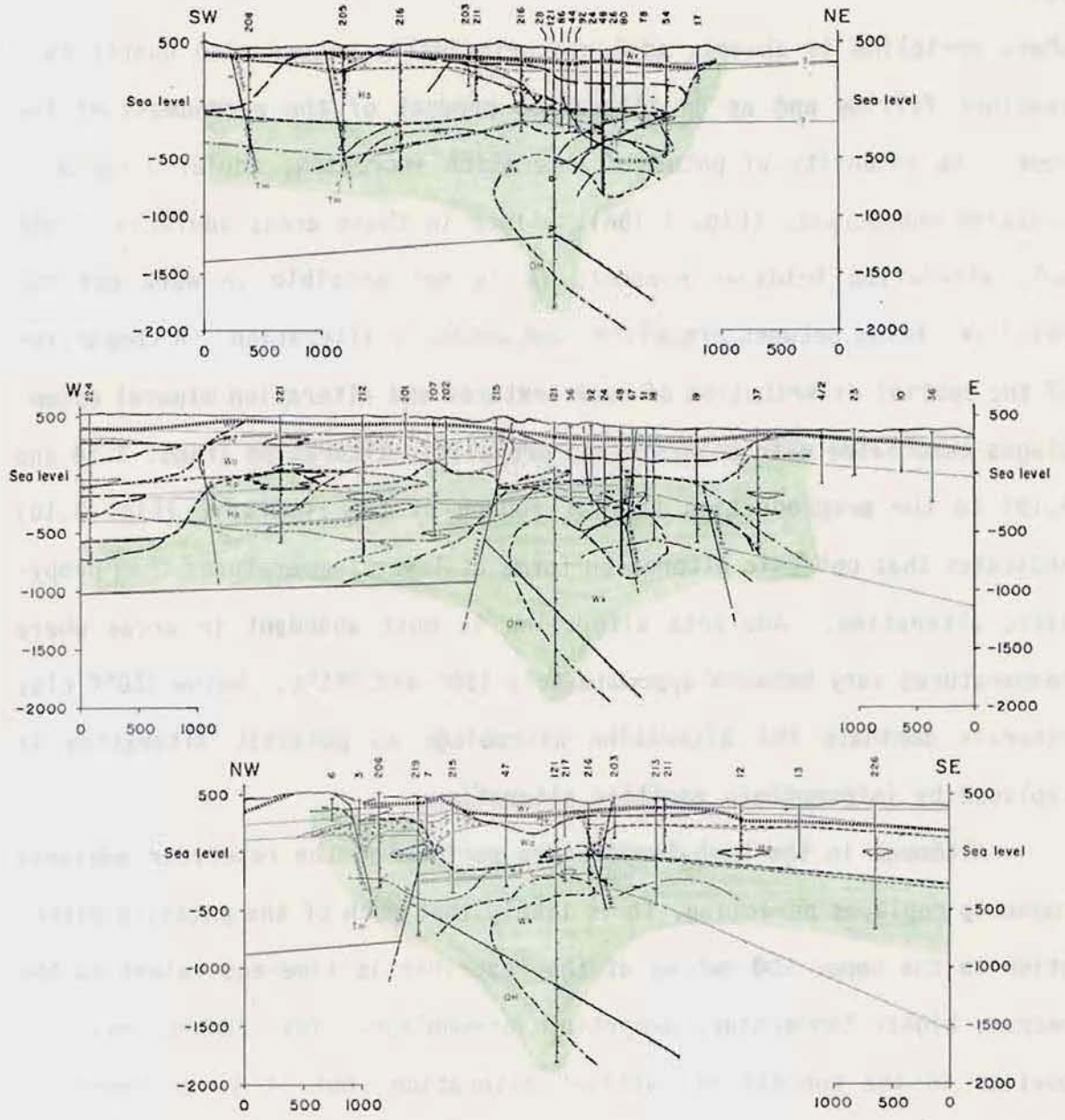

Figure 3.14. Spatial distribution of propylitic (pericline) alteration within the Wairakei hydrothermal reservoir. The distribution of propylitic alteration is shown in green. See Figure 3.11 for location of the cross sections.

Potassic Alteration

Potassic alteration is identified by the replacement of either pericline or magmatic andesine by adularia. Where propylitic alteration preceded potassic alteration, typically at depths greater than ~500 metres, adularia replaces residual plagioclase and either replaces or forms overgrowths on pericline. In most of the upper 500 metres of the reservoir,

where pericline is absent, adularia principally occurs with quartz as a fracture filling and as an alteration product of the groundmass of the rock. As intensity of potassic alteration increases, adularia replaces andesine phenocrysts (Fig. 3.15A). Since in these areas adularia is the only alteration feldspar present, it is not possible to work out the relative timing between propylitic and potassic alteration. A comparison of the spatial distribution of rock textures and alteration mineral assemblages associated with potassic and propylitic alteration (Figs. 3.14 and 3.19) to the preproduction thermal zoning of the reservoir (Fig. 3.10) indicates that potassic alteration forms at lower temperatures than propylitic alteration. Adularia alteration is most abundant in areas where temperatures vary between approximately 150° and 245°C. Below 150°C clay minerals dominate the alteration assemblage as potassic alteration is replaced by intermediate argillic alteration.

Although in the high-temperature portion of the reservoir adularia commonly replaces pericline, it is likely that much of the potassic alteration in the upper 500 metres of the reservoir is time-equivalent to the deeper, higher temperature propylitic assemblage. This concept may seem obvious in the context of "active" alteration, but it is an important distinction which needs to be considered when dealing with mineral paragenesis in "fossil" geothermal systems such as the Nevada epithermal ore deposits at Round Mountain and Rawhide.

Alteration Mineral Assemblage

Potassic alteration may include a variety of minerals in equilibrium. Quartz and adularia are always present and are almost always accompanied by grothite (Al-titanite), chlorapatite, "white mica" (illite/sericite), clinochlore and pyrite (Figs. 3.15 to 3.17). Other minerals locally occurring as part of the potassic alteration assemblage are mordenite (see section on Zeolite Alteration), anatase-rutile, anhydrite, barite, biotite,

magnetite and zircon. Although hydrothermal grothite, monazite and chlorapatite almost always accompany adularia in potassically altered rocks, their abundances rarely exceed trace levels. The equilibrium assemblage which best characterizes potassic alteration at Wairakei is quartz-adularia-illite/sericite-grothite-apatite-anatase/rutile-pyrite.

Apatite

Magmatic and hydrothermal apatite are both present at Wairakei, but it is nearly impossible to differentiate between them by standard optical methods. However, it appears from textural relationships and mineral associations that magmatic and hydrothermal apatite may be differentiated on the basis of semiquantitative mineral chemical analysis. Hydrothermal apatite contains detectable to abundant chlorine whereas magmatic apatite is chlorine-deficient.

Monazite

Monazite occurs as micron-sized spherical to elliptical-shaped grains disseminated in hydrothermal veins and in the groundmass (Figs. 3.31 and 3.32); the largest hydrothermal monazite crystal identified was a skeletal grain ~10 microns by ~50 microns (Fig. 3.32 E and F). Because of the very fine grain size of monazite it is only detectable with the scanning electron microscope and, therefore, the spatial extent and abundance of monazite within the Wairakei reservoir is not known with certainty. However, in all known occurrences monazite is associated with potassic alteration, and monazite is most probably a common, albeit minor, component of the potassic alteration assemblage.

The hydrothermal monazite shown in Figure 3.32 E and F was the only crystal large enough to analyse quantitatively with the electron microprobe. This grain was analysed several times, and ultimately destroyed, while developing a procedure for quantitative analysis of REE-bearing

phases using the electron microprobe (see Appendix 4). Consequently only semi-quantitative data are available. The approximate composition of this Wairakei monazite is $(Ce_{0.4}La_{0.2}Nd_{0.2}Th_{0.1})PO_4$ with significant Si and trace amounts of Sm, Y, and Ca. Numerous other Wairakei monazites from different wells and lithologic units were probed by energy dispersive x-ray analysis, and in each case the above elements were detected. Considering these data, it appears that hydrothermal monazite at Wairakei has a relatively consistent composition.

Biotite

In general, detailed evaluations of the composition and occurrence of trace mineral phases associated with the major alteration assemblages were not completed during the course of this study. But low temperature hydrothermal biotite formed part of the potassic alteration assemblage at Iamalele and Wairakei and, in both cases, the maximum permissible crystallization temperatures were well below those described in the literature. The following discussion deals with the occurrence of low-temperature hydrothermal biotite associated with potassic alteration at relatively high levels within the Wairakei reservoir.

Hydrothermal biotite was identified in thin sections from wells 12, 34, 202, 208 and 226. The distribution of secondary biotite is restricted to the Haparangi Rhyolite and lower Huka Falls Formation in the southeastern portion of the reservoir. Secondary biotite generally occurs at depths varying between 300 and 500 metres, and, based on estimated preproduction reservoir isotherms, must have formed at temperatures ranging from ~160° to ~212°C. These temperatures are slightly lower than the maximum temperatures (225° to 250°C) predicted for the above depths from the hydrostatic liquid-vapour curve (see Appendix 7), but it is considered unlikely that hydrothermal biotite formed at temperatures much above 215°C.

Hydrothermal biotite is strongly pleochroic (brown-colourless to greenish brown-very pale greenish brown) and occurs as shreddy aggregates or radiating clusters of fine (<0.5 mm) prismatic crystals typically replacing groundmass minerals and glass. When present, hornblende and pyroxene (hypersthene?) are partially replaced by shreddy biotite. Most secondary biotite crystals are too small to allow one to obtain reliable interference figures and, therefore, optical identification was based on the mineral's habit, texture and strong pleochroism. None of the secondary biotite crystals showed signs of retrograde alteration.

Microprobe data were determined for hydrothermal biotite in only one thin section (125324) of Haparangi Rhyolite (Table 3.2). The analysis indicates aluminium-deficient fluorphlogopite. Since there is only a single analysis it is unclear whether the reported composition is representative of all of the low-temperature hydrothermal biotite at Wairakei. But considering that the analysed sample revealed no sign of retrograde alteration and that it is petrographically indistinguishable from secondary biotite crystals in the other thin sections, it is unlikely that major compo-

Table 3.2. Microprobe analysis (wt %) of hydrothermal biotite replacing groundmass microlites and glass in Haparangi Rhyolite. Sample 125324 collected at a depth of 445 m in well 12

SiO_2	TiO_2	Al_2O_3	FeO*	MnO	MgO	CaO	Na_2O	K_2O	F	Cl	Total
41.98	1.98	10.72	8.69	0.25	21.08	0.01	0.55	8.97	4.51	0.22	98.95

Cations based on 22 oxygen equivalents

Z			Y				X		
Si	Al^{IV}	Ti^{IV}	Ti^{VI}	Fe^{2+}	Mn	Mg	Ca	Na	K
6.114	1.840	0.046	0.171	1.058	0.030	4.576	0.001	0.156	1.667

F	Cl	Total			
2.540	0.055	18.254	Z	8.000	Mg/(Mg+Fe): 0.81
			Y	5.835	
			X	1.824	

Total iron reported as FeO*. The reported analysis represents an average of 5 spot analyses by electron microprobe of a single biotite grain.

sitional differences exist within the suite of hydrothermal biotites at Wairakei.

Chemical analyses of biotite collected from major "fossil" hydrothermal systems, mainly porphyry copper and porphyry molybdenum deposits, indicate that hydrothermal biotite is characteristically enriched in magnesium and fluorine when compared to associated magmatic biotite. In general, hydrothermal biotite is phlogopitic (Mg/(Mg+Fe) > 0.67) (Moore and Czmanske, 1973; Roberts, 1973; Bean, 1974; Jacobs and Parry, 1976) and has a moderately low titanium content, the abundance of titanium decreasing with decreasing biotite crystallization temperatures (Brimhall, 1977; Bean, 1982; Dilles, 1983). Hydrothermal biotite is further characterized by a trend toward increasing fluorine abundance with increasing Mg/(Mg+Fe) ratio (Munoz, 1984).

Munoz (1984) describes three parameters for evaluating fluorine enrichment in biotite. These are the fluorine intercept value $IV(F)_{bio}$, the chlorine intercept value $IV(Cl)_{bio}$ and the F/Cl intercept value $IV(F/Cl)_{bio}$. Representative ranges for these parameters for samples collected from several porphyry copper and porphyry molybdenum deposits, three active geothermal systems and four unaltered igneous rocks are shown in Table 3.3. Fluorine enrichment in biotite is characterized by lower

Table 3.3. Representative fluorine, chlorine and F/Cl values for hydrothermal biotite from selected mineral deposits and active geothermal areas, and for magmatic biotite from selected unaltered igneous rocks

Sample Type	$IV(F)_{bio}$	$-IV(Cl)_{bio}$	$IV(F/Cl)_{bio}$
Wairakei	1.05	5.17	6.22
Active Geothermal	0.98--2.54	4.09--4.45	6.20--6.52
Porphyry Copper	1.47--2.82	4.02--4.64	6.03--6.80
Porphyry Molybdenum	0.68--1.69	3.81--4.07	4.67--5.60
Unaltered Igneous	1.47--2.30	3.37--3.90	4.83--6.17

All of the data except that for Wairakei are from Munoz (1984), pages 481 and 482.

$IV(F)_{bio}$ and $IV(F/Cl)_{bio}$ values and less negative $IV(Cl)_{bio}$ values. The fluorine and F/Cl intercept values for Wairakei biotite are generally within the ranges given for the hydrothermal biotites (Table 3.3). However, the chlorine intercept values given for hydrothermal biotite are much lower than the Wairakei data. This probably reflects a lower chlorine content in the hydrothermal biotite from Wairakei than in hydrothermal biotite reported by Munoz (1984). The Wairakei data for each of the parameters fall outside the ranges given for the igneous biotites.

Considering the fluorine content of the geothermal fluid at Wairakei (see Table 3.4), the occurrence of fluorine-rich hydrothermal phlogopite is not surprising. However, the abundance of magnesium in the fluorphlogopite is somewhat unexpected because of the relatively low activity of Mg^{2+} within the reservoir fluid (see Table 3.8). Apparently Mg is strongly partitioned from fluid into the structure of hydrothermal biotite. The significance of the very low Al_2O_3 content of the Wairakei hydrothermal biotite cannot be evaluated without additional data. However, it appears that the tetrahedral vacancies resulting from insufficient Al^{3+} are adequately filled by Ti^{3+}, even though the titanium content of the Wairakei fluorphlogopite is similar to the titanium content of hydrothermal biotite from the Yerington and Ann Mason porphyry copper deposits which have "normal" Al_2O_3 contents (Dilles, 1983).

The formula for hydrothermal fluorphlogopite calculated from the microprobe analysis given in Table 3.3 is:

$$(K,Na,Ca)_{1.9}(Mg,Fe^{2+},Ti,Mn)_{5.8}[Si_{6.1}(Al,Ti)_{1.9}O_{22}](F_{2.5},Cl_{0.8},OH_{0.9}),$$

assuming that F, Cl and OH sum to 4.0.

Zircon

Hydrothermal zircon was identified in several thin sections (Fig. 3.18 B-E) where it appears to be part of the potassic alteration assemblage. Zircon generally occurs intergrown with chlorapatite, anatase and

Figure 3.15. Textures and mineral assemblages characteristic of potassic alteration; back scatter electron images. Photographic plates for Figure 3.15 are in the pocket at the back of Volume I.

A. Incipient replacement of an andesine (pl, medium grey) microphenocryst by adularia (ad, dark grey) and pyrite (py, white). Irregular white area at the upper right of the plagioclase grain is pyrite as are most of the small white spots in the groundmass. Microstringers and irregular replacement of plagioclase along cleavage planes and fractures by adularia ± pyrite is typical of the early stages of adularia (potassic) alteration; core sample 125736, well 211, 274 m, Haparangi Rhyolite.

B. Incipient replacement of andesine (pl, light grey) microphenocryst by adularia (ad, very light grey), grothite (gr, white) and apatite (ap, white). Note phenocryst overgrowths consisting of intergrown adularia and grothite. Surface texture to grain is the result of incomplete polishing. Polished areas in the groundmass are quartz (medium grey) intergrown with minor grothite (very light grey) and pyrite (white, lower left of plagioclase grain); core sample 125193, well 54, 733 m, Wairakei Ignimbrite 2.

C. Quartz (qz, dark grey, well polished) with trace chlorapatite (ap, white) microstringer with an inner envelope of illite (il, dark grey, textured) and an outer envelope of adularia (ad, light grey). Note euhedral crystal (rhombohedral) form of adularia; core sample 125719, well 216, 412 m, Haparangi Rhyolite.

D. Equilibrium intergrowth of quartz (qz, dark grey), adularia (ad, medium grey), grothite (white) and illite (il, dark grey, textured). This assemblage is characteristic of potassic alteration. Note rhombohedral crystal form of adularia, both in quartz and adjacent grothite. Holes in adularia result from crystal fragments removed during polishing; core sample 125719, well 216, 412 m, Haparangi Rhyolite.

E. Pervasive potassic alteration consisting of adularia (ad, white), quartz (qz, medium grey) and grothite (not visible). The quartz vein contains adularia, grothite and minor pyrite (white spots). Much of the quartz vein was removed during polishing; core sample 125708, well 17, 189 m, Huka Falls Formation rhyolite pumice breccia.

F. Magnified view of the area outlined in A. Grothite (gr, white) is now visible. Note the well-developed rhombohedral form of adularia.

G. Quartz (qz, medium grey) vein containing minor grothite, adularia and pyrite (very light grey to white spots). The vein has a narrow envelope of intergrown quartz, adularia (ad, white) and grothite (gr, white) adjacent to the vein which grades outward into pervasive disseminated alteration; core sample 125708, well 17, 189 m, Huka Falls Formation rhyolite pumice breccia.

H. Early propylitic alteration indicated by partial replacement of andesine (pl, dark grey) by quartz (qz, very dark grey) and pericline (ab, very dark grey) microveins and partial replacement of an amphibole(?) and adjacent andesine (pl, dark grey) grain by clinochlore (chl, medium grey veins), calcite (cal, light grey) and pyrite (white). Late potassic alteration identified by the replacement of pericline by adularia (ad, light grey) and andesine by adularia and grothite (gr, very light grey); core sample 125265, well 121, 1090 m, Wairakei Ignimbrite 2.

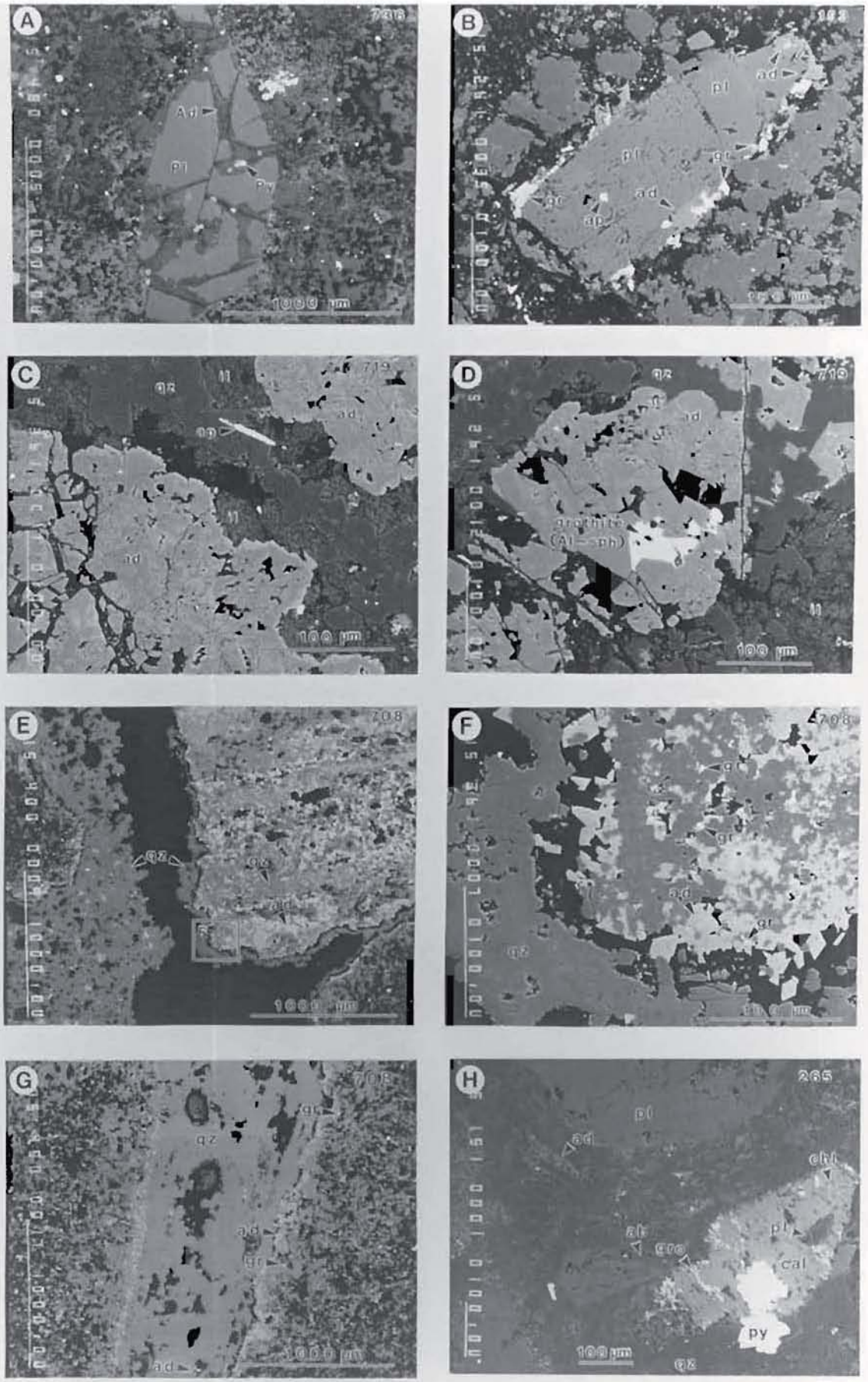
A
Ad
Pl
Py
1000 µm
B
pl
ad
gr
qz
ap
C
qz
ad
gr
100 µm
D
qz
ad
graphite
(Al – rich)
100 µm
E
qz
ad
F
F2
1000 µm
F
qz
gr
ad
qz
G
qz
qz
ad
gr
ad
1000 µm
H
pl
gd
chl
pl
zk
gro
cal
py
100 µm
qz

Figure 3.16. Textures and mineral assemblages characteristic of potassic alteration overprinting propylitic alteration; back scatter electron images. Photographic plates for Figure 3.16 are in the pocket at the back of Volume I.

A. Andesine phenocryst initially replaced by pericline (ab, dark grey). Pericline and andesine(?) almost totally replaced by adularia (ad, medium grey), grothite (gr, light grey irregular patches and veins) and pyrite (py, white). Groundmass replaced by quartz (qz, black), pericline, adularia, grothite and pyrite; core sample 125126, well 48, 582 m, Waiora Valley Andesite.

B. Magnified view of the area outlined in A. Note replacement of pericline (ab, black) by grothite (gr, light grey) and euhedral outline of adularia crystals around the perimeter of the grothite crystal at the bottom of the photograph. However, the irregular outline of the upper edge of the larger grothite crystal may indicate that grothite is replacing adularia. White spots within grothite are pyrite grains. Dark spot surrounding a small pyrite grain in the larger grothite crystal is the result of damage done to the crystal by the electron beam.

C. Andesine phenocryst in rhyolite pumice breccia replaced by the potassic alteration equilibrium assemblage grothite (gr, light grey)-quartz (qz, black)-adularia (ad, dark grey)-pyrite (py, white). Groundmass replaced by pericline (ab, black) and adularia documenting an earlier period of propylitic alteration; core sample 125708, well 17, 189 m, Huka Falls Formation rhyolite pumice breccia.

D. Near total replacement of the groundmass of the rhyolite pumice breccia is the result of potassic alteration superimposed on propylitic alteration. Propylitic alteration is indicated by the irregular intergrowths (equilibrium crystallization) of pericline (ab, dark grey) and adularia (ad, light grey), and potassic alteration is indicated by the occurrence of grothite (gr, white) intergrown with adularia. Note the occurrence of the relatively unaltered andesine (pl, medium grey) crystal fragment; core sample 125708, well 17, 189 m, Huka Falls Formation rhyolite pumice breccia.

E. Chlorite alteration of an amphibole phenocryst is probably related to early propylitic alteration; voids within the phenocryst were probably occupied by calcite which was eroded during polishing. The fuzzy nature of the groundmass results from abundant spherulitic adularia (a relatively rare texture). Groundmass adularia is intergrown with grothite (gr, light grey) and minor chlorapatite (not marked). Note grothite replacing an ilmenite (ilm, white) crystal. Andesine phenocrysts (pl, medium grey) are relatively unaltered; core sample 125193, well 54, 733 m, Wairakei Ignimbrite 2.

F. Magnified view of the area outlined in E. Note intergrown grothite (gr) and chlorapatite (ap). Andesine fragments (pl) are relatively unaltered.

G. Radiating acicular crystals of adularia (ad, light grey spherulites) intergrown with grothite (gr, very light grey). Adularia spherulites locally contain analcime (ac, medium grey) cores. Analcime is a comparatively rare (propylitic?) alteration mineral. Note magnetite (mt, white) and clinochlore (chl, medium grey fibrous veins) replacing a mafic (pyroxene?) microphenocryst; core sample 125193, well 54, 733 m, Wairakei Ignimbrite 2.

H. Very fine-grained adularia (ad, light grey) and barite (ba, white) replacing tuffaceous siltstone. Barite locally forms irregular and discontinuous veins comprised of individual barite crystals; core sample 125714, well 216, 183 m, Huka Falls Formation.

Figure 3.17. Textures and mineral assemblages characteristic of magnetite-destructive (potassic) alteration; back scatter electron images. Photographic plates for Figure 3.17 are in the pocket at the back of Volume I.

A. Amphibole phenocryst totally replaced by clinochlore (chl, thin medium grey "veins"), calcite (cal, medium grey), magnetite (mt, white)-ilmenite (ilm, white) and pyrite (py, white); calcite may postdate clinochlore. Groundmass replaced by the propylitic alteration assemblage quartz (qz, black)-pericline (ab, dark grey)-adularia (ad, light grey). For a description of post propylitic alteration see text for photographs B and C; core sample 125265, well 121, 1090 m, Wairakei Ignimbrite 2.

B. Magnified view of the area outlined in A. Hydrothermal magnetite (mt, white), ilmenite (ilm, white), clinochlore (chl, medium grey "veins"), calcite (cal, medium grey) and rare pyrite (py, white) replaced by grothite (gr, medium grey), chlorapatite (ap, medium grey with "high" relief) and anatase (at, light grey).

C. Magnified view of the area outlined in B. Ilmenite (ilm, white) replaced by grothite (gr, medium grey) and anatase (at, light grey). Note irregular grothite stringers which host micron-sized galena (gl, white) and cassiterite (cs, white) grains. Grothite also replaces chlorite and calcite indicating a relatively late (low-temperature) phase of titanite stability.

D. Hydrothermal(?) magnetite grain partially replaced by the assemblage grothite (gr, medium grey)-apatite (ap, medium grey with "high" relief)-anatase (at, light grey); core sample 125265, well 121, 1090 m, Wairakei Ignimbrite 2.

E. Magnetite (mt, white) crystal partially replaced by chlorapatite (ap, medium grey); note pronounced cleavage in magnetite, and that magnetite adjacent to the cleavage plane resists alteration. Groundmass altered to quartz and adularia (not shown) ; core sample 125193, well 54, 733 m, Wairakei Ignimbrite 2.

F. Grothite (gr, medium grey) and chlorapatite (ap, medium grey with "high" relief) replacing magnetite (mt, white) in andesine phenocryst hosted by pumiceous tuff breccia. Note adularia replacing andesine parallel to twinning; core sample 125709, well 17, 213 m, Member 5 of the Waiora Formation.

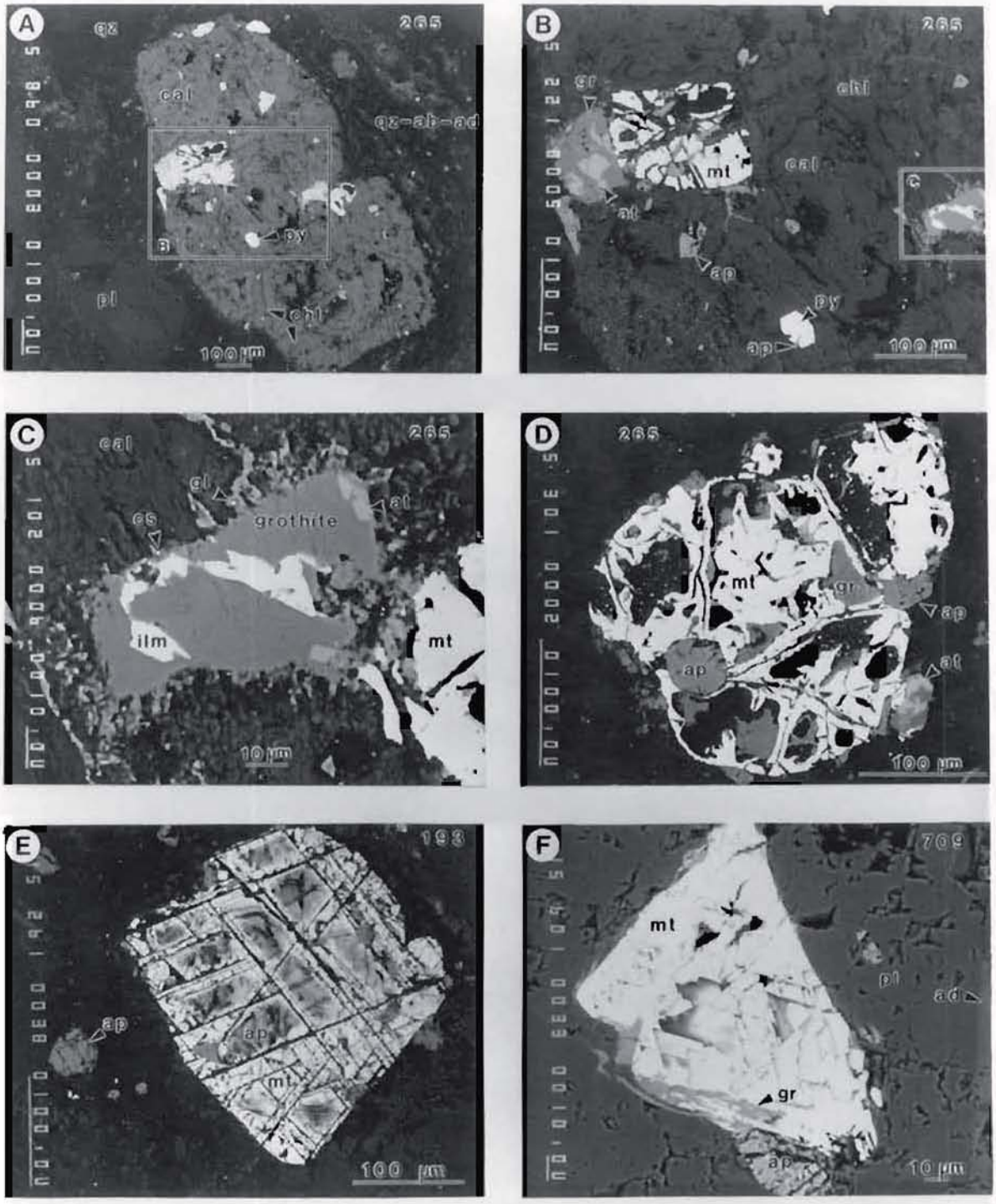

Figure 3.18. Textures and mineral assemblages characteristic of zircon (potassic) alteration; back scatter electron images. Photographic plates for Figure 3.18 are in the pocket at the back of Volume I.

A. Chlorapatite (ap, light to medium grey) alteration of hydrothermal magnetite (mt, white) associated with adularia (ad, dark grey) alteration of the groundmass of quartz-rich ignimbrite. Bulk rock alteration includes hydrothermal zircon and the replacement of grothite by ilmenite (not shown). Textured appearance of the groundmass is the result of an inadequately polished surface; core sample 125193, well 54, 733 m, Wairakei Ignimbrite 2.

B. Hydrothermal apatite and zircon replacing magnetite (?) in flow-banded rhyolite. Pseudohexagonal pattern adjacent to the zircon is ilmenite (ilm, light grey) and quartz (dark grey) replacing an amphibole phenocryst. Groundmass is altered to adularia (ad, medium dark grey) and quartz (qz, dark grey). Hydrothermal zircon is (locally) part of the potassic alteration assemblage, and is typically associated with abundant pyrite; core sample 125738, well 211, 396 m, Haparangi Rhyolite.

C. Mafic phenocryst in flow-banded rhyolite replaced by an outer zone of intergrown zircon (zr, white) and anatase (at, light grey), and an inner zone of chlorapatite (ap, medium grey). Plagioclase phenocrysts (pl, dark grey) are replaced by pericline (ab, dark grey), adularia (ad, light grey) and pyrite (py, white); core sample 125738, well 211, 396 m, Haparangi Rhyolite.

D. Groundmass of amphibole-bearing andesite replaced by equilibrium assemblage zircon (zr, white)-pyrite (py, white)-chlorapatite (ap, medium grey)-adularia (ad, dark grey)-quartz (qz, black). Large amphibole phenocryst replaced by intergrown grothite (gr, medium grey; pseudohexagonal pattern), quartz (black with smooth texture), chlorapatite, zircon and pyrite; core sample 125126, well 48, 582 m, Waiora Valley Andesite.

E. Pyrite inclusion in a hydrothermal zircon crystal; core sample 125193, well 54, 733 m, Wairakei Ignimbrite 2.

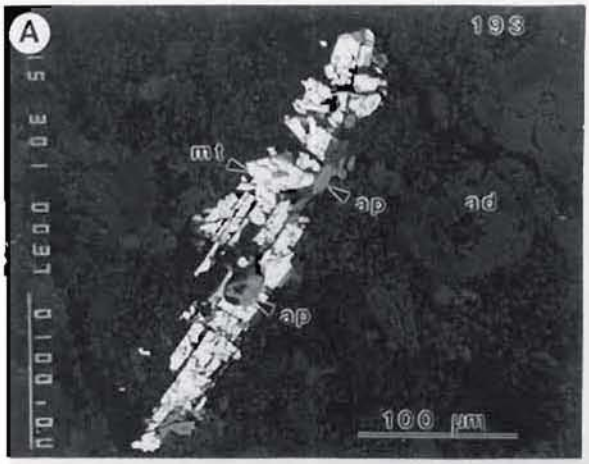

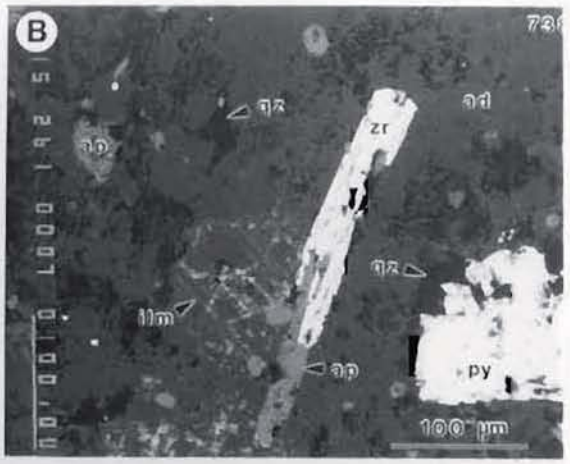

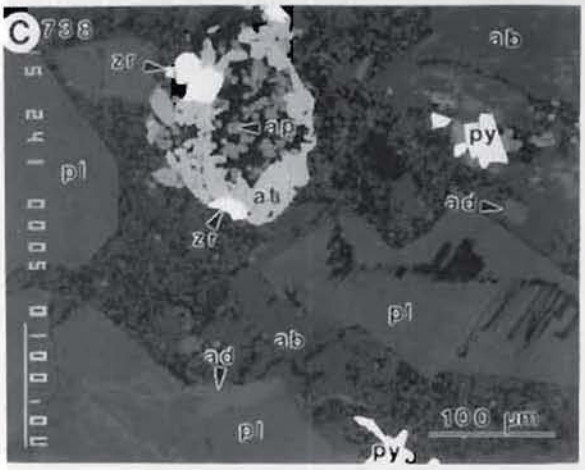

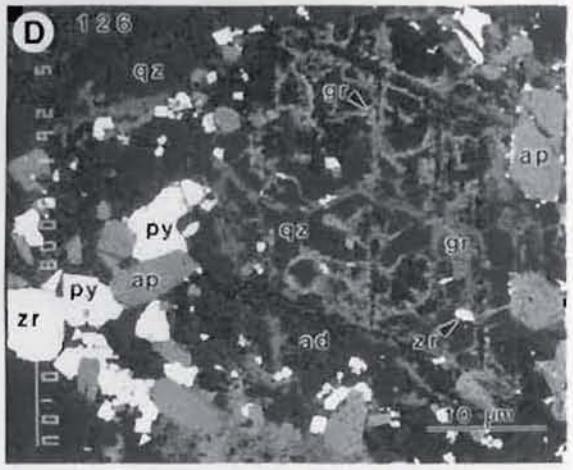

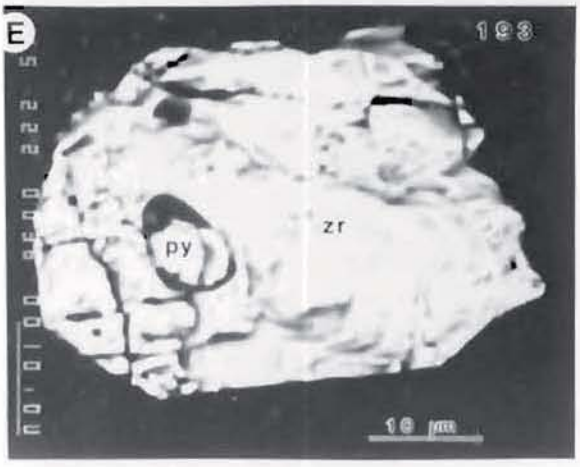

pyrite. Locally grothite and adularia are also intergrown with zircon, chlorapatite and pyrite (Fig. 3.18D). Because hydrothermal zircon crystals are generally less than 30 microns in maximum dimension, zircon was only positively identified with the electron microprobe. Consequently the spatial distribution and details of its occurrence were not determined.

Textural Relationships

In areas of incipient or weak potassic alteration, adularia characteristically replaces only the groundmass of the rock and perhaps the edges of tuffaceous rock fragments. As the intensity of potassic alteration increases, adularia selectively replaces plagioclase phenocrysts along cleavage and fracture planes, and may occur as "overgrowths" irregularly dispersed along crystal edges or as microveinlets within and adjacent to the crystal. Where potassic alteration is intense, plagioclase is totally replaced by adularia, and rock fragments and the groundmass are strongly replaced by fine- to relatively coarse-grained mosaics of adularia and quartz. The abundances of grothite and "white mica" also generally, but not always, increase as the abundances of quartz and adularia increase.

Potassic alteration exhibits numerous textural relationships, particularly at the scale required to identify the alteration minerals conclusively. Several of the more common rock and mineral textures, and a few of the less common or at least less well-known rock alteration textures are illustrated in Figures 3.15 through 3.18. These figures show the textures and equilibrium mineral assemblages which characterize potassic alteration in general (Figs. 3.15 and 3.16) and address some of the interesting but subtle aspects of potassic alteration such as magnetite destructive and apatite-zircon alteration (Figs. 3.17 and 3.18). Although the figures illustrate some very interesting "micro" chemical environments, these features have very little apparent effect on major alteration assemblages or the deposition of precious and base metals.

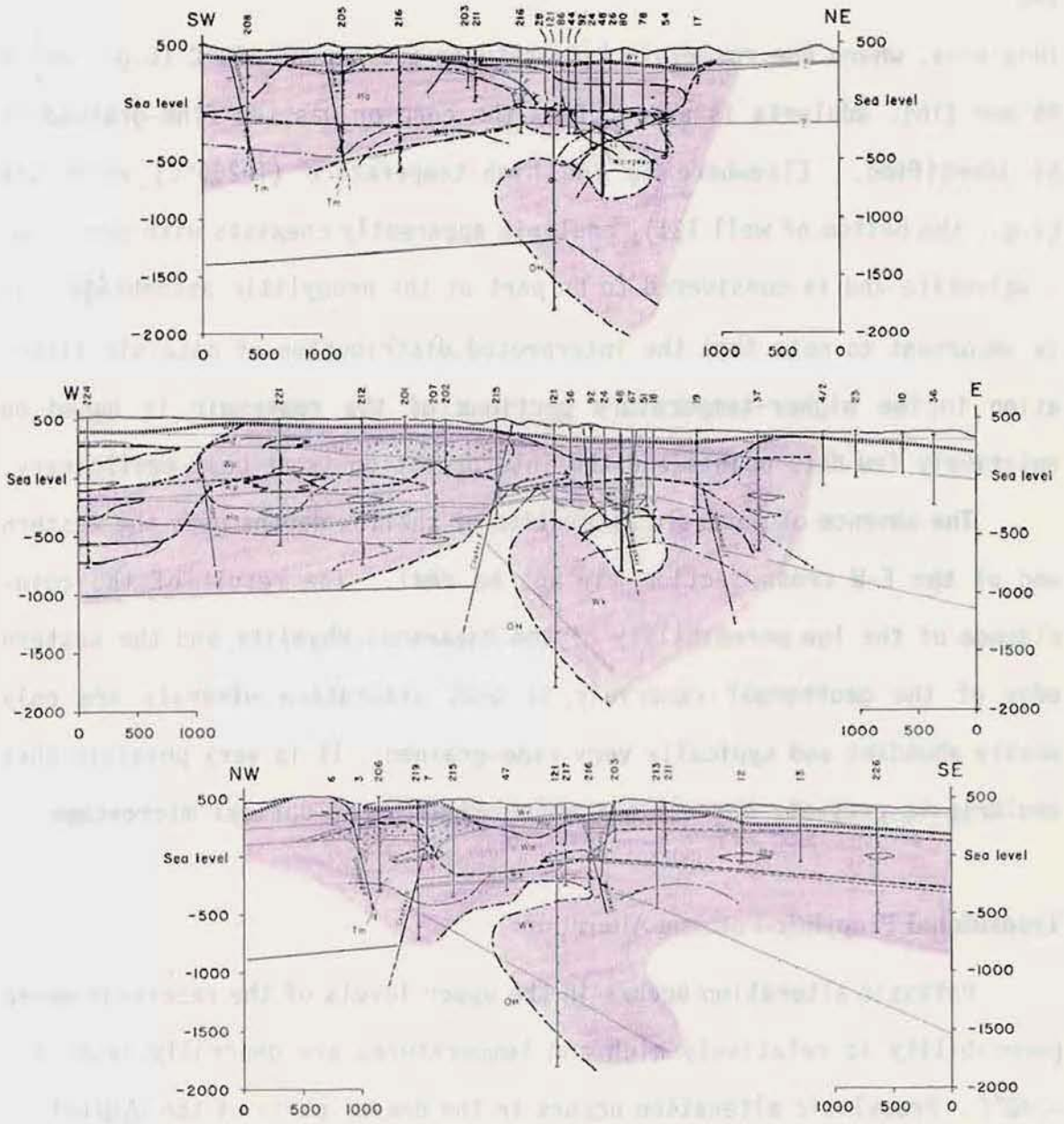

Figure 3.19. Spatial distribution of potassic alteration within the Wairakei hydrothermal reservoir. The distribution of potassic alteration is shown in purple. See Figure 3.11 for location of the cross sections.

Spatial Distribution

Potassic alteration occurs throughout most of the Wairakei reservoir. In general, the intensity of potassic alteration is much lower in the Wairakei Ignimbrite and Huka Falls Formation than in the Waiora Formation, a fact which probably reflects the lower permeability of the former units. It is apparent from Figure 3.19 that potassic alteration has not occurred in the central portion of the high-temperature (T≥250°C) reservoir. Within

this area, where the reservoir temperatures are around 250°C (e.g., wells 48 and 216), adularia is absent from the core or was too fine-grained to be identified. Elsewhere in the high-temperature (T≥260°C) reservoir (e.g., the bottom of well 121), adularia apparently coexists with pericline ± wairakite and is considered to be part of the propylitic assemblage. It is important to note that the interpreted distribution of potassic alteration in the higher-temperature portions of the reservoir is based on relatively few data points and the interpretation is at best preliminary.

The absence of potassic alteration at shallow depths near the western end of the E-W cross section may not be real. The result of the coincidence of the low permeability of the Haparangi Rhyolite and the western edge of the geothermal reservoir is that alteration minerals are only weakly abundant and typically very fine-grained. It is very possible that adularia is present, but was not observed with the optical microscope.

Transitional Propylitic-Potassic Alteration

Potassic alteration occurs in the upper levels of the reservoir where permeability is relatively high and temperatures are generally less than ~240°C. Propylitic alteration occurs in the deeper parts of the hydrothermal system where temperatures are high, typically greater than 240°C, and permeability varies from high (Waiora Formation) to relatively low (Wairakei Ignimbrite). Over a wide portion of the reservoir the areas of influence of potassic and propylitic alteration overlap, resulting in "transitional propylitic-potassic alteration" (Fig. 3.20). In the cooler peripheral parts of the reservoir ("low-temperature" transitional propylitic-potassic alteration) the most consistent feldspar paragenesis is the replacement of plagioclase by pericline ± adularia followed by the replacement of pericline and remnant plagioclase by adularia. This paragenetic sequence is apparently related to general decline in reservoir temperature, presumably reflecting the initial stage of reservoir collapse.

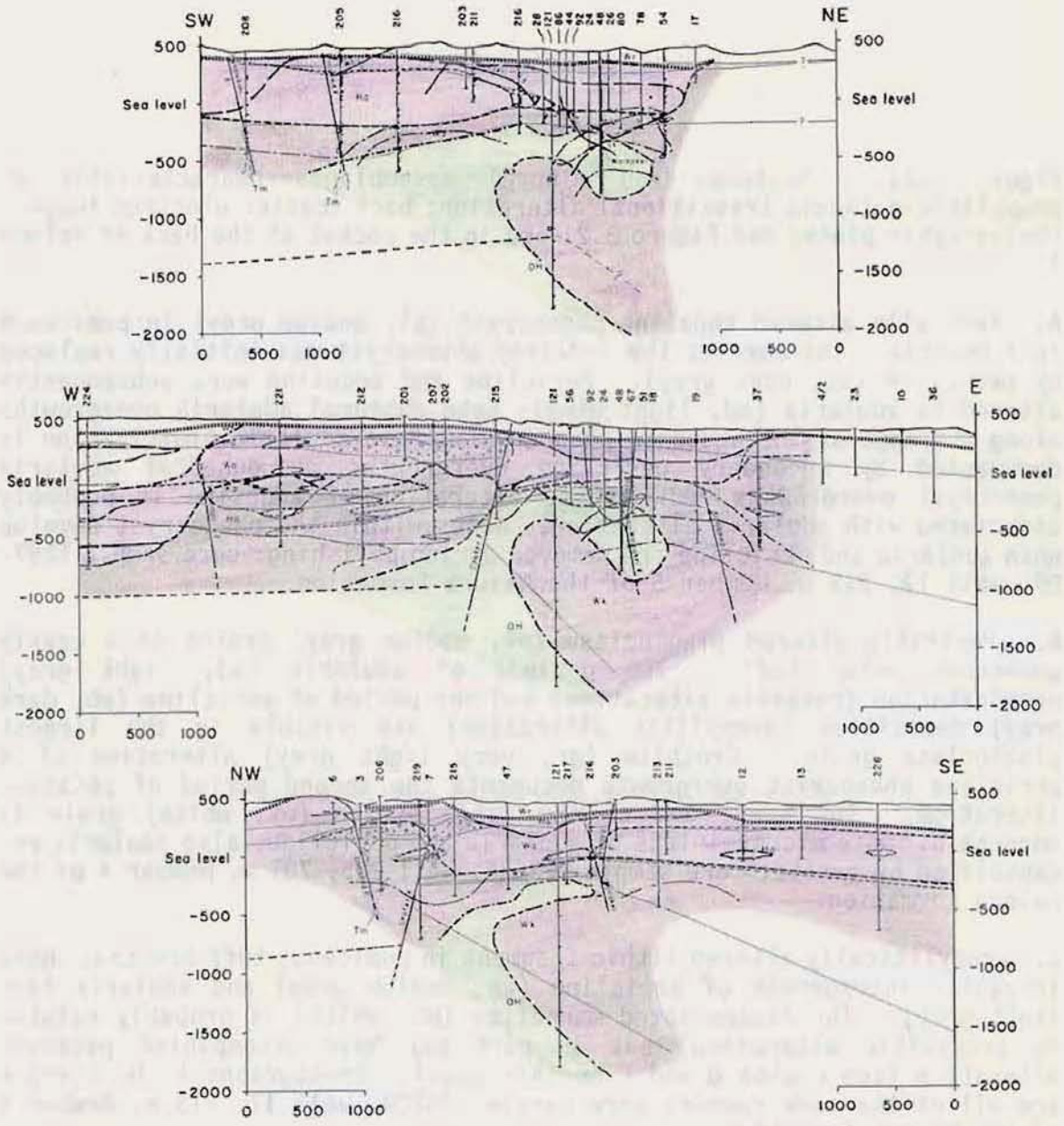

Figure 3.20. Spatial distribution of transitional propylitic-potassic alteration within the Wairakei hydrothermal reservoir. The distribution of propylitic alteration is shown in green and the distribution of potassic alteration is shown in purple. See Figure 3.11 for location of the cross sections.

Transitional propylitic-potassic alteration also occurs within the main high-temperature upflow zone for the reservoir; compare Figures 3.10 and 3.20. Rocks collected from this part of the reservoir have relatively complex textures which indicate that potassic alteration is locally overprinted by propylitic alteration. Further, feldspar alteration appears to have oscillated between pericline and adularia, i.e., adularia replaces and

Figure 3.21. Textures and mineral assemblages characteristic of transitional propylitic-potassic alteration; back scatter electron images. Photographic plates for Figure 3.21 are in the pocket at the back of Volume I.

A. Partially altered andesine phenocryst (pl, medium grey) in pumiceous tuff breccia. The core of the andesine phenocryst was initially replaced by pericline (ab, dark grey). Pericline and andesine were subsequently altered to adularia (ad, light grey); note euhedral adularia overgrowths along the edge of the andesine phenocryst. Post-adularia albitization is documented by secondary pericline overgrowths on euhedral adularia phenocryst overgrowths. Magnetite alteration of andesine is probably associated with adularia alteration. Holes within the phenocryst develop when adularia and pericline are removed during polishing; core sample 1257-09, well 17, 213 m, Member 5 of the Waiora Formation.

B. Partially altered plagioclase (pl, medium grey) grains in a weakly pumiceous silty tuff. Two periods of adularia (ad, light grey) precipitation (potassic alteration) and one period of pericline (ab, dark grey) deposition (propylitic alteration) are visible in the largest plagioclase grain. Grothite (gr, very light grey) alteration of a pericline phenocryst overgrowth documents the second period of potassic alteration. The exact age of the large pyrite (py, white) grain is uncertain. Note microveinlets of adularia and pericline, also adularia encapsulated by pyrite; core sample 125626, well 205, 701 m, Member 4 of the Waiora Formation.

C. Propylitically altered lithic fragment in pumiceous tuff breccia. Note irregular intergrowth of pericline (ab, medium grey) and adularia (ad, light grey). The disseminated magnetite (mt, white) is probably related to propylitic alteration, but in part may have accompanied potassic alteration (see photos D and F on this page). Photographs A, D, E and F are all of the same sample; core sample 125709, well 17, 213 m, Member 4 of the Waiora Formation.

D. Partially altered andesine phenocryst in pumiceous tuff breccia. See photographs E and F for alteration details; core sample 125709, well 17, 213 m, Member 4 of the Waiora Formation.

E. Magnified view of the area outlined in D. The right half of the andesine phenocryst was strongly replaced by pericline (ab, dark grey) ± adularia (ad, light grey). Pericline is partially altered to adularia. Note pericline overgrowths on adularia and the very thin magnetite (mt, white)-adularia veinlet which, in part, trends parallel to a twin plane.

F. Magnified view of the area outlined in D. Note: (1) adularia (ad, light grey) overgrowth on andesine (pl, medium grey; lower left portion of the photograph), (2) pericline (ad, dark grey) overgrowth on adularia (upper right corner of the photograph) and (3) irregular adularia-magnetite (mt, white) microstringers.

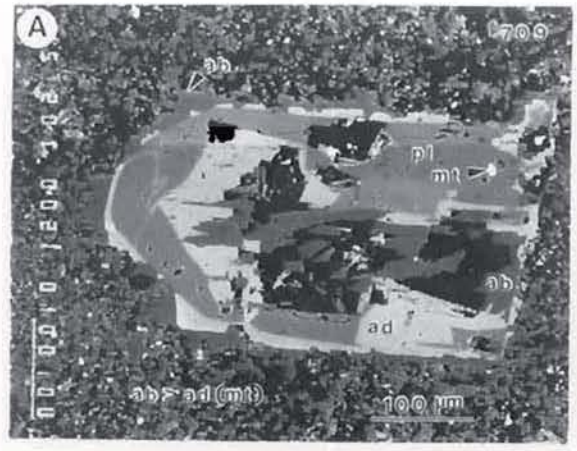

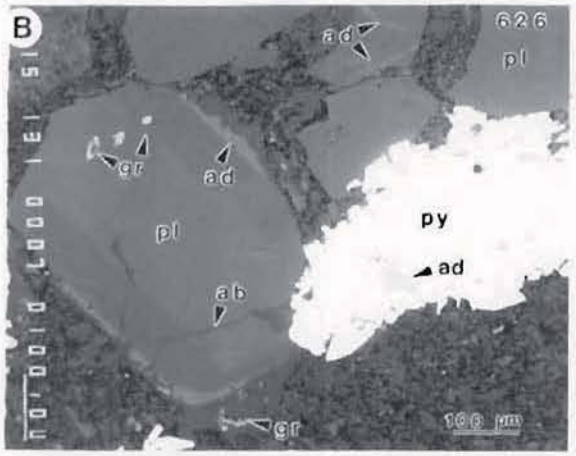

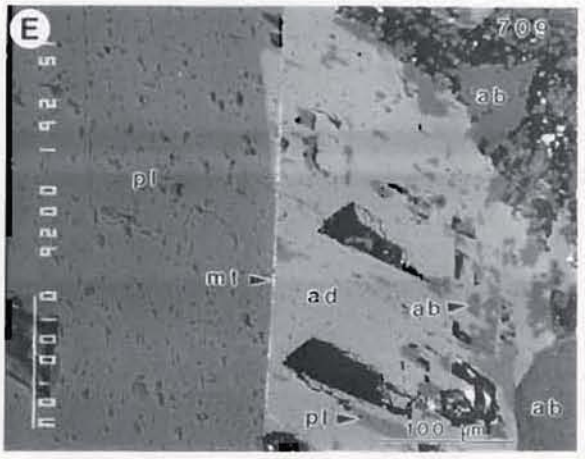

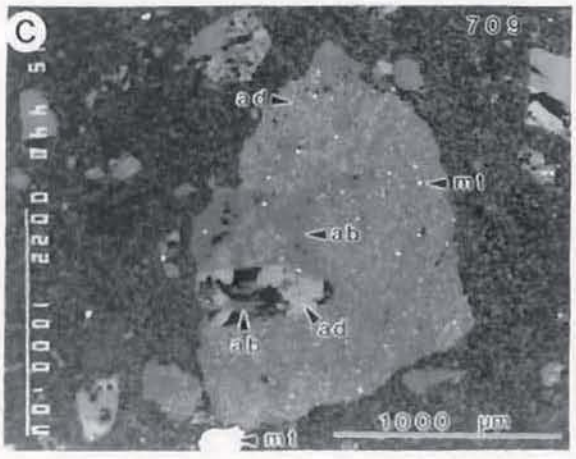

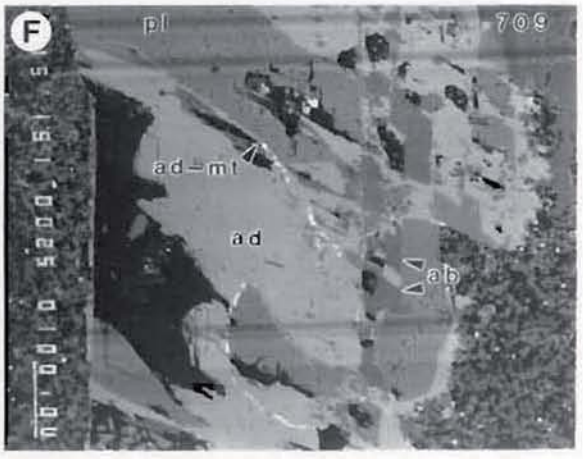

Figure 3.22. Textures and mineral assemblages characteristic of oxidized and reduced environments within potassic and transitional propylitic-potassic alteration; back scatter electron images. Photographic plates for Figure 3.22 are in the pocket at the back of Volume I.

A. Lithic fragment in pumiceous tuff breccia totally replaced by intergrown pericline (ab, dark grey), adularia (ad, light grey) and magnetite (mt, white). These minerals probably crystallized in equilibrium, but elsewhere in the sample pericline is clearly replaced by adularia. The groundmass is replaced by pericline (dominant) and adularia. The textured appearance of the groundmass is the result of an insufficiently polished surface; core sample 125709, well 17, 213 m, Member 5 of the Waiora Formation.

B. Andesine phenocryst (pl, medium grey) in pumiceous tuff breccia partially replaced by pericline (ab, dark grey) and adularia (ad, light grey); light streaks in plagioclase (right centre of phenocryst) are grothite (gr, light grey). Large grothite grain within the phenocryst is partially replaced by ilmenite; core sample 125709, well 17, 213 m, Member 5 of the Waiora Formation.

C. Andesine phenocryst (pl, medium grey) in pumiceous tuff breccia partially replaced by adularia (ad, light medium grey), magnetite (mt, white), grothite (gr, light grey) and chlorapatite (ap, very light grey); adularia is locally overgrown by pericline (ab, dark grey). Feldspar fragments contained within the holes in the phenocryst are composed of a mixture of andesine and adularia; core sample 125709, well 17, 213 m, Member 5 of the Waiora Formation.

D. Magnified view of the area outlined in C. Note the apparent equilibrium intergrowth of magnetite (mt) and chlorapatite (ap), see description of photograph E. Adularia (ad) microstringers surround the magnetite crystal enclosed in the box.

E. Magnified view of the area outlined in D. Although magnetite and grothite appear to be in equilibrium in photograph D, grothite (gr, medium grey) is replacing magnetite (mt, white); note (1) the irregular and rounded habit, (2) the obvious octahedral crystal lattice and (3) the abundance of grothite inclusions within the magnetite crystal. Adularia (ad, light grey) microstringers are now obvious.

F. Replacement of grothite (gr, medium grey) by ilmenite (ilm, white) and pyrite (py, white) associated with quartz-adularia alteration of plagioclase and the groundmass (not shown); hydrothermal pyrite and zircon are common in the sample. Reducing conditions may be related to locally abundant organic material entrained in the hydrothermal eruption breccia; core sample 125293, well 206, 308 m, Huka Falls Formation.

G. Hematite alteration of very fine-grained quartz-free rhyolite. Note the hematite microstringers, hematite replacement of biotite phenocrysts and hematite-silica replacement of ilmenite inclusions in the hornblende phenocryst. Groundmass is replaced by quartz (qz, dark grey) and adularia (ad, light grey); core sample 125696, well 218, 398 m, Karapiti Rhyolite.

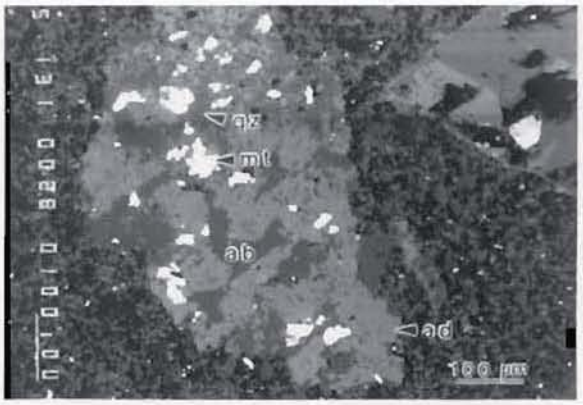

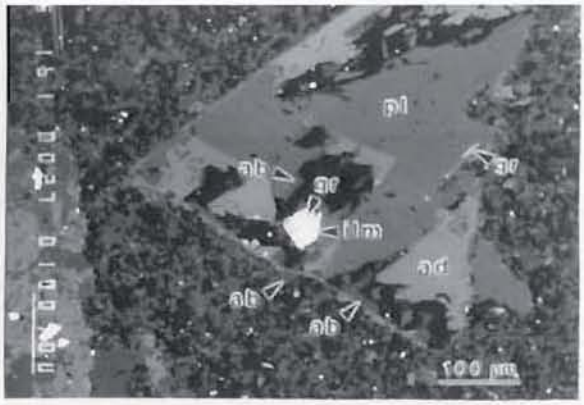

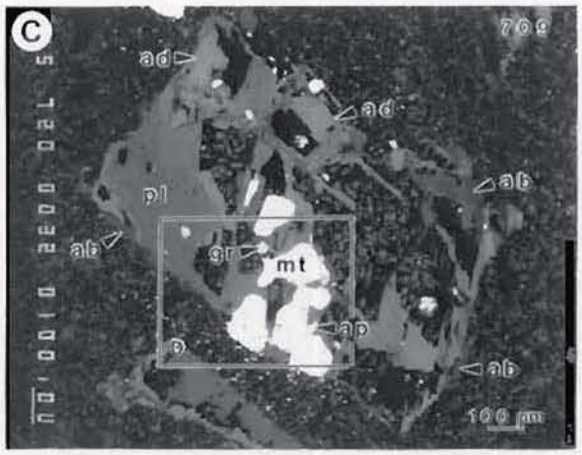

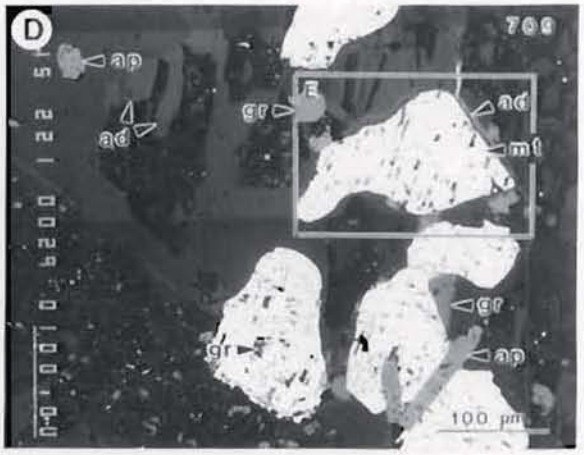

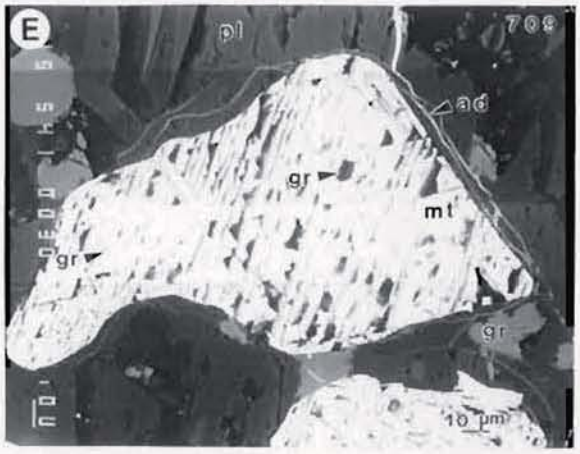

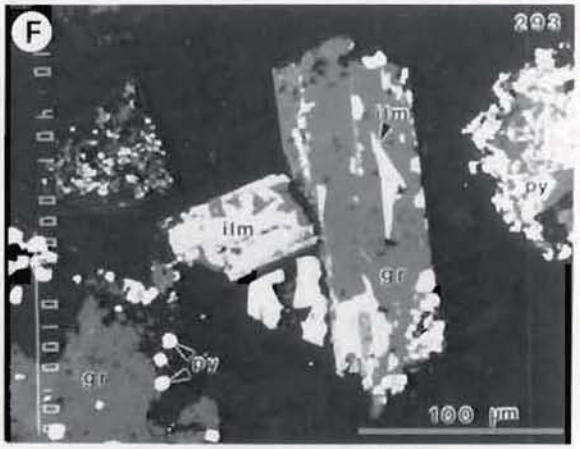

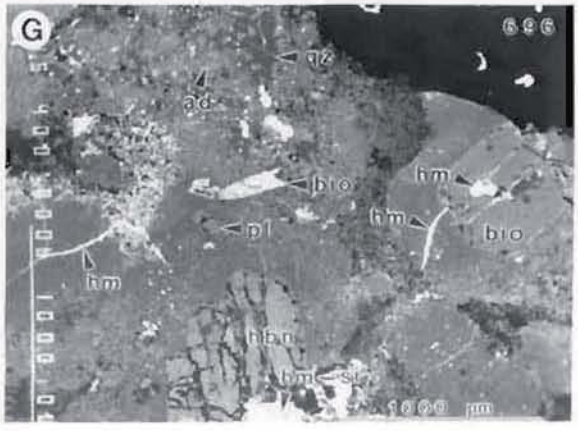

rims pericline and, in turn, is rimmed and replaced by pericline. Several of the more commonly observed rock textures in areas of transitional propylitic-potassic alteration are illustrated in Figures 3.21 and 3.22. The occurrence of "high-temperature" transitional propylitic-potassic alteration must be related to fluctuations in the temperature of the central portion of the reservoir. The effects that small variations in the temperature of the reservoir fluid may have on feldspar stability are discussed in more detail under Fluid-Mineral Equilibria.

Zeolite Alteration

One important aspect of hydrothermal alteration at Wairakei is the diversity and abundance of calcium zeolites. Wairakite, laumontite, mordenite and heulandite are the most abundant zeolites present. The stoichiometric compositions of these phases are shown in relationship to the other common calc-silicate phases in Figure 3.23. Mahon (1966) has shown that the silica content of the Wairakei hydrothermal fluid remains near quartz saturation regardless of the prevailing temperature, and it can be seen from Figure 3.23b that crystallization of the Ca-zeolites is favoured by a hydrothermal fluid which maintains or exceeds quartz saturation.

Since wairakite was discussed with propylitic alteration, only laumontite and mordenite will be discussed below. Heulandite was only identified from x-ray diffraction patterns generated on whole rock samples. Consequently a textural description of the occurrence of heulandite is not available, and there are insufficient x-ray diffraction samples to work out a reliable zoning pattern.

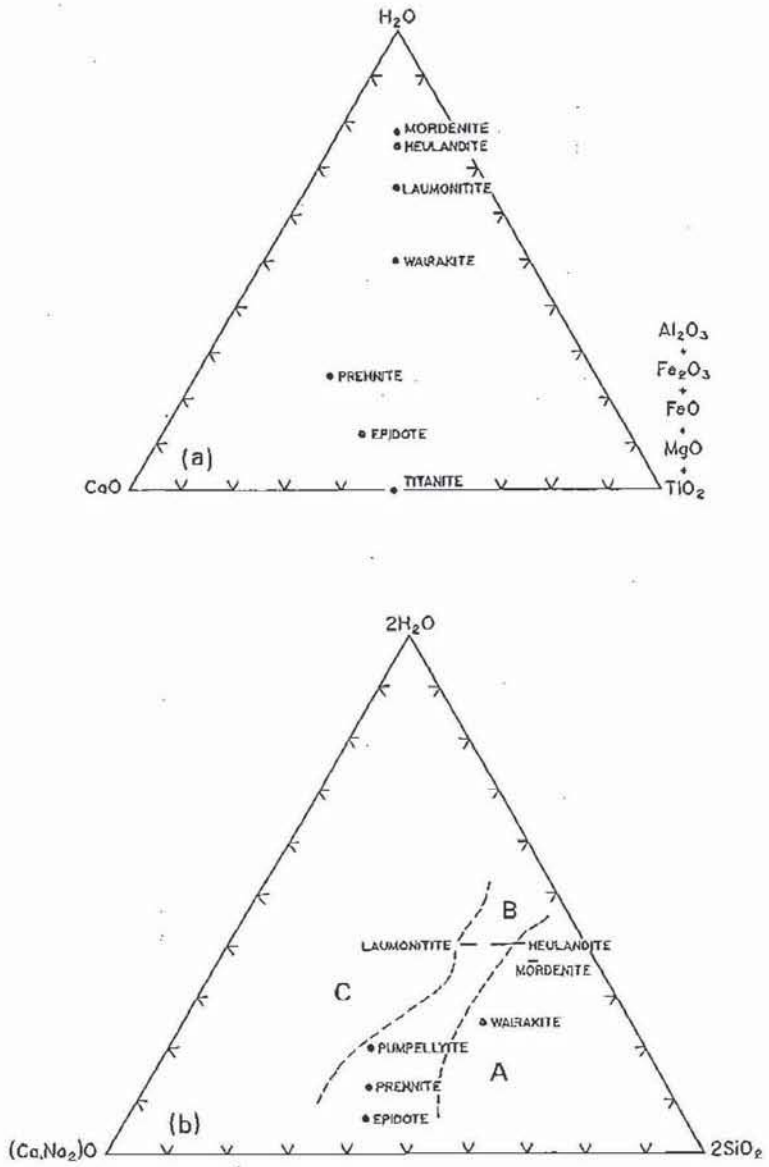

Figure 3.23. Compositions (in mole %) of the calc-silicate phases identified at Wairakei. Fields marked in diagram (b) identify minerals favoured by fluids which are (A) super-saturated, (B) saturated and (C) undersaturated with respect to quartz. Diagrams after Bird et al. (1984) (a) and Coombs et al. (1959) (b).

Alteration Mineral Assemblage and Textural Relationships

Mordenite was observed intergrown with quartz, adularia, clinochlore, pyrite, ilmenite, magnetite and possibly stilbite. The two most characteristic textures of mordenite are spheroidal aggregates of fine acicular crystals and horsetail plumes which form short discontinuous veins. The horsetail texture also occurs within larger through-going mordenite veins (Fig. 3.24A). Mordenite spherulites commonly nucleate on andesine pheno-

Figure 3.24. Textures and mineral assemblages characteristic of zeolite alteration; back scatter electron images. Photographic plates for Figure 3.24 are in the pocket at the back of Volume I.

A. Replacement of the groundmass and andesine phenocrysts (pl) of a vitrophyric quartz-bearing rhyolite by adularia (ad, light grey) and quartz (qz, medium grey). The thin quartz-adularia vein (top of photo, left of centre) is cut by a fibrous mordenite (mord, dark grey) vein with a weakly developed clinochlore (chl, white) envelope. The apparent peripheral quartz-adularia envelope on the mordenite vein is probably a quartz-adularia-lined fracture which reopened during mordenite-chlorite alteration. Very thin adularia stringers with mordenite envelopes (not visible in photo) are also present; core sample 125698, well 218, 671 m, Karapiti Rhyolite.

B. Laumontite (lmt, medium grey) ± quartz (qz, dark grey) replacing and filling open spaces around compositionally zoned andesine phenocrysts (pl, light to medium grey); core sample 125633, well 208, 216 m, Haparangi Rhyolite.

C. Complex microvein structure in which laumontite has precipitated along a fracture in a mordenite-adularia vein. This vein is composed of fibrous mordenite (mord, dark grey) grading into a fibrous intergrowth of mordenite (medium grey) and adularia (ad, light grey) with minor quartz (qz, dark grey), ilmenite (ilm, white) and magnetite (mt, white). Note massive mordenite replacement of the groundmass in the upper left corner of the photo; core sample 125633, well 208, 216 m, Haparangi Rhyolite.

D. Magnified view of the area outlined in C. Note that magnetite is the only Fe-Ti oxide associated with laumontite. The white spot within the large adularia crystal is barite (ba).

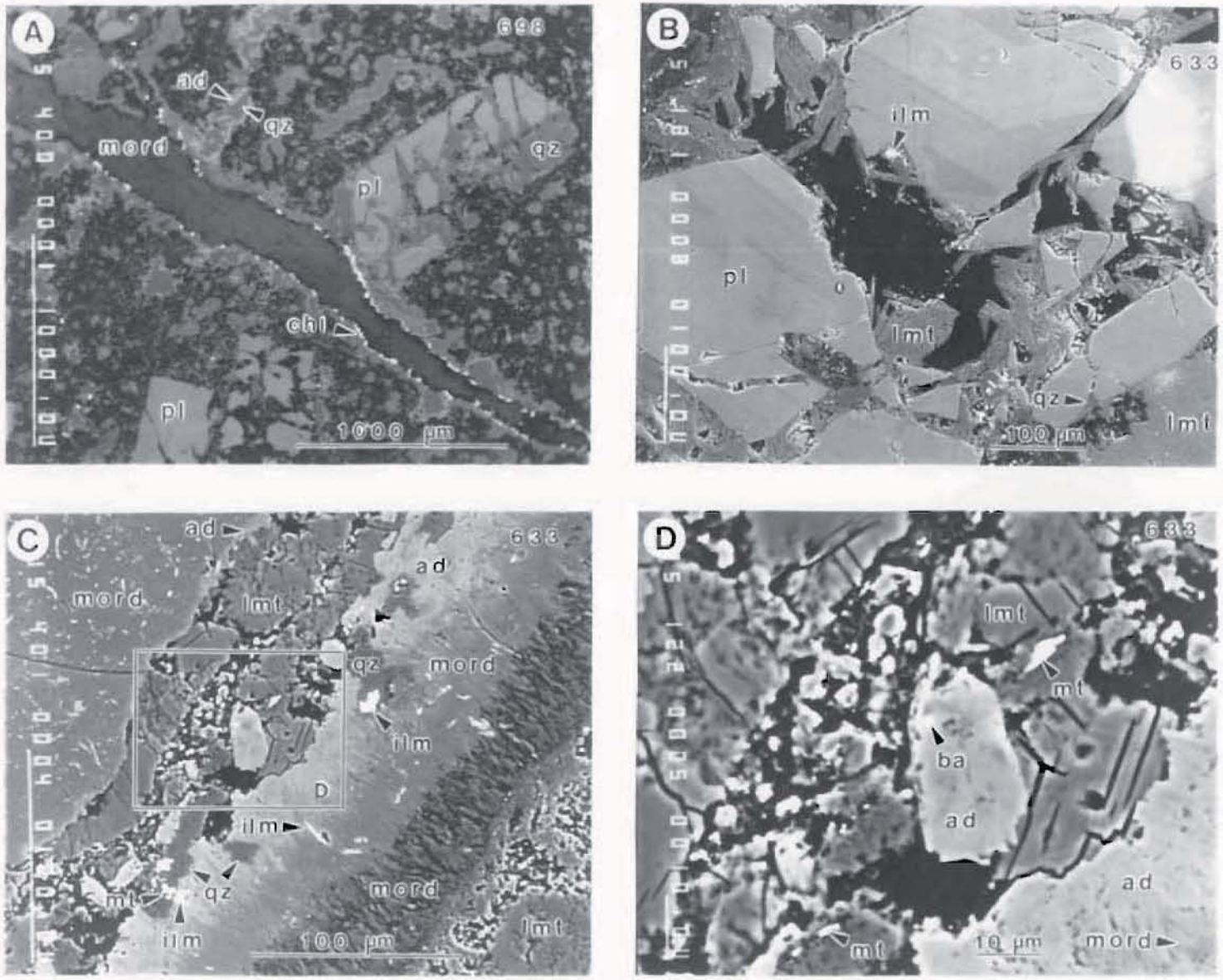
A
ad
qz
mord
qz
pl
chl
pl
1000 µm
B
ilm
pl
lmt
qz
100 µm
lmt
C
ad
ad
mord
lmt
qz
mord
ilm
D
ilm
mt
qz
mord
ilm
100 µm
lmt
D
lmt
mt
ba
ad
ad
mt
10 µm
mord

crysts or microphenocrysts, but also occur in the groundmass with no obvious association with plagioclase. A small percentage (<3%) of the groundmass spherulites have analcime cores. Mordenite, locally intergrown with clinochlore, montmorillonite and quartz, fills cavities and replaces silicic glass. Mordenite also forms elongated prismatic crystals which resemble laumontite. Pericline and mordenite are spatially associated in parts of the reservoir, but based on rock and mineral textures they do not appear to form in equilibrium.

Laumontite occurs as radial aggregates and discrete micro-veinlets, veins and open-space filling without noticeable signs of host rock/mineral replacement (Figs. 3.24B, C and D). The only minerals noted to crystallize in equilibrium with laumontite are quartz and magnetite. The exact relationship of laumontite to potassic alteration is not clear. Laumontite occurs in the lower temperature parts of the reservoir and, in a general sense, is probably time-equivalent to potassic alteration, but on a local scale laumontite veins fill fractures in or cut across adularia-mordenite veins and disseminated alteration. An alternative interpretation to the situation shown in Fig. 3.24C is that adularia-mordenite forms an envelope on the laumontite vein, but considering the "brecciated" texture of the laumontite vein, this interpretation is considered unlikely.

Spatial Zoning

The distribution of mordenite and laumontite alteration is shown in Figure 3.25 and Plate 6B. Clearly, a primary control on the distribution of mordenite is the occurrence of the Haparangi Rhyolite. It is not clear whether the chemical composition or the thermal environment of the Haparangi Rhyolite is the controlling factor on the distribution of mordenite. Because of the low permeability of the Haparangi Rhyolite, fluid/rock temperatures within it generally vary from approximately 150° to 220°C, which may be a critical temperature range for the formation of

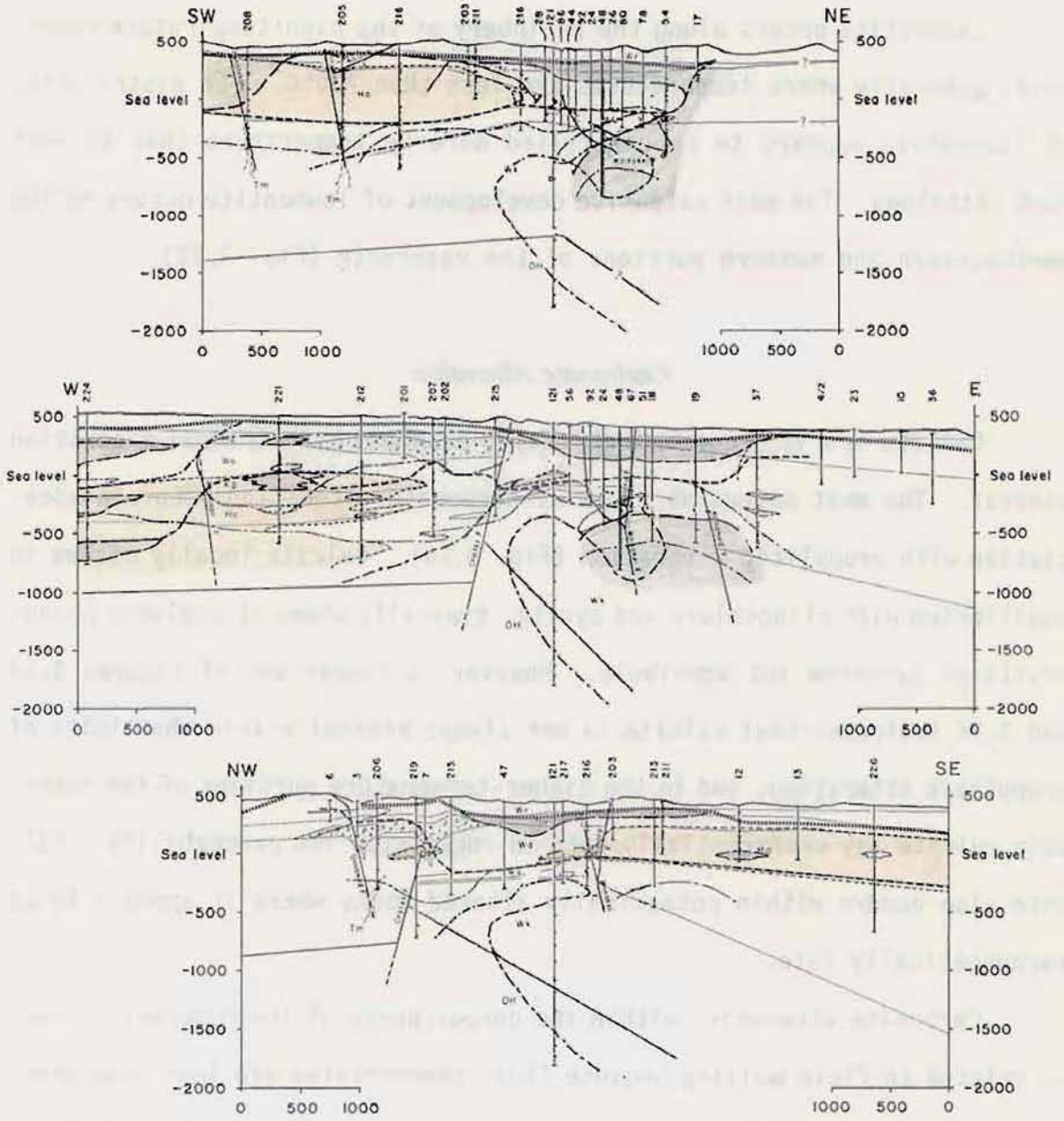

Figure 3.25. Spatial distribution of mordenite (orange) and laumontite (grey) alteration within the Wairakei hydrothermal reservoir. See Figure 3.11 for location of the cross sections.

mordenite. Mordenite does occur at higher temperatures (compare Figs. 3.10 and 3.25), but in these areas there is much less continuity to its distribution. Mordenite is absent from most of the high-temperature (T>250°C) reservoir. The development of mordenite alteration below the Haparangi Rhyolite in the west-central portion of the reservoir probably reflects the lower reservoir temperatures and thickening of the Waiora Formation west of the Crater fault.

Laumontite occurs along the periphery of the high-temperature reservoir, generally where temperatures are less than 230°C. The distribution of laumontite appears to be controlled more by temperature than by host rock lithology. The most extensive development of laumontite occurs in the northeastern and eastern portions of the reservoir (Fig. 3.25).

Carbonate Alteration

Calcite is a very common and locally abundant hydrothermal alteration mineral. The most extensive areas of carbonate alteration occur in association with propylitic alteration (Fig. 3.26). Calcite locally occurs in equilibrium with clinochlore and pyrite, typically where it replaces phenocrysts of pyroxene and amphibole. However, a comparison of Figures 3.14 and 3.26 indicates that calcite is not always present within the limits of propylitic alteration, and in the higher-temperature portions of the reservoir calcite may preferentially form in rocks with low permeability. Calcite also occurs within potassically altered rocks where it appears to be paragenetically late.

Carbonate alteration within the deeper parts of the reservoir cannot be related to fluid boiling because fluid temperatures are less than those required for hydrostatic boiling at these depths. It is likely that the formation of calcite in the upper 500 to 600 metres of the reservoir is partially related to the separation of CO_2 from the fluid, but this cannot be the sole controlling factor because calcite is absent from much of the area where the reservoir fluid is boiling. In general, the occurrence of calcite is probably a byproduct of simple alteration reactions involving plagioclase and mafic minerals.

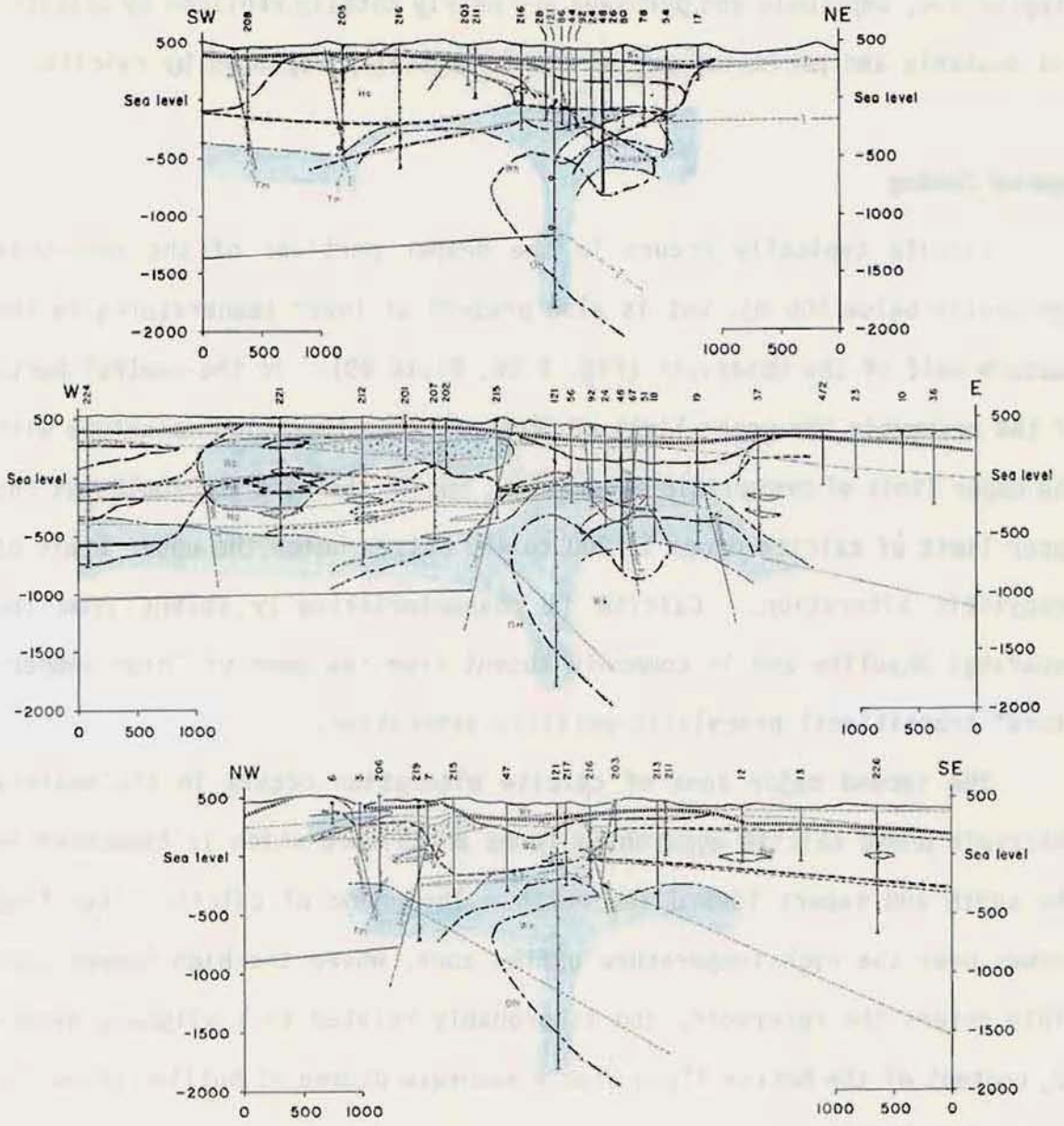

Figure 3.26. Spatial distribution of calcite (blue) alteration within the Wairakei hydrothermal reservoir. See Figure 3.11 for location of the cross sections.

Textural Relationships

Textures indicating calcite-secondary feldspar equilibrium are very rare at Wairakei, and calcite alteration is commonly a paragenetically late alteration event. In incipient carbonate alteration, randomly distributed, very fine-grained calcite replaces the groundmass. With increasing alteration intensity calcite replaces plagioclase phenocrysts along cleavage planes and within crystal cores. Where calcite alteration is intense,

plagioclase, amphibole and pyroxene are nearly totally replaced by calcite, and adularia and pericline are at least partially replaced by calcite.

Spatial Zoning

Calcite typically occurs in the deeper portions of the reservoir (generally below 500 m), but is also present at lower temperatures in the western half of the reservoir (Fig. 3.26; Plate 6B). In the central parts of the reservoir the upper limit of deep calcite alteration coincides with the upper limit of propylitic alteration, but in the west and southwest the upper limit of calcite drops to 200 to 400 metres below the upper limit of propylitic alteration. Calcite is characteristically absent from the Haparangi Rhyolite and is commonly absent from the zone of "high-temperature" transitional propylitic-potassic alteration.

The second major zone of calcite alteration occurs in the western reservoir where calcite apparently forms a manifold which is truncated to the south and tapers toward the north. This zone of calcite alteration occurs over the high-temperature upflow zone, where the high-temperature fluid enters the reservoir, and is probably related to a slightly higher CO_2 content of the hotter fluid plus a moderate degree of boiling above the rising hot fluid.

Mineral-Fluid Equilibria

One of the principal advantages of working on an active hydrothermal system is the availability of thermal and chemical data on the fluid. It is thus possible to evaluate the compatibility of the observed alteration mineral assemblages with the theoretical alteration products indicated by plotting the measured fluid composition on thermodynamic diagrams. This is the approach taken in this section.

Reservoir Chemistry

Fluid within the high-temperature reservoir maintains a near-neutral pH (pH ≈ 6.7 at T ≈ 260°C), is saturated with respect to quartz and is slightly undersaturated with respect to calcite (Ellis and Mahon, 1977; 1982). Chemical analyses of samples of the hydrothermal fluid collected from wells throughout the Wairakei geothermal area (Table 3.4) show that the fluid is relatively homogeneous with respect to most solutes and that in most cases only minor changes have occurred with time. In fact, after the removal of ~1 km^3 of ~250°C fluid the ionic concentrations of discharge waters had changed by only 1 to 2% (Ellis, 1979).

Salinity in the production reservoir is relatively constant. The preproduction high-temperature fluid contained ~0.011 moles per kilogram (mole/kg) CO_2 and ~0.0036 mole/kg H_2S which together comprised ~97% of the of the total dissolved gas, the remaining three percent being made up of NH_3, H_2, N_2, saturated hydrocarbons and the noble gasses (Ellis and Mahon, 1982). The deep fluid also contains ~0.008 parts per million (ppm) Fe, 0.35 ppm Al, 0.001 ppm Mn, 1.3 parts per billion (ppb) Cu and ~1.5 ppb Zn (Ellis and Mahon, 1982). When considering the ability of a dilute hydrothermal fluid to extensively alter large volumes of rock it is important to have an understanding of the magnitude of the transporting ability of the fluid. Estimates of the chemical (mass) output of fluid extracted from the Wairakei reservoir annually are 66,000 tonnes of Cl, 40,000 tonnes of Na, 16,000 tonnes of Si, 5,000 tonnes of K, 1,000 tonnes each of Ca and B, 150 tonnes of As and 4 kilograms (kg) of Hg (Ministry of Energy, 1985).

Calculated Reservoir Fluid Composition

Because the water analyses were generally collected from the well weirbox at atmospheric pressure and the steam is collected at close to reservoir pressure, the reported analyses must be calculated to reservoir

Table 3.4. Partial chemical analyses of reservoir fluid and steam for selected Wairakei wells

Well	Date	$pH_{(20)}$	mg/kg Fluid												
			Li	Na	K	Rb	Cs	Ca	Mg	F	Cl	SO_4	B	SiO_2	NH_3	HCO_3
12	9-52	7.6	9.2	1080	57	--	--	17	0.1	--	1820	24	23	296	--	36
12	12-61	--	8.5	1145	60	--	--	--	--	--	1929	--	--	--	--	--
19	9-56	--	9.9	850	105	--	--	--	--	--	--	--	--	285	--	--
19	9-59	8.1	14.0	1280	154	--	--	31.0	--	--	2028	--	--	--	0.55	20.0
19	11-68	8.6	--	1330	172	--	--	29.0	--	--	2312	--	--	--	--	--
27	8-56	--	12.0	1120	140	--	--	--	--	--	--	--	--	319	--	--
37	12-59	7.3	13.2	1315	142	--	--	36.0	0.02	--	2312	--	--	--	--	29.3
37	10-71	7.6	9.8	1197	103	1.52	2.17	--	0.04	--	2041	36.5	34.8	325	--	41.8
37	2-82	8.0	9.9	1305	--	1.39	2.24	60.0	0.03	--	2236	39.0	27.3	316	--	6.1
47	12-59	7.8	14.8	1315	245	--	--	17.0	0.03	--	2284	--	--	--	--	40.5
47	10-71	8.1	12.2	1330	216	2.87	2.68	--	0.02	--	2251	28.8	29.2	632	--	68.3
47	2-82	8.4	12.3	1308	198	2.80	2.59	24.7	0.01	--	2263	38.0	27.4	528	--	0.0
48	8-59	--	14.8	1320	250	--	--	16.0	0.06	--	2298	--	--	--	--	--
48	10-71	8.4	11.5	1250	197	2.53	2.42	--	0.01	--	2120	31.6	28.8	698	--	60.2
48	2-82	8.3	9.5	1008	145	1.78	1.82	16.3	0.01	--	1711	41.0	21.6	470	--	0.0
67	12-59	8.0	14.8	1260	228	--	--	16.0	0.09	--	2227	--	--	--	--	47.2
67	3-72	8.2	11.7	1207	187	2.48	2.60	22.8	--	--	2130	38.0	27.8	625	--	--
67	4-81	--	8.5	996	137	1.76	0.71	15.0	0.01	--	1600	39.0	20.8	463	--	--
78	12-59	7.9	14.8	1285	232	--	--	18.0	--	--	2284	--	--	--	--	42.8
78	10-71	7.8	12.0	1326	217	3.00	2.87	--	0.00	--	2269	34.5	33.4	648	--	61.2
80	3-60	--	14.8	1320	220	--	--	--	--	--	2269	35.0	--	--	--	--
80	12-72	8.5	9.4	961	84	1.21	1.40	24.2	0.02	--	1575	32.5	24.2	355	--	70.3
80	2-82	8.4	8.5	884	68	0.95	1.22	19.9	0.01	--	1430	36.0	17.5	296	--	18.1
92	11-62	--	--	1260	223	--	--	--	--	11.0	2226	--	28.8	560	--	--
92	3-72	8.1	11.5	1271	197	2.69	2.69	25.5	--	--	2190	35.5	29.4	546	--	--
92	2-82	8.3	11.5	1237	182	2.28	2.31	24.7	0.01	--	2132	34.0	27.7	526	--	1.5
121	5-69	8.5	9.8	1135	187	2.10	1.35	9.4	0.24	6.75	1844	24.0	26.0	720	0.80	16.0
205	11-59	--	14.8	1250	211	--	--	25.0	--	--	2170	--	28.0	--	0.24	--
206	8-60	8.2	13.4	1320	215	--	--	--	--	--	2198	--	--	570	--	44.3
211	8-60	6.8	13.4	1510	145	--	--	--	--	--	2567	--	--	480	--	13.5
212	5-62	--	--	1580	290	--	--	16.0	--	--	2726	--	--	665	--	--
215	9-61	8.1	15.4	1415	256	--	--	16.0	--	--	2482	--	--	700	--	20.0
219	7-62	--	--	1320	225	--	--	--	--	--	2252	--	--	460	--	--

Data from Henley et al., 1984. See Figure 3.11a and Plate 5 for well locations.

Table 3.4. Continued

Well	Date	Wellhead Pressure (b.g.)	Enthalpy (J/g)	Collection Pressure (b.g.)	mmoles/100 moles Steam				
					CO_2	H_2S	NH_3	H_2	CH_4
12	12-52	--	--	--	11	0.71	2.45	0.08	0.006
37	10-60	5.9	1470	5.9	194	6.50	--	--	--
37	2-71	5.2	2412	5.2	74.0	2.80	--	--	--
37	2-82	3.1	1051	1.3	71.7	2.56	0.46	--	--
47	1-60	15.7	1093	15.7	76.0	3.60	--	--	--
47	2-71	6.8	1003	5.3	14.0	1.50	--	--	--
47	3-82	5.0	1044	4.7	19.8	1.45	0.39	--	--
48	11-60	13.8	1107	13.8	75.0	3.60	--	--	--
48	2-71	7.7	1016	5.0	11.0	1.60	--	--	--
48	2-82	6.2	1071	6.2	10.4	1.58	1.13	--	--
67	9-60	15.5	986	15.5	89.0	3.30	--	--	--
67	2-71	11.7	1009	11.4	11.0	2.00	--	--	--
67	2-82	8.8	1022	8.1	13.6	1.76	0.51	--	--
80	5-61	15.2	1119	3.4	209	6.50	--	--	--
80	2-71	6.2	1286	5.2	134	4.75	--	--	--
80	2-82	5.7	1722	4.7	151	4.24	0.46	--	--
92	3-64	13.9	1123	13.7	59.0	3.30	--	--	--
92	2-71	5.9	1110	5.5	38.0	2.40	--	--	--
92	2-82	5.8	761	4.9	40.8	2.50	0.44	--	--
121	5-69	5.4	1030	5.2	136	7.82	--	--	--
205	5-61	8.1	1163	8.1	191	5.00	--	--	--
205	11-63	2.8	1210	1.9	112	3.50	--	--	--
206	5-61	13.8	1279	12.9	153	4.00	--	--	--
206	11-63	5.4	--	3.3	616	8.30	--	--	--
211	1-60	5.5	996	--	142	3.30	--	--	--
211	5-61	8.3	2396	0.7	169	7.90	--	--	--
211	11-63	1.0	2652	0.4	159	6.40	--	--	--
212	3-63	14.2	1105	2.9	76.0	2.50	--	--	--
212	3-64	9.4	1061	4.3	89.0	2.90	--	--	--
215	8-61	12.1	1149	8.6	137	3.80	--	--	--
215	2-64	12.1	1407	5.7	159	4.32	--	--	--
219	8-62	5.0	1433	3.0	65.0	2.85	--	--	--
219	11-63	4.1	1286	1.9	85.0	3.10	--	--	--

conditions. This was done following the methods outlined by Henley (1984a, b) and Henley and Brown (1985). Six water and steam analyses (Table 3.5) were selected for comparison to the observed alteration assemblages. The analyses were selected so that the data would be as representative of the geothermal reservoir as possible. Wells were selected in a transect across the reservoir and covered a range of maximum down-hole temperatures from 197° to 271°C. All of the samples were collected prior to 1962 to avoid potential production-related changes, primarily dilution and temperature reduction resulting from groundwater intrusion. In most cases water and steam samples were not collected at the same time, nor were the samples analysed for a consistent set of ions and gasses. Therefore, the two earliest and most complete analyses with the least temporal separation were selected. The calculated total discharge fluid composition for the six wells is shown in Table 3.6.

The most convenient way to compare the alteration mineral assemblages and the reservoir fluid data is by plotting the information on a series of activity diagrams drawn at particular temperature intervals from known thermodynamic data. Because the chemical reactions used to construct the activity diagrams are hydrolysis reactions which are typically written to conserve Al^{3+} and with quartz in excess, the axes of the activity diagrams are usually plotted as a ratio of the activity of an important cation (Na^+, K^+, Ca^{2+} or Mg^{2+}) to that of hydrogen.

Before activity ratios can be calculated from the data in Table 3.6, it is necessary to calculate the reservoir $pH_{(T)}$ for the temperature intervals selected for the diagrams. There are several methods of accomplishing this which vary from relatively complex (e.g., Henley, 1984c) to the simpler CO_2 dissociation method (Henley, 1984b; Henley and Brown, 1985) used here to derive the values in Table 3.7. The data in Table 3.7 compared very well with pH values determined by the calcite dissolution method using the log K values provided by Henley (1984b).

Table 3.5. Partial chemical analyses of Wairakei well discharge used to calculate activity ratios plotted in Figure 3.27

Well	Water Collection Pressure (b.g.)	$pH_{(20)}$	Enthalpy (J/g)	Discharge Water Composition (mg/kg) Na^+	K^+	Ca^{2+}	Mg^{2+}	HCO_3^-	CO_2	Date
15	0	7.5	1105	1230	118	30.0	0.02	25.5	--	12/59
27	0	8.1	1085	1320	220	16.8	0.05	33.0	0.4	8/60
37	0	7.3	1470	1315	142	36.0	0.02	29.3	--	12/59
67	0	8.0	986	1260	228	16.0	0.09	47.2	--	12/59
121	0	8.5	1030	1135	187	9.4	0.24	16.0	--	5/69
215	0	8.1	1149	1415	256	16.0	--	20.0	--	9/61

Well	Maximum Well Temperature (°C)	Steam Collection Pressure (b.g.)	Enthalpy (J/g)	Discharge Steam Composition (mmoles/kg) CO_2	H_2S	Date
15	197	5.4	1105	39.1	0.7	1/60
27	258	14.8	1085	67.2	2.3	8/60
37	246	5.9	1470	39.9	1.3	10/60
67	260	15.5	986	89.0	3.3	9/60
121	271	5.2	1030	13.6	0.8	5/69
215	250	8.6	1149	14.5	0.4	8/61

-- indicates no data. Data from Henley et al. (1984).

Table 3.6. Calculated total discharge fluid composition for well discharge data reported in Table 3.5

Well	(mg/kg) Na^+	K^+	Ca^{2+}	Mg^{2+}	HCO_3^-	CO_2	H_2S
15	979.1	93.9	23.9	0.016	20.3	351.0	4.8
27	1161.6	193.6	14.8	0.044	29.0	355.2	9.4
37	828.5	89.5	22.9	0.013	18.5	649.7	16.4
67	1184.4	214.3	14.1	0.085	44.4	242.9	7.0
121	930.7	153.3	7.7	0.197	13.1	107.7	4.9
215	1146.2	207.4	13.0	--	16.2	121.4	2.6

Well	(mmoles/kg) Na^+	K^+	Ca^{2+}	Mg^{2+}	HCO_3^-	CO_2	H_2S
15	42.59	2.40	0.60	0.0008	0.33	7.98	0.141
27	50.53	4.95	0.37	0.0021	0.48	8.07	0.276
37	36.04	2.29	0.57	0.0008	0.30	14.76	0.481
67	51.52	5.48	0.35	0.0035	0.73	5.52	0.205
121	40.48	3.92	0.19	0.0099	0.21	2.45	0.144
215	49.86	5.30	0.32	--	0.27	2.76	0.076

Well discharge data recalculated following the methods outlined in Henley (1984a, b) and Henley and Brown (1985).

Table 3.7. Calculated reservoir pH values for well discharge data reported in Table 3.5

Well	Calculated Reservoir pH			
	$pH_{100°C}$	$pH_{200°C}$	$pH_{250°C}$	$pH_{300°C}$
15	4.88	5.69	6.21	6.75
27	5.04	5.85	6.37	6.91
37	4.57	5.38	5.91	6.44
67	5.38	6.19	6.71	7.25
121	5.20	6.01	6.53	7.07
215	5.25	6.06	6.59	7.12

Calculations follow the CO_2 dissociation method described by Henley (1984b) and Henley and Brown (1985). Log K values are from Fournier (1985).

Table 3.8. Ion activities calculated from well discharge data presented in Table 3.6

Well	$m_{Na^+}(0.7)$	$m_{K^+}(0.7)$	$m_{Ca^{2+}}(0.27)$	$m_{Mg^{2+}}(0.27)$
15	0.02981	0.00168	0.000161	0.00000022
27	0.03537	0.00347	0.000100	0.00000054
37	0.02523	0.00160	0.000154	0.00000027
67	0.03606	0.00384	0.000095	0.00000095
121	0.02834	0.00274	0.000051	0.00000216
215	0.03490	0.00371	0.000086	--

Well	$m_{H^+}(0.8)$			
	100°C	200°C	250°C	300°C
15	0.00001054	0.00000163	0.00000062	0.000000142
27	0.00000730	0.00000113	0.00000034	0.000000098
37	0.00002154	0.00000417	0.00000098	0.000000290
67	0.00000334	0.00000052	0.00000016	0.000000045
121	0.00000505	0.00000098	0.00000024	0.000000068
215	0.00000450	0.00000087	0.00000021	0.000000061

Activity coefficients (shown above in parentheses) taken from Henley (1984b) and Henley and Brown (1985). Hydrogen ion concentration corresponds to calculated reservoir pH (Table 3.7).

The computed ion activities are shown in Table 3.8. The activity coefficients were taken from lists presented in Henley (1984b) and Henley and Brown (1985). Unfortunately these works give more than one activity coefficient for each ion. A few activity ratios were calculated using the different numbers with the result that differences in the final activity ratios were generally insignificant. The computed activity ratios for six

Table 3.9. Activity ratios calculated from Wairakei water and steam analyses given in Table 3.5

Well	$\log(a_{Na^+}/a_{H^+})$	$\log(a_{K^+}/a_{H^+})$	$\log(a_{Ca^{2+}}/a^2_{H^+})$	$\log(a_{Mg^{2+}}/a^2_{H^+})$
		T = 100°C		
15	3.45	2.20	6.16	3.30
27	3.69	2.68	6.27	4.01
37	3.07	1.87	5.52	2.76
67	4.04	3.06	6.95	4.93
121	3.75	2.73	6.30	4.93
215	3.89	2.92	6.63	--
		T = 200°C		
15	4.26	3.01	7.79	4.92
27	4.50	3.49	7.89	5.63
37	3.78	2.58	6.95	4.19
67	4.84	3.87	8.55	6.55
121	4.46	3.45	7.73	6.35
215	4.60	3.63	8.06	--
		T = 250°C		
15	4.68	3.44	8.63	5.76
27	5.02	4.01	8.94	6.67
37	4.41	3.21	8.21	5.45
67	5.36	4.39	9.59	7.59
121	5.07	4.06	8.95	7.57
215	5.22	4.25	9.29	--
		T = 300°C		
15	5.32	4.07	9.90	7.04
27	5.55	4.54	10.00	7.73
37	5.40	3.74	9.26	6.51
67	5.90	4.93	10.67	8.67
121	5.61	4.59	10.01	8.64
215	5.64	4.67	10.13	--

samples of Wairakei reservoir fluid are listed in Table 3.9. It is interesting to note that the various activity ratios calculated for a specific reservoir temperature vary very little between wells regardless of the portion of the reservoir the well is tapping and regardless of the maximum well feed temperature. These activity data further document the uniformity in the solute content of the Wairakei reservoir fluid.

Activity Diagrams

The activity diagrams (Figs. 3.27a to 3.27d) were constructed from the thermodynamic data presented in Bowers et al. (1984). Tables 3.10 and 3.11 present these data and the computed phase boundary reactions and log K values. The mineral phases plotted on the activity diagrams are a reasonable representation of the major and some of the minor alteration minerals identified in core samples. Unfortunately, one of the more important alteration minerals at Wairakei, mordenite, could not be plotted because thermodynamic data have not been determined for this mineral species (J.G. Liou, personal communication). The lack of recent data for smectite is also unfortunate. This data would be very useful since most hydrothermal systems contain abundant smectite as an alteration product. Also, since Na-, K-, Ca- and Mg-smectites exist, a smectite field could be plotted on each of the activity diagrams. An attempt was made to show the approximate location of the Na-montmorillonite field on Figure 3.27 by using the thermodynamic data published in Helgeson (1969). The Na-montmorillonite data for 100°C is relatively compatible with the Bowers et al. (1984) data, but at elevated temperatures the data sets are incompatible. Consequently, the Na-montmorillonite field shown on the higher temperature diagrams (Figs. 3.27b, c and d) is only approximate.

The only convention used in drawing the observed alteration mineral assemblages on the activity diagrams was that the activity ratios remained near phase boundary values. Consequently, the alteration assemblages do not extend very far into the phase field. For convenience the activity ratios (Table 3.9) for the reservoir fluid were grouped together into an "average" composition which was plotted on the activity ratio diagrams as a ruled box.

It is significant that the "average" Wairakei reservoir fluid overlaps the observed alteration mineral assemblages within a temperature range of ~275° to ~210°C on the activity diagrams. This indicates that the

described propylitic, potassic and higher temperature zeolite alteration mineral assemblages probably formed in equilibrium with the reservoir fluid.

Propylitic Alteration

Propylitic alteration was characterized by the presence of one or more of the indicator minerals (albite, wairakite, clinozoisite/epidote, prehnite) and was considered to occur at temperatures greater than 250°C. By comparing the activity diagrams for 250° and 300°C it can be seen that wairakite and clinozoisite (and epidote) only occur at temperatures >250°C. In fact, wairakite and clinozoisite first appear on the activity diagrams at 255°C and 260°C respectively. Thus it can be seen from the activity ratio diagrams that Steiner's (1977) medium rank alteration mineral wairakite cannot be a stable phase at temperatures between 230° and 240°C.

Another important mineral stability relationship apparent from Figures 3.27c and 3.27d is that as the Wairakei fluid temperature approaches 300°C it enters the stability area for calcite. This supports the concept that calcite may be an integral component of higher-temperature propylitic alteration and helps explain the common occurrence of calcite in the deeper and higher temperature portions of the reservoir.

Low-Temperature Alteration

The activity diagrams for 100°C show two important aspects of low-temperature alteration: (1) a laumontite phase field is still present and (2) if laumontite does form at low temperatures then calcite may also be present. This, however, is not supported by the spatial distributions of laumontite and calcite alteration; compare Figures 3.25 and 3.26. Since the "average" reservoir fluid does not plot near the laumontite phase field, it is possible that laumontite is only a metastable phase in the low-temperature periphery of the reservoir and that reservoir temperatures

Table 3.10. Hydrolysis reactions and log K values for minerals used in constructing Figure 3.27

Mineral	Abbreviation	Reaction	Log K ($P = P_{SAT}$) 100°C	200°C	250°C	300°C
Albite	ALB	$NaAlSi_3O_8 + 4H^+ = Na^+ + Al^{3+} + 3SiO_{2(qtz)} + 2H_2O$	10.25	6.47	5.04	3.51
Calcite	CALC	$CaCO_3 + 2H^+ = Ca^{2+} + CO_{2(aq)} + H_2O$	9.09	8.77	8.67	8.39
Clinochlore (14Å)	CHL(14Å)	$Mg_5Al(AlSi_3O_{10})(OH)_8 + 16H^+ = 5Mg^{2+} + 2Al^{3+} + 3SiO_{2(qtz)} + 12H_2O$	56.62	37.69	31.88	26.07
Clinozoisite	CLNZ	$Ca_2Al_3Si_3O_{12}(OH) + 13H^+ = 2Ca^{2+} + 3Al^{3+} + 3SiO_{2(qtz)} + 7H_2O$	37.63	22.97	17.33	11.34
Grossular	GROSS	$Ca_3Al_2Si_3O_{12} + 12H^+ = 3Ca^{2+} + 2Al^{3+} + 3SiO_{2(qtz)} + 6H_2O$	46.44	32.21	26.80	21.21
Kaolinite	KAOL	$Al_2Si_2O_5(OH)_4 + 6H^+ = 2Al^{3+} + 2SiO_{2(qtz)} + 5H_2O$	8.61	3.31	1.22	-1.20
K-Feldspar	K-SPAR	$KAlSi_3O_8 + 4H^+ = K^+ + Al^{3+} + 3SiO_{2(qtz)} + 2H_2O$	8.19	5.13	3.92	2.57
Laumontite	LAUM	$Ca(Al_2Si_4O_{12})\cdot 4H_2O + 8H^+ = Ca^{2+} + 2Al^{3+} + 4SiO_{2(qtz)} + 8H_2O$	19.98	12.10	9.11	5.88
Muscovite	MUSC	$KAl_2(AlSi_3O_{10})(OH)_2 + 10H^+ = K^+ + 3Al^{3+} + 3SiO_{2(qtz)} + 6H_2O$	15.72	7.19	3.83	0.00
Na-montmorillonite	Na-MONT	$3Na_{0.33}Al_{2.33}Si_{3.67}O_{10}(OH)_2 + 22H^+ = Na^+ + 7Al^{3+} + 11SiO_{2(qtz)} + 14H_2O$	35.06	--	--	--
Phlogopite	PHLOG	$KMg_3(AlSi_3O_{10})(OH)_2 + 10H^+ = K^+ + 3Mg^{2+} + Al^{3+} + 3SiO_{2(qtz)} + 6H_2O$	36.38	25.44	21.32	17.04
Prehnite	PREHN	$Ca_2Al(AlSi_3O_{10})(OH)_2 + 10H^+ = 2Ca^{2+} + 2Al^{3+} + 3SiO_{2(qtz)} + 6H_2O$	31.77	21.00	16.88	12.51
Pyrophyllite	PYROPH	$Al_2Si_4O_{10}(OH)_2 + 6H^+ = 2Al^{3+} + 4SiO_{2(qtz)} + 4H_2O$	9.62	3.72	1.39	-1.22
Quartz	QTZ	$3SiO_{2(qtz)} = 3SiO_{2(aq)}$	9.30	7.29	6.57	6.03
Wairakite	WAIR	$Ca(Al_2Si_4O_{12})\cdot 2H_2O + 8H^+ = Ca^{2+} + 2Al^{3+} + 4SiO_{2(qtz)} + 6H_2O$	22.45	12.80	9.13	5.31

All thermodynamic data except for Na-montmorillonite are from Bowers et al. (1984). Na-montmorillonite data are from Helgeson (1969).

Table 3.11. Reactions and log K values used to construct phase boundaries in Figure 3.27

Reaction	Log K ($P = P_{SAT}$) 100°C	200°C	250°C	300°C
Albite				
$2ALB + 2H^+ + H_2O = KAOL + 2Na^+ + 4QTZ$	11.89	9.63	8.86	8.22
$ALB + K^+ = K\text{-}SPAR + Na^+$	2.06	1.34	1.12	0.94
$3ALB + 2H^+ + K^+ = MUSC + 3Na^+ + 6QTZ$	15.03	12.22	11.29	10.53
$7ALB + 6H^+ = 3Na\text{-}MONT + 6Na^+ + 10QTZ$	36.69	--	--	--
Clinochlore (14Å)				
$CHL(14Å) + 8H^+ + 2Na^+ + 3QTZ = 2ALB + 5Mg^{2+} + 8H_2O$	36.12	24.75	21.80	19.05
$CHL(14Å) + 4H^+ + 3Ca^{2+} = GROSS + 5Mg^{2+} = 6H_2O$	10.18	5.48	5.08	4.68
$CHL(14Å) + 10H^+ = KAOL + 5Mg^{2+} + QTZ + 7H_2O$	48.01	34.38	30.66	27.27
$CHL(14Å) + 8H^+ + 2K^+ + 3QTZ = 2K\text{-}SPAR + 5Mg^{2+} + 8H_2O$	40.24	27.43	24.04	20.93
$CHL(14Å) + 8H^+ + Ca^{2+} + QTZ = LAUM + 5Mg^{2+} + 4H_2O$	36.64	25.59	22.77	20.19
$3CHL(14Å) + 28H^+ + 2K^+ = 2MUSC + 15Mg^{2+} + 3QTZ + 2H_2O$	138.42	98.69	87.98	78.21
$7CHL(14Å) + 68H^+ + 2Na^+ + QTZ = 6Na\text{-}MONT + 35Mg^{2+} + 56H_2O$	326.22	--	--	--
$CHL(14Å) + 6H^+ + 2Ca^{2+} = PREHN + 5Mg^{2+} + 6H_2O$	24.85	16.69	15.00	13.56
$CHL(14Å) + 8H^+ + Ca^{2+} + QTZ = WAIR + 5Mg^{2+} + 4H_2O$	34.17	24.89	22.75	20.76
Clinozoisite				
$CLNZ + H^+ + 3Na^+ = 3ALB + 2Ca^{2+} + H_2O$	6.88	3.56	2.21	0.81
$2CLNZ + 2H^+ + 6QTZ + 10H_2O = 3WAIR + Ca^{2+}$	7.91	7.54	7.27	6.75
Grossular				
$GROSS + 4H^+ + 2Na^+ + 3QTZ = 2ALB + 3Ca^{2+} + 2H_2O$	25.94	19.27	16.72	14.19
$GROSS + 4H^+ + 2K^+ = 2K\text{-}SPAR + 3Ca^{2+} + 2H_2O$	30.06	21.95	18.96	16.07
$GROSS + 2H^+ = PREHN + Ca^{2+}$	14.67	11.21	9.92	8.70
K-Feldspar				
$3K\text{-}SPAR + 2H^+ = MUSC + 2K^+ + 6QTZ$	8.85	8.20	7.93	7.71
Laumontite				
$LAUM + 2H^+ = KAOL + Ca^{2+} + 2QTZ + 3H_2O$	11.37	8.79	7.89	7.08
$3LAUM + 4H^+ + 2K^+ = 2MUSC + 3Ca^{2+} + 6QTZ + 12H_2O$	28.50	22.00	19.67	17.64
$LAUM + 2H^+ = PYROPH + Ca^{2+} + 4H_2O$	10.36	8.38	7.72	4.66
Muscovite				
$2MUSC + 2H^+ + 3H_2O = 3KAOL + 2K^+$	5.61	4.45	4.00	3.60
$7MUSC + 4H^+ + 3Na^+ + 12QTZ = 9Na\text{-}MONT + 7K^+$	4.86	--	--	--
Na-montmorillonite				
$6Na\text{-}MONT + 2H^+ + 7H_2O = 7KAOL + 2Na^+ + 8QTZ$	9.85	--	--	--
Phlogopite				
$2PHLOG + 4H^+ = CHL(14Å) + 2K^+ + Mg^{2+} + 3QTZ$	16.14	13.19	10.76	8.01
$3PHLOG + 20H^+ = MUSC + 2K^+ + 9Mg^{2+} + 6QTZ + 12H_2O$	93.42	69.13	60.13	51.12
Prehnite				
$PREHN + 2H^+ + 2Na^+ + 3QTZ = 2ALB + 2Ca^{2+} + 2H_2O$	11.27	8.06	6.80	5.49
$3PREHN + 4H^+ = 2CLNZ + 2Ca^{2+} + 3QTZ + 4H_2O$	20.05	17.06	15.98	14.85
$PREHN + 2H^+ + 2K^+ + 3QTZ = 2K\text{-}SPAR + 2Ca^{2+} + 2H_2O$	15.39	10.74	9.04	7.37
$PREHN + 2H^+ + QTZ + 2H_2O = LAUM + Ca^{2+}$	11.79	8.90	7.77	6.63
$3PREHN + 10H^+ + 2K^+ = 2MUSC + 6Ca^{2+} + 3QTZ + 6H_2O$	63.87	48.62	42.98	37.53
$PREHN + 2H^+ + QTZ + 2H_2O = WAIR + Ca^{2+}$	9.32	8.20	7.75	7.20
Wairakite				
$WAIR + 2H^+ = KAOL + Ca^{2+} + 4H_2$	13.84	9.49	7.91	6.51
$WAIR + 2H^+ = PYROPH + Ca^{2+} + 4H_2O$	12.83	9.08	7.74	6.53

Reactions and log K values calculated from the data presented in Table 3.10.

Figure 3.27a. (Facing page) Activity diagrams for the aqueous species (A) K^+, Na^+, and H^+, (B) K^+, Mg^{2+} and H^+, (C) Ca^{2+}, K^+ and H^+, (D) Mg^{2+}, Na^+ and H^+, (E) Ca^{2+}, Mg^{2+} and H^+ and (F) Ca^{2+}, Na^+ and H^+ at 100°C and quartz saturation. The mineral phase boundaries are calculated from the thermodynamic data in Table 3.11. Values of $a_{Ca^{2+}}/a^2_{H^+}$ for precipitation of calcite at mco_2 concentrations of 0.03 and 0.003 are shown as dashed lines. The two values cover the range in mco_2 concentrations of the water analyses in Table 3.6. "Average" activity ratios for the Wairakei reservoir fluid (ruled box) are estimated for the aqueous species concerned from data in Table 3.6. Stippled areas approximate the given alteration assemblage thought to be in equilibrium at this temperature; these assemblages were estimated from thin section analyses (see Appendix 1). Mineral phases are 14Å-clinochlore (14Å-CHL), clinozoisite (CLNZ), grossular (GROSS), K-feldspar (K-SPAR), kaolinite (KAOL), laumontite (LAUM), muscovite (MUSC), Na-montmorillonite (Na-MONT), pericline (ALB), phlogopite (PHLOG), prehnite (PREHN), quartz (QTZ), wairakite (WAIR).

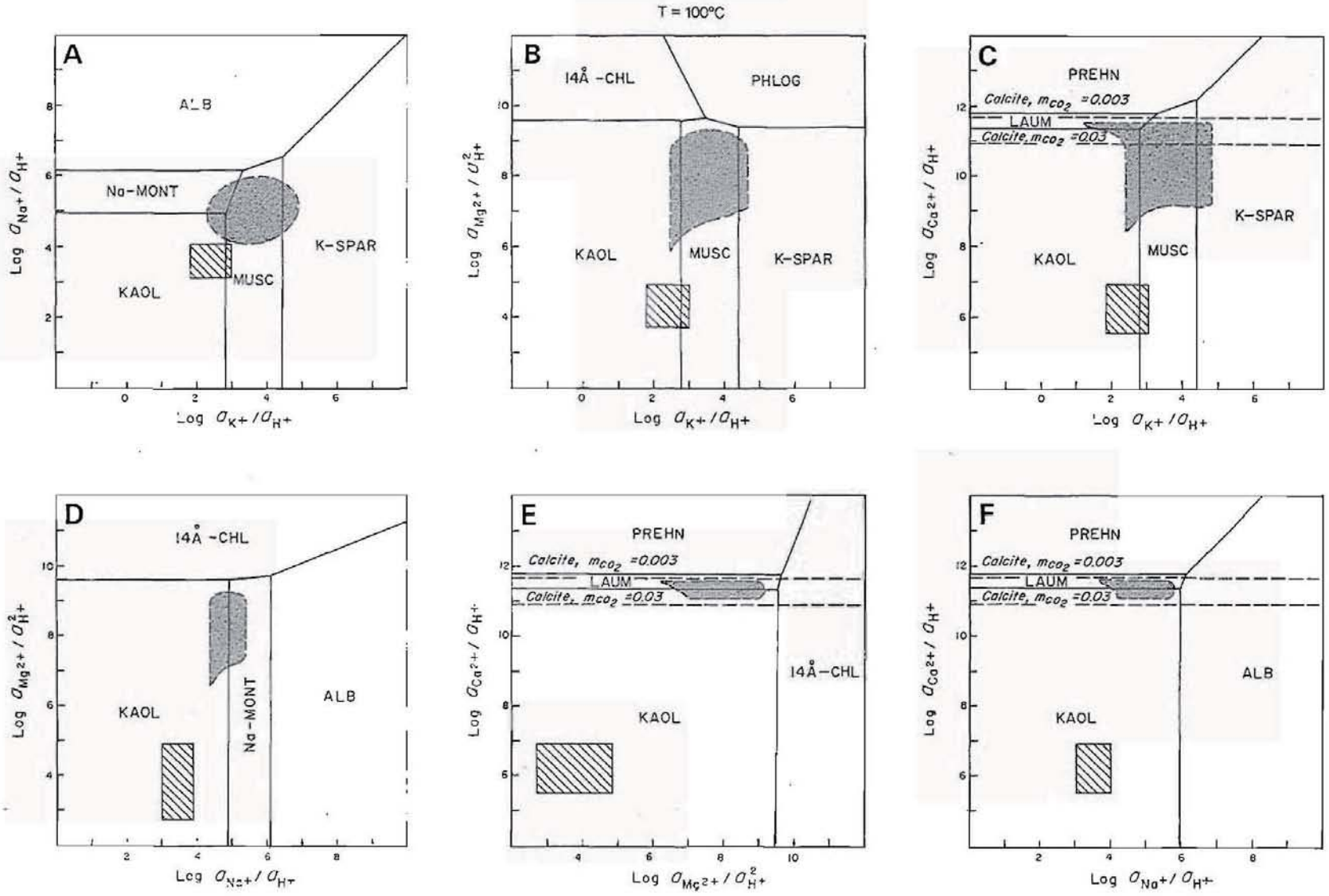
T = 100°C
A
ALB
Na-MONT
K-SPAR
KAOL
MUSC
Log a_{Na^+}/a_{H^+}
Log a_{K^+}/a_{H^+}
B
14Å -CHL
PHLOG
KAOL
MUSC
K-SPAR
Log $a_{Mg^{2+}}/a_{H^+}^2$
Log a_{K^+}/a_{H^+}
C
PREHN
Calcite, m_{CO_2} =0.003
LAUM
Calcite, m_{CO_2} =0.03
K-SPAR
KAOL
MUSC
Log $a_{Ca^{2+}}/a_{H^+}$
Log a_{K^+}/a_{H^+}
D
14Å -CHL
KAOL
Na-MONT
ALB
Log $a_{Mg^{2+}}/a_{H^+}^2$
Log a_{Na^+}/a_{H^+}
E
PREHN
Calcite, m_{CO_2} =0.003
LAUM
Calcite, m_{CO_2} =0.03
14Å-CHL
KAOL
Log $a_{Ca^{2+}}/a_{H^+}$
Log $a_{Mg^{2+}}/a_{H^+}^2$
F
PREHN
Calcite, m_{CO_2} =0.003
LAUM
Calcite, m_{CO_2} =0.03
ALB
KAOL
Log $a_{Ca^{2+}}/a_{H^+}$
Log a_{Na^+}/a_{H^+}

Figure 3.27b. (Facing page) Activity diagrams for the aqueous species (A) K^+, Na^+, and H^+, (B) K^+, Mg^{2+} and H^+, (C) Ca^{2+}, K^+ and H^+, (D) Mg^{2+}, Na^+ and H^+, (E) Ca^{2+}, Mg^{2+} and H^+ and (F) Ca^{2+}, Na^+ and H^+ at 200°C and quartz saturation. The mineral phase boundaries are calculated from the thermodynamic data in Table 3.11. Values of $a_{Ca^{2+}}/a^2_{H^+}$ for precipitation of calcite at mco_2 concentrations of 0.03 and 0.003 are shown as dashed lines. The two values cover the range in mco_2 concentrations of the water analyses in Table 3.6. "Average" activity ratios for the Wairakei reservoir fluid (ruled box) are estimated for the aqueous species concerned from data in Table 3.6. Stippled areas approximate the given alteration assemblage thought to be in equilibrium at this temperature; these assemblages were estimated from thin section analyses (see Appendix 1). Mineral phases are 14Å-clinochlore (14Å-CHL), clinozoisite (CLNZ), grossular (GROSS), K-feldspar (K-SPAR), kaolinite (KAOL), laumontite (LAUM), muscovite (MUSC), Na-montmorillonite (Na-MONT), pericline (ALB), phlogopite (PHLOG), prehnite (PREHN), quartz (QTZ), wairakite (WAIR).

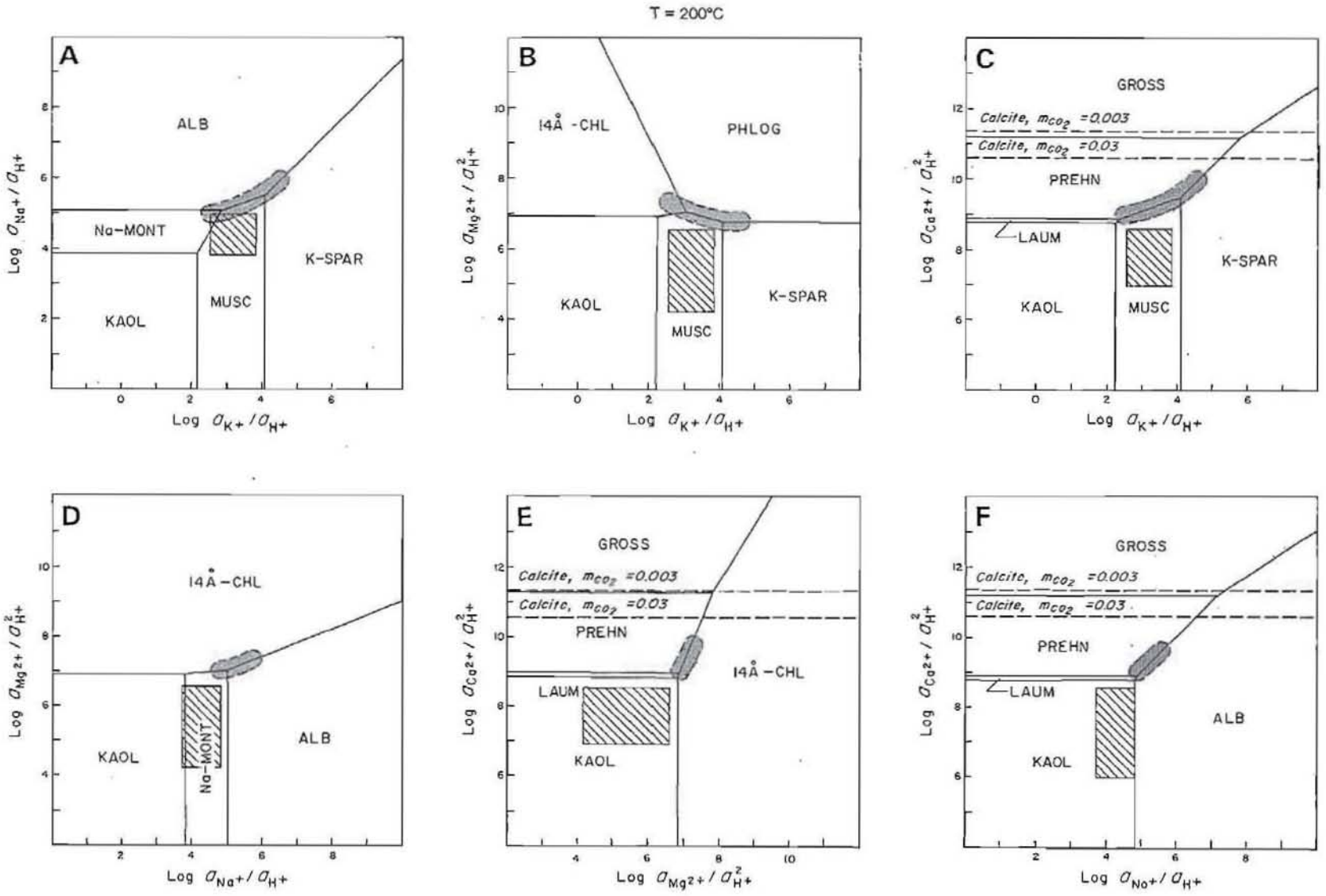
T = 200°C
A
ALB
Na-MONT
K-SPAR
KAOL
MUSC
Log a_{Na^+}/a_{H^+}
Log a_{K^+}/a_{H^+}
B
14Å -CHL
PHLOG
KAOL
K-SPAR
MUSC
Log $a_{Mg^{2+}}/a^2_{H^+}$
Log a_{K^+}/a_{H^+}
C
GROSS
Calcite, m_{CO_2} =0.003
Calcite, m_{CO_2} =0.03
PREHN
LAUM
KAOL
MUSC
K-SPAR
Log $a_{Ca^{2+}}/a^2_{H^+}$
Log a_{K^+}/a_{H^+}
D
14Å -CHL
KAOL
Na-MONT
ALB
Log $a_{Mg^{2+}}/a^2_{H^+}$
Log a_{Na^+}/a_{H^+}
E
GROSS
Calcite, m_{CO_2} =0.003
Calcite, m_{CO_2} =0.03
PREHN
14Å -CHL
LAUM
KAOL
Log $a_{Ca^{2+}}/a^2_{H^+}$
Log $a_{Mg^{2+}}/a^2_{H^+}$
F
GROSS
Calcite, m_{CO_2} =0.003
Calcite, m_{CO_2} =0.03
PREHN
LAUM
ALB
KAOL
Log $a_{Ca^{2+}}/a^2_{H^+}$
Log a_{Na^+}/a_{H^+}

Figure 3.27c. (Facing page) Activity diagrams for the aqueous species (A) K^+, Na^+, and H^+, (B) K^+, Mg^{2+} and H^+, (C) Ca^{2+}, K^+ and H^+, (D) Mg^{2+}, Na^+ and H^+, (E) Ca^{2+}, Mg^{2+} and H^+ and (F) Ca^{2+}, Na^+ and H^+ at 250°C and quartz saturation. The mineral phase boundaries are calculated from the thermodynamic data in Table 3.11. Values of $a_{Ca^{2+}}/a^2_{H^+}$ for precipitation of calcite at mCO_2 concentrations of 0.03 and 0.003 are shown as dashed lines. The two values cover the range in mCO_2 concentrations of the water analyses in Table 3.6. "Average" activity ratios for the Wairakei reservoir fluid (ruled box) are estimated for the aqueous species concerned from data in Table 3.6. Stippled areas approximate the given alteration assemblage thought to be in equilibrium at this temperature; these assemblages were estimated from thin section analyses (see Appendix 1). Mineral phases are 14Å-clinochlore (14Å-CHL), clinozoisite (CLNZ), grossular (GROSS), K-feldspar (K-SPAR), kaolinite (KAOL), laumontite (LAUM), muscovite (MUSC), Na-montmorillonite (Na-MONT), pericline (ALB), phlogopite (PHLOG), prehnite (PREHN), quartz (QTZ), wairakite (WAIR).

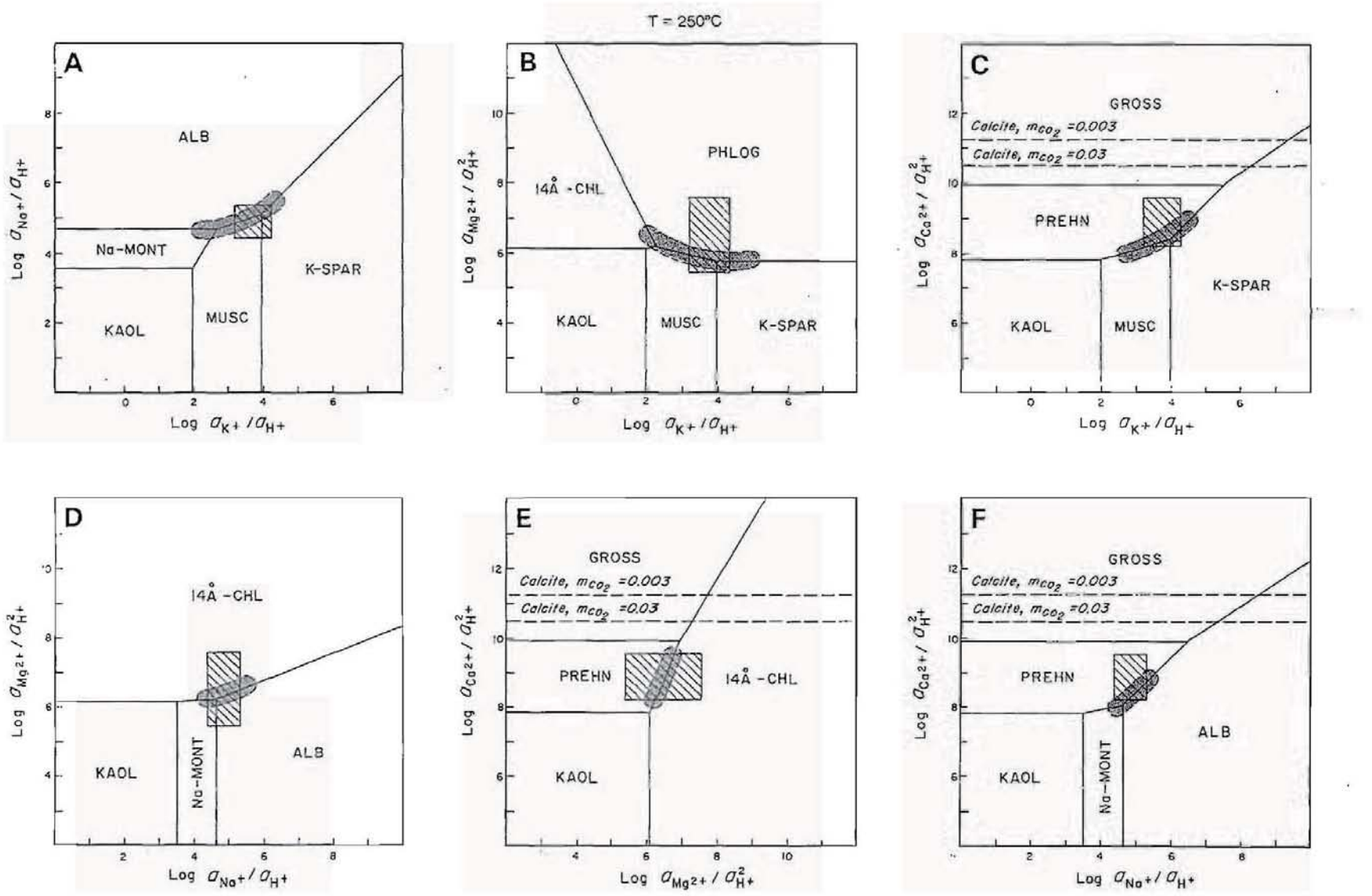
T = 250°C
A
ALB
Na-MONT
K-SPAR
KAOL
MUSC
Log a_{Na^+}/a_{H^+}
Log a_{K^+}/a_{H^+}
B
PHLOG
14Å -CHL
KAOL
MUSC
K-SPAR
Log $a_{Mg^{2+}}/a_{H^+}^2$
Log a_{K^+}/a_{H^+}
C
GROSS
Calcite, m_{CO_2} =0.003
Calcite, m_{CO_2} =0.03
PREHN
K-SPAR
KAOL
MUSC
Log $a_{Ca^{2+}}/a_{H^+}^2$
Log a_{K^+}/a_{H^+}
D
14Å -CHL
KAOL
Na-MONT
ALB
Log $a_{Mg^{2+}}/a_{H^+}^2$
Log a_{Na^+}/a_{H^+}
E
GROSS
Calcite, m_{CO_2} =0.003
Calcite, m_{CO_2} =0.03
PREHN
14Å -CHL
KAOL
Log $a_{Ca^{2+}}/a_{H^+}^2$
Log $a_{Mg^{2+}}/a_{H^+}^2$
F
GROSS
Calcite, m_{CO_2} =0.003
Calcite, m_{CO_2} =0.03
PREHN
ALB
KAOL
Na-MONT
Log $a_{Ca^{2+}}/a_{H^+}^2$
Log a_{Na^+}/a_{H^+}

Figure 3.27d. (Facing page) Activity diagrams for the aqueous species (A) K^+, Na^+, and H^+, (B) K^+, Mg^{2+} and H^+, (C) Ca^{2+}, K^+ and H^+, (D) Mg^{2+}, Na^+ and H^+, (E) Ca^{2+}, Mg^{2+} and H^+ and (F) Ca^{2+}, Na^+ and H^+ at 300°C and quartz saturation. The mineral phase boundaries are calculated from the thermodynamic data in Table 3.11. Values of $a_{Ca^{2+}}/a^2_{H^+}$ for precipitation of calcite at mco_2 concentrations of 0.03 and 0.003 are shown as dashed lines. The two values cover the range in mco_2 concentrations of the water analyses in Table 3.6. "Average" activity ratios for the Wairakei reservoir fluid (ruled box) are estimated for the aqueous species concerned from data in Table 3.6. Stippled areas approximate the given alteration assemblage thought to be in equilibrium at this temperature; these assemblages were estimated from thin section analyses (see Appendix 1). Mineral phases are 14Å-clinochlore (14Å-CHL), clinozoisite (CLNZ), grossular (GROSS), K-feldspar (K-SPAR), kaolinite (KAOL), laumontite (LAUM), muscovite (MUSC), Na-montmorillonite (Na-MONT), pericline (ALB), phlogopite (PHLOG), prehnite (PREHN), quartz (QTZ), wairakite (WAIR).

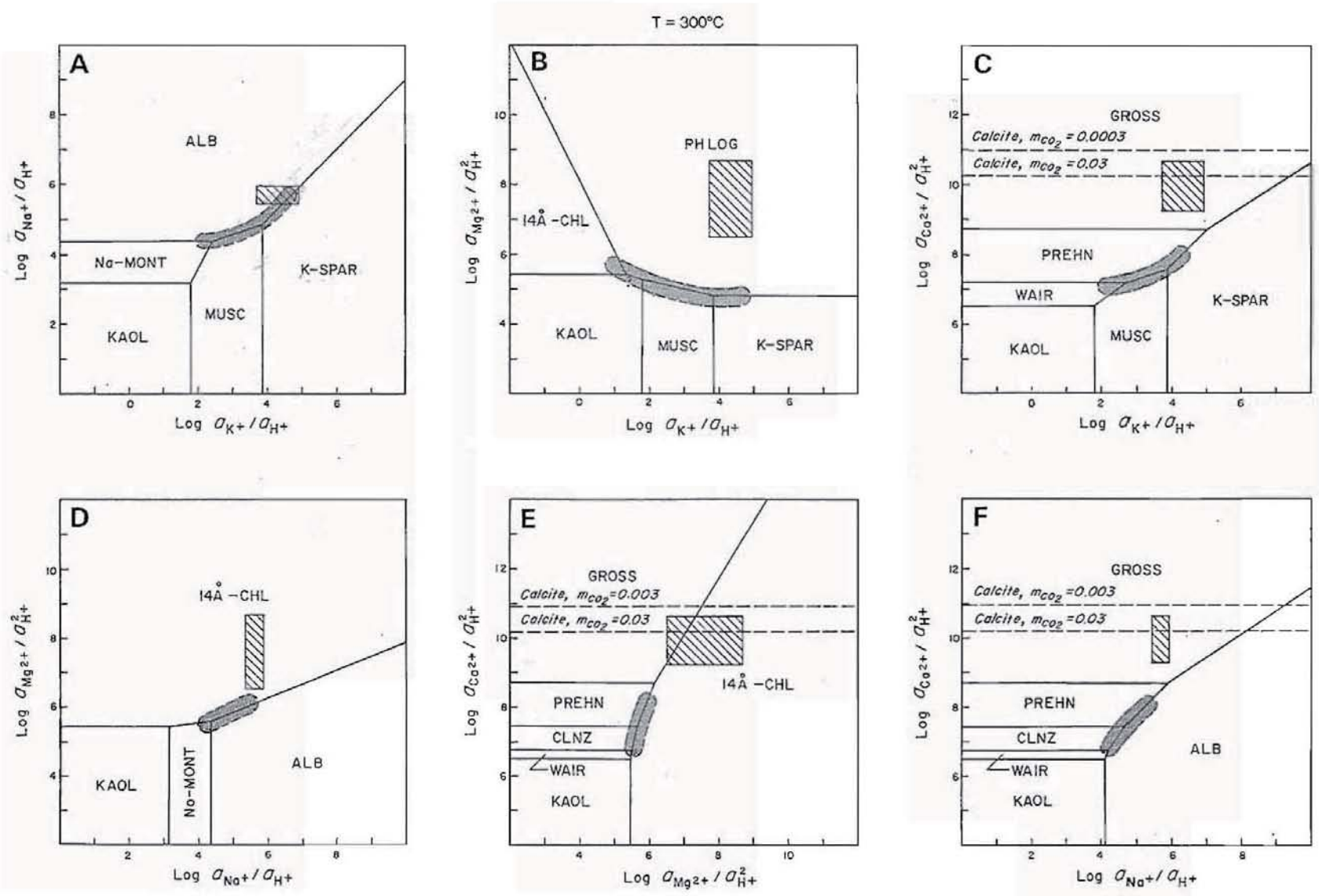
T = 300°C
A
ALB
Na-MONT
K-SPAR
KAOL
MUSC
Log a_{Na^+}/a_{H^+}
Log a_{K^+}/a_{H^+}
B
PHLOG
14Å -CHL
KAOL
MUSC
K-SPAR
Log $a_{Mg^{2+}}/a_{H^+}^2$
Log a_{K^+}/a_{H^+}
C
GROSS
Calcite, m_{CO_2} = 0.0003
Calcite, m_{CO_2} = 0.03
PREHN
WAIR
KAOL
MUSC
K-SPAR
Log $a_{Ca^{2+}}/a_{H^+}^2$
Log a_{K^+}/a_{H^+}
D
14Å -CHL
KAOL
No-MONT
ALB
Log $a_{Mg^{2+}}/a_{H^+}^2$
Log a_{Na^+}/a_{H^+}
E
GROSS
Calcite, m_{CO_2}=0.003
Calcite, m_{CO_2} =0.03
14Å -CHL
PREHN
CLNZ
WAIR
KAOL
Log $a_{Ca^{2+}}/a_{H^+}^2$
Log $a_{Mg^{2+}}/a_{H^+}^2$
F
GROSS
Calcite, m_{CO_2} =0.003
Calcite, m_{CO_2} =0.03
PREHN
CLNZ
WAIR
KAOL
ALB
Log $a_{Ca^{2+}}/a_{H^+}^2$
Log a_{Na^+}/a_{H^+}

were higher when laumontite formed. This is very likely since the Wairakei reservoir was in its waning stage prior to production discharge. However, the local occurrence of calcite with laumontite (and mordenite) at high levels within the reservoir (see Figs. 3.25 and 3.26) may indicate that fluid in the upper portion of the reservoir has a different composition from that calculated in Table 3.9. Since the intrusion of "cold" groundwater or "acid-sulphate" water is not known to occur in the upper zone of calcite alteration (Fig. 3.10), it is unlikely that the reservoir fluid varies substantially from the "average" value. The upper zone of calcite alteration, in part, may be the result of adiabatic cooling (boiling). A comparison of Figures 3.10 and 3.26 shows that the upper zone of calcite alteration occurs above the high-temperature upflow zone of the reservoir. It is possible that the upwelling higher temperature fluid contained slightly increased amounts of dissolved CO_2 and that, as the fluid rose and cooled by boiling, the partitioning of CO_2 into the vapour phase was strong enough to decrease the solubility of calcite to the point at which it precipitated.

Alkali Feldspar Equilibrium

The coincidence of the "average" reservoir fluid with the albite and K-spar fields on the activity diagrams for temperatures above ~225°C indicates that either or both minerals may precipitate. As noted earlier, the results of reservoir monitoring programmes carried out during the first 25 years of production indicate that the chemical composition of the Wairakei reservoir is relatively uniform throughout. Further, the chemical composition of the fluid changes very slowly and dramatic changes in the fluid chemistry are unlikely to occur (Ellis, 1979). Considering this, the fluid which produced propylitic alteration must have been nearly equivalent to the fluid that produced potassic alteration.

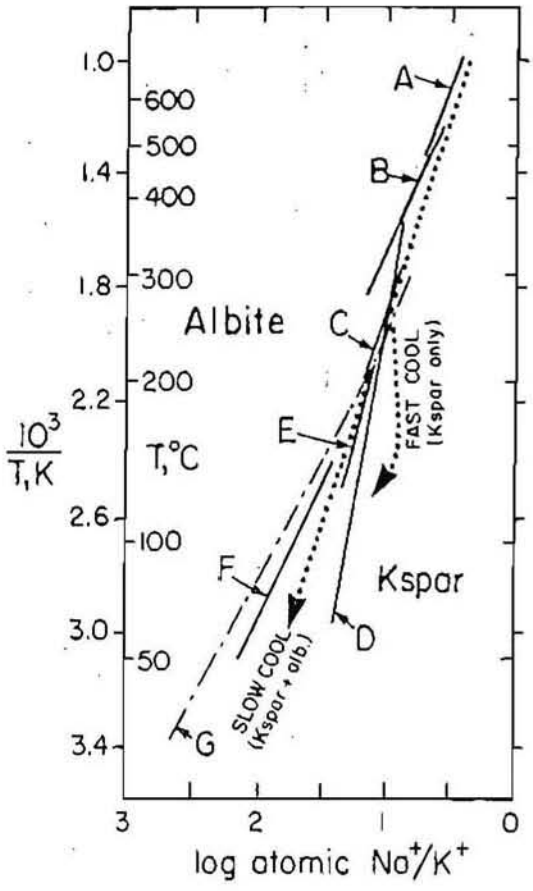

Figure 3.28. Relation between Na/K and temperature in fluid coexisting with alkali feldspars (from Sander, 1988b). Solid lines are from (A) Orville (1963), (B) Hemley (1967), (C) Ellis (1970), (D) Ellis and Mahon (1967), (E) White (1965) and (F) White (1965). Dash-dot line (G) is the calculated phase boundary of Fournier and Truesdell (1973). Variations in the slope and positioning of the lines are due to differences in experimental conditions and to differences in the compositions and structural state of the feldspars. Dotted line was constructed by Sander (1988b) to show the general stability fields of albite and K-feldspar. Cooling trends are discussed in the text.

The reservoir condition that most likely affects feldspar equilibrium is temperature. One way to visualize the effects that temperature may have on the stability of the alkali feldspars in equilibrium with a hydrothermal fluid is to apply the Na/K geothermometer in reverse. Normally the measured Na/K ratio of a geothermal fluid is used to estimate the temperature of the deep reservoir (Hemley, 1967; Fournier and Truesdell, 1973), but the concept may also be used to evaluate alkali feldspar equilibrium. Figure 3.28 summarizes the relationship between the Na/K ratio and temper-

ature. It can be seen from the diagram that the precipitation of pericline (Albite) and adularia (K-spar) may be explained by simple variations in the temperature of the fluid at a relatively constant Na/K ratio. Three possibilities exist. If the fluid is heated or cooled slowly, equilibrium between pericline and adularia is maintained and both minerals precipitate. However, if the fluid cools rapidly, equilibrium is not maintained and only adularia precipitates. A third possibility which is not shown on the diagram is that if the fluid (rock) is heated rapidly, then only pericline will precipitate. The first two possibilities quite satisfactorily explain the oscillation between pericline-stable and adularia-stable alteration assemblages in "transitional propylitic-potassic alteration". The third possibility is also important because it may help explain the occurrence of pericline at relatively shallow levels in the northern portion of the reservoir. If the reservoir was heated rapidly by an upwelling high-temperature fluid, it is likely that pericline would precipitate at the expense of adularia until equilibrium was regained.

Low Temperature Hydrothermal Biotite

Secondary hydrothermal biotite was identified in core samples from the relatively low temperature (T<225°C) portions of the reservoirs at both Iamalele and Wairakei. In both cases secondary biotite occurred in quartz-free rhyolite. At Iamalele hydrothermal biotite replaces primary amphibole and forms overgrowths on magmatic biotite contained in the flow-banded Mona Malala rhyolite dyke(?). At Wairakei biotite alteration occurs as fine-grained shreddy clusters of crystals replacing the groundmass and mafic mineral phenocrysts in the composite lavas of the Haparangi Rhyolite. At both locations the quartz-free rhyolite units cut across or are intercalated within thick sequences of rhyolitic ignimbrite.

As noted earlier, the secondary biotite at Wairakei formed at temperatures <225°C. If reservoir temperatures in the near-surface environment

at Iamalele conform to the equilibrium vapour-liquid curve for water, then the temperature at which hydrothermal biotite formed must be less than 225°C, just as at Wairakei.

The occurrence of low temperature (T ≈ 200°C) hydrothermal biotite within the geothermal reservoirs at Wairakei and Iamalele is significant because secondary biotite generally forms at temperatures greater than ~300°C (Roberts, 1973; Bean, 1974; Kendall, 1976; Hoagland and Elders, 1978; Henley and Ellis, 1983). However, it can be seen from the $a_{Mg^{2+}}/a^2_{H^+}$ versus $a_{K^+}/a^2_{H^+}$ diagrams in Figures 3.27b and c that the "average" Wairakei reservoir fluid enters the phlogopite phase field at a temperature of ~205°C. Two minerals considered to be in equilibrium with phlogopite from analyses of several polished sections are adularia and white mica. Significantly, phlogopite-adularia-white mica (muscovite) is the assemblage indicated by the location of the "average" Wairakei fluid in Figures 3.27b and c (diagram B) for temperatures between approximately 205° and 260°C. Unfortunately water analyses of the "deep" reservoir fluid at Iamalele are not available and a similar comparison between the fluid composition and theoretical phase relationships could not be completed.

In addition to the occurrences at Iamalele and Wairakei, low temperature (T less than ~250°C) hydrothermal biotite has been identified associated with distal potassic alteration related to the Yerington and Ann Mason porphyry copper deposits in Nevada, U.S.A. (J.H. Dilles, personal communication) and at the Dieng geothermal system in Indonesia (Fauzi, 1985)[5]. At Jefferson Canyon in the Toquima caldera complex (Nevada, U.S.A.) potassically altered rhyolite ash-flow tuff contains disseminated euhedral biotite. The biotite is pleochroic, shows no obvious optical sign of significant retrograde alteration and appears to coexist with quartz and

---

[5]Fauzi (1985) notes that although the measured reservoir temperatures for "low-temperature" hydrothermal biotite range from 235° to 260°C, it is possible that secondary biotite formed at temperatures near 315°C.

and adularia which crystallized at temperatures ranging from 200° to 250°C (D.R. Boden, personal communication).

The occurrences of secondary biotite cited above, which are supported by the fluid-mineral equilibria shown in Figures 3.27b and c, indicate that low-temperature hydrothermal biotite may be more common than previously thought.

Metallization

In the following section trace and minor element data are presented for about 500 bulk rock samples from Wairakei. Descriptions and locations of the samples are given in Appendix 1 and the chemical data are tabulated in Appendix 3. The locations of most of the samples of drill core and cuttings are plotted on Plate 6C. Ore minerals were identified in polished thin sections of several samples and the locations of these sites are marked on Plates 6B and 6C.

Steam Production Equipment

Steam used to power the electrical generators is separated from the geothermal fluid by rapidly reducing the confining pressure on the fluid (flashing). Following steam separation the residual liquid (T ~140°C) is transferred via pipeline to silencers where the fluid is reduced to atmospheric pressure prior to discharge from the production area. During the steam separation process metal-rich scale is deposited on the interior walls of the wellhead production equipment and amorphous silica (siliceous sinter) precipitates on the walls of the silencer weirbox (Fig. 3.29) and hot water drains (Fig. 3.1). Both the metal-rich scale and siliceous precipitate contain strongly anomalous amounts of gold, silver, platinum group metals and a variety of other elements including most of the rare earths.

Figure 3.29. Photograph of production wellhead equipment in the central bore field at Wairakei; view is to the northwest. (For a schematic drawing of wellhead equipment see Figure 3.31). Vertical cylinders in central and right foreground are cyclone separators which separate the steam from the two-phase fluid. The steam leaves through the bottom of the separator and travels via pipeline (pipes traversing the centre of the photograph) to the generating station located about 3 km to the east of the photograph. The fluid leaves the separator through the pipe extending from half way up the column and enters the water tank which is connected by a series of valves to either the silencers (wooden columns emitting steam) or a secondary separation system (flash plant; stainless steel cylinders behind wooden silencer in left foreground). The fluid is reduced to atmospheric pressure in the silencer and exits the base into a weirbox (not shown) and subsequently into the hot water drain (upper extreme right of photograph, identified by faint rising steam). Twin silencers (white) in the centre of the photograph are coated with silica precipitated directly from the discharging fluid. Yellowish white siliceous precipitate piled on the ground (1) adjacent to the twin silencers to the right of the silica-coated silencers and (2) adjacent to the separator in the centre foreground has been removed from the silencers. Siliceous precipitate piled on the ground near the hot water drain was removed from the drain. The siliceous sinter shown in the photograph is strongly anomalous in gold, silver and a variety of other metals.

Siliceous Precipitates

Approximately 125 samples of siliceous precipitate were collected from silencers, weirboxes and hot water drains. Very little petrography was done on the siliceous precipitates, since most of them were composed of amorphous silica or cristobalite. The samples were analysed to deter-

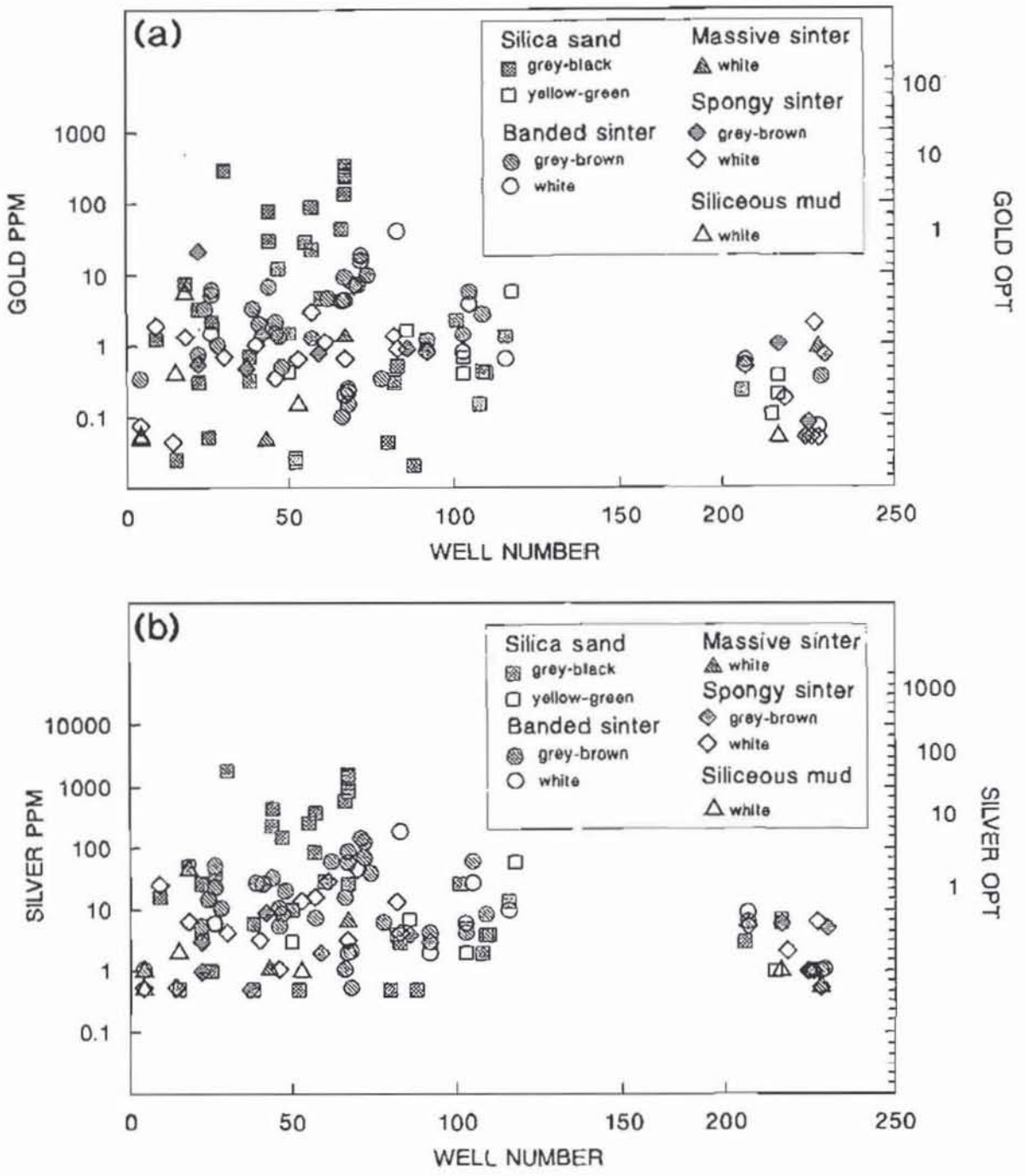

Figure 3.30. Gold (a) and silver (b) content of siliceous precipitate collected from silencers and hot water drains at Wairakei.

mine the abundances of several trace elements (see Appendix 3). The data for gold and silver are plotted in Figure 3.30. All of the samples contained anomalous gold values, and most contained very high values. These data are important because they document that the hydrothermal fluid at

Wairakei is capable of "leaching", transporting and depositing a wide variety of elements.

Several of the samples were analysed for the platinum group elements. Because of interferences from other elements, particularly gold and silver, the detection limits for platinum and palladium were very high, but still three samples contained detectable values of platinum and palladium (see Table 3.12).

Metal-rich Scale

Metal-rich scale from the back-pressure plate (Fig. 3.31) of well 66 was collected during 1984. Analyses of similar material from the Broadlands geothermal area (Brown, 1986) revealed that the scale contained impressive amounts of gold and silver among other economically important elements, but the only mineralogical analysis of the sample consisted of X-ray diffraction determinations. Since two quantitative analyses of the metal-rich scale from well 66 and well 67 at Wairakei indicated gold and silver contents of 1362 grams per tonne (g/t) Au, 5088 g/t Ag and 1939 g/t Au, 3792 g/t Ag respectively (P.J. Roberts, written communication), I wanted to find out whether the metal-rich scale was an amorphous "dumping"

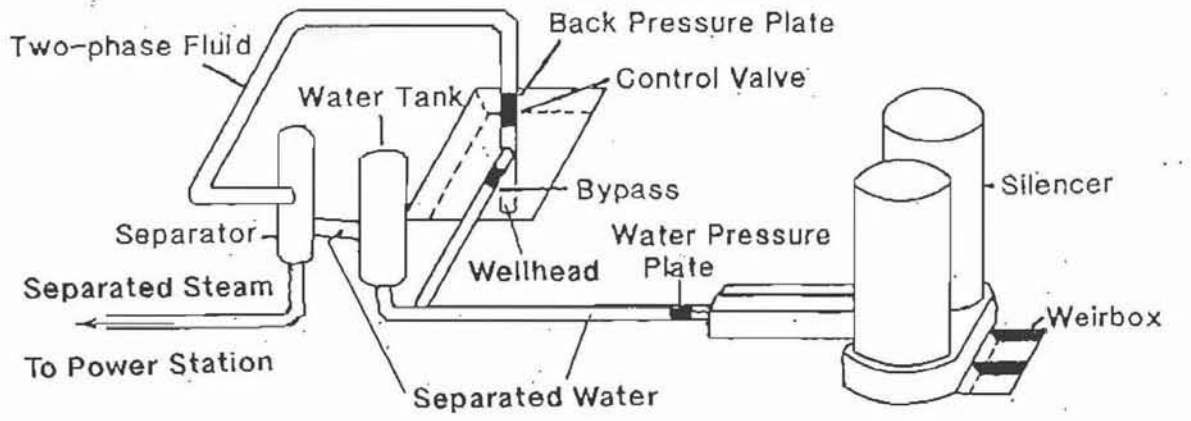

Figure 3.31. Schematic drawing of the wellhead production equipment required to separate steam from the two-phase fluid. Diagram modified from Brown (1986; Figure 1, page 980).

Table 3.12. Partial trace element composition (ppm) of siliceous precipitate collected from silencers and hot water drains at Wairakei

Well	Au	Ag	Pt	Pd	Se	As	Sb	Cu	Pb	Zn	Type	Sample Number
18	6.70	60	<0.05	3.100	4.5	310	78	29	32	120	Sand	125018
	7.00	63	<0.04	0.120	4.0	320	74	31	34	120	Sinter	125343
30	260	1880	--	--	240	120	45	5600	1480	1040	Sand	125025
44	78.1	441	--	--	--	890	492	1070	374	690	Sand	125368
	30.5	232	--	--	--	290	30	1130	240	296	Sand	125369
47	12.5	153	--	--	--	210	19	510	120	700	Sand	125385
55	29.2	262	--	--	--	80	13	1120	250	153	Sand	125393
57	89.2	382	--	--	--	100	6	2100	770	560	Sand	125400
66	46.1	600	--	--	--	250	70	2750	520	730	Sand	125388
67	330	1611	--	--	--	--	--	2600	--	--	Sand	10383
	137	1490	--	--	--	200	22	3400	815	570	Sand	125395
	8.40	52	1.0	<0.05	8.0	24	160	150	32	50	Sinter	125032
70	3.10	26	<0.08	0.040	1.9	29	210	150	34	65	Sinter	125035
83	41.8	192	--	--	--	25	9	770	29	158	Sinter	125366
217	0.510	9.5	<0.6	<0.011	<1.0	2000	61	40	140	38	Pyrite	125344

Sample type: Siliceous sand and sinter and rock fragments collected from the bottom of the silencer (Sand), siliceous sinter collected from the interior walls of a silencer or weirbox (Sinter), pyrite separated from silica sand and sulphide discharged from well 217 (pyrite). -- = not analysed. Pt and Pd analyses by neutron activation.

Table 3.13. Composition and textural characteristics of minerals contained in metal-rich scale from the back pressure plate of Wairakei well 66

Mineral	Composition	Trace metals	Textural characteristics
Cu-SULPHIDES			
bornites	$Cu_{5.8}Fe_{0.2}S_{4.0}$ to $Cu_{4.9}Fe_{0.7}S_{4.4}$	Au, Ag, As, Sb, Ni, Pb	Early formed grains
chalcopyrite	$CuFeS_{2.2}$	Co, Zn, Ag, Pb, Se, Au, Ag	Rims on and inclusions in magnetite
Pb-SULPHIDES			
argentiferous galena	$Pb_{0.9}S$	Ag, Se, Zn	<10μ inclusions in chalcopyrite; contains submicron-size inclusions of aguilarite
Fe-SULPHIDES			
pyrrhotite	$Fe_{0.8}S$	None detected	Elongated crystals; contained in silicious precipitate
pyrite	$FeS_{2.1}$	Pb	Euhedral crystals; contained in siliceous precipitate
Ni-SULPHIDES			
millerite	$Ni_{1.1}S$	As, Sb, Fe, Pb	Early formed crystals; encapsulated in bornite
SELENIDES			
aguilarite	$Ag_{2.9}(Fe,Cu,Pb,Zn,Co)_{1.0}SeS_{1.5}$	Au, Zn, Pb	Inclusions in galena
Ag-SULPHOSALTS			
polybasite (?)	$(Ag,Cu,Fe)_{9.8}(Sb,As)_{3.3}S_{11.0}$	None detected	Irregular crystals; substantially nonstoichiometric
pyrargyrite (?)	$Ag_{6.0}Sb_{2.0}S_{10.0}$	None detected	Irregular crystals; substantially nonstoichiometric
Cu-SULPHOSALTS			
tetrahedrite	$Cu_{2.4}(Sb,As)S_{3.5}$	Ag, As, Zn, Pb, Pt	Rims on and possibly replaces bornite; rims on niccolite; rims on breithauptite
Ni-ARSENIDES			
niccolite	$Ni_{1.1}(As,Sb)$	Sb, Fe, Pb, S, Te, Zn, Au, Ag	Major mineral phase; rims on, replacement of, or fracture filling in bornite
maucherite	$Ni_{<3}As_2$	Au, Ag, Sb, Pt, Fe, Pb	Occurs locally
breithauptite	NiSb	As	Rims on niccolite

of precious and other elements or if actual mineral phases existed. The results of preliminary electron microprobe and reflected light microscopic analyses of the scale from well 66 are summarized in Table 3.13 (see Appendix 3 for additional data).

It was surprising to find that not only a few minerals had formed, but a suite of economically important minerals was present (Fig. 3.32).

Figure 3.32. Photomicrographs (A,B,C,D) and back scatter electron images (E,F) of metal-rich scale removed from a back pressure plate from well 66.

A. Hematite-silica (bluish white) "core" with fine mesh of acicular crystals of magnetite (light bluish white) radiating outward from the "core". Magnetite crystals and locally hematite-silica are surrounded by a band of chalcopyrite crystals (bright white to yellowish white). The chalcopyrite contains microscopic grains of galena which in turn host micron-sized grains of aguilarite. Field of view ~1 mm.

B. Chalcopyrite (yellow) grain containing abundant inclusions of argentiferous galena (white). Field of view ~1 mm.

C. Bornite (bluish brown) is rimmed and replaced by niccolite (flesh). Field of view ~3 mm.

D. Bornite (bluish brown) rimmed and replaced by niccolite (pinkish white) in the large grain in upper right. Elsewhere bornite rimmed or replaced by tetrahedrite (beige). Small yellow inclusions in bornite are chalcopyrite. Field of view ~3 mm.

E. Niccolite (dark) with breithauptite rim (dark); note gradational contact. Black spot is a witness mark made by the electron microprobe. Bright spots along the edge of the niccolite portion of the crystal are micron-sized grains of electrum.

F. Bornite (dark) rimmed by niccolite (light). Micron-sized grains in centre of the bornite crystal are electrum.

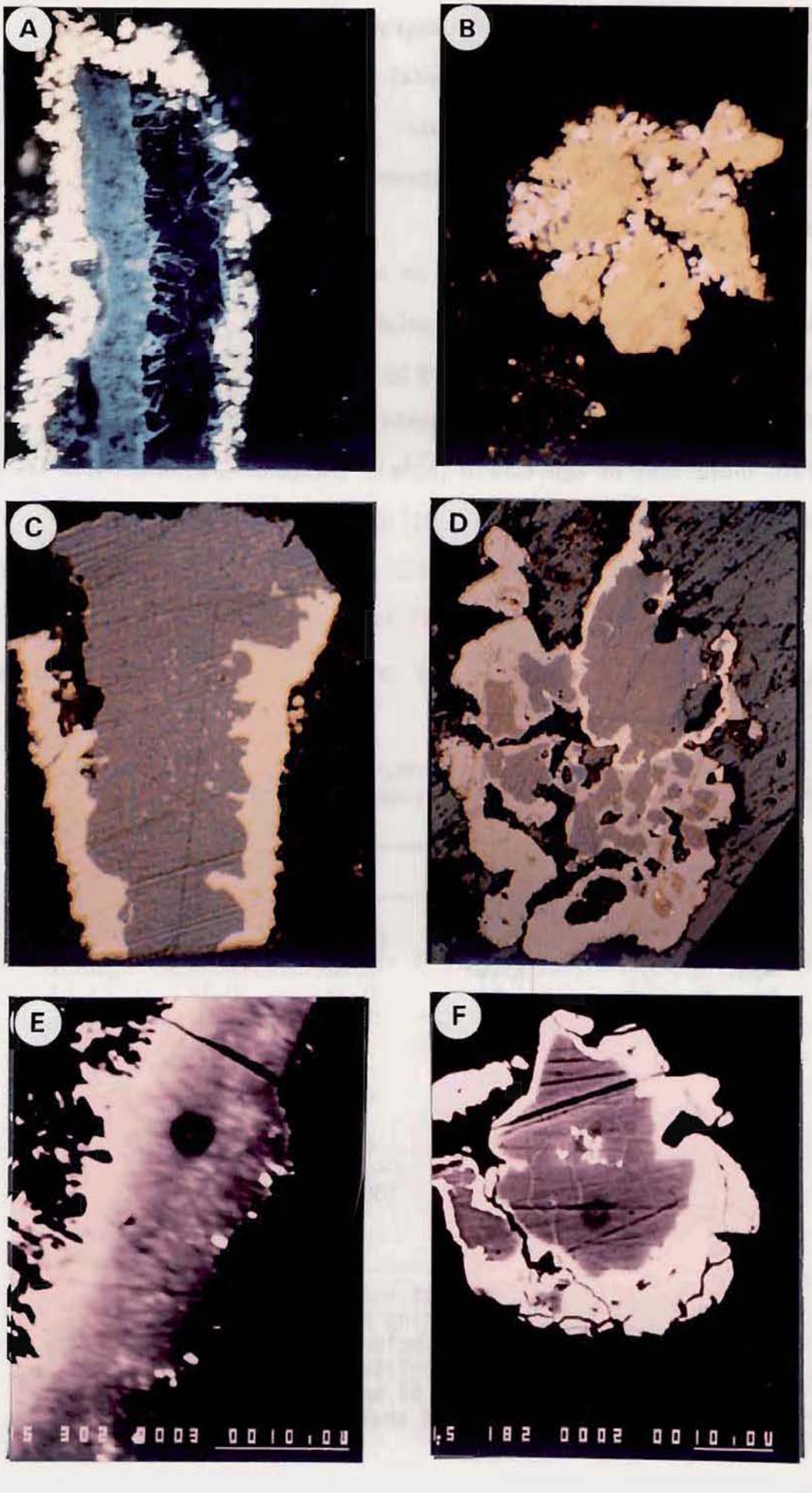
A
B
C
D
E
F

Ag:Au ratios of ~3:1, while later niccolite contains electrum with Ag:Au ratios of 7:1 to 10:1. There is a consistent time-dependent substitution of As for Sb in niccolite such that mineral rims are enriched in Sb and may grade into breithauptite (NiSb)(Fig. 3.32D). Within this sequence precious metals, generally silver-rich electrum (Table 3.14), occur as <1 micron (μ) inclusions in bornite (Fig. 3.32E), chalcopyrite (Fig. 3.32F), tetrahedrite, niccolite and breithauptite (Fig. 3.32D).

Hydrothermal Reservoir

Approximately 225 samples of drill core and cuttings were analysed for a wide variety of elements including many of the rare earths. Gold grades encountered deep within the reservoir at Wairakei are commonly low (<0.01 to 0.04 ppm). In only two of 225 samples analysed did the gold content of reservoir rocks exceed 0.04 ppm (Figs. 3.33a and b). The two higher gold values (0.12 and 0.13 ppm) occurred in core taken from well 54. These samples came from areas which are in or adjacent to steep geothermal gradients which probably result from local mixing with cooler groundwater (areas above and below 200°C isotherm in centre part of the well in Fig. 3.10). Both samples show mineral textures consistent with transitional potassic-propylitic alteration.

Ore minerals were identified in polished sections of core collected from several different wells located throughout the reservoir (Figs. 3.34 and 3.35). All of the samples which contained economically important minerals were collected from the zone of transitional potassic-propylitic alteration. The minerals which are associated with transitional alteration are extremely fine-grained, generally <5 μ, and include argentite, electrum, gold-palladium alloy, chalcopyrite, galena, monazite, cassiterite and sphalerite.

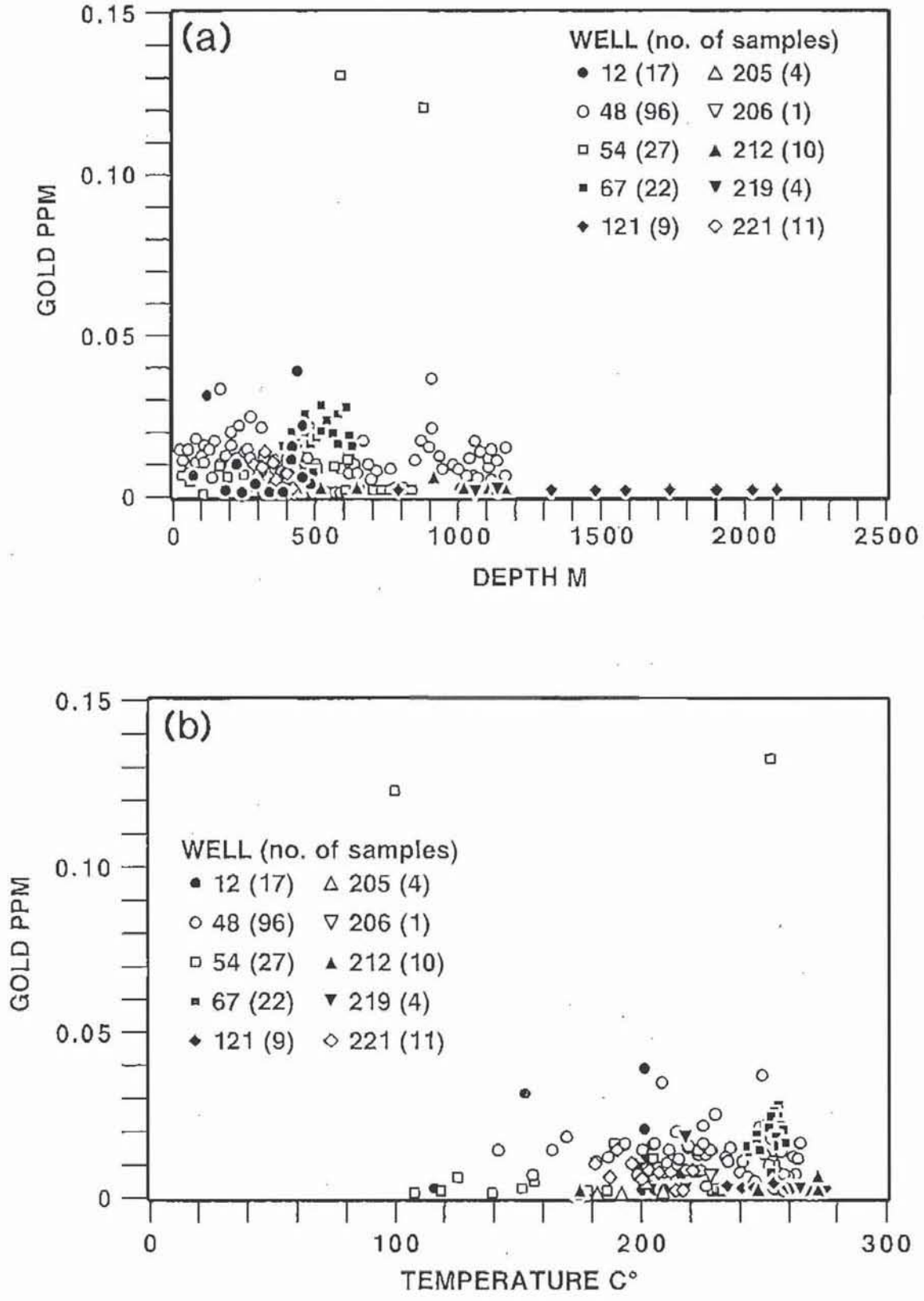

Figure 3.33. Graph of gold content versus depth (a) and temperature (b) for 225 core and cuttings samples collected from the Wairakei reservoir.

Rare Earth Elements

Rare earth elements (REE) and Y data were determined by bulk rock neutron activation for 75 samples of drill core and cuttings and 17 samples of siliceous precipitate (sinter) collected from wellhead production equipment. La, Ce, Nd, Sm, Eu, Tb, Yb and Lu data and chondrite-normalized abundance patterns for a group of representative samples are presented in Table 3.15 and Figure 3.36.

In general, the bulk rock samples have similar REE patterns regardless of lithology. This may reflect a common magmatic source for the volcanic rocks or REE homogenization due to hydrothermal alteration. The common occurrence of hydrothermal monazite in potassically altered rocks supports the concept of REE homogenization due to hydrothermal alteration.

REE patterns for the hydrothermally altered samples retain the overall characteristics of unaltered pumice collected from the Taupo Pumice (sample 125206). However, the slope of the REE patterns of many of the altered samples deviates slightly from that of the Taupo Pumice, reflecting variable degrees of REE mobility. The most common change involves a small depletion of the heavy REEs and corresponding enrichment of the light REEs. Typical REE abundance patterns for the hydrothermally altered rocks have La values ~60 times that of the average chondrite and relatively low La/Sm and Tb/Lu ratios. The most notable difference between the unaltered Taupo Pumice and the hydrothermally altered samples is in the abundance of Eu. At the present time, there are insufficient data to quantify the extent of REE mobility for specific alteration assemblages, but qualitatively, variations in the abundance of Eu correlate with the abundance of certain alteration minerals. The most important alteration effects include (1) the development of a positive Eu anomaly when either pericline or illite/muscovite is abundant (Fig. 3.34), (2) the retention of the initial bulk rock REE pattern during silicification and mordenite alteration and (3) a

Figure 3.34. Typical occurrences of gold-palladium and hydrothermal monazite in transitional propylitic-potassic alteration; back scatter electron images. Photographic plates for Figure 3.34 are in the pocket at the back of Volume I.

A. Pericline (Ab)-clinochlore (chl) veinlet (propylitic alteration) invading pumiceous silty tuff. Plagioclase grains completely replaced by pericline (light grey) which in turn is replaced by adularia (white, see medium-sized grain in lower left); adularia overgrowths on albite are cross cut by pericline microveins (not shown). The euhedral pyrite (py) grain which is surrounded by pericline may be associated with adularia (potassic) alteration. The occurrence of hydrothermal monazite (mz) and gold-palladium (Au-Pd) are discussed below; core sample 125626, well 205, 701 m, Member 4 of the Waiora Formation.

B. Magnified view of the area outlined in A. Pericline (Ab)-clinochlore (chl) veinlet "cross cut" by an adularia (ad) microvein (light grey). Hydrothermal monazite (mz) occurs along the contact between pericline and adularia. The gold-palladium (Au-Pd) grain is probably related to adularia-monazite (potassic) alteration, but may be earlier, i.e., related to propylitic alteration. Textured appearance of pericline outside the fracture is the result of an inadequately polished surface.

C. Magnified view of the area outlined in B.

D. Hydrothermal monazite associated with quartz (qz)-adularia (ad) (potassic) alteration of the groundmass of a spherulitic, quartz-free rhyolite. Voids may have contained phyllosilicates (illite-smectite), but are most likely due to incomplete polishing; core sample 125694, well 218, 701 m; Karapiti Rhyolite.

E. Quartz (qz, dark grey)-adularia (ad, light grey) veinlets containing disseminated pyrite (py, larger white grains; dominant) and monazite (mz); note weakly zoned vein envelopes with adularia predating quartz. Hydrothermally altered fault(?) breccia; core sample 125630, well 205. 899 m, Te Mihi Rhyolite.

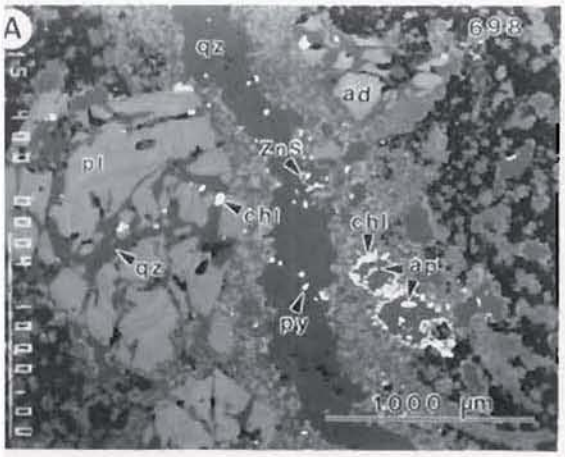

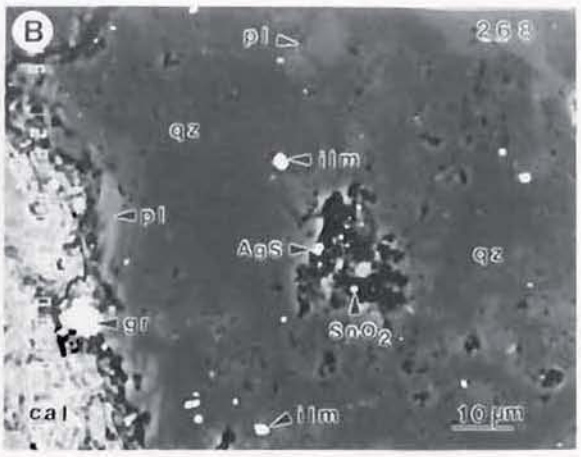

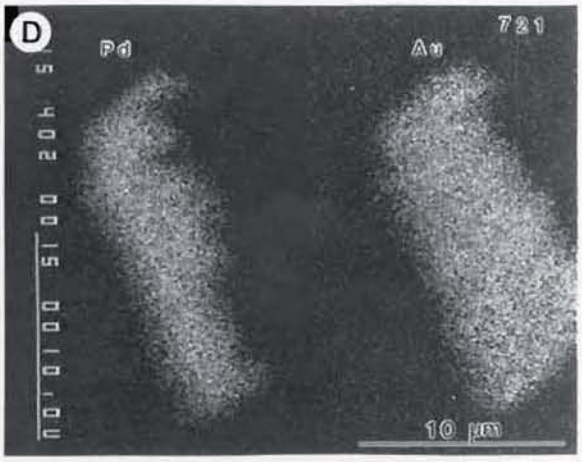

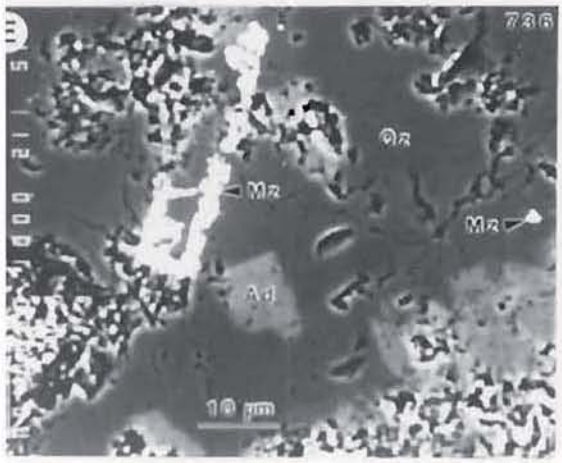

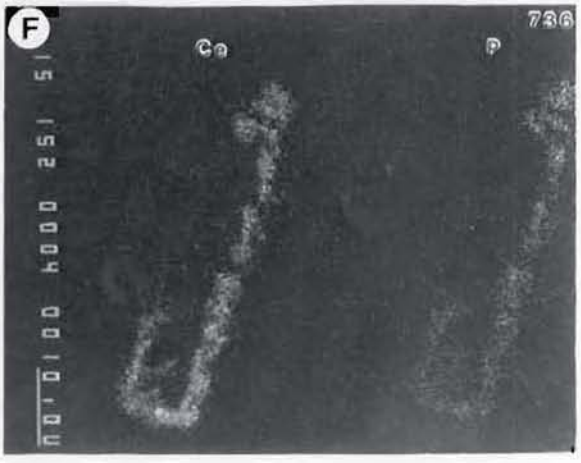

Figure 3.35. Examples of precious, platinum group, base and rare earth element mineralization associated with potassic alteration; back scatter electron images. Photographic plates for Figure 3.35 are in the pocket at the back of Volume I.

A. Quartz (qz, dark grey)-sphalerite (ZnS, white)-pyrite (py, white, dominant) vein with quartz-adularia (ad, light grey) envelope (potassic alteration) pervading flow-banded quartz-free rhyolite. Large andesine phenocryst (pl) replaced by the assemblages quartz-pyrite-clinochlore (chl, white) and quartz-adularia (minor) along vein envelope. Mafic minerals (amphibole?) replaced by the assemblage quartz-clinochlore-pyrite-chlorapatite (ap). Andesine phenocrysts (upper right) and groundmass replaced by the assemblage adularia-quartz-pyrite. Unpolished areas are black; core sample 125698, well 218, 671 m, Karapiti Rhyolite.

B. Groundmass of quartz-rich ignimbrite replaced by quartz (qz, dark grey)-hosting argentite (AgS), cassiterite (SnO_2) and ilmenite (ilm); note remnant andesine (pl, medium grey). Calcite (cal) and grothite (gr) replace a mafic phenocryst (amphibole?) on the left side of photo; core sample 125268, well 121, 1541 m, Wairakei Ignimbrite I.

C. Andesine phenocryst in a sandy lithic tuff replaced by quartz (qz, black background)-adularia (not shown) alteration hosting a zoned gold-palladium (Au-Pd) grain. Bulk rock alteration includes: (1) an early propylitic assemblage (albite-epidote-chlorite-pyrite), (2) an intermediate aged potassic assemblage (quartz-adularia-wairakite-illite-pyrite), and (3) late calcite alteration; core sample 125721, well 216, 457 m, Member 4 of the Waiora Formation.

D. Palladium (Pd) and gold (Au) x-ray intensity images of Figure C.

E. Replacement of groundmass feldspar and interstitial glass of a spherulitic flow-banded rhyolite by the equilibrium assemblage quartz (qz)-adularia (ad)-monazite (mz). Rough surface areas due to inadequate polishing; core sample 125736, well 211, 274 m, Haparangi Rhyolite.

F. Cerium (Ce) and phosphorous (P) x-ray intensity images of Figure E.

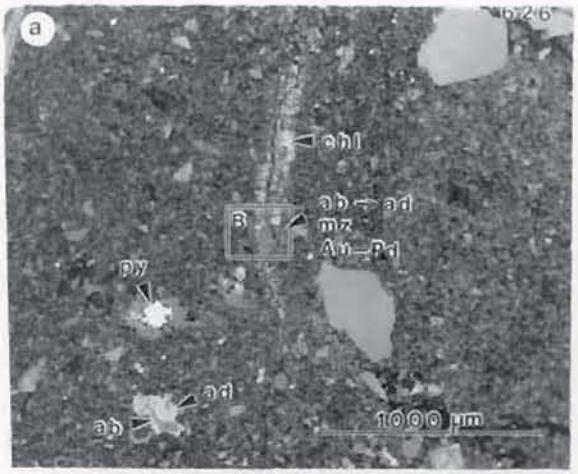

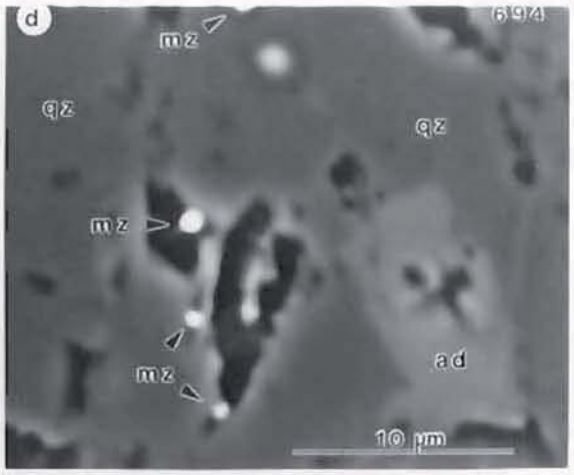

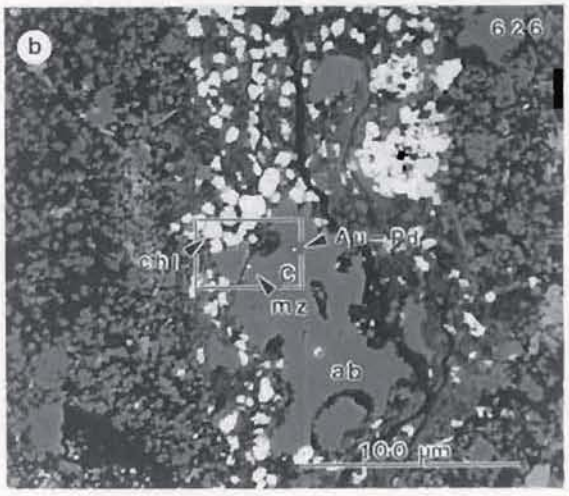

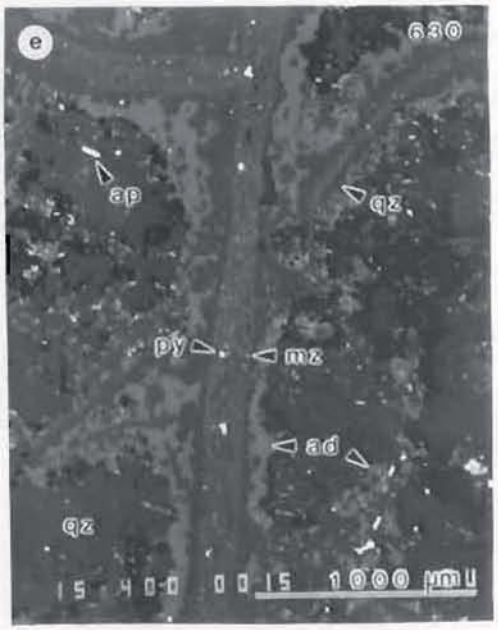

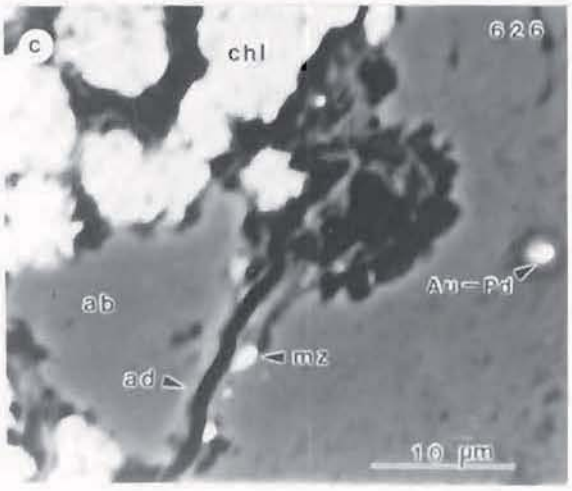

Table 3.15. Selected rare earth element data for representative bulk rock and siliceous precipitate samples

Unit	La/Sm	Tb/Lu	La (ppm)	LaCN	Sm (ppm)	SmCN	Tb (ppm)	TbCN	Lu (ppm)	LuCN	Well number	Sample number
Tp	3.2	0.8	28.0	90	5.45	28	0.8	17	0.67	21	surface	206
Wr	3.8	0.8	18.6	60	3.10	16	0.4	8	0.36	11	54	141
Hu	3.6	1.0	20.2	65	3.56	18	0.6	13	0.40	12	54	148
Wa5	3.5	0.9	26.0	84	4.62	24	0.7	15	0.55	17	12	349
Ha	3.6	0.8	20.3	65	3.59	18	0.5	11	0.40	12	205	246
Wa4	3.8	0.9	21.2	68	3.55	18	0.5	11	0.60	11	54	150
Wv	3.8	1.2	18.6	60	3.04	16	0.6	13	0.34	11	48	127
Wa3	3.2	1.0	19.1	62	3.81	20	0.6	13	0.41	13	54	169
Kp	3.9	1.0	26.7	86	4.47	23	0.9	19	0.59	18	212	307
Wa2	3.4	0.8	12.4	40	2.29	12	0.3	6	0.27	8	54	176
Wk3	4.8	0.6	15.1	49	1.99	10	0.2	4	0.24	7	54	191
Wk2	4.5	0.8	16.7	54	2.36	12	0.3	6	0.25	8	48	133
Oh	3.9	1.2	22.6	73	3.61	19	0.7	15	0.41	13	121	271
Sinter	6.0	1.2	1.0	3	0.10	0.5	0.05	1.1	0.03	0.9	28	024
Sinter	3.8	1.1	2.5	8	0.40	2.1	0.10	2.1	0.06	1.9	62	031
Sinter	25.0	1.4	1.6	5	0.04	0.2	0.10	2.1	0.05	1.6	67	032
Sinter	4.3	2.7	1.0	3	0.14	0.7	0.04	0.8	0.01	0.3	70	035
Sinter	5.0	2.3	0.6	2	0.08	0.4	0.10	2.1	0.03	0.9	72	036

Rock units are Taupo Pumice (Tp); Wairakei Breccia (Wr); Huka Falls Formation (Hu); Waiora Formation, Member 5 (Wa5), Member 4 (Wa4), Member 3 (Wa3), and Member 2 (Wa2); Haparangi Rhyolite (HA); Waiora Valley Andesite (Wv); Karapiti Rhyolite (Kp); Wairakei Ignimbrite, Member 3 (Wk3) and Member 2 (Wk2); Ohakuri Group (Oh). All sinter samples are siliceous. Sample numbers are preceded by the prefix 125, e.g., 206 is sample 125206.

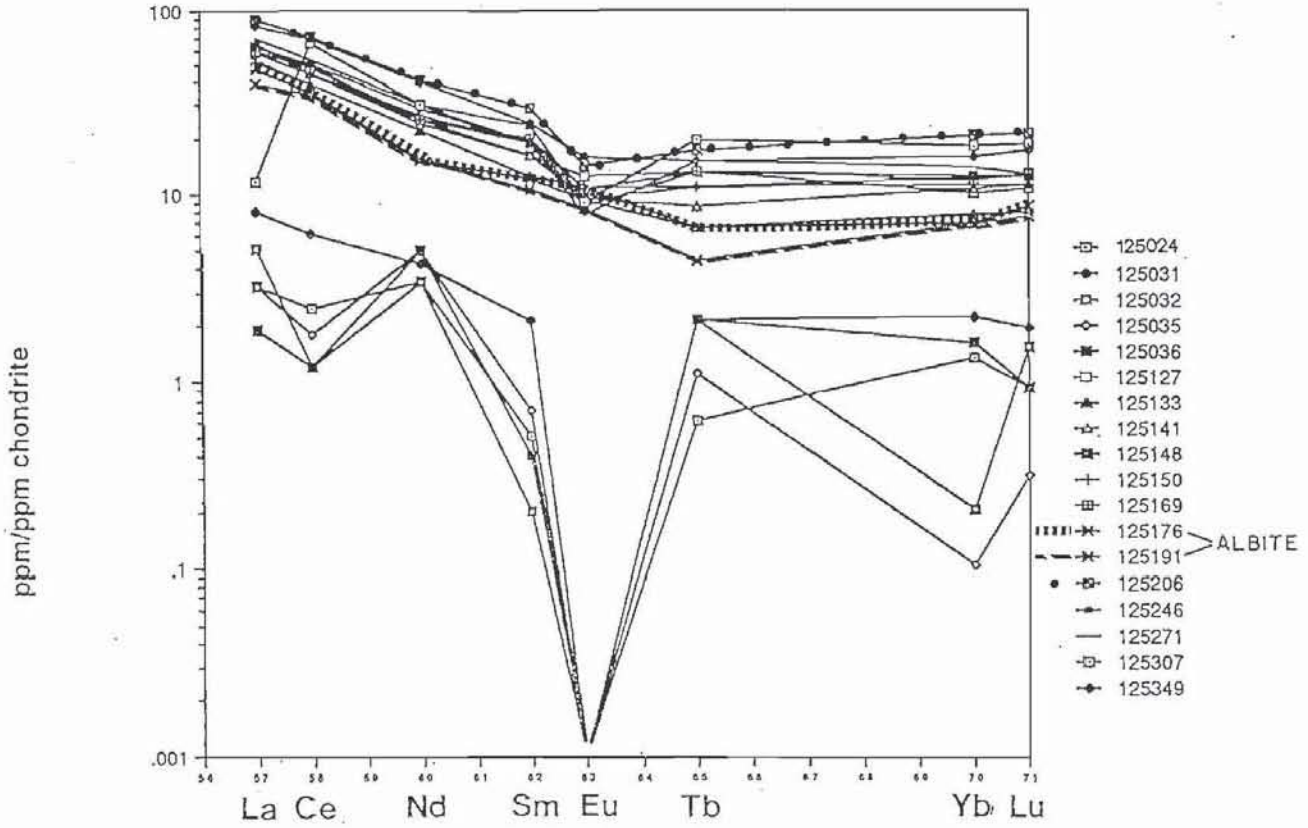

Figure 3.36. Chondrite normalized REE patterns for one representative bulk rock (core) sample from each lithologic unit at Wairakei and five siliceous precipitate samples collected from production wellhead equipment; see Table 3.15 for sample descriptions. Refer to Appendix 1 for detailed lithologic descriptions and Appendix 3 for geochemical data. Note: (1) the similarity in REE patterns for rocks collected from the geothermal reservoir, regardless of lithology, (2) the extreme negative Eu anomalies for the siliceous precipitates and (3) the slight positive Eu anomalies for samples 125176 and 125191.

slight decrease in the abundance of Eu when adularia is a major component of the altered rock.

As compared to the bulk rock data, siliceous precipitate has an order of magnitude lower REE content, a slight depletion of the light REEs relative to the heavy REEs and an extreme negative Eu anomaly (Eu <0.05 ppm; see Fig. 3.36). Except for trace amounts, Eu is either not transported in or not deposited by the hydrothermal fluid within the production equipment. The reason for this is not clear, but Eu^{2+} may have been selectively concentrated in early-formed pericline (Sverjensky, 1984). Alternatively, Eu may have been concentrated in illite during potassic alteration. Potassic alteration is common in most portions of the reservoir from which the geothermal fluid is withdrawn, and since illite is a common hydrothermal mineral associated with potassic alteration it is very possible that illite at least contributes to the low levels of Eu.

Discussion

The diversity and abundance of metals, particularly gold and silver, deposited within the production wellhead equipment clearly documents the ability of a low salinity and low total sulphur reservoir fluid to transport and deposit ore-grade quantities of economically important elements. In fact, very small-scale high-grade ore bodies are currently forming within the production equipment. In contrast with this high-grade metallization, only trace amounts of gold (<0.04 g/t) and silver (<1.0 g/t) are being deposited within the reservoir. The major causes of precious metal precipitation at the wellhead are obvious, but the cause of metal deposition within the reservoir is less clear.

In the wellhead equipment metal-rich scale containing gold and silver grades as high as 1939 g/t (56.6 troy ounces per ton (ozt/t)) and 5088 g/t (148.4 ozt/t) occur near the back pressure plate where the fluid confining pressure is reduced from ~7.2 to 5.5 bar absolute (b.a.) as ~20 wt % of the

fluid volatilizes to steam. The precious metal content of the pipe scale decreases with increasing distance from the back pressure plate; this happens very rapidly on the upstream side (Brown, 1986). Metallization is much more extensive on the downstream side of the back pressure plate, with metal-rich scale or metalliferous siliceous sinter coating most of the internal surfaces between the back pressure plate and the weirbox. This observation implies that metal deposition is controlled by (1) rapid decompression of the fluid (flashing) and (2) the reduction in fluid temperature which accompanies decompression. The importance of these controls to metal precipitation is further illustrated by the abundance of metal deposited in the silencers as the fluid is reduced from ~2.7 b.a. to atmospheric conditions. The reduction in fluid temperature from ~260°C to ~140°C accompanying this transition reduces the solubility of gold substantially (Brown, 1986).

Controls on metal deposition within the preproduction reservoir at Wairakei are much less obvious than within the wellhead equipment. The deposition of gold (silver is generally below detection limits of standard analytical procedures) appears to have been relatively uniform throughout the reservoir above a depth of ~1200 metres and at temperatures ranging from ~265°C to ~140°C (Fig. 3.33). Ore minerals (gold-palladium, argentite, sphalerite, galena and chalcopyrite) were only identified in thin sections of rocks which came from areas of transitional propylitic-potassic alteration, although Figure 3.33 clearly shows that gold was also deposited at shallower levels where its precipitation is associated with potassic alteration. Phase separation (boiling) does not appear to be a viable mechanism for gold precipitation within the Wairakei reservoir since the reservoir fluid does not begin to evolve a vapour phase until it reaches a depth of ~700 metres ($T_{MAX} \approx 265°C$), whereas gold is deposited in approximately equal amounts above and below this level. In fact, gold solubility increases with small to moderate degrees of boiling (Brown, 1988).

The larger grain size of precious and base metals deposited within the zone of transitional propylitic-potassic alteration and the slightly higher abundance of these elements may indicate that minor fluctuations in reservoir temperature which result in transitional propylitic-potassic alteration also cause an increase in metal deposition. There is also an indication that gold was precipitating at a greater rate as a result of fluid mixing in and adjacent to the zone of "cold" water intrusion in well 54, but much more data are required to evaluate this hypothesis.

Spatial distribution of propylitic and potassic alteration, supported by preliminary palaeo-reservoir temperatures (T_H data), indicate that although the preproduction reservoir at Wairakei was slowly cooling, it was a relatively steady-state system with near-equilibrium conditions existing between the precipitation and leaching of gold. These steady-state conditions are reflected in the relatively uniform distribution of gold at very low grades throughout the Wairakei reservoir regardless of rock type.

Chapter 4

DISCUSSION AND CONCLUSIONS

INTRODUCTION

In Chapter 4 two main topics are discussed. These are (1) the degree to which active high-temperature geothermal systems are modern analogues for epithermal precious metal deposits and (2) the occurrence and petrogenesis of a suite of high-Mg lavas from southeastern Papua New Guinea. Although these topics are unrelated, and the second clearly a diversion from the main theme of my dissertation, both topics are important aspects of my Ph.D. research, and therefore are brought together in this chapter.

The first part of Chapter 4 follows directly from the first two chapters. In this chapter the characteristics of hydrothermal alteration and metallization identified within the high-temperature geothermal reservoirs at Iamalele (P.N.G.) and Wairakei (N.Z.) are compared with similar information for the mid-Tertiary precious metal deposits at Rawhide and Round Mountain (U.S.A.). Observations made during these comparative studies are employed in answering three fundamental questions. (1) Are there any active high-temperature geothermal systems that contain significant quantities of precious metals at economic concentrations? (2) To what extent are the current geothermal-based models applicable to the genesis of epithermal precious metal deposits? And (3), if significant quantities of gold and silver at economic concentrations do not occur within the high-temperature reservoirs of active geothermal systems, what prohibits the precipitation of these metals?

The second part of Chapter 4 contains a discussion of the occurrence of a suite of high-Mg lavas in southeastern Papua New Guinea. During my study of the volcanic stratigraphy of western Fergusson Island in the

D'Entrecasteaux Islands of Papua New Guinea a few of the calc-alkalic lavas sampled contained unusually high abundances of certain transition elements, most notably Mg, Cr and Ni. Further study showed that these rocks were actually part of a suite of magnesium-rich lavas that could be traced from Egum Atoll in the Coral Sea to the highlands of the Owen Stanley Range. In addition, the chemistry and mineralogy of these rocks were similar to the chemistry and mineralogy of high-Mg lavas from other sectors of the Circum-Pacific Rim. Detailed studies of high-Mg calc-alkalic lavas from Japan and Chile had shown that those rocks were primary magmas generated in the upper mantle, and as such are a fundamental component of island arc terranes. Since the high-Mg lavas from southeastern Papua New Guinea are remarkably uniform in composition, particularly considering their extensive spatial distribution, it was apparent that their origin must involve a fundamental tectonic process. Because unraveling this process and the chemistry of the high-Mg lavas may have significant implications for the genesis of volcanic arc magmas, I elected to investigate the origin of these rocks in relative detail.

ACTIVE GEOTHERMAL SYSTEMS AS THE PRECURSORS OF EPITHERMAL GOLD-SILVER DEPOSITS

Introduction

Geothermal systems have been considered the modern analogues of epithermal ore deposits for nearly forty years (e.g. White, 1955). This is the case because the physical conditions which characterize the epithermal ore-forming environment are remarkably similar to the conditions prevailing in active geothermal systems. Most genetic models for epithermal precious metal deposits, particularly deposits occurring in volcanic terranes (e.g., Henley and Ellis, 1983; Hayba et al., 1985), are firmly based on chemical and hydrologic data collected from high-temperature, liquid-dominated geothermal systems such as Wairakei (Steiner, 1977), Broadlands (Browne,

1969) and Steamboat Springs (Schoen and White, 1967). But despite extensive exploration during the 1970s and 1980s, substantial quantities of gold ore have not been identified within the high-temperature reservoirs of the geothermal systems from which the precious metal models were developed.

White (1981) suggested four possible reasons why active geothermal systems are not forming ore deposits on the scale of those contained in their fossil equivalents, the epithermal systems: (1) deposits of ore grade and quantity do exist in active systems but have not yet been recognized; (2) most geothermal exploration has involved systems with surface discharge, and perhaps in these "leaky" systems most of the gold is discharged at the surface; (3) large high-grade ore deposits form only in specially favourable tectonic and geochemical environments which do not exist in explored active geothermal systems; (4) most gold and silver occurs late in the paragenetic sequence and has not been deposited in the high-temperature active systems. In the remainder of this chapter each of these possible explanations is evaluated by comparing the geologic setting and hydrothermal alteration and metallization occurring within the geothermal reservoirs at Iamalele and Wairakei with similar observations made at the mid-Tertiary precious metal deposits of Rawhide (Black et al., 1991) and Round Mountain (Sander and Einaudi, 1990). These precious metal deposits are located in Nevada, U.S.A., and were chosen for comparison because they are representative of a large number of volcanic-hosted epithermal gold-silver deposits located throughout the western U.S.A., because both areas have been well studied and because detailed descriptions of these deposits have been published recently.

Potential for the Discovery of Economic Precious Metal Mineralization in High-Temperature Geothermal Systems

Areas of high surface heat flow have been explored as potential sources of geothermal power in many parts of the world (Fig. 4.1). The

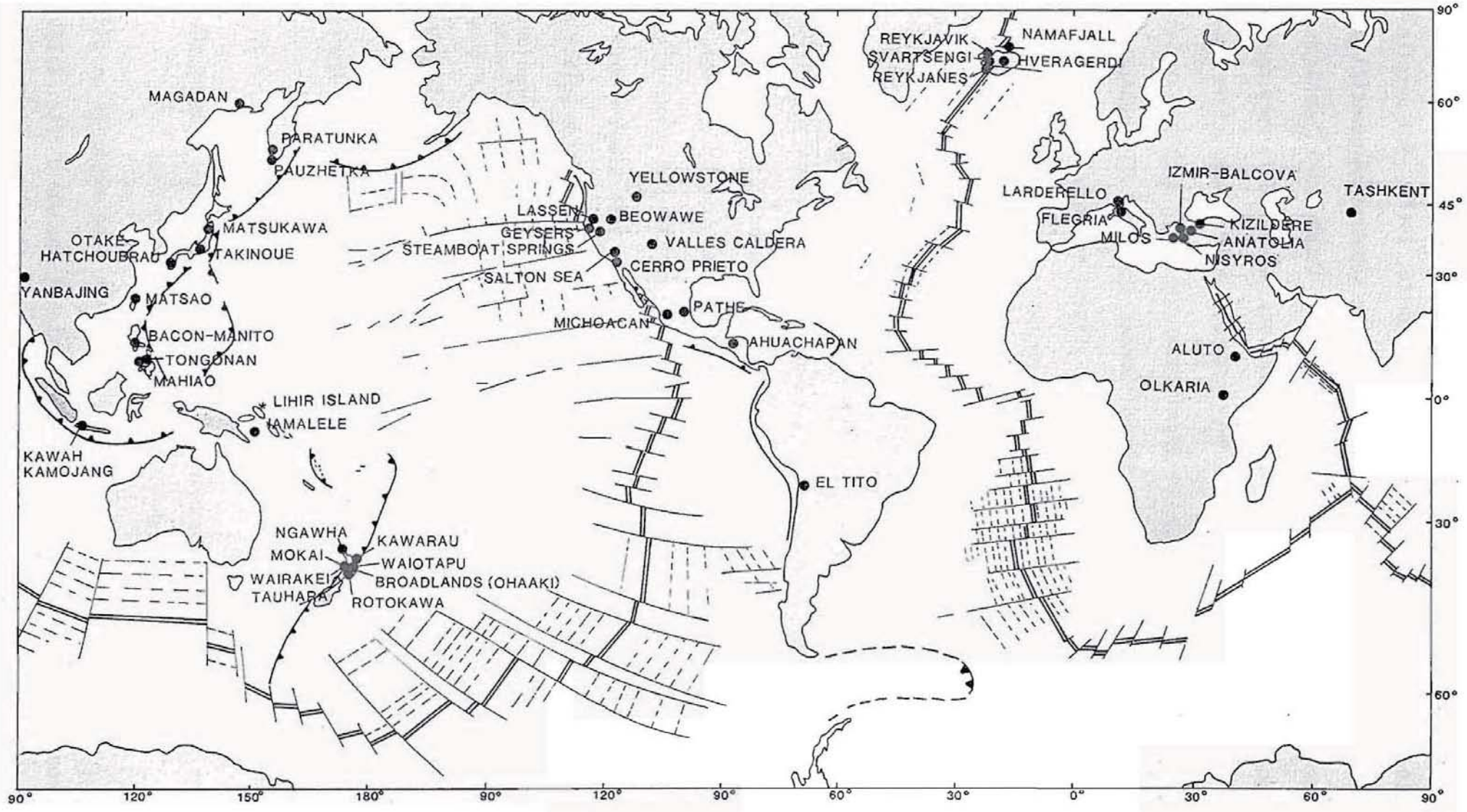
MAGADAN
PARATUNKA
PAUZHETKA
MATSUKAWA
OTAKE
HATCHOUBRAU
TAKINOUE
YANBAJING
MATSAO
BACON-MANITO
TONGONAN
MAHIAO
LIHIR ISLAND
IAMALELE
KAWAH
KAMOJANG
NGAWHA
KAWARAU
MOKAI
WAIOTAPU
WAIRAKEI
BROADLANDS (OHAAKI)
TAUHARA
ROTOKAWA
YELLOWSTONE
LASSEN
BEOWAWE
GEYSERS
STEAMBOAT SPRINGS
VALLES CALDERA
SALTON SEA
CERRO PRIETO
PATHE
MICHOACAN
AHUACHAPAN
EL TITO
REYKJAVIK
NAMAFJALL
SVARTSENGI
HVERAGERDI
REYKJANES
LARDERELLO
IZMIR-BALCOVA
TASHKENT
FLEGRIA
MILOS
KIZILDERE
ANATOLIA
NISYROS
ALUTO
OLKARIA
90°
60°
45°
30°
0°
30°
60°
90°
90°
120°
150°
180°
90°
120°
90°
60°
30°
0°
30°
60°
90°

Figure 4.1. (Facing page) World map showing the location of several well-known high-temperature geothermal fields. Many of the geothermal fields shown have been described extensively and the references provided below do not necessarily contain the most detailed account of the particular geothermal area. The references are included as a starting point for further research and are listed alphabetically by geothermal area. Ahuachapan (Weissberg et al., 1979); Aluto (Hochstein et al., 1983); Anatolia (Ellis, 1979); Bacon-Manito (Lawless et al., 1983; Leach et al., 1985); Beowawe (Cole and Ravinsky, 1984); Broadlands/Ohaaki (Browne, 1969, 1973); Cerro Prieto (Elders et al., 1978); El Tatio (Ellis, 1979); Flegria (Ellis, 1979); Geysers (Ellis, 1979); Hveragerdi (Ellis, 1979); Iamalele (this paper); Izmir-Balcova (Yilmazer et al., 1989); Kawah Kamojang (Healy and Mahon, 1982; Sudarman and Hochstein, 1983); Kawerau (Christenson, 1987); Kizildere (Ellis, 1979); Larderello (Ellis, 1979); Lassen (Muffler et al., 1982); Magadan (Ellis, 1979); Mahiao (Seastres, 1982); Matsao (Chen, 1970); Matsukawa (Ellis, 1979); Michoacan (Ellis, 1979); Milos (Economides et al., 1983b); Mokai (Mongillo and Clelland, 1984); Nanafjall (L.J.P. Muffler, written communication); Ngawha (Ellis and Mahon, 1966); Nisyros (Economides et al., 1983a); Olkaria (Browne, 1984); Panzhetka (Ellis, 1979); Paratunka (Weissberg et al., 1979); Pathe (Weissberg et al., 1979); Reykjanes (Bjornsson et al., 1970); Reykjavik (Ellis, 1979); Rotokawa (Krupp and Seward, 1987); Salton Sea (McKibben and Elders, 1985); Steamboat Springs (Schoen and White, 1967); Takinoue (Muramatsu, 1984); Tashkent (Ellis, 1979); Tauhara (Henley and Stewart, 1983); Tongonan (Weissberg et al., 1979); Valles Caldera (Dondanville, 1978); Waiotapu (Hedenquist, 1983); Wairakei (Grindley, 1965; Steiner, 1977); Yangbajing (Weissberg et al., 1979); Yellowstone (Honda and Muffler, 1970).

geothermal fields shown in Figure 4.1 are well documented and well-known, but extensive chemical data bases also exist for a number of less well-known high-temperature systems; e.g., Liao et al. (1986) lists 35 high-temperature geothermal areas which have been investigated in the West Yunnan Province of China alone. Typically exploration wells are completed to a depth of ~1,000 metres, but several high-temperature reservoirs (Rotokawa, Latera, Cerro Prieto) have been drilled to depths exceeding 2,500 metres. Trace element analyses are not routinely completed on drill cuttings and core samples, but data on several elements important to the understanding of and exploration for epithermal ore deposits (in particular Au, Ag, As, Sb and Hg) are available for most of the major geothermal systems.

The larger, high-temperature geothermal fields, particularly those from which electrical power is produced (e.g. Wairakei), are comparable in size to the hydrothermal systems which produced the largest epithermal precious metal deposits (e.g. Round Mountain), and as such, possess the greatest potential for the discovery of economic gold-silver mineralization. Yet, significant concentrations of ore-grade (>1 gram per tonne (g/t); 0.029 troy ounce per ton (ozt/t)) gold mineralization have not been identified in any of the high-temperature active systems. The explored high-temperature geothermal fields include the largest active hydrothermal systems known. Considering the variability in the geologic settings (e.g., Ellis, 1979) and the geochemical data bases available for the explored systems (e.g., Schoen and White, 1967; Browne, 1969; Elders et al., 1978; Krupp and Seward, 1987), it is unlikely that there are any undiscovered major high-temperature geothermal systems that contain economic concentrations of precious metals. However, a major gold deposit spatially associated with a moderate temperature geothermal system was recently discovered on Lihir Island in New Ireland Province of Papua New Guinea.

At Lihir the relationship between current geothermal activity and gold mineralization is complex and not well understood.

Lihir Island, Papua New Guinea

The only active hydrothermal system known to host economic precious metal mineralization is on Lihir Island in Papua New Guinea (Fig. 4.1). The Ladolam deposit, located on the east coast of Lihir Island, is a major disseminated gold deposit (>1440 kilograms (>42 million ounces) of contained gold; Niugini Mining Limited, 1988) spatially associated with the breached caldera of the Luise volcano. Economic concentrations of gold occur in hydrothermal breccias associated with the cupola zone of a 350 ka monzonitic stock which intrudes cogenetic alkalic volcanic rocks (Wallace et al., 1983; Williamson, 1983; Davies and Ballantyne, 1987). Gold mineralization is related to a wide range of hydrothermal alteration assemblages (advanced argillic, intermediate argillic, silicic, potassic and propylitic) with the highest grade mineralization occurring in areas where the propylitic and potassic assemblages overlap (Shatwell, 1987). Low-grade gold mineralization is reported to be associated with intermediate argillic alteration at moderate depths, whereas high-grade mineralization accompanies advanced argillic alteration in the near-surface environment (Davies and Ballantyne, 1987).

Low- to moderate-temperature geothermal activity is associated with the Luise caldera and the Ladolam gold deposit. The maximum reservoir temperature measured within the Ladolam deposit is 231°C, which corresponds remarkably well to the maximum reservoir temperature (230°C) determined from water analyses by Na-K-Si geothermometry (Davies and Ballantyne, 1987). The chemistry of the current reservoir fluid indicates that it is primarily meteoric water (Davies and Ballantyne, 1987), but the abundance of anhydrite in the deeper portions of the ore deposit indicates that the hydrothermal fluid which deposited most of the gold contained a significant

Figure 4.2. Hot spring at the northwestern edge of Acid Lake in the Yaluwana thermal area at Iamalele, see Figure 2.10 for location map. The yellow precipitate is a sol rich in As. Samples of siliceous sand containing the same yellowish precipitate assayed 8.25% As, 34 ppm Sb and 121 ppm Hg.

Figure 4.3. Eastern bore field at Wairakei. The mounds of yellowish-white material are spongy siliceous sinter which precipitated in the hot water drains. Gold precipitates from the discharge fluid within ~100 metres of the weirbox at temperatures <130°C. As and Sb precipitate from the fluid at much lower temperatures. A sample of siliceous precipitate removed from the hot water drain near the small trees growing along the drain on the left side of the photograph assayed in ppm: 0.08 Au, 1.0 Ag, 1510 As and 52 Sb.

seawater component (Shatwell, 1987). Although gold mineralization is associated spatially with the current geothermal activity, it is not clear that gold was deposited under these conditions. K-Ar age dates indicate that most of the gold was deposited between 350 and 100 ka (Davies and Ballantyne, 1987).

Metal Loss through Surface Discharge in High-Temperature Geothermal Systems

One possible explanation for the absence of economic precious metal mineralization in the high-temperature active systems is that the gold and silver which would normally be deposited within the reservoir is lost through surface discharge. It has been shown that surface features, such as sinter terraces and areas of strong hydrolytic alteration, associated with most of the high-temperature geothermal systems commonly contain high concentrations of Au, Ag, As, Sb and Hg (White, 1981).

The results of geochemical sampling around surface discharge features at Iamalele (Fig. 4.2) and Wairakei indicate that the metals contained in the escaping fluid were quickly fixed, either by incorporation in clay altered rock or by coprecipitating encapsulation in siliceous sinter. Chemical data for siliceous sinter collected from wellhead production equipment and hot water drains at Wairakei (Fig. 4.3) showed that precious and base metals carried by the production fluid at Wairakei precipitated within 10 to 150 metres of the weirbox. Within the production wellhead equipment, precipitation of base and precious metals is related to the instantaneous decompression (flashing) and related cooling of the discharged fluid. Precipitation of Au, Ag, As and Sb remaining in the fluid after flashing is controlled by fluid cooling.

These data indicate that most of the gold and silver carried in the hydrothermal fluid rapidly precipitates when exposed to the surface environment and is not removed by surface runoff. Therefore, unless

removed by erosion, which is unlikely to have occurred in most of the active systems, the majority of the gold discharged from the high-temperature reservoir should remain in or near the surface discharge areas. It is clear that high concentrations of gold (10 to >60 g/t) can occur in surface discharge features (e.g., Hedenquist, 1983; Krupp and Seward, 1987), but the total volume of this material is extremely small when compared to the volume of the hydrothermal reservoir or palaeoreservoir. Since there are no known active high-temperature geothermal systems with economic (grade and tonnage) accumulations of precious metals at the surface or within the very near-surface environment it is unlikely that significant quantities of gold are lost from deep reservoirs through surface discharge.

Tectonic Setting and Geochemical Environment of Active and "Fossil" Hydrothermal Systems

One reason why the active geothermal systems may be barren of economic gold mineralization is that large high-grade precious metal deposits form only in specially favourable tectonic and geochemical environments which do not exist in the explored active geothermal systems (White, 1981). To evaluate this possibility the geology, hydrothermal alteration and metallization of the Iamalele and Wairakei geothermal systems were compared with similar features of the mid-Tertiary epithermal precious metal deposits of Rawhide (Black et al., 1991) and Round Mountain (Sander and Einaudi, 1990) which are located in Nevada, U.S.A.

Selection of Areas for Comparison

In selecting an epithermal precious metal deposit for comparison with Iamalele and Wairakei it was important to ensure that it (1) occurred in a similar geologic and geochemical environment, (2) was representative of a large number or "class" of deposits, and (3) had been studied in detail.

An additional consideration is that equilibrium mineral assemblages characteristic of the epithermal environment must vary with the temperature (depth) of formation. In general, hydrothermal alteration occurring in precious metal deposits that formed at shallow depths (100 to 500 m) below the palaeosurface (Rawhide) is characterized by the "potassic" assemblage quartz-adularia-illite/sericite-pyrite-sphene-apatite-anatase ± calcite. In most instances high-level potassic alteration is overprinted by extensive intermediate argillic alteration. Hydrothermal alteration occurring in deposits that formed at depths greater than ~500 metres below the palaeosurface (Round Mountain) is generally more complex, consisting of a higher-temperature propylitic assemblage (quartz-albite-adularia-epidote-chlorite-pyrite-anatase ± calcite) which is generally overprinted by the lower temperature potassic assemblage and minor intermediate argillic alteration. Because both of these levels of exposure are present within the Wairakei reservoir it was necessary to consider the alteration effects at both Rawhide and Round Mountain to complete the comparison of active and "fossil" epithermal systems. To illustrate the relationship between Wairakei, Rawhide and Round Mountain, the approximate size and depth of formation of ore-grade mineralization at Rawhide and Round Mountain are plotted on a long section through the Wairakei reservoir (Fig. 4.4).

At Rawhide economic gold-silver mineralization is hosted by andesite lavas, lithic tuffs and volcaniclastic rock associated with a major andesite to rhyolite volcanic centre. Although andesitic lavas only occupy a small percentage of the total reservoir volume at Iamalele and Wairakei, the effects of hydrothermal alteration at Iamalele and in the upper levels of the Wairakei reservoir are remarkably similar to the effects of hydrothermal alteration at Rawhide. The comparison of Wairakei to Round Mountain is particularly appropriate because both systems are associated with major rhyolitic caldera complexes and the effects of hydrothermal alteration within these systems are nearly identical.

Figure 4.4. (Facing page) Comparison of the Wairakei geothermal reservoir with schematic representations of the ore zones at Rawhide and Round Mountain. Boxes representing the approximate vertical and horizontal extent of ore-grade mineralization at Rawhide (ruled) and Round Mountain (stippled) are plotted at approximately the same areas within the Wairakei reservoir where the ore zones occurred in their respective mid-Tertiary reservoirs. The area depicted for the Rawhide deposit is the long dimension; the narrow dimension is approximately half of the length. The ore deposit at Round Mountain is nearly equidimensional.

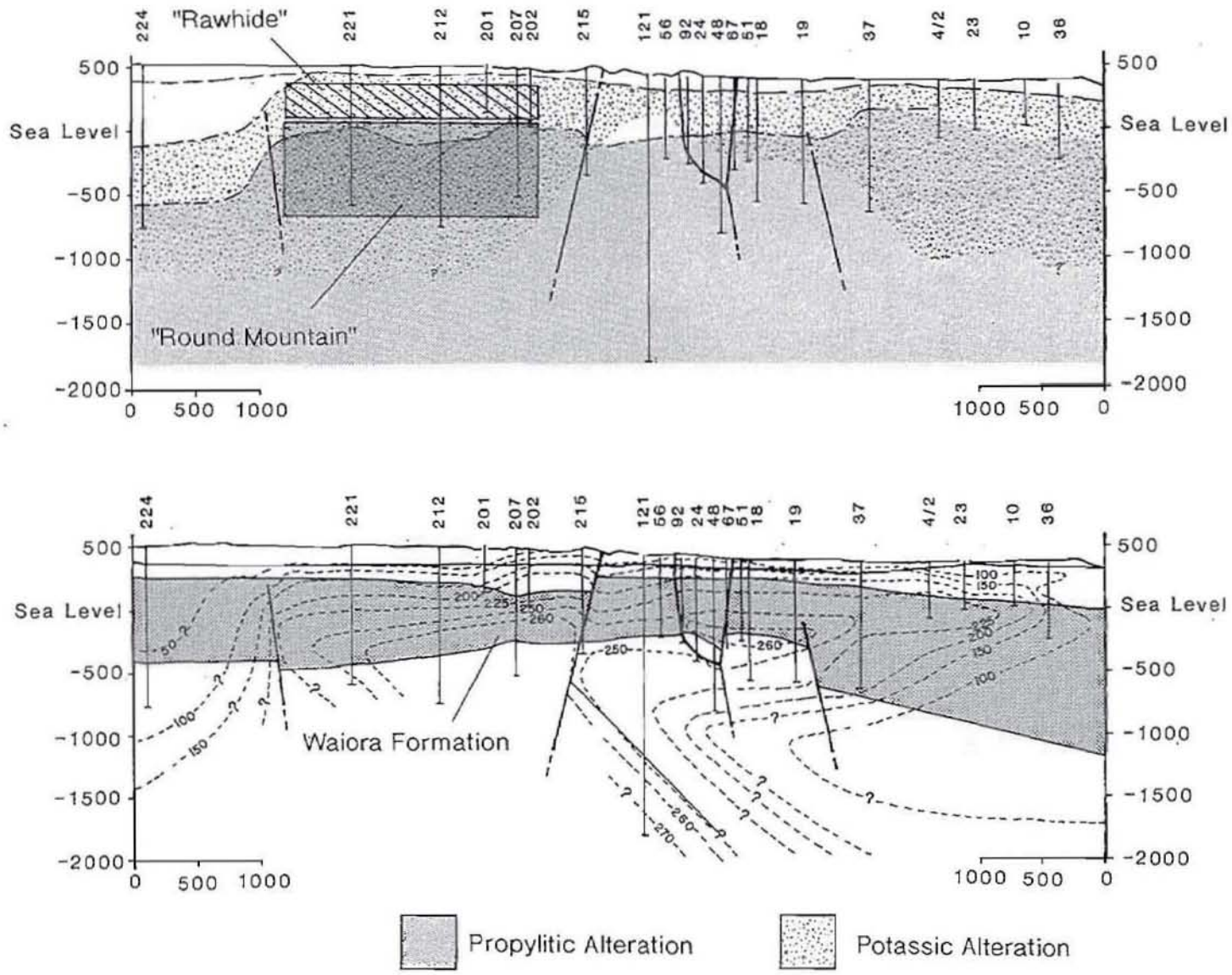
224
"Rawhide"
221
212
201
207
202
215
121
56
92
24
48
67
51
18
19
37
4/2
23
10
36
500
Sea Level
-500
-1000
-1500
-2000
"Round Mountain"
0 500 1000
1000 500 0
Waiora Formation
Propylitic Alteration
Potassic Alteration

Rawhide and Round Mountain are representative of the most common type of volcanic-hosted epithermal precious metal deposit referred to as "adularia-sericite-type" (Hayba et al., 1985; Berger, 1988). Iamalele and Wairakei are representative of one of the most common types of geothermal system, the "low-gas, terrestrial magma-related system" type (Henley, 1985; Henley and Berger, 1988), which is the geothermal equivalent of the adularia-sericite-type gold-silver deposit. Recent detailed information is available on both Rawhide (Black, 1988; Black et al., 1991) and Round Mountain (Sander, 1988b; Sander and Einaudi, 1990). Because of the strong similarities between Iamalele, Wairakei, Rawhide and Round Mountain, conclusions derived from the comparison of these systems are applicable to a majority of epithermal precious metal deposits.

Tectonic Setting and Regional Geology

The salient features of the regional and district-scale geology of Iamalele, Wairakei, Rawhide and Round Mountain are summarized below and in Tables 4.1 and 4.2. Detailed accounts of the geology, hydrothermal alteration and metallization occurring in each of these areas may be found in Chapters 2 (Iamalele) and 3 (Wairakei) of this dissertation, Black (1988) and Black et al. (1991) (Rawhide), and Sander (1988b) and Sander and Einaudi (1990)(Round Mountain).

Iamalele

The D'Entrecasteaux Islands occur in a very complex boundary zone between the Indo-Australian and Pacific plates. Post-Cretaceous(?) tectonism in the southern Solomon Sea has involved periods of subduction, obduction and, most recently, extension (Davies et al., 1984, Smith and Milsom, 1984). Geothermal activity related to recent extension and associated volcanism occurs on many of the D'Entrecasteaux Islands, with the most extensive areas of geothermal activity occurring on the southeastern and western

Table 4.1. Volcano-tectonic and structural setting of the Iamalele and Wairakei geothermal areas and the Rawhide and Round Mountain epithermal precious metal deposits

Hydrothermal System	Tectonic Setting	Volcanic Centre	Caldera	Volcanic and Structural Setting	Volcanic Age
Iamalele (Fergusson Island, D'Entrecasteaux Islands, P.N.G.)	Post-subduction extension	Kukuia-Goodenough	Suggested but not documented, probable multiple collapse	Eastern margin of the Kukuia-Goodenough volcanic centre, within proposed Iamalele caldera	~6.0 Ma to <400 ka
Wairakei (North Island, N.Z.)	Subduction-related extension	Maroa and Taupo	Yes, multiple collapse	Southeastern margin of the Maroa caldera volcano and northern margin of the Taupo caldera volcano	~330 ka to 186 A.D.
Rawhide (Nevada, U.S.A.)	Basin and Range extension	Rawhide	Uncertain	Northeastern margin of the Rawhide Volcanic Centre, along northern boundary of the Walter Lane structural zone	22.5 to 14.5 Ma
Round Mountain (Nevada, U.S.A.)	Basin and Range extension	Toquima	Yes, multiple collapse	Five km south of the southwestern margin of the Moores Creek and Jefferson calderas	27.2 to 23.6 Ma

Rawhide data from Black (1988) and Black et al. (1991). Round Mountain data from Sander (1988b) and Sander and Einaudi (1990).

Table 4.2. Geology of the geothermal reservoirs at Iamalele and Wairakei and the palaeoreservoirs at Rawhide and Round Mountain

Hydrothermal System	High-Temperature Reservoir Dimensions L x W x D m	Lithology	Hydrothermal Breccias	Lacustrine Environment	Structural Geology
Iamalele (Fergusson Island, D'Entrecasteaux Islands, P.N.G.)	7000 x 3000 x >200	Rhyolitic ignimbrites, domes, obsidian lava and volcaniclastic rocks; minor andesitic lavas; capped by marine and lacustrine volcaniclastic rocks	Abundant hydrothermal eruption breccias and hydraulic fracturing	Periodic(?), moderate accumulations late in the volcanic sequence	Numerous, dominantly(?) small displacement normal faults, possibly radial to a central caldera
Wairakei (North Island, N.Z.)	7000 x 5000 x ≥1000	Rhyolitic ignimbrites, lavas and volcaniclastic rocks; minor andesitic lava; capped by lacustrine volcaniclastic rocks	Abundant hydrothermal eruption breccias, minor hydraulic fracturing	Periodic, major accumulations occur late in the volcanic sequence	Numerous, dominantly small displacement normal oblique-slip faults
Rawhide (Nevada, U.S.A.)	2500 x 1000(?) x >300	Andesitic tuffs and lavas; minor rhyolitic ignimbrite, lavas, domes and dikes; intercalated with and capped by lacustrine volcaniclastic rocks	Abundant hydraulic fracturing, probable hydrothermal eruption breccias	Major accumulations occur late in the volcanic sequence	Abundant high to moderate angle normal and oblique-slip faults; post-mineral faulting offsets positions of the ore zone
Round Mountain (Nevada, U.S.A.)	≥5000 x ≥3000 x ≥1000	Rhyolitic ignimbrite; capped by lacustrine volcaniclastic rocks	Moderate hydraulic fracturing	Major(?) accumulations late in the volcanic sequence	Abundant dominantly small to moderate displacement high angle normal faults

Rawhide data from Black (1988) and Black et al. (1991). Round Mountain data from Sander and Einaudi (1990).

margins of Fergusson Island. Iamalele, which is located in the coastal lowlands of west-central Fergusson Island (Fig. 4.5), is one of the two largest geothermal areas on Fergusson Island. The hydrothermal reservoir formed within a relatively flat-lying sequence of Late Pleistocene to Holocene, dacite to rhyolite ignimbrites, air fall tuffs and tuffaceous volcaniclastic rocks which occupy the central portion of the inferred Seymour Bay caldera (Fig. 4.6; Plate 1). The ignimbrite sequence is intercalated with andesite lavas and intruded by flow-banded rhyolites which are probably feeder zones for the late rhyolite flow domes. Formation of the Iamalele reservoir is probably related to accumulation of lacustrine and shallow marine volcaniclastic sedimentary rocks which formed a relatively impermeable cap to the underlying highly porous tuffaceous rocks.

Wairakei

New Zealand straddles the boundary between the Indo-Australian and Pacific plates (Fig. 3.3). In the North Island the major manifestation of this boundary is the Taupo Volcanic Zone, which developed in response to localized extension related to westward directed subduction of the Pacific Plate (Cole, 1986). Wairakei is one of several major high-temperature geothermal systems (Fig. 4.7) which developed in response to Late Pleistocene to Holocene volcano-plutonic activity within the central Taupo Volcanic Zone (Rogan, 1982: Wilson et al., 1984). The Wairakei reservoir lies within a diffuse border zone between the Maroa and Taupo caldera volcanoes, where it is localized in a voluminous sequence of rhyolitic ignimbrites, air fall tuffs and tuffaceous volcaniclastic rocks intercalated with andesite and rhyolite lavas (Plate 6A). The high-temperature reservoir is largely restricted to the Waiora Formation where rising hydrothermal fluids controlled by major faults and formational boundaries expanded in subhorizontal aquifers which developed within porous, poorly-welded tuffs and tuffaceous volcaniclastic horizons. An important control on the develop-

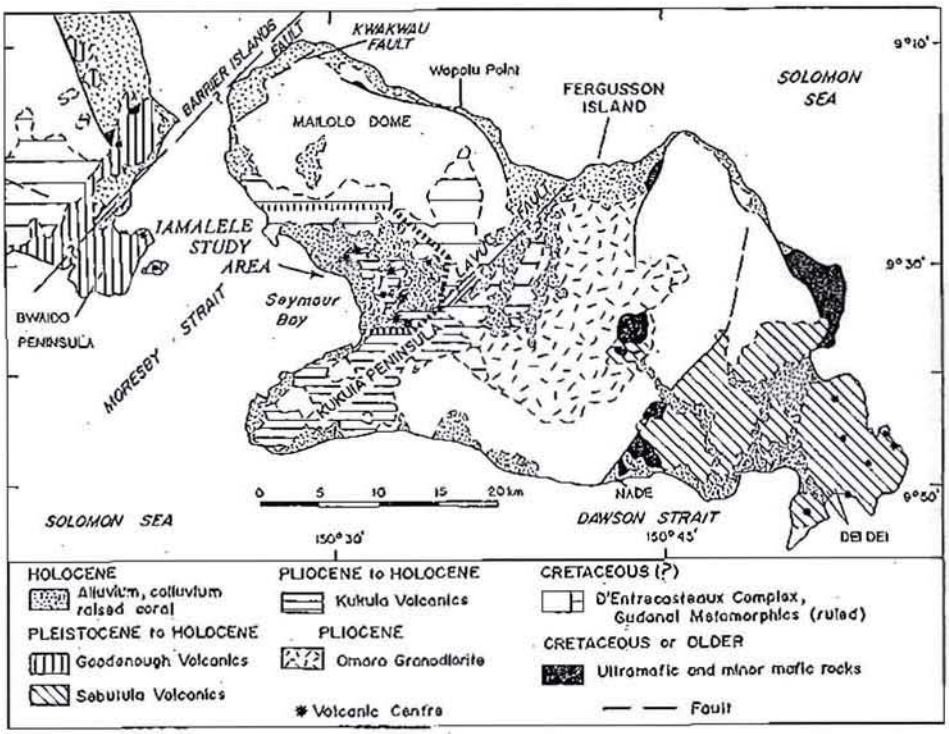

Figure 4.5. Location of the Iamalele geothermal area (striped outline) and simplified geology of Fergusson Island and the southeastern tip of Goodenough Island. Geology after Davies (1973).

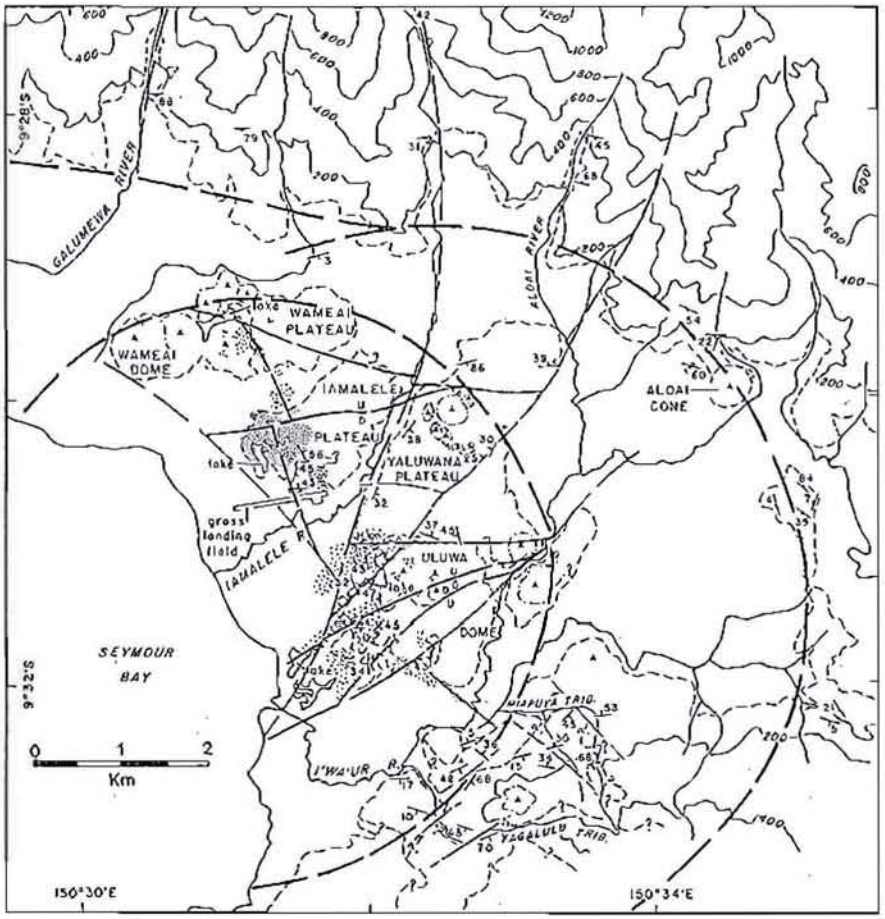

Figure 4.6. Structural setting of west-central Fergusson Island. Heavy dashed lines are inferred ring structures, thinner long-dashed lines are normal faults. Geologic units can be identified by comparing the figure to Plate 1.

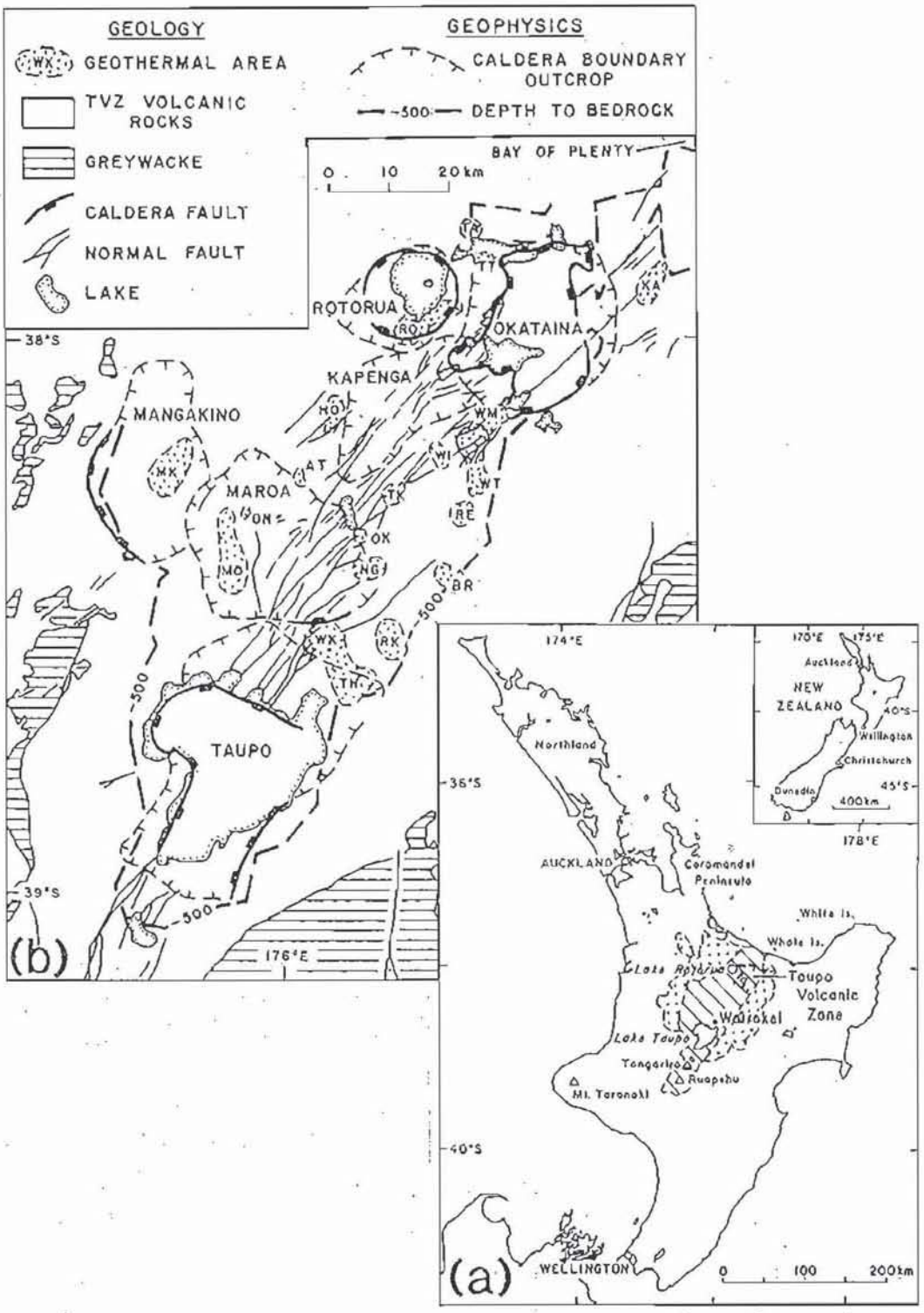

Figure 4.7. Location of the Wairakei geothermal area (WK) with respect to: a) the Taupo Volcanic Zone (TVZ) and b) the major caldera volcanoes and geothermal systems within the TVZ. Stippled area in Figure 4.7a represents the approximate distribution of related volcanic rocks that occur outside the central graben inferred from geophysics. Figure drawn from data developed by New Zealand Geological Survey (1972), Wilson et al. (1984) and Mongillo and Clelland (1984). Geothermal areas are Atiamuri (AT), Broadlands (BR), Horohoro (HO), Kawerau (KA), Mangakino (MK), Mokai (MO), Ngatamariki (NG), Ongaroto (ON), Orakeikorako (OK), Reporoa (RE), Rotokawa (RK), Rotorua (RO), Tahara (TH), Taheke (TA), Te Kopia (TK), Tikitere (TT), Wairakei (WK), Waikite (WI), Waimangu (WM) and Waiotapu (WT).

ment of the current geothermal reservoir was the accumulation of a sequence of thinly to moderately thick bedded clastic and volcaniclastic rocks (Huka Falls Formation) which form a relatively impermeable cap to the upwardly migrating fluid.

Rawhide

The Rawhide epithermal gold-silver deposit is located in the Basin and Range Province near the intersection of the northern boundary of the Walker Lane structural zone (Locke et al., 1940; Albers, 1967; Stewart, 1980) and the northeastern margin of the Rawhide volcanic centre (Ekern and Byers, 1986)(Figs. 4.8 and 4.9). Calc-alkalic pyroclastic and associated volcaniclastic rocks, lavas, and hypabyssal intrusives forming the Rawhide volcanic centre cover an area of approximately 6.5 by 12 kilometres and are elongated in a northwesterly direction parallel to the Walker Lane (Black et al., 1991). Much of the volcanic complex appears to be composed of a complex sequence of lavas interlayered with flow-domes. Specific calderas have not been identified within the Rawhide volcanic centre, although Black et al. (1991) note that emplacement of portions of the volcanic pile is related to a series of nested arcuate structures. Stratigraphy in the vicinity of the Rawhide deposit consists of a "basal" sequence of poorly welded ash tuffs and crystal lithic lapilli ash tuffs, and volcaniclastic sedimentary rocks (lithic tuff in Figure 4.9) with an aggregate thickness exceeding 245 metres (Black et al., 1991). The lithic tuff unit is overlain by andesite lavas which in turn are overlain by tuffaceous sedimentary rocks and volcanic breccia (Fig. 4.9). The spatial distribution of the various types of hydrothermal alteration and metallization indicate that the palaeohydrothermal reservoir developed preferentially within poorly welded tuffaceous rocks or strongly fractured brittle andesite flows.

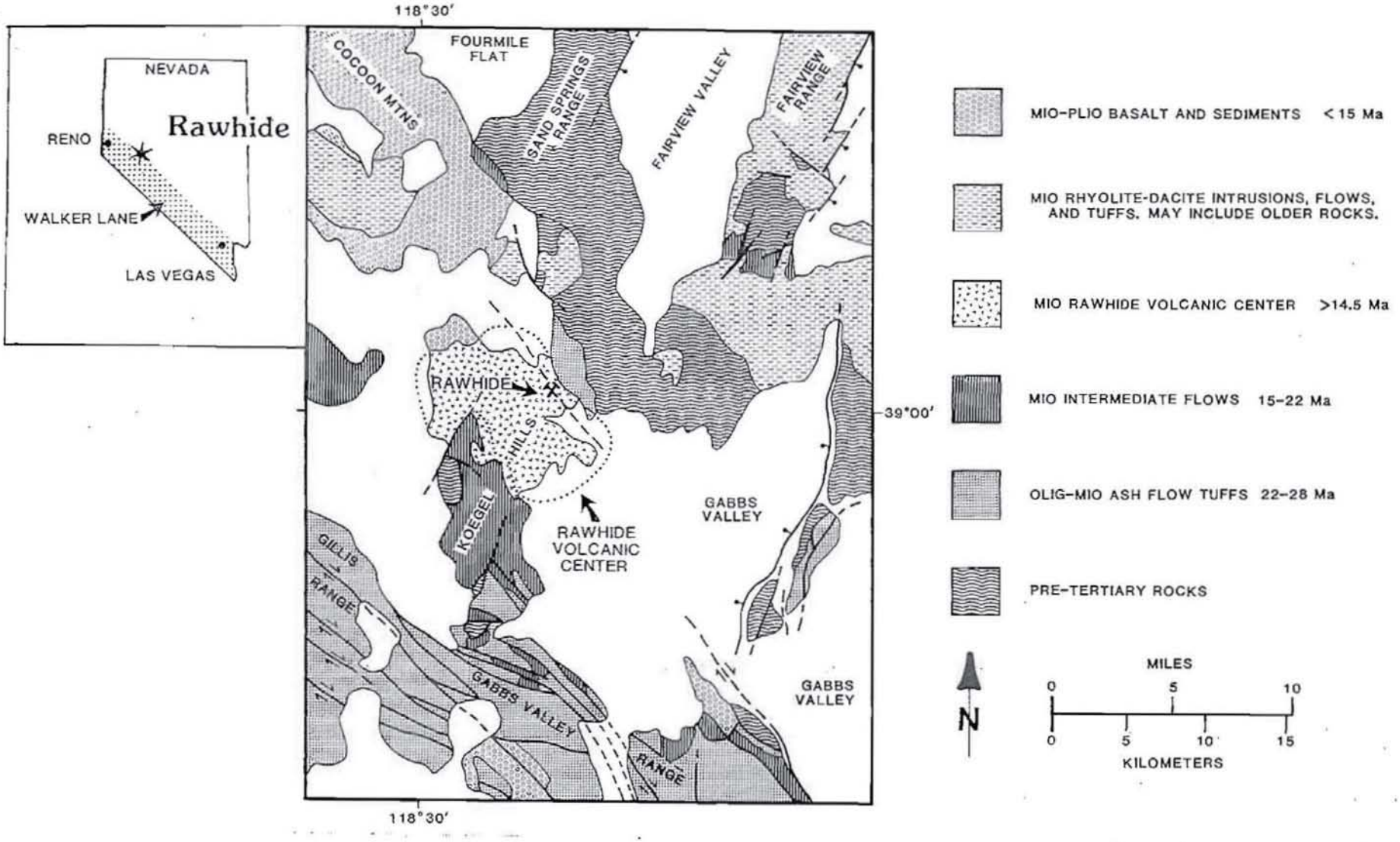

Figure 4.8. Location map and regional geology in the vicinity of the Rawhide gold-silver deposit. Figure reproduced from Black et al. (1991) with permission of the authors.

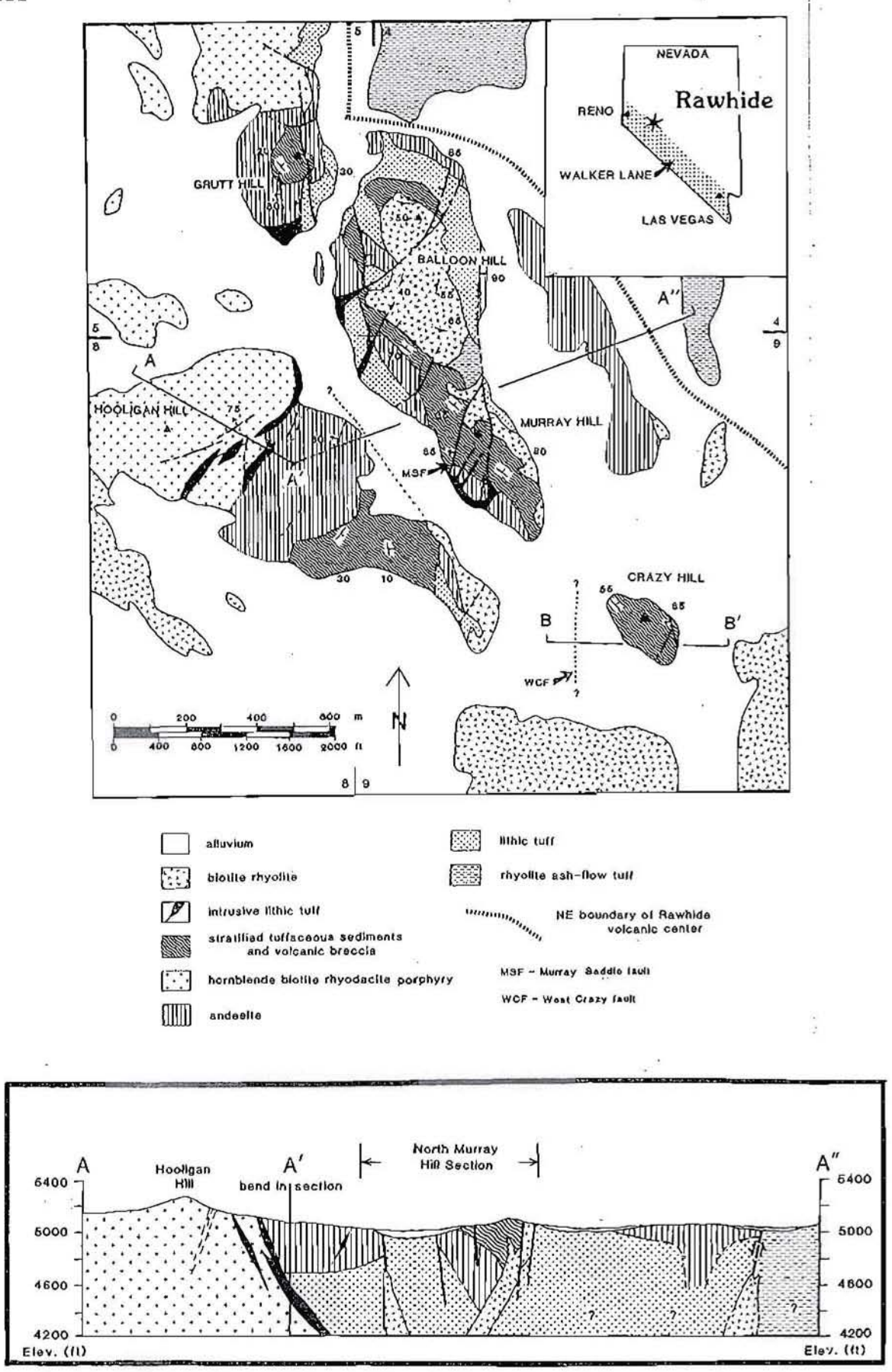

Figure 4.9. Location map and simplified geology of the Rawhide gold-silver deposit. Figure reproduced from Black et al. (1991) with permission of the authors.

Round Mountain

The Round Mountain precious metal deposit is spatially associated with the Toquima caldera complex (Fig. 4.10) which consists of three nested, non-resurgent calderas formed during repeated eruptions of high-silica rhyolite ignimbrite between 27.2 and 23.5 Ma (Boden, 1986). Gold-silver mineralization is hosted by the tuff of Round Mountain which is an early (26.7 Ma) outflow product of the Mount Jefferson caldera (Boden, 1986). The tuff of Round Mountain is a single cooling unit ~300 metres thick in the mine area (Fig. 4.11) consisting of a lower poorly welded tuff, middle densely welded tuff and a thin upper poorly welded tuff (Sander and Einaudi, 1990). In the mine area the tuff of Round Mountain was overlain by a sequence of finely-bedded volcaniclastic siltstone and sandstone. The style and spatial distribution of hydrothermal alteration and precious metal mineralization (Sander and Einaudi, 1990) indicate that the lower poorly welded tuff formed the high-temperature reservoir. The densely welded tuff partially capped the deep reservoir with the overlying volcaniclastic rocks forming the upward seal to the hydrothermal system. Steeply dipping fractures and small-displacement, oblique-slip faults, which aided in localizing gold-silver mineralization (Sander and Einaudi, 1990), document the occurrence of minor tectonism concomitant with hydrothermal activity.

Discussion

The present geologic environments of the Iamalele and Wairakei geothermal areas are very similar to the mid-Tertiary geologic environments of the Rawhide and Round Mountain gold-silver deposits (Chapter 2; Wilson, et al., 1984; Boden, 1986; Mills et al., 1988). Each area occurs within a major calc-alkalic volcanic centre from which voluminous rhyolitic ignimbrites and air fall tuffs were erupted. Maroa, Taupo and Toquima are major, nonresurgent caldera volcanoes with nested margins reflecting

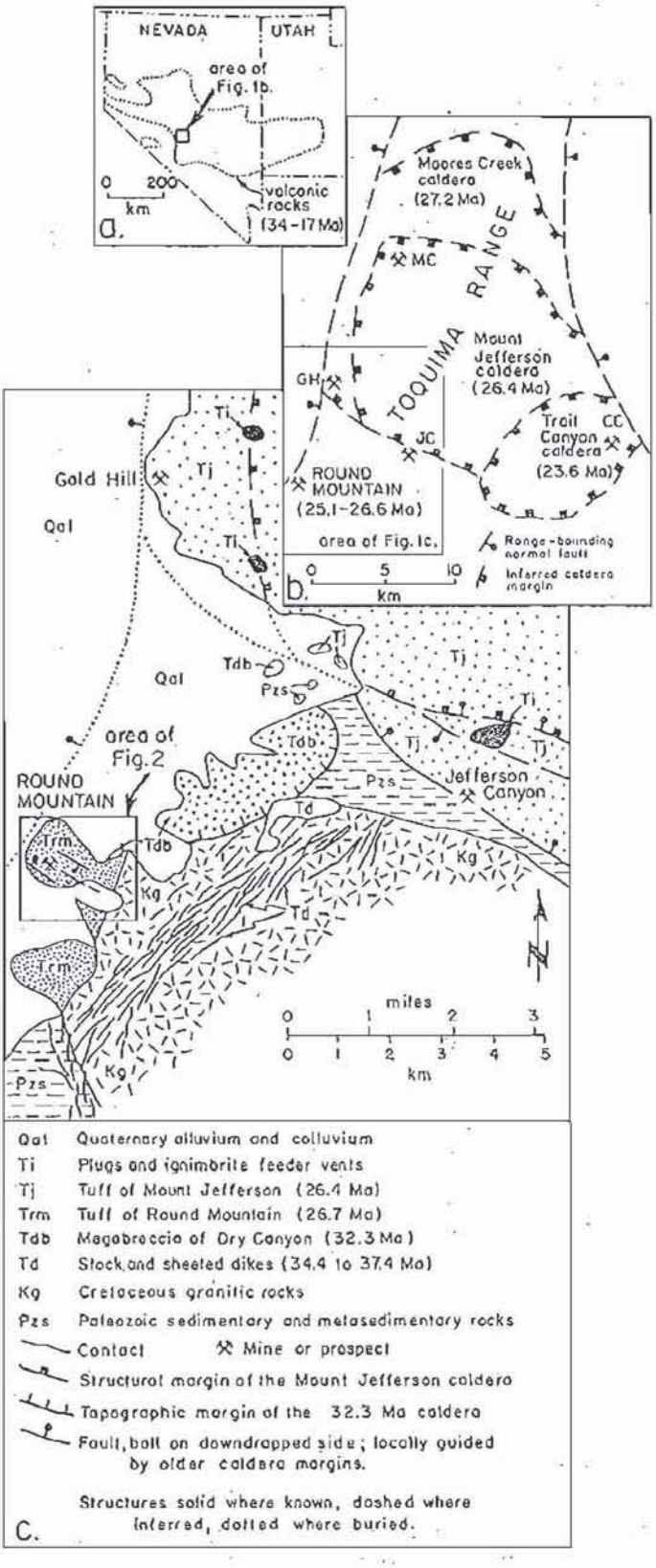

Figure 4.10. Location of the Round Mountain gold-silver mine with respect to Nevada, U.S.A. (a) and the Toquima caldera complex (b). Geology of the western flank of the Toquima Range is shown in (c). Figure reproduced from Sander and Einaudi (1990) with permission of the authors.

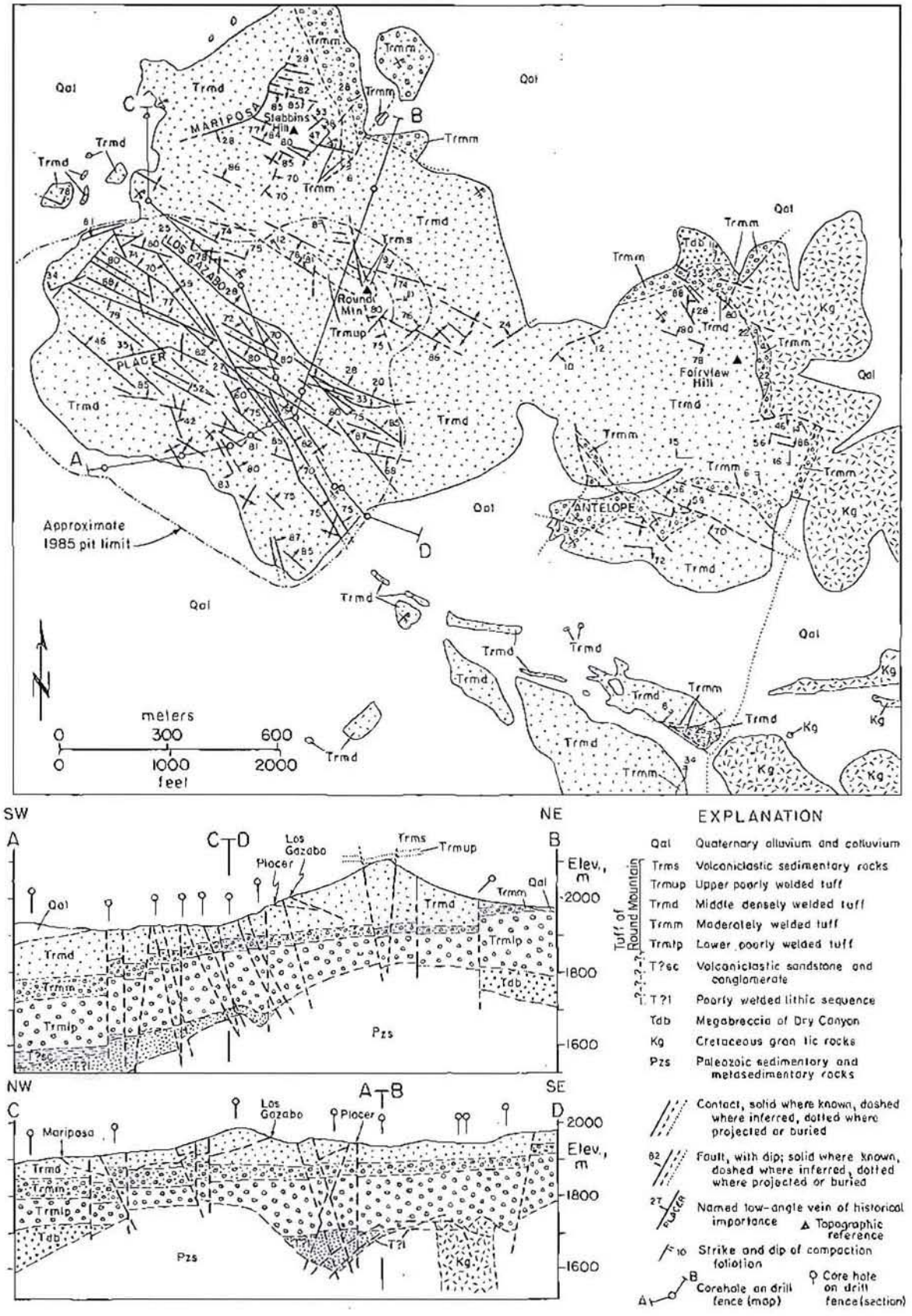

Figure 4.11. Generalized geology of the Round Mountain gold-silver mine. Figure reproduced from Sander and Einaudi (1990) with permission of the authors.

multiple pyroclastic eruptions and related caldera collapse (Wilson et al., 1984; Boden, 1986). The spatial distribution of volcanic rocks at the Iamalele and Rawhide volcanic centres is, in part, controlled by large-diameter ring fractures, interpreted to be possible caldera margins (Chapter 2; Black et al. 1991). Further, the complex interfingering of intermediate to felsic lavas and flow domes which characterizes the Rawhide volcanic centre (Black et al., 1991) closely resembles the style and composition of post-caldera effusive volcanism at the Iamalele, Maroa and Taupo volcanic centres.

The hydrothermal reservoirs (palaeoreservoirs) at Iamalele, Wairakei, Rawhide and Round Mountain are similar with respect to size, host rocks and hydrology (palaeohydrology), see Tables 4.1 to 4.3. In each case hydrothermal activity followed volcanism and caldera collapse by less than a million years and was localized by major structural boundaries (caldera margins), by active faults, and especially by the spatial coincidence of faults and caldera margins. The systems were formed by upwelling hydrothermal plumes, guided by faults and/or formational contacts which expanded into large reservoirs within subhorizontal, volcanic aquifers. The source of heat to drive convection at Iamalele, Wairakei, Round Mountain and probably Rawhide is at least a few thousand metres below the reservoir (palaeoreservoir).

The close similarities in tectonic setting, geology and reservoir hydrology between the geothermal areas and the precious metal deposits described above eliminate one of White's (1981) hypotheses: that active geothermal systems are barren of economic gold-silver mineralization because the tectonic and geologic environments required to form precious metal deposits do not exist in the explored geothermal systems.

Table 4.3. Characteristics of hydrothermal alteration occurring in the geothermal reservoirs at Iamalele and Wairakei and in the palaeoreservoirs at Rawhide and Round Mountain

Hydrothermal System	Age of Hydrothermal System (Ma)	Duration of Hydrothermal Activity (Ma)	Depth (Palaeodepth) to top of High-Temperature Reservoir (m)	Maximum Reservoir (Palaeoreservoir) Temperature (°C)	Major Types of Hydrothermal Alteration
Iamalele (Fergusson Island, D'Entercasteaux Islands, P.N.G.)	<0.4	<0.4, probably <0.15	>100	>200	potassic, intermediate argillic, advanced argillic
Wairakei (North Island, N.Z.)	<0.2	<0.2, probably <0.15	400-500	~310	propylitic, potassic, zeolite, advanced argillic (minor)
Rawhide (Nevada, U.S.A.)	15.7 ± 0.6	<1.0 (?)	>100	~250	potassic, intermediate argillic, silicic, advanced argillic (minor)
Round Mountain (Nevada, U.S.A.)	26.6 ± 0.6 to 25.1 ± 0.8	<1.0	300-400	~275	propylitic, potassic, intermidiate argillic, silicic

Rawhide data from Black (1988) and Black et al. (1991); palaeoreservoir temperature, J.E. Black personal communication. Round Mountain data from Sander (1988b) and Sander and Einaudi (1990).

High-Level Hydrothermal Systems

The term "high-level" herein applies to hydrothermal alteration and metallization occurring in the upper ~400 metres of a hydrothermal reservoir, and at temperatures less than ~240°C[6]. The equilibrium mineral assemblages and intensity of hydrothermal alteration identified in the upper levels of the Wairakei reservoir and at Rawhide are similar. "Ore" minerals which occur in production wellhead equipment and at high levels within the Wairakei reservoir are also similar to the ore minerals identified at Rawhide, the major difference being the enhanced abundance of these minerals within the Rawhide deposit.

Because the stratigraphic units which "cap" the high-temperature reservoirs of productive geothermal systems have low permeabilities and relatively low rock temperatures, little emphasis is placed on sampling these areas during drilling. As a result, there are very few data relating to the styles and intensity of hydrothermal alteration and metallization occurring in the very near-surface (upper ~100 m) environment at Wairakei. Therefore, to complete the comparison between the high-level hydrothermal environment of active geothermal systems and that of Rawhide, it was necessary to incorporate data from Iamalele.

In the following sections descriptions of hydrothermal alteration and metallization at Rawhide are summarized from Black (1988) and Black et al. (1991).

---

[6]The 240°C temperature was determined from thermodynamic relationships of the observed equilibrium alteration assemblages and measured temperatures within the upper portions of active geothermal systems. Reconnaissance fluid inclusion geothermometry on potassically altered rocks from Rawhide indicate maximum palaeoreservoir temperatures in the range of 240° to 250°C with many temperatures in the 190° to 210°C range (J.E. Black, written communication). Estimated preproduction reservoir temperatures for high-level potassic alteration at Wairakei range from 150° to 245°C. These data conform to the theoretical temperatures (~225° to <250°C) determined from the boiling point-for-depth relationship for depths less than ~300 m.

Hydrothermal Alteration

In accordance with the usage of Meyer and Hemley (1967), high-level hydrothermal alteration at Iamalele, Wairakei and Rawhide may be divided into three principal types. These are, in order of decreasing temperature and increasing activity of H^+, potassic, intermediate argillic and advanced argillic. At Rawhide, Black et al. (1991) subdivided quartz-adularia alteration into potassic and silicic assemblages depending on the abundance of quartz. For simplicity, and because the equilibrium mineral assemblages for potassic and silicic alteration are equivalent, the two types of quartz-adularia alteration described at Rawhide are discussed collectively under the heading of Potassic Alteration.

Structural Controls

The development of high-level alteration at Iamalele and Wairakei is controlled by primary porosity and to a lesser degree by fracture permeability. At Rawhide fracture permeability is the primary control on the distribution of hydrothermal alteration and metallization in the andesite lavas, whereas primary permeability (mainly porosity) is the dominant control in lithic tuffs and volcaniclastic sedimentary rocks. The importance of fracture permeability as a primary control at Rawhide reflects the brittle nature of the andesite lavas which host much of the bulk mineable ore. In each of the three areas potassic alteration is the earliest. Intermediate argillic alteration is widespread and locally pervasive at Iamalele and Rawhide but is in general weakly developed at Wairakei. For the most part intense clay alteration is structurally controlled. At Iamalele and Rawhide advanced argillic alteration is paragenetically late and its distribution is strongly controlled by fracture permeability, brecciation and faults. Extensive advanced argillic alteration at Wairakei is generally restricted to surface discharge features.

Potassic Alteration

Potassic alteration may include a variety of minerals in equilibrium, but quartz and nearly stoichiometric adularia are always present. Adhering to the usage of Meyer and Hemley (1967), the essential alteration assemblage characteristic of high-level potassic alteration at Iamalele, Wairakei and Rawhide is quartz-adularia-illite/sericite-pyrite. Quartz is characteristically the most abundant component of the potassic alteration assemblage. The abundance of quartz is highly variable and potassic alteration may grade into silicification, particularly along or near major fractures or fracture systems. However, even in areas of pervasive silicification and in the selvages of quartz veins small euhedral rhombs of adularia are invariably present (e.g., see Figure 3.15E and F). Illite is also very common in silicified rock and may be locally abundant.

Incipient potassic alteration at Iamalele, Wairakei and Rawhide is characterized by the partial replacement of the rock matrix or groundmass and perhaps the edges of tuffaceous rock fragments by quartz and adularia. As the intensity of potassic alteration increases, adularia selectively replaces plagioclase phenocrysts along cleavage and fracture planes, and may occur as "overgrowths" irregularly dispersed along crystal perimeters or as microveinlets within or adjacent to the crystal (e.g. see Figure 3.15A and B). Where potassic alteration is pervasive, adularia totally replaces plagioclase and most of the groundmass is replaced by relatively fine-grained mosaics of quartz and adularia.

Iamalele: Potassic alteration is present in the Iamalele drill core below a depth of ~80 metres and is represented by the assemblage quartz-adularia-illite/sericite-anhydrite-pyrite. Quartz, adularia and illite are the most abundant components of potassic alteration and below ~130 metres maintain a relatively constant ratio of (quartz:adularia:illite) 45:25:10. Most of the remaining 20% is made up of clay minerals associated with intermediate argillic alteration and pyrite. Pyrite generally constitutes

1 to 2% of the altered rock, but in areas of strong fracturing or brecciation the abundance of pyrite may locally exceed 5%. Minor to trace components of potassic alteration include anhydrite and biotite.

Wairakei: Potassic alteration is represented by a more diverse suite of minerals at Wairakei than at Iamalele and Rawhide. The most common potassic alteration assemblage is quartz-adularia-illite/sericite-grothite (Al-titanite)-chlorapatite-anatase/rutile-pyrite. In addition to these minerals mordenite, 14Å-clinochlore, calcite, barite, anhydrite, monazite, pyrrhotite, marcasite, biotite, magnetite and zircon locally occur in equilibrium with quartz and adularia. Of these minerals, only mordenite, 14Å-clinochlore, calcite and barite exceed a trace percentage (>1%) of the altered rock.

Rawhide: The most common potassic alteration assemblage at Rawhide is quartz-adularia-illite/sericite-apatite-pyrite. In addition to these minerals calcite is locally abundant and monazite constitutes a trace component. Nearly all of the primary feldspar is at least partially replaced by adularia, indicating that potassic alteration occurs throughout the Rawhide deposit (Black et al., 1991). Illite is more abundant near the centre of the deposit and calcite is more abundant in the peripheral areas (Black et al., 1991).

Intermediate Argillic Alteration

Intermediate argillic alteration at Iamalele, Wairakei and Rawhide is manifested by the replacement of primary feldspar (plagioclase and sanidine), mafic minerals and portions of the groundmass by quartz, smectite (typically montmorillonite), kaolinite, illite and pyrite. The occurrence of residual(?) adularia in areas of relatively strong clay alteration (e.g., at Rawhide; Black et al., 1991) indicates that potassium feldspar may be locally metastable. Clay alteration is much more common at Iamalele and Rawhide than at Wairakei, a fact that suggests that rela-

tively low (palaeo)reservoir temperatures are important to the formation of clay minerals in high-level hydrothermal systems.

The intensity of intermediate argillic alteration appears to be related to rock permeability. The most intense development of clay alteration is associated with brecciated intrusive contacts, major faults and fracture systems, hydrothermal breccias and lithologic units with relatively high porosity.

Iamalele: The major mineral species associated with intermediate argillic alteration are quartz, beidellite, montmorillonite, vermiculite and possibly illite. Barite and anhydrite appear to coexist with beidellite and illite. Textural relationships indicate that smectite replaces primary and secondary feldspar and the groundmass or matrix of the rock. Quartz and beidellite are the major components of the drill core at depths between 85 and 125 metres (Fig. 2.14). Beidellite is most abundant within fault and shear zones where it may constitute up to 37% of the total rock volume. Vermiculite is present in the core below 110 metres and is particularly abundant in the major fault zones below ~120 metres and in the lower (>170 m) hydrothermal breccias. In these areas vermiculite accounts for 10 to 35% of the rock. Within the lower hydrothermal breccias vermiculite replaces montmorillonite.

Wairakei: Weak intermediate argillic alteration occurs throughout the upper portion of the Wairakei reservoir, with clay minerals being most abundant in areas where preproduction temperatures were less than ~150°C. The most common minerals associated with intermediate argillic alteration are 14Å-montmorillonite and mixed-layer illite-smectite. These minerals are locally accompanied by minor amounts of halloysite, kaolinite and cristobalite. Illite is generally associated with potassic alteration, but at shallow levels along the western margin of the reservoir illite accompanies intermediate argillic alteration.

Rawhide: Intermediate argillic alteration is the dominant alteration type at Rawhide and is the result of multiple events including supergene acid leaching (Black et al., 1991). In general, illite, kaolinite and chlorite are the most abundant hypogene clay minerals. Mixed-layer illite-smectite and montmorillonite are also related to hypogene processes, but are less abundant (Black et al., 1991). Clay alteration affects primary plagioclase, mafic phenocrysts and the groundmass, but adularia and quartz are unaffected (Black, et al., 1991). Intermediate argillic alteration is most well developed along the margins of the system (Fig. 4.12) and within the more permeable tuffs and volcaniclastic rocks. Less commonly, strong intermediate argillic alteration is associated with major faults and fracture systems.

Advanced Argillic Alteration

Kaolinite, alunite and poorly-ordered silica are the major constituents of advanced argillic alteration at Iamalele, Wairakei and Rawhide (usage of Meyer and Hemley, 1967). At Iamalele and Wairakei poorly-ordered silica is either lussatite or cristobalite, except in the very near-surface environment (depths less than ~5 m) where opal may be abundant. At Rawhide poorly-ordered silica is either chalcedony or opal (Black et al., 1991). Typically one of the characteristic minerals (kaolinite, alunite or poorly-ordered silica) is much more abundant than the remainder of the suite and may constitute >95% of the altered rock; e.g., see Figure 2.14.

Advanced argillic alteration commonly occurs as fracture or vein filling and as narrow envelopes on porcelaneous veins formed mainly of poorly-ordered silica, alunite and kaolinite. Initially alteration occurs along faults and throughgoing fractures, but as the intensity of alteration increases the entire rock may be replaced. Where advanced argillic alteration is weakly developed, kaolinite partially replaces illite, mixed-layer illite-smectite and smectite, as magmatic feldspar and the groundmass or

matrix of the rock are partially replaced by the assemblage kaolinite-alunite-poorly-ordered silica ± pyrite. As alteration intensity increases the advanced argillic alteration assemblage expands away from the fractures and veins to form irregular pods or zones which may extend outward from the structure a few centimetres to more than 5 metres. Late porcelaneous veins consisting of poorly-ordered silica and alunite, with or without kaolinite, are characteristic of areas of moderate to pervasive advanced argillic alteration.

Iamalele: Advanced argillic alteration is the dominant type of alteration exposed in rock outcrops and is the only alteration type present in the upper ~80 metres of core recovered from the Iamalele drill hole. The principal components of advanced alteration are kaolinite, alunite, lussatite and cristobalite. These minerals are typically associated with minor amounts of pyrite, opal (locally abundant on the surface), gibbsite, brucite, jarosite, goethite and hematite. Hydrothermal breccias consisting solely of alunite, cristobalite and kaolinite are a common feature of near-surface (depths <75 m) hypogene alteration at Iamalele. The breccias, which resulted from hydraulic fracturing, are composed of clasts of cristobalite, lussatite and alunite supported in a lussatite-kaolinite, lussatite-alunite or alunite matrix (Figs. 2.14 and 2.15). Pyrite related to advanced argillic alteration occurs as disseminated grains, as fine stringers crosscutting alunite or cristobalite, and as clots filling small

Figure 4.12. (Facing page) Relationship between geology, hydrothermal alteration and gold mineralization at the Rawhide precious metal deposit. (A) Geologic cross section. Tbr is a flow-banded biotite rhyolite. Tstc1 refers to lapilli tuff and tuff breccia with minor interbeds of siliceous siltstone. Tstc2 refers to well-bedded volcaniclastic siltstone and sandstone with minor ash tuff beds. (B) Distribution of silicification and intermediate argillic alteration. Potassic alteration is present throughout the cross section, although the abundances of quartz and adularia vary. Potassic alteration is the most intense in areas of strong silicification. (C) Gold distribution. See Figure 4.9 for cross section location. Reproduced from Black et al. (1991) with permission of the authors.

CRAZY HILL CROSS SECTION

GEOLOGY

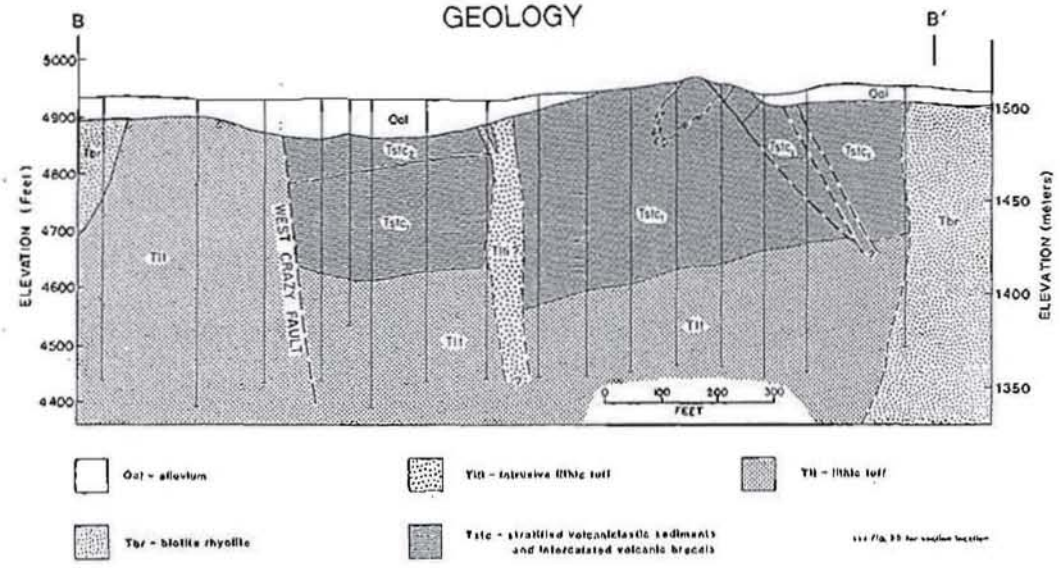

HYDROTHERMAL ALTERATION

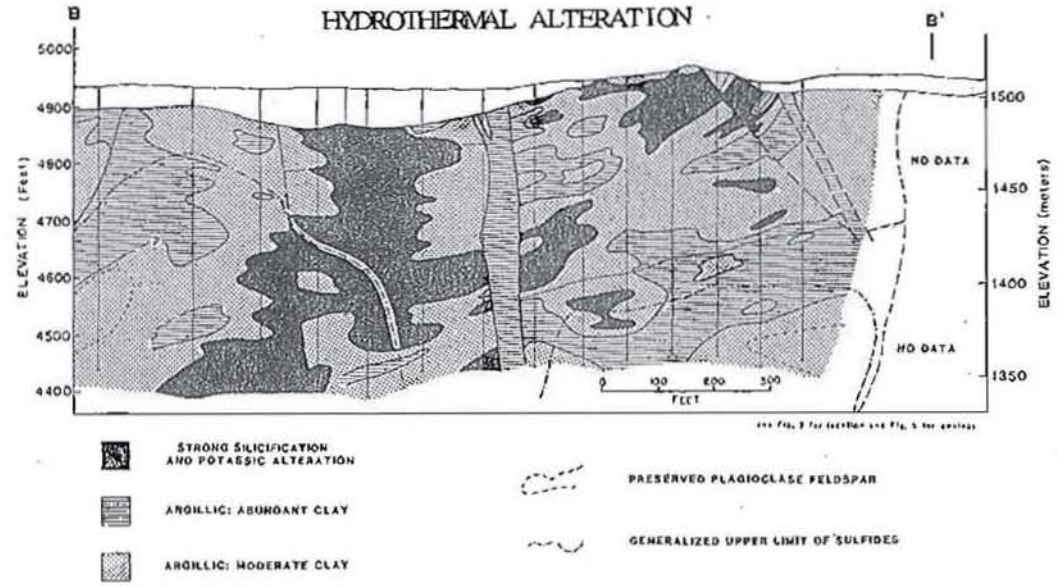

GOLD DISTRIBUTION

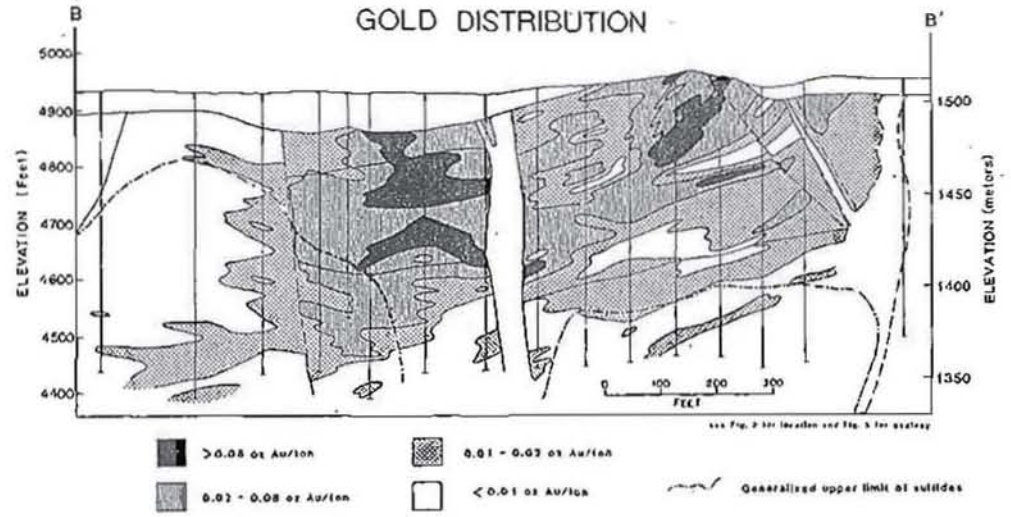

open spaces in the hydrothermal breccias. Late porcelaneous veins crosscut all alteration types and breccia features except the kaolinite-alunite-cristobalite-pyrite hydrothermal breccias. Irregular pods of kaolinite-alunite-lussatite ± opal alteration commonly extend outward from the porcelaneous veins and fractures for 1 to 10 centimetres, but where the rock was highly fractured or very porous, intense advanced argillic alteration may affect large areas, e.g., see Plate 3. Extensive areas of advanced argillic alteration are generally surrounded by a halo of intermediate argillic alteration.

Wairakei: Advanced argillic alteration is well developed in surface exposures where it is associated with the active thermal features and in areas where fluid discharge occurred in the relatively recent past. During my investigation of the high-level hydrothermal alteration at Wairakei, minerals and textures characteristic of advanced argillic alteration were not identified in polished sections or by x-ray diffraction analysis of samples of drill core and cuttings. However, Steiner (1977) notes that within the Wairakei reservoir kaolinite, alunite, opal and hydrated iron oxides are locally present at depths <65 metres (Steiner, 1977).

Rawhide: Advanced argillic alteration at Rawhide is represented by the assemblage kaolinite-alunite ± chalcedony, quartz or opal (Black et al., 1991); chalcedony and quartz probably recrystallized from hydrous silica phases (Sander and Black, 1988). Kaolinite-alunite-silica alteration is not extensively developed and occurs only in the upper portion of the ore deposit where irregular pod-like areas of kaolinite-alunite-chalcedony alteration may extend outward from veins and fractures for a few centimetres to a few metres (Black et al., 1991).

From observations of cross-cutting vein relationships Black et al. (1991) concluded that advanced argillic alteration was the result of a late supergene process, possibly post-dating hydrothermal activity. But advanced argillic alteration is paragenetically late even in the active

systems (e.g., Iamalele) and, since conclusions drawn from vein relationships provide only relative ages, it is possible that advanced argillic alteration at Rawhide may be a hypogene alteration assemblage.

If the advanced argillic alteration at Rawhide is the result of the hypogene process which deposited precious metals, it is possible that very little material has been eroded from the top of the deposit since it formed.

Metallization

It is not feasible to make a direct comparison of metallization occurring at Iamalele and Wairakei to metallization occurring at Rawhide because of the low abundances of ore minerals in the active systems. However, metallization paragenesis in each of these areas is comparable, and many of the economically important minerals identified at Rawhide also occur within the Wairakei reservoir and production wellhead equipment (Table 4.4).

Precious metal mineralization is genetically related to potassic alteration at Iamalele, Wairakei and Rawhide. In each of the areas ore and sulphide gangue minerals typically occur as (1) fine disseminations and fracture coatings and (2) disseminated grains and very thin stringers within quartz-adularia veins. Disseminated mineralization typically occurs in pumiceous tuffs and volcaniclastic rocks with high primary porosity or enhanced porosity related to vapour phase alteration during cooling of the pyroclastic units. Fracture-controlled quartz-adularia veins develop preferentially in the more brittle rocks (e.g., lavas, densely welded tuffs and hypabyssal intrusives) where high permeability has developed as a result of tectonic or magmatic-related fracturing. Quartz-adularia veining locally grades into open space filling as vein intensity increases along formational contacts and in tectonic or hydrothermal breccias. Quartz is

Table 4.4. Characteristics of metallization occurring in the geothermal reservoirs at Iamalele and Wairakei and in the palaeoreservoirs at Rawhide and Round Mountain

Hydrothermal System	Ore Minerals	Approximate Au:Ag Ratio	Ore Deposit		
			Tons ($\times 10^6$)	Gold (ozt/ton)	Silver (ozt/ton)
Iamalele (Fergusson Island, D'Entercasteaux Islands, P.N.G.)	Electrum, arsenopyrite, stibnite, pyrite	Not determined	None discovered		
Wairakei (North Island, N.Z.)	Reservoir: Gold-palladium alloy, argentite, galena, sphalerite, cassiterite, monazite, pyrrhotite, pyrite, marcasite	1:10	None		
	Production Equipment: Electrum, aguilarite, polybasite, pyrargyrite, trechmannite, tetrahedrite, niccolite, millerite, maucherite, breithauptite, bornite, chalcopyrite, galena, pyrrhotite, pyrite, marcasite				
Rawhide (Nevada, U.S.A.)	Electrum, embolite, cerargyrite, aguilarite, acanthite, pyrargyrite, perceite, tetrahedrite, argentojarosite, jalpaite, chalcopyrite, galena, sphalerite, molybdenite, monazite, pyrrhotite, pyrite, marcasite	1:10	29.4 29.9	0.040 0.032	0.36 0.23
Round Mountain (Nevada, U.S.A.)	Electrum, Au-Ag tellurides, pyrargyrite, tetrahedrite, arsenopyrite, realgar, chalcopyrite, galena, sphalerite, pyrrhotite, pyrite, marcasite	1:10	275	0.032	Not determined

Rawhide data from Black (1988) and Black et al. (1991). Round Mountain data from Sander (1988a) and Sander and Einaudi (1990).

generally the most abundant gangue mineral associated with both disseminated and structurally-controlled metallization.

Minor amounts of gold and silver are also deposited during intermediate argillic and advanced argillic alteration. Precious metals may be concentrated locally in areas of strong hydrolytic alteration, but their overall abundances are generally low. Where intermediate argillic alteration overprints potassic alteration it is difficult to ascertain the percentage of the gold that is related to a particular alteration assemblage, and it is possible that significant quantities of gold and silver may be genetically related to intermediate argillic alteration. Precious metals may certainly attain economic concentrations in areas of intense advanced argillic alteration. However, advanced argillic alteration is generally not extensively developed in the "adularia-sericite-type" of epithermal precious metal deposit and consequently areas of advanced argillic alteration do not constitute a significant source of economic precious metal mineralization. This is not true for the "acid-sulphate-type" of epithermal precious metal deposits (Hayba et al., 1985).

Iron sulphides (pyrite >> marcasite > pyrrhotite) are the most abundant sulphide phases associated with gold-silver mineralization, although trace amounts of chalcopyrite, galena, sphalerite and molybdenite may be present. Arsenopyrite, stibnite, cinnabar and other As, Sb and Hg sulphides may also accompany high-level alteration and gold-silver mineralization.

Iamalele

The upper portion of the Iamalele reservoir, at least in the area adjacent to the diamond drill hole, is well zoned with respect to hydrothermal alteration and metallization (Fig. 2.14). Altered rocks generally contain 1 to 5% disseminated and fracture-controlled pyrite, but pyrite may exceed 20% of the rock in quartz veins and in narrow fault zones where

intermediate argillic alteration is intense. The occurrence of antimony and arsenic appears to be correlated with the distribution of pervasive potassic alteration. However, more detailed examination reveals that stibnite is typically intergrown with mixed-layer illite-smectite indicating that the deposition of antimony is actually associated with intermediate argillic alteration of potassically altered rocks. Trace amounts of arsenic and antimony also accompany advanced argillic alteration. Mercury mineralization is primarily restricted to areas of advanced argillic alteration, where the abundance of mercury is directly related to that of kaolinite. Minor amounts of mercury also occur in potassically altered rocks where arsenic values are high.

Wairakei

Precious and base metal mineralization occurring at Wairakei is directly related to potassic alteration. Analytically detectable metallization is ubiquitous throughout the potassically altered portions of the reservoir (Figs. 3.33, 4.13 and 4.14), but ore minerals large enough ($\approx 0.1\mu$) to be identified readily by use of the scanning electron microscope or electron microprobe are rare. With the exception of the iron sulphides, the distribution of identifiable ore minerals is generally restricted to intermediate levels within the reservoir (transitional propylitic-potassic alteration); see Metallization section under Round Mountain. Precious and base metals are common contaminants of iron sulphide minerals (Stanton, 1972) and since minor amounts ($\leq 1\%$) of pyrite commonly accompany high-level potassic alteration, it is possible that much of the analytically detectable metallization associated with high-level potassic alteration is contained within pyrite. Although much more common in transitional propylitic-potassic alteration, hydrothermal monazite is an important trace mineral associated with high-level potassic alteration at Wairakei. Monazite occurs as micron-sized grains and discontinuous microstringers in

quartz-adularia-pyrite veins (Fig. 3.34E) and as disseminated micron-sized grains in areas of pervasive quartz-adularia alteration (Figs. 3.34D and 3.35E). Hydrothermal monazite may be a common trace mineral associated with high-level potassic alteration, but because it typically occurs as micron-sized grains, its occurrence in most epithermal precious metal deposits may be overlooked. However, hydrothermal monazite associated with potassic alteration has been identified recently at the epithermal gold-silver deposits of Rawhide (J.E. Black, personal communication) and Mesquite (S. Manske, personal communication). At Rawhide the alteration and textural characteristics of hydrothermal monazite are identical to those of secondary monazite occurring at Wairakei.

Rawhide

The following descriptions are paraphrased from Black et al. (1991). At Rawhide, economic precious metal mineralization is genetically related to potassic alteration and closely associated with silicification. Gold and silver occur as (1) fracture-controlled (quartz-adularia vein and vein stockwork) mineralization and (2) uniformly disseminated (pervasive quartz adularia alteration) mineralization. Fracture-controlled metallization developed preferentially in brittle rocks with low primary permeability (andesite lava). Disseminated ore is generally restricted to highly permeable lithic tuffs and volcaniclastic sedimentary rocks. The primary sulphide ore minerals at Rawhide are electrum, acanthite (Ag_2S) and the silver sulphoselenide aguilarite (Ag_4SeS); in the oxidized portion of the deposit the primary ore minerals are cerargyrite (AgCl) and embolite (Ag(Br,Cl)). Pyrite is the most abundant sulphide mineral, occurring as fracture coatings, fine disseminated grains and small stringers. Pyrite commonly accounts for 1 to 5% of the altered rocks. Trace amounts of chalcopyrite, galena, sphalerite, molybdenite, pyrrhotite, marcasite and

Figure 4.13. (Facing page) Down-hole distribution of selected trace and minor elements determined from drill cuttings and core from Wairakei well 48. The analytical data are given in Appendix 3.

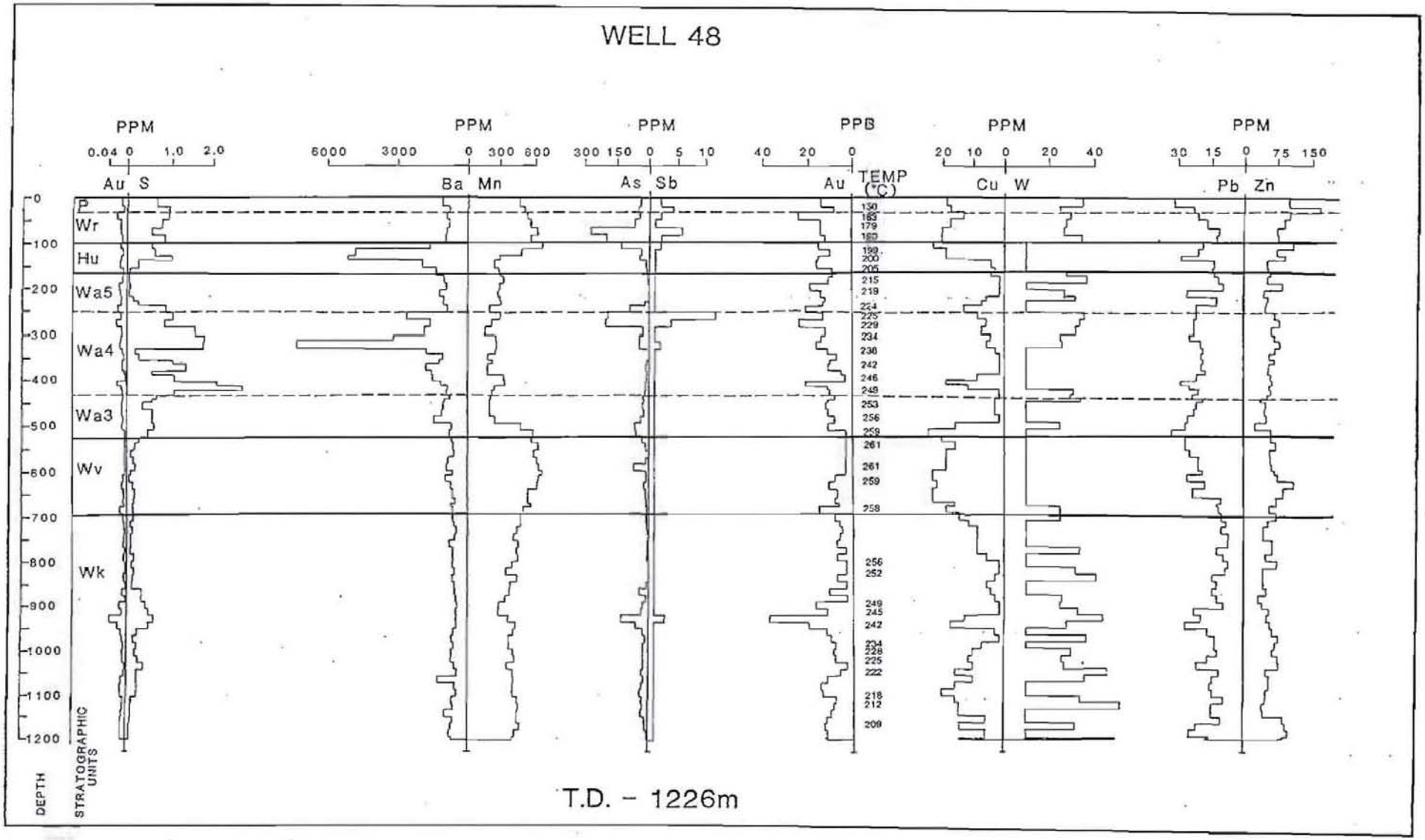
WELL 48
PPM
0.04 0 1.0 2.0
Au S
PPM
6000 3000 0 300 600
Ba Mn
PPM
300 150 0 5 10
As Sb
PPB
40 20 0
Au
TEMP (°C)
PPM
20 10 0 20 40
Cu W
PPM
30 15 0 75 150
Pb Zn
P
Wr
Hu
Wa5
Wa4
Wa3
Wv
Wk
0
100
200
300
400
500
600
700
800
900
1000
1100
1200
DEPTH
STRATOGRAPHIC UNITS
T.D. - 1226m

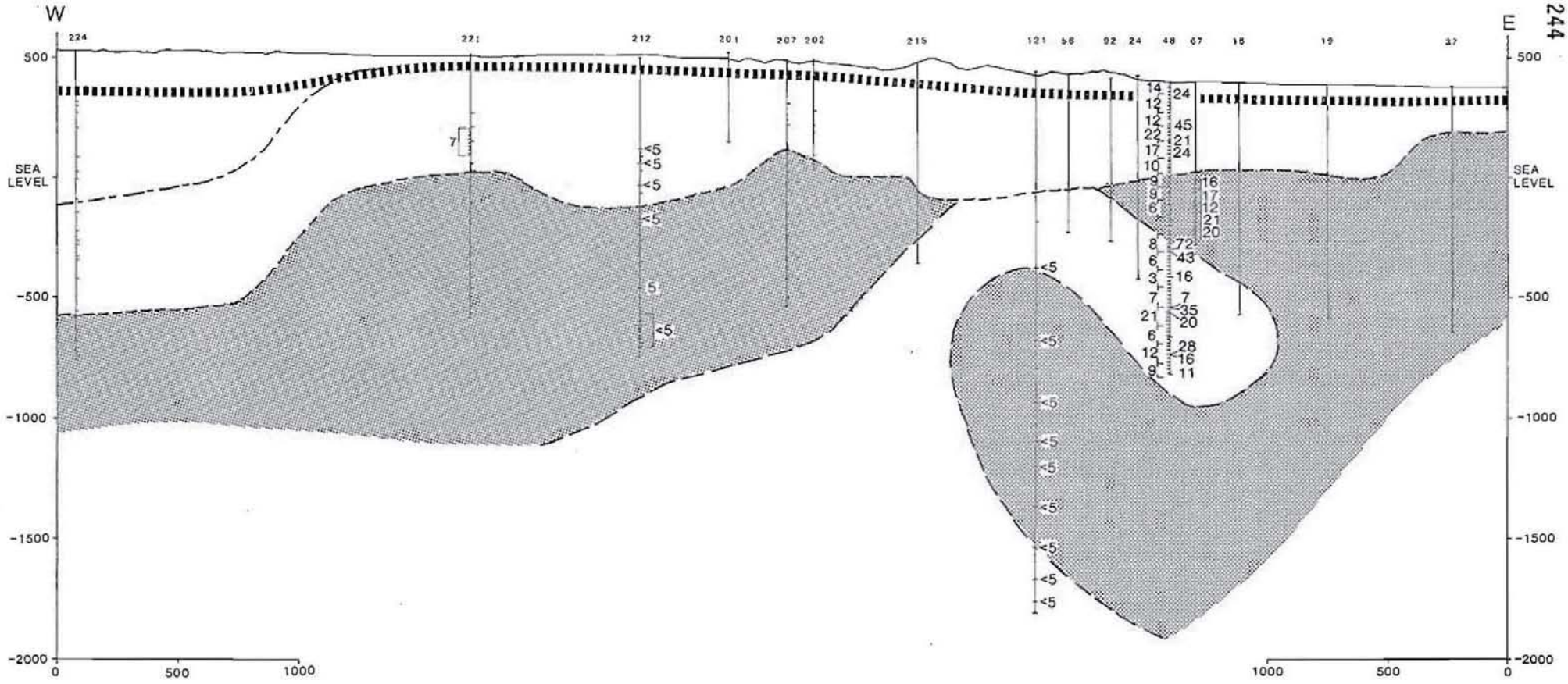

Figure 4.14. Gold geochemical data for core (numbers on right side of drill hole) and cuttings (numbers on left side of drill hole) samples from four Wairakei wells. Note that smaller values are associated with the drill cuttings. This implies that much of the gold is localized in veins or along fractures which tend to be abraded during drilling and that much of the gold is "partitioned" into the drilling mud which is not sampled. Other symbols show the upper limit of (1) hydrothermal alteration (thick striped line), (2) potassic alteration (long and short dashed line) and (3) propylitic alteration (short dashed line). See Figure 3.20 for comparison.

numerous other ore minerals (Table 4.4) also accompany potassic alteration at Rawhide.

Discussion

It is evident from the studies of Iamalele, Wairakei and Rawhide that precious metal mineralization is genetically related to potassic alteration, and that enhanced gold and silver grades are likely to occur in areas of strong silicification. High-level hydrothermal alteration occurring at Iamalele and in the upper portions of the Wairakei reservoir closely resembles hydrothermal alteration which occurred in the palaeo-reservoir at Rawhide, with the only significant difference between the two geothermal systems and Rawhide being the quantity of gold and silver present.

At Wairakei the spatial distribution of hydrothermal alteration and incipient gold-silver metallization is dominantly controlled by primary porosity, whereas at Rawhide the distribution of hydrothermal alteration and economic gold-silver mineralization is a function of (1) fracture permeability in the brittle andesite lavas, with gold and silver grades proportional to the fracture density, and (2) primary porosity in the tuffaceous and volcaniclastic rocks, with gold grades relatively uniformly distributed throughout the rock (Black et al., 1991). The strong correlation between economic mineralization and rock fracturing in the andesite lavas at Rawhide may indicate that economic concentrations of gold and silver developed as a result of fluid cooling related to disruption of the reservoir hydrology by a tectonic and/or a magmatic event.

Although the characteristics of potassic, intermediate argillic and advanced argillic alteration are very similar at Iamalele, Wairakei and Rawhide, one difference is the occurrence of abundant zeolites at Wairakei. This contrasts strongly with the rare occurrence of zeolite minerals at Iamalele and the apparent absence of zeolite alteration in and adjacent to

economic gold-silver mineralization at Rawhide. The two most abundant zeolites which occur at relatively low temperatures within the Wairakei reservoir are mordenite ($(Na_2,K_2,Ca)[Al_2Si_{10}O_{24}]\cdot 7H_2O$) and laumontite ($Ca[Al_2Si_4O_{12}]\cdot 4H_2O$). Mordenite is clearly part of the potassic assemblage, and may account for more than 25% of the rock. In general, mordenite occurs where reservoir temperatures are <230°C, but it is stable over a temperature range of <150° to >260°C, indicating minimal thermal control on its distribution. A comparison of Figures 3.5 and 3.25 indicates that the spatial distribution of mordenite clearly reflects a strong lithologic control. Laumontite is a common alteration mineral in the peripheral (lower temperature) portions of the Wairakei reservoir (Fig. 3.25), where it appears to postdate potassic alteration. The occurrence of laumontite is apparently an independent type of late alteration unrelated to intermediate argillic alteration. The spatial distribution of laumontite alteration commonly traverses formational boundaries and appears to be controlled primarily by temperature. Laumontite may occur at temperatures ranging up to 250°C, but it is most abundant where reservoir temperatures are less than ≈200°C.

The range in temperatures over which laumontite and mordenite are stable (~150° to ~230°C) certainly existed within the hydrothermal reservoir at Rawhide during potassic alteration and precious metal deposition. Why then are zeolite minerals absent from the altered rocks at Rawhide? Three possible reasons are readily apparent: (1) the composition of the host rocks inhibited the formation of zeolite minerals, (2) erosion has removed those portions of the palaeoreservoir which contained zeolite alteration or (3) the combined effect of reservoir hydrology (primarily permeability) and fluid chemistry prohibited the development of zeolite alteration. The first possibility is unlikely to be a major factor because even though a large part of the economic gold-silver mineralization at Rawhide occurs in andesite lava(s), rhyolitic pyroclastic rocks, hypabyssal

intrusives and flow domes are abundant and do not host zeolite alteration. Further, laumontite alteration was identified in samples of andesitic lava and hypabyssal dykes (Waiora Valley Andesite) which occur within the Wairakei reservoir. The second possibility is a viable reason for the absence of low temperature zeolites like laumontite. The peripheral portions of the palaeoreservoir may have been removed by erosion during unroofing of the Rawhide ore deposit, and exploration drill holes were not completed to sufficient depths to intersect the base of the palaeoreservoir. However, erosion cannot account for the absence of the higher temperature zeolites such as mordenite. Overall the third possibility seems to be the most reasonable option. A comparison of the size and location of the Rawhide ore body with the dimensions of the preproduction reservoir at Wairakei (Fig. 4.4) and the distribution of zeolite alteration (Fig. 3.25) shows that similar areas within the Wairakei reservoir are also devoid of zeolite minerals. This theory is supported further by the rarity of zeolites in the drilled portion of the Iamalele reservoir.

Because the effects of hydrothermal alteration at Iamalele and Wairakei closely resemble the effects of hydrothermal alteration at Rawhide, it is unlikely that significant differences existed in the thermochemical environments of their respective reservoirs. The only significant difference between the two geothermal systems and Rawhide are the absence of economic gold-silver mineralization and the lack of extensive rock fracturing in the hydrothermal reservoirs at Iamalele and Wairakei. These differences may imply that a relatively simple structural event could be the catalyst required to convert a portion of a high-level geothermal reservoir into an epithermal precious metal deposit.

Intermediate-Level Hydrothermal Systems

The term "intermediate-level" applies to hydrothermal alteration and metallization occurring at depths between ~400 and ~1500 metres and at tem-

peratures greater than ~200°C. Maximum reservoir temperatures at these depths generally range from ~250° to ~325°C[7]. The types of hydrothermal alteration and alteration paragenesis characteristic of intermediate levels within the Wairakei reservoir and the palaeoreservoir at Round Mountain are strikingly similar. "Ore" minerals occurring in production wellhead equipment and at intermediate levels within the reservoir at Wairakei are also similar to the ore minerals described from Round Mountain, the major difference being the much greater abundance of gold and silver at Round Mountain.

In the following discussion descriptions of hydrothermal alteration and metallization at Round Mountain are from data presented by Sander (1988b) and Sander and Einaudi (1990).

Hydrothermal Alteration

Hydrothermal alteration which occurs at intermediate levels within high-temperature reservoirs as a result of the interaction of rock with a low salinity, near-neutral pH fluid generally results in an "equilibrium" assemblage in which at least one feldspar phase is stable. Adhering to the usage of Meyer and Hemley (1967), intermediate-level alteration may be divided into two principal types reflecting the stable feldspar species. In order of decreasing temperature and activity of H^+ these two types are propylitic and potassic.

---

[7]The 200°C temperature was determined from thermodynamic relationships of the observed equilibrium alteration assemblages, measured temperatures within the upper portions of active geothermal systems and fluid inclusion homogenization temperatures determined for propylitic and potassic alteration occurring at Round Mountain. The temperature range of ~250° to ~300°C is consistent with maximum measured temperatures recorded at many of the high-temperature geothermal reservoirs, but temperatures as high as ~370°C have been recorded at Mexicali (Ellis, 1979). The maximum reservoir temperature measured at Wairakei is 271°C (well 121, 2240 m), however, reconnaissance fluid inclusion homogenization temperature data indicate that the deeper reservoir attained a maximum temperature of ~310°C. Fluid inclusion homogenization temperatures determined for Round Mountain indicate that the maximum reservoir temperature was ~275°C (Sander and Einaudi, 1990).

The terminology used in the descriptions that follow differs slightly from the terminology employed by Sander (1988b) and Sander and Einaudi (1990). In accordance with the usage of Shelley (1975), the terms adularia and pericline are used to refer respectively to potassium and sodium feldspar which have crystallized from hydrothermal solutions and are of near stoichiometric composition. Sander (1988b) and Sander and Einaudi (1990) refer to hydrothermal Na-feldspar as albite. These authors use adularia to refer to hydrothermal K-feldspar, but also use the terms Ksp(I) and Ksp(II) in reference to adularia associated with propylitic (KspI) and potassic (KspII) alteration.

Structural Controls

In general, the spatial distributions of propylitic alteration at Wairakei and Round Mountain are similar, with major structures and formation boundaries providing the fundamental control. Away from these structural features propylitic alteration proceeds intergranularly, a process which can best be described as a soaking event. At Wairakei potassic alteration is primarily controlled by porosity, and alteration intensity decreases as rock porosity decreases. Fracture-controlled alteration is of minor importance at intermediate levels within the Wairakei reservoir. However, at Round Mountain both porosity and fracture-permeability are important controls on the distribution of potassic alteration, and rock properties dictate the prevailing style of alteration.

Propylitic Alteration

Propylitic alteration is the earliest and highest temperature (T $\geq$250°C) rock alteration that occurs at intermediate levels within the Wairakei reservoir and at Round Mountain. At both locations propylitic alteration is represented by the equilibrium assemblage quartz-pericline-adularia-chlorite-epidote-pyrite-anatase/rutile. The core samples shown

in Figures 4.15 and 4.16 are typical examples of propylitically altered rock. The replacement textures which are essential to the identification of propylitic alteration at Round Mountain are (1) the replacement of plagioclase by pericline (albite) and (2) the replacement of sanidine by adularia (KspI) ± pericline. Magmatic sanidine is not known to occur in the reservoir rocks at Wairakei, and therefore propylitic alteration is identified solely by the alteration of plagioclase to pericline ± quartz ± adularia. Mineralogical differences between propylitic alteration at Wairakei and at Round Mountain are the occurrence of wairakite ($Ca[Al_2Si_4O_{12}]\cdot 2H_2O$), prehnite ($Ca_2Al[AlSi_3O_{10}](OH)_2$), illite-sericite and montmorillonite at Wairakei, and the abundance of calcite at Round Mountain. Additional subtle differences include the composition of chlorite, which is clinochlore at Wairakei and brunsvigite at Round Mountain (Sander, 1988b) and the occurrence of clinozoisite, zoisite and magnetite only at Wairakei. These mineralogical differences may imply that the activities of Ca^{2+} and Al^{3+} are slightly higher and the activities of Mg^{2+} and Fe^{3+} are slightly lower in the Wairakei fluid than in the fluids that were associated with propylitic alteration at Round Mountain.

Wairakei: At Wairakei propylitic alteration occurs in the higher-temperature portions of the reservoir at depths generally greater than 500 metres (Fig. 3.14). Propylitic alteration may be characterized by the replacement of plagioclase by twinning-controlled intergrowths of pericline-adularia-quartz ± epidote, prehnite, clinochlore and magnetite (Figs. 4.17A, 3.21A, D, E and F). In feldspar alteration the relative percentages of individual replacement minerals vary, but pericline or wairakite is always the most abundant. The groundmass and rock fragments are typically replaced by irregular intergrowths of all the minerals listed above, but quartz and adularia are commonly the most abundant alteration minerals (Figs. 3.16D, 3.21C and 3.22A). Additional minerals locally occurring in apparent equilibrium with pericline and/or wairakite are

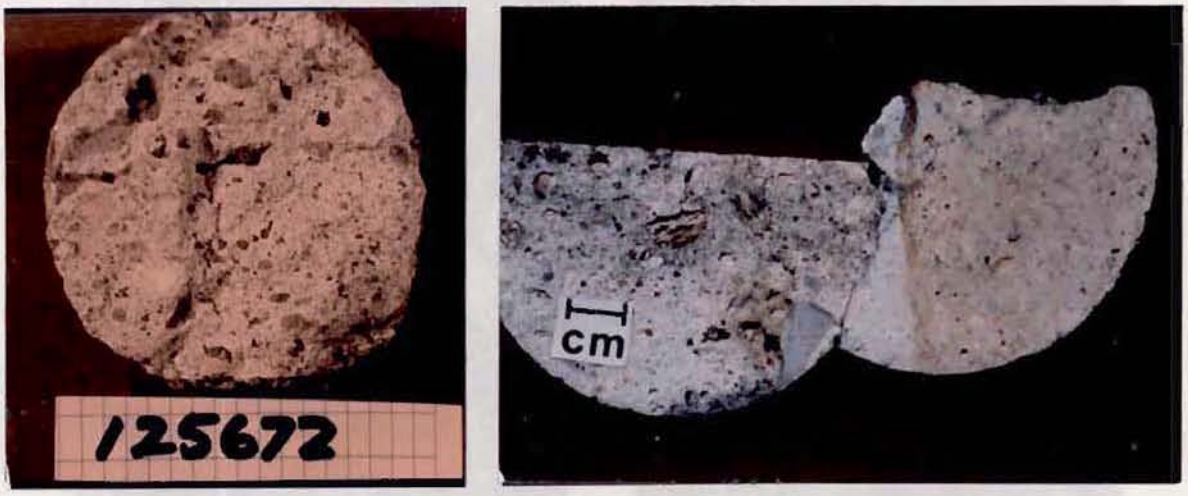

Figure 4.15. Characteristic rock alteration occurring at intermediate levels within the hydrothermal reservoir at Wairakei and the palaeo-reservoir at Round Mountain. Photograph on the left (Wairakei) shows rock textures characteristic of transitional propylitic-potassic alteration in pumiceous ignimbrites of the Waiora Formation. Photograph on the right (Round Mountain) contrasts typical ore-grade potassically altered propylitized poorly-welded tuff (left) and clay-choked (intermediate argillic alteration) poorly welded tuff (right). Pumice textures in the ore-grade sample were preserved during early vapour phase alteration. Clay-choked poorly welded tuff does not contain economic concentrations of gold.

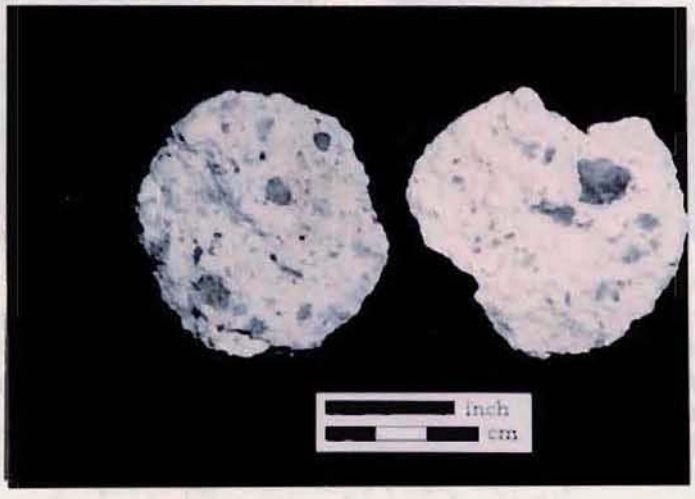

Figure 4.16. Characteristic rock alteration occurring at intermediate levels within the hydrothermal reservoir at Wairakei (left) and the palaeo-reservoir at Round Mountain (right). The photograph shows rock textures characteristic of propylitic alteration in poorly-welded pumiceous ignimbrites. Feldspar phenocrysts are replaced by pericline and adularia, lithic fragments are replaced by chlorite ± pyrite, and the groundmass is replaced by the assemblage quartz-pericline-adularia-chlorite-pyrite-calcite.

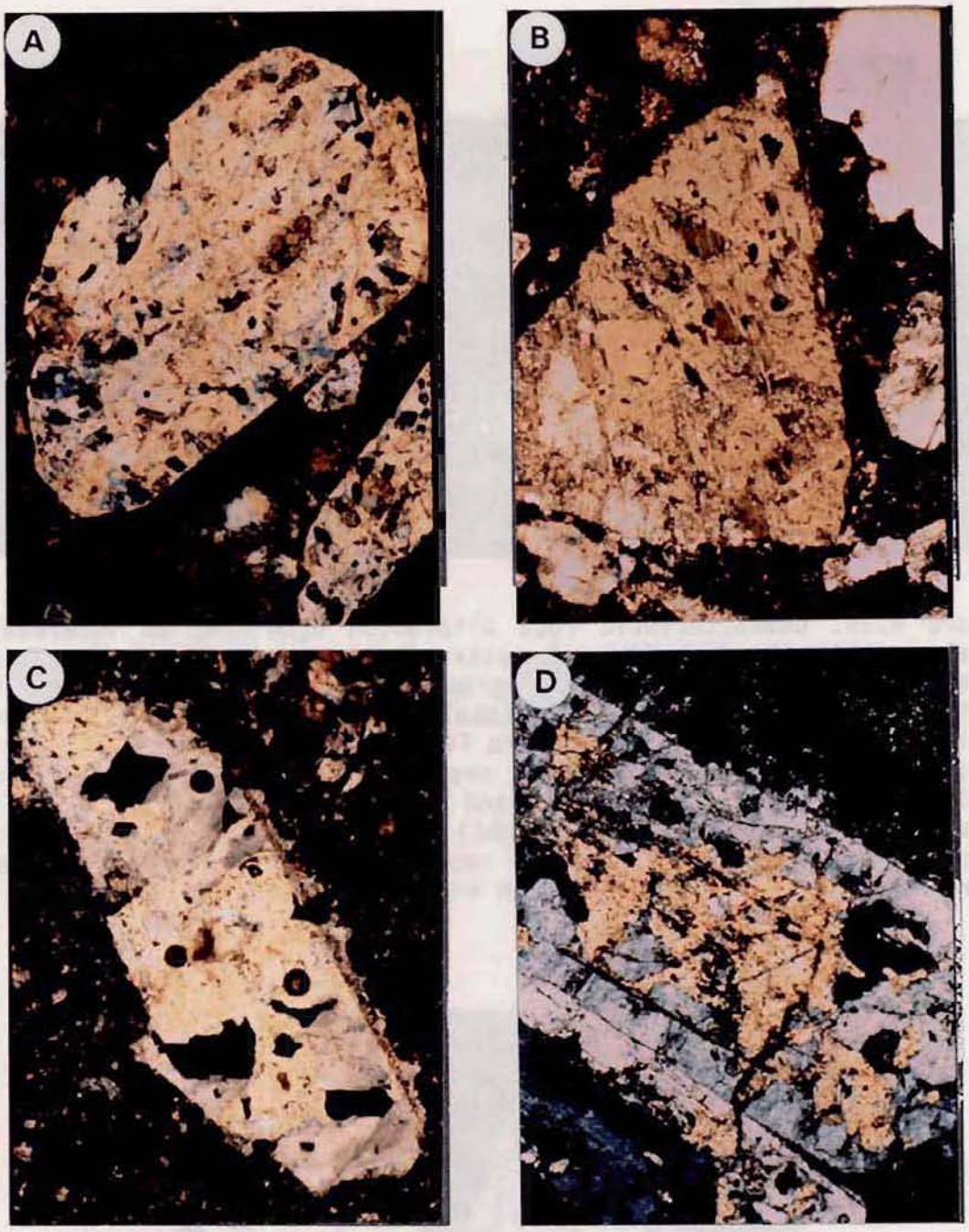

Figure 4.17. Photomicrographs of key feldspar replacement textures. (A) Wairakei: propylitic alteration of andesine phenocryst replaced by the equilibrium assemblage pericline (yellow), wairakite (light grey area in lower left corner of large phenocryst) and epidote (areas with high birefringence); blue areas are stained epoxy. Sample from Te Mihi Rhyolite, well 206, at 809 m. (B) Round Mountain: propylitic (Ksp I) alteration of andesine phenocryst replaced by pericline (yellow) and calcite (white patches in lower corner of the large phenocryst); irregular dark grey areas with twinning are residual andesine. Sample from densely welded tuff. (C) Wairakei: potassic alteration of previously propylitically altered andesine phenocryst. Adularia (mottled grey areas) partially replacing pericline (yellow); black areas are holes where adularia was plucked from the section. Sample from pumiceous sandstone (Member 3, Waiora Fm.), well 206, at 656 m. (D) Round Mountain: potassic (Ksp II) alteration of previously propylitically altered plagioclase phenocryst. Adularia (light grey) replacing pericline (yellow); black areas are holes in the section. Sample from lower poorly welded tuff.

clinozoisite, zoisite, and possibly illite-sericite, montmorillonite and leucoxene. The intensity of propylitic alteration varies from weak in less permeable units to intense in areas where the fluid/rock ratio has remained high, e.g., in the high-temperature upflow zone which feeds the reservoir.

Below ~1500 metres the abundance of pericline decreases rapidly, and at depths greater than ~2000 metres pericline alteration grades into strong silicification consisting of the assemblage quartz-pericline-adularia-illite-pyrite ± wairakite, chlorite and calcite. If the high-temperature reservoir is in its waning stages and, as suggested in Chapter 3, collapsing from the bottom up, it is possible that the deep silicification event is in part related to a potassic overprint on propylitic alteration. Further evidence in support of a deep potassic event is the existence of quartz-adularia stringers and the common occurrence and local abundance of grothite (Al-titanite) which is an important component of the potassic alteration assemblage. It may be possible to extend this scenario to include incipient intermediate argillic alteration. Below a depth of ~2000 metres core and cuttings samples from well 121 locally contain abundant mixed-layer illite-smectite and less commonly montmorillonite. It is possible that these minerals form part of the propylitic equilibrium assemblage, but the replacement of epidote and chlorite by smectite and calcite is more consistent with a "late" intermediate argillic alteration event.

Round Mountain: At Round Mountain propylitic alteration is the earliest hydrothermal alteration. It occurred at temperatures between ~250° and ~275°C and is represented by the equilibrium assemblage quartz-pericline (albite)-adularia (KspI)-chlorite-calcite-pyrite-rutile ± epidote (Sander, 1988b). Propylitic alteration is identified by the concurrent partial to total replacement of (1) sanidine by adularia ± calcite, pericline and epidote (2) plagioclase by pericline ± chlorite (brunsvigite) and calcite (Fig. 4.17B), (3) biotite and other mafics by brunsvigite ± pyrite, rutile, calcite and epidote, and (4) magnetite by

brunsvigite + pyrite (Sander and Einaudi, 1990). Within the limits of the ore body propylitic alteration is pervasive and its distribution is directly dependent upon palaeoreservoir temperatures (Sander and Mitchell, 1988).

On a deposit-wide scale the spatial distribution of propylitic alteration at Round Mountain is structurally controlled, forming extensive halos on major faults and joint sets (Fig. 4.18). However, on a more detailed scale propylitic alteration proceeded intergranularly or along unconnected microfractures. This is particularly evident in the poorly welded tuff where propylitic alteration is pervasive (Sander and Einaudi, 1990). Bulk rock permeability is a key factor in the distribution of propylitic alteration at Round Mountain. This is documented by the occurrence of propylitic alteration as "envelopes" on major structural zones in the densely welded tuff and as pervasive replacement of the poorly welded tuff (Sander and Einaudi, 1990). The intensity of propylitic alteration decreases laterally away from the limits of ore-grade mineralization. This is manifested initially by the disappearance of epidote followed by a gradual decrease in the abundance of minerals associated with the assemblage (Sander and Einaudi, 1990).

Potassic Alteration

Intermediate-level potassic alteration at Wairakei and Round Mountain is represented by the alteration assemblage quartz-adularia-white mica (illite/sericite)-pyrite-rutile. At both locations potassic alteration is identified by the replacement of magmatic plagioclase and pericline by nearly stoichiometric adularia. Potassic alteration at Round Mountain is also identified by the replacement of magmatic sanidine by adularia (Sander and Einaudi, 1990). Adularia associated with potassic alteration is indistinguishable from that associated with propylitic alteration. At Wairakei this accentuates the difficulty in determining whether the adularia that replaces plagioclase is related to propylitic or potassic alteration, and

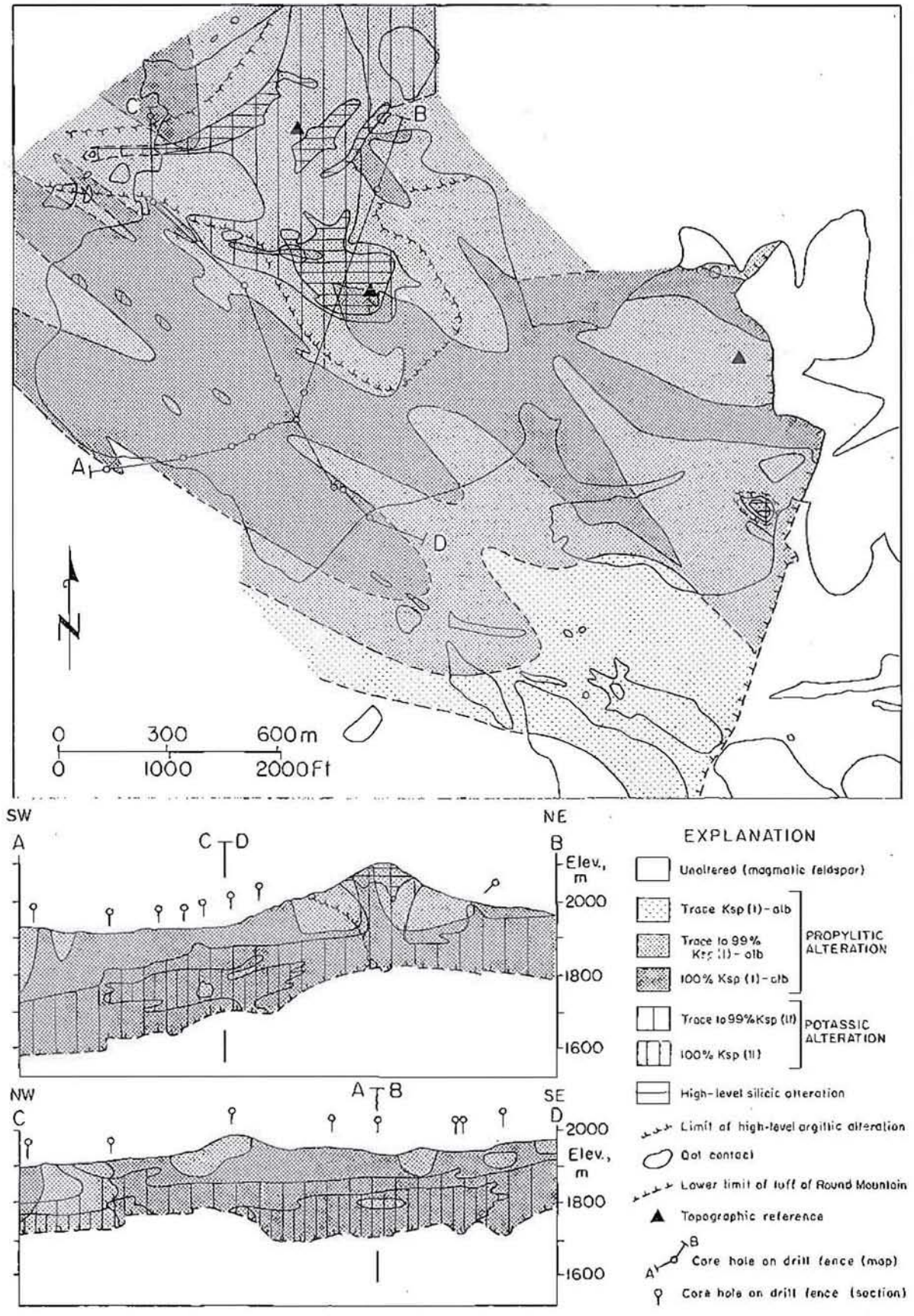

Figure 4.18. Spatial distribution of hydrothermal alteration assemblages at the Round Mountain epithermal gold-silver deposit. The effects of lithologic versus structural control on the distribution of propylitic and potassic alteration is apparent when this figure is compared with Figure 4.11.

the only textural relationship which is conclusive of potassic alteration is the replacement of pericline by adularia. At Round Mountain the identification of potassic alteration is less ambiguous because pervasive propylitic alteration was more extensive and both magmatic sanidine and plagioclase occurred in the tuff of Round Mountain. The occurrence of magmatic plagioclase and sanidine is important because (1) during propylitic alteration plagioclase was replaced by pericline but not by adularia, and sanidine remained unaltered and (2) during potassic alteration pericline, residual plagioclase and sanidine were all replaced by adularia. Thus, the presence of two magmatic feldspars allowed Sander and Einaudi to establish a clear paragenetic sequence.

The principal differences between potassic alteration at Wairakei and at Round Mountain are the intensity of alteration and the occurrence of fracture-controlled alteration in the densely welded tuff at Round Mountain. Mineralogical differences include (1) the occurrence of mordenite, grothite, clinochlore and monazite at Wairakei and their apparent absence at Round Mountain and (2) the abundance of calcite at Round Mountain.

Wairakei: Potassic alteration at Wairakei is widely distributed and locally pervasive at depths between ~500 and ~1500 metres within the reservoir. Intermediate-level potassic alteration is represented by the assemblage quartz-adularia-illite/sericite-grothite-pyrite-anatase which is always present. In addition mordenite, clinochlore and chlorapatite are commonly present and locally abundant. Trace amounts of anhydrite, magnetite and zircon may also form part of the intermediate-level potassic assemblage. Intermediate-level potassic alteration is similar to high-level potassic alteration with one important exception. This is that precious and base metal minerals are only known to occur with intermediate-level potassic alteration. The most obvious alteration texture signifying potassic alteration is the replacement of pericline by adularia (Fig. 4.15C).

At intermediate levels within the high-temperature reservoir the effects of propylitic and potassic alteration overlap. Within this "transitional zone" potassic alteration generally postdates the propylitic assemblage, but relatively complex mineral textures indicating cyclic deposition of the propylitic and potassic assemblages are not uncommon (Figs. 3.21 and 3.22). These "cyclic" textures are referred to as transitional propylitic-potassic alteration which is characterized by cyclic overgrowths of adularia and pericline along the rims of plagioclase phenocrysts. The sequence most commonly observed is pericline-adularia-pericline, but in a few samples the sequence ends with a second period of adularia alteration.

Round Mountain: At Round Mountain potassic alteration is represented by the assemblage quartz-adularia (KspII)-calcite-white mica (illite/sericite)-pyrite-rutile and is recognized by the replacement of plagioclase, sanidine and pericline (Fig. 4.17D) by nearly stoichiometric adularia (Sander and Einaudi, 1990). During potassic alteration magmatic biotite and brunsvigite are replaced by white mica which approaches muscovite in composition (Sander and Einaudi, 1990). Repetitive overprints of potassic and propylitic alteration similar to those occurring in areas of transitional propylitic-potassic alteration at Wairakei were not noted at Round Mountain.

Potassic alteration is only weakly developed at the surface and in the densely welded tuff in areas that are not in close proximity to major fracture sets and faults, but is pervasive in the poorly welded tuff (Fig. 4.18). The spatial distribution of potassic alteration indicates that the densely welded tuff was an effective aquitard which allowed hydrothermal fluids to permeate the underlying poorly welded tuff, and demonstrates the importance of fracture permeability in rock units with low primary permeability.

Metallization

At Wairakei and Round Mountain small amounts of gold and silver were deposited during propylitic alteration, but the majority of precious metal mineralization (at Round Mountain) is directly associated with potassic alteration. Within the Wairakei reservoir precious and base metal minerals were only identified in rocks affected by transitional propylitic-potassic alteration. A similar situation exists at Round Mountain where the distribution of ore-grade gold and silver mineralization corresponds to the areas where potassic alteration overprints the propylitic assemblage.

Wairakei

Gold and silver are being deposited at very low grades (<0.01 to ~0.04 g/t) throughout the Wairakei reservoir (Figs. 3.33, 4.13 and 4.14), but precious metal minerals were identified only in a few locations. These minerals are gold-palladium alloy and argentite (Ag_2S). A few isolated occurrences of sphalerite, galena and chalcopyrite were also noted within the limits of transitional propylitic-potassic alteration. Micron-sized grains of hydrothermal monazite are relatively common alteration products at intermediate levels within the reservoir. Precious metal-, base metal- and REE-bearing minerals occur as (1) quartz-pyrite-sphalerite veins with quartz-adularia ± pyrite envelopes, (2) quartz-argentite-cassiterite (SnO_2)-ilmenite replacement of the groundmass, (3) quartz-pericline-adularia-monazite-gold-palladium alloy microveins and groundmass replacement, (4) grothite-anatase-apatite-galena replacements of iron-titanium oxide minerals and groundmass. Examples of some of these occurrences are shown in Figures 3.34 and 3.35.

Samples of metal-rich scale and siliceous sinter collected from wellhead production equipment contained numerous ore minerals including electrum, Ag sulphides and selenides, Cu, Pb, Zn and Ni sulphides, Ag and

Cu sulphosalts and Ni arsenides (Fig. 3.32, Table 4.4). Minerals identified in the metal-rich scale are hosted by hydrous iron and silica oxides.

Round Mountain

The total amount of recoverable gold in the system at Round Mountain exceeds 372,000 kg (10.85 million troy ounces; Table 4.4), with the vast majority of this amount occurring in the ore body that supports the present open pit mine (H. Elson, personal communication). Gold and silver occur in sheeted sets of quartz-adularia-pyrite veins in the densely welded tuff and also occur as very fine disseminated mineralization accompanying pervasive quartz-adularia-pyrite alteration in poorly welded tuff. Economic precious metal mineralization accompanied potassic alteration. Deposition of gold and silver occurred during the transition from propylitic to potassic alteration as temperatures declined from about 265° to less than 200°C within the deeper portions of the palaeoreservoir (Sander and Einaudi, 1990). Studies conducted in conjunction with recent mine development support the findings of Sander (1988b) that gold-silver mineralization at Round Mountain occurred in a single hydrothermal event and is not the result of multiple periods of alteration and metallization (H. Elson, personal communication). The relationship between hydrothermal alteration and gold-silver mineralization is apparent from a comparison of Figures 4.18 and 4.19.

Discussion

The physical environments of the preproduction high-temperature reservoir at Wairakei and the palaeoreservoir at Round Mountain are remarkably similar with respect to alteration mineral assemblages and the sequence of alteration events. At both locations the reservoir (palaeoreservoir) of hot water at 250°C or more was three to five kilometres in diameter, 400 metres or more below the surface (palaeosurface) and more

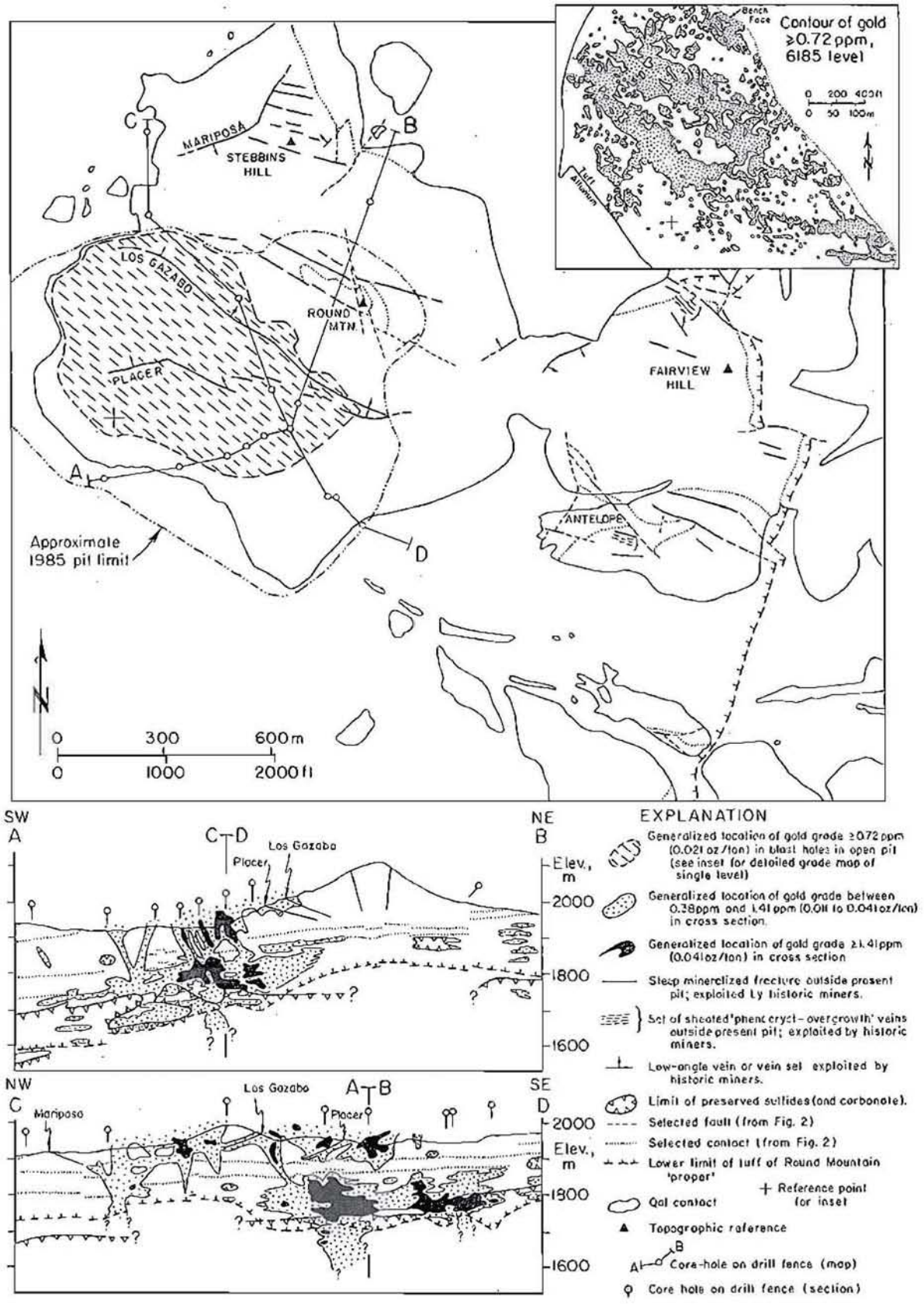

Figure 4.19. Relationship between hydrothermal alteration and precious metal mineralization at the Round Mountain epithermal gold-silver deposit. Figure reproduced from Sander and Einaudi (1990; Figure 3, page 290) with permission of the authors.

than 400 metres thick (Sander and Mitchell, 1988). Reservoir fluids sampled by wells at Wairakei are exceedingly dilute (a few tenths of a weight percent equivalent NaCl, with low ΣC and ΣS; Henley et al., 1984; Hedenquist and Henley, 1985). Fluids at Round Mountain are also inferred to have been dilute and low in ΣC (Sander and Einaudi, 1990).

The major alteration types identified at intermediate levels within the Wairakei reservoir and within and adjacent to economic gold-silver mineralization at Round Mountain are propylitic and potassic. At Wairakei propylitic alteration is represented by the assemblage quartz-pericline-adularia-clinochlore-pyrite ± wairakite, epidote/clinozoisite, mordenite, calcite and anatase. Propylitic alteration typically occurs at temperatures ≥250°C and is pervasive in the high-temperature reservoir where its intensity is directly related to primary permeability (mainly porosity). Potassic alteration generally overprints propylitic alteration and is represented by the assemblage quartz-adularia-illite/sericite-pyrite ± mordenite, clinochlore, calcite and anatase.

Propylitic alteration at Round Mountain is characterized by the assemblage quartz-pericline-adularia-chlorite-calcite-pyrite-rutile ± epidote, is pervasive and occurs at temperatures ≥250°C. Its intensity is directly dependent upon local palaeoreservoir temperature (Sander and Mitchell, 1988). Fracture-controlled potassic alteration overprints propylitic alteration and consists of the equilibrium assemblage quartz-adularia-illite/sericite-calcite-pyrite-rutile. Hydrothermal fluids which formed propylitic and potassic alteration were similar in composition; the only difference was the rate of cooling (Fig. 3.28). Slow cooling from 270°C produced propylitic alteration, with pericline and adularia in equilibrium, whereas fast cooling produced potassic alteration with adularia forming at the expense of pericline (Sander and Einaudi, 1990).

The single major difference between Wairakei and Round Mountain is in the amount and style of gold-silver mineralization. Gold is being

deposited at Wairakei in economically insignificant amounts but locally at high grades, within geothermal production equipment and less commonly within surface discharge zones ("hot springs"). Gold grades encountered at intermediate levels within the high-temperature reservoir are low (<0.01 to ~0.04 g/t; Fig. 3.33). Only two samples of reservoir rock contained more than 0.04 g/t gold. Importantly, the two higher gold values (0.12 and 0.13 g/t) occurred within and adjacent to steep geothermal gradients which suggests the influence of local mixing with cooler groundwater.

Precious metals contained in the ore body presently being mined at Round Mountain were deposited several hundred metres below the palaeo-surface in what would be called the reservoir of an active system (Sander and Mitchell, 1988). Gold and silver were deposited during the transition from propylitic to potassic alteration as palaeoreservoir temperatures declined from ~265° to less than 200°C (Sander and Einaudi, 1990). Quartz-adularia-pyrite-calcite were stable together throughout the transition from propylitic to potassic alteration, establishing firm limits on the changes in pH and fO_2 that could have accompanied cooling (Fig. 4.20). The mineralogical relationships illustrated on the diagrams in Figure 4.20 indicate that reduced gold solubility was not related to major changes in pH or ion activities. Boiling or fluid mixing with descending acidic waters also was unlikely to have been an important factor in the precipitation of gold, leaving temperature decline as the major cause of gold deposition at Round Mountain (Sander and Einaudi, 1990). The most important cause of the temperature decline was disruption of reservoir conditions due to intrusion of cold groundwater along sets of fractures that developed in response to regional tectonic stresses (Sander and Einaudi, 1990). The model proposed by Sander and Einaudi (1990) for the genesis of the Round Mountain gold-silver ore body is shown in Figure 4.21.

Metallization at Wairakei occurs at temperatures between ~265° and 225°C in a transitional alteration zone where potassic assemblages over-

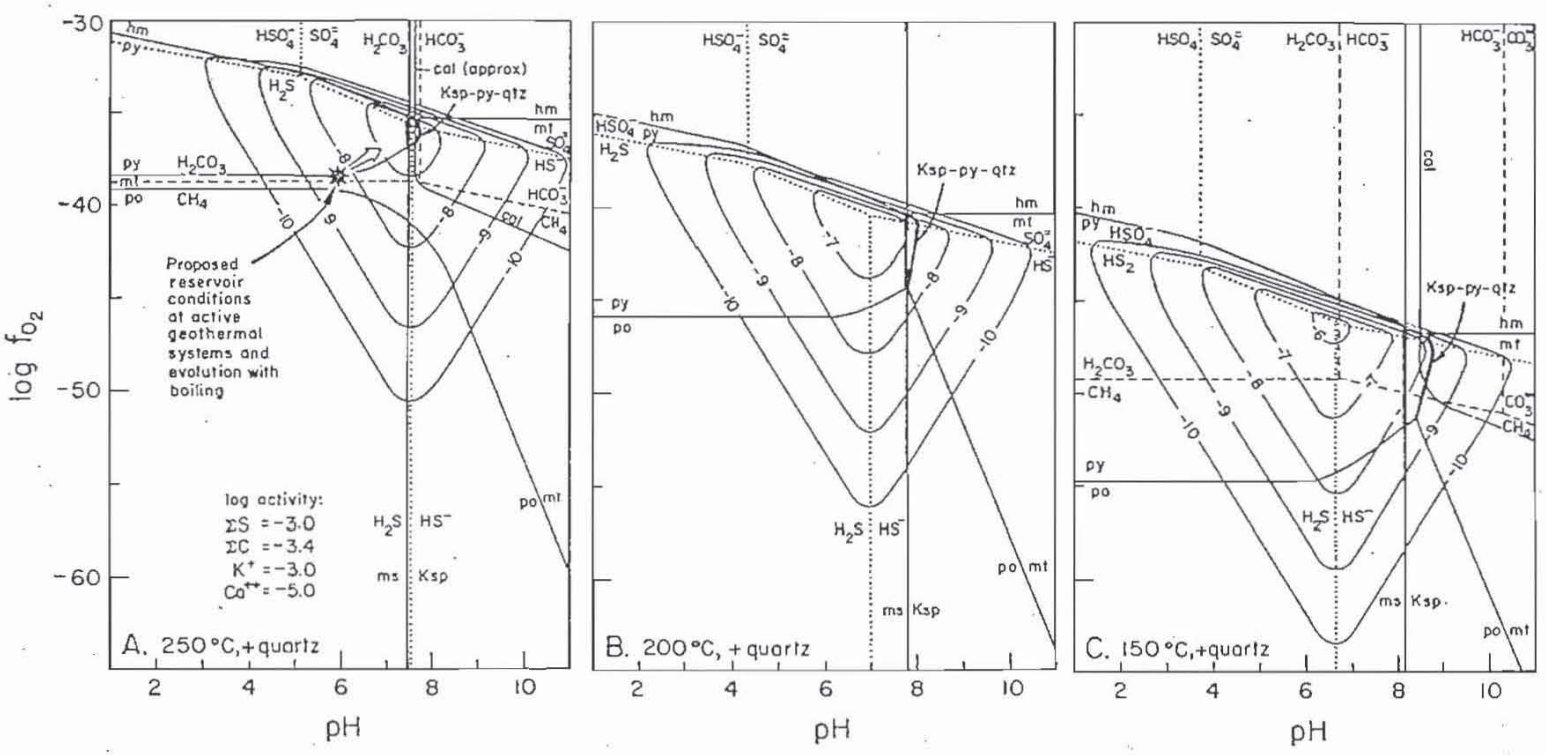

Figure 4.20. Log fO_2-pH diagrams constructed for fluid composition typical of carbon- and sulphur-poor (low gas) geothermal systems and consistent with broad compositional constraints at Round Mountain: A) relations at 250°C; B) relations at 200°C; C) relations at 150°C. Diagrams represent equilibria along the liquid-vapour curve for pure water. Abbreviations: hematite (hm); magnetite (mt); pyrite (py); pyrrhotite (po); calcite (cal); muscovite (ms); K-feldspar (high sanidine) (Ksp). Figure reproduced from Sander and Einaudi (1990; Fig. 12, page 305) with permission of the authors.

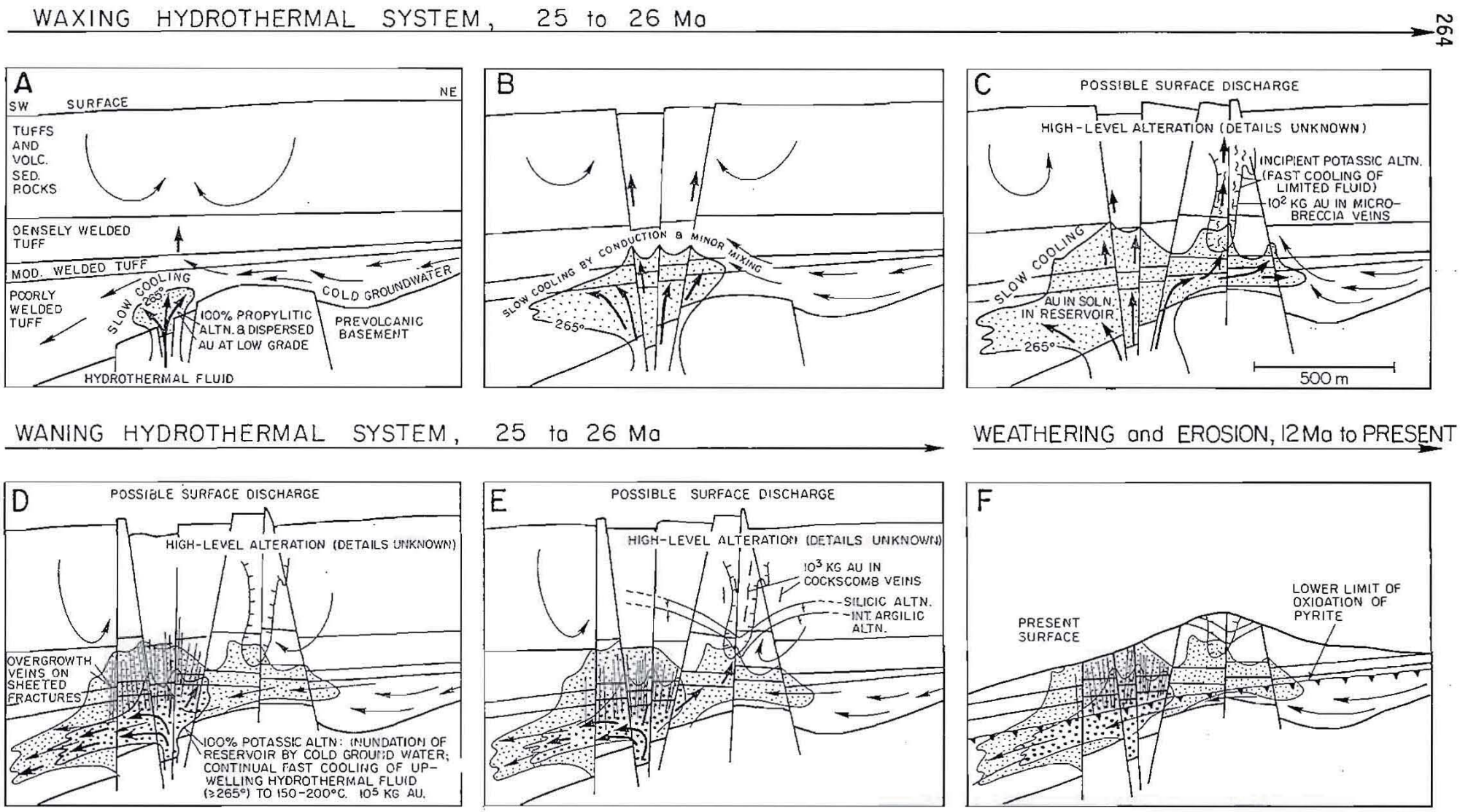

Figure 4.21. Model for the development of the Round Mountain hydrothermal system in space and time. Figure reproduced from Sander and Einaudi (1990; Fig. 15, page 309) with permission of the authors.

print propylitic alteration. However, the transition from propylitic to potassic alteration at Wairakei is more complex than this transition at Round Mountain. At Wairakei changing reservoir conditions have resulted in cyclic precipitation of secondary feldspar. These repeated cycles of propylitic and potassic alteration probably reflect minor temperature fluctuations within the high-temperature reservoir and may represent alternate periods of cooling and of relative thermal stability. Although only one transition from propylitic to potassic alteration was observed at Round Mountain (Sander and Einaudi, 1990), minor textural evidence of a period of cyclic reservoir conditions may have been obliterated during the focused cooling event which forced the precipitation of gold and silver. By their very definition the high-temperature active geothermal systems have not experienced this period of focused cooling during which economic concentrations of gold and silver are deposited. In the scenario proposed by Sander and Einaudi (1990) Figure 4.21C illustrates the evolutionary stage of the preproduction reservoir at Wairakei, the only difference being that Wairakei lacks gold-rich microbreccia veins.

The similarities in tectonic setting, geologic and hydrologic environment, and types and styles of the alteration and metallization which are occurring within the high-temperature reservoir at Wairakei and which have occurred in the palaeoreservoir at Round Mountain eliminate the possibility that ore deposits form only in specially favourable tectonic and geochemical environments which do not exist in explored active geothermal systems. It may be, rather, that the precipitation of significant quantities of gold and silver at economic grades requires the temporal and spatial coincidence of a "typical" active hydrothermal system with a relatively simple structural event, and that such a coincidence has not occurred in the explored active high-temperature geothermal systems.

Implications for Precious Metal Exploration

Understanding the spatial distribution of above-background values of several "pathfinder" elements, particularly Au, Ag, As, Sb and Hg, is of utmost importance in exploring for epithermal precious metal deposits. These elements typically form halos surrounding economic concentrations of gold and silver and thus they provide an important guide to locating ore. However, all surface geochemical anomalies are not directly related to large high-grade ore deposits and, in fact, they are more commonly associated with subeconomic mineralization. Furthermore, ore-grade geochemical anomalies at the surface may overlie subeconomic mineralization.

Many high-temperature active geothermal systems provide excellent examples of strong surface geochemical anomalies which are unrelated to economic mineralization. In many of the high-temperature geothermal systems in New Zealand gold is being deposited at high grades but in insignificant amounts at shallow levels within surface discharge zones ("hot springs")(e.g., Ohaaki (Broadlands): Browne (1973) and Brown (1986, 1988); Kawerau: Christenson (1987); Rotokawa: Krupp and Seward (1987); Waiotapu: Hedenquist (1983) and Wairakei: Chapter 3). However, rock samples containing economic precious metal grades over significant intervals have not been identified in any of the deep reservoirs of the systems listed above.

Geochemical Anomalies Related to Surface Discharge Features

Extensive surface sampling within the Iamalele geothermal area defined several areas with very high surface geochemical anomalies. One of these areas occurred along the western and northern flanks of the Uluwa flow dome in the Yaluwana thermal area (Figs. 2.10 and 2.13). In addition to finding strong As, Sb and Hg anomalies in soil and rock chip samples, native gold was recovered from sand and gravel deposits in all of the small streams and dry gullies which drained or had drained active areas of intense hydrolytic alteration or thermal springs. Gold assay values

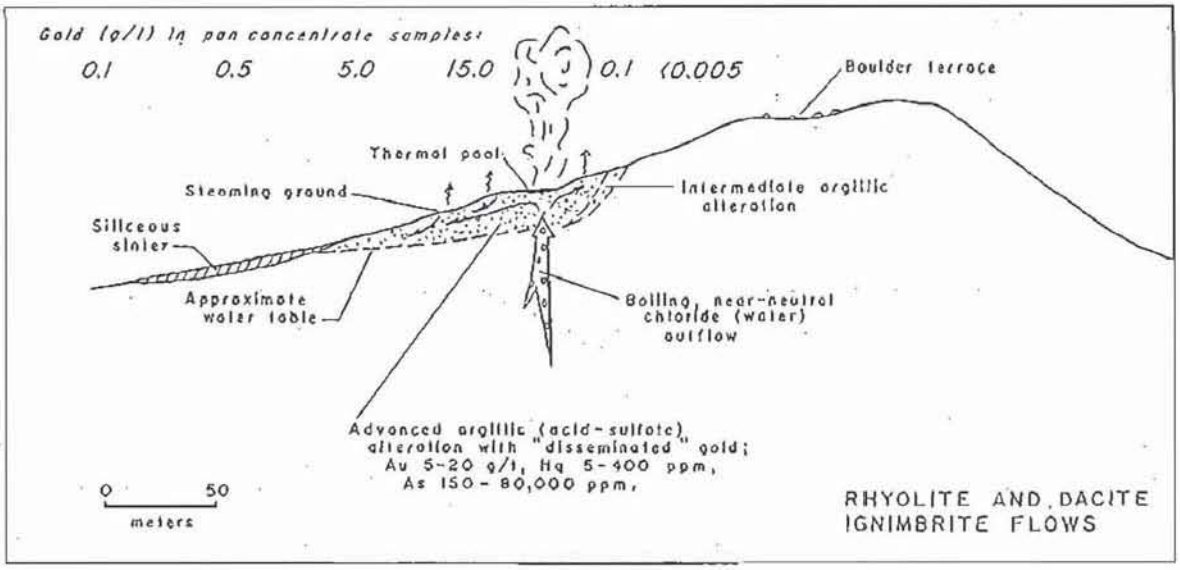

Figure 4.22. Schematic cross section through the Uluwa flow dome showing the relationship between active thermal springs and the spatial distribution of gold in stream sediment (pan concentrate) samples.

measured from sediment collected from these streams and gullies increased upstream until the thermal area was reached, then decreased immediately above the thermal area to <0.03 g/t (Fig. 4.22). These data indicate that gold is readily deposited in the relatively cool ($T \leq 100°C$), low pH surface environments, and strongly support a geothermal source for the surface gold at Iamalele.

In the near-surface environment the deposition of gold is reported to occur in response to a combination of boiling and the mixing of a near-neutral, relatively high-temperature reservoir fluid with cooler, acidic near-surface waters (e.g., Henley and Ellis, 1983). To demonstrate the effectiveness of this process, phase fields for the essential minerals of potassic and advanced argillic alteration are plotted on two isothermal log fO_2-pH diagrams (Fig. 4.23).

The coexistence of adularia, illite/sericite, pyrite and anhydrite (potassic alteration) restricts the chemical environment within which the minerals may form to a very narrow area near the intersection of the H_2S-SO_4 species boundary and the K-feldspar-muscovite boundary (Fig. 4.23A).

Figure 4.23. (Facing page) Isothermal log fO_2-pH diagrams constructed for temperatures of 225°C and 150°C. Stippled areas indicate the stability fields constrained by the potassic equilibrium assemblage quartz-adularia-illite/sericite-andydrite-pyrite-stibnite (A) and by the advanced argillic equilibrium assemblage alunite-kaolinite-lussatite-pyrite-barite (B). Diagrams (C) and (D) are simplified versions of (A) and (B) respectively showing gold solubility contours. Shaded areas in diagrams (C) and (D) represent the stability fields defined for potassic and advanced argillic alteration respectively. When possible, solute activities were estimated from water analyses of local thermal springs when possible. Diagram is based on published thermodynamic data for sulphur species (Robie and Waldbaum, 1968); iron and sulphur species, K-feldspar-muscovite, muscovite-kaolinite, barite and anhydrite solubility (Helgeson, 1969); kaolinite-alunite (Hemley et al., 1969); sulphur species (Ellis and Giggenbach, 1971); kaolinite-alunite (Helgeson et al., 1978); pyrite + stibnite-berthierite (Barton and Skinner, 1979).

The stability field for the advanced argillic alteration assemblage is also restricted to a relatively narrow area by the coexistence of alunite, pyrite and barite (Fig. 4.23B[8]). It is apparent from Figure 4.23C that the stability field for the observed potassic alteration assemblage coincides with the region of maximum gold (bisulphide) solubilities, and it is unlikely that a significant amount of gold will precipitate from the fluid under these conditions. However, gold solubilities are very low within the stability field defined by the observed advanced argillic alteration assemblage (Fig. 4.23D). Under these acidic near-surface conditions all but a very minor amount of gold carried by a rising hydrothermal fluid would precipitate (Fig. 4.24).

From the relationships indicated by Figures 4.23 and 4.24 it is apparent that in the near-surface environment significant quantities of gold may precipitate from a fluid which at depth would be slightly under-

[8]The stippled area in Figure 4.23B represents the log fO_2-pH conditions under which the alunite breccias formed at Iamalele. The assemblage alunite-cristobalite is commonly the dominant alteration assemblage in areas of intense hydrolytic alteration associated with active thermal features. In locations where kaolinite coexists with alunite and cristobalite the stippled area would be reduced to a narrow band along the boundary between kaolinite and alunite + cristobalite. The resulting area would be restricted at low pH by the solubility of barite and at higher fO_2 by the hematite-pyrite phase boundary.

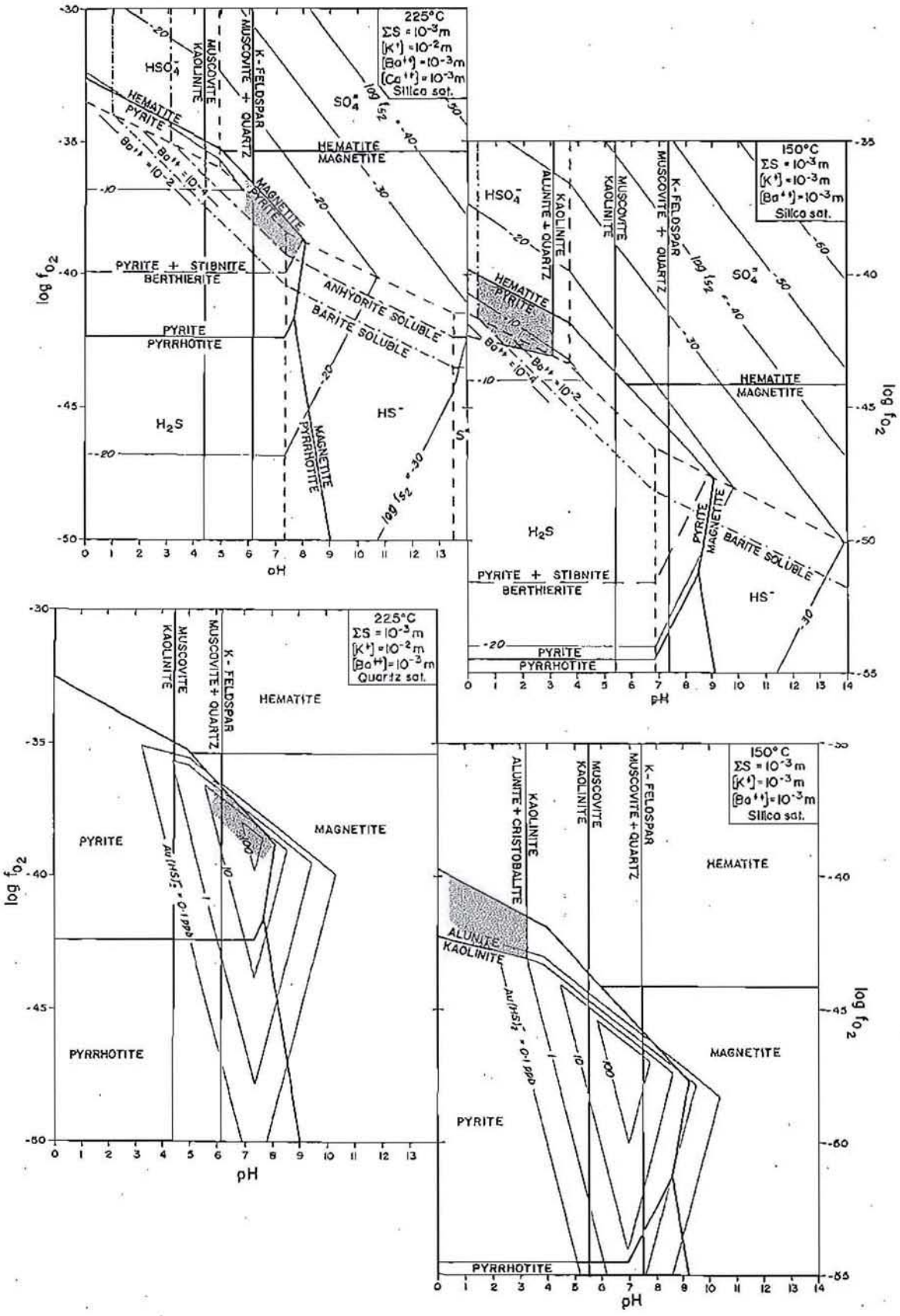
225°C
ΣS = 10⁻³m
[K⁺] = 10⁻²m
[Ba⁺⁺] = 10⁻³m
[Ca⁺⁺] = 10⁻³m
Silica sat.
HSO4⁻
SO4⁼
KAOLINITE
MUSCOVITE
K-FELDSPAR
MUSCOVITE + QUARTZ
HEMATITE
PYRITE
MAGNETITE
HEMATITE
MAGNETITE
PYRITE + STIBNITE
BERTHIERITE
ANHYDRITE SOLUBLE
BARITE SOLUBLE
PYRITE
PYRRHOTITE
H2S
HS⁻
MAGNETITE
PYRRHOTITE
log fS2
log fO2
pH
150°C
ΣS = 10⁻³m
[K⁺] = 10⁻³m
[Ba⁺⁺] = 10⁻³m
Silica sat.
ALUNITE + QUARTZ
KAOLINITE
MUSCOVITE
MUSCOVITE + QUARTZ
K-FELDSPAR
HEMATITE
PYRITE
MAGNETITE
BARITE SOLUBLE
PYRITE + STIBNITE
BERTHIERITE
PYRITE
PYRRHOTITE
225°C
ΣS = 10⁻³m
[K⁺] = 10⁻²m
[Ba⁺⁺] = 10⁻³m
Quartz sat.
KAOLINITE
MUSCOVITE
K-FELDSPAR
MUSCOVITE + QUARTZ
HEMATITE
PYRITE
MAGNETITE
PYRRHOTITE
Au(HS)2⁻ = 0·1 ppb
150°C
ΣS = 10⁻³m
[K⁺] = 10⁻³m
[Ba⁺⁺] = 10⁻³m
Silica sat.
ALUNITE + CRISTOBALITE
KAOLINITE
MUSCOVITE
MUSCOVITE + QUARTZ
K-FELDSPAR
HEMATITE
ALUNITE
KAOLINITE
MAGNETITE
PYRITE
PYRRHOTITE
Au(HS)2⁻ = 0·1 ppb

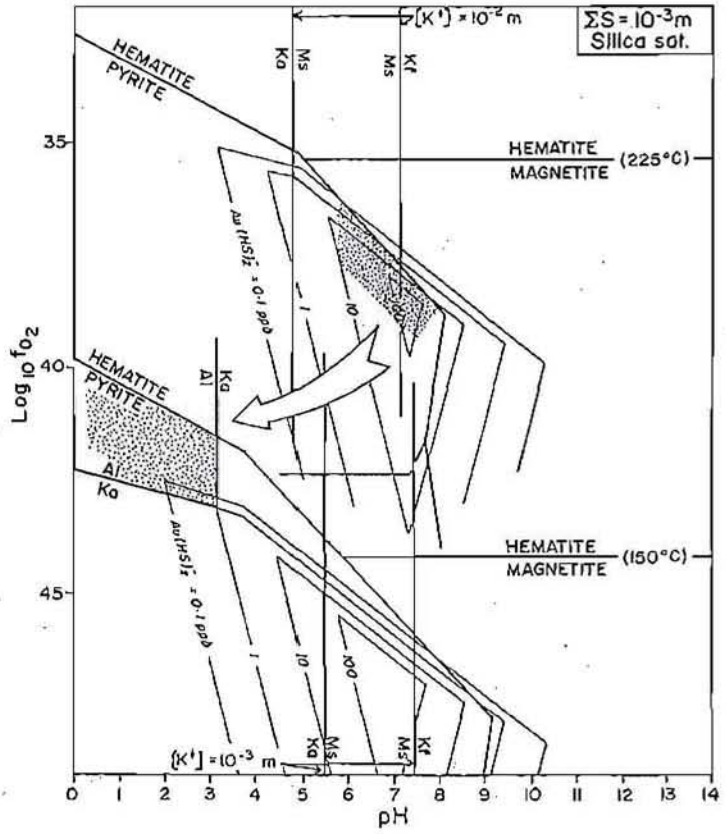

Figure 4.24. Log fO_2-pH diagram simplified from Figure 4.23 and showing the expected decrease in the solubility of gold bisulphide as the activity of H^+ and the relative oxidation state of the fluid increase.

saturated with respect to gold carried as bisulphide complex. This may account for the occurrence of locally abundant gold in surface samples taken from many of the major geothermal areas even though the high-temperature reservoirs of these systems contain only trace amounts of gold. This may also explain why only trace levels (5 to 43 parts per billion (ppb)) of gold were detected in the Iamalele drill hole, when surface samples from the same area contained up to 1000 ppb gold.

Conclusions

Despite the similarities between geothermal systems and precious metal deposits, significant quantities of gold are not being deposited in the active systems, except in the near-surface environment. White (1981) presented four possible reasons why active geothermal systems are not obviously forming ore bodies on the scale of those contained in their

fossil equivalents, the epithermal systems. By comparing the active systems of Iamalele and Wairakei to the epithermal gold-silver deposits of Rawhide (Black et al., 1991) and Round Mountain (Sander and Einaudi, 1990), three of the four possibilities may be ruled out: incomplete knowledge of active systems, excessively "leaky" active systems, and markedly dissimilar geologic settings. The remaining reason, that gold is paragenetically late in hydrothermal systems and has not yet been deposited in active systems, is a good explanation and can be restated in terms of recent findings at Iamalele, Wairakei, Rawhide and Round Mountain. Within the high-temperature reservoir of waxing or steady-state (active) systems, gold remains in solution or is dispersed at low grades, although near the surface minor amounts of gold may be deposited at high grades as relatively small amounts of fluid rise into localized discharge zones. In contrast, within deep reservoirs of waning systems where continually upwelling hydrothermal fluid is cooled by groundwater over a protracted mixing history, large quantities of gold at mineable grades are deposited and are more likely to be preserved. Indeed, epithermal deposits are "fossil" geothermal systems, and it is during the process of being "fossilized" by the inundation described at Round Mountain that they become ore deposits.

HIGH-Mg LAVAS IN THE LATE CENOZOIC VOLCANIC ARC ASSOCIATIONS OF PAPUA NEW GUINEA

Introduction

The volcanic rocks generated at convergent plate boundaries (arc-type rocks) constitute one of the most complex suites of the major igneous associations. This reflects the range of tectonic possibilities and the variety of components which may contribute to magma generation during active plate convergence. Although there is not universal agreement about the

petrogenesis of arc-type magmas, there is a general consensus that they are the result of multi-component systems to which the upper mantle, subducted ocean lithosphere and, in some cases, crust and ocean-floor sediments variably contribute. These major petrogenetic factors tend to have a unique blend in any particular geologic setting, and, in general, the complexity of preceding geologic history is reflected in the chemistry of the magmas erupted at the surface. The following discussion addresses the occurrence and genetic significance of magnesium-rich lavas generated at convergent plate margins by focusing on the high-Mg lavas that occur in the late Cenozoic volcanic stratigraphy of southeastern Papua New Guinea (Fig. 4.25).

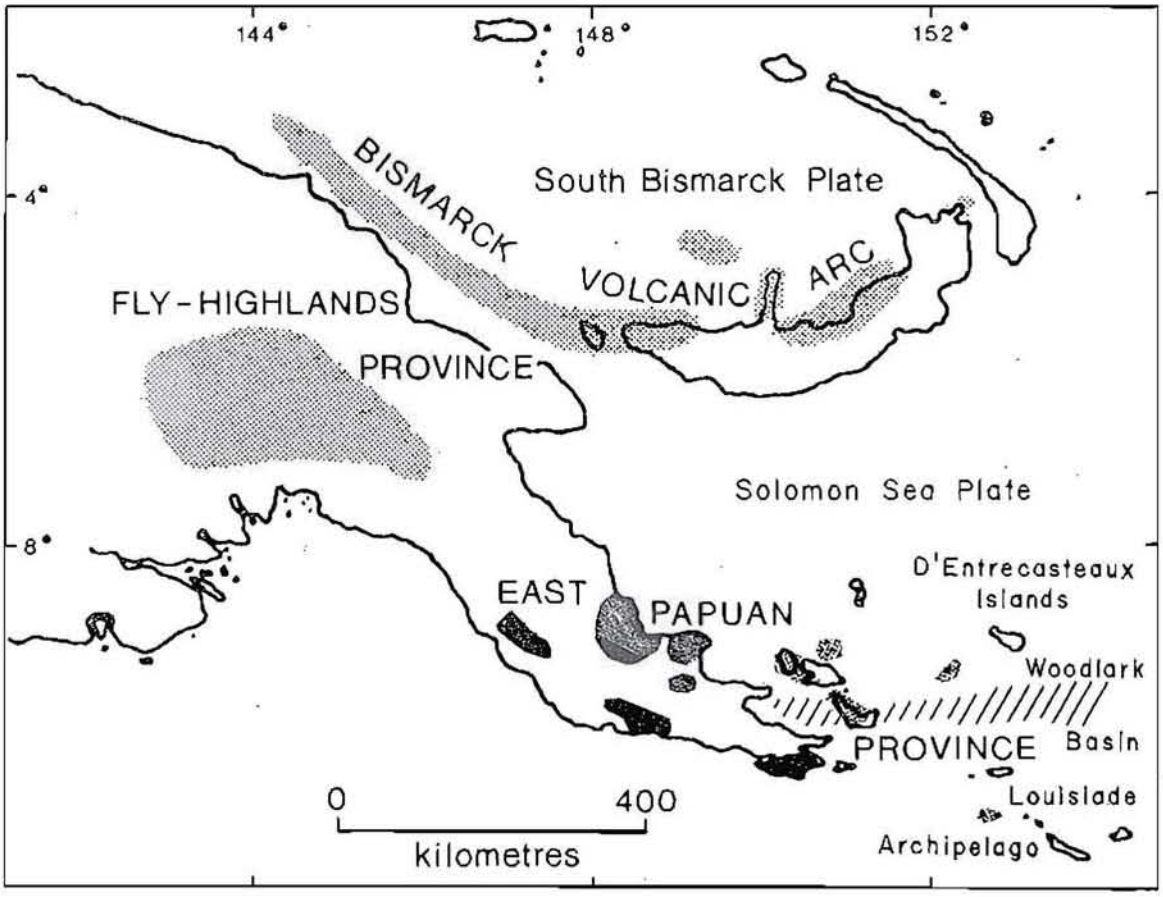

Figure 4.25. Distribution of late Cenozoic arc-type rocks (stipple) in Papua New Guinea (after Johnson, 1979). Location of the northern and southern (dark stipple) volcanic belts within the east Papuan volcanic province is according to Smith (1976b). Hachures show areas of Quaternary extension (after Davies et al., 1984).

High-Mg Lavas in Arc-Type Associations

One generally recognized chemical characteristic of arc-type volcanic rocks is their relatively low content of certain transition elements, principally Mg, Cr and Ni. Recently this view has been challenged by the recognition of high-Mg lavas in several areas around the circum-Pacific rim (Fig. 4.26). These high-Mg lavas range from basalt to low-silica dacite in composition and are characterized by high Cr (~150 to >600 ppm) and Ni (~80 to >350 ppm) abundances, and FeO*/MgO and CaO/MgO ratios near unity[9]. The lavas are typically phenocryst-poor (<10%) and contain simple phenocryst assemblages within which olivine, clinopyroxene or, less commonly, orthopyroxene is the dominant phase.

Table 4.5 summarizes the occurrence of high-Mg lavas in several of the major arc systems of the circum-Pacific rim. A study of these occurrences revealed several significant characteristics of arc-type high-Mg lavas. (1) High-Mg lavas do not appear to be restricted to any specific type of arc. They are found as a component of the magmatic association in relatively simple arcs (e.g., Indonesia, Aleutian Peninsula and South Shetland Islands), in complex arcs (e.g., Papua New Guinea, Japan and New Zealand) and in continental margin settings (e.g., western North America, Mexico, Peru and Chile). (2) Where they occur, the high-Mg rocks form an integral part of their suite and share the gross chemical characteristics of their magmatic association (e.g., see Table 4.6). This is an important point since high-Mg lavas are found as a component of all of the principal recognized arc-type associations (island arc tholeiite, calc-alkalic, and high-K alkalic). (3) High-Mg lavas encompass a range of rock types, typically basalt to andesite, but also include low-silica dacite. Considering the occurrences summarized in Table 4.5, high-Mg lavas appear to be relatively common at convergent plate boundaries, but in the past have been

[9]FeO* is total iron as FeO.

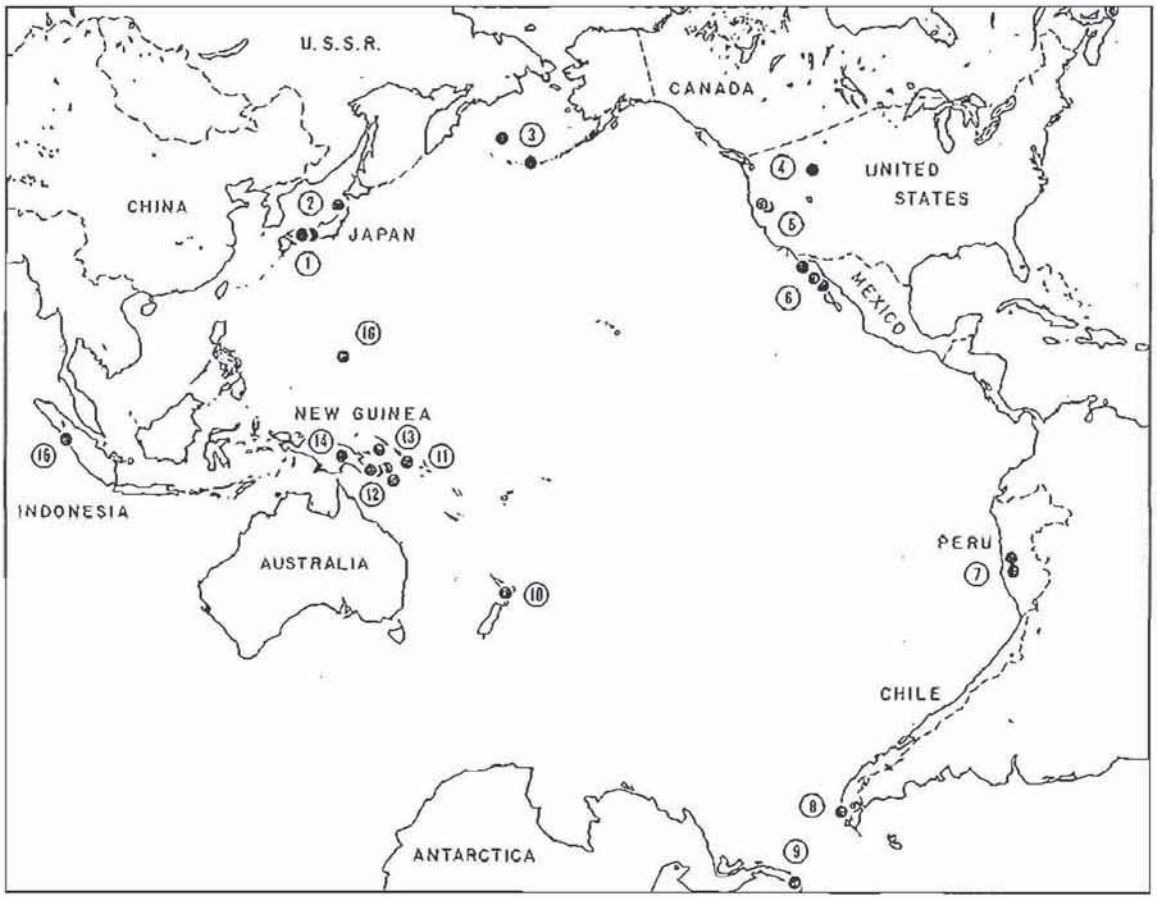

Figure 4.26. Location of high-Mg lavas summarized in Table 4.5.

commonly overlooked or interpreted as being either partial cumulates or contaminated magmas.

Nomenclature of Magnesium-Rich Arc-Type Lavas

Magnesium-rich arc-type rocks of the circum-Pacific region have been referred to by a variety names: magnesian andesites (Kay, 1978; Tatsumi and Ishizaka, 1982a; Johnson et al., 1983); sanukitioids (Tatsumi and Ishizaka, 1981); high-magnesian andesites (Tatsumi and Ishizaka, 1982b); high-magnesium andesite (Meen and Eggler, 1987); and bajaites (Saunders et al., 1987). Furthermore, in a number of cases high-Mg lavas in arc-type associations have been referred to as boninitic or boninite-like, e.g., Johnson et al., 1983. To avoid this confusion and problems arising from the compositional variability (basalt to dacite) of the lavas, the purely descrip-

Table 4.5. Occurrence of high-Mg lavas, circum-Pacific rim

	Locality	High-Mg Lithologies	Associated Lithologies	Association	Age	Tectonic Setting		Reference
1.	Southern Japan	Basalt to andesite	Andesite	Arc tholeiite to calc-alkalic	Middle Miocene	Active subduction	*	Tatsumi and Ishizaka (1981, 1982a)
2.	Northeastern Japan	Basalt to basaltic andesite	Basaltic andesite to andesite	Calc-alkalic	Holocene	Active subduction	*	Aoki and Fugimaki (1982)
3.	Aleutian Islands	Basaltic andesite to andesite	Basalt to andesite	Arc tholeiite to calc-alkalic	Middle Miocene to Pliocene	Active subduction	*	Kay (1978)
4.	Montana	Andesite to rhyolite	Basaltic andesite	Calc-alkalic to high-K calc-alkalic	Late Cretaceous	Orogenesis		Meen and Eggler (1987)
5.	Northern California	Basalt to andesite	Basalt to rhyolite	Calc-alkalic	Pliocene to Holocene	Active subduction		Smith and Carmichael (1968)
6.	Baja California	Basaltic andesite to andesite	Basalt to andesite	Calc-alkalic to high-K calc-alkalic	Late Miocene to Holocene	Post-subduction	*	Saunders et. al. (1987)
7.	Peru	Basaltic andesite	Basalt to rhyolite	Calc-alkalic to high-K calc-alkalic	Late Cenozoic	Active subduction		Noble et. al. (1975)
8.	Southern Chile	Basalt to basaltic andesite	Basalt to andesite	Calc-alkalic	Miocene to Holocene	Active subduction		Puig et. al. (1984)
9.	Antarctic Peninsula	Basaltic andesite to andesite	Basalt to rhyolite	Arc tholeiite	Mesozoic to Quaternary	Active subduction		Tarney et. al. (1982)
10.	New Zealand	Basalt	Basalt to andesite	Calc-alkalic	Quaternary	Active subduction		Graham and Hackett (1987)
11.	Solomon Islands	Basalt to andesite	Basalt to andesite	Arc tholeiite	Late Tertiary to Holocene	Active subduction		Cox and Bell (1972)
12.	Southeastern Papua New Guinea	Basalt to dacite	Basalt to rhyolite	High-K calc-alkalic to high-K alkalic	Late Cenozoic	Uplift and crustal extension	*	Smith and Mitchell (1989)
13.	Northern New Britain	Basalt to dacite	Basalt to rhyolite	Arc tholeiite to calc-alkalic	Late Cenozoic	Active subduction		Johnson (1977)
14.	Papua New Guinea Highlands	Basalt to andesite	Basalt to dacite	High-K calc-alkalic to high-K alkalic	Late Cenozoic	Orogenesis		Mackenzie and Chappell (1972)
15.	Eastern Indonesia	Basalt to basaltic andesite	Basalt to dacite	Calc-alkalic to high-K calc-alkalic	Late Tertiary to Quaternary	Active subduction		Morris et. al. (1983)
16.	Mariana Islands	Basalt to basaltic andesite	Basalt to dacite calc-alkalic	Arc tholeiite to Holocene	Eocene to	Active subduction	*	Shiraki et. al. (1978)

Note: Numbers correspond to localities shown in Figure 4.26. Asterisks signify authors who specifically identified the presence of high-Mg lavas.

tive prefix *high-Mg* should be used to recognize the existence of magnesium-rich rocks among arc-type igneous associations in the same way that high-K has been used to identify suites of rocks with that particular characteristic, e.g., high-Mg dacite or high-Mg tholeiitic basalt.

High-Mg Lava or Boninite?

High-Mg arc-type volcanic rocks and boninites are magnesium-rich, relatively silica-rich rocks, and both occur in several areas around the circum-Pacific rim (Kuroda et al., 1978; Sun and Nesbitt, 1978; Jenner, 1981; Tatsumi and Ishizaka, 1982a; Cameron, 1985; Dobson, 1986). It is important to recognize that in both mineralogy and chemistry the high-Mg rocks discussed in this section are quite distinct from boninites. High-Mg lavas occur in volcanic arcs and correlate with subduction-related tectonic environments, whereas, although boninites do occur in volcanic arcs (Mariana arc; Dobson, 1986), they are generally associated with ophiolites and appear to be more closely related to obduction (Cameron, 1985). Table 4.6 presents the mean chemical analyses for calc-alkalic, high-Mg calc-alkalic and boninite lavas from southeastern Papua New Guinea. These data illustrate the overall tendency for high-Mg lavas to retain the chemical signature of the arcs in which they occur and show that the only chemical similarity between arc-type high-Mg lavas and boninites is their intermediate silica content. It is also apparent that in contrast to the high-Mg lavas, the boninites were derived from a depleted mantle source. High-Mg lavas and boninites are independent rock types and it is incorrect to refer to arc-type magnesium-rich rocks as having "boninitic affinities" unless they are derived from a depleted mantle source.

Table 4.6. Mean chemical composition of calc-alkalic and boninite lavas from southeastern Papua New Guinea

	Calc-alkalic		Boninite
	Arc-type (n = 21)	High-Mg (n = 40)	(n = 43)
Oxides (wt %)			
SiO_2	58.55	57.81	57.61
TiO_2	1.17	1.00	0.25
Al_2O_4	17.47	15.47	8.38
FeO*	5.99	6.04	9.59
MnO	0.11	0.10	0.20
MgO	3.40	6.51	17.83
CaO	6.45	6.74	4.94
Na_2O	4.26	3.70	0.83
K_2O	2.24	2.27	0.33
P_2O_5	0.36	0.36	0.04
Total	100.00	100.00	100.00
Elements (ppm)			
Ba	795	873	48
Rb	51	51	6
Sr	692	821	100
Th	6	8	0.6
Zr	228	194	0.2
Nb	6	5	2
Y	29	21	5
La	44	49	3
Ce	70	74	7
Sc	14	14	30
V	137	132	156
Cr	49	299	1775
Ni	30	155	378
Mg Number	54.4	69.4	79.6

Calc-alkalic rock analyses were determined by X-ray fluorescence spectrometry. Major element data were normalized to a volatile-free basis. Number of analyses is given by n. FeO* is total Fe as FeO. Mg number (mol 100 MgO/[MgO + FeO]) was computed for $Fe_2O_3/FeO = 0.20$. Calc-alkalic data are from Smith (1976b) and Appendix 3. Boninite data are from Jenner (1981).

Tectonic Setting of Papua New Guinea

Papua New Guinea Mainland and New Britain

Papua New Guinea is one of the more complex regions of the circum-Pacific rim, with late Cenozoic tectonism involving several minor plates caught up in a major zone of interaction between the Pacific and Indo-Australian plates (Johnson and Molnar, 1972; Curtis, 1973). The tectonic

evolution of southeastern Papua New Guinea involves subduction (possibly with a reversal in polarity), obduction and rifting, the complexities of which are not totally resolved (Davies et al., 1984; Smith and Milsom, 1984). Concurrent with tectonic activity, arc-type volcanism has occurred in widely separated areas of Papua New Guinea, principally in the Bismarck volcanic arc, in the Fly-Highlands province and in the east Papuan volcanic province (Johnson, 1979) (Fig. 4.25). The Bismarck volcanic arc is clearly associated with active subduction resulting from interaction between the Solomon Sea and South Bismarck micro-plates (Johnson, 1979). Although not obviously associated with present day subduction, the Fly-Highlands province straddles a suture between the Indo-Australian plate and the Bismarck Sea microplate, interpreted as a Cenozoic collision zone (Hamilton, 1979).

In southeastern Papua New Guinea tectonism has resulted in the juxtaposition of an unusual variety of latest Mesozoic and Cenozoic volcanic rock associations, which include ultramafic, mafic, plutonic, metamorphic and tholeiitic to peralkaline volcanic rocks. The essential features of the geological basement of the Papuan peninsula are a core of moderate to high-grade metamorphic rocks overlain by an obducted sheet of ultramafic and associated MORB-type basalts; these rocks are Late Mesozoic and lower Tertiary in age (Davies, 1973; Davies and Smith, 1976). The archipelagos lying to the east and southeast of the Papuan peninsula show, to varying degrees, the fragments of this general sequence. Late Cenozoic uplift, possibly associated with a tensional tectonic stress, has resulted in spectacular doming of the metamorphic rocks, which on the Papuan peninsula and on the larger islands form metamorphic core complexes of medium- to high-grade schist and gneiss (Davies and Smith, 1971).

Southeastern Papua New Guinea

The Papuan peninsula extends southeastward from the Fly-Highlands province, following the boundary between the Indo-Australian plate and

Solomon Sea microplate, and is bounded on either side by lower Tertiary oceanic crust (Papuan Ultramafic Belt). The onshore geologic record is complex and fragmentary, and the sequence and nature of events are open to multiple interpretations (Smith, 1982; Davies et al., 1984; Smith and Milsom, 1984). Tectonic activity began during the late Mesozoic or early Tertiary in response to collision between the Indo-Australian and Pacific plates. A simplified interpretation of the major tectonic events inferred from the geology of the Papuan peninsula and islands in the southwestern Solomon Sea include (1) formation of the Coral Sea Basin and accumulation of a thick volcano-sedimentary prism (D'Entrecasteaux Complex) during the Eocene (Davies, 1973; Smith and Milsom, 1984), (2) burial metamorphism of the sedimentary prism as a consequence of the emplacement (obduction) of the Papuan Ultramafic Belt during Eocene-Oligocene time (Davies, 1980) and (3) late Cenozoic extension, uplift and unroofing of the D'Entrecasteaux Complex and subsequent calc-alkalic and peralkaline volcanism accompanying opening of the Woodlark Basin (Luyendyk et al., 1973; Smith and Milsom, 1984). Palaeotectonic reconstructions involving both southward (Hamilton, 1979) and northward dipping (Davies et al., 1984) late Cenozoic subduction systems have been proposed. However, evidence for either hypothesis is equivocal and open to interpretation (Smith, 1982; Smith and Milsom, 1984). An additional complexity is the existence of a peralkaline rhyolite association in the D'Entrecasteaux Islands which appears to be a magmatic response to Quaternary extension associated with spreading in the Woodlark Basin (Smith, 1976a; Smith et al., 1977).

Late Cenozoic Volcanism in Southeastern Papua New Guinea

The major late Cenozoic magmatic event in southeastern Papua New Guinea is represented by mid-Miocene to Recent volcanic and minor intrusive rocks. Arc-type volcanic rocks are exposed in six areas representing distinct eruptive centres or clusters of eruptive centres. These are the

western Calvados Islands, Egum Atoll, Normanby Island, Amphlett Islands, the Moresby Strait area of the D'Entrecasteaux Islands and the Cape Nelson and Lamington-Hydrographers-Managlase areas on the Papuan peninsula (Fig. 4.27). The volcanic rocks of southeastern Papua New Guinea form an association which is essentially arc-type and dominantly andesite, but ranging in composition from basalt to rhyolite. Although the volcanic centres differ with respect to age and/or the relative abundance of rock types, there is no systematic pattern to the variations (Smith, 1982; Smith and Milsom, 1984).

Because the eastern centres are less well represented, there is a sampling bias which might affect an analysis of space-time variation in the distribution and chemical composition of the rocks; that is that the samples from the two easternmost centres may not be representative of the volcano or volcanic episode. However, with the exception of these centres the sample collection is considered to be representative of the rocks forming each centre.

The following description of the volcanic geology of the Calvados Islands, Egum Atoll, Normanby Island, Amphlett Islands and western Fergusson Island are summarized from Smith (1976b), unpublished data provided by I.E.M. Smith (written communication), the regional geologic map of the D'Entrecasteaux Islands (Davies, 1973) and my unpublished data.

Calvados Islands

Volcanogenic conglomerate, agglomerate and tuff with subordinate lava flows crop out on several islands within a radius of about 8 kilometres near the western end of the Calvados Island chain. These rocks represent the easternmost and oldest (11.4 Ma, sample 33603; Smith and Compston, 1982) centre in the northern part of the east Papuan volcanic province. Rock types include aphyric to slightly porphyritic pyroxene and hornblende

andesite and pyroxene dacite. The maximum aggregate thickness of the exposed volcanic rocks is approximately 200 metres.

Egum Atoll

Egum Atoll lies about 175 kilometres to the northwest of the Calvados Islands. It is a typical atoll made up of reefs and low-lying coral islands which rise from ocean depths of 2000 metres to enclose a large lagoon containing small (0.5 km^2 or less) volcanic islets. The islets are composed of jointed, generally porphyritic, hornblende andesites which are presumably the emergent tip of a much larger andesitic volcano. Radiometric dating of one lava flow gave a late Pliocene age (2.85 Ma, 33608; Smith, 1973).

Normanby Island

Normanby Island is the easternmost of the three main islands in the D'Entrecasteaux Islands and is made up mainly of pre-Tertiary metamorphic and ultramafic rocks. A variety of volcanic rocks with a maximum thickness of 200 metres overlie the pre-Tertiary basement in the central and western parts of the island. Microfossils from interbedded limestone indicate a late Miocene age (Tertiary "e" stage; Davies, 1969), and limited radiometric dating has yielded a Pliocene age (3 Ma; Smith, 1973) for the overlying volcanic rocks. There is no sign of constructional volcanic land forms on Normanby Island. Rock types range from basalt to rhyolite, but are mainly pyroxene-bearing basalt and andesite with subordinate hornblende andesite and dacite. The late Miocene lavas are typically porphyritic, whereas the late Pliocene rocks consist of older aphyric to sparsely porphyritic lavas overlain by porphyritic dacite and alkali dacite.

Figure 4.27. (Facing page) Generalized geology of the D'Entrecasteaux Islands, Calvados Islands and Egum Atoll. Geology compiled from Davies and Ives (1965), Smith (1976b). See Appendix 1 for sample descriptions. In Appendix 1 600 series samples are prefixed by 33 and 800 series samples are prefixed by 125, e.g., 603 is 33603, 802 is 125802.

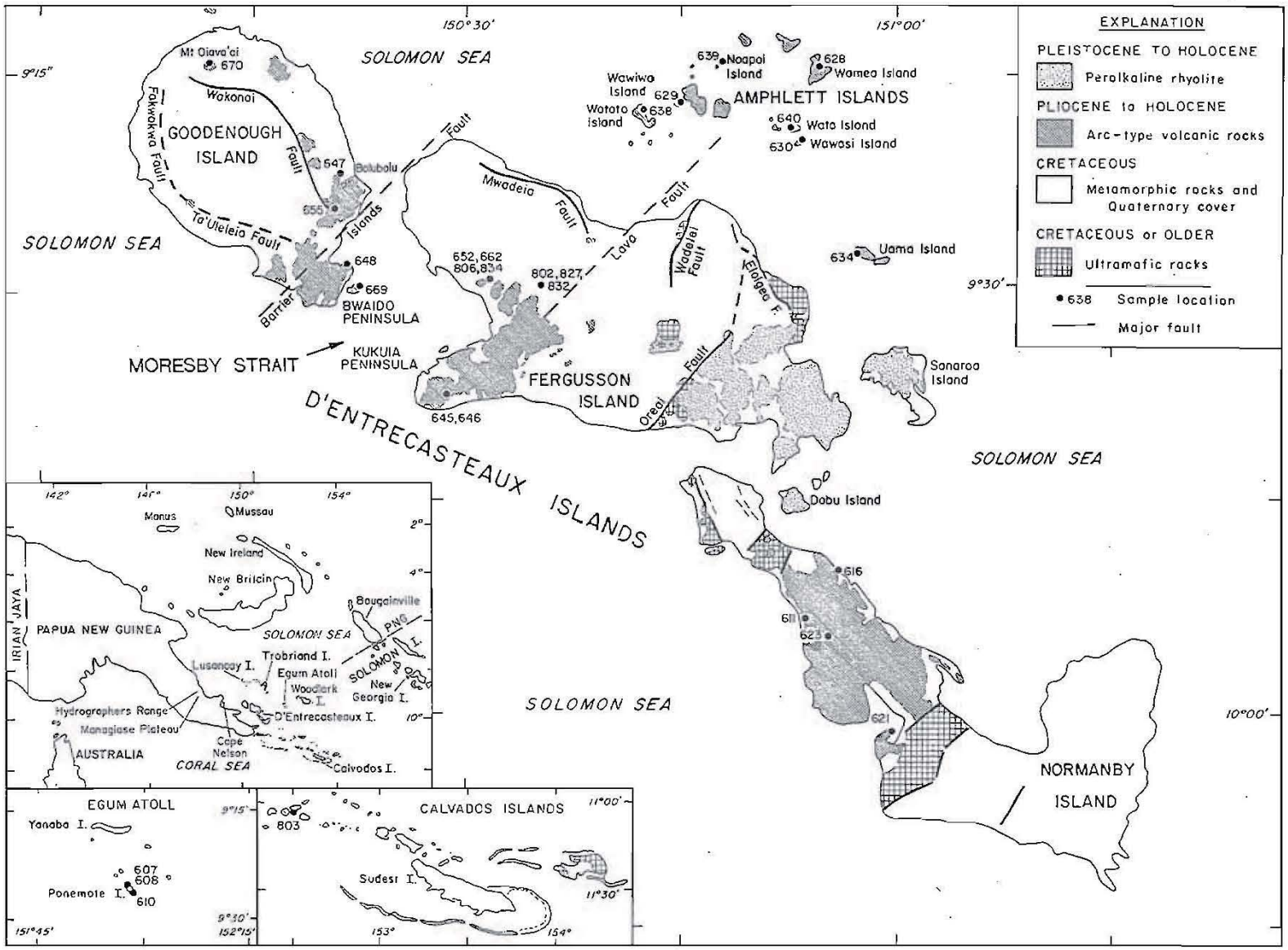
EXPLANATION
PLEISTOCENE TO HOLOCENE
Peralkaline rhyolite
PLIOCENE to HOLOCENE
Arc-type volcanic rocks
CRETACEOUS
Metamorphic rocks and Quaternary cover
CRETACEOUS or OLDER
Ultramafic rocks
638 Sample location
Major fault
SOLOMON SEA
GOODENOUGH ISLAND
Mt Oiava'ai 670
Wakonoi
Fakwokwa Fault
Ta'Uteleia Fault
Barrier
Islands
Fault
Bolubolu
647
655
648
669
BWAIDO PENINSULA
MORESBY STRAIT
KUKUIA PENINSULA
Mwadeia Fault
Lava Fault
652,662
806,834
802,827,
832
FERGUSSON ISLAND
645,646
Wadelai Fault
Elaogea F.
Oreoi Fault
AMPHLETT ISLANDS
Wawiwa Island
629
Watoto Island
638
639 Noapoi Island
628 Wamea Island
640 Wata Island
630 Wawasi Island
634 Uama Island
Sanaroa Island
D'ENTRECASTEAUX ISLANDS
Dobu Island
616
611
623
621
NORMANBY ISLAND
9°15'
9°30'
10°00'
150°30'
151°00'
142°
146°
150°
154°
2°
4°
10°
Manus
Mussau
New Ireland
New Britain
PAPUA NEW GUINEA
IRIAN JAYA
Bougainville
PNG
SOLOMON SEA
Trobriand I.
Lusancay I.
Egum Atoll
Woodlark I.
SOLOMON I.
New Georgia I.
Hydrographers Range
Managlase Plateau
D'Entrecasteaux I.
Cape Nelson
AUSTRALIA
CORAL SEA
Calvados I.
EGUM ATOLL
Yanaba I.
607
608
Ponemote I.
610
9°15'
9°30'
151°45'
152°15'
CALVADOS ISLANDS
11°00'
803
Sudest I.
11°30'
153°
154°

Amphlett Islands

The Amphlett Islands are on the northern side of the D'Entrecasteaux Island group and are entirely volcanic. The islands appear to be remnants of an andesitic stratovolcano, a concept which is supported by the spatial distribution of the islands and the existence of a large positive Bouguer gravity anomaly (Davies, 1973) centred on the Amphlett group. The exposed volcanic sequence is early Pliocene in age (3.6 to 4.0 Ma; Smith and Compston, 1982). Rock types exposed in massive to vesicular lava flows and intercalated agglomerate beds include basaltic andesite, andesite and dacite. The lavas are typically porphyritic, but relatively aphyric varieties occur on most of the islands of the Amphlett group and on Uama Island.

Western D'Entrecasteaux Islands

Volcanic rocks occur extensively on western Fergusson Island and on the southeastern tip of Goodenough Island. On Fergusson Island volcanic rocks occur mainly in the southwestern and west-central portions of the island, but isolated outcrops also occur near the centre of the island and along the north coast. The largest contiguous area of volcanic rocks is on the Kukuia Peninsula, where the Kukuia Volcanics attain their maximum exposed thickness of ~600 metres. The volcanic rocks rest on an undulating, pre-Tertiary metamorphic basement of moderate relief. No volcanic land forms have been recognized on the peninsula, although Davies and Ives (1965) have suggested that some of the peaks at the western end may be volcanic plugs or necks. Radiometric ages for the volcanic rocks exposed on the Kukuia Peninsula span a range from 6.27 to 0.4 Ma (Smith and Compston, 1982).

The Iamalele area lies to the north of the Kukuia Peninsula, and is an alluvium-covered lowland except for several small steep-sided cumulodomes and volcanic plateaus. Here, high-Mg lavas are intercalated with ignimbrite deposits, and also form small eruptive centres deposited on both

metamorphic basement and the ignimbrites. Volcanic rocks in the Iamalele area are the youngest units of the Kukuia Volcanics. Geothermal features are prevalent in the western half of the area and are among the most active in southeastern Papua New Guinea. Because of the presence of youthful volcanic land forms and geothermal activity the volcanic rocks in the Iamalele area are probably late Pleistocene to Holocene in age. The late Cenozoic volcanic rocks of western Fergusson Island are dominated by rhyolite, but include subordinate basaltic andesite, andesite and dacite.

Volcanic rocks crop out along the margins of the metamorphic core of Goodenough Island. The most extensive development of volcanic rocks is on the Bwaido Peninsula where they attain a maximum exposed thickness of ~600 metres. Elsewhere the volcanic rocks occur as small cones or flows adjacent to the major faults or form isolated hills on the extensive alluvial apron surrounding the central metamorphic core complex. These volcanic rocks may be as old as Pleistocene, especially in the thick section on Bwaido Peninsula where volcanic landforms are absent, but many of the small eruptive centres on Goodenough Island are undoubtedly very recent.

East Papuan Volcanic Arc

Petrographic and geochemical data have been used to divide the late Cenozoic arc-type association of southeastern Papua New Guinea into two volcanic belts (Fig. 4.25), a northern belt dominated by high-K andesite and a southern belt dominated by K-rich basalt (shoshonite)(Smith, 1982). Allowing for the effects of Quaternary rifting, these two belts are interpreted to be components of a single volcanic arc within which there is considerable temporal and compositional diversity.

Northern Volcanic Belt

The northern volcanic belt is composed of a diverse suite of rocks which includes basalt (10%), basaltic andesite (25%), andesite (45%),

dacite (15%) and rhyolite (5%). "Normal" calc-alkalic and high-Mg extrusive rocks occur throughout the northern volcanic belt. The basalts, basaltic andesites and some andesites are commonly porphyritic vesicular rocks containing sparse to abundant phenocrysts of plagioclase (An_{75-50}), olivine, pale-green clinopyroxene and orthopyroxene, and in some lavas, microphenocrysts of spinel and/or iron-titanium oxide minerals. The phenocrysts are set in a groundmass of labradorite, clinopyroxene, iron-titanium oxide minerals, less commonly orthopyroxene and, in a few samples, olivine. Hornblende-bearing lavas ranging from andesite to dacite are also an important component of the association. One lava (sample 33636), which is chemically transitional between a "normal" and a high-Mg calc-alkalic composition, contains hornblende which is Ti- and Mg-rich, approaching kaersutite in composition. The hornblende-bearing lavas are typically highly porphyritic and contain phenocrysts of plagioclase (An_{60-30}), brown hornblende, biotite and iron-titanium oxide minerals in a groundmass dominated by plagioclase but containing clinopyroxene, orthopyroxene and rare olivine or quartz. Phenocrysts are generally restricted to three or four phases but a few andesites and dacites contain exceedingly complex phenocryst assemblages including hornblende, biotite, two pyroxenes and olivine, in addition to plagioclase. Many of the andesitic rocks in the northern volcanic belt are characterized by the presence of complexly zoned and commonly corroded feldspar phenocrysts and, less commonly, clusters (autoliths) of one or more of the phenocrystic phases. Hornblendite and rare dunite inclusions are an additional feature of some lavas (Jakes and Smith, 1970; Arculus et al., 1983). Rhyolites are closely associated with the andesites and dacites in the Moresby Strait area of the D'Entrecasteaux Islands (Fig. 4.27). For a detailed description of the rhyolite petrography, see Smith and Johnson (1981) and the section on silicic volcanism in this chapter.

All of the volcanic centres in the northern volcanic belt have erupted andesite, accompanied in most areas by basaltic andesite with or without subordinate basalt and dacite. These rocks form a suite characterized by high alkali contents and comparatively high K_2O/Na_2O ratios (Fig. 4.28; Table 4.7). In terms of Peccerillo and Taylor's (1976) classification they form a high-K calc-alkalic association. The ferromagnesian elements (Ti, Fe, Mn, Mg, V, Cr, and Ni) and Ca and P show a positive correlation with each other and a clearly defined inverse relationship with the abundances of Si, K and incompatible trace elements. The abundances of large ion lithophile (LIL) elements are high but fall within the range for high-K andesites given by Jakes and White (1972). Rare earth element (REE) abundance patterns show a characteristic light-element enrichment. Initial $^{87}Sr/^{86}Sr$ ratios range from 0.7038 to 0.7044 with a mean of 0.7041 (Smith and Compston, 1982), although higher values have been reported for a few volcanic centres on the Papuan peninsula (Page and Johnson, 1974).

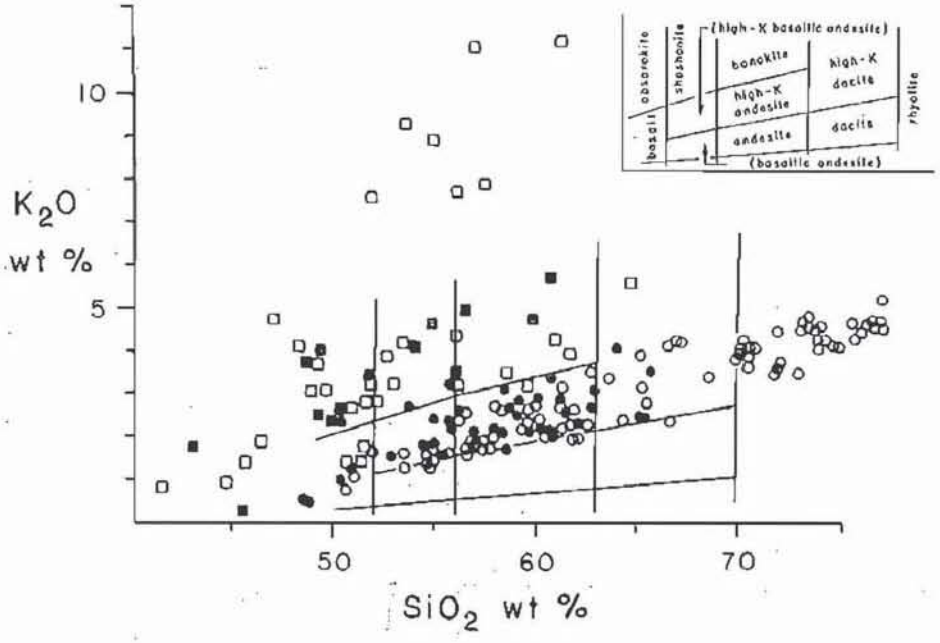

Figure 4.28. K_2O-SiO_2 variation in late Cenozoic arc-type volcanic rocks from the east Papuan volcanic province. Solid symbols are high-Mg rocks, circles are northern volcanic belt rocks, squares are southern volcanic belt rocks. Data sources are Jakes and Smith (1970), Smith (1972), Smith (1976b), Davies and Smith (1976), Appendix 3. Inset shows nomenclature of arc-type rocks after Peccerillo and Taylor (1976).

Table 4.7. Chemical analyses of andesitic rocks from the northern

	Outlying Islands		Normanby Island			Amphlett Islands					
SAMPLE NO.	33604	33605	33613	33618	33620	33636	33637	33642	33650	33660	125805
wt %											
SiO_2	59.20	63.50	51.90	54.62	58.20	58.98	59.44	64.29	52.80	55.45	55.74
TiO_2	0.82	0.48	2.00	1.36	1.20	0.95	1.00	0.62	1.26	1.18	1.18
Al_2O_3	15.00	16.70	16.50	16.73	17.60	15.74	16.48	16.20	18.00	17.84	18.49
Fe_2O_3	3.90	1.55	4.00	2.97	1.96	4.24	2.48	2.48	2.43	2.49	6.96
FeO	1.75	2.20	4.50	3.65	3.95	1.03	3.33	1.41	4.40	3.84	--
MnO	0.09	0.07	0.13	0.12	0.12	0.07	0.08	0.05	0.13	0.11	0.12
MgO	4.50	2.20	4.20	4.17	2.95	3.94	3.55	2.60	5.01	3.93	3.25
CaO	5.75	4.20	7.95	7.50	6.00	4.94	6.06	3.87	9.17	7.71	7.32
Na_2O	3.20	3.50	4.05	4.22	4.10	4.08	4.34	4.56	3.80	4.00	3.90
K_2O	2.65	3.10	1.61	2.20	2.15	3.28	1.93	2.42	1.27	1.67	1.53
P_2O_5	0.32	0.25	0.74	0.49	0.33	0.39	0.21	0.20	0.39	0.30	0.25
LOI	2.57	1.91	2.82	1.41	1.38	1.74	1.07	0.85	0.79	1.32	0.90
Total	99.75	99.66	100.40	99.44	99.94	99.38	99.97	99.55	99.45	99.84	99.64
Trace Elements (ppm)											
Ba	925	915	699	704	856	1352	574	804	579	586	585
Rb	60	99	26	40	54	82	40	62	23	36	37
Sr	315	1250	807	803	668	1065	612	668	666	594	609
Pb	34	37	10	18	16	35	14	17	13	13	11
Th	8	13	3	8	5	15	2	4	3	5	5
Zr	nd	nd	198	245	213	250	168	167	161	189	201
Nb	nd	nd	7	9	6	6	5	5	5	5	8
Y	22	18	26	25	22	16	17	21	22	21	36
La	21	32	32	30	31	54	23	45	26	23	63
Ce	52	63	59	68	57	84	50	57	47	50	46
V	138	77	257	176	113	90	108	66	186	153	130
Cr	136	42	68	54	35	188	105	139	46	43	69
Ni	20	26	40	43	7	86	38	92	37	26	28
Zn	72	66	88	80	75	75	67	70	45	73	73

-- = element not determined, nd = element not detected. Total Fe by XRF, FeO by titration, Fe_2O_3

In terms of MgO-SiO_2 covariance of the basaltic and intermediate lavas forming the northern volcanic belt, the high-Mg group can be clearly separated from the remainder of the suite by an empirically derived line with the formula MgO = (-0.433 x SiO_2) + 29.14 (Fig. 4.29). Thus discriminated, high-Mg lavas comprise approximately one-third of the 150 analysed samples from the northern volcanic belt. The high-Mg lavas vary in chemical composition from basalt to dacite, but the majority are basaltic andesite and andesite. Compared with other lavas from the northern volcanic belt, the high-Mg group tends to be more sparsely porphyritic and contains a higher percentage of chrome spinel, magnesian olivine and clinopyroxene, iron-titanium oxides, and interstitial glass. Characteristic of these lavas are anomalously high but variable abundances of Cr (158 to 592 ppm) and Ni (80 to 343 ppm), and Mg numbers (mol 100 MgO/[MgO+FeO],

volcanic belt of the east Papuan volcanic province

Fergusson Island							Goodenough Island				
33667	125810	125833	125830	139015	33643	33673	33649	33654	33657	33671	
											wt %
57.01	57.50	57.71	62.17	63.11	64.45	64.63	50.47	53.70	54.22	60.29	SiO_2
1.13	1.11	1.02	1.06	0.87	0.60	0.87	1.64	1.67	1.02	1.15	TiO_2
17.61	17.42	16.75	17.38	16.82	16.08	16.02	19.21	17.15	17.62	16.54	Al_2O_3
2.32	6.31	3.01	5.37	4.55	1.91	2.95	4.33	2.34	1.79	2.54	Fe_2O_3
3.59	--	2.95	--	--	1.92	1.46	2.54	5.40	5.87	2.55	FeO
0.11	0.10	0.10	0.09	0.09	0.09	0.09	0.11	0.14	0.14	0.12	MnO
3.72	3.47	3.90	0.67	1.11	3.05	1.51	4.59	3.99	4.51	2.64	MgO
6.96	6.74	6.72	3.76	3.72	4.13	4.02	8.91	8.30	9.02	4.03	CaO
4.17	3.72	3.68	5.11	5.15	4.54	4.60	3.76	3.97	3.09	5.19	Na_2O
1.66	2.52	2.52	2.37	2.41	2.49	2.76	1.58	1.53	1.33	3.14	K_2O
0.28	0.44	0.37	0.38	0.29	0.22	0.27	0.51	0.34	0.30	0.46	P_2O_5
1.23	0.67	0.20	1.07	1.03	0.68	0.88	2.17	1.26	0.61	0.84	LOI
99.79	100.00	98.93	99.43	99.15	100.16	100.06	99.82	99.79	99.52	99.49	Total
											ppm
612	964	1057	734	1891	943	825	680	596	582	995	Ba
39	57	54	65	66	62	71	36	38	20	85	Rb
571	1209	1127	544	560	651	486	843	493	922	505	Sr
9	15	18	16	16	17	16	7	11	9	19	Pb
3	11	11	6	7	5	9	2	4	1	10	Th
197	303	304	231	229	189	201	184	219	149	380	Zr
4	5	6	4	7	5	4	5	4	2	9	Nb
28	22	25	30	26	20	30	21	29	23	33	Y
33	86	110	35	36	41	52	28	24	22	56	La
54	129	141	62	60	69	65	39	52	44	99	Ce
130	187	162	73	54	63	85	176	180	215	84	V
39	23	77	4	4	124	3	101	23	15	61	Cr
26	24	36	nd	5	81	8	72	34	14	33	Ni
65	68	62	49	76	59	61	59	77	71	64	Zn

by difference.

Fe_2O_3/FeO = 0.20) in the range of 64 to 76 (see Appendix 3 for bulk rock data). The compositional trends of the high-magnesium lavas either overlap or, at high silica values, converge on the trends shown by the remainder of the suite (Fig. 4.30). It is significant that apart from higher abundances of Mg, Cr and Ni, and lower abundances of Ti, Al and Na, the high-Mg lavas have virtually the same chemical compositions as those forming the remainder of the suite.

Southern Volcanic Belt

The southern volcanic belt differs from the northern in that rocks of intermediate to felsic composition are less common and that the basaltic rocks are petrographically distinct. The following petrologic description of the southern belt rocks is summarized from Smith (1976b) and information provided by I.E.M. Smith (written communication). Typical of the southern

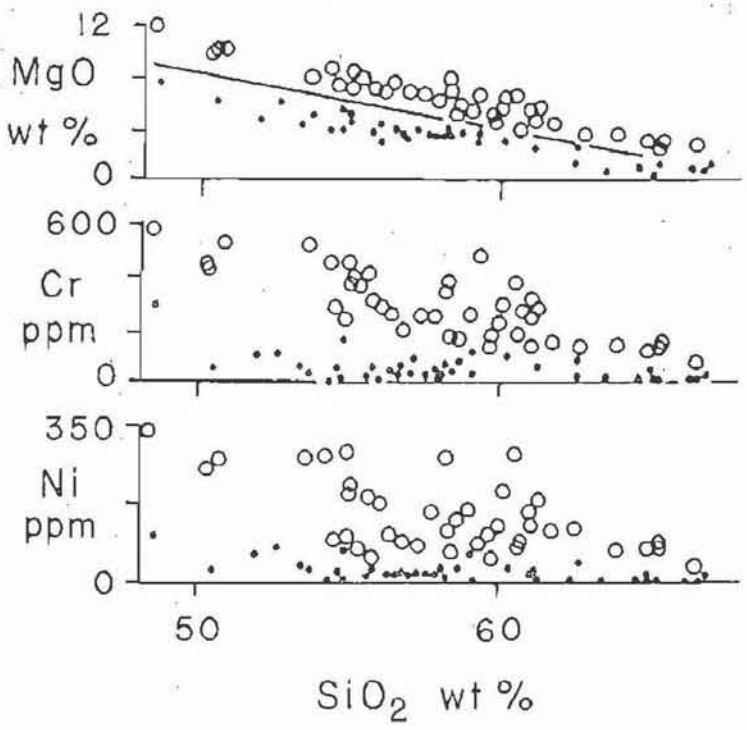

Figure 4.29. Variation in MgO, Cr and Ni with respect to SiO_2 in lavas from the northern volcanic belt of the east Papuan volcanic province. The line separates high-Mg lavas (open circles) from the remainder of the suite; rhyolites are not plotted.

belt are highly porphyritic basalts containing phenocrysts of pale-green salitic clinopyroxene typically accompanied by smaller phenocrysts of olivine and/or plagioclase. Small phenocrysts and microphenocrysts of iron-titanium oxide minerals are also present in many of the samples. The groundmass of these rocks consists of labradorite microlites with interstitial K-feldspar, iron-titanium oxide minerals, minor clinopyroxene and accessory apatite. The groundmass may also contain small crystals of biotite and/or a medium to dark brown glass. Rocks of intermediate composition are typically porphyritic and contain phenocrysts of biotite, hornblende, clinopyroxene, iron-titanium oxide minerals and, rarely, olivine. Rhyolite has not been noted from the southern volcanic belt (Smith, 1982).

Intrusive rocks associated temporally and spatially with the volcanic terrane of the southern volcanic belt have been described by Smith (1972) and Davies and Smith (1976). The intrusive phases range from pyroxenite

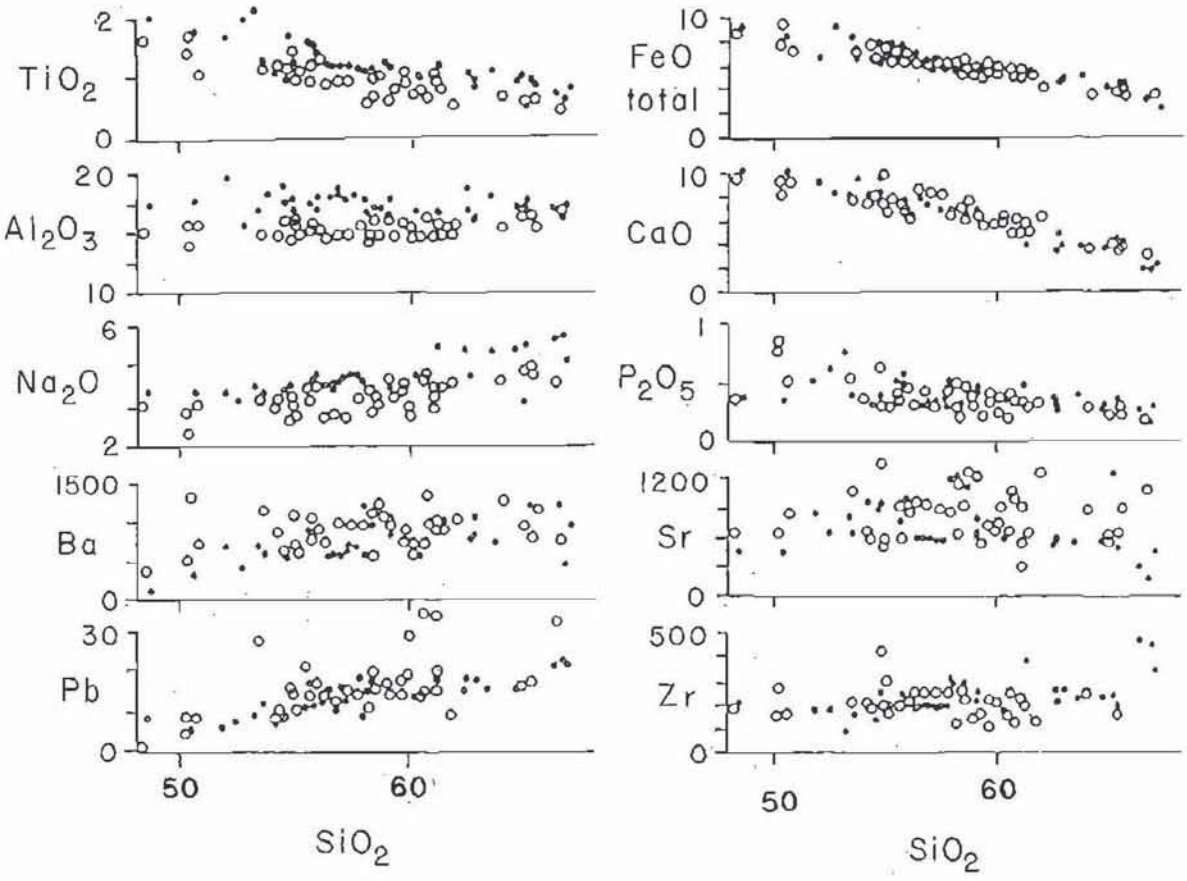

Figure 4.30. Variation in major oxides (wt %) and trace elements (ppm) with respect to SiO_2 (wt %) in lavas from the northern volcanic belt of the east Papuan volcanic province; open circles are high-Mg samples.

and gabbro to syenite, and occur as small plutons and swarms of porphyry dykes.

Although the volcanic and associated intrusive rocks from the southern volcanic belt are more basaltic and have higher K_2O/Na_2O ratios than those from the northern volcanic belt, they share the same general characteristics of high LIL-element abundances and enriched light REE patterns. $^{87}Sr/^{86}Sr$ ratios are comparable to, but more variable than, those in the northern volcanic belt (Smith and Compston, 1982). Using the discriminant formula derived for the northern volcanic belt, the suite of rocks from the southern volcanic belt also contains lavas which are relatively high in MgO, Cr and Ni (Fig. 4.31).

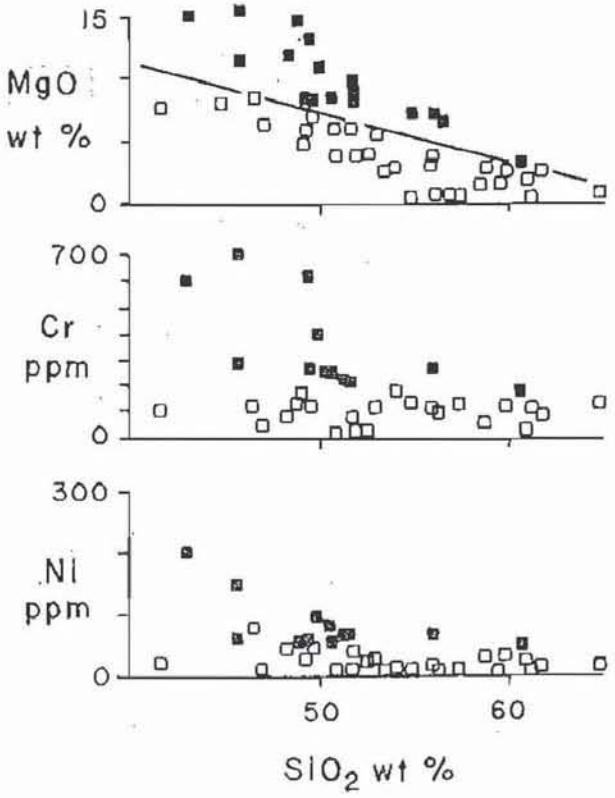

Figure 4.31. Variation in MgO, Cr and Ni with respect to SiO_2 in lavas from the southern volcanic belt of the east Papuan volcanic province. Solid symbols represent high-Mg samples.

High-Mg Lavas in Arc-type Settings of Papua New Guinea

Since Johnson et al. (1983) had noted the occurrence of a high-Mg lava at Bamus volcano in New Britain, the criteria for establishing the presence of high-Mg lavas in the east Papuan volcanic province were applied to published chemical analyses from the Bismarck volcanic arc and the Fly-Highlands province (Fig. 4.25) to assess the relative abundance of high-Mg lavas in these arc-type terranes.

The lithologies exposed in the Bismarck volcanic arc range from basalt to rhyolite and are arc-tholeiite to low-K calc-alkalic in character (Johnson et al., 1978a). An analysis of the major element compositions of the Bismarck volcanic arc (Johnson, 1977) indicates that in terms of the criteria established for the late Cenozoic volcanic belt(s) in southeastern

Papua New Guinea a significant proportion of analyses show the same high-Mg character (Fig. 4.32).

The Fly-Highlands volcanic province consists of a group of large, mainly andesitic volcanoes. Published geochemical data from these volcanoes (Mackenzie and Chappell, 1972; Mackenzie, 1976) include analyses which show a high-Mg character according to the criteria established for the east Papuan volcanic province. These rocks also form an integral part of the petrologic suites in which they occur.

The discriminant line derived for the suite of analysed rocks from the northern volcanic belt of the east Papuan volcanic province may not be directly applicable to other volcanic arcs. However, it does serve as a reference line to show that other major arc-type volcanic associations in Papua New Guinea include a proportion of rocks which contain relatively high contents of MgO.

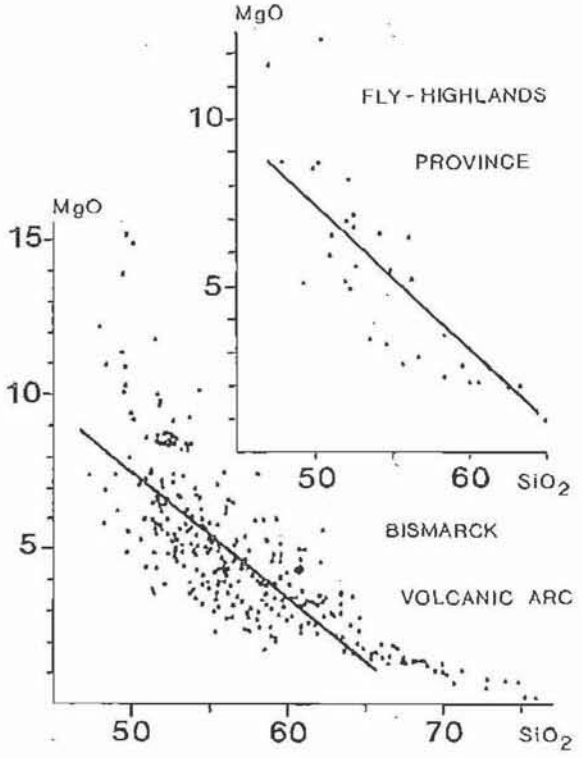

Figure 4.32. Variation in MgO (wt %) with respect to SiO_2 (wt %) in rocks from the Bismarck volcanic arc (Johnson, 1977) and the Fly-Highlands province (Mackenzie and Chappell, 1972; Mackenzie, 1976). The line separates a high-Mg character according to the criteria established for the east Papuan volcanic province (Fig. 4.29). The high-Mg lavas form an integral part of the Fly-Highlands petrologic suites.

Petrology of High-Mg Lavas
Northern Volcanic Belt, East Papuan Volcanic Arc

High-Mg lavas within the northern volcanic belt are petrographically distinct from the remainder of the suite even though the rocks are spatially and temporally inseparable. However, within the suite of high-Mg lavas there is notably little petrographic variation. High-Mg lavas are typically aphyric to sparsely porphyritic rocks containing less than 10% phenocrysts and/or microphenocrysts. The phenocrysts which do occur in these lavas are limited to four phases, olivine (Fo_{93-71}), clinopyroxene (Di_{91-72}), orthopyroxene (En_{91-81}) and plagioclase (An_{78-45}), with plagioclase being much less abundant than are the other phenocryst phases. These minerals characterize the following phenocryst assemblages: (1) olivine-clinopyroxene-plagioclase (dominant), (2) clinopyroxene-olivine and (3) orthopyroxene-clinopyroxene-olivine (uncommon). Lavas containing phenocrysts of only olivine or clinopyroxene are also uncommon. Microphenocrysts of chrome spinel and/or iron-titanium oxide minerals occur in many of the high-Mg lavas. The phenocrysts are dispersed in a hypocrystalline to pilotaxitic trachytoid groundmass of labradorite, clinopyroxene and calcium-poor pyroxene with both inclined and straight extinction (pigeonite), iron-titanium oxide minerals, and in some samples olivine; fresh, dark brown glass is also a common constituent in the high-Mg lavas. In a very few samples rare crystals of quartz and sanidine occur in the groundmass. The only hydrous mineral phase identified in the high-Mg lavas was iddingsite.

Clusters (glomerocrysts and autoliths) of two or more of the microphenocryst phases olivine, clinopyroxene, plagioclase and rarely chromite are common in many of the high-Mg lavas and may account for 15% of the phenocryst total. In some of the larger autoliths the microphenocrysts are intertwined with and surrounded by very fine networks of acicular calcic-plagioclase.

Only one sample (33639) contained an accidental inclusion (dunite). The source of the dunite clast, which contained small forsterite "veins", is unclear. It may be either a mantle xenolith or a fragment of a metamorphic tectonite from the Papuan Ultramafic Belt.

Bulk Rock Chemistry

Bulk rock chemical data for the Late Cenozoic andesitic rocks of the east Papuan volcanic province are shown in Table 4.8; additional data may be found in Smith (1976b), Smith (1982) and in Appendix 3. The geochemistry which applies to both "normal" and high-Mg calc-alkalic rocks from the northern volcanic belt was discussed under the heading Northern Volcanic Belt. The following discussion pertains specifically to the high-Mg rocks of the northern volcanic belt.

Major Elements

The high-Mg rocks of the northern volcanic belt are high-K calc-alkalic, with relatively high K_2O/Na_2O ratios and SiO_2 contents which range from 47 to 61 wt % (Table 4.8). One characteristic of the high-Mg rocks is that their FeO^*/MgO and, in particular, CaO/MgO ratios maintain a relatively constant value (~1) over a substantial range in SiO_2 and $Na_2O + K_2O$. This suggests that the magmas were buffered to a rather narrow range for Fe, Mg and Ca. Al_2O_3/TiO_2 ratios are similar to MORB values reported by Sun et al. (1979), whereas K_2O/TiO_2 ratios are much higher and reflect potassium enrichment.

Minor and Trace Elements

The trace element content of the high-Mg lavas is similar to that of "normal" calc-alkalic rocks except that Ni (80 to 343) and Cr (158 to 592) are characteristically high. Cr/Ni ratios are typically similar to mantle

Table 4.8. Chemical analyses of high-Mg lavas from the northern

	Outlying Islands		Normanby Island		Amphlett Islands						
SAMPLE NO.	33607	33603	33611	33616	33628	33629	33630	33634	33638	33645	33646
wt %											
SiO_2	56.63	58.70	48.80	54.10	52.39	53.42	54.64	58.43	59.55	47.51	47.91
TiO_2	0.60	0.71	1.68	1.12	1.15	1.23	0.94	0.81	0.75	1.64	2.00
Al_2O_3	14.16	14.60	13.70	14.70	14.67	14.53	15.20	14.60	14.58	15.00	17.13
Fe_2O_3	3.54	1.70	4.35	0.69	4.51	2.83	4.50	3.01	2.65	2.39	2.90
FeO	1.91	4.05	5.30	6.45	3.04	4.97	2.19	3.26	2.93	6.41	6.28
MnO	0.12	0.09	0.15	0.14	0.12	0.13	0.12	0.10	0.08	0.15	0.15
MgO	7.79	6.45	9.65	8.05	7.94	8.60	6.96	6.77	6.64	11.77	7.69
CaO	6.81	6.15	8.05	7.70	7.66	7.46	7.34	5.62	4.92	9.37	10.03
Na_2O	3.76	3.00	2.50	3.05	3.56	3.31	3.92	3.64	4.20	3.40	3.89
K_2O	2.05	2.15	2.25	1.58	2.66	1.79	2.33	2.23	2.05	0.52	0.48
P_2O_5	0.28	0.22	0.84	0.31	0.52	0.37	0.40	0.20	0.20	0.37	0.37
CO_2	0.13	0.15	0.07	0.42	0.05	0.09	0.08	0.03	bd	0.23	0.23
LOI	2.08	1.66	2.32	1.48	1.02	0.94	0.88	0.99	1.32	0.94	0.77
Total	99.86	99.63	99.66	99.79	99.31	99.67	99.52	99.69	99.87	99.70	99.83
Fe_2O_3/FeO	1.85	0.42	0.82	0.11	1.48	0.57	2.05	0.92	0.90	0.37	0.46
Mg Number	76.0	70.6	68.5	70.2	69.9	70.4	69.8	70.2	72.2	74.0	64.2
Trace Elements (ppm)											
Ba	1116	613	1327	608	1160	882	1061	837	707	388	154
Rb	41	55	56	41	61	33	41	42	47	13	5
Sr	1126	914	660	620	1063	670	929	558	667	657	463
Pb	12	30	9	11	28	9	22	15	15	1	9
Th	5	9	6	3	15	4	8	9	4	bd	bd
Zr	124	--	268	172	215	214	196	175	160	188	205
Nb	3	--	14	6	7	7	7	6	4	3	4
Y	13	18	25	21	17	21	17	15	23	27	28
La	34	18	51	24	54	29	44	30	40	16	12
Ce	49	40	87	34	96	53	76	45	36	21	48
Sc	11	15	22	22	18	20	22	16	14	24	29
V	97	142	213	160	159	162	126	124	91	156	206
Cr	344	310	442	377	536	457	421	488	393	592	303
Ni	288	211	260	80	288	291	194	92	291	343	109
Cu	192	45	41	17	39	27	50	16	28	48	47
Zn	65	81	84	80	81	85	77	74	76	64	73

-- = element not determined, bd = element below detection. Total Fe by XRF, FeO by titration, Mg number [Mol. 100 MgO/(MgO + FeO)] calculated assuming $Fe_2O_3/FeO = 0.20$.

peridotite values obtained using the Cr and Ni abundances estimated for peridotite by Goles (1967). Vanadium abundances are moderate to high and correlate well with the abundances of FeO, MnO and TiO_2 indicating that the concentrations of these elements are partly a function of the abundance of iron-titanium oxide minerals.

Rare Earth Elements

In general the rare earth element (REE) abundances in the high-Mg rocks of the northern volcanic belt indicate light rare earth element (LREE) enrichment with moderate to strong fractionation relative to chondrite data, whereas the heavy rare earth elements (HREE) are enriched but

volcanic belt of the east Papuan volcanic province

Fergusson Island							Goodenough Island				
125832	125827	125802	33652	125806	33662	125834	33647	33648	33655	33670	
											wt %
53.79	54.18	54.93	53.53	55.91	56.16	56.25	49.39	50.28	53.88	57.67	SiO_2
0.98	0.97	0.97	1.43	0.93	0.96	0.94	1.43	1.11	1.15	0.69	TiO_2
15.80	15.53	15.72	14.17	14.47	14.70	14.70	15.53	15.62	15.82	14.65	Al_2O_3
2.46	2.74	1.51	2.32	2.73	3.08	3.55	3.03	3.77	1.07	2.27	Fe_2O_3
4.20	3.85	4.85	3.91	3.65	3.27	2.90	5.11	3.94	6.03	4.29	FeO
0.10	0.16	0.11	0.11	0.13	0.11	0.10	0.13	0.14	0.13	0.12	MnO
8.48	8.39	8.67	6.87	7.55	6.89	6.59	9.76	10.06	7.35	7.16	MgO
6.60	7.41	7.56	9.61	8.61	8.31	8.15	9.34	9.22	7.97	7.11	CaO
3.33	3.29	3.67	2.87	3.04	3.09	2.91	3.16	3.44	3.54	3.14	Na_2O
1.82	1.88	1.75	2.33	2.06	2.13	2.08	0.98	1.24	1.67	1.68	K_2O
0.31	0.32	0.32	0.62	0.31	0.43	0.29	0.76	0.52	0.34	0.20	P_2O_5
--	--	--	0.69	--	0.03	--	0.03	0.06	0.02	0.05	CO_2
0.53	-0.20	-0.67	0.86	-0.23	0.55	0.49	0.80	0.36	0.68	0.74	LOI
98.41	94.67	99.38	99.32	99.15	99.71	98.94	99.45	99.76	99.65	99.77	Total
0.59	0.71	0.31	0.59	0.75	0.94	1.22	0.59	0.96	0.18	0.53	Fe_2O_3/FeO
73.6	73.6	74.6	70.4	72.2	70.3	69.5	72.1	74.0	68.6	70.1	Mg Number
											ppm
706	652	609	1088	767	995	962	549	740	619	576	Ba
53	44	48	53	42	43	45	11	23	40	39	Rb
514	594	582	1346	962	946	910	675	856	608	650	Sr
15	15	16	15	15	13	16	5	9	11	12	Pb
6	16	6	15	8	6	10	bd	6	6	3	Th
206	303	195	428	253	257	252	161	170	188	130	Zr
5	3	11	6	3	4	6	3	4	6	2	Nb
21	23	22	20	32	28	96	22	21	22	40	Y
28	24	31	207	91	104	361	25	40	32	39	La
50	50	61	311	115	114	367	50	71	61	41	Ce
24	--	--	20	28	21	28	23	25	22	23	Sc
132	130	159	206	178	170	169	193	204	173	171	V
403	385	472	245	265	208	260	457	540	291	393	Cr
225	210	301	110	113	97	89	262	281	98	120	Ni
42	--	--	141	100	72	84	51	47	24	87	Cu
59	65	106	70	66	66	62	71	74	75	70	Zn

Fe_2O_3 by difference, negative LOI indicates a weight gain,

unfractionated (Fig. 4.33; Table 4.9). The chondrite normalized patterns for the high-Mg lavas have similar slopes with minor to no negative Eu anomalies. A few of the patterns possibly show a slight negative Ce anomaly. However, the rocks vary significantly in the degree of enrichment (ΣREE = 128 to 1149) and LREE/HREE fractionation ($(La/Lu)_{CN}$ = 7.6 to 34.4). Compared with the "normal" calc-alkalic rocks of the northern volcanic belt, the high-Mg rocks exhibit the maximum degree of variation in both ΣREE enrichment and LREE/HREE fractionation.

In part, the differences in the degree of REE enrichment among the high-Mg rocks may be attributable to variations in the abundances of olivine and clinopyroxene since the crystal-liquid partitioning coefficients for these two minerals show an inverse relationship. Clinopyroxene

tends to be enriched in the REE, in particular the HREE, relative to the melt, whereas olivine tends to partition all of the rare earth elements into the melt (Humphris, 1984).

Because the total REE content and REE enrichment and fractionation are essentially independent of chemical composition, and because the chondrite normalized patterns have at most very minimal negative Eu anomalies of the bulk rock, the REE contents of the high-Mg andesitic rocks probably

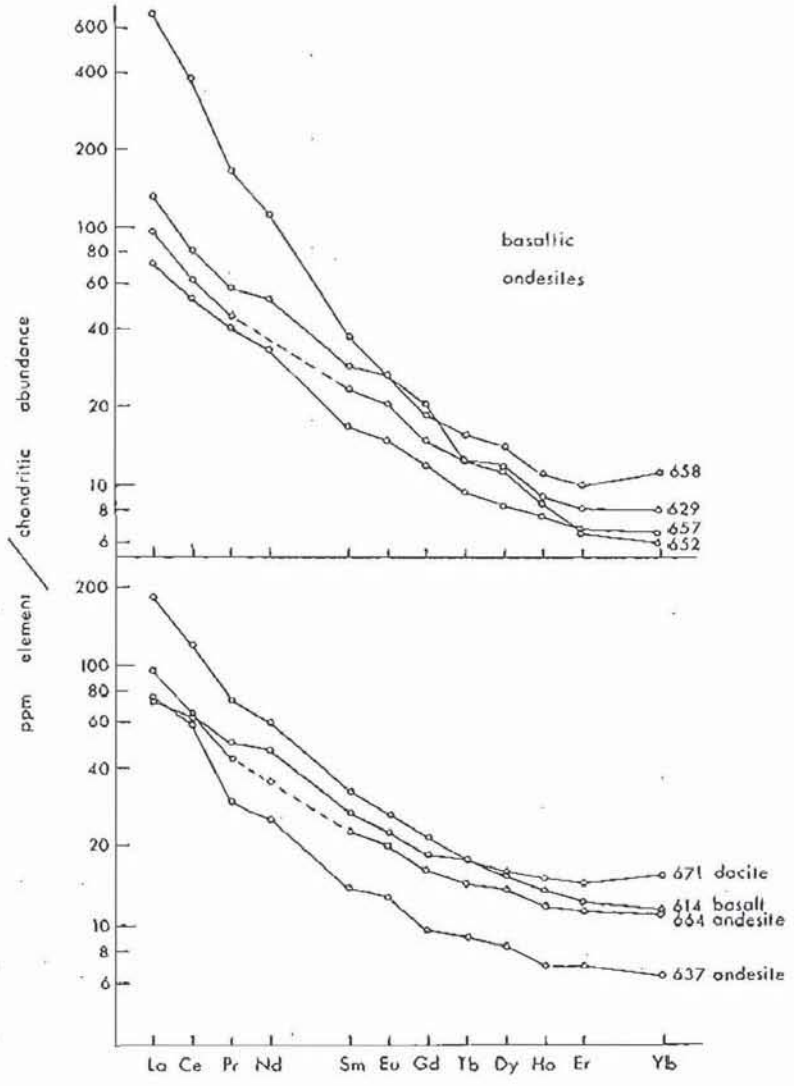

Figure 4.33. Chondrite normalized rare earth element abundance patterns for andesitic rocks from the northern volcanic belt of the east Papuan volcanic province, from Smith (1976b, page 90). The rare earth element data for these samples and additional data for the Iamalele area of western Fergusson Island are given in Appendix 3. When using Appendix 3 add the prefix 33 to the sample numbers shown in Figure 4.33, e.g., 658 = 33658.

Table 4.9. Rare earth element data for andesitic lavas from the northern volcanic belt of the east Papuan volcanic province

SAMPLE NO.	33629	33652	125806	125832	125834
ppm La	29	207	91	28	361
Ce	53	311	115	50	367
Pr	5.5	19.7	18	7	77
Nd	--	65.1	49	22	218
Sm	4.9	7.8	7.77	5.04	34.2
Eu	1.5	2	1.22	1.00	7.16
Gd	3.8	5.3	8	5	30
Tb	0.61	0.62	0.7	0.8	4.3
Dy	3.7	3.5	4.7	3.3	23.7
Ho	0.66	0.63	1.0	1.0	4.5
Er	1.7	1.4	3.5	2.0	11.0
Tm	--	--	0.5	0.5	1.5
Yb	1.6	1.2	2.29	1.85	8.19
Lu	--	--	0.33	0.38	1.41
Hf	4.0	7.9	7.7	5.0	7.0
Ta	--	--	bd	bd	bd
Nb	--	--	20	10	10
Cs	0.4	0.6	1.7	2.6	2.2
Co	--	--	80	46	35

-- = element not determined, bd = element below detection. Samples 33629 and 33652 are from Smith (1976b).

reflect the composition of the initial melt (Smith, 1976b). Further, the chondrite normalized patterns for the high-Mg lavas are similar to the calculated trends for the equilibrium (batch) melting of a garnet lherzolite source (Hanson, 1980). The differences between the patterns may be explained by varying the volume of the partial melt. The patterns suggest 5% or less for the melt volume.

Radiogenic Isotopes

Neodymium and Strontium

The $^{143}Nd/^{144}Nd$ and $^{87}Sr/^{86}Sr$ ratios for southeastern Papua New Guinea lavas plot along the mantle array (Fig. 4.34). This is significant because it indicates (1) that there is a mantle component to the isotopic signature of Nd and Sr, (2) that very little, if any, contamination of the magmas

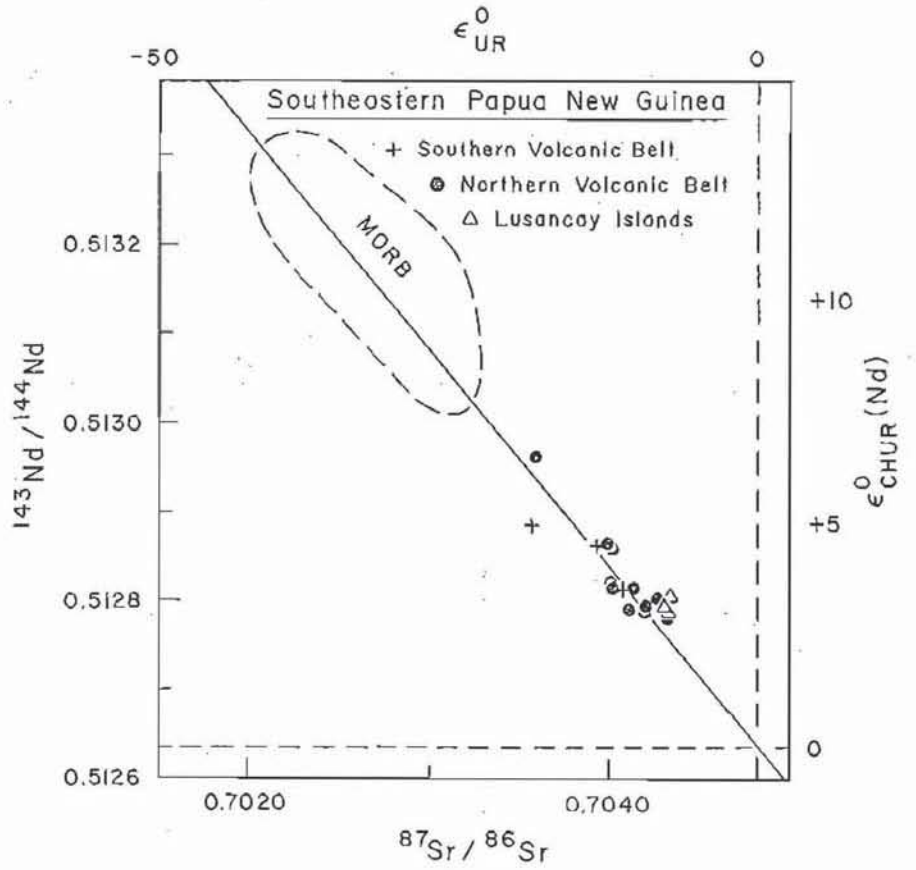

Figure 4.34. $^{143}Nd/^{144}Nd$ and $^{87}Sr/^{86}Sr$ ratios for lavas from the east Papuan volcanic province. Unpublished data from I.E.M. Smith (written communication). All $^{143}Nd/^{144}Nd$ ratios were corrected for isotopic fractionation to $^{146}Nd/^{144}Nd$. MORB boundary and mantle array from Faure (1986).

occurred as they rose through the thick sequence of metamorphic rocks (D'Entrecasteaux Complex; Precambrian source) prior to eruption and (3) that there is no apparent seawater component to the isotopic ratios. The ratios plot outside the MORB field indicating that the source is not MORB alone. There is an apparent correlation between the age of the sample and the Nd-Sr ratio, but additional age dating is required to establish this conclusively. The $^{87}Sr/^{86}Sr$ ratios for lavas from the northern volcanic belt range from 0.703595 to 0.704321 indicating a relatively primitive and totally oceanic source. These values correlate very well with the $^{87}Sr/^{86}Sr$ ratios (0.70398 to 0.70414) reported by Smith and Compston (1982) for the northern volcanic belt.

Lead

Lavas from the northern volcanic belt of the east Papuan volcanic province have high isotopic ratios for $^{206}Pb/^{204}Pb$ (18.30 to 18.91), $^{207}Pb/^{204}Pb$ (15.51 to 15.60) and $^{208}Pb/^{204}Pb$ (38.09 to 38.70), which plot well outside the range of MORB. The $^{207}Pb/^{204}Pb$ and $^{208}Pb/^{204}Pb$ ratios are plotted against $^{206}Pb/^{204}Pb$ ratio in Figure 4.35. These data show that the rocks from the east Papuan volcanic province define trends which also plot well away from the trend for mantle-derived Pacific Ocean Basin basalts. The lead isotope data for lavas from southeastern Papua New Guinea are more radiogenic than typical MORB lead, and considering that the fields for ocean floor sediment and for the andesitic rocks of the northern volcanic

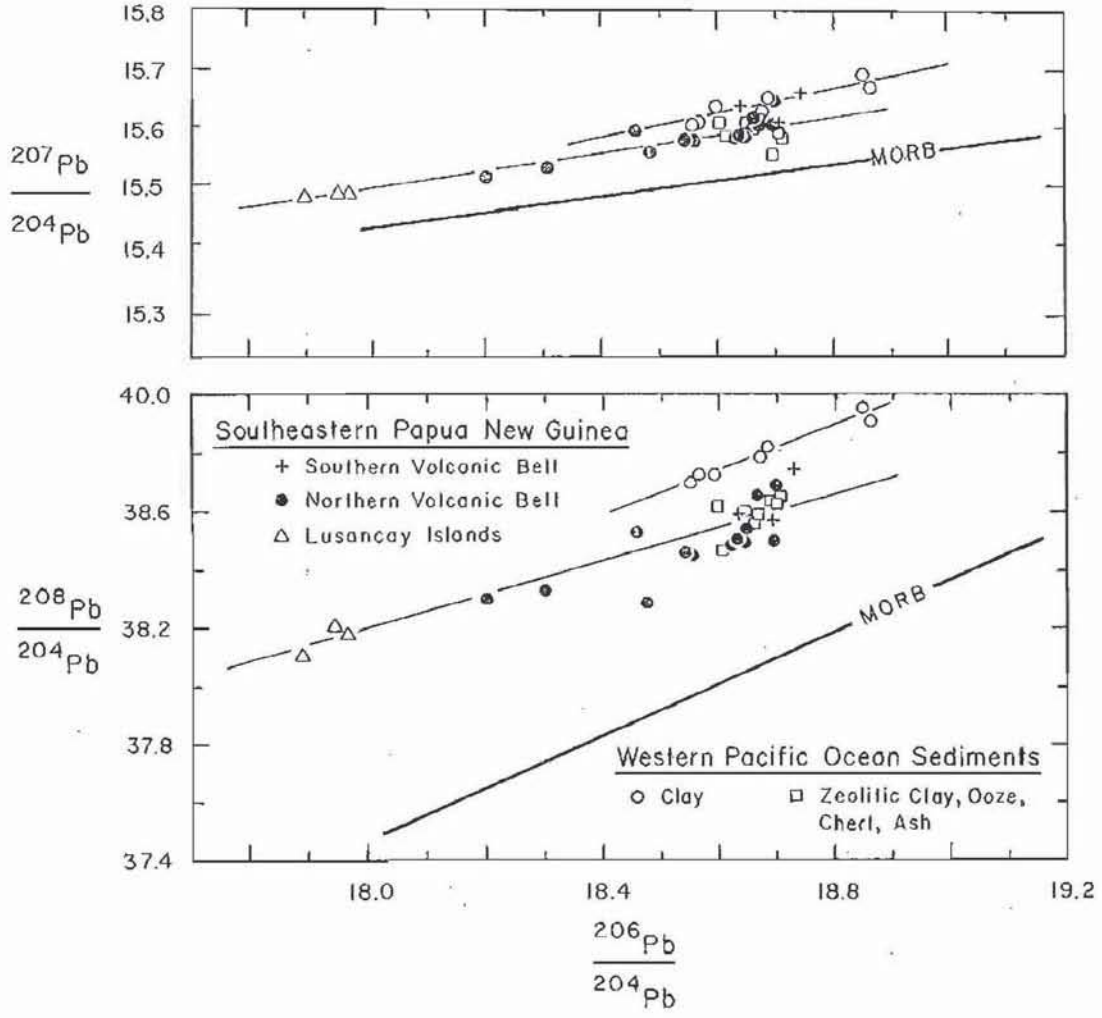

Figure 4.35. $^{207}Pb/^{204}Pb$ (a) and $^{208}Pb/^{204}Pb$ (b) ratios plotted against $^{206}Pb/^{204}Pb$ for lavas from the east Papuan volcanic province. Unpublished data from I.E.M. Smith (written communication). Western Pacific Ocean sediment data from Meijer (1976).

belt overlap (Fig. 4.35), the data appear to indicate significant contamination of a mantle source by ocean floor sediment.

Mineral Chemistry

Spinel

Spinel was the first liquidus phase to crystallize from the high-Mg magmas. Small (<150μ) euhedral crystals of chromite, reddish-brown hercynite and rare chromian magnetite locally form microphenocrysts, but more

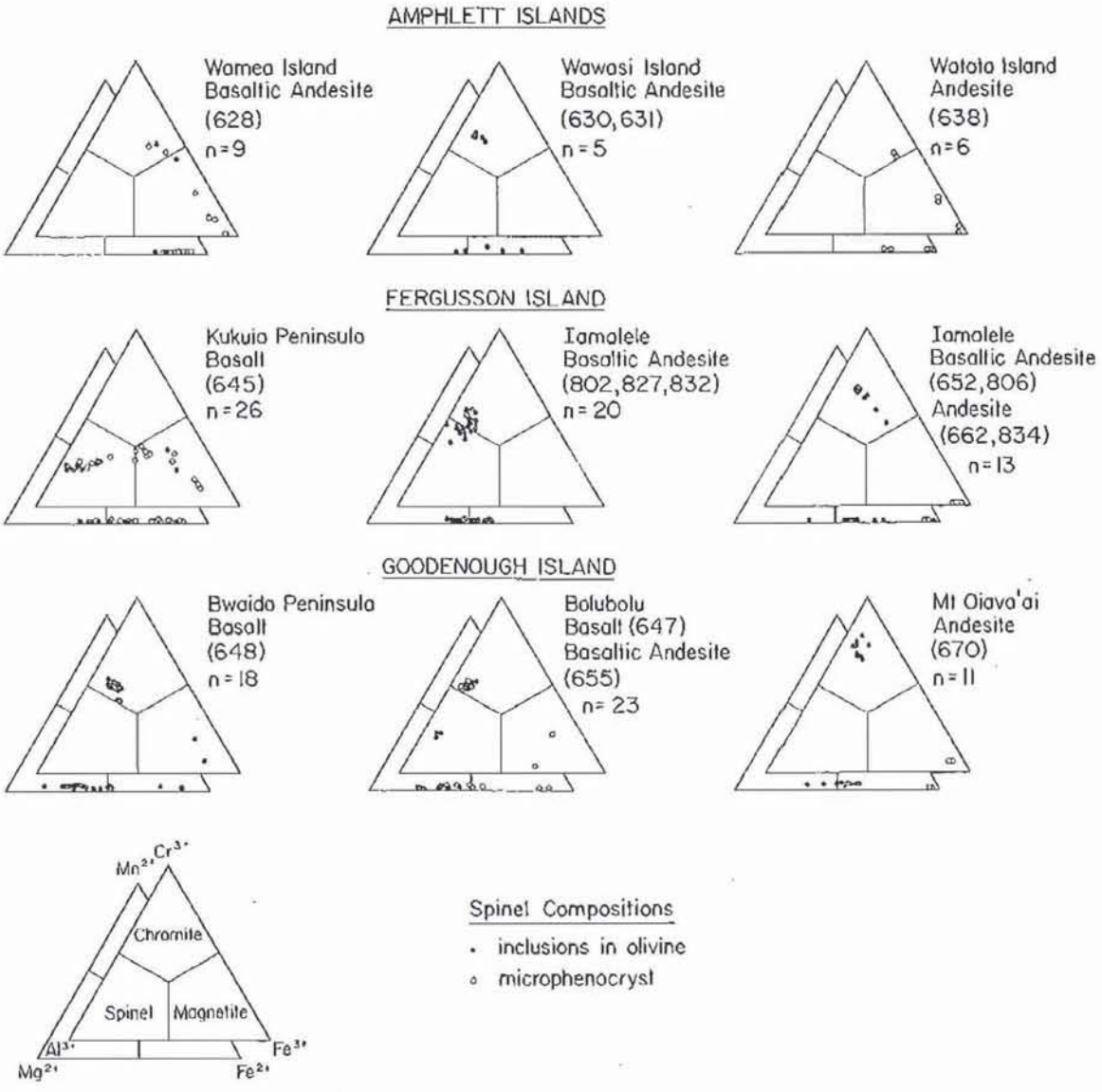

Figure 4.36. Compositional range of spinel in high-Mg lavas from the northern volcanic belt of the east Papuan volcanic province. See Figure 4.27 for sample locations and Appendix 4 for the analytical data and structural formulas. When using Appendix 4 add 33 to 600 samples and 125 to 800 samples, e.g., 628 = 33628 and 802 = 125802.

Table 4.10. Chemical analyses of spinel in high-Mg lavas from the northern volcanic belt of the east Papuan volcanic province

SAMPLE NO.	33628	33638		33645		33647	33648	33670	125802	
wt %	Phen.	Phen.	Incl.	Phen.	Phen.	Incl.	Incl.	Incl.	Incl.	Phen.
SiO_2	0.09	0.15	0.09	--	0.10	0.11	0.13	--	0.06	0.25
TiO_2	3.40	13.47	1.62	4.05	20.79	0.67	0.47	0.37	0.80	0.77
Al_2O_3	7.96	1.21	30.35	29.69	2.93	42.82	20.77	11.75	19.34	25.79
Cr_2O_3	32.96	8.49	20.08	18.19	3.20	19.32	43.27	54.91	41.89	35.93
V_2O_3	0.28	0.42	0.11	0.13	0.48	0.09	0.10	0.07	0.09	0.10
FeO*	48.47	71.02	36.83	35.44	65.53	16.94	19.13	17.62	23.93	24.06
MnO	0.40	0.24	0.33	0.31	0.53	0.14	0.14	0.15	0.18	0.20
MgO	4.26	1.13	9.33	10.37	3.85	18.91	14.80	14.27	12.27	12.05
CaO	--	0.05	--	--	--	--	0.08	--	0.03	0.08
NiO	--	0.14	0.11	0.13	0.17	0.23	0.18	0.14	0.16	0.09
Sum	97.82	96.32	98.85	98.31	97.58	99.23	99.07	99.28	98.75	99.32
Recalculated analyses (ulvospinel basis)										
Fe_2O_3	21.34	32.48	14.70	12.96	23.46	7.55	7.13	6.22	8.24	6.47
FeO	29.27	41.80	23.60	23.78	44.43	10.15	12.72	12.02	16.52	18.23
Total	99.96	99.58	100.32	99.61	99.94	99.99	99.79	99.90	99.58	99.96

-- = element below detection, FeO* = total Fe as FeO, Incl. = inclusion in olivine, Phen. = microphenocryst. Fe_2O_3/FeO recalculation follows Carmichael (1967), see Appendix 4. Na_2O and K_2O were below detection in all analyses. These data were selected from the 131 spinel analyses plotted in Figure 4.36. For additional data and structural formulas see Appendix 4.

characteristically occur as small (<100μ) inclusions or clusters of inclusions in olivine. Olivine phenocrysts generally contain less than 10 spinel inclusions, but in some rocks spinel may occupy up to 15 percent (rare) of an olivine phenocryst. Considering these occurrences it is likely that spinel crystals provided nucleation sites for early crystallizing olivine. Cr-spinel is absent in many olivine phenocrysts and is extremely rare or absent in phenocrystic phases which crystallized after olivine, indicating that crystallization of spinel ceased prior to or shortly after olivine began to precipitate.

Spinels show a wide range in composition which documents a trend toward Cr^{3+}, Al^{3+} and Mg^{2+} depletion and Fe^{3+} and Fe^{2+} enrichment with time (Fig. 4.36; Table 4.10). Compositional gaps in the crystallization trends probably reflect the relatively small sample populations. Chromite is present in all of the samples except 33645 which is a transitional basalt (Smith, 1976b). The crystallization trend for spinel in sample 33645 is also unique in that it shows a moderate enrichment in Cr during the early

stages of crystallization, followed by the normal trend toward iron enrichment during the later stages of crystallization.

In general the spinel crystals are too small to allow quantitative determination of the extent of chemical zoning. The larger spinel inclusions and microphenocrysts which were analysed showed either normal or reverse zoning with Cr abundances varying between ~1 and ~8 wt %. Typical variations in the abundance of Cr in spinel inclusions within a single olivine phenocryst ranged from <1 to ~4 wt %.

Olivine

Olivine occurs as euhedral and rare skeletal phenocrysts which may contain (rare) inclusions of clinopyroxene. In a few samples olivine is rimmed by, and in the case of smaller grains, completely replaced by iddingsite, indicating that oxidizing conditions existed in some of the magmas; iddingsite is the only oxidized phase present in the high-Mg lavas implying a magmatic origin.

Compositionally zoned euhedral nickel-bearing olivine (Fo_{92-78}) occurs in nearly all of the high-Mg lavas (Fig. 4.37; Table 4.11). In zoned crystals the cores tend to have higher Mg/(Mg+Fe) ratios and higher Ni contents than the rims, but olivine phenocrysts with reverse chemical zoning are

Table 4.11. Chemical analyses of olivine in high-Mg lavas from the

SAMPLE NO.	33607		33628		33638		33645			
wt %	Core	Rim	Core	Rim	Core	Rim	Core	Rim	Gm	Core
SiO_2	40.28	40.33	39.20	38.85	38.75	38.33	39.80	38.87	36.01	39.11
TiO_2	--	--	--	--	--	--	0.06	--	--	--
Al_2O_3	--	--	--	--	--	--	0.08	0.07	0.45	0.07
Cr_2O_3	na	na	--	--	--	--	--	0.07	--	--
FeO*	11.23	11.52	10.28	14.76	14.85	17.17	11.90	15.98	26.51	10.79
MnO	0.19	0.12	0.14	0.18	0.17	0.21	0.22	0.30	--	0.17
MgO	48.30	48.03	49.51	46.03	44.99	43.73	46.72	44.54	36.89	49.12
CaO	--	--	0.13	0.14	0.13	0.14	0.24	0.20	--	0.30
Na_2O	na	na	--	--	--	--	--	--	--	--
NiO	na	na	0.33	0.23	0.39	0.32	0.23	0.22	--	0.16
Total	100.00	100.00	99.59	100.19	99.28	99.90	99.25	100.25	99.86	99.72
Mg/(Mg+Fe)	0.89	0.88	0.90	0.85	0.84	0.82	0.87	0.83	0.71	0.89

na = element not analysed, -- = element below detection, FeO* = total Fe as FeO, core and rim =
The data in Table 4.11 were selected from the 364 olivine analyses plotted in Figure 4.37. For

always present. The phenocryst phases are more magnesian than the associated groundmass grains (Fo_{80-70}). The calcium content of olivine phenocrysts increases slightly from core to rim generally varying from ~0.15 to 0.30 wt %, although a few values up ~0.60 wt % were measured. Olivine composition appears to be unrelated to either the SiO_2 content or the age of the rock.

Considering Mg-Fe partitioning, olivine in most of the high-Mg lavas appears to be in chemical equilibrium with the host magma (Fig. 4.38). The olivine data plotted in Figure 4.38 bracket the 0.30 K_D line (Roeder and Emslie, 1970) remarkably well, although disequilibrium conditions may be indicated for a few of the samples (e.g. 638 and 670). Since the Fe^{2+}/Mg ratio of the bulk rock was used to approximate that of the magma, the mean Fe^{2+}/Mg ratio for olivine phenocrysts and groundmass should plot below and above the K_D line respectively. This relationship is demonstrated by the data for samples 647 and 655; reliable groundmass olivine compositions were not available for most samples. Phenocryst data for four samples (630, 645, 652 and 806) plot above the K_D line, which could signify olivine-melt disequilibrium at the time of their eruption. However, for each of the samples (except 645) mineral textures and the composition of coexisting minerals suggest equilibrium conditions prevailed. Sample 33645, the

northern volcanic belt of the east Papuan volcanic province

33647		33648		33670		125802		125834		
Rim	Gm	Core	Rim	Core	Rim	Core	Rim	Core	Rim	wt %
39.91	38.54	39.89	38.09	40.35	38.50	38.28	39.62	39.30	39.31	SiO_2
--	--	--	--	--	--	--	--	--	--	TiO_2
--	--	0.07	0.08	--	--	0.07	0.05	--	--	Al_2O_3
--	--	--	--	--	--	--	--	--	--	Cr_2O_3
9.64	21.93	9.54	9.15	6.93	15.60	17.00	11.21	10.73	10.84	FeO*
0.25	0.35	0.18	0.16	--	0.22	0.23	0.19	0.13	0.20	MnO
49.47	39.00	49.75	51.52	52.00	44.92	44.09	48.50	49.15	49.04	MgO
0.27	0.15	0.15	0.19	0.09	0.11	0.07	0.19	0.14	0.15	CaO
--	--	0.04	0.07	--	--	--	--	--	--	Na_2O
0.27	--	0.35	0.42	0.47	0.10	0.14	0.31	0.38	0.36	NiO
99.81	99.97	99.97	99.68	99.84	99.45	99.88	100.07	99.83	99.90	Total
0.90	0.76	0.90	0.91	0.93	0.84	0.82	0.89	0.89	0.89	Mg/(Mg+Fe)

phenocrysts, Gm = groundmass, V_2O_3 and K_2O were below detection in all analyses.
additional data and structural formulas see Appendix 4.

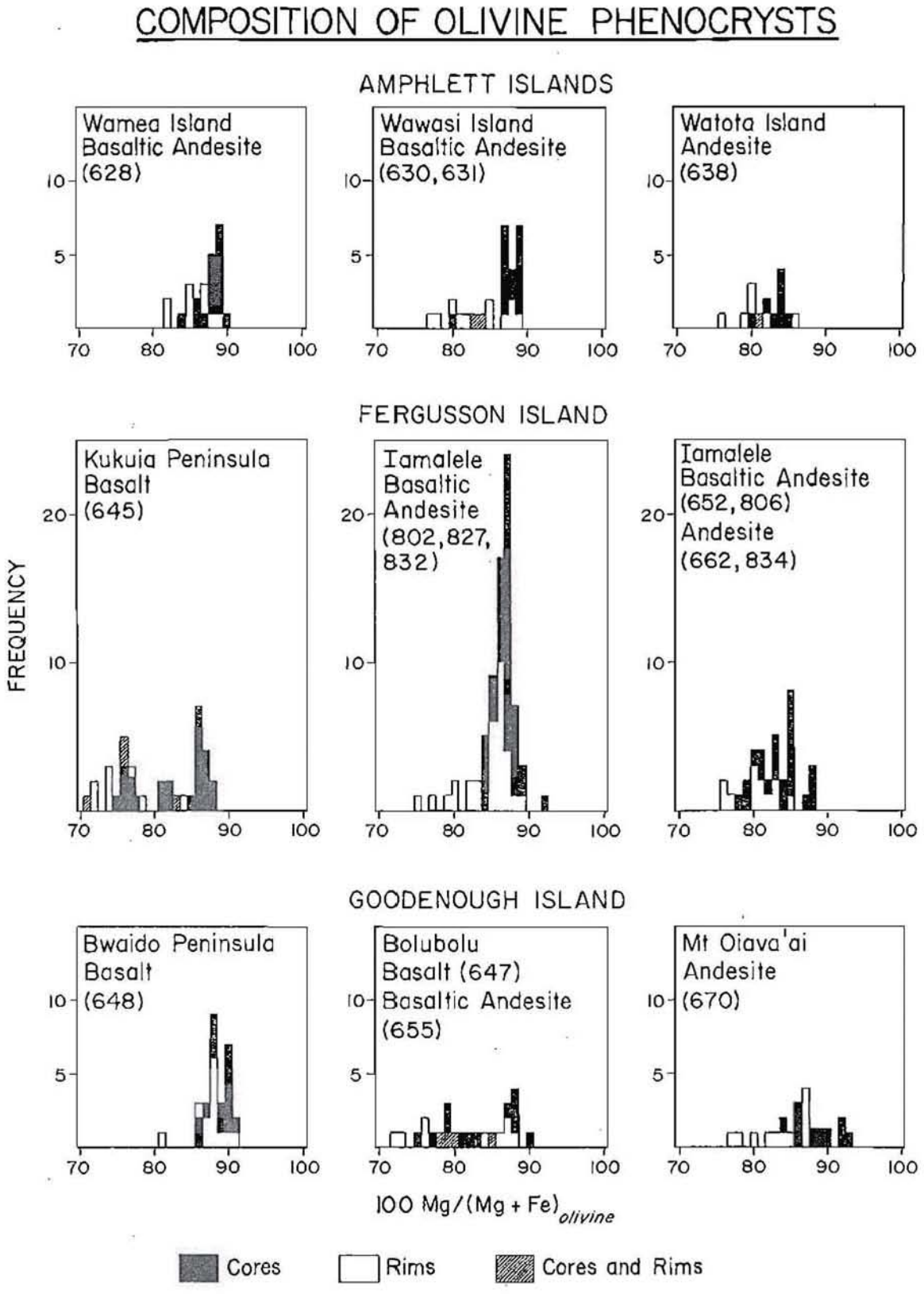

Figure 4.37. Compositional range of olivine phenocrysts in high-Mg lavas from the northern volcanic belt of the east Papuan volcanic province. See Figure 4.27 for sample locations and Appendix 4 for the analytical data and structural formulas. When using Appendix 4 add 33 to 600 samples and 125 to 800 samples, e.g., 628 = 33628 and 802 = 125802.

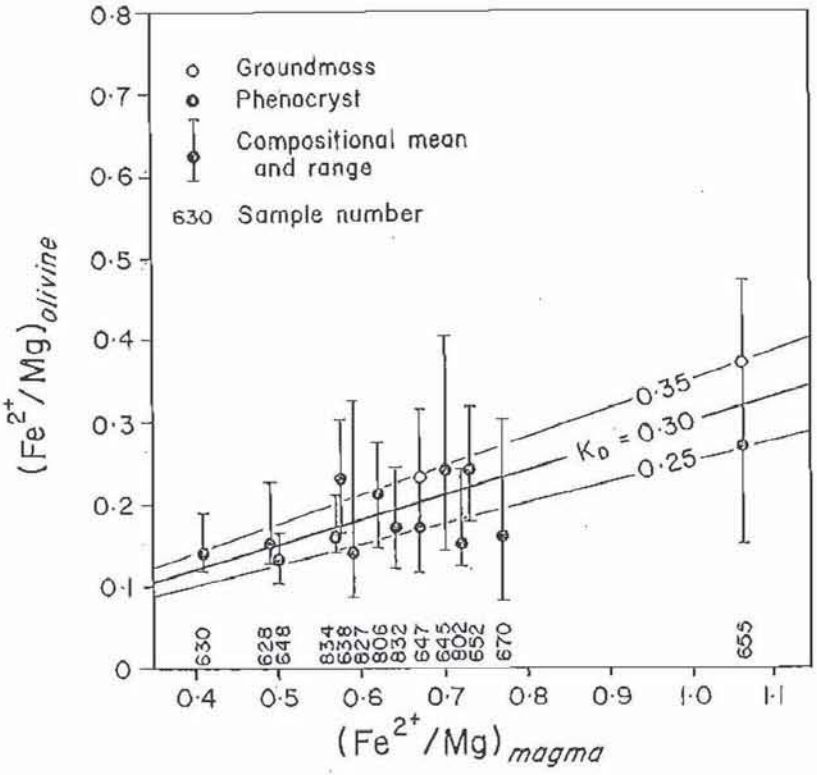

Figure 4.38. Partitioning of Fe^{2+} and Mg between olivine phenocrysts and the magma for high-Mg lavas from the northern volcanic belt of the east Papuan volcanic province. Fe^{2+}/Mg was estimated from the Fe^{2+} and Mg content of the bulk rock. See Tables 4.8 and 4.11 and Appendices 3 and 4 for the analytical data. When using Appendix 4 add 33 to 600 samples and 125 to 800 samples, e.g., 628 = 33628 and 802 = 125802.

transitional basalt, contains a bimodal population of olivine in which one population has lower Fe/(Fe+Mg) ratios and is not in equilibrium with the host magma.

Phenocrystic and groundmass olivine in several samples (628, 647, 648, and 832) are at least partially altered to iddingsite. In these samples the chemical composition of unaltered olivine phenocryst and groundmass phases are in equilibrium with the melt, indicating that Mg lost during magmatic oxidation was retained in the magma.

Xenoliths were observed at only one locality (33639) in the northern volcanic belt. Microprobe analyses of a dunite xenolith in sample 33639 indicate that the olivine is a high-Ni forsterite (Fo_{93-91}). Such olivine compositions are permissive for derivation of this inclusion from either

Table 4.12. Chemical analyses of clinopyroxene in high-Mg volcanic province

SAMPLE NO.	33628		33647			33648		
wt %	Core	Gm	Core	Rim	Gm	Core	Rim	Gm
SiO_2	53.91	52.46	50.30	47.71	51.12	50.46	49.14	50.21
TiO_2	0.51	--	1.08	1.50	1.30	0.79	0.75	1.21
Al_2O_3	1.77	2.05	5.06	5.91	3.15	4.68	3.99	5.77
Cr_2O_3	0.52	--	0.11	0.19	--	1.11	0.89	0.50
V_2O_3	--	--	0.09	0.07	--	0.07	0.06	--
FeO*	4.10	7.89	6.41	6.86	8.03	4.59	4.16	5.79
MnO	0.15	--	0.14	0.12	--	0.13	0.10	--
MgO	17.98	16.95	15.49	15.70	14.31	15.25	16.60	14.65
CaO	21.58	20.53	20.68	20.36	20.37	22.51	22.59	21.50
Na_2O	0.22	--	0.46	0.55	0.89	0.32	0.32	--
NiO	--	--	--	--	--	--	0.06	--
Sum	100.74	99.88	99.82	98.97	99.17	99.91	98.66	99.63
								Recalculated
Fe_2O_3	0.05	1.86	1.85	5.71	1.62	1.31	4.62	--
FeO	4.05	6.21	4.75	1.72	6.57	3.41	--	5.79
Total	100.74	100.06	100.01	99.54	99.33	100.04	99.12	99.63
Mg/(Mg+Fe)	0.89	0.79	0.81	0.80	0.76	0.86	0.88	0.82

-- = element below detection, FeO* = total Fe as FeO, core and rim = phenocrysts, The data in Table 4.12 were selected from the 311 pyroxene analyses plotted in

the metamorphic tectonites of the Papuan Ultramafic Belt or from the upper mantle.

Clinopyroxene

Clinopyroxene phenocrysts and microphenocrysts are typically pale green euhedral to subhedral crystals. Clinopyroxene phenocrysts locally contain small inclusions of olivine, but inclusions of spinel were not observed. Crystallization of clinopyroxene probably postdates precipitation of chromite and Cr-rich spinel and, by inference, also postdates the initiation of olivine crystallization.

Endiopside and diopside are the most common clinopyroxene phenocrysts, whereas groundmass grains show a wider compositional range extending to Ca-poor pyroxene (Fig. 4.39). The only exception to this is the transitional basalt (645) which contains phenocrysts of salite and magnesium-pigeonite. Most phenocrysts contain between 0.5 and 1.0 wt % Cr_2O_3 and many contain trace amounts of NiO (Table 4.12). Additional

lavas from the northern volcanic belt of the east Papuan

33670		125802			125834			
Core	Rim	Core	Rim	Gm	Core	Rim	Gm	wt %
52.34	52.29	50.45	52.88	52.08	52.40	53.02	54.06	SiO_2
0.34	0.39	0.85	0.37	0.59	0.32	0.33	0.27	TiO_2
2.65	2.71	4.58	1.93	3.01	1.68	2.22	4.67	Al_2O_3
0.58	0.43	0.83	0.26	0.42	0.59	0.70	--	Cr_2O_3
0.06	--	0.05	--	--	0.03	--	--	V_2O_3
5.52	5.93	4.42	4.78	5.36	3.52	3.65	14.74	FeO*
0.16	0.17	0.11	0.13	0.19	0.08	0.14	0.55	MnO
17.60	16.94	16.69	18.63	15.84	19.04	18.74	21.60	MgO
20.24	20.62	21.19	20.50	22.43	21.38	20.91	3.33	CaO
0.23	0.31	0.29	0.24	--	0.26	0.31	0.66	Na_2O
--	--	0.06	0.07	--	0.07	0.04	--	NiO
99.72	99.79	99.52	99.79	99.92	99.37	100.06	99.88	Sum
analyses								
1.29	1.41	1.92	2.21	--	3.59	1.95	14.74	Fe_2O_3
4.36	4.66	2.69	2.79	5.36	0.29	1.89	--	FeO
99.85	99.93	99.71	100.01	99.92	99.73	100.25	99.88	Total
0.85	0.84	0.87	0.87	0.84	0.91	0.90	0.72	Mg/(Mg+Fe)

Gm = groundmass, Fe_2O_3 recalculation follows Robinson (1980).
Figure 4.39. For additional data and structural formulas see Appendix 4.

characteristics of clinopyroxene are moderate to high Al_2O_3 (4 to 7 wt %), low TiO_2 (<2 wt %) and relatively constant CaO (19.7 to 22.6 wt %) abundances.

The Mg/(Mg+Fe) ratio of clinopyroxene is slightly lower than that of the associated olivine, but preliminary calculations of Fe-Mg partitioning between clinopyroxene phenocrysts and their host magmas indicate that the clinopyroxene was in equilibrium with the magma. The Mg-Fe compositional variation between clinopyroxene phenocrysts and groundmass is greater than that of olivine, which is consistent with later crystallization. Variations in calculated Fe^{3+}/Fe^{2+} ratios for clinopyroxene phenocrysts may reflect variable oxidation states of the magmas; see Table 4.12 for examples.

Orthopyroxene

Coexisting orthopyroxene and clinopyroxene phenocrysts were present in only one of the high-Mg lavas sampled (see sample 33638 in Figure 4.39).

Figure 4.39. (Facing page) Compositional range of pyroxene phenocrysts in high-Mg lavas from the northern volcanic belt of the east Papuan volcanic province. See Figure 4.27 for sample locations and Appendix 4 for the analytical data and structural formulas. When using Appendix 4 add 33 to 600 samples and 125 to 800 samples, e.g., 628 = 33628 and 802 = 125802.

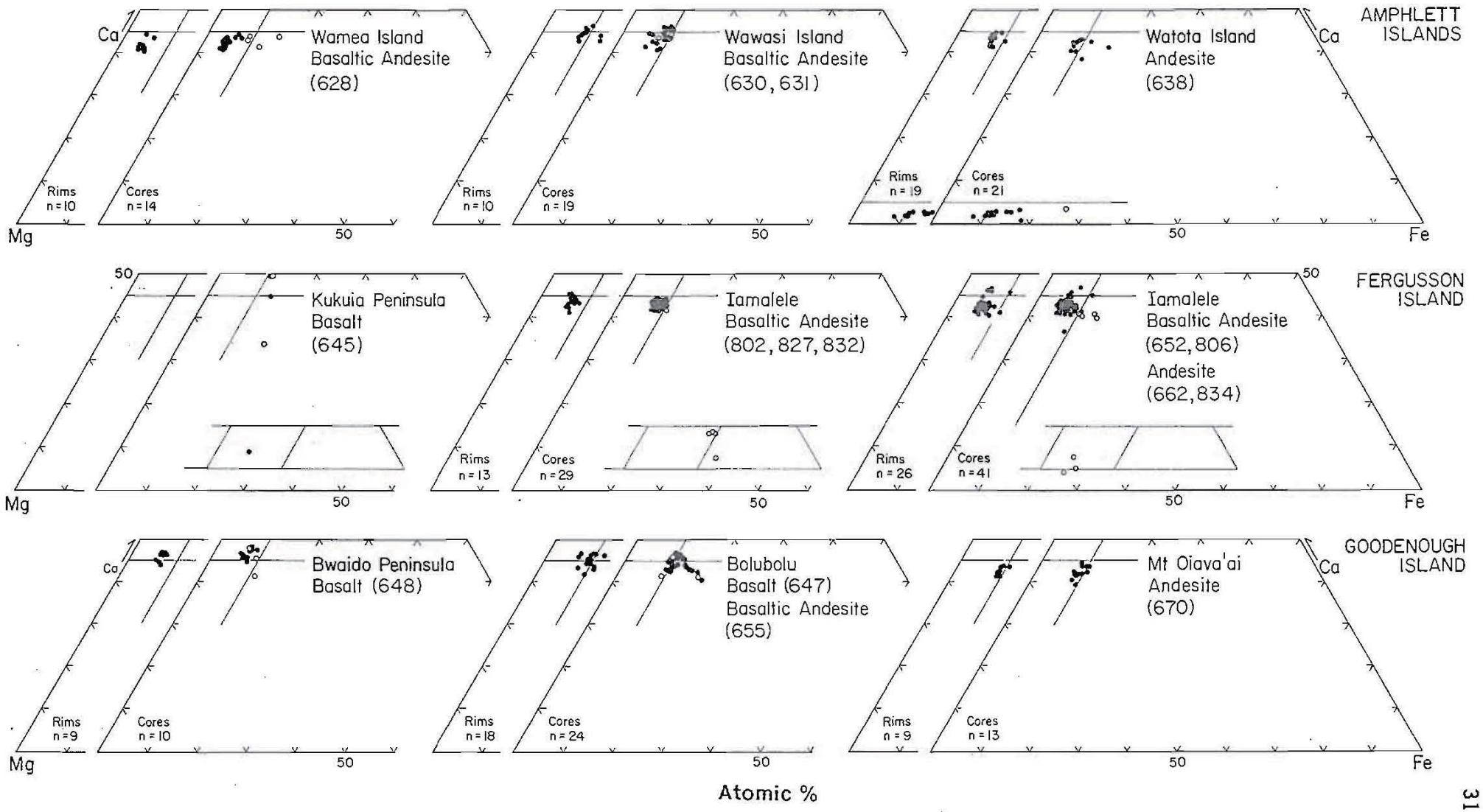
AMPHLETT ISLANDS
Wamea Island Basaltic Andesite (628)
Wawasi Island Basaltic Andesite (630, 631)
Watota Island Andesite (638)
FERGUSSON ISLAND
Kukuia Peninsula Basalt (645)
Iamalele Basaltic Andesite (802, 827, 832)
Iamalele Basaltic Andesite (652, 806)
Andesite (662, 834)
GOODENOUGH ISLAND
Bwaido Peninsula Basalt (648)
Bolubolu Basalt (647)
Basaltic Andesite (655)
Mt Oiava'ai Andesite (670)
Ca
Mg
Fe
50
Rims n=10
Cores n=14
Rims n=10
Cores n=19
Rims n=19
Cores n=21
Rims n=13
Cores n=29
Rims n=26
Cores n=41
Rims n=9
Cores n=10
Rims n=18
Cores n=24
Rims n=9
Cores n=13
Atomic %

Table 4.13. Chemical analyses of coexisting phenocrysts and groundmass pyroxene in high-Mg lavas from Watota Island (33638), northern volcanic belt, east Papuan volcanic province

	Endiopside		Enstatite		Bronzite		Bronzite
wt %	Core	Rim	Core	Rim	Core	Rim	Gm
SiO2	52.60	52.80	56.29	55.55	55.20	55.18	54.99
TiO2	0.41	0.37	0.09	0.06	0.22	0.20	0.25
Al2O3	2.62	2.52	1.49	1.56	1.42	1.35	0.53
Cr2O3	0.67	0.65	0.65	0.69	0.33	0.37	--
FeO*	5.24	4.90	5.31	5.46	9.37	9.54	16.84
MnO	0.09	0.11	0.08	0.11	0.18	0.19	0.30
MgO	18.21	17.67	35.06	34.77	31.59	32.32	25.26
CaO	19.71	20.25	0.76	0.89	1.27	1.32	1.80
Na2O	0.40	0.39	--	--	--	--	--
NiO	--	--	0.32	0.24	--	--	--
Sum	99.95	99.66	100.05	99.33	99.58	100.47	99.97
			Recalculated analyses				
Fe2O3	1.80	0.88	1.97	2.70	1.42	3.16	16.84
FeO	3.62	4.11	3.54	3.03	8.09	6.70	--
Total	100.13	99.75	100.25	99.60	99.72	100.79	99.97
Mg/(Mg+Fe)	0.86	0.87	0.92	0.92	0.86	0.86	0.73

-- = element below detection, FeO* = total Fe as FeO, core and rim = phenocrysts, Gm = groundmass, -- = oxide not present in recalculation. Fe2O3/FeO recalculation follows Robinson (1980). V2O3 and K2O were below detection in all analyses. For additional data and structural formulas see Appendix 3.

In general orthopyroxene (En_{91-81}) has a moderate to high Cr content and low TiO_2 and Al_2O_3 contents (Table 4.13). NiO abundances were below detection except for enstatite which contained a surprisingly high percentage of NiO. The only groundmass grain that was successfully analysed had a much lower Mg/(Mg + Fe) ratio (0.73). Fe^{3+}/Fe^{2+} recalculations predict that the groundmass grain contains only ferric iron.

Iron-Titanium oxides

Titaniferous magnetite and ilmenite characteristically occur as constituents of the groundmass and as small microphenocrysts. Titaniferous magnetite also occurs as euhedral inclusions in olivine and clinopyroxene (rare) phenocrysts, although this mode of occurrence is relatively uncommon. In a few samples Ti-bearing magnetite formed irregular-shaped skeletal crystals (rare) in the groundmass which probably developed during quenching of the lava.

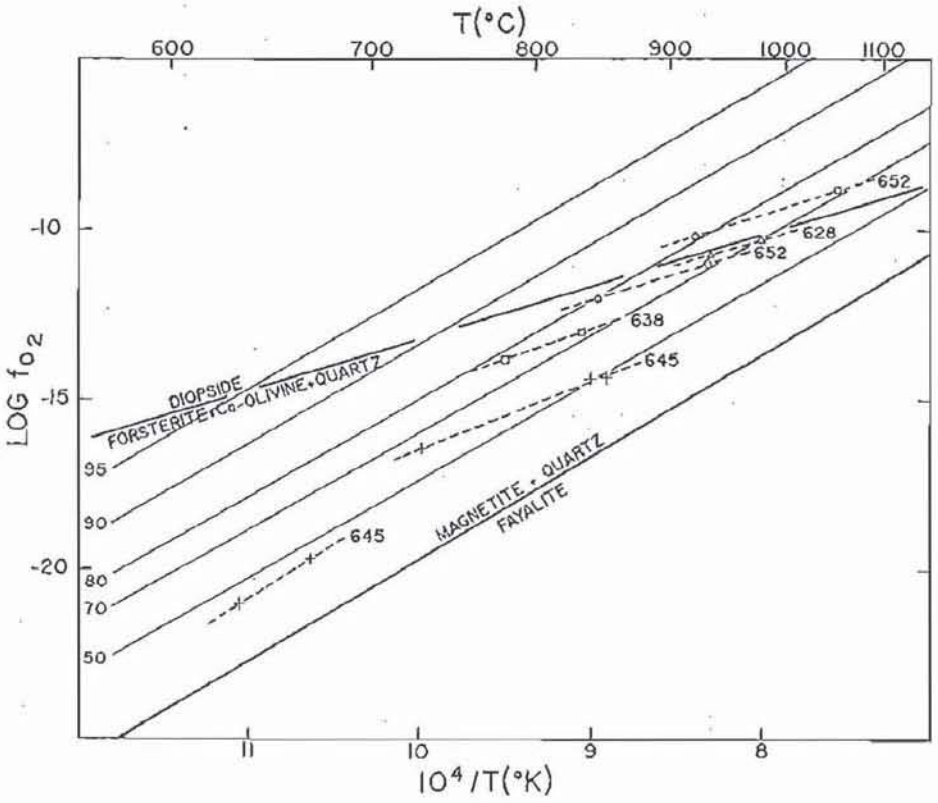

Figure 4.40. fO_2-T-X diagram for olivine phenocrysts in high-Mg lavas from the northern volcanic belt of the east Papuan volcanic province; fO_2-T data are for coexisting magnetite-ilmenite. Isocomposition curves are given in mole percent forsterite and were calculated using data from Nitsan (1974).

Except for ilmenite exsolution lamellae in magnetite, ilmenite was not observed as an included phase in any mineral. Ilmenite is absent from the high-Mg lavas which contain abundant spinel. Considering the data in Appendix 3 it appears that the abundance of ilmenite in the high-Mg lavas increases as the SiO_2 content of the bulk rock increases.

Many of the high-Mg lavas analysed contained coexisting magnetite and ilmenite. In most cases mineral textures (euhedral grain boundaries or exsolution lamellae) indicated that magnetite and ilmenite were in equilibrium, and for these phases T-fO_2 conditions were calculated (I.E.M. Smith, written communication) or measured from the fO_2-T-X projection for coexisting Fe-Ti oxide constructed by Buddington and Lindsley (1964) and Ghiorso and Carmichael (1981). The results of these calculations show a consistent trend of increasing oxidation state of the magma with increasing crystallization (Fig. 4.40; Table 4.14). Two important aspects of Figure 4.40 are

Table 4.14. Analyses of coexisting iron-titanium oxide of the east Papuan province

SAMPLE NO.	33645		33645		33628		33628	
wt %								
SiO_2	0.10	0.05	--	--	--	--	--	--
TiO_2	20.79	52.11	12.21	53.44	15.51	41.63	13.38	41.63
Al_2O_3	2.93	0.10	10.40	--	1.57	0.47	2.54	0.47
Cr_2O_3	3.20	0.24	16.87	0.18	3.92	1.97	10.36	1.97
V_2O_3	0.48	--	na	na	na	na	na	na
FeO*	65.53	39.38	51.49	39.70	71.61	48.70	65.61	48.70
MnO	0.53	0.50	0.79	0.73	0.66	0.85	0.72	0.85
MgO	3.85	7.17	6.20	5.74	2.89	3.94	3.76	3.94
CaO	--	0.06	--	0.15	0.16	--	--	--
NiO	0.17	0.09	--	--	--	--	--	--
Sum	97.58	99.70	97.96	99.94	96.32	97.56	96.37	97.56
								Recalculated
Fe_2O_3	23.46	6.47	19.32	3.12	34.66	21.28	31.33	21.28
FeO	44.43	33.55	34.10	36.89	40.42	29.55	37.42	29.55
Total	99.94	100.34	99.89	100.25	99.79	99.69	99.51	99.69
Mol.% Usp	56.72	--	31.39	--	42.91	--	36.66	--
Mol.% M_2O_3	--	6.19	--	3.10	--	22.45	--	22.45
								Fe-Ti oxide
T deg. C	900		700		1050		990	
-Log fO_2	13.0		18.0		8.5		10.0	

-- = element below detection, FeO* = total Fe as FeO. Data determined on Carmichael (1967). Temperature and oxygen fugacity calculations follow Ghiorso

(1) that the data (except 33645) plot within a narrow compositional range for olivine (Fo_{80-70}) and (2) that the slopes of the cooling trends approximate the slope of the reaction forsterite + Ca-olivine + quartz $\rightleftharpoons$ diopside:

$$Mg[SiO_4]_{1/2} + Ca[SiO_4]_{1/2} + SiO_2 \rightleftharpoons CaMgSi_2O_6.$$

It is also significant that the cooling trend established for sample 33645 is approximately parallel to the fayalite-magnetite-quartz buffer reaction. All of the rocks except 33645 contain olivine, clinopyroxene and magnetite in apparent equilibrium, whereas 33645 contains a bimodal population of olivine, as well as magnetite and rare, primarily groundmass clinopyroxene.

Plagioclase

Compositionally zoned plagioclase (An_{88-45}) constitutes a small portion of the total phenocryst population in the high-Mg lavas. Plagioclase phenocrysts characteristically show extensive internal melting (sieve tex-

minerals in high-Mg lavas from the northern volcanic belt

33638		33638		33652		33652		
								wt %
--	--	--	--	--	--	--	0.93	SiO_2
11.99	46.38	7.99	46.38	13.89	31.24	8.26	41.82	TiO_2
1.49	--	5.12	--	1.58	1.16	1.87	0.15	Al_2O_3
8.58	0.20	26.00	0.20	0.15	0.18	0.14	--	Cr_2O_3
na	na	na	na	na	na	na	na	V_2O_3
72.71	49.15	51.48	49.15	78.43	60.50	83.19	51.96	FeO*
0.69	0.66	0.85	0.66	0.44	0.85	0.43	0.62	MnO
0.96	1.55	5.75	1.55	1.28	1.60	0.44	2.52	MgO
--	--	--	--	--	0.10	--	--	CaO
--	--	0.34	--	--	--	--	--	NiO
96.42	97.94	97.53	97.94	95.77	95.63	94.33	98.00	Sum
analyses								
35.90	12.07	24.18	12.07	40.74	40.29	50.53	20.41	Fe_2O_3
40.40	38.29	29.72	38.29	41.78	24.25	37.72	33.60	FeO
100.01	99.15	99.95	99.15	99.86	99.67	99.39	100.05	Total
33.65	--	21.16	--	39.04	--	23.54	--	Mol.% Usp
--	11.70	--	11.70	--	40.39	--	19.35	Mol.% M_2O_3
geothermometer								
840		725		1250		875		T deg. C
13.0		15.5		6.0		11.5		-Log fO_2

microphenocrysts and groundmass crystals. Fe_2O_3 recalculation follows and Carmichael (1981). For additional data and structural formulas see Appendix 3.

tures) indicating feldspar-melt disequilibrium. Petrographic and electron microprobe data (Appendix 4) show that reverse zoning is also a common feature of the plagioclase phenocrysts. Bytownite (An_{88-83}) microphenocrysts are a constituent of some high-Mg lavas, typically occurring in autoliths (e.g., sample 33657). Calcic plagioclase appeared relatively early in the crystallization history of the high-Mg lavas, but the initiation of plagioclase crystallization may have postdated the main phase of olivine precipitation. Although there is no textural evidence with which to establish the timing of plagioclase crystallization, theoretical calculations indicate that olivine crystallizing with pyroxene and plagioclase will tend to be Fe-rich (Hanson and Langmuir, 1978), and olivine in the high-Mg rocks is Mg-rich. However, groundmass olivine, which most likely crystallized with plagioclase, is enriched in iron with respect to olivine phenocrysts. The common occurrence of reversely zoned plagioclase phenocrysts indicates that the crystals circulated within the magma chamber.

The fact that groundmass plagioclase is dominantly labradorite indicates that the lavas were erupted before extensive differentiation of the magmas occurred.

Petrogenesis of the Southeastern Papua New Guinea Lavas

Among the rocks forming the late Cenozoic arc-type volcanic association of southeastern Papua New Guinea are high-Mg lavas ranging in composition from basalt to dacite. In the northern volcanic belt the high-Mg rocks form part of a volcanic suite which may be characterized as high-K calc-alkalic. In the southern volcanic belt the high-Mg rocks constitute part of an overall shoshonitic assemblage. A petrogenetic model for the high-Mg lavas must satisfy the following observations: (1) they are an integral part of a long-lived volcanic association which includes both high-K calc-alkalic and shoshonitic rocks, and (2) the mechanism of their genesis effectively discriminates a few elements which are either preferentially concentrated or depleted relative to the remainder of the association. The mechanisms which are most likely to affect a rising magma are mixing, contamination, crystal fractionation and/or crystal accumulation.

Modified Mantle Source

The high-Mg lavas are enriched in Mg, Cr and Ni, but have Cr/Ni ratios and incompatible element abundances typical of arc-type volcanic rocks, suggesting their derivation by a subduction-like process. The FeO^*/MgO and Al_2O_3/TiO_2 ratios, the abundance of transition elements, and the high incompatible element contents of the high-Mg lavas require that they be generated from a previously undepleted mantle source. K_2O/TiO_2 ratios indicate chemical modification of the mantle source by a potassium-bearing hydrous fluid which was probably derived from dehydrating, subducted lithosphere.

The dominance of olivine and clinopyroxene and corresponding paucity of orthopyroxene and plagioclase in the high-Mg magmas is consistent with their derivation from undepleted mantle peridotite modified by hydrous fluids evolving from dehydrating lithosphere. Hydrous solutions containing K^+, Na^+ and Ca^{2+} enhance the stability of olivine and pyroxene relative to orthopyroxene and plagioclase respectively, by lowering the activity of SiO_2 (Ewart, 1979; Mysen, 1982). An increase in the activity of SiO_2 favours the crystallization of orthopyroxene following the reaction:

$$Mg_2SiO_2 + SiO_2 \rightleftharpoons 2MgSiO_3 + I/2\ O_2.$$

The only sample with orthopyroxene phenocrysts (33638) contains only a minor amount of olivine, which is in chemical disequilibrium with the melt. The dominance of orthopyroxene in this sample suggests that a lower oxidation state and higher activity of SiO_2 reduced the stability of olivine in the magma; high silica activity may imply a lower K_2O content of the magma (Ewart, 1979). Significantly, sample 33638 has the highest SiO_2 content and is the only non-high-K calc-alkalic high-Mg lava collected from the Amphlett Islands.

Variations in CaO content of olivine (Appendix 3) suggest that olivine crystallized under relatively constant temperature and pressure (Stormer, 1973) at moderate to deep levels within the lithosphere (Simkin and Smith, 1970). These interpretations are supported by the Al_2O_3 content of clinopyroxene in the high-Mg rocks. Since the Al_2O_3 content of clinopyroxene increases with increasing pressure of crystallization (Thompson, 1974), the moderately high and relatively consistent Al_2O_3 content of the clinopyroxene phenocrysts from the high-Mg lavas suggests that they formed at moderate lithospheric depths and that the parental magmas or magma chambers were either generated or existed at relatively similar depths throughout southeastern Papua New Guinea. Further, the similarity in clinopyroxene compositions in all of the high-Mg rocks suggests the existence of a relatively uniform source region for magma generation

throughout southeastern Papua New Guinea since the bulk composition of the melt is also a controlling factor in the composition of clinopyroxene (Campbell and Borley, 1974). It is important to remember that, although there is very little variation in the chemical composition of individual phenocrysts within any of the phenocryst species which characterize the high-Mg lavas, the abundances of certain trace elements, most notably the rare earth elements, may vary markedly between the lavas, even when erupted from the same vent or cluster of vents (e.g., see samples 125806 and 125834 in Appendix 3).

Weak to moderate negative cerium and europium anomalies occur in a few of the chondrite normalized REE patterns for andesitic rocks of the northern volcanic belt (Fig. 4.41). Cerium was analysed by X-ray fluorescence spectrometry and neutron activation and the analytical results of these methods compared favourably (see Appendix 3). However, there is some question as to the extent of the Ce anomalies because of uncertainty in the accuracy of praseodymium analyses. There is no apparent reason to suspect the validity of the Eu_{CN} anomalies.

There are several possible causes for both the Ce and Eu anomalies. Negative europium anomalies are characteristic of crystal fractionation of several minerals, in particular plagioclase (Henderson, 1984), but extensive fractionation did not enter into the petrogenesis of the high-Mg rocks (see below). Negative cerium anomalies are less common, and most commonly related to hydrothermal alteration or weathering (Fleet, 1984), but all of the rocks analysed for petrogenetic purposes were unaltered and unweathered. One possibility is that both the negative Ce and negative Eu anomalies were inherited from subducted seawater or ocean floor sediments (see Fig. 4.41).

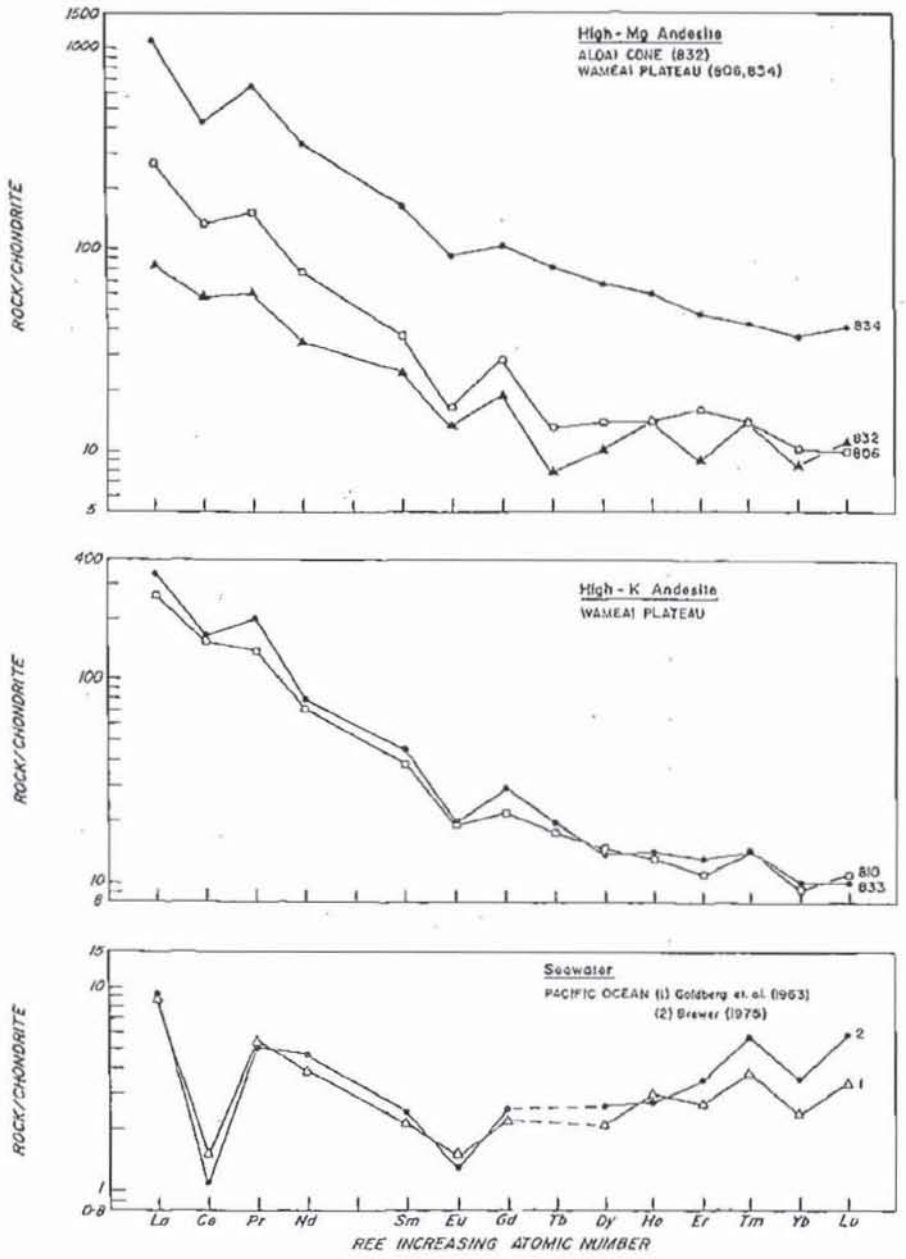

Figure 4.41. Chondrite normalized rare earth element abundance patterns for andesitic rocks from the northern volcanic belt of the east Papuan volcanic province and for Pacific Ocean sea water.

Delayed Magmatism

Although there is a continuing moderate level of arc-type volcanic activity in the east Papuan volcanic province (Smith, 1981), there is no suggestion of active subduction in the present-day pattern of seismicity. However, there is no doubt that after the late Mesozoic the area underwent major convergence which has resulted in crustal thickening. In order to resolve the apparent contradictions, Johnson et al. (1978b) and Smith

(1982) suggested that active subduction is not necessarily an immediate precondition for the type of magmatism seen in southeastern Papua New Guinea, but that it may be the result of partial melting of a source which was generated during an earlier convergent event. This delayed magmatism model resolves the apparent conflict in the juxtaposition of late Cenozoic magmatic associations (Smith et al., 1977), and explains the occurrence of young, typically arc-type volcanic rocks in an area not undergoing active plate convergence. Similar petrogenetic models have been proposed for the Indonesian Banda arc (Silver et al., 1985) and the northern New Hebrides arc (Barsdell et al., 1982).

Contamination

Arculus et al. (1983) have argued convincingly that high MgO, Cr and Ni in some of the lavas forming Mount Lamington in the northern volcanic belt of southeastern Papua New Guinea are the result of contamination from the subjacent Papuan Ultramafic Belt. They cite the presence of ultramafic mineral clusters in the rocks and present numerical models in support of the hypothesis. Mafic mineral clusters also occur in some of the high-Mg lavas in the D'Entrecasteaux Islands, but petrographic and geochemical data indicate that in this case the mineral clusters are comagmatic in origin (autoliths). Olivine and pyroxene contained in the mineral clusters are optically and compositionally identical to the phenocrysts with which they occur, and no remnant metamorphic textures were found which would suggest that olivine or pyroxene were derived from underlying ultramafic tectonites. Normal and reverse chemical zoning (Mg/Mg+Fe), albeit minor, are characteristic features of the larger crystals of olivine and pyroxene whether they occur in clusters or as phenocrysts. I interpret these data to indicate that the olivine and pyroxene are magmatic in origin. The compositional range and extent of chemical zoning of olivine and pyroxene in the high-Mg lavas are similar, however, to those of the same minerals

in the ultramafic cumulates from the Papuan Ultramafic Belt (England and Davies, 1973). Thus contamination remains a possibility, but ultramafic cumulates comprise less than 10 percent of the Papuan Ultramafic Belt (England and Davies, 1973) and it is unlikely that their spatial distribution is as extensive as that of the high-Mg lavas. Further, the Al_2O_3 content of clinopyroxene contained in the high-Mg lavas (0.8 to 7.1 wt %) is significantly higher than that of clinopyroxene in the ultramafic cumulates (0.8 to 2.6 wt %). Finally, the overlapping compositions for most chemical components of the lavas and the separation of the compositional trends into two discrete groups on a MgO-SiO_2 plot would not be expected if the high magnesium contents in the lavas were the result of a random process such as contamination. Only one of the analysed samples (33639) from the northern volcanic belt contained an ultramafic xenolith, and this lava is not magnesium-rich. I propose that contamination cannot be a general explanation for the occurrence of high-Mg lavas in southeastern Papua New Guinea.

Fractional Crystallization

The high MgO, Cr, Ni and Mg-numbers of relatively aphyric (high-Mg) lavas preclude significant fractionation of the mafic phases. Preliminary geochemical modelling indicates that the high-Mg lavas are not the result of high-pressure fractionation (R.L. Nielsen, written communication). It is, therefore, unlikely that the high-Mg lavas have evolved from a "normal" series by low-pressure fractionation. However, an important consideration in regard to a general petrogenetic model for the formation of the northern volcanic belt is that the petrographic data and preliminary geochemical modelling (R.L. Nielsen, written communication) do permit the derivation of the "normal" arc-type lavas from high-Mg parent magmas by high-pressure crystal fractionation. As noted earlier (see section entitled Northern Volcanic Belt) the only significant difference between the high-Mg lavas

and the "normal" calc-alkalic lavas is the higher abundance of MgO, Cr, and Ni in the former. It was also shown in the section on Petrology of the High-Mg Lavas that these elements are concentrated in olivine and pyroxene phenocrysts, and therefore, fractionation of these phases would substantially lower the MgO, Cr and Ni content of the resulting magma. Microprobe analyses indicate that the chemical compositions of olivine and pyroxene phenocrysts in the "normal" calc-alkalic lavas are similar and, in many examples, identical to those of the high-Mg lavas (Fig. 4.42; Appendix 3). Reaction textures indicate that in most cases the mafic phenocrysts in the "normal" series rocks are not in equilibrium with the host magma. The presence of negative europium anomalies in the chondrite normalized REE patterns for some of the unaltered and unweathered "normal" series andesitic lavas suggests that plagioclase fractionation has occurred. The size of the negative Eu anomaly increases significantly for dacite compositions. These observations support the hypothesis that the "normal" series rocks were derived from high-Mg parental magmas by crystal fractionation.

Crystal Accumulation

The accumulation of olivine and pyroxene by crystal settling is a viable means of increasing the MgO, Cr and Ni content of a magma. The occurrence of mafic autoliths in some of the high-Mg lavas from the east Papuan volcanic province supports this hypothesis. However, on the basis of petrographic evidence and Fe-Mg exchange partitioning, the olivine (Fo_{-87}) and clinopyroxene contained in the high-Mg lavas were in equilibrium with a melt composition equivalent to the erupted whole rock composition. This observation implies that minimal crystal accumulation (or fractionation) occurred. Further, Mg-numbers in the range of 66 to 75 are similar to those of a melt that was in equilibrium with the upper mantle (Wass, 1980).

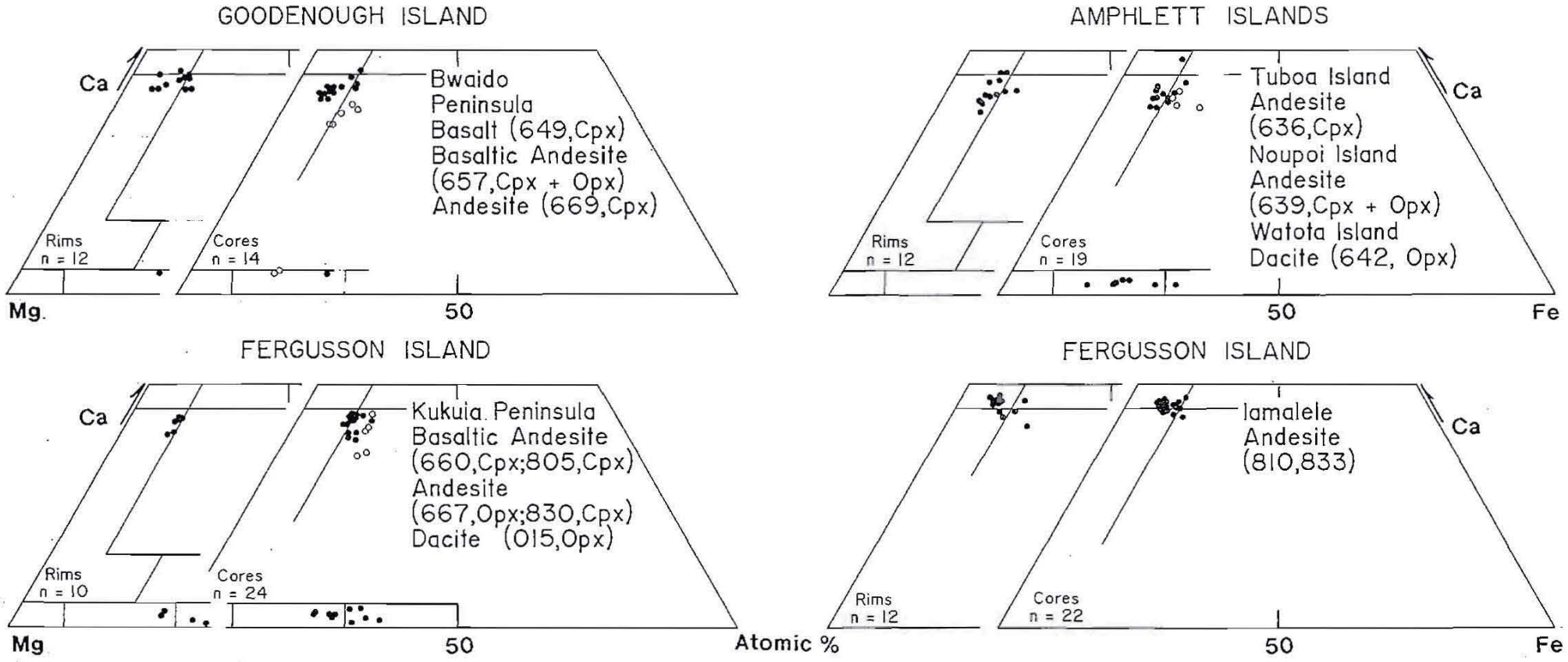

Figure 4.42. Composition of pyroxene in "normal" series calc-alkalic andesitic lavas from the northern volcanic belt of the east Papuan volcanic province. All of the rocks represented on the diagram contain <6.0 wt % MgO, but have variable Cr and Ni contents ranging in abundance from levels expected for the high-Mg rocks (320 ppm Cr and 164 ppm Ni) to values of 15 ppm Cr and 14 ppm Ni (see Appendix 3 for additional data).

Two Component Mixing

If the mafic phases, melt and upper mantle are in equilibrium, then a two component mixing hypothesis comparable to the restite model for the origin of granites may be applicable. Two component mixing is not contamination by pre-existing material but the mixing of a partial melt with components of the crystalline residuum with which it is in equilibrium. The mixing process offers a way by which chemical components which are normally not associated can become correlated. If the high MgO, Cr and Ni content of the high-Mg lavas is related to inclusion of residual source material, then the incompatible element content of the melt fraction is independent of the Ni and Cr content of the whole rock (melt plus some crystalline residuum). The major argument against two component mixing is that the olivine and pyroxene crystals appear to be of magmatic origin based on (1) the existence of chemical zoning and (2) the occurrence of chromite, spinel and rare clinopyroxene inclusions in olivine, and olivine and rare spinel inclusions in clinopyroxene.

Primary Magma

Whole-rock and mineral chemical compositions of high-Mg lavas indicate that olivine and clinopyroxene phenocrysts have crystallized from a melt with approximately the composition of their hosts, and that both could have equilibrated with a mantle source. The primitive nature of the lavas is also reflected in the common occurrence of chromite inclusions in olivine, the occurrence of chromite microphenocrysts in some samples, and the near MORB values for FeO^*/MgO, Al_2O_3/TiO_2 and CaO/TiO_2 ratios. However, comparatively high K_2O/TiO_2 ratios and incompatible element concentrations indicate the involvement of a more evolved source. The relative abundance of REE and enrichment of LREE is consistent with calculated trends for small volume partial melts (batch melting) of garnet lherzolite (Hanson, 1980). These data suggest that the high-Mg lavas represent initial

(primary) magmas generated by hydrous partial melting of undepleted upper mantle or of subduction-modified mantle.

Conclusions

Analysis of MgO-SiO_2 covariance in the suite of rocks from the northern volcanic belt in southeastern Papua New Guinea has allowed the empirical derivation of a discriminant line separating relatively magnesium-rich rocks from the remainder of the suite. In all of the arc-type settings in Papua New Guinea for which data are available, high-Mg lavas form an integral part of the volcanic associations and cannot be separated as a temporally or spatially distinct event. The high-Mg lavas, at least locally, form a significant component of all of the main arc-type associations in which they occur. These observations must be incorporated into any general theory for the origin of magmas in convergent plate tectonic settings.

Saunders et al. (1987) noted that in all known instances the generation of high-Mg magmas may be related to high heat flow associated with subduction of young ocean lithosphere (e.g., ridge subduction). The work in southeastern Papua New Guinea discussed in this section documents the occurrence of high-Mg lavas in a region where subduction or attempted subduction of a spreading centre is not a factor in palaeotectonic reconstructions. I consider the high-Mg magmas to have formed from a subduction-modified mantle source in response to incipient tensional stresses associated with the westward migration of spreading in the Woodlark Basin (Luyendyk et al., 1973). The existence of intercalated high-Mg and "normal" arc-type lavas indicates that some of the primary magmas rose rapidly to the surface and retained their initial chemical signature, whereas others rose more slowly, permitting crystal fractionation to occur prior to eruption. The genesis of high-Mg lavas in other areas also may be related to tensional environments. Clearly, in several of the high-Mg

lava localities cited earlier extension is at least a transient feature of the tectonic setting.

REFERENCES CITED

Albers, J.P., 1967, Belt of sigmoidal bending and right-lateral faulting in the western Great Basin: Geological Society of America Bulletin, v. 78, p. 143-156.

Allis, R.G., 1979, Thermal history of the Karapiti area, Wairakei: New Zealand Division of Scientific and Industrial Research Geophysics Division Report 137, 38 p.

--- 1981, Changes in heat flow associated with exploitation of Wairakei geothermal field, New Zealand: New Zealand Journal of Geology and Geophysics, v. 24, p. 1-19.

--- 1982a, Geologic controls on shallow hydrologic changes at Wairakei Field: Proceedings of the Pacific Geothermal Conference 1982 incorporating the 4th New Zealand Geothermal Workshop, Part 1, Auckland, p. 139-144.

--- 1982b, Wairakei geothermal field: heat flow, *in* DSIR Geothermal Coordination Group, ed., Geothermal developments in New Zealand - background papers for participants on the Pacific Geothermal Conference Tours: Geothermal Institute, University of Auckland, p. 94-97.

Allis, R.G., and Webber, S., 1984, Shallow temperature measurements at Wairakei and Broadlands fields: New Zealand Department of Scientific and Industrial Research Geophysics Division Report No. 197, 27 p.

Aoki, K., and Fujimaki, H., 1982, Petrology and geochemistry of calc-alkaline andesite of presumed upper mantle origin from Itinomegata, Japan: American Mineralogist, v. 67, p. 1-3.

Arculus R., Johnson, R.W., Chappell, B.W., McKee, C.O., and Sakai, H., 1983, Ophiolite-contaminated andesites, trachybasalts and cognate inclusions of Mount Lamington Papua New Guinea: anhydrite-amphibole bearing lavas and the 1951 cumulodome: Journal of Volcanology and Geothermal Research, v. 4, p. 215-247.

Baird, H.F., 1951, Geothermal project report of aeromagnetic surveys of the Wairakei-Taupo thermal area conducted by magnetic survey Christchurch: Department of Scientific and Industrial Research, unpublished report, 2 p.

Banwell, C.J., 1955, Physical investigations, *in* Grange, L.I., compiler, Geothermal steam for power in New Zealand: New Zealand Geological Survey Bulletin 117, chapter 6, p. 45-74.

Banwell, C.J., Cooper, E.R., Thompson, G.E.K., and McCree, K.J., 1957, Physics of the New Zealand thermal area: New Zealand Department of Scientific and Industrial Research Bulletin 123, 110 p.

Banwell, C.J., and MacDonald, W.J.P., 1965, Resistivity surveys in New Zealand thermal areas: Proceeding of the 8th Commonwealth Mining and Metallurgical Congress Paper 213, p. 1-7.

Banwell, C.J., and Thompson, G.E.K., 1959, Changes in natural thermal activity near the Karapiti area, Wairakei: Department of Scientific and Industrial Research Thermal Laboratory unpublished report, 7 p.

Barsdell, M., Smith, I.E.M., and Sporli, K.B., 1982, The origin of reversed geochemical zoning in the northern New Hebrides volcanic arc: Contributions to Mineralogy and Petrology, v. 81, p. 148-155.

Barton, P.B., Jr. and Skinner, B.J., 1979, Sulfide mineral stabilities: *in* Barnes, H.L., ed., Geochemistry of hydrothermal ore deposits: John Wiley & Sons, p. 278-403.

Bean, R.E., 1974, Biotite stability in the porphyry copper environment: Economic Geology, v.69, p. 241-256.

--- 1982, Hydrothermal alteration in silicate rocks: *in* Titley, S.R., ed., Advances in geology of the porphyry copper deposits, southwestern North America: University of Arizona Press, Tucson, p.117-138.

Beck, A.C., and Robertson, E.I., 1955, Geology and geophysics, *in* Grange, L.I., compiler, Geothermal steam for power in New Zealand: New Zealand Geological Survey Bulletin 117, Chapter 2, p. 15-20.

Benseman, R.F., 1959, Estimating the total heat output of natural thermal regions: Journal of Geophysical Research, v. 62, p. 1057-1062.

Berger, B.R., 1988, Lithological and tectonic setting of epithermal gold-silver deposits in western North America: *in* Goode, A.D.T., and Bosma, L.I., compilers, Bicentennial Gold 88 Extended Abstracts Oral Programme: Geological Society of Australia Abstracts Series Number 22, p. 154-160.

Bird, D.K., and Norton, D.L., 1981, Theoretical prediction of phase relations among aqueous solutions and minerals: Salton Sea geothermal system: Geochimica et Cosmochimica Acta, v. 45, p. 1479-1493.

Bird, D.K., Schiffman, P., Elders, W.A., Williams, A.E., and McDowell, S.D., 1984, Calc-silicate mineralization in active geothermal systems: Economic Geology, v. 79, p. 671-695.

Bjornsson, S., Arnorsson, S., and Tomasson, J., 1970, Exploration of the Reykjanes thermal brine area: Geothermics (Special Issue 2), v.2 (Pt. 2), p. 1640-1650.

Black, J.E., 1988, Mineralization and high-temperature alteration at the Rawhide Au-Ag deposit, Mineral County, Nevada: Unpublished M.S. thesis, Stanford University, Stanford, California, U.S.A., 101 p.

Black, J.E., Mancuso, T.K., and Gant, J.L., 1991, Geology and mineralization at the Rawhide Au-Ag deposit, Mineral County, Nevada, *in* Raines, G.L., Lisle, R.E., Shafer, R.W., and Wilkinson, W.H., Geology and Ore Deposits of the Great Basin Symposium Proceedings: Geologic Society of Nevada, Reno, Nevada, p. 1123-1144.

Boden, D.R., 1986, Eruptive history and structural development of the Toquima caldera complex, central Nevada: Geological Society of America Bulletin, v. 97, p. 61-74.

Bolton, R.S., 1970, The behaviour of Wairakei geothermal field during exploitation: Proceedings of the United Nations Symposium on the Development and Utilization of Geothermal Resources, Pisa, Geothermics Special Issue 2, p. 1426-1436.

--- 1982, Fracturing in Wairakei geothermal field, New Zealand, *in* Fractures in geothermal reservoirs: Proceedings of the Geothermal Resources Council Workshop, Hawaii, 27-28 August, v. 12, p. 85-101.

Bowers, T.S., Jackson, K.J., and Helgeson, H.C., 1984, Equilibrium activity diagrams for coexisting minerals and aqueous solutions at pressures and temperatures to 5 kb and 600 C: Springer-Verlag, Berlin, 397 p.

Briggs, N.D., 1976, Welding and crystallisation zonation in Whakamaru Ignimbrite, Central North Island, New Zealand: New Zealand Journal of Geology and Geophysics, v. 19, p. 189-212.

Brimhall, G.H., 1977, Early fracture-controlled disseminated mineralization at Butte, Montana: Economic Geology, v. 72, p. 37-59.

Brown, K.L., 1986, Gold deposition from geothermal discharges in New Zealand: Economic Geology, v. 81, p. 979-983.

--- 1988, Kinetics of gold precipitation from hydrothermal solutions, *in* Goode, A.D.T., and Bosma, L.I., compilers, Bicentennial Gold 88 Extended Abstracts Oral Program: Geological Society of Australia Abstracts Series Number 22, p. 199-204.

Browne, P.R.L., 1969, Sulfide mineralization in a Broadlands geothermal drill hole, Taupo volcanic zone, New Zealand: Economic Geology, v. 64, p. 156-159.

--- 1973, The geology, mineralogy and geothermometry of the Broadlands Geothermal Field, Taupo Volcanic Zone, New Zealand: Unpublished Ph.D. dissertation, Victoria University, Wellington, New Zealand.

--- 1984, Subsurface stratigraphy and hydrothermal alteration of the eastern section of the Olkaria geothermal field, Kenya: Proceedings of the 6th New Zealand Geothermal Workshop 1984, University of Auckland Geothermal Institute in conjunction with the Centre for Continuing Education, p. 33-42.

Browne, P.R.L., and Ellis, A.J., 1970, The Ohaki-Broadlands hydrothermal area, New Zealand: mineralogy and related geochemistry: American Journal of Science, v. 269, p. 97-131.

Bruce, J.A., and Shorland, F.B., 1932, Utilisation of natural heat resources in thermal regions: New Zealand Journal of Agriculture, v. 45, 272-278.

Buddington, A.F., and Lindsley, D.H., 1964, Iron-titanium oxide minerals and synthetic equivalents: Journal of Petrology, v. 5, p. 310-357.

Cameron, W.E., 1985, Petrology and origin of primitive lavas from the Troodos ophiolite, Cyprus: Contributions to Mineralogy and Petrology, v. 89, p. 239-255.

Campbell, I.H., and Borley, G.D., 1974, The geochemistry of pyroxenes from the lower layered series of the Jimberlana Intrusion, Western Australia: Contributions to Mineralogy and Petrology, v. 47, p., 281-297.

Carmichael, I.S.E., 1967, The iron-titanium oxides of salic volcanic rocks and their associated ferromagnesian silicates: Contributions to Mineralogy and Petrology, v. 14, p. 36-64.

Cathles, L.M., 1977, An analysis of the cooling of intrusives by ground-water convection which includes boiling: Economic Geology, v. 72, p. 804-826.

Chen, C.H., 1970, Geology and geothermal power potential of the Tatun volcanic region: Geothermics (Special Issue 2), v. 2 (Pt. 2), p. 1134-1143.

Christenson, B.W., 1987, Fluid-mineral equilibria in the Kawerau hydrothermal system, Taupo volcanic zone, New Zealand: Unpublished Ph.D. dissertation, University of Auckland, Auckland, New Zealand.

Christiansen, R.L., 1979, Cooling units and composite sheets in relation to caldera structure: Geological Society of America Special Papers, v. 180, p. 29-42.

Cole, D.R., and Ravinsky, L.I., 1984, Hydrothermal alteration zoning in the Beowawe geothermal system, Eureka and Lander Counties, Nevada: Economic Geology, v. 79, p. 759-767.

Cole, J.W., 1979, Structure, petrology and genesis of Cenozoic volcanism, Taupo Volcanic Zone, New Zealand--a review: New Zealand Journal of Geology and Geophysics, v. 22, p. 631-657.

--- 1984, Taupo-Rotorua Depression: an ensialic marginal basin of North Island, New Zealand, *in* Kokelaar, B.P., and Howells, M.F., eds., Marginal basin geology: volcanic and associated sedimentary and tectonic processes in modern and ancient marginal basins: Special Publication of the Geological Society of London, v. 16, p. 109-120.

--- 1986, Distribution and tectonic setting of late Cenozoic volcanism in New Zealand, *in* Smith, I.E.M., ed., Late Cenozoic volcanism in New Zealand: Wellington, Royal Society of New Zealand Bulletin 23, p. 7-20.

--- 1989, Crustal structure and volcanism in the Taupo volcanic zone, New Zealand *in* Continental magmatism abstracts: New Mexico Bureau of Mines and Mineral Resources Bulletin 131, p. 55.

Cole, J.W., and Lewis, K.B., 1981, Evolution of the Taupo - Hikurangi subduction system: Tectonophysics, v. 72, p. 1-21.

Coombs, D.S., Ellis, A.J., Fyfe, W.S., and Taylor, A.M., 1959, The zeolite facies, with comments on the interpretation of hydrothermal syntheses: Geochimica et Cosmochimica Acta, v. 17, p. 53-107.

Cox, K. G., and Bell, J.D., 1972, A crystal fractionation model for basaltic rocks of the New Georgia Group, British Solomon Islands: Contributions to Mineralogy and Petrology, v. 37, p. 1-13.

Craig, H., 1963, The isotopic geochemistry of water and carbon in geothermal areas, *in* Nuclear geology in geothermal areas: Spoleto Conference on Nuclear Geology in Geothermal Areas, p. 95-138.

Cullington, A.L., 1954, The geothermal field in New Zealand at epoch 1950.5: New Zealand Department of Scientific and Research Memorandum no. 2.

Curtis, J.W., 1973, Plate tectonics and the Papua New Guinea-Solomon Islands region: Geological Society of Australia Journal, v. 20, p. 21-36.

Davies, H.L., 1969, Normanby Island reconnaissance petrography: Australia Bureau of Mineral Resources Record 1969/46 (unpublished).

--- 1973, Fergusson Island, Papua New Guinea: Bureau of Mineral Resources, Geology and Geophysics, 1:250,000 Geological Series--Explanatory Notes, Sheet SC/56-6, 25 p.

--- 1980, Crustal structure and emplacement of ophiolite in southeastern Papua New Guinea: *in* Allegre, C.J., et al., conveners, Orogenic mafic-ultramafic association: Colloques Internationaux du Centre National de la Recherche Scientifique, Paris, no. 272, p. 17-33.

Davies, H.L., and Ives, D.J., 1965, The geology of Fergusson and Goodenough Islands, Papua: Australian Bureau of Mineral Resources, Geology and Geophysics Report No. 82, 65 p.

Davies, H.L., and Smith, I.E., 1971, Geology of eastern Papua: Geological Society of America Bulletin, v. 82, p. 3299-3312.

Davies, H.L., and Smith, I.E.M., 1976, Geology of the southeast Papuan mainland: Australian Bureau of Mineral Resources, Geology and Geophysics Bulletin 165, 86 p.

Davies, H.L., Symonds, P.A., and Ripper, I.A., 1984, Structure and evolution of the southern Solomon Sea region: Bureau of Mineral Resources Journal of Australian Geology and Geophysics, v. 9, p. 49-68.

Davies, R.M., and Ballantyne, G.H., 1987, Geology of the Ladolam gold deposit Lihir Island, Papua New Guinea: Proceedings of the Australasian Institute of Mining and Metallurgy Pacific Rim Congress 87, 26-29 August, Gold Coast, Queensland, Australia, p. 943-949.

Dawson, G.B., and Dickinson, D.J., 1970, Heat flow studies in thermal areas of the North Island of New Zealand: Proceedings of the United Nations Symposium on the Development and Utilization of Geothermal Resources, Pisa, Geothermics Special Issue 2, p. 466-474.

Dawson, G.B., and Fisher, R.G., 1964, Diurnal and seasonal ground temperature variations at Wairakei: New Zealand Journal of Geology and Geophysics, v. 7, p. 144-154.

Dilles, J.H., 1983, Petrology and geochemistry of the Yerington batholith and the Ann-Mason porphyry copper deposit, western Nevada: Unpublished Ph.D. dissertation, Stanford University, Stanford, California, U.S.A., 389 p.

Dobson, P.F.,1986, The petrogenesis of boninite: a field, petrologic, and geochemical study of the volcanic rocks of Chichi-Jima, Bonin Islands, Japan: Unpublished Ph.D. dissertation, Stanford University, Stanford, California, U.S.A., 163 p.

Dondanville, R.F., 1978, Geological characteristics of the Valles Caldera geothermal system, New Mexico: Geothermal Resources Council Transactions, v. 2, p. 157-160.

Economides, M.J., Ehlig-Economides, C.A., Koutroupis, N., Speliotis, G., Ungemach, P., and Vrouzi, R., 1983a, Preliminary assessment of the geology and reservoir characteristics of the geothermal field on Nisyros Island, Greece: Proceedings of the 5th New Zealand Geothermal Workshop 1983, University of Auckland, p. 31-33.

Economides, M.J., Ehlig-Economides, C.A., Spelioti, G., and Vrouzi, R., 1983b, Resource evaluation and development plans for a 120 MW geothermal power plant on Milos Island, Greece: Proceedings of the 5th New Zealand Geothermal Workshop 1983, University of Auckland, p. 35-42.

Edwards, A.K.M., 1950, Report on investigation of sulphur deposits, Iamalele-Fagalulu district, Fergusson Island: Bureau of Mineral Resources of Australia Record 1950, 29 p.(unpublished).

Ekren, E.B., and Byers, F.M., Jr., 1986, Geologic map of the Murphys Well, Pilot Cone, Copper Mountain, and Poinsettia Spring quadrangles, Mineral County, Nevada: U.S. Geological Survey Miscellaneous Investigations Series Map I-1576, scale 1:48,000.

Elder, J., 1981, Geothermal systems: London, Academic Press, 508 p.

Elders, W.A., Hoagland, J.R., and Olson, E.R., 1978, Hydrothermal mineralogy and isotopic geochemistry in the Cerro Prieto geothermal field, Mexico: Geothermal Resources Council Transactions, v. 2, p. 177-180.

Ellis, A.J., 1962, Interpretation of gas analysis from the Wairakei hydrothermal area: New Zealand Journal of Science, v. 5, p. 434-450.

--- 1969, Present-day hydrothermal systems and mineral deposition, *in* Jones, M.J., ed., Mining and petroleum geology: Institution of Mining and Metallurgy (London), Proceedings of the 9th Commonwealth Mining and Metallurgical Congress 1969, v.2, p. 211-240.

--- 1970, Quantitative interpretation of chemical characteristics of hydrothermal systems: Geothermics (Special Issue 2), v. 2, p. 516-528.

--- 1979, Explored geothermal systems: *in* Barnes, H.L., ed., Geochemistry of hydrothermal ore deposits, 2nd ed.: New York, John Wiley & Sons, p.632-683.

Ellis, A.J., and Giggenbach, W.F., 1971, Hydrogen sulfide ionization and sulfur hydrolysis in high temperature solutions: Geochimica et Cosmochimica Acta, v. 35, p. 247-260.

Ellis, A.J., and Mahon, W.A.J., 1966, Geochemistry of the Ngawha hydrothermal area: New Zealand Journal of Science, v. 9, p. 440-456.

--- 1967, Natural hydrothermal systems and experimental hot-water/rock interactions (Part II): Geochimica et Cosmochimica Acta, v. 31, p. 519-539.

--- 1977, Chemistry and geothermal systems: New York, Academic Press, 392 p.

--- 1982, Wairakei geothermal field: chemistry, *in* DSIR Geothermal Coordination Group, ed., Geothermal developments in New Zealand - background papers for participants on the Pacific Geothermal Conference Tours: Geothermal Institute, University of Auckland, p. 97-104.

Ellis, A.J., and Wilson, S.H., 1955, The heat from the Wairakei-Taupo thermal region calculated from the chloride output: New Zealand Journal of Science and Technology, v. B36, p. 622-631.

--- 1960, The geochemistry of alkali metal loss in the Wairakei hydrothermal system: New Zealand Journal of Geology and Geophysics, v. 3, p. 593-617.

England, R.N., and Davies, H.L., 1973, Mineralogy of ultramafic cumulates and tectonites from eastern Papua: Earth and Planetary Science Letters, v. 17, p. 416-425.

Eslinger, E.V., and Savin, S.M., 1973, Mineralogy and oxygen isotope geochemistry of the hydrothermally altered rocks of the Ohaki-Broadlands, New Zealand geothermal area: American Journal of Science, v. 273, p. 240-267.

Ewart, A., 1965, Mineralogy and petrogenesis of the Whakamaru Ignimbrite in the Maraetai area of the Taupo Volcanic Zone, New Zealand: New Zealand Journal of Geology and Geophysics, v. 8, p. 611-677.

--- 1979, A review of the mineralogy and chemistry of Tertiary-Recent dacitic, latitic, rhyolitic, and related salic volcanic rocks, *in* Barker, F., ed., Trondhjemites, dacites and related rocks: Amsterdam, Elsevier, p. 13-121.

Faure, G., 1986, Principles of isotope geology, 2nd ed.: New York, John Wiley & Sons, 589 p.

Fauzi, A., 1989, Composition of hydrothermal igneous biotites, and their occurrence in borehole no. 1, Dieng, Indonesia: *in* Browne, P.R.L., and Nicholson, K., eds., Proceedings of the 11th New Zealand Geothermal Workshop 1989, University of Auckland, p. 301-303.

Field, C.W., and Fifarek, R.H., 1984, Light stable-isotope systematics in the epithermal environment, *in* Berger, B.R., and Bethke, P.M., eds., Geology and geochemistry of epithermal systems: Reviews in Economic Geology, v. 2, p. 99-128.

Fisher, R.G., 1964, Geothermal heat flow at Wairakei during 1958: New Zealand Journal of Geology and Geophysics, v. 7, p. 128-184.

Fisher, W.M., 1955, Production of steam from drill holes at Wairakei, *in* Grange, L.I., compiler, Geothermal steam for power in New Zealand: New Zealand Geological Survey Bulletin 117, Chapter 7, p. 75-102.

Fleet, A.J., 1984, Aqueous and sedimentary geochemistry of the rare earth elements, *in* Henderson, P., ed., Rare earth element geochemistry: Amsterdam, Elsevier, p. 343-373.

Fournier, R.O., 1981, Application of water geochemistry to geothermal exploration and reservoir engineering, *in* Ryback, L., and Muffler, L.J.P., eds., Geothermal systems: principles and case histories: New York, John Wiley & Sons, p. 109-143.

--- 1985, Carbonate transport and deposition in the epithermal environment: *in* Berger, B.R., and Bethke, P.M., Geology and geochemistry of epithermal systems: Reviews in Economic Geology, v.2, p. 63-72.

Fournier, R.O., and Truesdell, A.H., 1973, An empirical Na-K-Ca geothermometer for natural waters: Geochimica et Cosmochimica Acta, v. 37, p. 1255-1275.

Froggatt, P.C., 1983, Toward a comprehensive Upper Quaternary tephra and ignimbrite stratigraphy in New Zealand using electron microprobe analysis of glass shards: Quaternary Research, v. 19, p.188-200.

Gant, J.L., 1986, Geologic report, Rawhide West, Mineral County, Nevada: Unpublished report, Kennecott Exploration, 14 p.

Gerard, V.B., and Lawrie, J.A., 1955, Aeromagnetic surveys in New Zealand, 1949-1952. Geophysical Memoir 3: Wellington, New Zealand Department of Scientific and Industrial Research.

Ghiorso, M.S., and Carmichael, I.S.E., 1981, A Fortran IV computer program for evaluating temperatures and oxygen fugacities from the compositions of coexisting iron-titanium oxides: Computers & Geosciences, v. 7, p. 123-129.

Giggenbach, W.F., Gonfiantini, R., Jangi, B.L., and Truesdell, A.H., 1983, Isotopic and chemical composition of Parbati Valley geothermal discharges, NW Himalaya, India: Geothermics, v. 12, p. 199-222.

Glover, R.B., 1970, Interpretation of gas compositions from the Wairakei field over 10 years: Proceedings of the United Nations Symposium on the Development and Utilization of Geothermal Resources, Pisa, Geothermics Special Issue 2, p. 1355-1366.

--- 1971, Interpretation of gas compositions from the Wairakei Field over 10 years: Geothermics (Special Issue 2), v. 2(2), p. 1355-1366.

--- 1977, Chemical and physical changes at Geyser Valley, Wairakei, and their relationship to changes in borefield performance: New Zealand Department of Scientific and Industrial Research Bulletin 218, p. 19-26.

Goles, G.G., 1967, Trace elements in ultramafic rocks, *in* Wyllie, P.J., ed., Ultramafic and related rocks: New York, John Wiley & Sons, p. 352-262.

Graham, I.J., and Hackett, W.R., 1987, Petrology of calc-alkaline lavas from Ruapehu Volcano and related vents, Taupo Volcanic Zone, New Zealand: Journal of Petrology, v. 28, p. 531-567.

Grange, L.I., 1937, The geology of the Rotorua-Taupo subdivision, Rotorua and Kaimanawa divisions: New Zealand Geological Survey Bulletin, v. 37, 138 p.

--- 1955, Introduction, *in* Grange, L.I., compiler, Geothermal steam for power in New Zealand: New Zealand Geological Survey Bulletin 117, Chapter 1, p. 9-14.

Grant, M.A., 1977, Two-phase linear geothermal pressure transients - a comparison with single-phase transients: Society of Petroleum Engineers Paper SPE 6972.

--- 1979, Interpretation of downhole measurements in geothermal wells: New Zealand Department of Scientific and Industrial Research Applied Mathematics Division Report No. 88, 66 p.

--- 1980, Notes on the Wairakei wells 1-63: New Zealand Department of Scientific and Industrial Research, Geothermal Circular MAG28, 42 p.

--- 1982, The recharge to the Wairakei reservoir: Proceedings of the Pacific Geothermal Conference, Auckland University.

--- 1984, Preliminary modelling of Wairakei reinjection: Unpublished New Zealand Department of Scientific and Industrial Research Applied Mathematics Division Report, 18 p.

Grant, M.A., and Horne, R.N., 1980, The initial state and response to exploitation of Wairakei geothermal field: Transactions of the Geothermal Resources Council, v. 4, p. 333-336.

Grapes, R.H., Sissons, B.A., and Wellman, H.W., 1987, Widening of the Taupo Volcanic Zone, New Zealand, and the Edgecumbe earthquake of March 1987: Geology, v. 15, p. 1123-1125.

Gregg, D.R., 1958, Natural heat flow from the thermal areas of the Taupo sheet district: New Zealand Journal of Geology and Geophysics, v. 1, p. 65-75.

Grindley, G.W., 1959, Geologic map of New Zealand 1:63,360, Sheet N85-Waiotapu. New Zealand Department of Scientific and Industrial Research, Wellington.

--- 1965, The geology, structure, and exploitation of the Wairakei geothermal field, Taupo, New Zealand: New Zealand Geological Survey Bulletin no. 75, 131 p.

--- 1982, The deeper structure of the Wairakei geothermal field: Proceedings of the Pacific Geothermal Conference 1982 incorporating the 4th New Zealand Geothermal Workshop, Part 1, p. 69-74.

Hamilton, W., 1979, Tectonics of the Indonesian region: U.S. Geological Survey Professional Paper 1078, p. 293-304.

Hanson, G.N., 1980, Rare earth elements in petrogenetic studies of igneous systems: Annual Review of Earth and Planetary Science Letters, v. 8, p. 371-406.

Hanson, G.N., and Langmuir, C.H., 1978, Modelling of major elements in mantle-melt systems using trace element approaches: Geochimica et Cosmochimica Acta, v. 42, p. 725-741.

Hatherton, T., MacDonald, W.J.P., and Thompson, G.E.K., 1966, Geophysical methods in geothermal prospecting in New Zealand: Bulletin of Volcanology, v. 29, p. 485-497.

Hayba, D.O., Bethke, P.M., Heald, P., and Floey, N.K., 1985, Geologic, mineralogic, and geochemical characteristics of volcanic-hosted epithermal precious-metal deposits: *in* Berger, B.R., and Bethke, P.M., eds., Geology and geochemistry of epithermal systems: Reviews in Economic Geology, v. 2, p. 129-167.

Healy, J., 1956, Preliminary account of hydrothermal conditions at Wairakei, New Zealand: Proceedings of the 8th Pacific Science Congress, p. 214-217.

--- 1962, Structure and volcanism in the Taupo Volcanic Zone, New Zealand: Crust of the Pacific Basin, American Geophysical Union, Geophysical Monograph no. 6, p. 151-157.

--- 1964, Geothermal energy: New Zealand Engineering, v. 19, p. 55-60.

--- 1984, Wairakei geothermal field in review: New Zealand Geological Survey Geothermal Circular JH/10, 53 p.

Healy, J., and Mahon, W.J.A., 1982, Kawah Kamojang geothermal field, West Java: Proceedings of the Pacific Geothermal Conference 1982 incorporating the 4th New Zealand Geothermal Workshop 1982, Part 2, University of Auckland, p. 313-319.

Hedenquist, J.W., 1983, Waiotapu, New Zealand: the geochemical evolution and mineralization of an active hydrothermal system: Unpublished Ph.D. dissertation, University of Auckland, Auckland, New Zealand, 242 p.

Hedenquist, J.W., and Henley, R.W., 1985, The importance of CO_2 on freezing point measurements of fluid inclusions: evidence from active geothermal systems and implications for ore deposition: Economic Geology, v. 80, p. 1379-1406.

Helgeson, H.C., 1968, Geologic and thermodynamic characteristics of the Salton Sea geothermal system: American Journal of Science, v. 266, p. 129-166.

--- 1969, Thermodynamics of hydrothermal systems at elevated temperatures and pressures: American Journal of Science, v. 267, p. 790-804.

Helgeson, H.C., Delany, J.M., Nesbitt, H.W., and Bird, D.K., 1978, Summary and critique of the thermodynamic properties of rock-forming minerals: American Journal of Science, v. 278-A, 229 p.

Hemley, J.J., 1967, Aqueous Na/K ratios in the systems K_2O-Na_2O-Al_2O_3-SiO_2-H_2O: Geological Society of America Abstracts with Programs, Annual Meeting, New Orleans, p. 94-95.

Hemley, J.J., Hostetler, P.B., Gude, A.J., and Mountjoy, W.T., 1969, Some stability relations of alunite: Economic Geology, v. 64, p. 599-612.

Henderson, P., ed., 1984, Rare earth element geochemistry: Amsterdam, Elsevier, 510 p.

Henley, R.W., 1984a, Chemical structure of the geothermal systems: *in* Henley, R.W., Truesdell, A.H., Barton, P.B., Jr. and Whitney, J.A., Fluid-mineral equilibria in hydrothermal systems: Reviews in Economic Geology, v. 1, p. 9-28.

--- 1984b, Hydrolysis reactions in hydrothermal fluids: *in* Henley, R.W., Truesdell, A.H., Barton, P.B., Jr. and Whitney, J.A., Fluid-mineral equilibria in hydrothermal systems: Reviews in Economic Geology, v. 1, p. 65-82.

--- 1984c, pH calculations for hydrothermal fluids: *in* Henley, R.W., Truesdell, A.H., Barton, P.B., Jr. and Whitney, J.A., Fluid-mineral equilibria in hydrothermal systems: Reviews in Economic Geology, v. 1, p. 83-98.

--- 1985, The geothermal framework of epithermal deposits: *in* Berger, B.R., and Bethke, P.M., eds., Geology and geochemistry of epithermal systems: Reviews in Economic Geology, v. 2, p. 1-24.

Henley, R.W., and Berger, B.R., 1988, Advances in the understanding of epithermal precious-metal deposits: *in* Goode, A.D.T., and Bosma, L.I., compilers, Bicentennial Gold 88 extended abstracts oral programme: Geological Society of Australia Abstracts Series Number 22, p. 277-283.

Henley, R.W., and Brown, K.L., 1985, A practical guide to the thermodynamics of geothermal fluids and hydrothermal ore deposits: *in* Berger, B.R., and Bethke, P.M., Geology and geochemistry of epithermal systems: Reviews in Economic Geology, v. 2, p. 25-44.

Henley, R.W., and Ellis, A.J., 1983, Geothermal systems ancient and modern: a geochemical review: Earth Science Reviews, v. 19, p. 1-50.

Henley, R.W., Hedenquist, J.W., and Roberts, P.J, eds., 1986, Guide to the active epithermal (geothermal) systems and precious metal deposits of New Zealand: Berlin-Stuttgart, Monograph Series on Mineral Deposits, No. 26, 211 p.

Henley, R.W., Singers, W.A., Brown, K.L., and Finlayson, J.B., 1984, Analytical data for Wairakei well discharges and natural features, 1950-1982: New Zealand Department of Scientific and Industrial Research Report CD 2351, 197 p.

Henley, R.W., and Stewart, M.K., 1983, Chemical and isotopic changes in the hydrology of the Tauhara geothermal field due to exploitation at Wairakei: Journal of Volcanology and Geothermal Research, v. 15, p. 285-314.

Hoagland, J.R., and Elders, W.A., 1978, Hydrothermal mineralogy and isotopic geochemistry of Cerro Prieto geothermal field Mexico, I. Hydrothermal mineral zonation: Geothermal Resources Council Transactions, v. 2, p. 283-286.

Hochstein, M.P., 1982, Wairakei geothermal field: geophysical structure, *in* DSIR Geothermal Coordination Group, ed., Geothermal developments in New Zealand - background papers for participants on the Pacific Geothermal Conference Tours: Geothermal Institute, University of Auckland, p. 91-93.

Hochstein, M.P., Caldwell, G., and Kifle, K., 1983, Minimum age of the Aluto geothermal system (Ethiopia) from fossil temperatures beneath a deep lateral outflow: Proceedings of the 5th New Zealand Geothermal Workshop 1983, University of Auckland, p. 209-212.

Honda, S., and Muffler, L.J.P., 1970, Hydrothermal alteration in core from research drill hole Y-1, Upper Geyser Basin, Yellowstone National Park, Wyoming: American Mineralogist, v. 55. p. 1714-1737.

Humphris, S.E., 1984, The mobility of rare earth elements in the crust, *in* Henderson, P., ed., Rare earth element geochemistry: Amsterdam, Elsevier, p. 317-342.

Hunt, T.M., 1970, Gravity changes at Wairakei geothermal field, New Zealand: Geological Society of America Bulletin, v. 81, p. 529-536.

--- 1975, Repeat gravity measurements at Wairakei, 1961-1974: Department of Scientific and Industrial Research Geophysics Division Report 111.

--- 1977, Recharge of water in Wairakei geothermal field determined from repeat gravity measurements: New Zealand Journal of Geology and Geophysics, v. 20, p. 303-317.

Irvine, T.N., and Baragar, W.R.A., 1971, A guide to the chemical classification of the common volcanic rocks: Canadian Journal of Earth Sciences, v. 8, p. 523-548.

Jacobs, D.C., and Parry, W.T., 1976, A comparison of the geochemistry of biotite from some Basin and Range stocks: Economic Geology, v.71, p. 1029-1035.

Jakes, P., and Smith, I.E., 1970, High potassium calc-alkaline rocks from Cape Nelson, eastern Papua: Contributions to Mineralogy and Petrology, v. 28, p. 259-271.

Jakes, P., and White, A.J.R., 1972, Major and trace element abundances in volcanic rocks of orogenic areas: Geological Society of America Bulletin, v. 83, p. 29-40.

Jenner, G.A., 1981, Geochemistry of high-Mg andesites from Cape Vogel, Papua New Guinea: Chemical Geology, v. 33, p. 307-332.

Johnson, R.W., 1977, Distribution and major-element chemistry of late Cainozoic volcanoes at the southern margin of the Bismarck Sea, Papua New Guinea: Australia Bureau of Mineral Resources Report 188, 170 p.

--- 1979, Geotectonics and volcanism in Papua New Guinea: A review of the late Cainozoic: Australia Bureau of Mineral Resources Journal of Australian Geology and Geophysics, v. 4, p. 181-207.

Johnson, R.W., Mackenzie, D.E., and Smith, I.E.M., 1978a, Volcanic rock associations at convergent plate boundaries: reappraisal of the concept using case histories from Papua New Guinea: Geological Society of America Bulletin, v. 89, p. 96-106.

--- 1978b, Delayed partial melting of subduction-modified mantle in Papua New Guinea: Tectonophysics, v. 46, p. 197-216.

Johnson, R.W., Macnab, R.P., Arculus, R.J., Ryburn, R.J., Cooke, R.J.S., and Chappell, B.W., 1983, Bamus volcano, Papua New Guinea: dormant neighbour of Uluwan, and magnesian andesite locality: Geologische Rundschau, v. 72, p. 207-237.

Johnson, T., and Molnar, P., 1972, Focal mechanisms and plate tectonics of the southwest Pacific: Journal of Geophysical Research, v. 77, p. 5000-5032.

Kay, R.W., 1978, Aleutian magnesian andesites: implications of a melting-mixing model for recycling in the crust-upper mantle: Journal of Volcanology and Geothermal Research, v. 4, p. 117-132.

Kendall, C., 1976, Petrology and stable isotope geochemistry of three wells in the Buttes area of the Salton Sea geothermal field Imperial Valley, California, U.S.A.: Unpublished Ph.D. dissertation, University of California, Riverside, California, U.S.A., 210 p.

Kohn, B.P., 1973, Some studies on New Zealand Quaternary pyroclastic rocks: Unpublished Ph.D. dissertation, Victoria University, Wellington, New Zealand.

Krupp, R.E., and Seward, T.M., 1987, The Rotokawa geothermal system, New Zealand: An active epithermal gold-depositing environment: Economic Geology, v. 82, p. 1109-1129.

Kuroda, M., Shiraki, K., and Urano, H., 1978, Boninite as a possible calc-alkaline magma: Bulletin of Volcanology, v. 41, p. 563-575.

Lawless, J.V., Bromley, C.J., Leach, T.M., Licup, A.C., Jr., Cope, D.M., and Recio, C.M., 1983, Bacon-Manito geothermal field: a geoscientific exploration model: Proceedings of the 5th New Zealand Geothermal Workshop 1983, University of Auckland, p. 97-102.

Leach, T.M., Umali, D.U., and del Rosario, R.C., 1985, Epithermal mineral zonation in an active island arc: the Bacon-Manito geothermal systems, Philippines: Proceedings of the 7th New Zealand Geothermal Workshop 1985, University of Auckland, p. 109-114.

Lewis, J.F., 1968, Tauhara Volcano, Taupo Zone, part I - geology and structure: New Zealand Journal of Geology and Geophysics, v. 11, p. 212-224.

Liao, Z., Tong, W., Liu, S., and Zhao, F., 1986, Research for high temperature hydrothermal systems in west Yunnan Province (P R China): Proceedings of the 8th New Zealand Geothermal Workshop 1986, University of Auckland, p. 213-217.

Locke, A., Billingsley, P.R., and Mayo, E.B., 1940, Sierra Nevada tectonic patterns: Geological Society of America Bulletin, v. 51, p. 513-540.

Lorenz, V., 1986, On the growth of maars and diatremes and its relevance to the formation of tuff rings: Bulletin of Volcanology, v. 48, p. 265-274.

Luyendyk, B.P., Macdonald, K.C., and Bryan, W.B., 1973, Rifting history of the Woodlark basin in the southwest Pacific: Geological Society of America Bulletin, v. 84, p. 1125-1134.

Mackenzie, D.E., 1976, Nature and origin of late Cainozoic volcanoes in western Papua New Guinea, *in* Johnson, R.W., ed., Volcanism in Australasia: Amsterdam, Elsevier, p. 221-238.

Mackenzie, D.E., and Chappell, B.W., 1972, Shoshonitic and calc-alkaline lavas from the highlands of Papua New Guinea: Contributions to Mineralogy and Petrology, v. 35, p. 50-62.

Mahon, W.A.J., 1962, The carbon dioxide and hydrogen sulphide content of steam from drill holes at Wairakei: New Zealand Journal of Science, v. 5, p. 85-98.

--- 1966, Silica in hot water discharged from drill holes at Wairakei, New Zealand: New Zealand Journal of Science, v. 9, p. 135-144.

Mahon, W.A.J., and Glover, R.B., 1965, The chemistry of geothermal fluids discharged from drill holes at Wairakei, New Zealand: Proceedings of the Commonwealth Mining and Metallurgical Congress, 8th Australia-New Zealand, New Zealand Section, paper number 209, 10 p.

Martin, R.C., 1961, Stratigraphy and structural outline of the Taupo Volcanic Zone: New Zealand Journal of Geology and Geophysics, v. 4, p. 449-478.

McKibben, M.A., and Elders, W.A., 1985, Fe-Zn-Cu-Pb mineralization in the Salton Sea geothermal system, Imperial Valley, California: Economic Geology, v. 80, p. 539-559.

Meijer, A., 1976, Pb and Sr isotopic data bearing on the origin of volcanic rocks from the Mariana island-arc system: Geological Society of America Bulletin, v. 87, p. 1358-1369.

Meen, J.K., and Eggler, D.H., 1987, Petrology and geochemistry of the Cretaceous Independence volcanic suite, Absaroka Mountains, Montana: clues to the composition of the Archean sub-Montana mantle: Geological Society of America Bulletin, v. 98, p. 238-247.

Mercer, J.W., Pinder, G.F., and Donaldson, I.G., 1975, A Galerkin finite-element analysis of the hydrothermal system at Wairakei, New Zealand: Journal of Geophysical Research, v. 80, p. 2608-2621.

Meyer, C., and Hemley, J.J., 1967, Wall rock alteration, *in* Barnes, H.L., ed., Geochemistry of hydrothermal ore deposits: New York, Holt, Rinehart, and Winston, p. 166-235.

Mills, B.A., Boden, D.R., and Sander, M.V. 1988, Alteration and precious metal mineralization associated with the Toquima caldera complex, Nye County, Nevada, *in* Schafer, R.W., Cooper, J.J., and Vikre, P.G., eds., Bulk-mineable precious metal deposits of the western United States: Geological Society of Nevada Symposium Proceedings, Sparks, Nevada, April 6-8, 1987, p. 303-311.

Milsom,, J., and Smith, I.E., 1975, Southeastern Papua: generation of thick crust in a tensional environment?: Geology, v. 3, p. 117-120.

Ministry of Energy, 1984, Wairakei geothermal power station: 25 years' operation: Wellington, Electricity Division, Ministry of Energy, 14 p.

--- 1985, Power from the earth: Information Services, Electricity Division, Ministry of Energy, Wellington, 50 p.

Ministry of Works and Development, Geothermal Projects Office, Wairakei, 1984, Wairakei geothermal field--summary of production and reservoir data 1978-1984: Unpublished government report, Wairakei Seminar 26-27/9/1984, 64 p.

Mitchell, P.A., and Yousif, H.S., 1985, Geology and geochemistry of the Iamalele area, D'Entrecasteaux Islands, Papua New Guinea [Abstract]: Geological Society of New Zealand, Miscellaneous Publication 32A, p. 62.

Modriniak, N., and Studt, F.E., 1959, Geological structure and volcanism of the Taupo-Tarawera district: New Zealand Journal of Geology and Geophysics, v. 2, p. 654-684.

Mongillo, M.A., and Clelland, L., 1984, Concise listing of information on the thermal areas and thermal springs of New Zealand: Department of Scientific and Industrial Research Geothermal Report 9, 228 p.

Moore, W.J., and Czmanske, G.K., 1973, Compositions of biotites from unaltered and altered monzonite rocks in the Bingham mining district: Economic Geology, v. 68, p. 269-274.

Morris, J.D., Jezek, P.A., Hart, S.R., and Gill, J.B., 1983, The Halmahera island arc, Molucca Sea collision zone, Indonesia: a geochemical survey, *in* Hayes, D.E., ed., The tectonic evolution of southeast Asian seas and islands, Part 2: American Geophysical Union Geophysical Monograph, v. 27. p. 373-387.

Muffler, L.J.P., Nehring, N.L., Truesdell, A.H., Janik, C.J., and Clynne, M.A., 1982, The Lassen geothermal system: Proceedings of the 4th New Zealand Geothermal Workshop 1982, Part 2, University of Auckland Geothermal Institute in conjunction with the Centre for Continuing Education, p. 349-356.

Muffler, L.J.P., and White, D.E., 1969, Active metamorphism of Upper Cenozoic sediments in the Salton Sea geothermal field and the Salton Trough, southeastern California: Geological Society of America Bulletin, v. 80, p. 157-182.

Munoz, J.L., 1984, F-OH and Cl-OH exchange in micas with applications to hydrothermal ore deposits: *in* Bailey, S.W., ed., Micas: Reviews in Mineralogy, v. 13, p. 469-494.

Muramatsu, Y., 1984, Fluid inclusion study in the Takinoue geothermal field, Iwate Prefecture, Japan: an application to the estimate of the present underground temperature: Proceedings of the 6th New Zealand Geothermal Workshop 1984, University of Auckland, p. 21-25.

Mysen, B.O., 1982, The role of mantle anatexis, *in* Thorpe, R.S., ed., Andesites: orogenic andesites and related rocks: Chichester, U.K., John Wiley & Sons, p. 489-522.

New Zealand Geological Survey, 1972, North Island (first edition) Geological Map of New Zealand 1:1,000,000: Department of Scientific and Industrial Research, Wellington, New Zealand.

Nitsan, U., 1974, Stability field of olivine with respect to oxidation and reduction: Journal of Geophysics Research, v. 79, p. 706-711.

Niugini Mining Limited, 1988, Lihir Island: Niugini Mining Limited Annual Report 1988, p. 4-7.

Noble, D.C., Bowman, H.R., Hebert, A.J., Silberman, M.L., Heropoulos, C.E., Fabbi, B.P., and Hedge, C.E., 1975, Chemical and isotopic constraints on the origin of low-silica latite and andesite from the Andes of central Peru: Geology, v. 3, p. 501-520.

Northey, D.J., 1982, Seismic studies of the structure beneath Lake Taupo: Unpublished Ph.D. dissertation, Victoria University, Wellington, New Zealand.

Norton, D.L., 1982, Fluid and heat transport phenomena typical of copper-bearing pluton environments: southeastern Arizona, *in* Titley, S.R., ed., Advances in geology of the porphyry copper deposits, southwestern North America: Tucson, University of Arizona Press, p. 59-72.

O'Neil, J.R., and Silberman, M.L., 1974, Stable isotope relations in epithermal Au-Ag deposits: Economic Geology, v. 69, p. 902-909.

Orville, P.N., 1963, Alkali ion exchange between vapor and feldspar phases: American Journal of Science, v. 261, p. 201-237.

Page, R.W., and Johnson, R.W., 1974, Strontium isotope ratios of Quaternary volcanic rocks of Papua New Guinea: Lithos, v. 7, p. 91-100.

Peccerillo, A., and Taylor, S.R., 1976, Geochemistry of Eocene calc-alkaline volcanic rocks from the Kastamonu area, northern Turkey: Contributions to Mineralogy and Petrology, v. 58, p. 63-81.

Pritchard, P.W., 1963, Geological reconnaissance of Fergusson and Goodenough Islands: Bureau of Mineral Resources of Australia Record 1963, 58 p (unpublished).

Pritchett, J.W., Garg, S.K., and Brownell, D.H., Jr., Rice, L.F., Rice, M.H., Riney, T.D., and Hendrickson, R.R., 1976, Geohydrological environmental effects of geothermal power production -- phase IIA: Systems, Science and Software, Report SSS-R-77-2998.

Pritchett, J.W., Rice, L.F., and Garg, S.K., 1978, Reservoir engineering data: Wairakei geothermal field, New Zealand: Systems, Science and Software Report, SSS-R-78-3591, 2 volumes, 850 p.

--- 1979, Summary of reservoir engineering data: Wairakei geothermal field, New Zealand: Systems, Science and Software Report, 25 p.

--- 1980, Reservoir simulation studies: Wairakei geothermal field, New Zealand: Systems, Science and Software Report SSS-R-80-4313, 103 p.

Puig, A., Herve, M., Suarez, M., and Saunders, A.D., 1984, Calc-alkaline and alkaline Miocene and calc-alkaline Recent volcanism in the southernmost Patagonian Cordillera, Chile: Journal of Volcanology and Geothermal Research, v. 21, p. 149-163.

Pullar, W.A., 1981, Recent earth movements in Whakatane graben suggested by tephra markers and surficial deposits, *in* Howorth, R., Froggatt, P., Vucetich, C.G., and Collen, J.D., eds., Proceedings of the tephra workshop, June 30-July 1, Victoria University of Wellington: Wellington, Victoria University, Geology Department Publication 20, p. 110-113.

Risk, G.F., Rayner, H.H., Stagpoole, V.M., Graham, D.J., Dawson, G.B., and Bennie, S.L., 1983, Resistivity survey of the Wairakei geothermal field: New Zealand Department of Scientific and Industrial Research Geophysics Division, Unpublished Working Notes, 16 p.

Roberts, S.A., 1973, Pervasive early alteration in the Butte district, Montana: *in* Guidebook for the Butte field meeting, Society of Economic Geology: Butte, Montana, Anaconda Company, p. HH1-HH8.

Robertson, A., 1984, Analysis of subsurface compaction and subsidence at Wairakei geothermal field, New Zealand: Unpublished M.S. thesis, Auckland University, Auckland, New Zealand, 123 p.

Robertson, E.I., 1951, Gravity survey of the Wairakei-Taupo area, *in* Results of geothermal investigations Wairakei Taupo area: Wellington, Department of Scientific and Industrial Research Geophysics Division unpublished report, 9 p.

Robie, R.A., and Waldbaum, D.R., 1968, Thermodynamic properties of minerals and related substances at 298.15°K (25°C) and one atmosphere (1.013 bars) pressure and at higher temperatures: U.S. Geological Survey Bulletin 1259, 256 p.

Robinson, P., 1980, The compositional space of terrestrial pyroxenes - internal and external limits, *in* Prewitt, C.T., ed., Pyroxenes: Mineralogical Society of America Reviews in Mineralogy, v. 7, p. 419-494.

Roedder, E., 1979, Fluid inclusions as samples of ore fluids, *in* Barnes, H.L., ed., Geochemistry of hydrothermal ore deposits, 2nd ed.: New York, John Wiley & Sons, p. 684-737.

Roeder, P.L., and Emslie, R.F., 1970, Olivine-liquid equilibrium: Contributions to Mineralogy and Petrology, v. 29, p. 275-289.

Rogan, M., 1982, A geophysical study of the Taupo Volcanic Zone, New Zealand: Journal of Geophysical Research, v. 87, p. 4073-4088.

Roobol, M.J., Wright, J.V., and Smith, A.L., 1983, Calderas or gravity-slide structures in the Lesser Antilles island arc?: Journal of Volcanology and Geothermal Research, v. 19, p. 121-134.

Sander, M.V., 1988a, Geologic setting and relation of epithermal gold-silver mineralization to wall rock alteration at the Round Mountain mine, Nye, County, Nevada, *in* Schafer, R., and Cooper, T., eds., Bulk-mineable precious metal deposits of the western United States: Geological Society of Nevada Proceedings of Symposium held April, 1987, Sparks, Nevada.

--- 1988b, Epithermal gold-silver mineralization, wall-rock alteration, and geochemical evolution of hydrothermal fluids in the ash-flow tuff at Round Mountain, Nevada: Unpublished Ph.D. dissertation, Stanford University, Stanford, California, U.S.A., 283 p.

Sander, M.V., and Black. J.E., 1988, Crystallization and recrystallization of growth-zoned vein quartz from epithermal systems - implications for fluid inclusion studies: Economic Geology, v. 83, p. 1052-1060.

Sander, M.V., and Einaudi, M.T., 1990, Epithermal deposition of gold during transition from propylitic to potassic alteration at Round Mountain, Nevada: Economic Geology, v. 85, p. 285-311.

Sander, M.V., and Mitchell, P.A., 1988, Close resemblance between the active geothermal system at Wairakei, New Zealand, and the Tertiary epithermal Au-Ag deposit at Round Mountain, Nevada, U.S.A.--except for amount, position, and timing of Au mineralisation, *in* Goode, A.D.T., and Bosma, L.I., compilers, Bicentennial Gold 88 Extended Abstracts Oral Program: Geological Society of Australia Abstracts Series Number 22, p. 290-297.

Saunders, A.D., Rogers, G., Marriner, G.F., Terrell, D.J., and Verma, S.F., 1987, Geochemistry of Cenozoic to Recent volcanic rocks, Baja California, Mexico: Implications for the petrogenesis of post subduction magmas: Journal of Volcanology and Geothermal Research, v. 32, p. 223-245.

Schiffman, P., Bird, D.K., and Elders, W.A., 1985, Hydrothermal mineralogy of calcareous sandstones from the Colorado River delta in the Cerro Prieto geothermal system, Baja California, Mexico: Mineralogical Magazine, v. 49, p. 435-449.

Schiffman, P., Elders, W.A., Williams, A.E., McDowell, S.D., and Bird, D.K., 1984, Active metasomatism in the Cerro Prieto geothermal system, Baja California, Mexico: a telescoped low-pressure, low-temperature metamorphic facies series: Geology, v. 12, p. 12-15.

Schoen, R., and White, D.E., 1967, Hydrothermal alteration of basaltic andesite and other rocks in drill hole GS-6, Steamboat Springs, Nevada: U.S. Geological Survey Professional Paper 575-B, p. 110-119.

Schoen, R., White, D.E., and Hemley, J.J., 1974, Argillization by descending acid at Steamboat Springs, Nevada: Clays and Clay Minerals, v. 22, p. 1-22.

Seastres, J.S., Jr., 1982, Subsurface geology of the Nasuju-Sogongon sector, Southern Negros geothermal field, Philippines: Proceedings of the 4th New Zealand Geothermal Workshop 1982, Part 1, University of Auckland Geothermal Institute in conjunction with the Centre for Continuing Education, p. 173-178.

Self, S., and Healy, J., 1987, Wairakei Formation, New Zealand: stratigraphy and correlation: New Zealand Journal of Geology and Geophysics, v. 30, p. 73-86.

Seward, T.M., 1973, Thio complexes of gold and the transport of gold in hydrothermal ore solutions: Geochimica et Cosmochimica Acta, v. 37, p. 379-399.

--- 1988, The hydrothermal chemistry of gold and its implications for ore formation, *in* Goode, A.D.T., and Bosma, L.I., compilers, Bicentennial Gold 88 Extended Abstracts Oral Program: Geological Society of Australia Abstracts Series Number 22, p. 197-198.

Shatwell, D., 1987, Epithermal gold mineralisation and late Cenozoic magmatism in the Melanesian outer arc: Proceedings of the Australasian Institute of Mining and Metallurgy Pacific Rim Congress 87, 26-29 August, Gold Coast, Queensland, Australia, p. 393-398.

Shelley, D., 1985, Optical mineralogy, 2nd ed.: Amsterdam, Elsevier, 321 p.

Shiraki, K., Kuroda, N., Maruyama, S., and Urano, H., 1978, Evolution of the Tertiary volcanic rocks in the Izu-Mariana are: Bulletin of Volcanology, v. 41, p. 548-561.

Silver, E.A., Gill, J.B., Schwartz, D., Prasetyo, H., and Duncan, R.A., 1985, Evidence for a submerged and displaced continental borderland, north Banda Sea, Indonesia: Geology, v. 13, p. 687-691.

Simkin, T., and Smith, J.V., 1970, Minor element distribution in olivine: Journal of Geology, v. 78, p. 301-325.

Smith, A.L., and Carmichael, I.S.E., 1968, Quaternary lavas from the southern Cascades, western U.S.A.: Contributions to Mineralogy and Petrology, v. 19, p. 212-238.

Smith, E.G.C., and Webb, T.H., 1986, The seismicity and related deformation of the central volcanic region, North Island, New Zealand, *in* Smith, I.E.M., ed., Late Cenozoic volcanism in New Zealand: Wellington, Royal Society of New Zealand Bulletin 23, p. 112-133.

Smith, I.E.M., 1972, High potassium intrusives from southeastern Papua: Contributions to Mineralogy and Petrology, v. 34, p. 167-176.

--- 1973, Late Cainozoic volcanism in the southeast Papuan Islands: Bureau of Mineral Resources, Australia, record 1973/67 (unpublished).

--- 1976a, Peralkaline rhyolites from the D'Entrecasteaux Islands, Papua New Guinea, *in* Johnson, R.W., ed., Volcanism in Australasia: Amsterdam, Elsevier, p. 275-285.

--- 1976b, Volcanic rocks from southeastern Papua: the evolution of volcanism at a plate boundary: Unpublished Ph.D. dissertation, Australian National University, Canberra, Australia, 290 p.

--- 1981, Young volcanoes in eastern Papua, *in* Johnson, R.W., ed., Cooke-Ravian volume of volcanological papers: Geological Survey of Papua New Guinea Memoir 10, p. 257-265.

--- 1982, Volcanic evolution in eastern Papua: Tectonophysics, v. 87, p. 315-333.

Smith, I.E.M., Chappell, B.W., Ward, G.K., and Freeman, R.S., 1977, Peralkaline rhyolites associated with andesitic arcs of the southwest Pacific: Earth and Planetary Science Letters, v. 37, p. 230-236.

Smith, I.E.M., and Compston, W., 1982, Strontium isotopes in Cenozoic volcanic rocks from southeastern Papua New Guinea: Lithos, v. 15, p. 199-206.

Smith, I.E.M., and Johnson, R.W., 1981, Contrasting rhyolite suites in the late Cenozoic of Papua New Guinea: Journal of Geophysical Research, v. 86, p. 10257-10272.

Smith, I.E.M., and Milsom, J.S., 1984, Late Cenozoic volcanism and extension in eastern Papua, *in* Kokelaar, B.P., and Howells, M.F., eds., Marginal basin geology: volcanic and associated sedimentary and tectonic processes in modern and ancient marginal basins: Geological Society of London Special Publication 16, p. 163-171.

Smith, I.E.M., and Mitchell. P.A., 1989, High-magnesium lavas in the late Cenozoic volcanic arc associations of southeastern Papua New Guinea: Neues Jahrbuch fur Mineralogie Monatshefte, v. 11, p. 481-497.

Smith, R.L., 1979, Ash-flow magmatism: *in* Chapin, C.E., and Elston, W.E., eds., Ash-flow tuffs: Geological Society of America Special Paper 180, p. 5-27.

Smith, R.L., and Bailey, R.A., 1968, Resurgent cauldrons, *in* Coats, R.R., Hay, R.L., and Anderson, C.A., eds., Studies in volcanology: Geological Society of America Memoir 116, p. 613-662.

Stanley, E.R., 1920, Geology of Fergusson Island (Moratau): Bulletin of the Territory of Papua, 6 p.

Stanton, R.L., 1972, Ore petrology: New York, McGraw-Hill Book Company, 713 p.

Steiner, A., 1953, Hydrothermal rock alteration at Wairakei, New Zealand: Economic Geology, v. 49, p. 1-13.

--- 1955, Hydrothermal rock alteration, *in* Grange, L.I., compiler, Geothermal Steam for Power in New Zealand: New Zealand Geological Survey Bulletin 117, Chapter 3, p. 21-26.

--- 1968, Clay minerals in hydrothermally altered rock at Wairakei, New Zealand: Clays and Clay Mineralogy, v. 16, p. 193-213.

--- 1977, The Wairakei geothermal area, North Island, New Zealand: its subsurface geology and hydrothermal rock alteration: New Zealand Geological Survey Bulletin 90, 136 p.

Stern, T., 1985, Subsurface volcanic structures on the western margin of the Central Volcanic Region near Nangakino: New Zealand Geophysical Society 1985 Symposium Abstracts, p. 26.

Steven, T.A., and Lipman, P.W., 1976, Calderas of the San Juan volcanic field, southwestern Colorado: United States Geological Survey Professional Paper 958, 35 p.

Stewart, J.H., 1980, Geology of Nevada: a discussion to accompany the geologic map of Nevada: Nevada Bureau of Mines and Geology, Special Publication 4, 136 p..

Stewart, M.K., 1978, Stable isotopes in waters from the Wairakei geothermal area, New Zealand, *in* Stable isotopes in earth sciences: New Zealand Department of Scientific and Industrial Research Bulletin 220, p. 113-119.

--- 1984, Isotopic geochemistry at Wairakei--a hydrological model of the system: Unpublished notes, Wairakei Seminar 26-27/9/1984, 13 p.

Stipp, J.J., 1968, The geochronology and petrogenesis of the Cenozoic volcanics of North Island, New Zealand: Unpublished Ph.D. dissertation, Australian National University, Canberra, Australia.

Stormer, J.C., 1973, Calcium zoning in olivine and its relationship to silica activity and pressure. Geochimica et Cosmochimica Acta, v. 37, p. 1815-1821.

Studt, F.E., 1951, Magnetic surveys in the Wairakei Taupo area, *in* Results of geothermal investigations Wairakei Taupo area: Wellington, New Zealand, Department of Scientific and Industrial Research, 7 p.

Sudarman, S., and Hochstein, M.P., 1983, Geophysical structure on the Kamojang geothermal field (Java): Proceedings of the 5th New Zealand Geothermal Workshop 1983, University of Auckland, p. 225-230.

Sun, S.S., and Nesbitt, R.W., 1978, Geochemical regularities and genetic significance of ophiolitic basalts: Geology, v. 6, p. 689-693.

Sun, S.S., Nesbitt, R.W., and Sharaskin, A.Y., 1979, Geochemical characteristics of mid-ocean ridge basalts: Earth and Planetary Science Letters, p. 119-138.

Sverjensky, D.A., 1984, Europium redox equilibria in aqueous solution: Earth and Planetary Science Letters, v. 67, p. 70-78..

Tarney, J., Weaver, S.D., Saunders, A.D., Pankhurst, R.J., and Barker, P.F., 1982, Volcanic evolution of the northern Antarctic Peninsula and the Scotia arc, *in* Thorpe, R.S., ed., Andesites: John Wiley & Sons, p. 371-400.

Tatsumi, Y., and Ishizaka, K., 1981, Existence of andesitic primary magma: an example from southwest Japan: Earth and Planetary Science Letters, v. 53, p. 124-130.

--- 1982a, Magnesian andesite and basalt from Shoda-Shima island, southwest Japan, and their bearing on the genesis of calc-alkaline andesites: Lithos, v. 15, p. 161-172.

--- 1982b, Origin of high magnesian andesites in the Setouchi volcanic belt, southwest Japan: I. Petrological and chemical characteristics: Earth and Planetary Science Letters, v. 60, p. 293-304.

Taylor, H.P., Jr., 1974, The application of oxygen and hydrogen isotope studies to problems of hydrothermal alteration and ore deposition: Economic Geology, v. 69, p. 843-883.

Thompson, B.H., 1889, Narrative of an exploring expedition to the Louisiade and D'Entrecasteaux Islands: Proceedings of the Royal Geographic Society of London, v. 11, 9 p.

Thompson, G.E.K., Banwell, C.J., Dawson, G.B., and Dickinson, D.J., 1961, Prospecting of hydrothermal areas by surface thermal surveys: Proceedings of the U.N. Conference on New Sources of Energy, paper 35/G/54.

Thompson, R.N., 1974, Some high-pressure pyroxenes: Mineralogical Magazine, v. 39(307), p. 768-787.

Torgersen, T., Lupton, J.E., Sheppard, D.S., and Giggenbach, W.F., 1982, Helium isotope variations in the thermal areas of New Zealand: Journal of Volcanology and Geothermal Research, v. 12, p. 283-298.

Truesdell, A.H., 1984, Chemical geothermometers for geothermal exploration, *in* Henley, R.W., Truesdell, A.H., Barton, P.B., Jr. and Whitney, J.A., Fluid-mineral equilibria in hydrothermal systems: Economic Geology, Reviews in Economic Geology, v. 1, p. 31-43.

Wallace, D.A., Johnson. R.W., Chappell, B.W., Arculus, R.J., Perfit, M.R., and Crick, I.H., 1983, Cainozoic volcanism of the Tabar, Lihir, Tanga and Feni Islands, Papua New Guinea: geology, whole-rock analyses, and rock-forming mineral compositions: Bureau of Mineral Resources, Geology and Geophysics, report 243, p. 1-61.

Wass, S.Y., 1980, Geochemistry and origin of xenolith-bearing and related alkali basaltic rocks from the Southern Highlands, New South Wales, Australia: American Journal of Science, v. 280-A, p. 639-666.

Weissberg, B.G., Browne, P.R.L., and Seward, T.M., 1979, Ore metals in active geothermal systems, *in* Barnes, H.L., ed., Geochemistry of hydrothermal ore deposits, 2nd ed.: New York, John Wiley & Sons, p. 738-780.

White, D.E., 1955, Thermal springs and epithermal ore deposits: Economic Geology, 50th anniversary volume, p. 99-154.

--- 1965, Saline waters of sedimentary rocks, *in* Fluids in subsurface environments--a symposium: American Association of Petrology and Geology Memorandum 4, p. 342-366.

--- 1981, Active geothermal systems and hydrothermal ore deposits: Economic Geology, 75th anniversary volume, p. 392-423.

Williamson, A., 1983, Thermal activity of Lihir Island, New Ireland Province: Geological Survey of Papua New Guinea, report 83/15, p. 1-21.

Wilson, C.J.N., 1986, Reconnaissance stratigraphy and volcanology of ignimbrites from Mangakino Volcano, *in* Smith, I.E.M., ed., Late Cenozoic volcanism in New Zealand: Wellington, Royal Society of New Zealand Bulletin 23, p. 179-193.

Wilson, C.J.N., Houghton, B.F., and Lloyd, E.F., 1986, Volcanic history and evolution of the Maroa - Taupo area, central North Island, *in* Smith, I.E.M., ed., Late Cenozoic volcanism in New Zealand: Wellington, Royal Society of New Zealand Bulletin 23, p. 194-223.

Wilson, C.J.N., Rogan, A.M., Smith, I.E.M., Northey, D.J., Nairn, I.A., and Houghton, B.F., 1984, Caldera volcanoes of the Taupo Volcanic Zone, New Zealand: Journal of Geophysical Research, v.89, p. 8463-8484.

Wilson, S.H., 1955, Chemical investigations, *in* Grange, L.I., compiler, Geothermal Steam for Power in New Zealand: New Zealand Geological Survey Bulletin 117, Chapter 4, p. 27-42.

Yilmazer, S., Gevrek, A.I., and Sahinci, A., 1989, Clay mineralogy and hydrothermal alteration studies of the Izmir-Balcova geothermal field, Turkey: *in* Browne, P.R.L., and Nicholson, K., eds., Proceedings of the 11th New Zealand Geothermal Workshop 1989, University of Auckland, p. 317-320.

N. Jb. Miner. Mh.	Jg. 1989, H. 11	481–497	Stuttgart, November 1989

High-magnesium lavas in the late Cenozoic volcanic arc associations of southeastern Papua New Guinea

By Ian E. M. Smith, Auckland, and Peter A. Mitchell, Christchurch

With 7 figures and 3 tables in the text

Smith, Ian E. M. & Mitchell, Peter A.: High-magnesium lavas in the late Cenozoic volcanic arc associations of southeastern Papua New Guinea. – N. Jb. Miner. Mh., 1989, H. 11, 481–497, Stuttgart 1989.

Abstract: Southeastern Papua New Guinea contains an unusual variety of late Cenozoic volcanic associations reflecting complex plate motions during late Mesozoic and Cenozoic times. The major association is mid-Miocene to Recent in age and is high-K calc-alkalic to shoshonitic in character; rock types range from basalt to rhyolite with andesite predominant. Detailed geochemical study of these rocks has revealed the presence of lavas which are high in MgO, Cr and Ni forming an integral part of this arc-type association. The high concentrations of these elements relative to typical arc-related rocks are thought to reflect the chemical composition of a primary melt rather than phenocryst accumulation or contamination by ultramafic material. A review of the literature shows that high-Mg lavas occur in other volcanic arcs of Papua New Guinea, and that, in each case, these lavas share the overall chemical characteristics of the volcanic arc in which they occur. High-Mg lavas appear to be an integral part of many circum-Pacific arc-type volcanic associations. They have been identified in a variety of broadly arc-type tectonic settings including the full range of geochemically identified arc-type magmatic associations. Although in some cases accumulation of mafic phases or contamination by subjacent ultramafic material can be appealed to as an explanation for these rocks, neither hypothesis is convincing as a general explanation. The high-Mg lavas appear to represent parental magmas to typical arc-type rock series in many arc-type tectonic settings.

Key words: Papua New Guinea, arc-type, high-Mg andesite.

Introduction

A widely quoted chemical characteristic of arc-type volcanic rocks is their relatively low content of certain transition elements, principally Mg, Cr and Ni. Recently, this view has been challenged by the recognition of high-Mg lavas in the arc-type volcanic associations of the Aleutian Islands (Kay, 1978; Reid & Nye, 1986; Gust & Perfit, 1987), Japan (Tatsumi & Ishizaka, 1981, 1982 a, 1982 b; Aoki & Fujimaki, 1982) and as part of comparable associations in continental settings (Mexico, Saunders et al., 1987; U.S.A., Meen &

0028-3649/89/1989-0481 $ 4.25

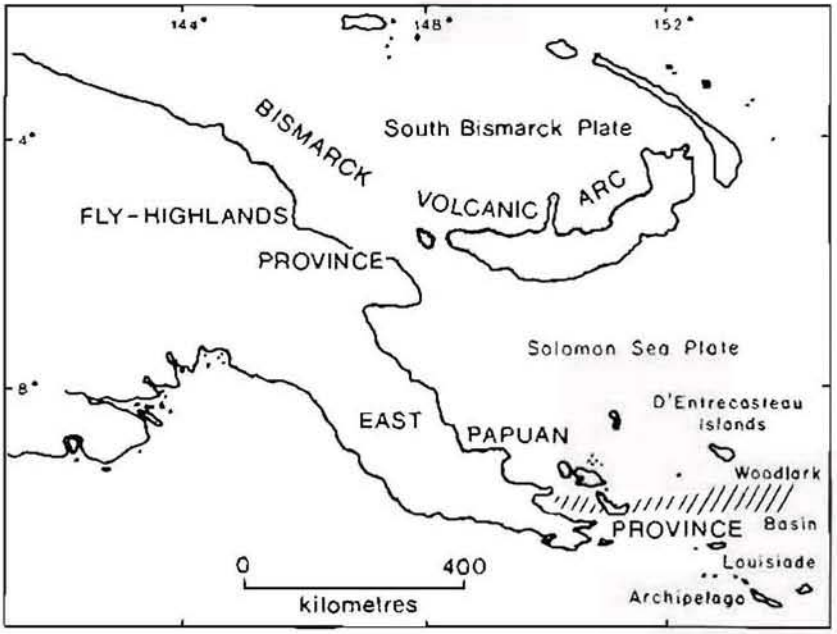

Fig. 1. Distribution of late Cenozoic arc-type rocks (shown stippled) in Papua New Guinea, after JOHNSON (1979); areas of Quaternary extension (hatched pattern) after DAVIES et al. (1984).

EGGLER, 1987). Magnesium-rich lavas have also been described but not explicitly recognized from a number of areas around the circum-Pacific rim; for example, northern California, U.S.A. (SMITH & CARMICHAEL, 1968), the New Georgia Group islands, Solomon Islands (COX & BELL, 1972). A review of the literature suggests that high-Mg lavas may be widespread among circum-Pacific arc-type volcanic associations, but because they are commonly a subordinate or even a rare component of the suite in which they occur, their importance has been overlooked.

High-Mg lavas in the context of this paper are arc-type volcanic rocks ranging from basalt through basaltic andesite to andesite and characterized by MgO, Ni and Cr contents which are markedly higher than those normally found in arc-type rocks. The high-Mg lavas described in this paper are typically less porphyritic and more olivine rich than other rocks of the associations in which they occur.

Here we describe high-Mg lavas from the late Cenozoic volcanic stratigraphy of southeastern Papua New Guinea (Fig. 1) and use their compositions to define the abundances of MgO relative to SiO_2 which characterize them. We also

review the occurrence of high-Mg lavas associated with convergent plate tectonic settings elsewhere in the Pacific rim and suggest that high-Mg lavas are an important component of many typical arc-type volcanic associations.

Volcanism in Papua New Guinea

Late Cenozoic tectonism in Papua New Guinea (PNG) has been modelled in terms of a number of minor plates caught up in a major zone of interaction between the Pacific and Indo-Australian plates (JOHNSON & MOLNAR, 1972; CURTIS, 1973). Concurrent with tectonic activity, arc-type volcanism has occurred in widely separated areas of PNG, principally the Bismarck volcanic arc, the Fly-Highlands province and the east Papuan province (JOHNSON, 1979) (Fig. 1). The Bismarck volcanic arc is clearly associated with active subduction resulting from interaction between the Solomon Sea and South Bismarck micro-plates (JOHNSON, 1979). Although not obviously linked to present day subduction, the Fly-Highlands province straddles a suture between the Indo-Australian plate and the Bismarck Sea micro-plate which has been interpreted as a Cenozoic collision zone (HAMILTON, 1979).

The Papuan peninsula, extends southeastward from the Fly-Highlands province, straddles the boundary between the Indo-Australian plate and Solomon Sea micro-plate, and is bounded on either side by Lower Tertiary oceanic crust. The onshore geological record is complex and fragmentary; paleotectonic reconstructions involving both southward HAMILTON, 1979) and northward dipping (DAVIES et al., 1984) late Cenozoic subduction systems have been proposed but evidence for either hypothesis is equivocal and open to alternative interpretation (e.g. SMITH, 1983; SMITH & MILSOM, 1984). We favor an hypothesis of southward dipping subduction in mid- to late Miocene times and a transition to a late Tertiary and Quaternary extensional tectonic regime associated with spreading in the Woodlark Basin.

The major late Cenozoic magmatic event in southeastern PNG is represented by mid-Miocene to Recent volcanic and minor intrusive rocks. These form an association which is essentially arc-type and dominantly andesite, but includes a range of lithologies from basalt to rhyolite. Petrographic and geochemical data have been used to divide the late Cenozoic arc-type association of southeastern PNG into a northern belt dominated by high-K indesite, and a southern belt in which K-rich basalt (shoshonite) is the predominant rock type (SMITH, 1983). These two belts are interpreted to be a single volcanic association in which there is considerable temporal and compositional diversity.

The northern volcanic belt is composed of basalt (10%), basaltic andesite (25%), andesite (45%), dacite (15%) and rhyolite (5%). The basalts, basaltic andesites and some andesites are typically porphyritic, vesicular rocks containing sparse to abundant phenocrysts of plagioclase (An_{75-50}), olivine, pale

green clinopyroxene and orthopyroxene; microphenocrysts of spinel and/or iron–titanium oxides occur in some of the lavas. Hornblende-bearing lavas ranging from andesite to dacite are also an important component of the association. The hornblende-bearing lavas are typically highly porphyritic and contain phenocrysts of plagioclase (An_{60-30}), brown hornblende, biotite and iron–titanium oxides. Phenocrysts are generally restricted to three or four phases, but a few andesites and dacites contain exceedingly complex phenocryst assemblages including hornblende, biotite, two pyroxenes and olivine in addition to plagioclase. Rhyolites are closely associated with the andesites and dacites in the Moresby Strait area of the D'Entrecasteaux Islands; for a detailed description of their petrography see SMITH & JOHNSON (1981).

Table 1. Mean chemical composition of calc–alkaline and boninite lavas from southeastern Papua New Guinea.

	Calc–alkaline		
Wt.%	Arc-type (n = 40)	High-Mg (n = 43)	Boninite (n = 21)
SiO_2	58.55	57.81	57.61
TiO_2	1.17	1.00	0.25
Al_2O_3	17.47	15.47	8.38
FeO*	5.99	6.04	9.59
MnO	0.11	0.10	0.20
MgO	3.40	6.51	17.83
CaO	6.45	6.74	4.94
Na_2O	4.26	3.70	0.83
K_2O	2.24	2.27	0.33
P_2O_5	0.36	0.36	0.04
	100.00	100.00	100.00
ppm			
Ba	795	873	48
Rb	51	51	6
Sr	692	821	100
Th	6	8	0.6
Zr	228	194	0.2
Nb	6	5	2
Y	29	21	5
La	44	49	3
Ce	70	74	7
Sc	14	14	30
V	137	132	156
Cr	49	299	1775
Ni	30	155	378
Mg-Number	54.4	69.4	79.6

Calc–alkaline rock analyses were determined by XRF. Major element analyses normalized to a volatile-free basis. n is the number of analyses. FeO* is total Fe as FeO. Mg-number [Mol. 100 MgO/(MgO + FeO)] is computed for $Fe_2O_3/FeO = 0.20$. Boninite data are from JENNER (1981).

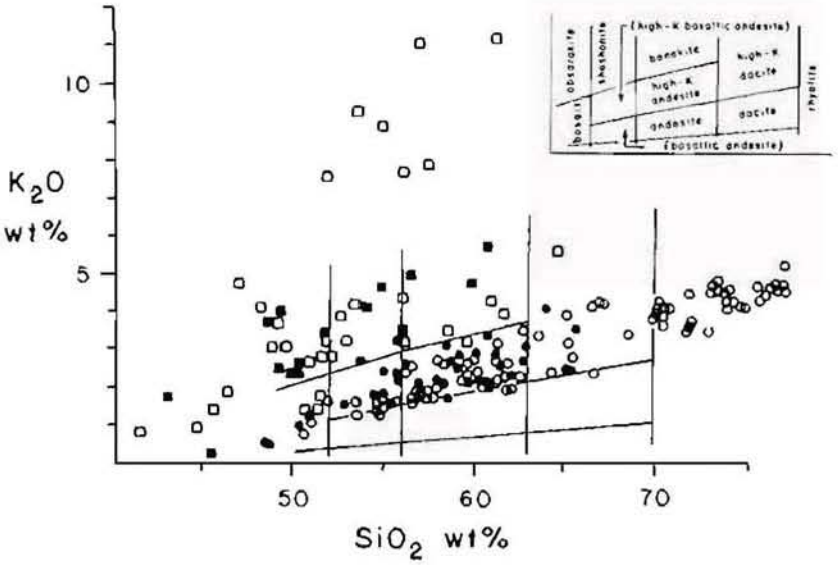

Fig. 2. K_2O-SiO_2 variation in late Cenozoic arc-type volcanic rocks from the east Papuan volcanic province. Solid symbols are high-Mg rocks, circles are northern volcanic belt rocks, squares are southern volcanic belt and associated intrusive rocks. Data sources are JAKES & SMITH (1970), SMITH (1972), DAVIES & SMITH (1976) and authors' unpublished data. Inset shows nomenclature of arc-type rocks after PECCERILLO & TAYLOR (1976).

All of the volcanic centers in the northern volcanic belt have erupted andesite; in most centers, andesite is accompanied by basaltic andesite with or without subordinate basalt and dacite. These rocks form a suite characterized by high alkali contents and comparatively high K_2O/Na_2O ratios (Table 1); in terms of PECCERILLO & TAYLOR's (1976) classification they form a high-K calc-alkaline association (Fig. 2). The ferromagnesian elements (Ti, Fe, Mn, Mg, V, Cr and Ni), and Ca and P show a positive correlation with each other and a clearly defined inverse relationship with the abundances of Si, K and incompatible trace elements. The abundances of large-ion incompatible elements are high, but fall within the range for high-K andesites given by JAKES & WHITE (1972).

Lavas with relatively high contents of MgO occur intercalated with "normal" lavas and are an inseparable part of the association. Compared with other lavas from the northern volcanic belt, this high-Mg group tends to be more sparsely porphyritic and to contain a higher percentage of chrome spinel, magnesian olivine and clinopyroxene, iron–titanium oxides and interstitial glass. On a plot of MgO vs. SiO_2 the high-Mg lavas can be clearly separated from the remainder of the suite. A line drawn through the data to separate

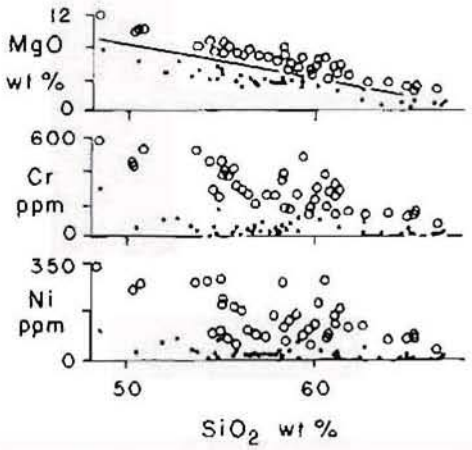

Fig. 3. Variation in MgO, Cr and Ni with respect to SiO_2 in samples from the northern volcanic belt of the Papuan volcanic province. The line separates high-Mg lavas (open circles) from the remainder of the suite; rhyolites are not plotted.

these petrographically defined groups is described by the formula $MgO = (-0.433 \times SiO_2) + 29.14$ (Fig. 3). There is no rigorous mathematical basis for this empirically derived line; it serves as a reference separating the high-Mg lavas from the remainder of the suite. The mean of analysed high-Mg lavas are compared with the mean of analysed "normal" lavas in Table 1.

High-Mg lavas comprise approximately one third of the 150 analyzed samples from the northern volcanic belt; they constitute an estimated 15 % of the total volume of exposed volcanic rocks. The high-Mg lavas vary in chemical composition from basalt to dacite, but the majority are basaltic andesite and andesite. Intrinsic to these lavas are anomalously high, but variable, abundances of Cr (158 to 592 ppm) and Ni (80 to 343 ppm), and Mg-numbers (mol. 100 MgO/(MgO + FeO), $Fe_2O_3/FeO = 0.20$) in the range 64 to 76. The compositional trends of the high-Mg lavas either overlap, or, at high silica values, converge on the trends shown by the remainder of the suite (Fig. 4). It is significant that apart from higher abundances of Mg, Cr and Ni, and lower abundances of Ti, Al and Na, the high-Mg lavas have essentially the same chemical compositions as those forming the remainder of the suite.

The southern volcanic belt differs from the northern in that rocks of intermediate to felsic composition are less common and that the basaltic rocks are petrographically distinct. Typical of the southern belt are highly porphyritic basalts containing phenocrysts of pale green salitic clinopyroxene commonly accompanied by smaller phenocrysts of olivine and/or plagioclase. Rocks of intermediate composition are characteristically porphyritic and contain phe-

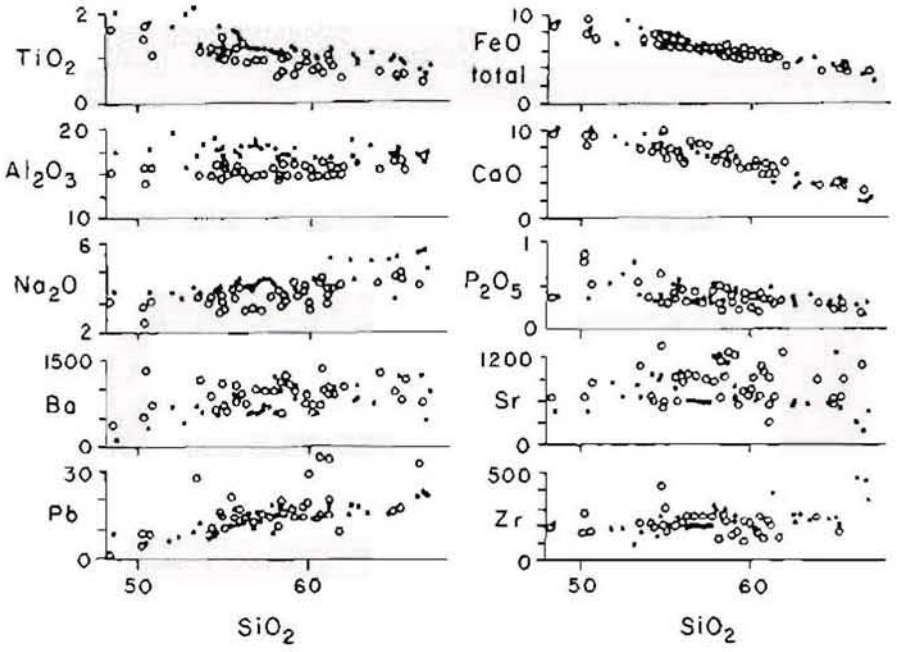

Fig. 4. Variation in selected major oxides (Wt.%) and trace elements (ppm) with respect to SiO_2 (Wt.%) in samples from the northern volcanic belt of the east Papuan province; open circles are high-Mg samples.

nocrysts of biotite, hornblende, clinopyroxene, iron–titanium oxides and, rarely, olivine. Rhyolite has not been noted from the southern volcanic belt.

Intrusive rocks associated temporally and spatially with the volcanic rocks of the southern volcanic belt have been described by SMITH (1972). They range from pyroxenite and gabbro to syenite, and occur as small plutons and swarms of porphyry dikes.

Although the volcanic and associated intrusive rocks from the southern volcanic belt are more basaltic and have higher K_2O/Na_2O ratios than those from the northern volcanic belt, they share the same general chemical characteristics. Using the discriminant line derived for the northern volcanic belt, the suite of rocks from the southern volcanic belt also contains lavas which are relatively high in MgO, Cr and Ni (Fig. 5).

Discussion

Among the rocks forming the late Cenozoic arc-type volcanic association of southeastern PNG we have recognized high-Mg lavas ranging in composition

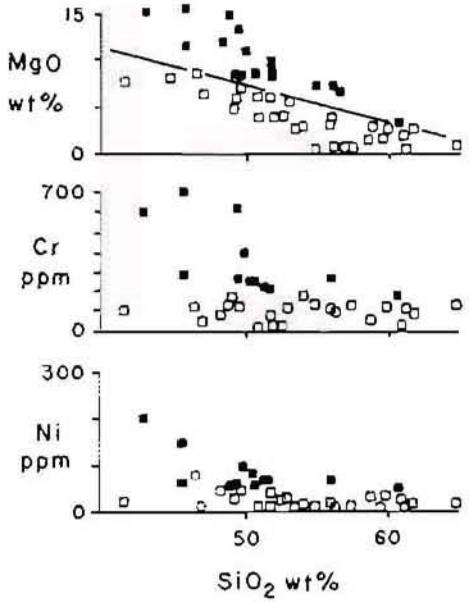

Fig. 5. Variation in MgO, Cr and Ni with respect to SiO_2 in lavas and intrusions from the southern volcanic belt of the east Papuan province. Solid symbols represent high-Mg samples.

from basalt to dacite. In the northern volcanic belt these occur with rocks which may be characterized as high-K calc–alkaline, and in the southern volcanic belt they form part of a shoshonitic group. A petrogenetic model for the high-Mg lavas must satisfy the following observations: 1) they are an integral part of a long-lived volcanic association which includes both high-K calc–alkaline and shoshonitic rocks, and 2) the mechanism of their genesis effectively discriminates a few elements which are preferentially enriched relative to the remainder of the association.

Mg/Fe ratios of olivine phenocrysts and host rocks follow the pattern predicted by Roeder & Emslie (1970) and the olivine is interpreted as an early phase crystallized from a magma with approximately the composition of the host rock. Mg-numbers of high-Mg basalts and basaltic andesites are compatible with equilibrium with mantle olivine. The primitive nature of these lavas is also reflected in common occurrence of chromite or Cr-spinel inclusions in olivine, and near-MORB values for FeO^*/MgO, Al_2O_3/TiO_2 and CaO/TiO_2. These petrographic and compositional characteristics preclude a cumulate origin for the high-Mg lavas and also argue against contamination by ultramafic material within the crust. We suggest instead that the Papuan high-Mg

lavas represent a series in which the more mafic members represent primary magmas generated by hydrous partial melting of undepleted upper mantle, or of subduction-modified mantle.

High-Mg lavas are uncommon in arc-type associations. One explanation for their occurrence in Papua may be that the present tectonic regime is one of extension and rapid uplift (Smith, 1983; Davies et al., 1984). In this environment magmas may rise relatively rapidly thereby retaining their high-Mg character whereas more commonly arc-type magmas undergo CAMS fractionation and contamination with crustal material as they rise through the crust.

Although there is a continuing moderate level of arc-type volcanic activity in the east Papuan province (Smith, 1981) there is no suggestion of active subduction in the present day pattern of seismicity. However, there is no doubt that the area has undergone major convergence subsequent to the late Mesozoic which has resulted in crustal thickening. In order to resolve the apparent contradictions Johnson et al. (1978 b) and Smith (1983) suggested that active subduction is not necessarily an immediate precondition for the type of magmatism seen in southeastern PNG, but that it may be the result of partial melting of a source which was generated during an earlier convergent event.

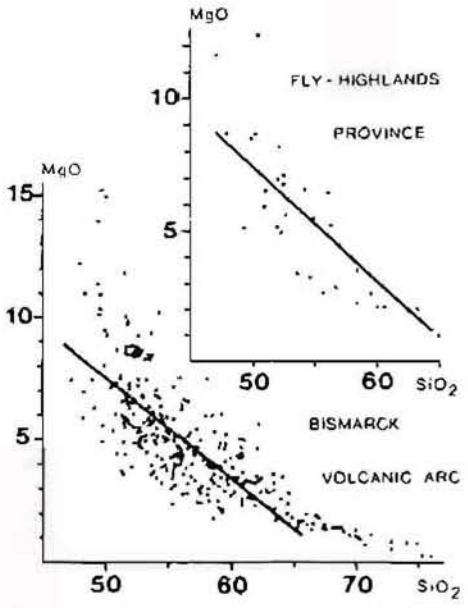

Fig. 6. Variation in MgO (Wt.%) with respect to SiO_2 (Wt.%) in samples from the Bismarck volcanic arc (Johnson, 1977) and the Fly-Highlands province (Mackenzie & Chappell, 1972; Mackenzie, 1976). The line separating the high-Mg field from the rest of the suite is taken from Fig. 4.

This delayed magmatism model resolves the apparent conflict in the juxtaposition of both arc-type and rift-type late Cenozoic magmatic associations (SMITH et al., 1977), and explains the occurrence of young, typically arc-type volcanic rocks in an area which is not at present undergoing active plate convergence.

High-magnesium lavas elsewhere in PNG

The lithologies exposed in the Bismarck volcanic arc range from basalt to rhyolite, and are arc-tholeiite to low-K calc–alkaline in character (JOHNSON et al., 1978 a). An analysis of the major element compositions of the Bismarck volcanic arc reported by (JOHNSON, 1977) shows that in terms of the criteria established for the late Cenozoic arc-type volcanics in southeastern PNG there is a significant proportion of analyses which show the same high-Mg character (Fig. 6).

The Fly-Highlands volcanic province consists of a group of large, mainly andesitic volcanoes. Although not presently associated with active subduction, their tectonic setting is considered to be one of plate convergence (HAMILTON, 1979). Published geochemical data from these volcanoes (MACKENZIE & CHAPPELL, 1972; MACKENZIE, 1976) include a proportion of analyses which show a high-Mg character according to the criteria established for the east Papuan volcanic province (Fig. 6). These high-Mg lavas form an integral part of the Fly-Highlands petrologic suites.

The discriminant line derived empirically for the suite of analyzed rocks from the northern volcanic belt of the east Papuan volcanic province may not be directly applicable to other volcanic arcs. However, it does serve as a reference line to show that all of the major arc-type volcanic associations in PNG include a proportion of rocks which contain relatively high contents of MgO.

High-magnesium lavas of the circum-Pacific rim

We have used the empirical compositional criteria by which the high-Mg lavas were defined in the calc–alkaline terrain of southeastern Papua New Guinea as a reference by which to recognize high-Mg lavas in other circum-Pacific arc-type volcanic associations. The result of this literature review is presented in Fig. 7 and Table 2. In only six of these examples (1, 2, 3, 6, 12, 17; Table 2) were the high-Mg lavas specifically identified in the original study.

The conventions followed in compiling Table 2 include classification of the arc-type rocks based on their silica content following the nomenclature of PECCERILLO & TAYLOR (1976), and subdivision of volcanic associations into island arc tholeiite, calc–alkaline, high-K calc–alkaline and high-K alkalic. The literature compilation of high-Mg lavas in Cenozoic circum-Pacific volcanic arcs

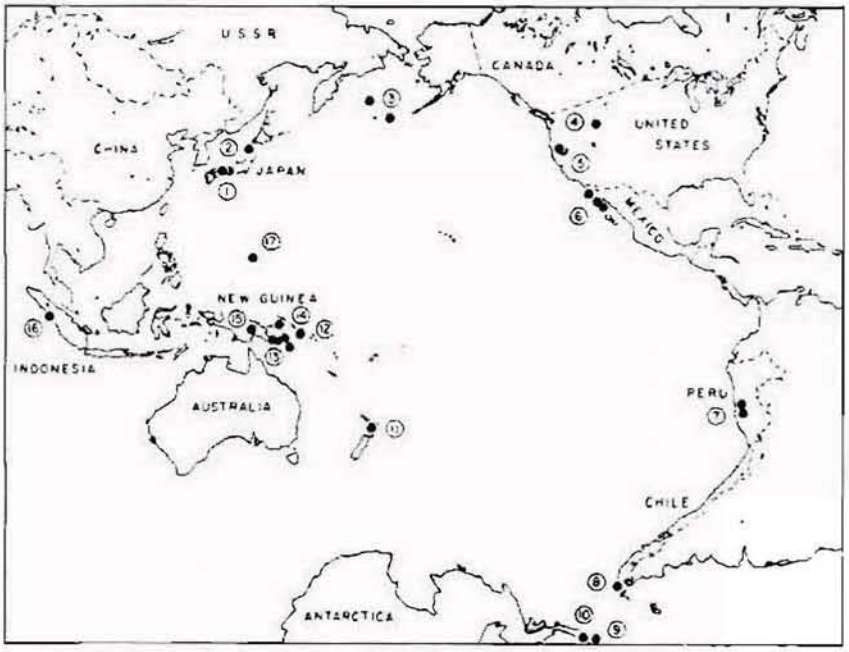

Fig. 7. Locations of high-Mg lavas summarized in Table 2.

(Fig. 7, Table 2) reveals several significant facts. 1) High-Mg lavas do not appear to be restricted to any specific type of arc. They are found as a component of the magmatic association in relatively simple arcs (e.g. Indonesia, Aleutian Peninsula and South Shetland Islands), in complex arcs (e.g. Papua New Guinea, Japan and New Zealand) and in continental margins (e.g. western North America, Mexico, Peru and Chile). 2) Where they occur, the high-Mg rocks form an integral part of their suite and share the gross chemical characteristics of their magmatic association. This is an important point since high-Mg lavas are found as a component of all of the principal recognized arc-type associations (island arc tholeiite, calc–alkaline, high-K alkaline). 3) High-Mg lavas encompass a range of rock types, typically basalt to andesite, but including low-silica dacite.

High-Mg lavas characteristically contain early-formed phenocrysts of olivine and clinopyroxene and thus are vulnerable to compositional modification by crystal fractionation processes. In order to preserve their magnesian character such magmas must rise rapidly from their source region. Although our general conclusion is that tectonic setting is not a contributing factor in the generation of high-Mg magmas, it may be important in controlling their rate of ascent and consequent degree of crystal fractionation.

Table 2. High-Mg lavas and associated rocks from localities around the circum-Pacific rim.

Locality	High-Mg Lithologies	Associated Lithologies	Association	Age	Tectonic Setting	Reference
1. Southern Japan	Basalt to andesite	Andesite	Arc tholeiite to calc–alkalic	Middle Miocene	Active subduction	*Tatsumi & Ishizaka (1981, 1982)
2. Northeastern Japan	Basalt to basaltic andesite	Basaltic andesite to andesite	Calc–alkalic	Recent	Active subduction	*Aoki & Fugimaki (1982)
3. Aleutian Islands	Basaltic andesite to andesite	Basalt to andesite	Arc theoleiite to calc–alkalic	Middle Miocene to Pliocene	Active subduction	*Kay (1978)
4. Montana	Andesite	Basaltic andesite to rhyolite	Calc–alkalic to high-K calc–alkalic	Late Cretaceous	Orogenesis	Mean & Eggler (1987)
5. Northern California	Basalt to andesite	Basalt to rhyolite	Calc–alkalic	Pliocene to Recent	Active subduction	Smith & Carmichael (1968)
6. Baja California	Basaltic andesite to andesite	Basalt to andesite	Calc–alkalic to high-K calc–alkalic	Late Miocene to Recent	Post-subduction	*Saunders et al. (1987)
7. Peru	Basaltic andesite	Basalt to rhyolite	Calc–alkalic to high-K calc–alkalic	Late Cenozoic	Active subduction	Noble et al. (1973)
8. Southern Chile	Basalt to basaltic andesite	Basalt to andesite	Calc–alkalic	Miocene to Recent	Active subduction	Puig et al. (1984)
9. South Shetland Islands	Basalt	Basalt to rhyolite	Arc-tholeiite	Quaternary	Back arc spreading	Weaver et al. (1979)
10. Antarctic Peninsula	Basaltic andesite to andesite	Basalt to rhyolite	Arc-tholeiite	Mesozoic to Quaternary	Active subduction	Tarney et al. (1982)
11. New Zealand	Basalt	Basalt to andesite	Calc–alkalic	Quaternary	Active subduction	Graham & Hackett (1987)
12. Solomon Islands	Basalt to andesite	Basalt to andesite	Arc-tholeiite	Late Tertiary to Recent	Active subduction	Cox & Bell (1972)
13. Southeastern Papual New Guinea	Basalt to dacite	Basalt to rhyolite	High-K calc–alkalic to high-K alkalic	Late Cenozoic	Uplift and crustal extension	*Smith & Mitchell (unpubl. data)
14. Northern New Britain	Basalt to dacite	Basalt to rhyolite	Arc-tholeiite to calc–alkalic	Late Cenozoic	Active subduction	Johnson (1977)
15. Papua New Guinea Highlands	Basalt to andesite	Basalt to dacite	High-K calc–alkalic to high-K alkalic	Late Cenozoic	Orogenesis	Mackenzie & Chappell (1972)
16. Eastern Indonesia	Basalt to basaltic andesite	Basalt to dacite	Calc–alkalic to high-K calc–alkalic	Late Tertiary to Quaternary	Active subduction	Morris et al. (1983)
17. Mariana Islands	Basalt to basaltic andesite	Basalt to dacite	Arc-tholeiite to calc–alkalic	Eocene to Recent	Active subduction	Shiraki et al. (1978)

Note: Numbers correspond to localities shown in Figure 7. Asterisks signify authors who specifically identified the presence of high-Mg lavas.

Nomenclature of magnesium-rich arc-type lavas

Magnesium-rich rocks of the circum-Pacific region have been referred to by a variety names: magnesian andesites (KAY, 1978; TATSUMI & ISHIZAKA, 1982 a; JOHNSON et al., 1983); sanukitioids (TATSUMI & ISHIZAKA, 1981); high-magnesian andesites (TATSUMI & ISHIZAKA, 1982 b); high-magnesium andesite (MEEN & EGGLER, 1987); and bajaites (SAUNDERS et al., 1987). To avoid any additional confusion, and to avoid problems arising from the compositional variability (basalt to dacite) of the lavas, we suggest the use of *high-Mg* to recognize the existence of magnesium-rich rocks among arc-type igneous associations in the same way that high-K has been used in the literature to identify suites of rocks with that particular character, e.g. high-Mg dacite.

As noted above, magnesium-rich volcanic rocks similar to the late Cenozoic high-Mg lavas in southeastern PNG occur in many other parts of the circum-Pacific region. An important feature in all of these areas is their intimate association with "normal" arc-type rocks, although in each area the association as a whole may have distinctive chemical characteristics. Boninites are also magnesium-rich, relatively silica-rich rocks, which occur in a number of circum-Pacific regions (KURODA et al., 1978; SUN & NESBITT, 1978; JENNER, 1981; BLOOMER & HAWKINS, 1987). It is important to recognize that the mineralogy and chemistry of the high-Mg rocks described and referred to in this paper are quite distinct from boninites. For example in the comparison of Papuan data (Table 1) the only chemical similarity between arc-type high-Mg lavas and boninites is their intermediate silica content. High-Mg lavas and boninites are unrelated rock types and we suggest that arc-type magnesium-rich rocks should not be referred to as having "boninitic affinities".

Conclusion

In all of the arc-type settings in PNG for which data are available, high-Mg lavas form an integral part of the volcanic associations and cannot be separated as a temporally or spatially distinct event. The importance of this is that high-Mg lavas, at least locally, form a significant component of the association in which they occur. This observation needs to be incorporated in any general theory for the origin of magmas in convergent plate tectonic settings.

SAUNDERS et al. (1987) noted that in all known instances the generation of high-Mg magmas in arc settings may be related to high heat flow associated with subduction of young ocean lithosphere (e.g. ridge subduction). Our work in southeastern PNG documents the occurrence of high-Mg lavas in a region where subduction or attempted subduction of a spreading center has not figured in paleotectonic reconstructions. We consider the high-Mg magmas to have formed from a subduction-modified, mantle source in a tectonic environment transitional to rifting associated with the westward migration of spread-

ing in the Woodlark Basin (LUYENDYK et al., 1973). The existence of intercalated high-Mg and "normal" arc-type lavas suggests that some of the primary magmas rose rapidly to the surface retaining their initial chemical signature, whereas others rose more slowly permitting crystal fractionation to occur prior to eruption. The genesis of high-Mg lavas in other areas also may be related to tensional environments. We note, that in several of the high Mg lava localities cited earlier, extension (rifting) is at least a transient feature of the tectonic setting.

On a broader scale we interpret the occurrence of high-Mg lavas in several of the major arc systems of the circum-Pacific rim to indicate that high-Mg lavas are a fundamental component of most, if not all, volcanic arcs associated with convergent plate margins. The petrological significance of high-Mg lavas in any particular arc-type association is probably not a constant. In some cases they may be cumulates, whereas in others, high-Mg lavas may be the result of contamination by subjacent ultramafic material (e.g. ARCULUS et al., 1983). However, in many of the occurrences noted in Table 2 the high-Mg rocks appeara to represent magmas which are parental to the other associated rocks. Because high-Mg lavas occur as an integral component of all of the geochemically defined arc-type magmatic associations in widely different arc-type tectonic settings we suggest that tectonic setting is not a major factor in determining the occurrence of high-Mg rocks as tentatively suggested by SAUNDERS et al. (1987).

In a number of cases high-Mg lavas in arc-type associations have been referred to as boninitic or boninite-like. We suggest that this is inappropriate and may create unnecessary confusion. We advocate the use of high-Mg as a prefix to rock terms consistent with the magmatic association in which the high-Mg lavas occur (e.g. high-Mg tholeiitic basalt, high-Mg banakite, etc.).

Acknowledgements

We thank B. M. BAKKEN, D. R. BODEN, S. D. WEAVER, A. L. GRUNDER and J. H. DILLES for helpful reviews of earlier drafts.

References

AOKI, K. & FUJIMAKI, H. (1982): Petrology and geochemistry of calc-alkaline andesite of presumed upper mantle origin from Itinomegata, Japan. – Amer. Miner., 67, 1–3.

ARCULUS, R., JOHNSON, R. W., CHAPPELL, B. W., MCKEE, C. O. & SARAI, H. (1983): Ophiolite-contaminated andesites, trachybasalts and cognate inclusions of Mount Lamington Papua New Guinea: anhydride–amphibole bearing lavas and the 1951 cumulodome. – J. of volcanology and Geothermal Res., 4, 215–247.

BLOOMER, S. H. & HAWKINS, J. W. (1987): Petrology and geochemistry of boninite series volcanic rocks from the Mariana Trench. – Contr. to Mineralogy and Petrology, 97, 361–377.

Cox, K. G. & Bell, J. D. (1972): A crystal fractionation model for basaltic rocks of the New Georgia Group, British Solomon Islands. – Contr. to Mineralogy and Petrology, **37**, 1–13.

Curtis, J. W. (1973): Plate tectonics and the Papua New Guinea–Solomon Islands region. – J. of the Geological Soc. of Australia, **20**, 21–36.

Davies, H. L., Symonds, P. A. & Ripper, I. A. (1984): Structure and evolution of the southern Solomon Sea region. – Bur. of Miner. Resources J. of Austral. Geology and Geophysics, **9**, 49–68.

Graham, I. J. & Hackett, W. R. (1987): Petrology of calc–alkaline lavas from Ruapehu Volcano and related vents, Taupo Volcanic Zone, New Zealand. – J. of Petrology, **28**, 531–567.

Gust, D. A. & Perfit, M. R. (1987): Phase relations of a high-Mg basalt from the Aleutian Island Arc: Implications for primary island arc basalts and high-Al basalts. – Contr. to Mineralogy and Petrology, **97**, 7–18.

Hamilton, W. (1979): Tectonics of the Indonesian region. – United States Geological Surv. Professional Pap., **1078**, 293–304.

Jakes, P. & Smith, I. E. (1970): High potassium calc–alkaline rocks from Cape Nelson, eastern Papua. – Contr. to Mineralogy and Petrology, **28**, 259–271.

Jakes, P. & White, A. J. R. (1972): Major and trace element abundances in volcanic rocks of orogenic areas. – Geological Soc. of America Bull., **83**, 29–40.

Jenner, G. A. (1981): Geochemistry of high-Mg andesites from Cape Vogel, Papua New Guinea. – Chem. Geology, **33**, 307–332.

Johnson, R. W. (1977): Distribution and major-element chemistry of late Cainozoic volcanoes at the southern margin of the Bismarck Sea, Papua New Guinea. – Bur. of Miner. Resources of Australia Report **188**, 170 pp.

– (1979): Geotectonics and volcanism in Papua New Guinea: a review of the late Cainozoic. – Bur. of Miner. Resources J. of Austral. Geology and Geophysics, **4**, 181–207.

Johnson, R. W., Mackenzie, D. E. & Smith, I. E. M. (1978 a): Volcanic rock associations at convergent plate boundaries: reappraisal of the concept using case histories from Papua New Guinea. – Geological Soc. of America Bull., **89**, 96–106.

– – – (1978 b): Delayed partial melting of subduction-modified mantle in Papua New Guinea. – Tectonophysics, **46**, 197–216.

Johnson, R. W., MacNab, R. P., Arculus, R. J., Ryburn, R. J., Cooke, R. J. S. & Chappell, B. W. (1983): Bamus volcano, Papua New Guinea: dormant neighbour of Uluwan, and magnesian andesite locality. – Geologische Rdsch., **72**, 207–237.

Johnson, T. & Molnar, P. (1972): Focal mechanisms and plate tectonics of the southwest Pacific. – J. of Geophysical Res., **77**, 5000–5032.

Kuroda, M., Shiraki, K. & Urano, H. (1978): Boninite as a possible calc–alkaline magma. – Bull. of Volcanology, **41**, 563–575.

Kay, R. W. (1978): Aleutian magnesian andesites: melts from subducted Pacific Ocean crust. – J. of Volcanology and Geothermal Res., **4**, 117–132.

Luyendyk, B. P., MacDonald, K. C. & Bryan, W. B. (1973): Rifting history of the Woodlark basin in the southwest Pacific. – Geological Soc. of America Bull., **84**, 1125–1134.

Mackenzie, D. E. (1976): Nature and origin of late Cainozoic volcanoes in western Papua New Guinea. – In: Johnson, R. W. (Ed.): Volcanism in Australasia, 221–238.

Mackenzie, D. E. & Chappell, B. W. (1972): Shoshonitic and calc–alkaline lavas from the Highlands of Papua New Guinea. – Contr. to Mineralogy and Petrology, **35**, 50–62.

MEEN, J. K. & EGGLER, D. H. (1987): Petrology and geochemistry of the Cretaceous Independence volcanic suite, Absaroka Mountains, Montana: clues to the composition of the Archean sub-Montana mantle. – Geological Soc. of America Bull., **98**, 238–247.

MORRIS, J. D., JEZEK, P. A., HART, S. R. & GILL, J. B. (1983): The Halmahera island arc, Molucca Sea collision zone, Indonesia: a geochemical survey. – In: HAYES, D. E. (Ed.): The tectonic evolution of southeast Asian seas and islands, Part 2. – Amer. Geophysical Union Geophysical Monograph **27**, 373–387.

NOBLE, D. C., BOWMAN, H. R., HEBERT, A. J., SILBERMAN, M. L., HEROPOULOS, C. E., FABBI, B. P. & HEDGE, C. E. (1975): Chemical and isotopic constraints on the origin of low-silica latite and andesite from the Andes of central Peru. – Geology, **3**, 501–520.

NYE, C. J. & REID, M. R. (1986): Geochemistry of primary and least fractionated lavas from Okmok Volcano, central Aleutians: Implications for arc magmagenesis. – J. of Geophysical Res., **91**, 10271–10287.

PECCERILLO, A. & TAYLOR, S. R. (1976): Geochemistry of Eocene calc-alkaline volcanic rocks from the Kastamonu area, northern Turkey. – Contr. to Mineralogy and Petrology, **58**, 63–81.

PUIG, A., HERVE, M., SUAREZ, M. & SAUNDERS, A. D. (1984): Calc-alkaline and alkaline Miocene and calc-alkaline Recent volcanism in the southernmost Patagonian Cordillera, Chile. – J. of Volcanology and Geothermal Res., **21**, 149–163.

ROEDER, P. L. & EMSLIE, R. F. (1970): Olivine-liquid equilibrium. – Contr. to Mineralogy and Petrology, **29**, 275–289.

SAUNDERS, A. D., ROGERS, G., MARRINER, G. F., TERRELL, D. J. & VERMA, S. P. (1987): Geochemistry of Cenozoic to Recent volcanic rocks, Baja California, Mexico: Implications for the petrogenesis of post-subduction magmas. – J. of Volcanology and Geothermal Res., **32**, 223–246.

SHIRAKI, K., KURODA, N., MARUYAMA, S. & URANO, H. (1978): Evolution of the Tertiary volcanic rocks in the Izu-Mariana arc. – Bull. of Volcanology, **41**, 548–561.

SMITH, A. L. & CARMICHAEL, I. S. E. (1968): Quaternary lavas from the southern Cascades, western U.S.A. – Contr. to Mineralogy and Petrology, **19**, 212–238.

SMITH, I. E. M. (1972): High potassium intrusives from southeastern Papua. – Contr. to Mineralogy and Petrology, **34**, 167–176.

– (1981): Young volcanoes in eastern Papua. – In: JOHNSON, R. W. (Ed.): Cooke-Ravian volume of volcanological papers. – Geological Survey of Papua New Guinea Memoir, **10**, 257–265.

– (1983): Volcanic evolution in eastern Papua. – Tectonophysics, **87**, 315–333.

SMITH, I. E. M., CHAPPELL, B. W., WARD, G. K. & FREEMAN, R. S. (1977): Peralkaline rhyolites associated with andesitic arcs of the southwest Pacific. – Earth and Planet. Sci. Let., **37**, 230–236.

SMITH, I. E. M. & JOHNSON, R. W. (1981): Contrasting rhyolite suites in the late Cenozoic of Papua New Guinea. – J. of Geophysical Res., **86**, 10257–10272.

SMITH, I. E. M. & MILSOM, J. S. (1984): Late Cenozoic volcanism and extension in eastern Papua. – In: Geological Soc. of Lond. Spec. Publ., **16**, 163–171.

SUN, S. S. & NESBITT, R. W. (1978): Geochemical regularities and genetic significance of ophiolitic basalts. – Geology, **6**, 689–693.

TARNEY, J., WEAVER, S. D., SAUNDERS, A. D., PANKHURST, R. J. & BARKER, P. F. (1982): Volcanic evolution of the northern Antarctic Peninsula and the Scotia arc. – In: ANDESITES, THORPE, R. S. (Ed.): John Wiley and Sons, 371–400.

TATSUMI, Y. & ISHIZAKA, K. (1981): Existence of andesitic primary magma: an example from southwest Japan. – Earth and Planet. Sci. Let., **53**, 124–130.

– – (1982 a): Magnesian andesite and basalt from Shodo-Shima island, southwest Japan, and their bearing on the genesis of calc–alkaline andesites. – Lithos, **15**, 161–172.

– – (1982 b): Origin of high-magnesian andesites in the Steouchi volcanic belt, southwest Japan, I. Petrology and chemical characteristics. – Earth and Planet. Sci. Let., **60**, 293–304.

WEAVER, S. D., SAUNDERS, A. D., PANKHURST, R. J. & TARNEY, J. (1979): A geochemical study of Magmatism associated with the initial stages of back-arc spreading: the Quaternary volcanics of Bransfield Strait, from South Shetland Islands. – Contr. to Mineralogy and Petrology, **68**, 151–169.

Manuscript received by the editor November 28, 1988; ready for print June 1989.

Author's addresses:

IAN E. M. SMITH, Department of Geology, University of Auckland, Private bag, Auckland, New Zealand.

PETER A. MITCHELL, Department of Geology, University of Canterbury, Private bag, Christchurch, New Zealand.